Dimensionnement fiabiliste sous chargements complexes : de la spécification à la validation

Emilien Baroux

▶ **To cite this version:**

Emilien Baroux. Dimensionnement fiabiliste sous chargements complexes : de la spécification à la validation. Génie mécanique [physics.class-ph]. Institut Polytechnique de Paris, 2023. Français. NNT : 2023IPPAX042 . tel-04257338

HAL Id: tel-04257338

https://theses.hal.science/tel-04257338v1

Submitted on 25 Oct 2023

HAL is a multi-disciplinary open access archive for the deposit and dissemination of scientific research documents, whether they are published or not. The documents may come from teaching and research institutions in France or abroad, or from public or private research centers.

L'archive ouverte pluridisciplinaire **HAL**, est destinée au dépôt et à la diffusion de documents scientifiques de niveau recherche, publiés ou non, émanant des établissements d'enseignement et de recherche français ou étrangers, des laboratoires publics ou privés.

INSTITUT POLYTECHNIQUE DE PARIS

NNT : 2023IPPAX042

Thèse de doctorat

Reliable design under complex loads: from specification to validation

Thèse de doctorat de l'Institut Polytechnique de Paris
préparée à l'École polytechnique

École doctorale n°626 École doctorale de l'Institut Polytechnique de Paris (EDIPP)
Spécialité de doctorat : Sciences et technologies industrielles

Thèse présentée et soutenue à Palaiseau, le Lundi 19 juin 2023, par

EMILIEN BAROUX

Composition du Jury :

Cédric Doudard Directeur de recherche, ENSTA Bretagne (IRDL)	Rapporteur
Franck Morel Directeur de recherche, Arts & Métiers Angers (LAMPA)	Rapporteur
Habibou Maitournam Directeur de recherche, ENSTA Paris (IMSIA)	Président de jury
Michele Sebag Directeur de recherche, Université Paris-Saclay (LRI)	Examinatrice
Cécile Mattrand Maître de conférence, SIGMA Clermont (Institut Pascal)	Examinatrice
Andrei Constantinescu Directeur de recherche, École Polytechnique (LMS)	Directeur de thèse
Patrick Pamphile Maître de conférence, Université Paris-Saclay (LMO)	Co-directeur de thèse
Laurent Rota Ingénieur chercheur, Stellantis	Co-encadrant industriel
Benoit Delattre Ingénieur chercheur, Stellantis	Co-encadrant industriel

« On peut, si on veut, ramener tout l'art de vivre à un bon usage du langage. »

Simone Weil, 1934

Acknowledgements

This thesis was conducted in the Laboratoire de Mécanique des Solides (LMS) of the Institut Polytechnique de Paris (IPP), and was co-supervised in the Laboratoire de Mathématiques d'Orsay (LMO) of the Université Paris-Saclay (UPS), where it was part of the team CELESTE of Inria Paris-Saclay. It was a collaboration with the automotive company Stellantis (formerly Groupe PSA) in the form of an industrial PhD convention (CIFRE). The project was funded jointly by Stellantis and the Association Nationale Recherche Technologie (ANRT).

I thank Cédric Doudard and Franck Morel for accepting to be the reviewers of this hefty manuscript, and for the very kind, dedicated and interesting exchanges on this topic. I thank Michèle Sebag, Cécile Mattrand and Habibou Maitournam for accepting to examine this thesis, for their interest and for the quality of their input during the defense.

I would like to thank Andrei Constantinescu for accepting to be my supervisor for this thesis at the LMS, as well as for his trust and optimism. I also thank Patrick Pamphile for accepting to co-supervise this thesis at the LMO, for the crucial mathematical and general inputs that he has provided, as well as for the time, energy and engagement that he has conscientiously invested in this project throughout these three years.

It was a great pleasure to share the environment at the LMS with Svetlana, Nikhil, Nicolas, Nina, Geoffrey, Phillip, Sam and all the other fellow PhD students and postdoctoral researchers that came and went in the lab. Thanks for all the activities, coffees and chats that we have shared. Je remercie chaleureusement l'équipe du secrétariat du LMS, Alexandra, Anna, Christiane, Danielle ainsi que tous les ingénieurs du labo, avec qui nous avons partagé d'importants moments de convivialité, et pour leur grande amabilité dans leurs missions. Je remercie également Jean-Pierre Bessis pour la curiosité qu'il a montré pour la thèse ainsi que pour la qualité de ses contributions philosophiques et des cours qu'il donne à l'École Polytechnique.

I must extend my warmest thanks to Benoit Delattre, initiator and original industrial tutor of the thesis at Stellantis, for his engagement, his unwavering trust and his outstanding pedagogic quality. I also thank Laurent Rota, who regularly followed then tutored the thesis at Stellantis, with excellent efficiency, pragmatism and consideration. I am grateful for all the moments and video chats shared with Agathe, Zoran, Olivier, Arnaud (x2), Vinay, Fernando and all the members of the original R&D team in structural mechanics. I also thank Ida Raoult, first for introducing me to this amazing team in 2019 and second for facilitating the administrative and scientific beginning of the thesis in 2020 as co-tutor. I thank Matteo Facchinetti and the members of the expertise network in structural integrity and reliability at Stellantis, and also Enora, Alexandre and Olivier, fellow PhD students of the network.

Indeed, our concomitant labor on several aspects of the topic at stake has helped to give this work more clout and meaning. Finally, I thank Jamila, Sandrine, Marco and all the PhD students of the Stellantis PhD network, for their engagement in ensuring optimal work conditions, scientific excellence and its promotion in the company, as well as camaraderie against all odds.

I thank Catherine du Boisbaudry for her curiosity, her friendliness, and for facilitating the beginning of my next professional endeavor. I thank Mickaël Le Jacq and Laurent Heck from Centigon Security Group for their trust and I look forward to collaborating with them.

I would like to thank the psychologist of the IPP, Sylvie Coussot, for her helpful outlook, her professional support and her refreshing commitment to improving the mental health of the students of the school - a sizable undertaking. It is no mystery that a fraction of PhD students may chronically be led to experience anxiety, self-pressure and doubt or to sacrifice work-life balance to productivity. These symptoms must no longer be deemed normal - such an idea is still conveyed sometimes, for instance by some members of the administration of a doctoral school [Cristia 2022]. They often denote a large amount of mental load, either on the shoulders of the doctoral student or their supervisors' or both. Loneliness, communication issues or hazy collaboration and/or management strategies may be causes, and all of those issues require a thorough bilateral redefinition of work dynamics.

Je remercie l'équipe de l'association d'aide à personnes dépendantes Espace Singulier pour leur engagement, leur bonne humeur contagieuse et leur intérêt sincère pour les bénévoles. Je remercie M. et Mme. Kagan, M. et Mme. Curvale - que j'ai pu accompagner dans le cadre des missions de l'association - pour leur intérêt et leur grande amabilité.

Je remercie également mes amis de l'ENSTA Paris et d'ailleurs : Thierry, Lucie, Juliette, Viviane, Camille, Louise, Benoit et le reste de la team "Ça ira" pour tous les moments partagés en métropole comme en province, Eugénie pour toutes ces pizzas et ces discussions passionnantes, les Copains du Phare, et enfin les anciens de Moriarty (merci Léonie pour ta motivation à nous rassembler régulièrement !), de la Lolita et de SalleT Alumni, pour leurs dynamiques uniques et à qui je souhaite bonne continuation. Special thanks to Georgia for her cheerful and dedicated friendship, and to Greg for his wit and good taste in general.

Je remercie enfin ma famille, d'abord cousins, nièces, tantes et oncles, qu'ils soient dans le nord ou en Floride, pour leur affection malgré la rareté de nos retrouvailles, ainsi que feu mes grands-parents pour ce patrimoine immatériel qu'ils ont courageusement construit et légué. Et je remercie tout particulièrement mes parents, mon frère et ma soeur, pour leur soutien, les diverses attentions qu'ils portent et leur amour indéfectible.

Contents

Acknowledgements **5**

Contents **7**

I General Introduction **13**
I.1 Industrial context . . . 13
I.2 Reliable design and validation for automotive parts . . . 15
I.3 Suspension and body failure by fatigue . . . 16
I.4 Stress-Strength Interference . . . 17
I.5 The need for a multidimensional approach . . . 19
I.5.1 Four ambitions . . . 19
I.5.2 An anchor point and a finish line . . . 19
I.6 Thesis strategy and outline . . . 20

List of Symbols **23**

II Fatigue analysis of a component submitted to a given load configuration **33**
II.1 Chapter introduction . . . 33
II.2 Cauchy stress tensors and stress concentration . . . 34
II.3 Mechanical phenomena associated with fatigue at the microscopic scale . . . 36
II.3.1 Microscopic crack nucleation, propagation . . . 36
II.3.2 Degradation of mechanical properties over time . . . 38
II.3.3 Plasticity and residual stress . . . 38
II.4 Fatigue analysis under cyclic loads . . . 40
II.4.1 Empirical characterization and S-N curves . . . 41
II.4.2 Representativeness of specimens used to characterize components . . . 43
II.4.3 Multiaxial fatigue criteria . . . 44
II.4.4 Probabilistic fatigue models . . . 46
II.5 Damage evaluation under multiaxial variable amplitude local loads . . . 47
II.5.1 Cycle counting and Rainflow matrices . . . 48
II.5.2 Miner Law . . . 50
II.5.3 Counting damage for multiaxial load configurations . . . 53
II.5.4 The effect of cycle means on damage . . . 53
II.5.5 Damage equivalents for a zone . . . 55
II.6 Fatigue analysis of control points in an industrial context . . . 56
II.7 Chapter conclusion . . . 57

III Fatigue characterization of a complex part under multi-input loads 59
III.1 Chapter introduction . . . 59
III.2 Global loads on the system . . . 60
III.2.1 Global load components . . . 60
III.2.2 Service loads . . . 62
III.3 Definition and objectives of fatigue characterization . . . 62
III.4 Mechanical response: from global to local loads . . . 64
III.5 Fatigue of a structure . . . 66
III.5.1 Damage models for the structure . . . 66
III.5.2 Pseudo-damage and local contexts . . . 67
III.6 Determination or choice of local contexts and fatigue vectors . . . 68
III.6.1 Global load cases . . . 68
III.6.2 Chosen local contexts in the thesis . . . 73
III.6.3 Discussion on the exhaustiveness of local contexts . . . 73
III.7 A new fatigue characterization variable: magnitude . . . 75
III.7.1 Motivation: the properties of pseudo-damage . . . 75
III.7.2 Definition of damage-equivalent magnitudes . . . 77
III.7.3 Magnitude radars . . . 79
III.8 Chapter conclusion . . . 82
III.8.1 Synthesis . . . 82
III.8.2 Transition: Stress or severity? . . . 83

IV Exploratory analysis of pseudo-fatigue in service 85
IV.1 Chapter introduction . . . 85
IV.2 Missions for personal vehicles . . . 86
IV.2.1 Mission factors: Driver, Trip and Payload . . . 86
IV.2.2 Road events . . . 88
IV.2.3 Road environments . . . 89
IV.3 Service load data . . . 89
IV.3.1 Direct service sampling: vehicle loans, connected vehicles . . . 89
IV.3.2 Measurement campaigns on aggregated trips . . . 90
IV.4 Statistical analysis of Driver-Trip interactions on segments of a trip . . . 91
IV.4.1 Separate road environment analyses . . . 92
IV.4.2 Multiple Factor Analysis . . . 104
IV.4.3 Population analysis . . . 115
IV.4.4 Discussion: the sampling of road environments . . . 122
IV.4.5 Synthesis of the multiple factor analysis . . . 127
IV.5 Chapter conclusion . . . 127

V Modeling the pseudo-fatigue induced by missions in service 129
V.1 Chapter introduction . . . 129
V.2 How to elaborate a model on a large population of lifelong missions? . . . 130
V.2.1 Restriction on the market and conservative pseudo-fatigue models . . . 130
V.2.2 Trip composition, trip sampling . . . 131
V.2.3 Vehicle life, aggregated trips . . . 132
V.3 Statistical analysis of driver severity for an aggregated trip . . . 134
V.3.1 Problem definition for an aggregated trip . . . 134

V.3.2 Prior observation of the magnitudes . . . 136
V.3.3 Principal Component Analysis . . . 141
V.3.4 Population analysis . . . 147
V.4 Population distribution . . . 150
V.4.1 Intrinsic versus conditional severity . . . 150
V.4.2 Model determination . . . 151
V.4.3 Distribution of variables of pseudo-fatigue . . . 155
V.5 The choice of an aggregated trip . . . 159
V.5.1 Alternative trip . . . 160
V.5.2 Comparison of pseudo-fatigue for different aggregated trips . . . 161
V.5.3 Section perspective: including a sampling of trips to the model . . . 170
V.6 Extrapolating trips to an objective lifetime . . . 172
V.6.1 The issue: aggregated trips are short . . . 172
V.6.2 Rainflow spectrum model identification . . . 173
V.6.3 Per magnitude spectral extrapolation by inverse transform sampling . . . 176
V.6.4 Perspective: modeling the variability in severity for one driver . . . 180
V.7 Chapter conclusion . . . 181
V.7.1 Synthesis . . . 181
V.7.2 Adapting the method to new markets . . . 182
V.7.3 Adapting the method to new variables . . . 183

VI Design and validation objectives for the reliability of automotive components 185
VI.1 Chapter introduction . . . 185
VI.2 The ingredients of reliable design . . . 187
VI.2.1 Standard loading histories and spectra . . . 187
VI.2.2 Customer correlation . . . 190
VI.2.3 Reliability analyses, state functions . . . 191
VI.2.4 Synthesis . . . 194
VI.3 Definition of the design and validation problems for complex systems . . . 194
VI.3.1 Complex systems . . . 194
VI.3.2 Towards multidimensional Stress and Strength . . . 195
VI.3.3 Risk of failure of a system . . . 197
VI.3.4 The design problem . . . 198
VI.3.5 The validation problem . . . 200
VI.3.6 Current limitations . . . 202
VI.4 Determination of design and validation objectives in a unidimensional framework 203
VI.4.1 Risk of failure and severe clusters . . . 203
VI.4.2 1D design objective . . . 205
VI.4.3 1D validation objective . . . 206
VI.4.4 Consequences for the elaboration of validation objectives . . . 208
VI.5 Application to previous models . . . 209
VI.5.1 Objective magnitude per simple component . . . 209
VI.5.2 Synthetic severe mission . . . 212
VI.5.3 Comparison of synthetic severe missions . . . 219
VI.6 Chapter conclusion . . . 223

VII Equivalent test loads for the validation of reliability **225**
VII.1 Chapter introduction . . . 225
VII.1.1 From objectives to loads . . . 225
VII.1.2 Testable loads, numerical and physical trials . . . 226
VII.1.3 Strong or weak fatigue equivalents . . . 227
VII.2 Analytical parametric loads: a literature review . . . 228
VII.2.1 1D formulation . . . 228
VII.2.2 Multidimensional perspectives . . . 230
VII.3 Proving grounds (PG) . . . 232
VII.3.1 Tracks . . . 233
VII.3.2 Track absolute magnitudes . . . 235
VII.3.3 PG schedules . . . 236
VII.4 Pseudo-fatigue equivalence . . . 238
VII.4.1 Restrictions of inputs, restrictions of contexts . . . 238
VII.4.2 Pseudo-damage and magnitude distances . . . 239
VII.4.3 Magnitude homogenization versus weighting . . . 240
VII.4.4 Optimization problem definition . . . 240
VII.5 Equivalent PG schedules for synthetic severe missions . . . 241
VII.5.1 Replicating measured or simulated missions . . . 241
VII.5.2 Replicating objective clients . . . 246
VII.5.3 Balanced PG schedules . . . 249
VII.6 Chapter conclusion . . . 252

VIII General conclusion **255**
VIII.1 Perspectives on fatigue characterization . . . 258
VIII.1.1 Mechanical hypotheses . . . 258
VIII.1.2 Alternative fatigue characterization . . . 259
VIII.2 Perspective on the statistical analysis of service loads . . . 260
VIII.2.1 Improving the sampling of Trip . . . 260
VIII.2.2 Improving the characterization of Trip . . . 260
VIII.2.3 Refined model of the outskirts of the population . . . 261
VIII.2.4 Quantitative identification of road events . . . 262
VIII.3 Perspectives on the reliable design of complex parts . . . 262

Bibliography **264**

Glossaries **279**
RAMS . . . 279
Material mechanics . . . 280
Rainflow . . . 280
Structural mechanics . . . 280
Personal vehicle service . . . 281
Reliability . . . 282
Automotive terms . . . 283

Acronyms **285**

A Elements of vehicle design in the field of RAMS **287**
A.1 RAMS functions and design . . . 287
A.1.1 Safety . . . 287
A.1.2 Availability and maintainability . . . 288
A.1.3 Durability and reliability . . . 289
A.1.4 Explicit and implicit performances, what the customer buys . . . 290
A.2 Car subsystems and development . . . 291
A.2.1 Architecture of the rolling chassis of a vehicle . . . 291
A.2.2 The development of a new vehicle . . . 295

B Loading concatenation **299**
B.1 Fatigue, variations and sequences - mechanical point of view . . . 299
B.2 Path effect in fatigue prediction . . . 302
B.3 Sequences of loads . . . 304
B.3.1 Block loads versus the randomness of events . . . 304
B.4 Rainflow counting algorithm . . . 305
B.5 Rainflow residual, properties and treatment . . . 307
B.6 Intermediary conclusion and the problem of concatenated loads . . . 309
B.7 Rainflow counting on concatenations of loads . . . 309
B.7.1 Definition of naive and chaotic schedules . . . 310
B.8 Effect of concatenation order on the pseudo-damages induced by a schedule . 312

C Data preparation **317**
C.1 Origin and structure of road load data . . . 317
C.2 Origin and elaboration of (reference) proving ground schedules . . . 318
C.3 Computing pseudo-damage and speed quantities . . . 318
C.4 Building the data tables . . . 320

D Multivariate statistics **321**
D.1 Cloud of individuals and scaling . . . 322
D.2 Correlation of variables . . . 323
D.3 Principal Component Analysis (PCA) . . . 325
D.3.1 Why PCA? . . . 325
D.3.2 Principal component determination . . . 326
D.3.3 Individuals on a principal space . . . 327
D.3.4 Principal components as variables . . . 328

E The effect of payload **331**
E.1 Difficulties in payload sampling and normalization . . . 331
E.2 Payload and vehicle model effects observed on proving grounds . . . 332
E.3 A conservative payload setting for the evaluation of service pseudo-fatigue . . 335

Chapter I

General Introduction

I.1 Industrial context

The rapid evolution of the automotive market is encouraging vehicle assemblers to increase the general efficiency of their development processes, in order to decrease the time-to-market for each new vehicle model.

On top of this competitive aspect, both customers and decision-makers formulate new demands and use paradigms that prompt the development and generalization of alternative engine technologies - battery-powered, hydrogen or hybrid vehicles. New urban use paradigms also encourage the creation of new vehicle platforms: smaller urban vehicles, sometimes even driver-less vehicles in restricted environments.

The economic movements of automotive companies (partnerships, investment, mergers), the growing assertion of the specific identity of vehicle brands as well as the general increase in engineering competence over the world, all these factors also lead international automotive companies like Stellantis to explore new markets in different regions of the world. New vehicle models must then be adapted to the specific environments, expectations and regulations of their targeted regions.

All of these changes in paradigms, technologies and market lead the company to ensure that its design references and validation protocols are adequate and robust.

The development of a new vehicle model is structured around the elaboration of solutions that satisfy the requirements of the system. Once the requirements are written for the system (specification), they are propagated into requirements at each sublevel of the conception (allocation), as shown in the V cycle (see Fig. I.1 and [Haskins and Forsberg 2007]).

Designing means settling on the full description of a new version of parts, organs or the system to develop. It is the task of the project teams, as they look for an optimal solution in terms of cost, verifying all the requirements of the subsystem at stake.

Once prototypes of these parts are available, they are tested to verify if they validate their associated requirements. If so, they are then integrated into the upper levels (organs), which in turn are validated according to their associated requirements, and so on. If validation

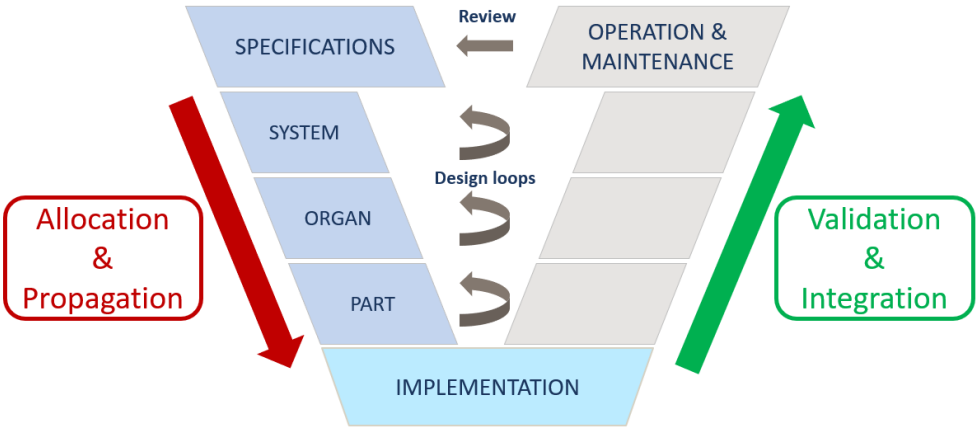

Fig. I.1: V-cycle paradigm for the conception of new systems

fails, the design is thought again and re-manufactured into a new prototype version.

Among the requirements of RAMS ensuring the safety, durability and availability of the vehicle, we focus on those that determine the reliability of parts composing its suspension and body (see Fig. I.2). The reliability of these organs denotes their ability to avoid failure or malfunction over a specified time objective under regular use conditions, also called service [Garvin 1987].

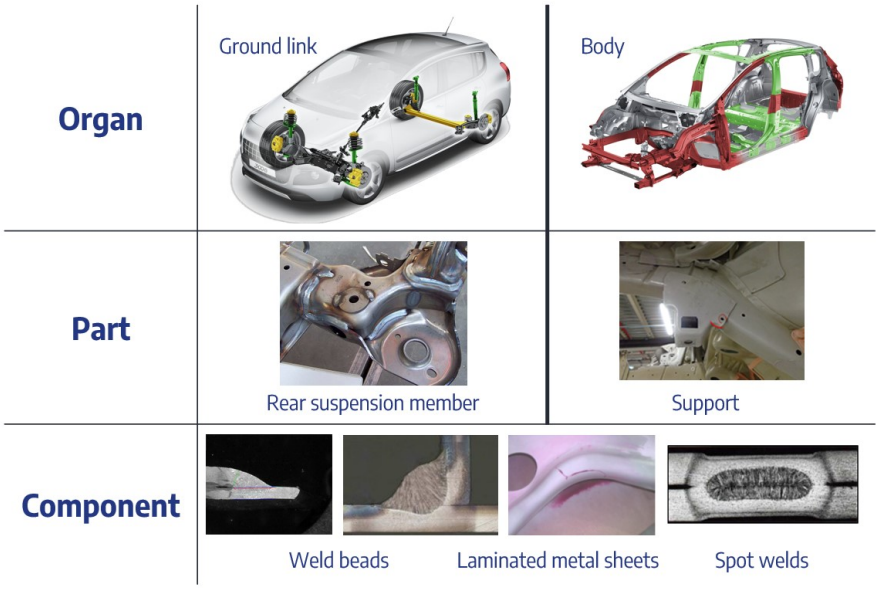

Fig. I.2: Suspension and body organs, and the distinction between part and component.

Suspension and body correspond to two carrier organs of the vehicle: their role is to maintain the integrity of the vehicle and to filter road and air-induced loads.

Unlike for crash performances or gas emissions, there is no definitive, conventional norm to specify adequate validation procedures nor criteria to assess the reliability of such passive subsystems (see [Beaumont 2013] §1.2). Moreover, personal vehicles are owned without a

thorough maintenance plan aimed at irreplaceable parts like suspensions and body. The catastrophic failure of these irreplaceable and unmaintainable carrier subsystems gravely endangers its users. Companies may be shunned or banned from countries and markets where their products appear to be weak and unsafe [Vatanen 2005].

Automotive companies must set and verify once and for all their own tolerance on the reliability of suspension and body parts, with respect to the knowledge of their conditions of usage in service, a compromise between price, weight and quality of materials and joints, and finally their available testing means.

Validation of the reliability of these organs must be ensured in a limited time with an increasing confidence at each conception level of the integration process. Robust validation procedures at early (lower) integration levels - parts - mean fewer unexpected failures in validation at later (upper) levels - organs and whole vehicle prototypes - and therefore fewer lengthy design loops. The validation method must also be coherent from one level of conception/integration to another: trials at an upper level of conception confirm the observations of trials performed at lower levels.

I.2 Reliable design and validation for automotive parts

In the case of organs that do not have a maintenance plan such as suspension and body, reliability is best characterized by their risk of failure (probability) in service before the lifetime objective of the system. Service denotes the population of plausible missions and associated loads that are considered devoid of abuse. This population is very diverse over the market of a vehicle model: Each user will drive differently, on different roads and with different payloads. This variability of missions begets a variability of road loads.

Failure of suspension and body organs is characterized by the occurrence of a macroscopic crack at any location of the structure. Components that are susceptible to be led to failure are illustrated in Fig. I.2: weld beads, spot welds and the edges of laminated metal sheets. Together, the suspension and the body contain a few dozen meters of weld beads, thousands of spot welds at diverse locations and a large geometrical diversity.

The welding process (gas metal arc or resistance welding) inevitably leads to the existence of microscopic notches at the toes of the weld after cooling down. However, the propagation of these microscopic defects is slow under repetitive mechanical loads. If the machining of metal sheets used in the manufacturing of a vehicle is well performed, cracks at the edge of the sheet are hard to initiate but easier to propagate.

The quality and final geometry of these components are variable from one location to another and from one issue of the vehicle model to another. This variability must also be taken into account to discuss the reliability of automotive organs.

Prior to the development of probabilistic reliable design, the strength of suspension and body parts was ensured by a maximalist or "rigid rule" approach [Svensson and Johannesson 2013]. The spirit of this approach was to ensure that the weakest issue of a part would still hold for its most severe known use cases. In that instant, the risk of failure of the

vehicle before its objective lifetime is strictly zero. In practice, this most severe use case was determined from an allegedly extremely severe reference. As for the weakest issue of a part, it was hard to characterize, both theoretically and physically. Anyhow, this method would lead the company to oversize the vehicle [Morel *et al.* 2010]. The probability that an extremely "severe" customer will be sold an extremely "weak" vehicle is extremely low.

Modern reliable design in the automotive industry follows a probabilistic approach. Reliability requirements take the form of a maximum acceptable risk of failure before an objective lifetime in service [Bignonnet and Thomas 2004]. The tolerance in terms of service loads, the acceptability of risk, the usual and expected lifetime of a system as well as its price, all these four aspects are considered simultaneously at the level of specifications to settle comprehensively on these objectives [Guarascio *et al.* 2007; Starr 1985].

I.3 Suspension and body failure by fatigue

Different failure mechanisms are identified and tracked in automotive parts [Beaumont 2013; Perroud 2009; Sonsino 2005] (see also Fig. I.3):

- Creep: for components submitted to long, sustained thermomechanical stresses [Binda 2010];
- Mechanical wear: for repetitive mobile contacts on soft materials (see tribology), for instance for vehicle gearboxes;
- Chemical or thermal modification of the microstructure, corrosion. Materials composing vehicle suspension and frame are usually coated to protect them from exterior hazards and the structure of the vehicle is designed to simplify the evacuation of water;
- Fatigue: microscopic propagation of defects under repeated thermomechanical loads that ultimately lead to macroscopic cracks.

The last one, fatigue, can be broken down in 3 domains based on the level and frequency of load variations: low cycle (10^3,10^4 variations), high cycle (10^5,10^6 variations) and gigacycle or vibratory fatigue ($> 10^7$ variations).

The reliability requirement for components of the suspension and body of a vehicle are only ensured for service loads, *i.e.* regular loads without abuse. The definition of service may be prone to cultural or regional interpretation. However, the company does set a threshold on global load levels that are deemed acceptable for service. A requirement on the maximum admissible amount of plastic deformation for loads below this threshold, is defined and tested, prior to reliability validation. The definition of these safety requirements notably ensures that all service loads do not induce macroscopical plastic deformations.

The parts of interest in this thesis are not submitted to heavy thermal or chemical loads susceptible to participate in their degradation, as opposed to powertrain parts for instance. Suspension and body parts are submitted to significant but not systematic single load events

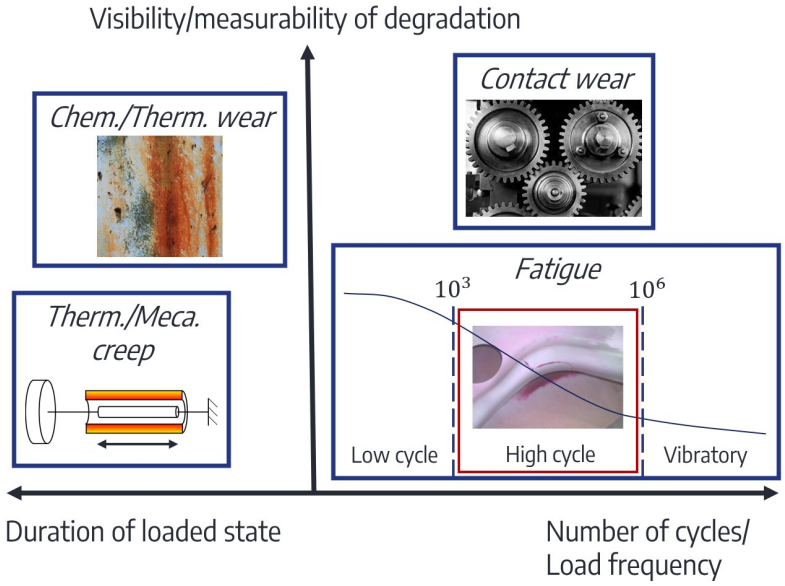

Fig. I.3: Modes of ruin to be considered in automotive subsystems submitted to thermo-chemo-mechanical loads, separated between degradation modes under maintained load states and temporary loads. Our domain of interest for the design of suspension and body parts is high cycle fatigue.

and loads due to road asperities. Their frequency is limited so that their number of variations falls in the low cycle and high cycle fatigue domains. Additional requirements in vibratory behavior ensure that the structure does not resonate under service frequencies, and thus that the levels in the very high cycle domain remain low enough. We will therefore focus on cold, high cycle metallic fatigue characterization.

Instead of implementing groundbreaking characterization models for the variety of phenomena at stake in the sensible zones of automotive structures, our priority is to clarify the hypotheses invoked or implied in current methods. We want to ensure that the indirect fatigue variables calculated from field data are indeed adequate and sufficient evaluations of the damage that a mission would induce on the sensible zones of a future vehicle.

I.4 Stress-Strength Interference

The major formalism implemented in the industry to conduct the probabilistic reliable design of automotive carrier parts is Stress-Strength Interference (SSI) methods. They were first introduced by [Lipson *et al.* 1967] and are widely used for the design of both electrical systems and structures submitted to mechanical loads.

For the design of the latter family of systems, a first univariate random variable is associated with the amount (potential) of damage induced by global loads on the weakest zone of a system [Bignonnet and Thomas 2001]. This variable is called Stress (not to be mixed up with Cauchy stress). It is sometimes named Severity or Load depending on constraints on

vocabulary. However, we will have to allocate these two other words to other variables. The main, defining, property of Stress is that it increases with the risk of failure of a structure.

Strength, also called Resistance, quantifies the highest level of Stress that a component to be designed can withstand without failing. It is built from knowledge of the component quality or from a characterization of its resistance under baseline load configurations, which must then be translated into a variable homogeneous to Stress.

Once this formalism is fully established, and only then, the risk of failure is given by the probability that the Stress surpasses the Strength, as shown in Fig. I.4.

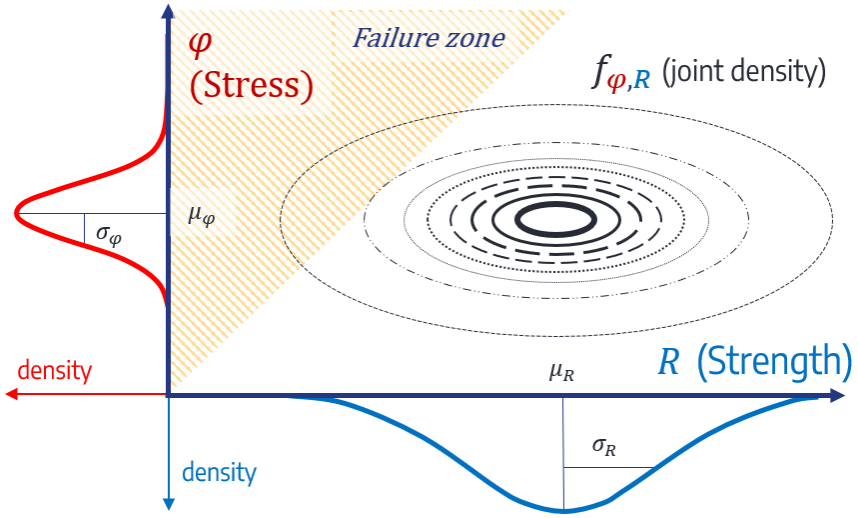

Fig. I.4: 1D Stress-Strength interference. Stress is distributed over the missions of a population. Strength is distributed over units/issues of a component/part/system

The distinction between Stress and Strength when discussing the failure of a vehicle allows to distinguish the sources of variability for this risk. Stress is variable due to the specificity of a client's uses and this variability is investigated and quantified by measurements in service. Strength is variable due to the manufacturing process and its variability derives from the manufacturing tolerances, as far as they are known. Stress and Strength are independent random variables. Indeed, the sale of a specific unit of a personal vehicle model is not determined, in terms of joint quality for instance, to the profile of the customer.

The major limitation of current implementations for our concern is the difficulty of defining Stress in the case of complex, partially known structures, such as vehicles that are yet to be designed. The need for a complex definition of Stress must yet be argued for. Moreover, the difficulties of evaluating Stress over service are not always introduced in an explicit manner with respect to the available data.

I.5 The need for a multidimensional approach

I.5.1 Four ambitions

Current methods used at Stellantis to quantify the variability of Stress in service have proven their efficiency for the adequate design of reliable personal combustion engine vehicles in the markets of Europe, Maghreb, South America and Asia. New geographical horizons require an update of the knowledge of real-life loads from available service measurements.

On the one hand, the determination of design references for the reliability of automotive subsystems must be initiated long before the start of a new vehicle project. On the other hand, the determination of adequate loading conditions for their validation must be adapted to the time scale of the project, *i.e.* be available within a short number of operations on a preliminary procedure. In both cases, an initial reference is required prior to knowing the design of the first parts of the structure. How can we establish a primitive characterization of the fatigue of a structure over a large variety of sensible zones, from an only partial knowledge of their interface loads and of their metallurgical and geometrical definitions?

Personal vehicle projects are associated to specific regions, with their own cultural specifics, regulations and road conditions. Through their segment or their power source (thermal or electrical), they may also target specific kinds of drivers and environments. How can we exploit the definition of missions of such systems to enhance the characterization of the multiple kinds of service fatigue that they induce?

The full application of SSI methods for the determination of adequate conditions for reliability validation requires a common ground between the characterization of Stress and that of Strength. How can we oppose the existing knowledge of the discrepancy of material quality to a richer characterization of the structural fatigue induced by a mission, and adapt the formulation of the risk of failure of a subsystem?

Ultimately, the company needs to provide the engineers with a limited base of regional design references for the first design phase of a new vehicle project. Such references must account for the objective levels over all subsystems and all failure modes. They take the form of proving ground schedules: concatenation of events associated with an artificial mission. How can we implement fatigue equivalents in a multi-dimensional framework to create design references that factorize a number of objectives for the reliability of the subsystems of a personal vehicle?

I.5.2 An anchor point and a finish line

To meet these four ambitions, the main limitation of current methods is their unidimensionality. This limits the versatility and quantity of information that it could bring to the contents of the mission in terms of multi-input load cases.

Global loads induced on a vehicle during a mission induce damage on several locations at once. Different kinds of simultaneous solicitations concentrate Cauchy stress at different sets of locations. Driving on different roads or having a different behavior at a crossroads changes

the directions, number of occurrences and level of wheel axle loads. A scalar definition for Stress cannot account for all the kinds of damages that missions can induce on all locations of the structure.

In order to unlock the possibility for a global and exhaustive analysis of multi-input service road loads, the key is an intermediary multidimensional fatigue characterization. Each dimension (pseudo-damage) would be related (proportional) to the fatigue (damage) induced on one set of sensible zones of the structure.

The endpoint of the characterization of service loads is the definition of an equivalent loading history, in the form of a schedule of events, that replicates one or several suitable validation objectives for the reliability of automotive components. This objective will take a form homogeneous to the intermediary fatigue characterization.

The fatigue characterization used to derive such equivalent loads must be relevant and exhaustive with respect to all high cycle fatigue phenomena at stake in the structure. It must be observable: available from measured or simulated wheel axle loads in service. Its dimensions must be physically interpretable, with respect to the load cases of the structures and to the obstacles and maneuvers that the vehicle encounters. We must prove that its distribution over a population of missions is well defined. We need to adapt this distribution to the sub-problems of reliable design, that is, to the framework of SSI and to the formula for the risk of failure of a subsystem. Finally, we need to translate this characterization into testable loads that reproduce the same fatigue as a mission of interest.

This significant agenda for our anchor point - fatigue characterization - motivates a complete investigation of the current method and a coherent framework for the evaluation of service usage and the determination of equivalent loads. We must ensure continuity between the different scientific domains at stake - solid mechanics, statistical learning, stochastic modeling, reliability and fatigue equivalence (optimization).

I.6 Thesis strategy and outline

This thesis belongs to a collaborative project combining the efforts of four industrial PhD students, their supervisors, as well as the expertise at Stellantis on structural integrity and reliability. Our goal is to provide the company with a thorough, robust and mechanically understandable method to improve the efficiency and confidence of reliable design and validation methods for any new personal car project.

We want to evaluate the fatigue induced on suspension and body parts by service loading histories. Locations of these parts that may be led to failure for some missions will be defined as sensible zones. We will propose a finite classification of these zones in terms of geometrical and material properties - local contexts. Each local context will be associated with a generic fatigue model. Sufficient ingredients of these fatigue models will be selected as our fatigue variables of interest - a fatigue characterization.

The variability of this characterization on a sample of missions is investigated through the lens of different mission factors, describing either the behavior of the driver, the compo-

sition of the trip or the number of passengers. Understanding the sources for the variability of our quantities of interest and the shape of the population will allow us to propose a model for their distribution, to be further implemented in a complete reliable design framework.

The ambition of the thesis is ultimately to determine adequate validation procedures - loads and thresholds above which a prototype fails validation - able to ensure the control of the risk of failure of new car projects depending on their target markets. Our privileged focus is the link between these test conditions and the acquired data on real-life usage (see Fig. I.5).

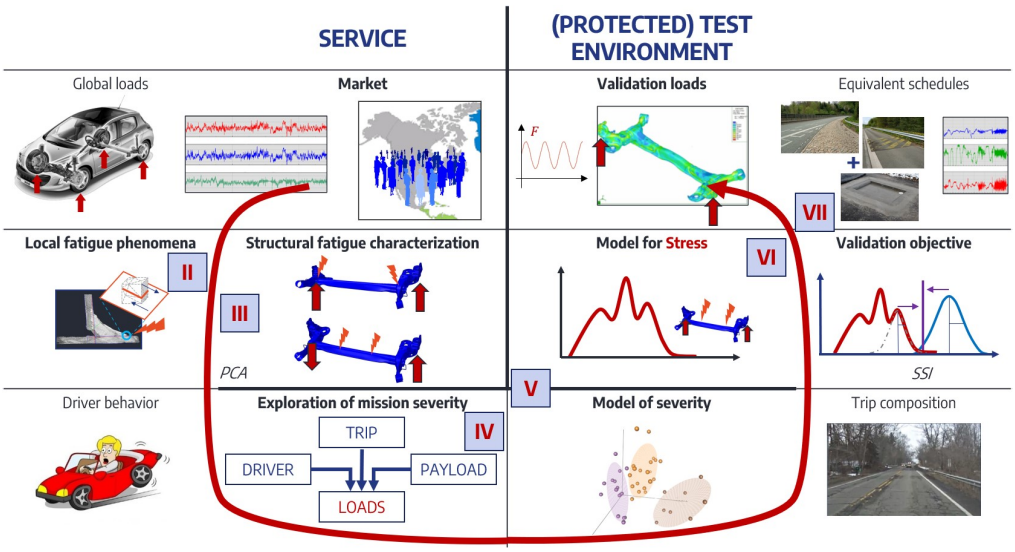

Fig. I.5: Structure of the thesis. The study starts with service loading histories and concludes with equivalent loading histories.

The mechanical framework and literature for the multiaxial fatigue analysis of single assemblies under variable amplitude local loads are presented in Chapter II. The goal is to present the phenomena at stake and to justify the fatigue variables chosen to describe their progression over the life of a vehicle.

The determination of an exhaustive quantification of the fatigue induced by multi-input loads on a diversity of local fatigue contexts throughout a complex structure is detailed in the rest of Chapter III. The main idea of the characterization is to measure the occurrence and level of various global load cases that deform the structure in a particular way. The result is a vector of variables of pseudo-fatigue calculated from the history of global loads on the vehicle. It contains all the sufficient and necessary information to evaluate the potential of fatigue that service loads can induce on all sensible zones of the structure.

A new approach to severity is enlightened in the exploratory analysis of pseudo-fatigue in Chapter IV. Available measurements of road load data are analyzed and interpreted with respect to the physical meaning of the variables we have previously defined. The content of the road is related to different road environments, such as urban, highway or back roads. An exploratory analysis is conducted through the implementation of Multiple Factor Analysis (MFA). It unveils a hierarchical structure of complex driver severity: Drivers distinguish themselves in their management of obstacles, maneuvers, traffic and speed, but also from one environment to another.

A distribution of the variables of pseudo-fatigue over a restriction of the populations of trips is elaborated in Chapter V. In order to overcome the lack of data on Driver Trip couples, we consider a conservative approach: the sampled drivers of the previous analysis are simulated on an aggregated trip. This trip is considered to represent the averaged content of a vehicle's life. The analysis is conservative if it overestimates the most severe observations of pseudo-fatigue over the population. Differences among drivers on this aggregated trip are investigated by a Principal Component Analysis (PCA) in order to reveal a multidimensional conditional driver severity. The distribution of the conditional severity over the population of drivers is built as a Gaussian mixture. The parameters of the mixture are determined from maximum likelihood estimation and the implementation of the Expectation-Maximization algorithm. The choice of the aggregated trip and its extrapolation to a vehicle lifetime are discussed at the end of the chapter.

In Chapter VI, we dive deeper into the current practice of reliable design in the literature. Then, we present a method to translate our previously determined mission-comprehensive distribution of severity into adequate Stress and Strength variables for the design of given subsets of the vehicle. The chapter culminates in the proposition of reliability validation objectives expressed in terms of severity and of pseudo-fatigue to reproduce on a prototype to test its resistance.

Finally, in Chapter VII, we recall the framework of fatigue-equivalent loads set up in [Genet (Le Corre) 2006; Raoult and Delattre 2020] to define loading procedures replicating these validation objectives and therefore suitable for the validation procedure of subsets of a vehicle. We elaborate equivalent schedules of proving ground events to replicate the pseudo-fatigue induced over the structure by synthetic severe missions of interest. Their content further helps to understand the content, in terms of loads and expected induced fatigue, of such new reference missions.

List of Symbols

Mathematical notations

$\{a,b\}$ Set containing a and b

$[a,b]$ Closed interval between a and b

$]a,b]$ resp. $[a,b[$ Half-closed interval between a and b, a excluded resp. b excluded

$[\![a,b]\!]$ Interval of integers from a to b

$(a_i)_{i\in[\![c,d]\!]}$ A vector or tuple built from the concatenation of several variables (not necessarily scalars). Vectors are written vertically

$\underline{a}$ Spatial vector or 1D tensor

$\vec{a}$ Load-related vector

$\overrightarrow{a}$ Structural fatigue characterization-related vector

$\vec{a}$ Any other kind of vector or tuple

$\underline{\underline{A}}$ 2D tensor

${}^T(a)$ Transposition of a vector or matrix

$a \cdot b$ Product of variables

$\vec{a} \bullet \vec{b} = \sum_i a_i \cdot b_i$ Simple contraction, a.k.a. scalar product

$\langle \vec{a} \mid \vec{b} \rangle = \sum_i a_i \cdot b_i$ Scalar product, alternative notation

$\vec{a} \bullet B = \left(\sum_i a_i \cdot b_{i,j}\right)_j$ Simple contraction with a matrix

$A : B = \sum_i \sum_j a_{i,j} b_{i,j}$ Double contraction

$\vec{e}_1 \otimes \vec{e}_2$ Dyadic product (fr. *produit tensoriel*)

$\widetilde{\vec{a}} = (\widetilde{a}_i)_{i\in[\![c,d]\!]}$ Unit vector or unit part of vector $\vec{a}$

$|a|$ Absolute value operator

$|\vec{a}| = \|\vec{a}\|_2$ Euclidian norm operator

$\|\vec{a}\|_?$ Any other norm operator

$|A|$ Determinant of A (if A is a squared matrix)

$\mathbb{R}$ Space of real numbers

$\mathbb{R}^0$ Space of positive real numbers, 0 included

$\mathbb{N}$ Space of natural integers

$\mathbb{U}^\kappa$ Space of real unit vectors of dimension κ

$\mathbf{A} = [a(i) \ \forall i \in [c,d]]$ A scalar timed sequence or history

$\vec{\mathbf{A}} = (\mathbf{A}_j)_{j \in [\![e,f]\!]}$ A vector time sequence or history

$\mathbf{A}||\mathbf{B}$ Concatenation of two time sequences or histories

Mechanical (local) quantities

Ω Spatial domain / Set of all points in a structure

$\underline{\underline{\varepsilon}}$ Green-Lagrange local deformation tensor, unused

$\underline{\underline{\sigma}}$ Cauchy local stress tensor

z A geographical location (a.k.a. zone) in the domain, associated with a Representative Element of Volume (REV)

$\left[\underline{\underline{\sigma}}\right]$ A Cauchy stress history

S (in S-N) Description of load / Cauchy stress for cyclic loading histories

N (in S-N) Number of repetitions of a load cycle

ΔS (in S-N) Range (peak-to-peak) of a cycle of S

ρ Load ratio, usually defined as the ratio between the minimum and the maximum of the load cycle (except in [Susmel and Lazzarin 2002])

$(N_0, \Delta S_0)$ Reference point of a Basquin model in an S-N graph

m Exponent used in a Basquin model

ΔS_u Ultimate strength of the component of interest

ΔS_∞ Endurance limit for the component of interest

N_∞ Number of cycles marking the beginning of the endurance domain

$f\left(\left[\underline{\underline{\sigma}}\right],\vec{k}_f\right)$ A fatigue criterion with parameters $\vec{k}_f$

τ A fatigue variable used in a fatigue criterion. Usually calculated from the instantaneous value of $\underline{\underline{\sigma}}$ or on the full history of $\underline{\underline{\sigma}}$ in a load cycle

$\underline{h}$ Normal vector of a local slip plane in a granular material

$\underline{u}$ Slip direction vector in a granular material

$\underline{\underline{H}}$ Tensor associated with the linear form on $\underline{\underline{\sigma}}$ that determines a linear fatigue variable

$D\left(z,\left[\underline{\underline{\sigma}}\right]\right)$ Damage induced on the zone z by the local loading history $\left[\underline{\underline{\sigma}}\right]$

Structural quantities

F Instantaneous scalar load / Global load component, usually one component of a point force (a.k.a. effort) at the input of a structure (*e.g.* wheel axles)

$\vec{F}$ Instantaneous vector load / Global load, usually a vector of efforts at the input of a structure

ϑ Moment component at wheel axle (unused)

$\mathbf{F} = [F(t),\ \forall t < T]$ A scalar loading history / Global loading component. The instant t is always considered to be positive

T Duration of a loading history

$\vec{\mathbf{F}} = (\mathbf{F}_j)_{j\in[\![1,n_F]\!]}$ A vector loading history / Global loading history

$\mathbb{F}$ Space of global loading histories for a personal vehicle

$\underline{\underline{K}}_{z,k}$ A (Cauchy stress) localization tensor associated with a zone z and to the k-th component of the global loads of a structure

$D\left(z,\vec{\mathbf{F}}\right)$ Damage induced by the global loading history $\vec{\mathbf{F}}$ on the zone z

φ One component of fatigue characterization, for a set of sensible zones of a structure

$\vec{\varphi} = (\varphi_k)_{k\in[\![1,\kappa]\!]}$ A fatigue characterization for a structure

$\vec{\alpha}_z$ Local absolute combination vector. Combined with the components of a global loading history, it determines the scalar history of a fatigue variable of interest for the fatigue analysis of zone z

$\widetilde{\vec{\alpha}}_z$ or $\widetilde{\vec{\alpha}}$ Combination vector associated with a global load case. Combined with the components of a global loading history, it determines the scalar history of a global load case, from which a pseudo-damage, proportional to the damage on z, can be calculated

γ_z or $\gamma = \left(\widetilde{\vec{\alpha}}_z, m_z\right)$ Local context, the joint information of a local combination vector and of a Basquin exponent, for instance associated with the calculation of the damage at zone z

$\breve{D}\left(z, \vec{\mathbf{F}}\right) = \breve{D}\left(\gamma_z, \vec{\mathbf{F}}\right)$ Pseudo-damage calculated on a local context γ_z, proportional to the damage of z.

$\mathbf{F}_\alpha$ History of a global load case, calculated using the local combination vector $\widetilde{\vec{\alpha}}$

$\vec{e}_k$ Elementary vector of the space $\mathbb{R}^\kappa$ such that $e_k = 1$ and $e_h = 0 \ \forall h \neq k$

$M\left(\gamma, \vec{\mathbf{F}}\right) = \sqrt[m]{\vec{\breve{D}}\left(\gamma, \vec{\mathbf{F}}\right)}$ Equivalent magnitude at intercept, calculated for a local context γ. The exponent m is the one stored in γ

$\vec{M} = \left(M_k\right)_{k \in [\![1,\kappa]\!]}$

θ_k Angle used for the construction of a local combination vector $\widetilde{\vec{\alpha}}_k$ from the linear combination of two global load components

Rainflow counting of a signal

$\mathrm{Rf}^0\ (\mathbf{F})$ Application of the Rainflow algorithm on a scalar loading history $\mathbf{F}$, prior to closure

$C^0(\mathbf{F}) = \left(\Delta F_i(\mathbf{F}), \mu_i(\mathbf{F})\right)_{i \in [\![1, n^0_{\mathrm{cyc}}]\!]}$ Counted cycles on a scalar loading history

$\Delta F_i(\mathbf{F})$ Range of the i-th Rainflow cycle

$\mu_i(\mathbf{F})$ Mean of the i-th cycle (unused)

n^0_{cyc} Number of Rainflow cycles prior to closure

R^0 Rainflow residual: sequence of turning points that could not be paired into Rainflow cycles

$\mathrm{Rf}^\bullet\ (\mathbf{F}) = C^\bullet(\mathbf{F}) = \left(\Delta F_i(\mathbf{F}), \mu_i(\mathbf{F})\right)_{i \in [\![1, n_{\mathrm{cyc}}]\!]}$ Application of the Rainflow algorithm on a scalar loading history $\mathbf{F}$, with closure

n_{cyc} Number of Rainflow cycles counted on a given history, following closure

$\mathrm{Rf}^\bullet\ (\mathbf{F}) = C^\bullet(\mathbf{F}) = \left(\Delta F_i, \mu_i, n_i(\mathbf{F})\right)_{i \in [\![1, n_{\mathrm{bin}}]\!]}$ Classed Rainflow algorithm, with closure. $n_i(\mathbf{F})$ is the number of cycles counted on the loading history $\mathbf{F}$ that fall in the i-th class. We use the same notation for the operator for both unclassed (two lines earlier) or classed Rainflow counts. The use of unclassed or classed Rainflow counts will be clarified contextually

n_{bin} Number of Rainflow classes

d_i Marginal damage associated with the i-th cycle or to the i-th class of a Rainflow count

H_i Cumulative number of Rainflow cycles counted for all classes between i and n_{bin}

(α,ν) (In Section V.6) Shape parameters of a load spectrum model

Personal vehicle mission description

$\mathbb{A}$ Service loads / The set of loading histories that are plausible and acceptable following the use of a vehicle

Q_j Static vertical charge (in Newtons) / Charge associated with the j-th wheel of the vehicle

$Q_{\text{tot}} = \sum_{j\in[\![1,4]\!]} Q_j$ Total charge of the vehicle / Payload

$\mathcal{T}$ Trip of the mission / Aggregated trip

l Distance in kilometers driven over a trip. Sometimes called "duration" in a metonymic fashion

$L\left(\gamma_k,\vec{\mathbf{F}}\right) = \sqrt[m_k]{1/l}\cdot M\left(\gamma_k,\vec{\mathbf{F}}\right)$ Load intensity calculated for the k-th local context on the trip associated with the global loading history $\vec{\mathbf{F}}$

$e \in [\![1,r]\!]$ Index of a trip $\mathcal{T}$ composed of r segments

$\vec{\mathbf{F}}_c^e$ Global loading history observed on the c-th driver on the e-th segment of the trip

Statistical quantities and operators - Chapter IV

$L_{ck}^e = L\left(\gamma_k,\vec{\mathbf{F}}_c^e\right)$ Observation of the load intensity on the k-th local context, for the c-th individual and on the e-th segment of the trip

$L_{c\bullet}^e = \left(L_{ck}^e\right)_{k\in[\![1,\kappa]\!]}$ Vector of all observed load intensities for the c-th individual on the e-th segment

$L_{\bullet k}^e = \left(L_{ck}^e\right)_{c\in[\![1,n]\!]}$ Vector of the observations of the k-th variable on all individuals on the e-th segment

$\mathcal{C} = L_{\bullet\bullet}$ Dataset of load intensities measured for a sample of drivers on a segmented trip

$\mathcal{C}_e = L_{\bullet\bullet}^e$ Data subset of load intensities calculated on the e-th segment of a trip

$\overline{L}_k^e$ resp. $s_{L_k}^e$ Empirical average resp. biased estimator of the standard estimation of the load intensities evaluated for the k-th local context over the population of drivers on the e-th segment of the trip

Var (A), covar (A,B), corr (A,B) Variance, covariance and correlation operators

$Z_{ck}^{L,e} = \frac{L_{ck}^e - \overline{L}_k}{s_{L_k}}$ Scaled load intensity calculated for the k-th local context on the c-th driver of the dataset and on the e-th segment of the trip

$\mathcal{C}'_e$ Data subset of scaled load intensities calculated on the e-th segment of a trip

$\overrightarrow{L}^{\text{ref}} = \left(L_k^{\text{ref}}\right)_{k\in[\![1,\kappa]\!]}$ Signature vector for the visualization of load intensities in a radar

$\breve{L}_{ck}^e$ Normalized load intensity for the k-th local context, toward visualization in a radar of the load intensity calculated on the c-th driver on the e-th segment

$A_{\mathcal{C}_e}$ Correlation matrix calculated on the data set $\mathcal{C}_e$

λ_h^e and $\overrightarrow{b}_h^e$ Eigenvalue resp. eigenvector of the correlation matrix $A_{\mathcal{C}_e}$

x_{hk}^e Coordinate of the h-th eigenvector $\overrightarrow{b}_h^e$ on the dimension corresponding to the k-th load intensity calculated on the e-th segment

$\overrightarrow{S}_{ch}^e$ Coordinate of the c-th driver on the h-th principal component determined from the separate analysis of the e-th segment of the trip

$A_{\mathcal{C}}$ Correlation matrix calculated on the dataset $\mathcal{C}$, after its normalization by the principal components of the separate analysis for each data subset $\mathcal{C}_e$ prior to the implementation of MFA

λ_h and $\overrightarrow{b}_h$ Eigenvalue resp. eigenvector of the correlation matrix $A_{\mathcal{C}}$

x_{hk} Coordinate of the h-th eigenvector $\overrightarrow{b}_h$ on the dimension corresponding to the k-th load intensity

$\overrightarrow{S}_{ch}$ h-th coordinate of intrinsic severity for the c-th driver following implementation of MFA on dataset $\mathcal{C}$

Statistical quantities and operators - Chapter V

M_{ck} Observation of the k-th equivalent magnitude on the c-th individual

$\overrightarrow{M}_{c\bullet} = (M_{ck})_{k\in[\![1,\kappa]\!]}$ Vector of all observed variables for the c-th individual

$M_{\bullet k} = (M_{ck})_{c\in[\![1,n]\!]}$ Vector of the observations of the k-th variable on all individuals

$\mathcal{C}_{\mathcal{T}} = \overrightarrow{M}_{\bullet\bullet}$ Dataset of equivalent magnitudes simulated over the trip $\mathcal{T}$

$\overline{M}_k$ resp. s_{M_k} Empirical average resp. biased estimator of the standard estimation of the equivalent magnitudes induced by the drivers on the trip $\mathcal{T}_1$

$v_k = s_{M_k}/\overline{M}_k$ Variation coefficient for the k-th equivalent magnitude observed on the dataset

$Z_{ck}^{M,1} = \frac{M_{ck}^e - \overline{M}_k}{s_{M_k}}$ Scaled equivalent magnitude for the k-th local context on the c-th driver on the trip $\mathcal{T}_1$

$\overrightarrow{M}^{\text{ref}} = \left(M_k^{\text{ref}}\right)_{k\in[\![1,\kappa]\!]}$ Signature vector for the visualization of equivalent magnitudes in a radar

$\mathcal{C}'_{\mathcal{T}}$ Scaled dataset of equivalent magnitudes simulated on trip $\mathcal{T}$

A^1 Correlation matrix calculated on the dataset $\mathcal{C}_{\mathcal{T}_1}$

λ_h and $\overrightarrow{b}_h$ Eigenvalue resp. eigenvector of the correlation matrix

$\Lambda = (\lambda_h)_{h\in[\![1,\kappa]\!]}$ Diagonal matrix containing all eigenvalues of the correlation matrix

x_{hk} Coordinate of the h-th eigenvector $\overrightarrow{b}_h$ on the dimension corresponding to the k-th equivalent magnitude

$\overrightarrow{S}_{ch}$ h-th coordinate of conditional severity for the c-th driver following implementation of PCA on dataset $\mathcal{C}_{\mathcal{T}_1}$

B Rotation matrix between the space of scaled equivalent magnitudes and the space of conditional severity

f Generic density function of a multivariate Gaussian variable

f_1 Density function for the conditional severity on Trip $\mathcal{T}_1$

$\overrightarrow{\mu}_y$ resp. Σ_y Mean vector resp. covariance matrix for the y-th core of a Gaussian mixture

π_y Fraction of the y-th core in a Gaussian mixture

w Algorithm step

$\epsilon_y\left(\overrightarrow{S}\right)$ Responsibility of the y-th core of a Gaussian mixture on the observation $\overrightarrow{S}$

Card Cardinal operator: number of elements in a finite set

B_p Restriction of the rotation matrix to its p first line (following for instance the determination of a number of dimensions of severity)

Λ_p Diagonal matrix containing the p first eigenvalues of the correlation matrix

$\delta\overrightarrow{Z}$ A direction in the space of scaled equivalent magnitudes

$\delta\overrightarrow{S}$ A severization direction / a direction in the space of conditional severity

$q(P_n) = q_n$ A quantile associated with a probability P_n

$\mathcal{N}$ A Gaussian law

$\mathcal{N}_0$ The standard Gaussian law

α_{P_n} A number of standard deviations used to determine the P_n-quantile of a Gaussian law

Reliability analysis for a system

$\mathcal{V}$ Vehicle model / System / Designed system

$\mathcal{Y}$ Subsystem / Part / Component / Designed subsystem

$\vec{\chi}$ Vector of base variables for the evaluation of system or subsystem failure

ι In a FORM/SORM framework: reliability index

$g_{\mathcal{V}}$ State function of the system $\mathcal{V}$

$g_{\mathcal{Y}}$ State function of the subsystem $\mathcal{Y}$

P_f Maximum admissible risk of failure in a requirement of reliability

φ Scalar fatigue characterization / Stress realization / Pseudo-fatigue component

$\vec{\varphi}$ Fatigue characterization / Realization of a multidimensional Stress / Pseudo-fatigue

$\vec{\Phi}$ Multivariate random variable of multidimensional Stress

$\mu_{\Phi,y}$ resp. $v_{\Phi,y}$ Mean resp. variation coefficient calculated on the y-th core of a Gaussian mixture modeling scalar Stress

$\mathbb{D}$ Space of multidimensional Stress

$\vec{r}$ Resistance / Strength realization

$\vec{R}$ Multivariate random variable of multidimensional Strength

μ_R resp. v_R Mean resp. variation coefficient of scalar Strength

$\mathbb{V}$ Space of parameters of design

$d\vec{\varphi}$ Measure over $\mathbb{D}$

$d\vec{r}$ Measure over $\mathbb{V}$

$\vec{a} \triangleright \vec{b}$ Asymmetrical endorelation between vectors of the same space that is true if $\exists k, a_k > b_k$

$(\mathcal{R}_{\mathcal{V}}) : ...$ A proposition / A requirement in reliability for the system $\mathcal{V}$. Can be true or false

$\left(V_{\mathcal{Y}}\left(\Phi_t\right)_{t\in[\![1,n_v]\!]}\right)$: ... A proposition / A procedure performed with a set of trials $\left(\Phi_t\right)_{t\in[\![1,n_v]\!]}$. Is true resp. false if the designed subsystem passes resp. fails the procedure

$\Phi_t = \left(\overrightarrow{\varphi}_t\right)_{t\in[\![1,n_v]\!]}$ A set of trials defined by their objectives $\overrightarrow{\varphi}_t$ in terms of pseudo-fatigue

$T = q\left(P_f/\pi_3\right)^{\mathcal{N}_0}$ Quantile of the standard Gaussian law associated with the probability P_f/π_3 in a unidimensional framework.

μ_R^* 1D design objective in term of nominal Strength

φ_n resp. M_n 1D validation objective in term of Stress resp. equivalent magnitude

P_n Probability that the Stress induced by a mission surpasses the validation objective φ_n of a procedure

P_0 Expected rate of failure of a subsystem when submitted to a mission equivalent to its validation objective

α_y Number of standard deviations that characterizes a high quantile of the y-th core of a Gaussian mixture for scalar Stress

β Number of standard deviations that characterizes a low quantile of scalar Strength

α_3^* Value of α_3 determined by the arbitrary choice of β to define an adequate validation procedure in a unidimensional framework

β^* Value of β determined by the arbitrary choice of α_3 to define an adequate validation procedure in a unidimensional framework

λ Any parameter participating in defining an analytical loading history in the search for equivalent loads

$e \in [\![1,g]\!]$ Index of a proving ground track used to build a schedule

$\vec{n}$ A combination vector containing number of repetitions of tracks in a schedule

$\overrightarrow{v}$ A reference vector of magnitudes used to modify the ponderation of each component in a norm on $\mathbb{R}^\kappa$

ψ A permutation

I_d^g Identity matrix of size g

G Matrix containing the pseudo-damage vectors for all tracks used to build an equivalent schedule

Chapter II

Fatigue analysis of a component submitted to a given load configuration

II.1 Chapter introduction

The first step in the development of a reliable design method is to define failure, as well as variables/predictors to evaluate it on missions. Metallic vehicle organs such as suspension and body are said to fail when they lose their integrity due to the apparition of any macroscopic crack. Investigating the phenomena at stake at the microscopic level - defect initiation and propagation - unveils quantities that are able to predict such an outcome. Introducing these quantities is the goal of this chapter.

Fatigue corresponds to mechanical phenomena that locally degrade or at least modify the properties and integrity of material components because of repeated solicitations. Fatigue is embodied by the apparition and/or propagation of defects in the material. Their growth may lead to a loss in functionality or in integrity of the system (see Fig. II.1). This phenomenon unfolds continuously throughout the life of the system in the absence of abuse, even if the material is solicited well below its limit of macroscopic elasticity.

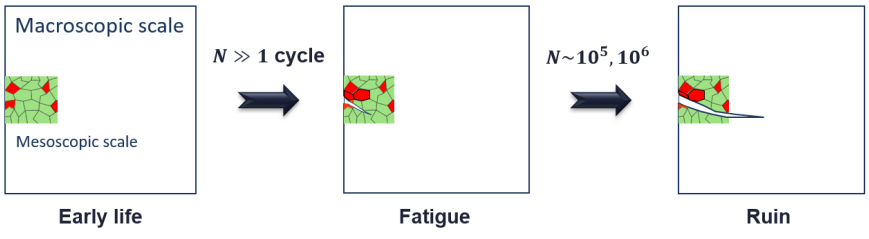

Fig. II.1: Propagation of a fissure in a granular material submitted to loads below the elastic limit of the material.

This elastic limit varies according to the quality and material of each part. So does the fatigue sensitivity of each zone to solicitations. We are therefore looking for predictive models that are suitable for the fatigue analysis of all kinds of zones of interest in the structure.

This chapter presents the ingredients to building predictive models for the fatigue analysis

of a stress concentration zone of the structure. The fatigue induced by road loads on automotive parts containing a variety of fallible components will be the discussion of Chapter III.

The structure of the chapter is as follows: Section II.2 introduces the description of local loads thanks to Cauchy stress tensors and to representative elements of volume (REV), and their meaning for material points in the structure. This classical mechanical formalism allows us to associate measurable variables to damaging phenomena. The usual definition of a stress concentration is herein modified to include all plausible load configurations of a structure to define stress concentration zones.

Section II.3 describes the different phenomena underlying fatigue degradation at the scale of the REV, and presents the different physical properties that these phenomena modify.

Fatigue analysis for simple components is separated in two sections in order to highlight the difference in types of local loads on the zone. The prediction of fatigue life under cyclic loads thanks to empirical or phenomenological models is presented in Section II.4. The evaluation of fatigue through the use of damage models for components submitted to local variable amplitude loads is presented in Section II.5.

§II.5.5 introduces 1D fatigue equivalents for simple components in order to illustrate damage models with an equivalent load variable. The implementation of local fatigue analysis in an industrial and numerical context is introduced in Section II.6, to understand what kind of predictors and numerical methods are used in practice.

II.2 Cauchy stress tensors and stress concentration

Under mechanical solicitations, the strain in a solid domain Ω causes inner force densities that try and push atoms in the domain back to their original relative positions [Forest *et al.* 2006; Maïtournam 2017]. In a given subdomain $\Omega_A \subset \Omega$, the inner force density $\underline{f}$ and the surface force density $\underline{t}$ are summarized by a symmetrical second-order Cauchy stress tensor $\underline{\underline{\sigma}}$ such that:

$$\underline{f} = \underline{\mathrm{div}}\left(\underline{\underline{\sigma}}\right) \text{ and } \underline{\underline{\sigma}} \cdot \underline{h} = \underline{t} \tag{II.2.1}$$

denoting $\underline{h}$ a normal vector of the surface of the subdomain; and $\underline{\mathrm{div}}$ the divergence operator applied to second-order tensors.

The stress tensor $\underline{\underline{\sigma}}$, defined in Eq. II.2.2, as well as its counterpart the strain tensor $\underline{\underline{\epsilon}}$, are the fundamental tools used to study the micro-structural behavior of materials under mechanical loads.

$$\underline{\underline{\sigma}} = \begin{pmatrix} \sigma_{11} & \sigma_{12} & \sigma_{13} \\ \sigma_{12} & \sigma_{22} & \sigma_{23} \\ \sigma_{13} & \sigma_{23} & \sigma_{33} \end{pmatrix} \tag{II.2.2}$$

The components of the Cauchy stress tensor represent the surface efforts, normal and transverse, applied on each face of a cubic element of volume, see Fig. II.2. A local axis system for the subdomain Ω_A is denoted (1,2,3). Any subset of the system can have its own local orientation. A specific convention for the univocal macroscopic system of a vehicle will be presented in Section III.2.

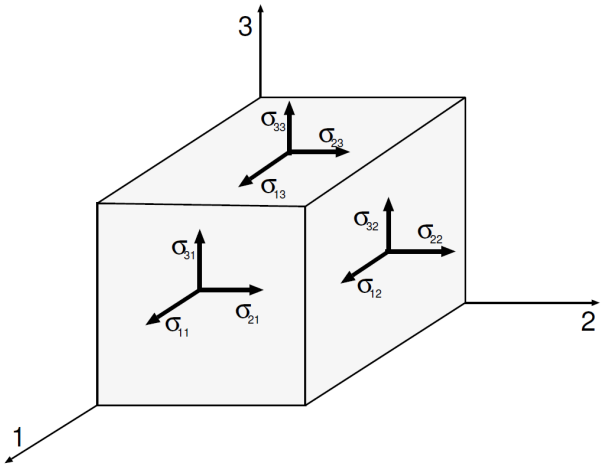

Fig. II.2: Each component of the stress tensor represents one of three solicitation directions on each face of a cubic reference volume

Atoms in solid metals are structured in grains - bulks of oriented crystals [Reynier 2013]. At the microscopic scale, the behavior of the material is therefore anisotropic. However, the very high density of grains in a macroscopic sample of material may lead to isotropy or orthotropy of mechanical properties (elasticity, Poisson effect, plasticity, fatigue resistance) at the macroscopic scale.

These granular materials are therefore homogenized by defining an intermediate scale between micro and macroscopic: the mesoscopic scale. A representative element of volume (REV) is defined as the smallest volume, containing a large number of grains, that is considered to be isotropic (see Fig. II.3). To each measure of local stress fields at a point of a structure is associated an REV of material at the corresponding location.

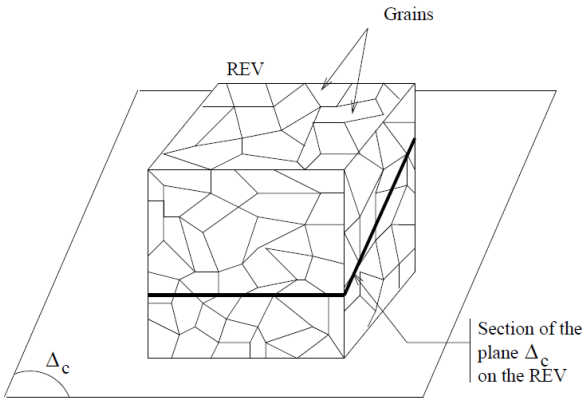

Fig. II.3: An REV is a representative volume of granular material [Genet (Le Corre) 2006]

In a structure, mechanical solicitations concentrate (Cauchy) stress at certain locations. There, a volume of material will show higher values and variations of stress than in its surroundings. A stress concentration denotes the close neighborhood of a local maximum of the Cauchy stress field when the domain is submitted to a given load configuration.

Two different load cases of the domain will ignite different sets of stress concentrations. We want to track all locations that may concentrate stress over a structure submitted to a variety of loads. Therefore, we name stress concentration zones z locations of the domain that are stress concentrations under specific loads. These stress concentration zones are typically located around part joints and edges - such as weld beads, spot welds and metal sheet edges in our parts of interest. For this reason, and the inevitable existence of microscopic defects created by their manufacturing processes (welding, machining or forging), these zones are of interest for failure prediction. We want to analyze their fatigue following a loading history on the system.

Stress concentration zones of a structure will have different volumes, depending on the size of the subset over which Cauchy stress is significant. This may be important for fatigue analysis, as larger volume of a given material will have a larger probability of containing larger microscopic defects. Thus the probability of initiating a crack following a given Cauchy stress history may increase. Design-wise, a larger volume of weld or a greater thickness of the sheet may however mitigate and therefore reduce local stress for a given mission.

II.3 Mechanical phenomena associated with fatigue at the microscopic scale

Understanding the physical process that leads to fatigue failure will allow us to identify ground truth variables, calculated from the Cauchy stress history of a stress concentration zone, to monitor or model degradation.

II.3.1 Microscopic crack nucleation, propagation

When a metallic material cools down following forming, welding or machining, the atoms agglomerate in crystals of various orientations. Defects such as inclusions, twins, voids and dislocations (Fig. II.4a) may appear at the microscopic level, inside and at the edge of the bulk material, inducing discontinuity in the granular structure.

As the material is loaded, such defects can be translated and/or coalesced. Atom bonds may break following local accumulation of dislocations. This leads to the initiation or expansion of voids inside the bulk material or cracks at its edges (Fig. II.4b).

The Cauchy stress field theoretically reaches infinite values at the notch of a void/crack. The Cauchy stress components' formulas at the vicinity of a notch can yet be written using prior knowledge on the size of the defect at the initial stage as well as a proportional term, the stress intensity factor, being a different value for each loading mode (Fig. II.4c) [Irwin 1957].

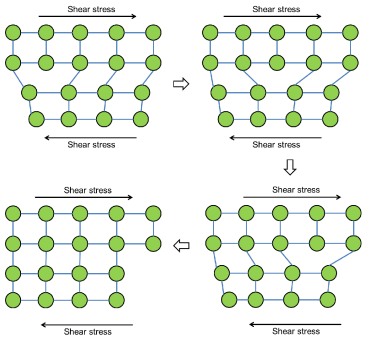

(a) Propagation of a dislocation [Singulani 2014]

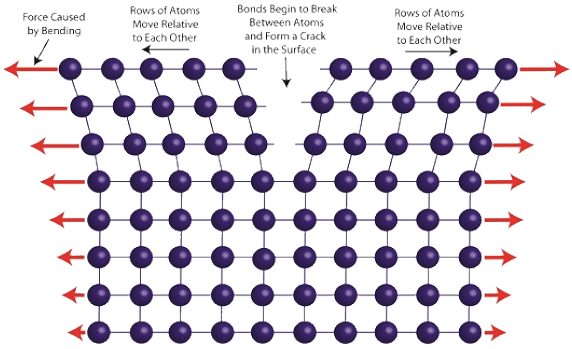

(b) Microscopic failure of atom bonds at the edge under tensile strain [O'Keefe 2012]

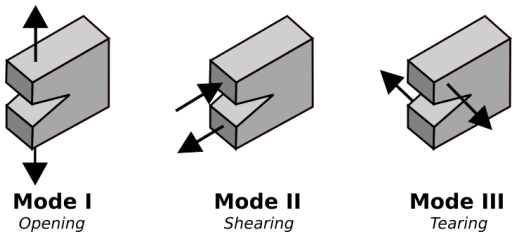

(c) Loading modes in the vicinity of a crack

Fig. II.4: Loaded behavior of crystalline structures

The stress intensity factor is often used to conduct the fatigue analysis of specimens with known defects. The Paris' Law [Paris and Erdogan 1963] links the growth rate of a crack to the concentration of stress at the crack tip, see figure II.5. Because of the dependence of this growth rate to the stress intensity factor at the location of the crack, most life prediction methods for welded assemblies propose to evaluate or model a stress intensity factor at the notch and link it to the lifetime of the weld [Fricke 2013; Hobbacher *et al.* 2016]. An example of full probabilistic design investigation for aeronautic components, using this strategy, can be found in [Mattrand 2011] Chap. 4.

As we may recall now and then in this manuscript, the industrial does not have access to precise knowledge on initial weld or sheet edge defect sizes. While being paramount to precise fatigue analysis of the zone, it is highly dependent on the context of the manufactured zone in the structure. Moreover, some assemblies may be elaborated by providers, following baseline norms and resistance criteria.

Let us delve further into methods of fatigue analyses to see when our available knowledge of component resistance kicks in. While being models applied on top of ground truth characterizations, the associated fatigue descriptors will prove to be satisfying for our goals in terms of fatigue analysis.

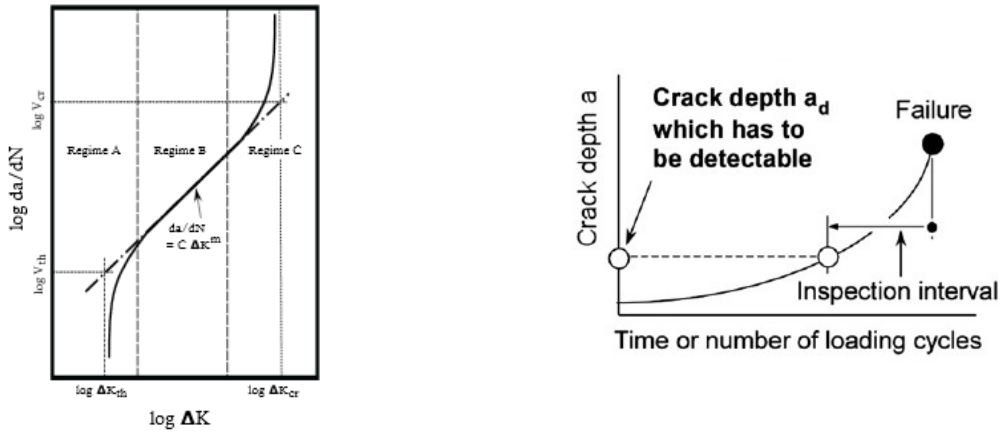

(a) As per crack growth rate against stress intensity factor

(b) As per crack size under a cyclic load of fixed amplitude [Zerbst *et al.* 2013]

Fig. II.5: Illustrations of the Paris Law

II.3.2 Degradation of mechanical properties over time

Changes in microstructure can be expected to modify the mechanical properties of the material, and therefore the response (in terms of stress and strain) of the structure to different kinds of loads. The modification of macroscopic mechanical properties is often called aging. Such modifications of material properties may be tracked to evaluate damage, using different kinds of monitoring instrumentations.

As evidenced in previous works [Pierron 2018], most properties of weld beads and other chassis system components are only degraded at the very end of their lives. Moreover, in this thesis, we will not handle "youth failures", caused by the eventual existence of a manufacturing defect. Vehicles are tested for youth defects shortly once they are assembled and through a larger test procedure on samples from the manufacturing chain.

Therefore, in our study, we consider that for the vast majority of the life of the system before failure, the kinematic and elastic properties of the structure remain constant. This amounts to approximating that the first and last phases of the bathtub curve (Fig. II.6) are negligible in time and repetitions compared to the fatigue life phase (see [Beaumont 2013] Chap. 2).

II.3.3 Plasticity and residual stress

Material degradation induced by local Cauchy stress histories can be quantified through elastoplastic models. Elasticity refers to the linear modeling of the first part of stress-strain curves and is a reversible phenomenon. Plasticity, being the non-linear behavior observed both macroscopically (as in Fig. II.8) and microscopically in metallic materials, stems from the irreversible accumulation and entanglement of dislocations. The frontier between the two

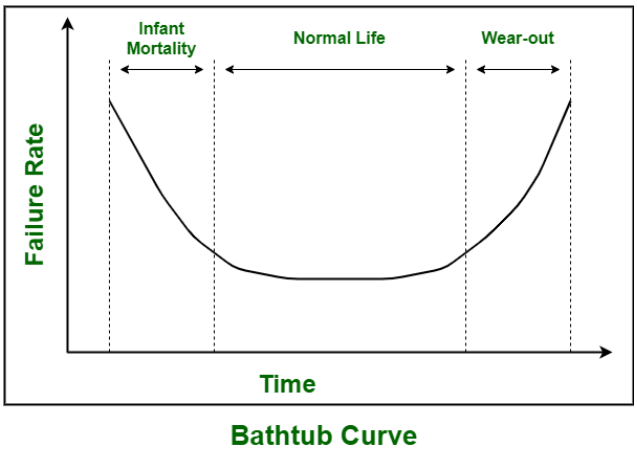

Fig. II.6: Bathtub curve: evolution of the failure rate of a system over its life cycle. Modifications of material properties at the first and last stage are not considered to conduct the fatigue analysis of our components in service

modeled sections (elasticity and plasticity) of the stress-strain curve is defined as the elastic limit.

At the macroscopic scale, the material seems to behave purely elastically when submitted to loads below its elastic limit. When dealing with thousands to millions of variations, even seemingly macroscopically elastic loads may repetitively induce plasticity at the microscopic level. This could garner into plasticity and/or the macroscopic apparition of cracks.

Plasticity shifts the load domains over which the material behaves elastically. Under periodic loads, this phenomenon is called hardening. There are two basic models for hardening of a material point under cyclic loadings. Kinematic hardening represents a translation of the elastic domain. Isotropic hardening represents its dilatation. Whether either or both of them are relevant to characterize the behavior of the point depends on its material properties and geometrical context (Fig. II.7).

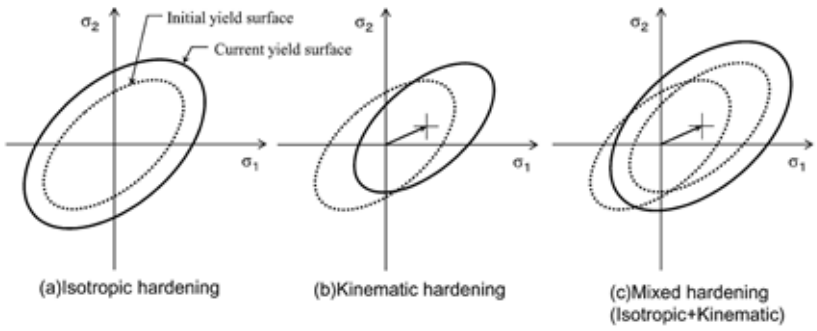

Fig. II.7: Isotropic, kinematic or mixed hardening following plasticity.

In low cycle fatigue, the amount of plastic energy dissipated through hardening is often taken as a parameter of fatigue analysis. For our components of interest, hardening occurs at the beginning of the life of the system, and sporadically, following a large solicitation in real-life usage. Therefore, we will not include hardening models in the problem, as we will

consider the system to be hardened at the beginning of its life. However, hardening justifies the physical sense behind the load variation tracking algorithm (Rainflow counting) that we will use in Section II.5 (see also Appendix B).

Residual stress is the stress state of the structure as long as it does not encounter external solicitation. In manufactured parts, it results from previous hardening and plasticizing events (see II.8). Components beginning their lives with tensile (positive) residual stresses are less resistant than components with compressive (negative) residual stresses for given loading histories. Therefore, residual stress at the beginning of the life of a structure may serve to quantify manufacturing quality, along with the difference between nominal and ultimate geometry. Automotive parts are submitted to post-processes like stress relieving or shot-peening to decrease their residual stress for the beginning of their life.

(a) Body crash box

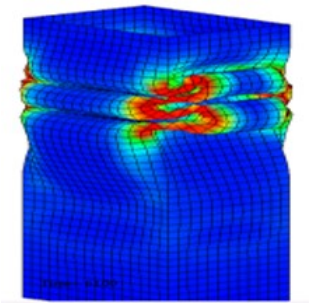

(b) Red zones highlight where the yield limit of the material was exceeded

Fig. II.8: Plasticity is observed macroscopically as a permanent modification of the component following a violent load case, here on a body crash box (fr. *absorbeur de choc*)

Knowledge on the actual residual stress of series production is limited for large structures, especially when their production is divided between providers and the car manufacturer. They can be estimated for a known manufacturing procedure [Merhy *et al.* 2014; Niane *et al.* 2012].

II.4 Fatigue analysis under cyclic loads

The previous section highlighted the micro-structural phenomena at hand in fatigue. Their monitoring requires a thorough knowledge of local geometry and material composition. These aspects may vary wildly for a given part manufactured several times and lead to large variability in lifetime. Therefore, we cannot use deterministic micro-mechanical models. We must manage random variables representing either ground truth properties or the lifetime of these components.

Let us disambiguate durability analysis and fatigue analysis. While both may consider the same degradation phenomena, durability controls the life expectancy of the system, while fatigue analysis predicts a probability of failure following a given loading history with a given duration.

First, we are only interested in the prediction of catastrophic failure of the system by mechanical fatigue during regular use. We ignore other failure scenarios like corrosion, or

other use conditions like abuse or accidents. Thus the lifetime of interest in our study is the fatigue lifetime.

Second, the requirement of interest for the system is a requirement in reliability. Reliability aims to control (as in regulate) the risk of failure of a system before a given fatigue lifetime objective. Hence the distribution of lifetime is not our direct concern.

Furthermore, in order to delve further into different practice in fatigue analysis, let us propose a distinction between empirical prediction models - based on the observation of fracture of a specimen - and phenomenological models.

Phenomenological models aim to build fatigue models, applied on macroscopic quantities like load ranges, fitted on the investigation of microscopic phenomena in a controlled environment. Therefore they track actual material properties or defect characterizations [Fernández-Canteli *et al.* 2021], providing materially realistic fatigue models that are best fitted to complex ruin mechanisms on well modeled microstructures. For instance, the exploitation of knowledge on the distribution of material defects for the prediction of component lifetime was investigated in several works [Charkaluk *et al.* 2014; El Khoukhi 2020; Shen *et al.* 2000; Szmytka *et al.* 2020].

Eventually, we will continue the work with empirical fatigue characterizations, as they correspond to the knowledge that is available in the company on the behavior of our components of interest.

II.4.1 Empirical characterization and S-N curves

We consider to be a well-defined component the joint knowledge of the geometry of a sample, material, microscopic arrangement, manufacturing process and tested load condition.

Load (S) versus number of cycles (N) graphs have been used since Wöhler [Wöhler 1860] to track the resistance of a component under cyclic input loads. An S-N scatter is built from fatigue trials of a given component under a given load case and several load levels (see Fig. II.9). The amount of cycle of a given load level to break a unit marks a points in the scatter. The y-axis of an S-N scatter can be taken as the effort range of an input load cycle, amplitude (half ranges), or any other proportional quantity. The x-axis is often represented in a logarithmic scale.

A Wöhler curve characterizes the life expectancy of a component under any cyclic load level for a given load case. Among the lifetime results of all units at a given load level, a Wöhler curve usually connects the median lifetime, such that there is at most an observed 50% of frequencies beyond the median. The intercept ΔS_u of the curve corresponds to the average ultimate strength of the component under said load case. A different modeling strategy fitting a model on the full scatter instead of level by level is presented in [Fouchereau *et al.* 2014].

The shape of the Wöhler curve for most steel components (butt welds in Fig. II.9) reveals three domains:

- Low cycle fatigue corresponds to non-adaptive material behaviors where the component is solicited beyond its macroscopic yield limit at each cycle;

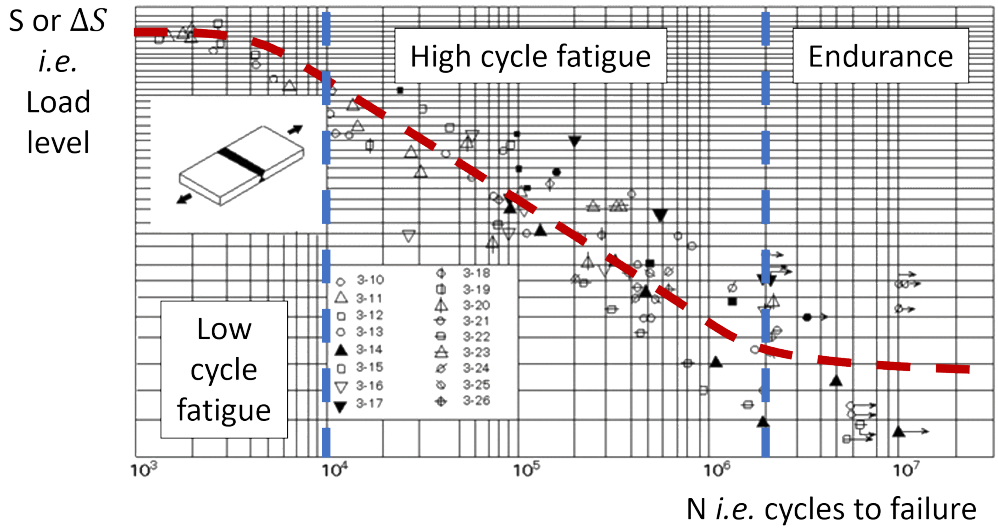

Fig. II.9: S-N scatters for different butt weld geometries under tensile loads [Može 2015]

- High cycle fatigue spans the high slope domain of the material;
- The endurance domain corresponds to the end or the convergence of the curve. Sometimes, studies are conducted in the very high cycle fatigue domain, beyond the second elbow of the curve, to design against vibratory fatigue.

Wöhler curves can be modeled using one of several models from the literature [Castillo and Fernández-Canteli 2009], depending on the domains of solicitations of the component. Under high cycle fatigue loads, a logarithmic Basquin model is most commonly used, characterized by a reference point $(N_0,\Delta S_0)$ and an exponent m. In a log-log graph, the exponent m denotes the slope of the curve in the high cycle fatigue domain.

$$1 = \frac{N \cdot \Delta S^m}{N_0 \cdot \Delta S_0^m} \tag{II.4.1}$$

The Basquin model is relevant for high cycle fatigue load levels. It overestimates lifetime under endurance loads and underestimates it in the low cycle domain. For instance, note that if a Basquin model is defined with a reference number of cycle $N_0 = 1$, then its intercept surpasses the ultimate strength of the component: $\Delta S_0 > \Delta S_u$. Other Wöhler curve models account for the endurance limit of the component (Stromeyer) and/or the low cycle fatigue behavior (Bastenaire).

A sample under bending or traction load cases will yield different exponents m, intercept ΔS_u and endurance threshold ΔS_∞. A different load ratio, usually defined as the ratio between cycle minimum and maximum, also yields a different Wöhler curve. We will develop on the handling of load ratio for fatigue analysis under automotive loads in §II.5.4. The generic fatigue behavior for a variety of load cases may be characterized for a given zone through interpolation between several models, calibrated on several load cases [Susmel and Lazzarin 2002].

If the Wöhler curve converges at high number of cycles to failure, the asymptote of the curve is called the endurance limit ΔS_∞. It exists for a large number of steel components and can be found, for any given cyclic load case, using StairCase and Locati families of characterization procedures (see [Beaumont 2013] Chap. 3).

Some components, however, do not exhibit an endurance limit. They merely display a change in slope of the Wöhler curve in the very high cycle domain and beyond [Sonsino 2007]. It is the case of most aluminum components. While loads below the otherwise observed endurance limit will not induce significant fatigue damage individually, ignoring them altogether on lifelong loading histories may underestimate the resistance of a component [Mayer *et al.* 2005].

The distinction between the high cycle fatigue domain and the unlimited endurance/vibratory fatigue domain, while approximate, is often conventionally set to a reference number of cycles N_∞. It is implied that a component surviving a number of cycles $N > N_\infty$ is solicited below its endurance limit and therefore will never be led to failure by the loading. For most of the recollection of works and practices at Stellantis, the reference number of cycle for the endurance domain is $N_\infty = 10^6$ cycles.

II.4.2 Representativeness of specimens used to characterize components

For the design of automotive structures, we need fatigue quantifiers that are adapted to the analysis of any kind of geometry and size of a joint or metal sheet edge. In order to find these variables, we need to prioritize characterizations of fatigue behavior from local variables instead of complete sample geometries.

Indeed, until now, we have discussed the fatigue of a given component, that is, a combination of a material, of a sample geometry, its manufacturing process and its load direction. The empirical characterization of such a component, yielding a traditional Wöhler curve, does not allow extrapolation to the material or to the manufacturing process' behavior under any geometry and any sample load case, yet. In order to exploit experimental trials on a component to its variants in a real structure, the experimental sample must be proven representative of the failure mode of its variants.

Said differently, instead of characterizing the lifetime of a component based on the parameters of macroscopic global loads on a sample, the characterization - the y-axis of the S-N scatter - must be based on local stress or even microscopic quantities. Once a local characterization is achieved, the Saint-Venant principle makes it valid for any variant in terms of global load conditions or sample geometry.

This is true for both fatigue lifetime and damage. In order to develop a generic damage model for the stress concentration zones of a structure (being, as far as we are concerned, weld beads, spot welds or metal sheet edges), the underlying fatigue characterization must handle the variety of these contexts' geometries and manufacturing parameters. For instance, reference Wöhler curves of weld beads, plotting effort level against cycles, are categorized by the International Institute of Welding (IIW) according to the geometry of the component [Hobbacher *et al.* 2016].

In the case of automotive structures submitted to complex multi-input loads, we will see in the next paragraphs that this representativeness of a fatigue characterization is only achieved with certainty if components are characterized for multiaxial load cases.

II.4.3 Multiaxial fatigue criteria

Without any information on its macroscopic context, an REV can be loaded in any direction. This direction will have a direct influence on the population of defects that will be propagated and how much. Moreover, the accumulation of defect propagation on different subsets of the REV, associated with different load directions, may or may not interfere on its effective fatigue life. Multiaxial fatigue criteria stem from this discussion or observation of the effect of multiple load directions.

While different Wöhler curves describe fatigue behaviors of single components under different load cases independently, multiaxial cyclic fatigue criteria take the succession of local load conditions in account in their formulation. They are derived from a theory of defect propagation (critical plane approaches) or of energetic cumulation (global approaches) (see [Weber 1999] Chap. 1), quite like phenomenological models as previously introduced.

These fatigue criteria evaluate whether a complex load cycle will lead the material to failure before the reference endurance number of cycles. Because they span a larger set of complex loads, they require calibration using more than one single test condition. The generic form of a multiaxial fatigue criterion is given by Eq. II.4.2.

$$f\left(\left[\underline{\underline{\sigma}}(t),\, t \in [0,T_0]\right], k_f\right) < 0 \tag{II.4.2}$$

denoting $\underline{\underline{\sigma}}(t)$ the instantaneous Cauchy stress tensor measured at a relevant location for the REV of interest; $\left[\underline{\underline{\sigma}}(t),\, t \in [0,T_0]\right]$ the successive states (history) of Cauchy stress values over a load cycle with period T_0; and k_f a material parameter.

A zone submitted to a given local loading history is critical if its associated fatigue criterion is not verified under such a loading history.

Several studies were conducted to evaluate and compare the performance of different fatigue criteria for cyclic fatigue characterization on reference components ([Weber 1999] Chap. 1 and [Papuga and Růžička 2008]). All fatigue criteria in the literature have their preferred applications in terms of component types and the loads they can endure. Some have more versatility with respect to more complex successions of local load cases [Dong *et al.* 2010; Mamiya *et al.* 2009; Susmel and D. Taylor 2011].

The choice of a criterion depends on available fatigue characterization in company expertise for applicable materials, manufacturing processes and geometries. In the absence of precise knowledge on the characteristics of components to consider, most conservative fatigue criteria can be considered roughly equivalent in terms of uncertainty (see [Weber 1999] Chap. 1).

Current available knowledge for the design of automotive components at Stellantis are based on the Dang Van II criterion [Dang-Van *et al.* 1989]. This strategy uses a property of Mohr circles to elude the search for a critical slip plane (see [Fauvin *et al.* 2020]). It consists

in evaluating a shear stress range τ_{Loc} that corresponds to the difference between the largest and smallest eigenvalues of the mesoscopic stress deviator $\underline{\underline{s}}$ (see Fig. II.10 a)).

$$P = \frac{\text{Tr}\left(\underline{\underline{\sigma}}\right)}{3} \tag{II.4.3}$$

$$\underline{\underline{s}} = \underline{\underline{\sigma}} - P \cdot \underline{\underline{1}} \tag{II.4.4}$$

$$\tau^{\text{Loc}} = \frac{1}{2} \cdot |\, s_I - s_{III} \,| \tag{II.4.5}$$

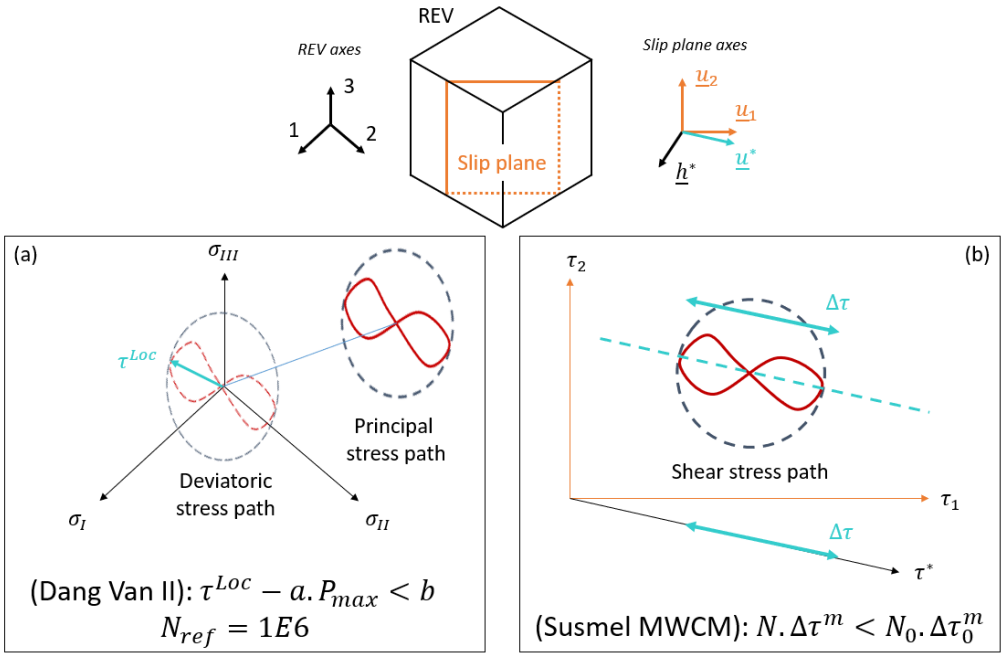

Fig. II.10: (a) Dang Van II criterion quantities calculated from a stress cycle (b) Shear stress on a critical slip direction used in a modified Wöhler curve model

denoting P the hydrostatic pressure; Tr the trace operator for a square matrix; s_I, s_{III} respectively the first and last eigenvalues of the stress deviator.

The hydrostatic pressure P is interpreted as the center of the mesoscopic shear stress path. The resolved shear stress τ^{Loc} is the radius of a circumscribed sphere around the shear stress path. Under hypothesis of local isotropy (all directions of the REV are critical), the Dang Van II criterion is written:

$$\max_{t\epsilon[0,T_0]} \left(\tau^{\text{Loc}}(t) + a \cdot P(t)\right) \leq b \tag{II.4.6}$$

a and b are material parameters and can be identified by evaluating the formula over two baseline fatigue tests: the endurance limit of the material under alternating $\rho = -1$ bending test f_{-1} and the endurance limit of the material under alternating $\rho = -1$ torsion tube test t_{-1}:

$$a = \frac{t_{-1} - \frac{f_{-1}}{2}}{\frac{f_{-1}}{3}} \qquad (II.4.7)$$
$$b = t_{-1}$$

If the criterion is not verified, the component is predicted to fail before the reference number of cycles with a probability greater than 50%.

A technical report from Groupe PSA showed an evaluation of the different Dang Van curves obtained when modifying the reference number of cycles [Augustins 2007] (see Fig. II.11).

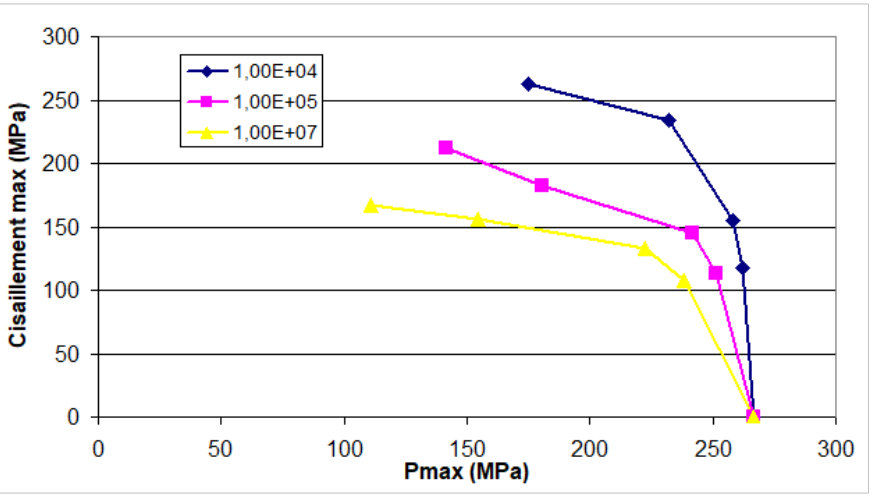

Fig. II.11: Critical points observed on the Dang Van diagram, obtained for 3 different reference life times, using four reference trials (left to right) $\rho = -1$, $\rho = -0.1$, $\rho = 0.2$ and $\rho = 0.4$ [Augustins 2007]

Further studies showed that the Dang Van II criterion yields non-conservative results for complex deviatoric stress paths [Dong *et al.* 2010], limiting its validity to near-unidimensional cyclic loads. This investigation is discussed in Appendix B.2. Another multiaxial variable presented later in §II.5.3 (see Fig. II.10 b)) shows better prediction results in the presence of such complex load cycles [Susmel and D. Taylor 2011].

II.4.4 Probabilistic fatigue models

Let us take a little step back with respect to the main problematic of the thesis. We want to control the risk of failure of a structure, let's say of a simple automotive component for instance, over a population of local loading histories it may endure in real life. We will look for validation load conditions, levels and criteria that ensure sufficient resistance of the component.

So far, assuming we would use cyclic validation loads and using previously defined fatigue criteria, we can only determine whether or not the component has more or less than a 50%

probability to fail before the reference number of cycles. This is a significant constraint on the definition of validation loads as it limits the range of possibilities in terms of pass criteria.

Probabilistic Wöhler curve models [Fouchereau *et al.* 2014] exploit the variability of S-N scatters to compare the risk of failure of the component under cyclic loads to a threshold of $X\%$.

When building the points of a Wöhler curve from an S-N scatter using a level by level approach, it is usually observed that the adequate probability law for specimen lifetime at a given level is a lognormal distribution. For a given lifetime objective, the distribution of specimen strength is modeled using a normal law (see Fig. II.12a).

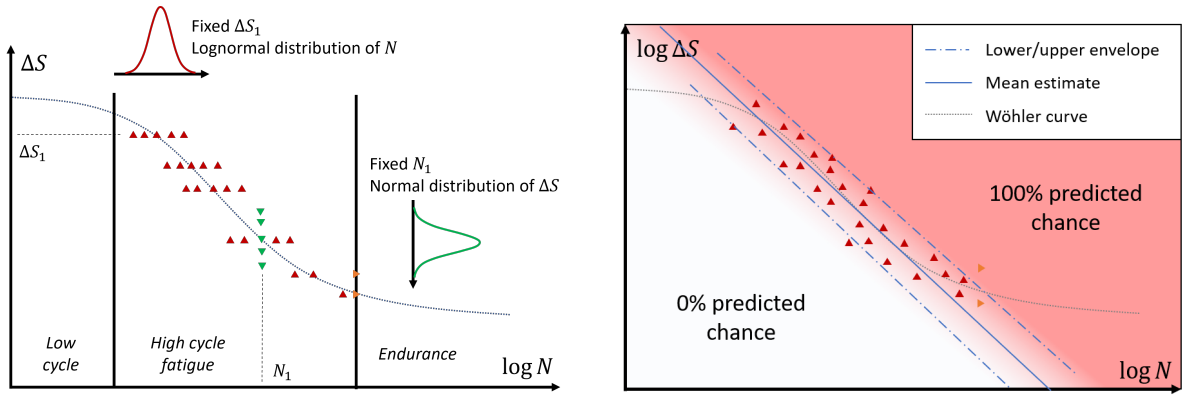

(a) 1D models used to distribute either range or number of cycles alone

(b) Probabilistic Basquin model

Fig. II.12: Stochastic fatigue models

For each load level, the parameters of a lognormal distribution of the cycles to failure can be estimated from the results of experimental characterizations. The $X\%$ quantiles of the distribution for different load levels can be connected or used to model a new $X\%$ Wöhler curve, as in II.12b (See [Beaumont 2013] Chap. 4 or [Benaouda *et al.* 2022]). Since fatigue criteria are calibrated using baseline fatigue tests as in Eq. II.4.7, the variability of these fatigue tests can be propagated into $X\%$ multiaxial criteria [Coudray *et al.* 2020]. The probabilistic modeling of a Dang Van II criterion allows defining test conditions such that the probability of failure of the tested component can be effectively compared to any probability between 0 and 1.

II.5 Damage evaluation under multiaxial variable amplitude local loads

The strategy underlying variable amplitude fatigue prediction is that each variation of the stress tensor is considered responsible of a fraction of material damage. Counting damage requires 1) defining a variable able to track quantitatively the evolution of local degradation 2) detecting and characterizing variations that may induce non negligible damage and 3) associating a marginal damage to each variation.

A popular method for the detection of variations in the history of a scalar variable towards evaluation of damage is Rainflow counting. §II.5.1 presents the definition and meaning of Rainflow cycles. §II.5.2 includes them in the evaluation of damage by cumulation from a known Wöhler curve for the component. In §II.5.3, we include the management of local multiaxiality to the framework of damage cumulation.

II.5.1 Cycle counting and Rainflow matrices

We distinguish between two kinds of variation tracking, each leading to different kinds of damage models: cycle counting (Rainflow counting and Miner-type damage cumulation methods) and local hardening tracking (cumulation of plastic hardening energy and Morel-type fatigue prediction).

Rainflow counting is the preferred method for cycle counting on a signal towards application of the linear cumulative damage law of Palgrem-Miner. From a material point of view, they are associated with the range of hysteresis cycles in a stress-strain diagram. Note that the Rainflow counting algorithm can be applied to any scalar signal, be it effort, stress or a quantity calculated from them.

Fig. II.13: From time history to nonchronological sequence of turning points

Rainflow counting is applied on the sequence of the turning points of a signal, regardless of the actual interval between these turning points, see Fig. II.13

A typical implementation of the Rainflow algorithm, called the four-point method [Rychlik 1987], associates extremum points of the signal together into Rainflow cycles, see figure II.14. Some extrema cannot be associated into cycles, they form the residual, an increasing-decreasing sequence of turning points that always contains the minimum and maximum of the signal [McInnes and Meehan 2008].

$$\mathrm{Rf}^0\ (\mathbf{F}) = \left(C^0(\mathbf{F}), R^0(\mathbf{F})\right) \tag{II.5.1}$$

$$C^0(\mathbf{F}) = \left(\Delta F_i(\mathbf{F}), \mu_i(\mathbf{F})\right)_{i\in[\![1,n^0_{\mathrm{cyc}}]\!]} \tag{II.5.2}$$

denoting ΔF_i and μ_i the range and the mean value of each cycle, respectively, and n^0_{cyc} the number of counted cycles on the scalar loading history $\mathbf{F}$. $R^0(\mathbf{F})$ denotes the residual of the signal after Rainflow counting and is an increasing-decreasing sequence of turning points. C^0 is the "unclosed" Rainflow count.

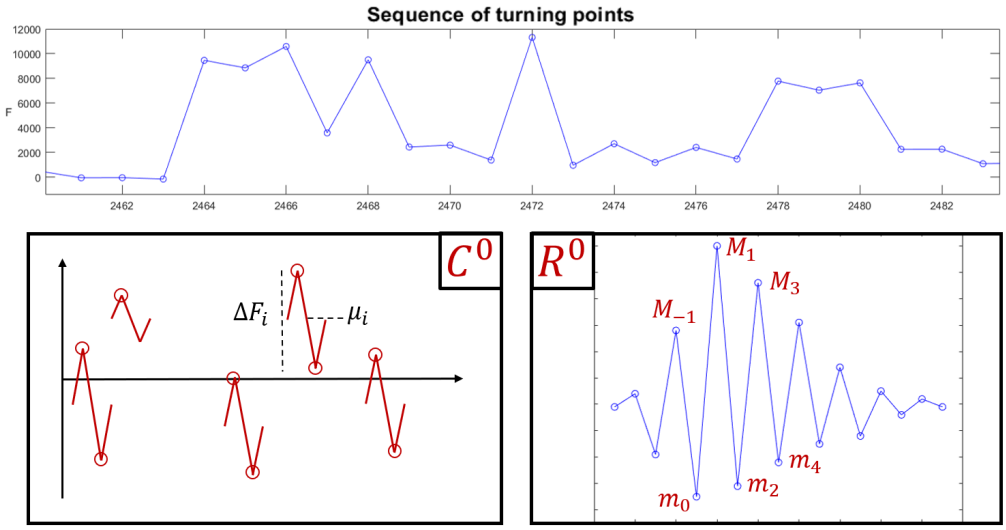

Fig. II.14: Rainflow cycles and residual of a sequence

Canonical cycle counting also usually doesn't retain the instant, and therefore the order, of counted cycles. However, most counting codes are able to memorize the location of cycle extrema in the output. The chosen damage cumulation law determines whether their instant matters or not.

The residual of a Rainflow counting can also be associated with a fraction of damage by "closing" it, *i.e.* by concatenating it with itself and counting new cycles on this concatenation. The efficiency of this method was investigated in [Marsh *et al.* 2016]. Since the residual always contains the global minimum and maximum of the signal, its contribution to overall damage induced by the signal can be very important. After closure, the Rainflow count on a signal is given by:

$$\mathrm{Rf}^\bullet\ (\mathbf{F}) = C^\bullet(\mathbf{F}) = \left(\Delta F_i(\mathbf{F}), \mu_i(\mathbf{F})\right)_{i\in[\![1,n_{\mathrm{cyc}}]\!]} \tag{II.5.3}$$

denoting $C^\bullet(\mathbf{F})$ the "closed" Rainflow count on signal $\mathbf{F}$; n_{cyc} the number of cycles following the addition of the new cycles obtained through closure of the residual $R^0(\mathbf{F})$.

Later in this thesis, we will need to evaluate the damage of concatenations of signals. The formula for an exact evaluation of Rainflow counting from the individual counts of signal parts is detailed in Appendix B. The main formula to keep in mind is:

$$C^0\left(\mathbf{F}_1||\mathbf{F}_2||...||\mathbf{F}_n\right) = \sum_j^n C^0\left(\mathbf{F}_j\right) + C^0\left(R^0(\mathbf{F}_1)||R^0(\mathbf{F}_2)||...||R^0(\mathbf{F}_n)\right) \tag{II.5.4}$$

$$R^0\left(\mathbf{F}_1||\mathbf{F}_2||...||\mathbf{F}_n\right) = R^0\left(R^0(\mathbf{F}_1)||R^0(\mathbf{F}_2)||...||R^0(\mathbf{F}_n)\right) \tag{II.5.5}$$

denoting $||$ the concatenation operator such that:

$$\mathbf{F}_1||\mathbf{F}_2 = \begin{bmatrix} F_1(t) \ \forall t \leq T_1 \\ F_2(t) \ \forall T_1 < t \leq T_2 \end{bmatrix} \tag{II.5.6}$$

In order to reduce the memory needed to store a Rainflow count, cycles are usually not saved individually but rather stored in counts in classes with set sizes, in terms of both cycle range and means, similarly to a histogram. We will refer to this practice as classed Rainflow counts.

By classing Rainflow counts thus, this allows us to normalize the number of classes used to characterize any loading history: therefore each Rainflow count always has the same number of classes n_{bin}. The classed Rainflow count prior to and following closure, respectively Rf^0 and Rf, are given by:

$$\text{Rf}^0\ (\mathbf{F}) = \left(C^0\left(\mathbf{F}\right), R^0\left(\mathbf{F}\right)\right) \tag{II.5.7}$$

$$C^0\left(\mathbf{F}\right) = \left(\Delta F_i, \mu_i, n_i^0\left(\mathbf{F}\right)\right)_{i\in[\![1,n_{\text{bin}}]\!]} \tag{II.5.8}$$

$$\text{Rf}^\bullet\ (\mathbf{F}) = \left(\Delta F_i, \mu_i, n_i(\mathbf{F})\right)_{i\in[\![1,n_{\text{bin}}]\!]} \tag{II.5.9}$$

denoting $n_i^0(\mathbf{F})$ and $n_i(\mathbf{F})$ the number of unclosed resp. closed Rainflow cycles counted in the class $(\Delta F_i, \mu_i)$ on the loading history $\mathbf{F}$. Note that the number of counted cycles on a loading history following closure is given by $n_{\text{cyc}}(\mathbf{F}) = \sum_{i=1}^{n_{\text{bin}}} n_i(\mathbf{F})$ and that $\forall i \in [\![1,n_{\text{bin}}]\!]$, $n_i(\mathbf{F}) \geq 0$.

Fig. II.15 shows common visualizations of closed Rainflow counts on a signal. A 2D Rainflow matrix displays the frequencies of Rainflow cycles for each class $(\Delta F_i, \mu_i)$. A 1D Rainflow matrix displays the frequencies of Rainflow ranges for each class (ΔF_i), following cumulation over all 2D classes $(\Delta F_i, \bullet)$. The symbol $\bullet$ means that all classes with same range ΔF_i but different cycle means μ_i are regrouped in a single class associated with ΔF_i. A 1D Rainflow spectrum is a reverse cumulative matrix of Rainflow ranges, cumulated from maximum range up to 0.

Note that the cumulation direction is non-trivial with respect to usual counting practice in other domains. In general, the cumulative matrix helps to alleviate the effect of outliers, at the far end of the distribution, on the shape of the spectrum. For the sake of fatigue analysis however, maximum ranges bear the most significance to the damage induced by a signal.

II.5.2 Miner Law

In this section, we consider the fatigue analysis of components submitted to local loads with a specific direction. However, the same discussion on representativeness and multiaxiality

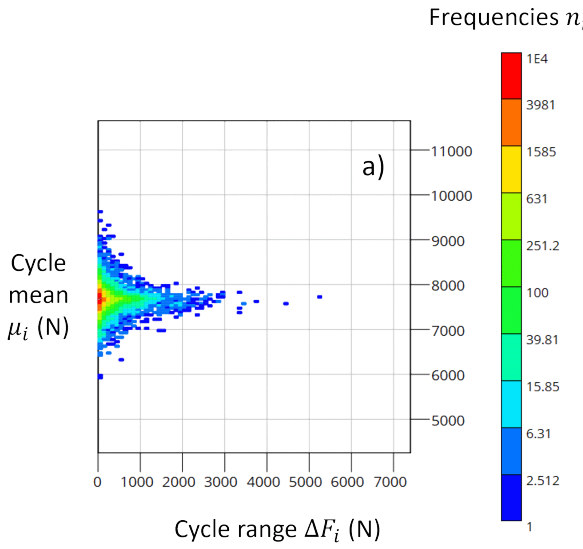

(a) 2D Rainflow matrix

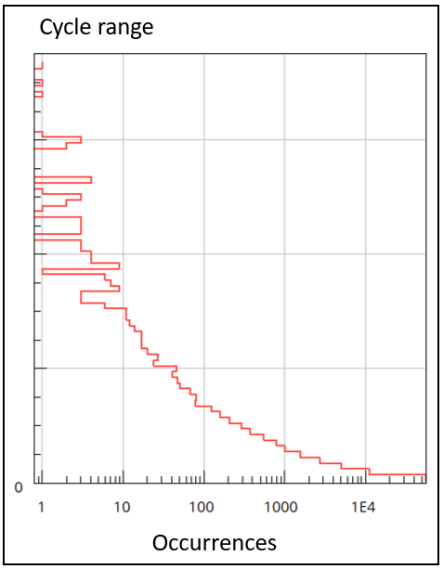

(b) 1D Rainflow (range) matrix

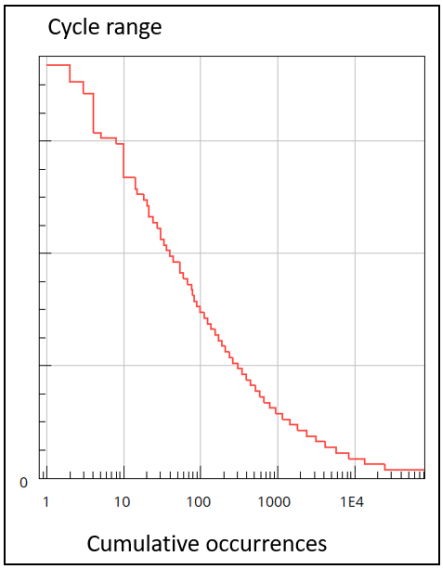

(c) Rainflow spectrum or reverse cumulative matrix

Fig. II.15: Three different visualizations of Rainflow counts

introduced in sections II.4.2 and II.4.3 is also important under variable amplitude loads. Multiaxiality will be tackled in this new fatigue framework in §II.5.3.

Let's consider a component and a Wöhler curve associated with it in a given load case (e.g. traction). The component is submitted to a unidimensional loading history **S** with variable amplitude falling in the high cycle domain. Let's consider a Basquin model of this Wöhler curve (Eq. II.4.1 in Section II.4).

The Palgrem-Miner law [Miner 1945] models the damage of the component by the sum of all marginal damages associated with each counted variation of the local load. The marginal damage of a cycle is given by the fraction of life time that it would represent under a cyclic

loading of the same level.

$$d(\Delta S_i) = d_i = \frac{1}{N(\Delta S_i)} \tag{II.5.10}$$

The value of $N(\Delta S_i)$ is given by a Basquin model of the Wöhler curve associated with this load case.

$$d_i = \frac{\Delta S_i^m}{N_0 \cdot \Delta S_0^m} \tag{II.5.11}$$

Therefore the total damage induced on the component is:

$$D = \sum_i^{n_{\text{cyc}}} d_i = \sum_i^{n_{\text{cyc}}} \frac{\Delta S_i^m}{N_0 \cdot \Delta S_0^m} \tag{II.5.12}$$

The component has a 50% chance of failure if the damage is equal to 1. N_0 is an expectation for the random resistance of the component under load level ΔS_0.

Miner's original method associates marginal damage to counted cycles independently to their order in the loading history. A given range is considered to deal the same damage should it appear at early or late cycles. When compared with the evolution of mechanical properties (§II.3.2) or crack propagation (§II.3.1), this is of course an abstraction, hence our calling Miner law a trivial damage metric.

Other methods to calculate the marginal damage of a counted cycle are detailed in [Fatemi and Yang 1998; Nadjitonon 2010]. Some trivial damage models are able to account for the damage previously inflicted when calculating the marginal damage of a counted cycle at some time of the history (Fig. II.16).

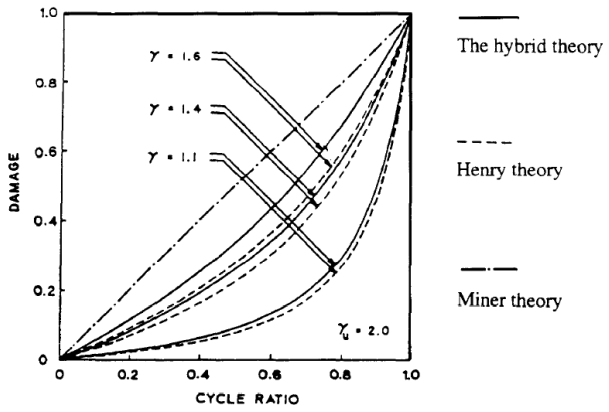

Fig. II.16: Different models for the marginal damaged to a given range depending on the instant of the cycle in the history [Fatemi and Yang 1998]

II.5.3 Counting damage for multiaxial load configurations

Most multiaxial fatigue criteria are elaborated from calculating a variable associated with local, mesoscopic fatigue-related phenomena. Indeed, the Dang Van criterion seeks the slip plane of the isotropic REV by maximizing a quantity of shear stress over all directions, then calculates a combination of this shear stress and of hydrostatic pressure and compares it to a threshold.

In [Meggiolaro and de Castro 2012], the authors propose to use ranges of cycles counted on the Von Mises stress value to evaluate the damage of a component under random amplitude multiaxial loads. The Miner law is directly applied to variations of multiaxial fatigue variables.

In order to compute damage (and later pseudo-damage) from variable amplitude loads, we propose the use of a predictive fatigue variable τ proportional to the Cauchy stress state of the component: projected shear stress on the critical crack propagation plane of a component (Fig. II.10 b)). Such a variable is used in [Susmel and Lazzarin 2002] to plot parametric Basquin models from the S-N scatter of components submitted to multiaxial loads. Such models are named modified Wöhler curves and their generic formula is given in Eq. II.5.15. The damage of an REV is evaluated using previously introduced Eq. II.5.12 on the history of projected shear stress calculated on a specific plane (normal vector $\underline{h}^*$) and slip direction $\underline{u}^*$:

$$\tau = \underline{u}^* \cdot \underline{\underline{\sigma}} \cdot \underline{h}^* \tag{II.5.13}$$

$$\rho = \frac{\sigma_{n,\max}}{\Delta\tau} \tag{II.5.14}$$

$$N \cdot \tau^{k(\rho)} = N_0 \cdot \tau_0(\rho)^{k(\rho)} \tag{II.5.15}$$

denoting ρ the stress ratio, $\sigma_{n,\max}$ and $\Delta\tau$ respectively the maximum value of normal stress and the range of projected shear stress over a cycle, both calculated on the critical plane of the component of interest; $k(\rho)$ the exponent of the model and $(N_0,\tau_0(\rho))$ a reference point in the curve. For a given sample, the parameters of the models are associated with the stress ratio ρ (Fig. II.17). The authors propose linear interpolation to estimate the parameters of a modified Wöhler curve for any stress ratio between baseline configurations.

The critical slip plane of a component is dependent on the loading history on the Representative Element of Volume. Determining this critical plane from a known local loading history is the first step of the evaluation of its damage. In §III.5.2, we will alleviate this operation thanks to the specificity of automotive structures in terms of local load directions.

The efficiency of modified Wöhler curves for the fatigue analysis of various metallic materials under load cycles highlighting multiaxial contributions was investigated in [Susmel and D. Taylor 2011].

II.5.4 The effect of cycle means on damage

The slope and intercept of a Basquin model of a Wöhler curve should be adapted to the stress ratio ρ (Eq. II.5.14) of the corresponding load cycle, in order to analyze the fatigue induced

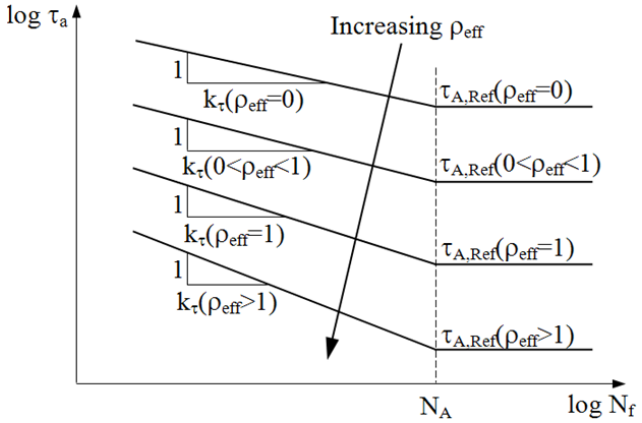

Fig. II.17: Modified Wöhler curve models for different load ratios ρ [Susmel and D. Taylor 2011]

on a component with precision. Indeed, each stress ratio corresponds to a different local load case of the component, and requires a new fatigue experimental base. Fatigue models are only valid in an application once they are proven representative for said application.

We need to have an idea on the expected variations in stress ratio over real-life loads for a vehicle, to determine the need for robustness in our calculation of marginal damage per stress cycle in Eq. II.5.11.

Two options are laid before us in order to decide on a damage cumulation strategy with respect to the effect of cycle means. If we can justify a low variety of Rainflow cycle means in real-life usage, we can consciously establish a fatigue analysis method that does not track changes in load cycle means. Otherwise, we would need to include the effect of cycle mean in the calculation of the marginal damage of a cycle. The chosen convention and its associated hypotheses will have to be roughly controlled for both the analysis of real-life loads and their replication in test conditions (test benches and proving grounds).

Haigh diagrams (Fig. II.18) are fatigue limit graphs that display an empirical or modeled relation between load cycle mean and the endurance limit in terms of load cycle range, for a component of interest [Sendeckyj 2001]. The author adequately refers to them as constant life diagrams, because the curve or the model connects so-called endurance limits for a given reference number of cycles.

Available Haigh characterizations for our components of interest are limited to uniaxial loads and it would be ambitious to consider them valid in the case of multiaxial fatigue models. Moreover, constant life diagrams establish a relation between properties of a component at the limit of endurance, not for any number of cycles. The second option would require further material characterizations or very strong assumptions.

In fact, loading histories in the service of personal vehicles are mostly expected to revolve around the static load configuration of the structure: flat and immobile. Moreover, the mass of the vehicle is not expected to change much, the only loss occurring over a driving episode being fuel consumption. Therefore, the static load configuration of the structure does not change with a frequency similar to load variations tracked by Rainflow counting. Thus, we can consider the hypothesis that Rainflow cycles counted on local (and later global) loading

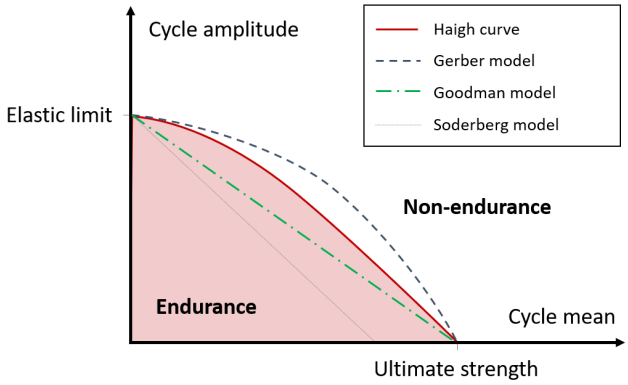

Fig. II.18: Models of the fatigue limit curve in the Haigh diagram

histories will not show a large variety of cycle means.

This hypothesis is corroborated by the shape of 2D Rainflow matrices applied to wheel axle loading histories (see Fig. II.15 a)). In most cases, high cycle ranges are associated with cycle means around the static value.

As mentioned in the previous paragraph, the parameters used to build a modified Wöhler curve model on a shear stress variable on the critical slip plane of a REV, are interpolated using a model that is linear on load ratio [Susmel and D. Taylor 2011]. Therefore, a small variation in cycle mean is expected to be similarly small in terms of marginal damage.

In the rest of this work, we will consider that the Rainflow means do not have a significant impact on the marginal damage induced by each Rainflow cycle.

II.5.5 Damage equivalents for a zone

Two different loading histories $\left[\underline{\underline{\sigma}}\right]_A$ and $\left[\underline{\underline{\sigma}}\right]_B$ can induce the same damage to a given zone z in a given structure (see [Lévai 2018] Chap. 4.4 and [Raoult and Delattre 2020]). The histories may even have different duration and cycle counts.

$$D(z,\left[\underline{\underline{\sigma}}\right]_A) = D(z,\left[\underline{\underline{\sigma}}\right]_B) \Leftrightarrow \sum_i^{n_{\text{cyc}}(A)} \Delta\tau_{i,A}^m = \sum_i^{n_{\text{cyc}}(B)} \Delta\tau_{i,B}^m \tag{II.5.16}$$

Let N_{ref} be a reference number of cycles. The 1D loading history made from N_{ref} repetitions of a sinus load with range $\Delta\sigma$ is equivalent to $\left[\underline{\underline{\sigma}}\right]$ if and only if the maximum shear stress range over all cutting planes of z is given by:

$$\tau_{eq} = \sqrt[m_z]{\frac{1}{N_{\text{ref}}} \cdot \sum_i^{n_{\text{bin}}} n_i \cdot \Delta\tau_i^m} \tag{II.5.17}$$

This 1D loading history can be associated with a location $(\tau_{eq},N_{\text{ref}})$ in an S-N graph and to a location $(\tau^{\text{Loc}},P_{max})$ in a $\tau - P$ diagram commonly used to plot Dang Van-like criteria.

Therefore, the loading can be predicted to lead the component to failure or not through comparison with an available model of the S-N curve associated with zone z for the variable $\Delta\tau$, or with an available Dang Van II criterion evaluated for a reference number of cycle N_{ref} (in practice we may expect N_{ref} to be large, at the far end of the high cycle domain $N_{\text{ref}} \approx 10^6$ cycles).

This backtracking procedure helps us predict the failure of a component under variable amplitude loading histories while using cyclic fatigue criteria.

II.6 Fatigue analysis of control points in an industrial context

In order to evaluate the failure propensity of joints, components and geometries in automotive structures under different variable amplitudes loading histories, engineers need an access to their material properties and the characterization of their fatigue behavior. The choice of fatigue variables to establish a method in reliable design depends on the availability of such data.

In an industrial setting, the cost and time to determine or buy new material characterizations must be confronted to the potential gains in freedom of design and cost of project development. The same principle goes for the calculation of quantities of interest to confront to these models. Being able to adapt the mechanical theory behind the elaboration of service severity to available resources and computing and experimental capacities is not a challenge, it is a necessity.

For instance, in physical trials, the most direct measures of local damage are the size of defects at the microscopic scale or the size of notches at crack initiation zones. These can be evaluated from samples with a correct static equipment, but access to sensors able to perform these measurements online on a sensor vehicle is limited. In practice, this sampling method is not applied to service measurements, and would be tedious to perform in a proving ground environment.

In numerical trials, consisting of finite element problems with various load conditions, the calculation of Cauchy stress tensors at crack initiation zones requires an acute description of the geometry at this location and a very refined mesh [Shams and Vormwald 2013]. Moreover, in the case of finite element calculations, the prediction of stress is only physically valid at some locations of the elements in the model, such as integration points (see [Zienkiewicz *et al.* 2005] Chap. 5). A measurement point in a location of interest for the evaluation of fatigue is called a control point. Several control points over a weld bead or any such weakness may refer to the same stress concentration zone.

There exists simplified numerical models of assemblies of interest, most importantly weld beads and spot welds [Mainnemare 2021], allowing the use of coarse meshes and to multiply the amount and complexity of numerical loads while curbing calculation duration. Such structural models [Coelho 2014; Palmonella *et al.* 2005; Turlier *et al.* 2018] may replace the weld with a numerical joint element, like a 1D rigid body in the case of the Fayard structural model for weld beads [Fayard 1996], see Fig. II.19.

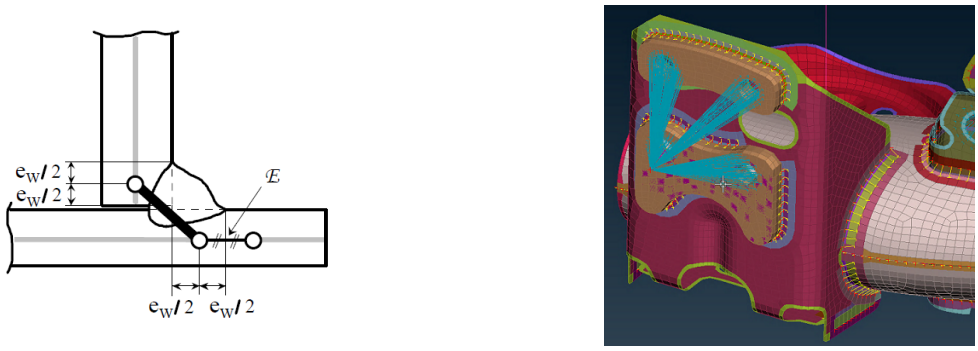

(a) Model definition [Fayard 1996] (b) Finite element model of a wheel mount

Fig. II.19: Fayard model of weld beads in a T configuration. The oblique element is a 1D rigid body element. The control point is at the center, here denoted E, of a shell element.

Naturally, such structural models are non-representative locally, and Cauchy stress coefficients or transformed variables, even when sampled on an integration point of a finite element inside the model, is not representative of the real local stress in an actual weld. Yet, the model can have roughly or exactly the same stiffness and have a very similar mechanical behavior as the original weld from a global point of view (see [Mainnemare *et al.* 2019] Chap. 2.3 or [Mainnemare *et al.* 2018]). Most importantly, structural stress models are elaborated to evaluate the fatigue behavior of the weld bead from measurements at specific control points [Dong 2001; Fayard 1996; Susmel and D. Taylor 2011].

At Stellantis, the component to design is submitted to a cyclic load. Structural Cauchy stress measured at the control points of structural models is translated into maximum hydrostatic pressure and range of mesoscopic shear stress over a cycle. These variables are used on baseline tests to fit a Dang Van II criterion as presented in §II.4.3. The samples used in these tests are reproductions of weld configurations met in the automotive industry with the same manufacturing procedure as serial components. Therefore, as explained in §II.3.3, the dispersion of the acquired fatigue model is representative of the variety of geometrical configurations and of the post-processes met in real structures. Thanks to hypotheses on the dispersion of the endurance limit of specimens of the joint at stake, a probabilistic version of the criterion is established as in §II.4.4.

The structural model used in the case of weld beads is the Fayard model. It was not designed to predict a failure at the root of the weld, only at its toes. Indeed, no root failure was observed at the time on the samples of interest submitted to typical load cases. The model is valid as long as the component modeled with it is only submitted to similar loads (traction) as test conditions. The model may otherwise behave in an unexpected manner [Turlier *et al.* 2018].

II.7 Chapter conclusion

We have presented in this chapter the various questions at stake when looking for a characterization of the propensity that a component has to fail under variable amplitude loads, and shown how these aspects were met in the industrial application. Our investigation culminates

in a local damage model that we can associate to degradation phenomena in our components of interest (see Fig. II.20).

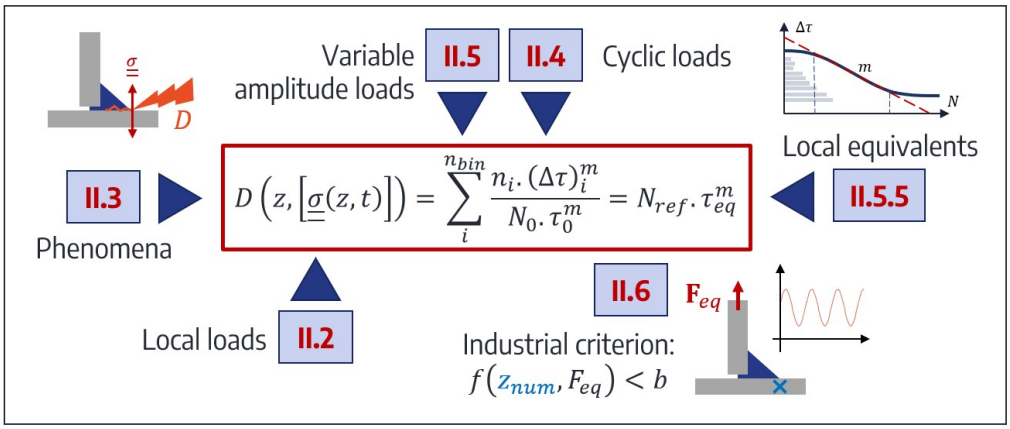

Fig. II.20: Overview of the chapter: the elements of a damaged model and its implementation for the fatigue analysis of a weld bead. F_{eq} denotes here the range of a cyclic loading history on the weld bead that replicates τ_{eq} at the location of interest z

The calculation of damage induced by a local loading history on a material zone effectively tracks the plausible apparition of a macroscopic crack initiated at the zone of interest. A damage model is the stacking of prior information on the failure mechanisms of a material, the manufacturing process of a component and on the type of local loads witnessed by the zone of interest in service. It also serves as an interface between equivalent loads that yield the same outcome for a specimen and between contexts that display the same fatigue behavior.

The relevance and conservativeness of linear damage cumulation for the fatigue life prediction of automotive parts submitted to variable amplitude loads is shown in [Pierron *et al.* 2020]. Moreover, because the marginal damage associated with each counted cycle is independent on the instants of cycle extrema in the history, its implementation is cheap in computation time, making it suitable for data sets of hour-long loading histories as presented in Section IV.3.

Chapter III

Fatigue characterization of a complex part under multi-input loads

III.1 Chapter introduction

In the previous chapter, we have presented the ingredients for the analysis of the fatigue induced on a stress concentration zone of a structure in a given load configuration.

An organ like the suspension or body of a personal vehicle contains several parts. These parts represent a large variety of stress concentration zones with their own associated fatigue models, material properties as well as encountered loading configurations in real life.

We have to find a way to characterize the fatigue of zones of interest of the structure, from variables that derive from the function of the system, *e.g.* from its input loads, defined in Section III.2.

However, the parts of a system do not have full material and geometrical definitions until designed. Even if they were, our knowledge of their characteristics in the case of a vehicle used for real-life measurements would be partial. Therefore, we seek an adequate fatigue characterization: an indirect evaluation of fatigue that has little dependency to the mechanical and fatigue strength properties of the fully designed system.

In Section III.3, we define sensible zones: stress concentration zones that may fail in service and therefore take part in the risk of failure of the structure. We will then define and justify the strategy of seeking a fatigue characterization that summarizes sufficient information on the fatigue of these sensible zones. This characterization will be suitable both for the analysis of real-life missions and for the definition of validation procedures in reliability, *i.e.* it will be our currency for the evaluation of pseudo-fatigue in Chapters IV and V and for the determination of design and validation objectives in Chapter VI.

In §III.5.1, the function of the system will allow us to enact adequate hypotheses to adapt the formula for local damage, introduced in Section II.5, to our application. There damage variables will then be replaced by their load-dependent factor and first characterization of fatigue, pseudo-damages, in §III.5.2.

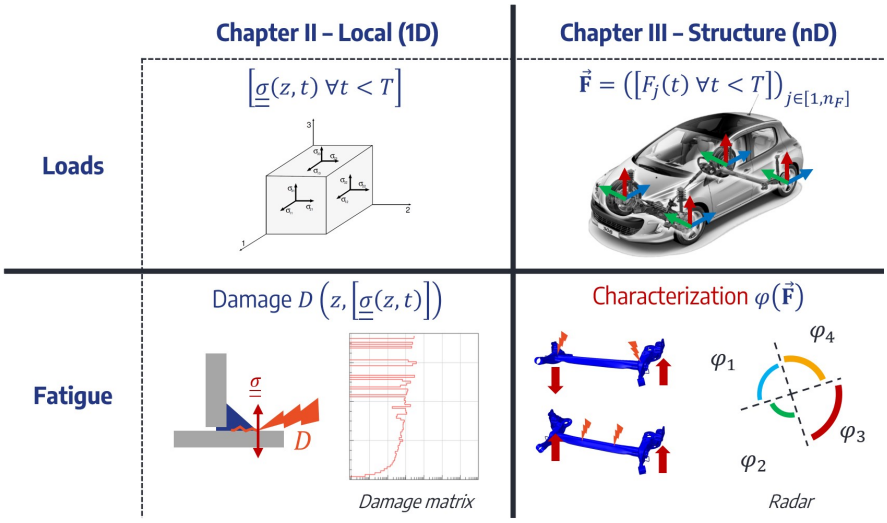

Fig. III.1: How does one discuss the fatigue of a partially known structure? The fatigue analysis of a zone yields a damage prediction. A fatigue characterization summarizes the fatigue induced by a global loading history on the whole structure.

A vehicle structure exhibits specific kinds of global load cases, associated with the function of the system. These global load cases deform the structure in specific ways and induce different stress concentrations. They are defined in §III.6.1. Under such global load cases, extrema of the local stress tensors of zones in the system will have privileged principal directions, and so will projected shear stress introduced in Eq. II.5.13.

Under appropriate hypotheses on the mechanical behavior of the structure, we can propose a first fatigue characterization verifying adequate properties for our application in the rest of Section III.6: a vector of pseudo-damages. In this section, sensible zones will be gathered in local contexts by their common mechanical parameters of interest.

In order to curb the mathematical properties of pseudo-damage, we will apply a small transformation on this variable in Section III.7 and define equivalent magnitudes. Finally, §III.7.3 introduces the graphical visualization of our newly acquired fatigue characterization.

III.2 Global loads on the system

III.2.1 Global load components

All exterior physical variables that have an effect on the function at stake of the vehicle are considered to be global loads. As such, systems overall can be submitted to thermal, chemical, mechanical, electromagnetic or even computational loads. In order to discuss the reliability of car chassis, we need to restrict these variables to those that have direct and exclusive effects on the fatigue of its subsystems.

We consider local Cauchy stress histories to be directly and exclusively linked to the fatigue of stress concentration zones (Section II.2) in the structure. We furthermore assume that local

stresses can be deduced from the histories of efforts on wheel axles, ignoring stresses from non-mechanical solicitations and mechanical loads from car aerodynamics, motor solicitations and user movements.

The global loads of the vehicles are therefore exclusively come down to efforts and moments at the four wheel axles (see Fig. III.2).

$$\vec{\mathbf{F}} = (\mathbf{F}_j)_{j\in[\![1,n_F]\!]} \quad \text{where} \quad \mathbf{F}_j = [F_j(t) \mid t \in [0,T]] \tag{III.2.1}$$

The labels used for global load components on personal vehicles are detailed in Tab. III.1. An example of a global loading history is presented in Fig. III.3.

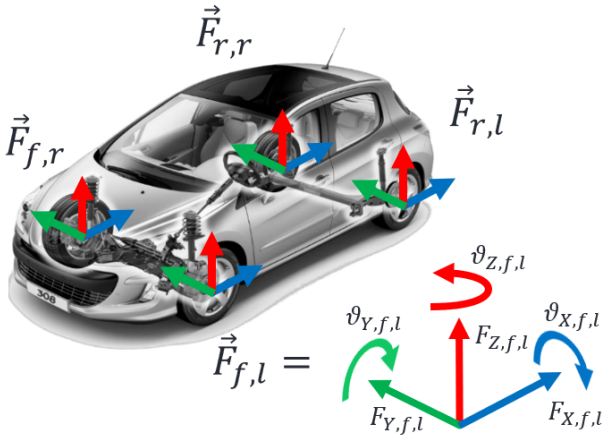

Fig. III.2: Global loads - convention for spatial directions

Component type	Front left	Front right	Rear left	Rear right
Efforts (N)	$\mathbf{F}_{X,f,l}$ $\mathbf{F}_{Y,f,l}$ $\mathbf{F}_{Z,f,l}$	$\mathbf{F}_{X,f,r}$ $\mathbf{F}_{Y,f,r}$ $\mathbf{F}_{Z,f,r}$	$\mathbf{F}_{X,r,l}$ $\mathbf{F}_{Y,r,l}$ $\mathbf{F}_{Z,r,l}$	$\mathbf{F}_{X,r,r}$ $\mathbf{F}_{Y,r,r}$ $\mathbf{F}_{Z,r,r}$
Moments (Nm) (unused)	$\vartheta_{X,f,l}$ $\vartheta_{Y,f,l}$ $\vartheta_{Z,f,l}$	$\vartheta_{X,f,r}$ $\vartheta_{Y,f,r}$ $\vartheta_{Z,f,r}$	$\vartheta_{X,r,l}$ $\vartheta_{Y,r,l}$ $\vartheta_{Z,r,l}$	$\vartheta_{X,r,r}$ $\vartheta_{Y,r,r}$ $\vartheta_{Z,r,r}$

Table III.1: Global load components for a personal vehicle

denoting f or r, l or r whether the effort (degrees of freedom X to Z) or moment (dof ϑ_X to ϑ_Z) is applied to the front or rear axles, on the left or right wheel (e.g. $F_{X,f,l}$); X, Y, Z directions associated respectively to longitudinal, lateral and vertical solicitations. $F_{X,\bullet,\bullet}$ is positive when the vehicle is decelerating and $F_{Z,\bullet,\bullet}$ is positive when the vehicle is pushed upwards, *e.g.* as a reaction to its weight. n_F is the total number of global load components.

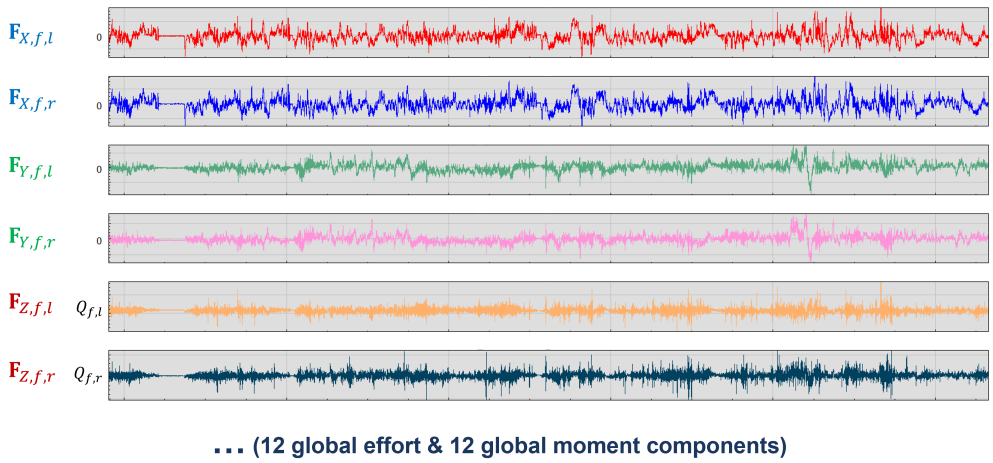

Fig. III.3: Example of a global loading history from service.

III.2.2 Service loads

The set of loading histories with any duration that stem from real-life use is called $\mathbb{A}$, service loads. As explained in the general introduction, service corresponds to all loads that are considered regular, acceptable during the use of a personal vehicle. The frontier between regular use and abuse is set by a threshold on maximum values of effort on the wheel axle, with a fraction of the mass of the vehicle being a parameter of the threshold. At this threshold, the designed components are first tested for absence of macroscopic plastic deformation, corresponding to another safety requirement of the system.

$$\vec{\mathbf{F}} \in \mathbb{A} \Rightarrow \forall t \in [0,T]\,,\ \forall j \in [\![1,n_F]\!],\ F_j(t) < k_j \cdot Q_j \tag{III.2.2}$$

denoting $k_j \cdot Q_j$ the level of the loads used for validation of non-plasticity; Q_j being the associated charge in Newton for the load component, representing a fraction of the weight of the vehicle.

This is a *negative* definition, *i.e.* an implication. Not all loads that do not lead the vehicle to yield are service loads. Indeed they also need to be realistic. What *positively* defines a service load is its plausibility on the road, *i.e.* the fact that it stems from the realization of a mission (see later §IV.2.1).

The generic set of loading histories with any duration that are plausibly input to automotive structures on the road, on proving grounds, on test benches or in numerical simulations is denoted $\mathbb{F}^{n_F} \supset \mathbb{A}$.

III.3 Definition and objectives of fatigue characterization

As explained in the introduction, suspension and body parts fail if a macroscopic crack appear at any stress concentration zone. The strength of one such part is the strength of its weakest

component. However, in the case of systems submitted to a very diverse population of pseudo-fatigue and for which the population of joints may be of independent qualities, there is no such thing as a weakest component over all specimens and for all of service pseudo-fatigue. This is even more true when the system is not yet designed.

The trick is to discuss the fatigue induced on the stress concentration zones of a part in terms of κ transformations of the input load components. These transformations will bring incomplete but sufficient knowledge of the fatigue induced on the structure.

While fatigue analysis predicts whether or not a component may fail before the end of a loading history, a fatigue characterization evaluates indirectly an amount of fatigue induced on an non-designed component. From there, if one wanted to conduct a fatigue analysis of the structure, fatigue characterization would have to be completed by information on the resistance of all its stress concentration zones (*i.e.* the material constants used in a damage model like the reference point $(N_0,\Delta\tau_0)$ of a Basquin model Eq. II.4.1).

A designed version of a vehicle model is denoted $\mathcal{V}$. This variable contains the joint information of all parts' geometries, materials, manufacturing qualities and the definition of their joints post-design. A function φ_k of the global loading history $\vec{\mathbf{F}}$ is a fatigue characterization for the vehicle model $\mathcal{V}$ if:

$$\exists z \in \mathcal{V},\ \exists f_{\mathcal{V}} \text{ such that } D\left(z,\vec{\mathbf{F}}\right) = f_{\mathcal{V}}\left(z,\varphi_k(\vec{\mathbf{F}})\right) \tag{III.3.1}$$

denoting D the damage function introduced in Section II.5; and $f_{\mathcal{V}}$ an unknown function completing the missing information on damage.

The objective of this chapter is to elaborate a fatigue characterization that helps us determine indirectly the fatigue induced on all the zones that may end up to be critical following service loads (see §II.4.3). In Section II.2, we have named stress concentration zones the locations in the structure that may be stress concentrations under a given loading history. Let us define a similar concept for zones of the structure that may be critical under a given service loading history:

Let z be a zone of a designed version of the vehicle model $\mathcal{V}$, accompanied with a fatigue criterion to determine for any global loading history whether or not it is a critical zone. Let $\mathbb{A}$ be the population of service loads. z is a sensible zone if there exists a global loading history $\vec{\mathbf{F}}^* \in \mathbb{A}$ such that z is critical.

As long as the final design of the system is not known, the set of sensible zones may at best be known only functionally. For instance the location of a weld bead may be known in advance, but not all parameters of the weld. Instead of making an inventory of the sensible zones of a structure and their material properties, the goal of fatigue characterization is to make sure that all have been accounted for.

Let us consider a dummy set of sensible zones $z \in \mathcal{V}$, $\mathcal{V}$ being unknown. Based on the previous definition, it corresponds to all the zones that we might need to check for failure in validation of their reliability, because they may all have a part in the risk of failure of the system.

The determination of suitable variables for the evaluation of Stress conditions and levels for all zones must meet three desiderata: First, the design of a part must help control the good resistance of all zones of the part; Second, the definition must be manageable by conception teams for the design of new parts; third, the definition must allow comparison of design references between different vehicle models or even segments. The two properties that satisfy such constraints are exhaustiveness and low structural dependency, defined as follows:

Property III.3.1 (Fatigue characterization exhaustiveness) *A characterization $\vec{\varphi}$ of the fatigue induced on a system $\mathcal{V}$ is exhaustive if:*

$$\forall z \in \mathcal{V},\ \forall \vec{\mathbf{F}} \in \mathbb{A},\ \exists j \in [\![1, Card(\vec{\varphi})]\!],\ D\left(z, \vec{\mathbf{F}}\right) = f\left(\mathcal{V}, \varphi_j(\vec{\mathbf{F}})\right)$$

Property III.3.2 (Low structural dependency) *A characterization $\vec{\varphi}$ of the fatigue induced on a system $\mathcal{V}$ has a low structural dependency if:*

$$\forall \mathcal{V}, \mathcal{V}' \text{ ensuring the same function},\ \forall \vec{\mathbf{F}} \in \mathbb{A},\ \vec{\varphi}_{\mathcal{V}}\left(\vec{\mathbf{F}}\right) = \vec{\varphi}_{\mathcal{V}'}\left(\vec{\mathbf{F}}\right) = \vec{\varphi}\left(\vec{\mathbf{F}}\right)$$

denoting $\mathcal{V}$ and $\mathcal{V}'$ any two different versions of the same vehicle project.

To sum up, we are looking for an exhaustive characterization of the fatigue induced by global loading histories $\vec{\mathbf{F}} \in \mathbb{F}^{n_F}$ (not just service loads) on suspension and body components of an automotive structure. The characterization must have low structural dependency. We also need these two properties to hold for the fatigue induced by any loading history, not only in service but also in test conditions (numerical simulation, test bench, proving grounds).

In order to obtain such a characterization, we need to model completely the relation between global loads of the system and the fatigue analysis of all its sensible zones.

III.4 Mechanical response: from global to local loads

Let us focus on the relation, called mechanical response or localization, between a given multi-input loading history $\vec{\mathbf{F}} = \left[\vec{F}(t)\ \forall t < T\right]$ and the local loading histories $\left[\underline{\sigma}\right](z) = [\sigma(z,t)\ \forall t < T]$ at each plausible crack initiation a.k.a. sensible zone z of a vehicle model $\mathcal{V}$.

The following localization method, as well as alternatives, are introduced and detailed in [Lévai 2018] Chap. 2.1.

We first consider car chassis structures to have a quasi-static response to service global loads, based on the rather low frequencies of non-vibratory loads. Therefore, instantaneous stresses are determined from instantaneous effort values (and not from the whole history of loads):

Hypothesis III.4.1 (Quasi-static structural response) *The structure is said to have a quasi-static response to multi-input global loads when the instantaneous value of every inner quantity of interest is determined by the instantaneous values of the global loads.*

$$\forall z \in \mathcal{V},\ \forall t < T,\ \underline{\underline{\sigma}}(z,t) = f\left(z, \vec{\mathbf{F}}(t)\right) \tag{III.4.1}$$

From a frequency point of view, a quasi-static structure has the same behavior as a full-pass dynamic system to service loads, while real mechanical systems are usually known to all be low-pass.

This quasi-static hypothesis is not available for the study of vibratory fatigue in the structure, because the corresponding frequency would be too high for the actual filtering frequency of a system. Still, design against vibratory fatigue failure requires different characterization methods and countermeasures to filter out eventual resonances in the system.

The quasi-static hypothesis is also hindered by violent events such as potholes or pavements, as they have a wider power density spectrum than regular road events. However, it is a conservative hypothesis, meaning it will overestimate the induced pseudo-fatigue. Indeed the larger frequencies contained in these single events would in reality be filtered by a low-pass dynamic structure.

In a second time, we also consider that the structure has an elastic response to service global loads. Indeed, we ignore material viscosity thanks to the hypothesis of quasi-static response. We ignore material plasticity by definition of the set of service loads $\mathbb{A}$.

We also ignore the effects of non-linear elements such as joint stops. While this last item seems arbitrary, it is actually another conservative hypothesis, because we overestimate stresses that would actually be filtered by joint stops. We will not consider the fatigue design of joint stops and bushings in this work. Besides, models for the fatigue analysis of rubber [Raoult 2005] are not presented in this manuscript.

Hypothesis III.4.2 (Elastic structural response) *If the structure has an elastic behavior, the value of every inner quantity of interest is given by the superposition of the contributions of each global load component.*

Under these two hypotheses, the structure has a linear mechanical response. This means that the local stress history at a point of such a structure is obtained at each instant from the superposition of the individual contributions of all load components:

$$\forall z \in \mathcal{V},\ \forall t < T,\ \underline{\underline{\sigma}}(z,t) = \sum_{j}^{n_F} \underline{\underline{K}}_{z,j} \cdot F_j(t) \tag{III.4.2}$$

denoting $\underline{\underline{K}}_{z,j}$ a linear localization tensor associated with the zone z and to a global load component $\mathbf{F}_j$. The coefficients of this tensor can be measured on a designed system by finite element calculations after application of the global load component $F_j(t)$ alone.

III.5 Fatigue of a structure

III.5.1 Damage models for the structure

The ingredients for defining relevant damage models for the characterization of the fatigue of sensible zones in a structure were given and justified in Chapter II. We recall them here to highlight the underlying hypotheses and give a complete definition of our fatigue models:

- We assume that the fatigue behavior of any sensible zone of interest z for the design of suspension and body subsystems, manufactured in a mass production environment, is well described using a modified Wöhler curve [Susmel and Lazzarin 2002] on a judicious local shear variable τ at a control point of the zone;
- We assume the existence of a Basquin model of the high cycle fatigue behavior from such a modified Wöhler curve, given by the formula $N \cdot \Delta\tau^m = N_0 \cdot \tau_0^m$ using a material reference point (N_0,τ_0);
- The local measure τ of the zone z is linearly dependent on local stress $\underline{\underline{\sigma}}(z,t)$ and this dependence is represented by the tensor $\underline{\underline{\underline{\underline{H}}}}$ such that $\tau(z,t) = \underline{\underline{\underline{\underline{H}}}} : \underline{\underline{\sigma}}(z,t)$, denoting : the double contraction operator for tensors. For instance, if the fatigue variable is a projected shear stress on the critical slip plane $(\underline{u}^*,\underline{h}^*)$, then $\underline{\underline{\underline{\underline{H}}}} : \underline{\underline{\sigma}}(z,t) = \underline{u}^* \cdot \underline{\underline{\sigma}}(z,t) \cdot \underline{h}^*$; if the fatigue variable contains a hydro-static pressure term, then $P(z,t) = \underline{\underline{\underline{\underline{H}}}}' : \underline{\underline{\sigma}}(z,t) = 1/3 \cdot \vec{1} \cdot \underline{\underline{\sigma}}(z,t) \cdot \vec{1}$;
- Variations of the local measure τ^* calculated for a critical degradation mode of the zone (such as a critical slip plane) are fit for cumulation using a trivial damage model;
- An REV may be significantly damaged by propagation of dislocations over a few critical slip planes $(\underline{u}^*,\underline{h}^*)$ but the damage calculated on each plane does not infer on the damage calculated on another plane at any moment of the local loading history;
- The local loading history is chaotic, therefore load sequence/hardening effects are negligible and the Rainflow counting algorithm associated with Miner law is best suited for damage computation. See Appendix B for more details on the importance of this hypothesis.

From these hypotheses and the localization method summarized in Eq. III.4.2, we can write our generalized damage model for any zone of interest in the structure:

$$\forall z \in \mathcal{V},\ \forall \vec{\vec{\mathbf{F}}} \in \mathbb{F}^{n_F},\ D(z,\vec{\vec{\mathbf{F}}}) = \sum_{i=1}^{n_{\text{cyc}}} \frac{\Delta\left(\underline{\underline{\underline{\underline{H}}}}_z : \left(\underline{\underline{\underline{\underline{K}}}}_{z,\bullet} \cdot \vec{\vec{\mathbf{F}}}\right)\right)_i^{m_z}}{N_0 \cdot \tau_0^{m_z}} \tag{III.5.1}$$

The geometry of a designed system is stored in the localization tensors $\underline{\underline{\underline{\underline{K}}}}_{z,\bullet}$, as well as in the fatigue measure tensor $\underline{\underline{\underline{\underline{H}}}}_z$ in terms of critical slip plane definition. The reference couple (N_0,τ_0) of the modified Wöhler curve informs us on the quality and more generally on the fatigue resistance of the zone of interest. These four variables are very design-dependent.

III.5.2 Pseudo-damage and local contexts

The form of Eq. III.5.1 hints at a factorization of design-dependent terms. For each zone z, let us define the local unit combination vector $\widetilde{\vec{\alpha}}_z$ and the local absolute combination vector $\vec{\alpha}_z$:

$$\vec{\alpha}_z = \sum_j^{n_F} \frac{\underline{\underline{H}}_z : \underline{\underline{K}}_{z,j}}{N_0 \cdot \tau_0^{m_z}} \tag{III.5.2}$$

$$\vec{\alpha}_z = |\vec{\alpha}_z| \cdot \widetilde{\vec{\alpha}}_z \tag{III.5.3}$$

Equation III.5.3 is a decomposition of the local absolute combination vector $\vec{\alpha}_z$ into norm $|\vec{\alpha}_z|$ and direction $\widetilde{\vec{\alpha}}_z$. One may choose either the Manhattan ($|\bullet|_1$) or Euclidian ($|\bullet|_2$) norm to define it, as long as the choice is consistent throughout the method. We can use these two previous equations to re-write the damage of a zone into:

$$\forall z \in \mathcal{V},\ D(z,\vec{\mathbf{F}}) = |\vec{\alpha}_z| \cdot \sum_i^{n_{\text{cyc}}} \Delta\left(\widetilde{\vec{\alpha}}_z \cdot \mathbf{F}\right)_i^{m_z} \tag{III.5.4}$$

In this damage formula for all sensible zones $z \in \mathcal{V}$, the norm $|\vec{\alpha}_z|$ of the local absolute combination vector $\vec{\alpha}_z$ compares the norm on stress magnification at zone z given by the double product $\left(\sum_j^{n_F} \underline{\underline{K}}_{z,j} : \underline{\underline{H}}\right)$ to the actual strength of the zone, given by the material factor $(N_0 \cdot \tau_0^{m_z})$.

The unit load combination $\widetilde{\vec{\alpha}}_z$ defined in Eq. III.5.3 weighs the influence of each global load component on the damage of zone z. In order to understand how the coefficients of this vector can be determined, we will associate this combination to usual load cases of the structure in the next §III.6.1.

Pseudo-damage $\breve{D}$, an intermediary variable introduced in [Johannesson and Speckert 2014] Chap. 3, is defined as:

$$\forall z \in \mathcal{V},\ \breve{D}(z,\vec{\mathbf{F}}) = \sum_i^{n_{\text{cyc}}} \Delta\left(\widetilde{\vec{\alpha}}_z \cdot \mathbf{F}\right)_i^{m_z} \tag{III.5.5}$$

The damage of a point is therefore the product of a material and structural mechanical term with pseudo-damage, a variable that is mostly dependent on the Rainflow cycles calculated on a linear combination of the global load components.

The last material parameter in the formula of pseudo-damage is the Basquin exponent m of the fatigue model associated with the studied failure mode of the zone z.

Several zones in the structure may have similar Basquin exponents, should they have the same crack initiation and propagation behaviors. Several zones may also have similar weightings of load components $\widetilde{\vec{\alpha}}_z$. Yet all these zones, being located in different spots of the structure, will not have equal magnification terms $|\vec{\alpha}_z|$.

We denote local context associated with the zone z the joint information of the unit combination vector $\widetilde{\vec{\alpha}}_z$ associated with the zone and Basquin exponent m_z: $\gamma(z) = (\widetilde{\vec{\alpha}}_z, m_z)$. We re-define the pseudo-damage associated with a local context γ as:

$$\breve{D}\left(\gamma, \vec{\mathbf{F}}\right) \sum_{i}^{n_{\text{cyc}}} \Delta\left(\widetilde{\vec{\alpha}} \cdot \vec{\mathbf{F}}\right)_i^m \tag{III.5.6}$$

A local context is made relevant by the subset of sensible zones in the structures that have proportional damages over the population of service loads $\mathbb{A}$:

$$\forall z \in \mathcal{V},\ \exists\left(\gamma, |\vec{\alpha}_z|\right), \forall \vec{\mathbf{F}} \in \mathbb{A},\ D\left(z, \vec{\mathbf{F}}\right) = |\vec{\alpha}_z| \cdot \breve{D}\left(\gamma, \vec{\mathbf{F}}\right) \tag{III.5.7}$$

Let us write our pseudo-damage cumulation using classed Rainflow ranges (§II.5.1), as will be the case in practice. The values of global loads in service are limited by the validation thresholds of service loads, Eq. III.2.2. Therefore, for all pseudo-damage formulas, we assume the existence of a generic set of Rainflow range classes $(\Delta F_i, \mu_i)_{i \in [\![1, n_{\text{bin}}]\!]}$ such that all Rainflow counts (Eq. II.5.2), on all plausible linear combinations $\widetilde{\vec{\alpha}}$ of global load components, can be re-written as a classed Rainflow count using the same generic set of Rainflow range classes (Eq. II.5.8). The formula for pseudo-damage then becomes:

$$\breve{D}\left(\gamma, \vec{\mathbf{F}}\right) = \sum_{i}^{n_{\text{bin}}} n_i\left(\widetilde{\vec{\alpha}} \cdot \vec{\mathbf{F}}\right) \cdot (\Delta F_i)^m \tag{III.5.8}$$

denoting $n_i\left(\widetilde{\vec{\alpha}} \cdot \vec{\mathbf{F}}\right)$ the Rainflow count for the i-th bin, *i.e.* the number of cycles counted on the scalar loading history $\widetilde{\vec{\alpha}} \cdot \vec{\mathbf{F}}$ the range of which falls into the class represented by ΔF.

III.6 Determination or choice of local contexts and fatigue vectors

III.6.1 Global load cases

The formula for damage written using combination vectors in Eq. III.5.4 shows that variations of a linear combination of global load components are directly linked to the damage of sets of sensible zones in the part, likewise for pseudo-damage in Eq. III.5.6. Combinations of global load components can be understood as load cases of the structure - global load cases.

As the vehicle is driven on the road, the structure will show specific deformation cases (see [Happian-Smith 2002] Chap. 6 or [Brown H. C. 2002] Chap. 5) in response to combinations of global loads. For instance, an in-phase combination of vertical loads on the right and left sides of a suspension axle (load case) will lead the cross member to bend (deformation case). An out-of-phase combination will lead it to twist, etc. (see Fig. III.4). These deformation cases will be associated with concentration of stresses at several locations of the structure,

and the repetitions of such structural deformation cases will induce damage at these zones. Each global load case will concentrate stress over a different set of zones. And each zone may concentrate stress under a different set of load cases.

Global load cases are non-measured effort histories calculated on measurements of the global load components of the system. They are defined by a unit combination vector $\widetilde{\alpha}$ such that:

$$\mathbf{F}_{\alpha_k} = \widetilde{\alpha}_k \cdot \vec{\mathbf{F}} \tag{III.6.1}$$

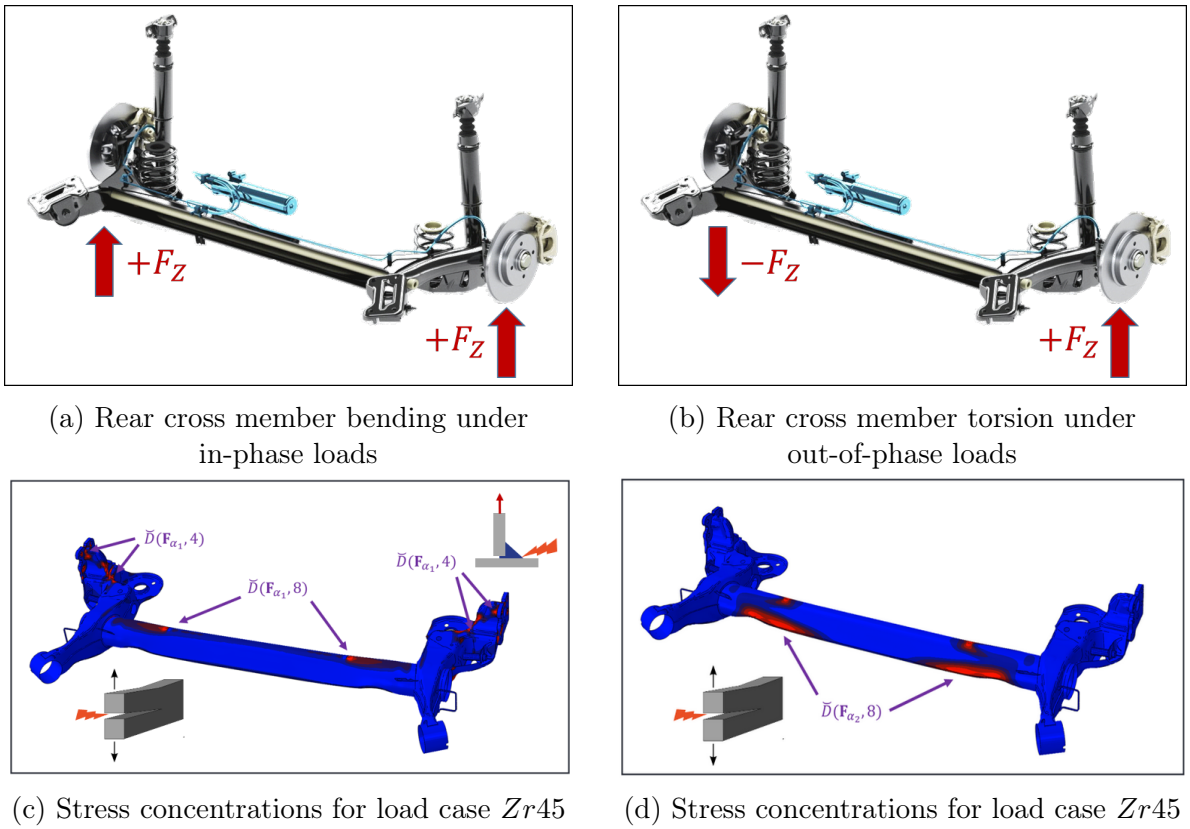

(a) Rear cross member bending under in-phase loads

(b) Rear cross member torsion under out-of-phase loads

(c) Stress concentrations for load case $Zr45$

(d) Stress concentrations for load case $Zr45$

Fig. III.4: Different load cases induce stress concentration at different sets of sensible zones. Pseudo-damage calculated from each load case factorizes the damage of subsets of zones that have similar fatigue models.

For instance, in the two examples given in Fig. III.4, the unit combination vectors are given by a) $\widetilde{\alpha}_{Zr45} = \sqrt{2}/2 \cdot (\vec{e}_{Z,r,l} + \vec{e}_{Z,r,r})$ for in-phase vertical loads on the rear axle and b) $\widetilde{\alpha}_{Zr135} = \sqrt{2}/2 \cdot (\vec{e}_{Z,r,l} - \vec{e}_{Z,r,r})$ for out-of-phase vertical loads, denoting $(\vec{e}_k)_{k\in[\![1,n_F]\!]}$ the elementary vectors associated with the base of the global load components on the vehicle. The combination quantities 45 and 135 denote angles as explained a little further in Eq. III.6.3.

Localization at a sensible zone z of a rigid structure located near a global load application point, like a weld bead on wheel posts, will prioritize load components corresponding to said application point. The local loading history at such a location can be approximated by the single contribution $\underline{\underline{K}}_{z,j} \cdot \mathbf{F}_j$, as in a uni-axial case. Following this principle, some global load

cases are defined from single components of the global loading history. 1D load cases are defined in Tab. III.2. For instance, for longitudinal solicitations on the left-hand side of the front suspension:

$$\begin{aligned} \mathbf{F}_{\alpha_k} &= \mathbf{F}_{X,f,l} \\ \text{such that } \exists z_k \in \mathcal{V},\ \breve{D}\left(z_k, \vec{\vec{\mathbf{F}}}\right) &= \sum_i n_i\left(\mathbf{F}_{\alpha_k}\right) \cdot \left(\Delta F_i\right)^m \quad \forall t < T \end{aligned} \tag{III.6.2}$$

A location far from global load application points will concentrate stress under global deformation cases, like cross member bending or torsion. These global load cases are associated with the combination of two global load components. The unit combination vector has therefore two non-null coefficients that can be written using an angle θ_k as follows:

$$\begin{aligned} \mathbf{F}_{\alpha_k} &= \cos\left(\theta_k\right) \cdot \mathbf{F}_{\bullet,f,l} + \sin\left(\theta_k\right) \cdot \mathbf{F}_{\bullet,f,r} \\ \text{such that } \exists z_k \in \mathcal{V},\ \forall t < T,\ \breve{D}\left(z_k, \vec{\vec{\mathbf{F}}}\right) &= \sum_i n_i\left(\mathbf{F}_{\alpha_k}\right) \cdot \left(\Delta F_i\right)^m \end{aligned} \tag{III.6.3}$$

The inspiration for using a sine-cosine decomposition to describe continuous load combinations stems from industrial experience (see also the localization method proposed in [Bellec *et al.* 2023]). In theory, it gives rise to an infinity of load cases, unless a finite set can be identified on a designed part. In §III.6.3, we will justify the relevance of discretizing this infinite set of load cases for the characterization of fatigue in service whilst retaining low structural dependency (§V.3.2). In Tab. III.3, we propose a physical interpretation of combinations for reference angles 45° (in-phase) and 135° (out-phase). Note that out-of-phase combinations for longitudinal (X) and lateral (Y) loads are not considered to be directly associated with the damage of any zone in the structure.

Parts with specific articulations will transmit some efforts to the rest of the structure. In that case, the concentration of stress at their sensible zones will not depend much on some components of the global loading history. For instance, stress concentration zones on the suspension arm are not dependent on vertical loads, despite the proximity of their application point, because vertical loads are filtered by another part of the suspension. Likewise, car body solicitations are mostly vertical. A suspension triangle-specific load case for the front suspension is written as follows:

$$\begin{aligned} \mathbf{F}_{\alpha_k} &= \cos\left(\theta_k\right) \cdot \mathbf{F}_{X,f,l} + \sin\left(\theta_k\right) \cdot \mathbf{F}_{Y,f,r} \\ \text{such that } \exists z_k \in \mathcal{V},\ \forall t < T,\ \breve{D}\left(z_k, \vec{\vec{\mathbf{F}}}\right) &= \sum_i n_i\left(\mathbf{F}_{\alpha_k}\right) \cdot \left(\Delta F_i\right)^m \end{aligned} \tag{III.6.4}$$

The relevance of such triangle-specific contexts depends on the possibility of designing the suspension system with a suspension arm. Such a solution can be different on the front and rear suspensions (see Appendix A.2).

Name	Code	Formula	Deformation case
1D front longitudinal	$Xf0$	$\mathbf{F}_{X,f,l}$	Bending around the Z-axis of left-hand front suspension parts
	$Xf90$	$\mathbf{F}_{X,f,r}$	- - - of right-hand front suspension parts
1D front lateral	$Yf0$	$\mathbf{F}_{Y,f,l}$	Shear along the Y-axis of left-hand front suspension parts
	$Yf90$	$\mathbf{F}_{Y,f,r}$	- - - of right-hand front suspension parts
1D front vertical	$Zf0$	$\mathbf{F}_{Z,f,l}$	Bending along the X-axis of left-hand front suspension parts
	$Zf90$	$\mathbf{F}_{Z,f,r}$	- - - of right-hand front suspension parts
1D lateral torsion (unused)	$\vartheta Yf0$	$\vartheta_{Y,f,l}$	Torsion along the Y-axis of left-hand front suspension parts
	$\vartheta Yf90$	$\vartheta_{Y,f,r}$	- - - of right-hand front suspension parts
1D rear longitudinal	$Xr0$	$\mathbf{F}_{X,r,l}$	Bending around the Z-axis of left-hand rear suspension parts
	$Xr90$	$\mathbf{F}_{X,r,r}$	- - - of right-hand rear suspension parts
1D rear lateral	$Yr0$	$\mathbf{F}_{Y,r,l}$	Shear along the Y-axis of left-hand rear suspension parts
	$Yr90$	$\mathbf{F}_{Y,r,r}$	- - - of right-hand rear suspension parts
1D rear vertical	$Zr0$	$\mathbf{F}_{Z,r,l}$	Bending along the X-axis of left-hand rear suspension parts
	$Zr90$	$\mathbf{F}_{Z,r,r}$	- - - of right-hand rear suspension parts
1D lateral torsion (unused)	$\vartheta Yr0$	$\vartheta_{Y,r,l}$	Torsion along the Y-axis of left-hand rear suspension parts
	$\vartheta Zf90$	$\vartheta_{Z,f,r}$	- - - of right-hand rear suspension parts

Table III.2: Personal vehicle 1D global load cases

Global load cases are denoted by a unit combination vector $\widetilde{\overline{\alpha}}_k$, as in Eq. III.5.3, and are labelled by their code (see tables III.2, III.3 and III.4). They correspond to new scalar loading histories $\mathbf{F}_{\alpha_k}$, direct inputs to the formula III.5.8 for pseudo-damage. These mathematical objects have a physical sense only thanks to all the hypotheses gathered in §III.5.1.

Name	Code	Formula	Deformation case
2D front longitudinal	$Xf45$	$\frac{\sqrt{2}}{2}(\mathbf{F}_{X,f,l}+\mathbf{F}_{X,f,r})$	Bending around the Z-axis of front suspension member
2D front lateral	$Yf45$	$\frac{\sqrt{2}}{2}(\mathbf{F}_{Y,f,l}+\mathbf{F}_{Y,f,r})$	Shear along the Y-axis - - -
2D front vertical	$Zf45$	$\frac{\sqrt{2}}{2}(\mathbf{F}_{Z,f,l}+\mathbf{F}_{Z,f,r})$	Bending along the X-axis - - -
	$Zf135$	$\frac{\sqrt{2}}{2}(\mathbf{F}_{Z,f,l}-\mathbf{F}_{Z,f,r})$	Torsion along the Y-axis - - -
2D rear longitudinal	$Xr45$	$\frac{\sqrt{2}}{2}(\mathbf{F}_{X,r,l}+\mathbf{F}_{X,r,r})$	Bending around the Z-axis of rear suspension member
2D rear lateral	$Yr45$	$\frac{\sqrt{2}}{2}(\mathbf{F}_{Y,r,l}+\mathbf{F}_{Y,r,r})$	Shear along the Y-axis - - -
2D rear vertical	$Zr45$	$\frac{\sqrt{2}}{2}(\mathbf{F}_{Z,r,l}+\mathbf{F}_{Z,r,r})$	Bending along the X-axis - - -
	$Zr135$	$\frac{\sqrt{2}}{2}(\mathbf{F}_{Z,r,l}-\mathbf{F}_{Z,r,r})$	Torsion along the Y-axis - - -

Table III.3: Personal vehicle 2D global load cases

Name	Code	Formula	Deformation case
Triangle loads front suspension	$XYfl$	$\frac{\sqrt{2}}{2}(\mathbf{F}_{X,f,l}+\mathbf{F}_{Y,f,l})$	Coupled deformation of left-hand front suspension arm
	$XYfr$	$\frac{\sqrt{2}}{2}(\mathbf{F}_{X,f,r}+\mathbf{F}_{Y,f,r})$	- - - of right-hand front suspension arm
Triangle loads rear suspension (unused)	$XYrl$	$\frac{\sqrt{2}}{2}(\mathbf{F}_{X,r,l}+\mathbf{F}_{Y,r,l})$	Coupled deformation of left-hand rear suspension arm
	$XYrr$	$\frac{\sqrt{2}}{2}(\mathbf{F}_{X,r,r}+\mathbf{F}_{Y,r,r})$	- - - of right-hand rear suspension arm
Body torsion (unused)	$Zf0$-$Zr90$	$\frac{\sqrt{2}}{2}(\mathbf{F}_{Z,f,l}+\mathbf{F}_{Z,r,r})$	Oblique body torsion
	$Zf90$-$Zr0$	$\frac{\sqrt{2}}{2}(\mathbf{F}_{Z,f,r}+\mathbf{F}_{Z,r,l})$	- - -

Table III.4: Extra personal vehicle global load cases

All load cases are to be tracked simultaneously over time. A variation in a global load component has an impact as both a single-wheel load case (Tab. III.2) and as a contribution to a combined load case (Tab. III.3 or III.4). Indeed, a single-wheel load case corresponds to the main contributor to a local loading history near the global application point, while a combined load case will be proportional to the local loading history far from the wheels.

However, global load cases built from the same global load components are not redundant in terms of load information. The sum of two loading components is maximum when both components are maximum at the same time. Likewise, both components may cancel their sum and maximize their difference if they are opposite at a given instant.

III.6.2 Chosen local contexts in the thesis

In this paragraph we propose a reference set of local contexts, built altogether and presented indistinctly from:

- industrial experience at Stellantis in terms of relevant load cases for structural fatigue characterization, sampled from §III.6.1;
- from alleged new load cases that may highlight new points of interest in the structure (load case overreach);
- and from previous studies on specific loads for vehicle subsystems such as the suspension arm.

The local contexts are presented in Tab. III.5. Local context derived from load cases associated with moments were not kept because of the number of available components in service data (see Section IV.3). Because they were added late in the thesis, the last line of the table is not included in the reference set of local contexts. The total number of local contexts for the reference set is $\kappa = 26$, setting the dimension for future analyses. This choice of local contexts will be the one exploited in the following Chapter IV.

Damage of zones with a high Basquin exponent is in majority induced by rare large variations in efforts. As we will show in the next paragraph, the difference in pseudo-damages is already apparent between calculations at exponents 4 and 8. However, because the amplitude of single high variations is volatile and hard to sample in service, formulas at high Basquin exponents turn out to be unstable and to vary wildly between similar missions.

We minimize the effect of the instability of such a fatigue characterization through the definition of equivalent magnitudes presented in Section III.7.

While the fatigue of metal sheet edges can be modeled by exponents of 15, we further replace them with models at exponent 8 to avoid these instabilities while maintaining a complementarity in terms of information between Basquin 4 and 8 pseudo-damages.

III.6.3 Discussion on the exhaustiveness of local contexts

In order to handle all plausible failure zones of the subsystem, and therefore to estimate accurately its risk of failure in service, we need to have a sufficient number of local contexts.

However, we may also expect some continuity and correlation between similar local contexts. Unit combination vectors that are close to one another in the unit sphere $\mathbb{U}^{n_F}$ will yield similar pseudo-damages.

Load case	Label	κ	Events	Zones	m
Front longitudinal	b4_FX_f0 (left) b4_FX_f90 (right) b4_FX_f45 (in-phase) b8_FX_f45	4	Maneuver: braking	Wheel mounts, suspension triangle	4, 8
Front lateral	b4_FY_f0 (left) b4_FY_f90 b4_FY_f45	3	Maneuver: cornering	Gussets, triangle joints	4
Front vertical	b4_FZ_f0, b4_FZ_f90 b4_FZ_f45 (in-phase) b4_FZ_f135 (out-of-phase) b8_FZ_f45, b8_FZ_f135	6	Obstacles: speed bump, ditch, pothole	Cross member edges and joints, wheel posts	4, 8, (15)
Rear solicitations	b4_FX_r0, b4_FX_r90 b4_FX_r45, b4_FY_r45 b4_FZ_r0, b4_FZ_r90 b4_FZ_r45, b4_FZ_r135 b8_FZ_r45, b8_FZ_r135	10	Obstacles: speed bump, ditch, pothole	Rear suspension parts	4, 8, (15)
Triangle specific	b8_FXY_fl45 b8_FXY_fr45	2	Coupled maneuvers	Front triangle edge	8
Body torsion (unused)			Twist event, pothole	Body spot welds	4
Total	$\gamma_k = \left(\widetilde{\alpha}_k, m_k\right)$	26			

Table III.5: Chosen local contexts for the suspension, for different solicitation directions and application points (front, rear, left, right). Basquin exponents in parentheses were replaced by 8, see the final paragraphs of the §III.6.2 for explanation. The last row was added late to the reference set and is arbitrarily ignored in most results.

Right now, we are preparing the ground for application of statistical analysis methods. Statistical correlation will make redundant variables invisible. What we need to do is feed our experimental plan with a sufficient amount of non-redundant information. We can settle on a discrete selection of contexts.

A sufficient (exhaustive) base of load cases for the fatigue characterization of all zones of a designed part can be elaborated incrementally. From a given set of sensible zones z of a system of interest $\mathcal{V}$, we can associate to each zone of interest a load case that causes this zone to concentrate Cauchy stress at a significant (damaging) level in a finite element calculation. From baseline load cases used in the industry (see §III.6.1), one can build a base of load cases $\left(\widetilde{\alpha} \cdot \vec{\mathbf{F}}\right)_{k \in [\![1, n_\alpha]\!]}$ until all sensible zones have been highlighted at least once.

Each load case highlights a different set of sensible zones in the structure, and these zones may have different fatigue behaviors, in terms of critical slip plane direction and of Basquin exponent as per our fatigue model. In other words, each local context brings a new information on the kind of fatigue that a multi-input loading history may induce on sensible zones of the structure.

It is also possible to "overreach" by adding more load cases and fatigue models in expectation of new zones of interest in future vehicle models, because of an expected change in vehicle technology for instance. This partially allows characterizing service loads measured previously, for a new vehicle with new technology and given severity profiles (analyzed in the next chapter). "Partially" is putting it lightly. As explained in Appendix E, new architecture and new technology may modify altogether the global loads submitted to a vehicle for a given mission, as well as the habits of driver and therefore the face of pseudo-fatigue. For a given loading history, an overreaching characterization is predictive. However, the prediction of the new loading histories in service on future systems may prove to be a difficult issue requiring a fair amount of new data and assumptions.

III.7 A new fatigue characterization variable: magnitude

III.7.1 Motivation: the properties of pseudo-damage

Figs. III.5 and III.6 show the two pseudo-damage matrices calculated on one Rainflow matrix corresponding to the count on a global load case ($Zf45$, front cross member bending), respectively with a Basquin exponent of 4 and 8.

A pseudo-damage matrix merely show the marginal damage associated with each Rainflow class (see §II.5.1 for definitions).

These graphs show the effect of the Basquin exponent m, the remaining material parameter of the fatigue model introduced in §III.5.1 and included in the definition of pseudo-damage, Eq. III.5.8. A larger exponent gives more importance in damage cumulation to Rainflow cycles with a large amplitude. This is physically associated with a difference in fatigue behavior (see Fig. III.7):

- A weld bead (Basquin exponent between 3 and 5) [Remes *et al.* 2020] always has initial micro-crack notches because of material retraction after manufacturing. Therefore, low to mild load variations above the endurance limit (see §II.4.1) will still induce non-negligible marginal damage.
- The edge of a metal sheet (Basquin exponent between 10 and 20 [Chmelko and Margetin 2020]) is usually not notched. A large load variation is necessary to initiate micro-cracks. Therefore low load variations will not induce a lot of marginal damage.

The power of ten of pseudo-damage is very different from a Basquin exponent to another. This does not, however, translate physically, because the norm of the absolute combination vector (Eq. III.5.2) and most importantly the denominator (the material factor $(N_0 \cdot \tau_0^{m_z})$) will also vary according to the exponent.

This is a problem for the purpose of comparison between similar clients, because the difference between pseudo-damage components will depend on the components' Basquin exponents.

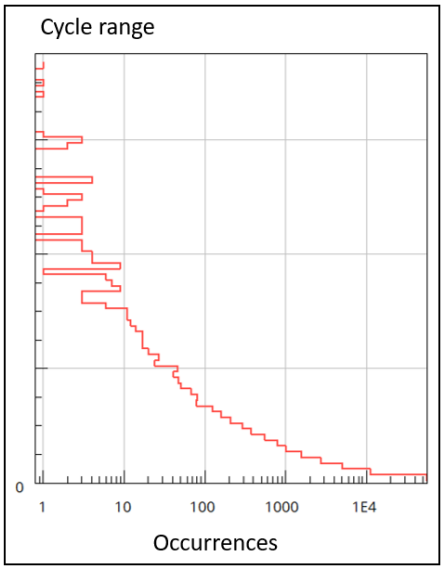

(a) 1D Rainflow matrix

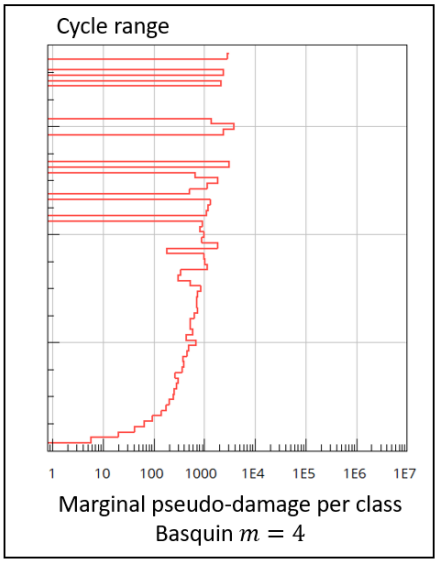

(b) Pseudo-damage matrix

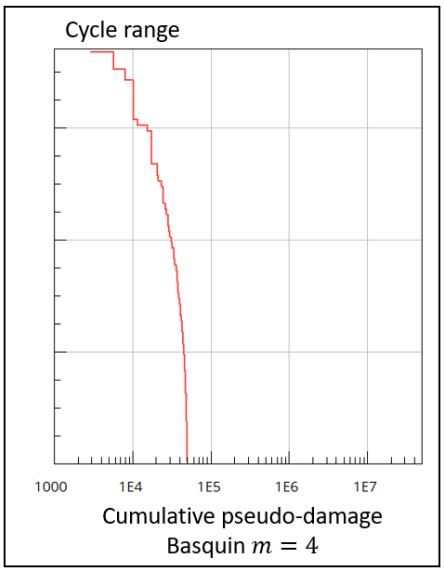

(c) Reverse cumulative pseudo-damage matrix

Fig. III.5: Example of calculation of a pseudo-damage matrix with a Basquin exponent $m = 4$

In §III.7.2, we propose a transformation of pseudo-damage into an effort quantity (in Newton), called equivalent magnitude, based on our introduction of 1D fatigue equivalents in Section II.5.5.

Nevertheless, even for components with the same exponent, the fatigue characterization will not be homogeneous over all load cases, as illustrated in §III.7.3.

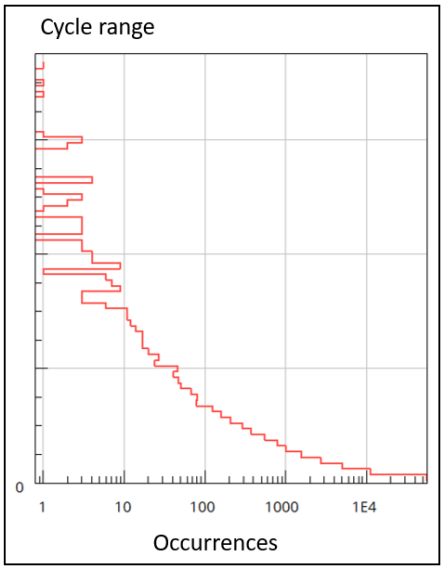

(a) 1D Rainflow matrix

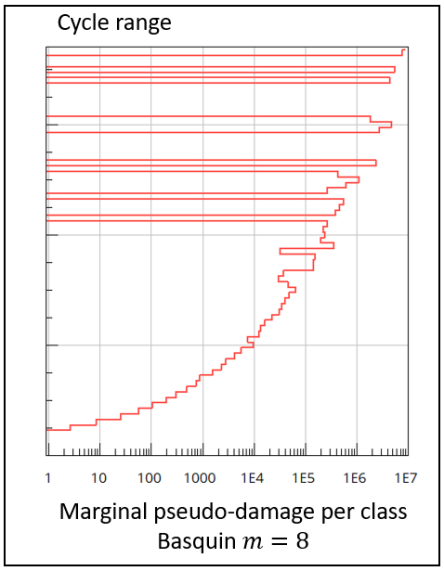

(b) Pseudo-damage matrix

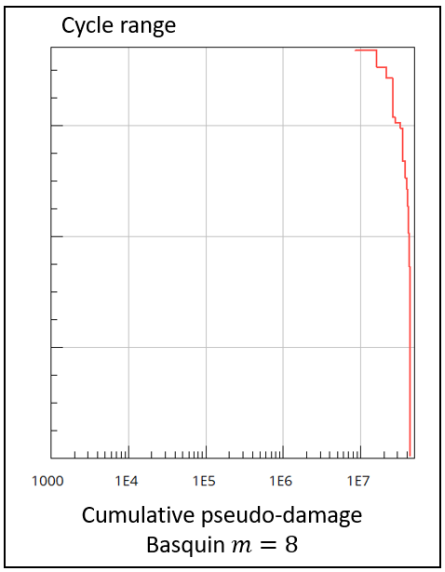

(c) Reverse cumulative pseudo-damage matrix

Fig. III.6: Example of calculation of a pseudo-damage matrix with a Basquin exponent $m = 8$

III.7.2 Definition of damage-equivalent magnitudes

A historical approach to fatigue characterization, similar to pseudo-damage calculation, was to evaluate, for unidimensional load conditions (for instance for each pseudo-damage individually and independently), an equivalent analytic cyclic loading inducing the same pseudo-damage (therefore the same damage) as the studied complex loading history:

$$N_{\text{ref}} \cdot \Delta F_{\text{ref}}\left(\gamma, \vec{\mathbf{F}}\right) = \sum_{i}^{n_{\text{bin}}} n_i \left(\widetilde{\alpha} \bullet \vec{\mathbf{F}}\right) \cdot (\Delta F)_i^m \tag{III.7.1}$$

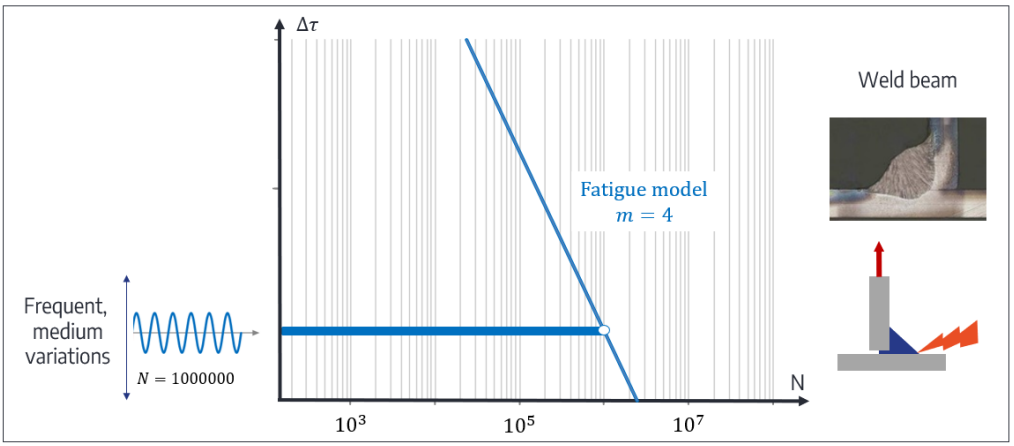

(a) Weld beads ($m = 4$)

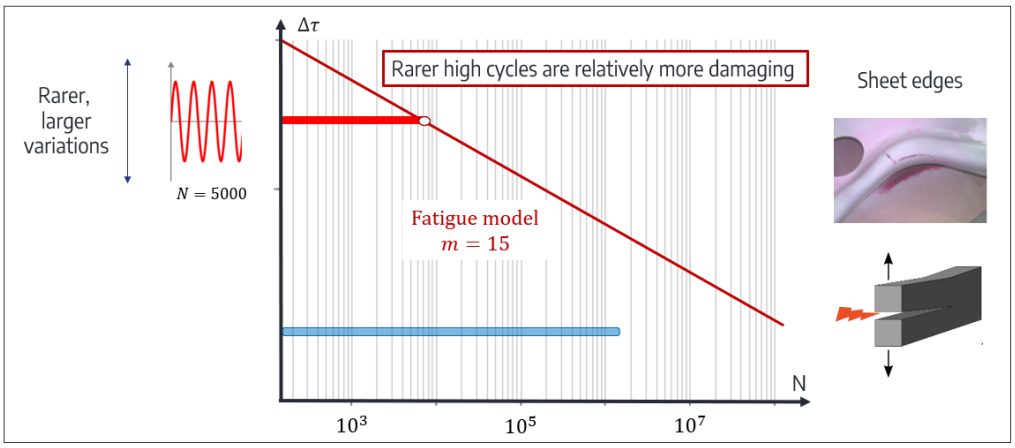

(b) Laminated sheet edges ($m = 15$)

Fig. III.7: Comparison of the marginal damage associated with rare high or to frequent low Rainflow ranges, in terms of relevance for the fatigue characterization of different types of sensible zones.

For $N_{ref} = 10^6$, the amplitude ΔF_{ref} denotes a historical value at Stellantis: the endurance equivalent load (EEL, internal denomination CFE). The choice of a reference number of cycles $N_{ref} = 10^6$ was considered to be the limit of endurance for most assemblies at stake in car chassis as explained in §II.4.1. This choice allowed the method to connect with endurance limit characterization procedures like StairCase and Locati, as well as endurance limit criteria like Dang Van II, established at $N_{ref} = 10^6$ (see §II.4.3).

The curve representing all solutions of this problem for couples $(N_{ref},\Delta F_{ref})$, extrapolated beyond the high cycle domain, is parallel to the Basquin model (see Figure III.8).

For unidimensional load conditions, fatigue equivalence is verified for the high cycle domain, i.e. $N_{ref} \in [10^4,10^6]$ (the actual value of limits are subject to discussions).

However, it is important to note that a κ-vector of pseudo-damage cannot be reproduced by κ individual unidimensional cyclic equivalents.

Therefore, and to avoid confusion with unidimensional fatigue equivalents, we make the arbitrary decision to calculate a similar quantity with $N_{ref} = 1$:

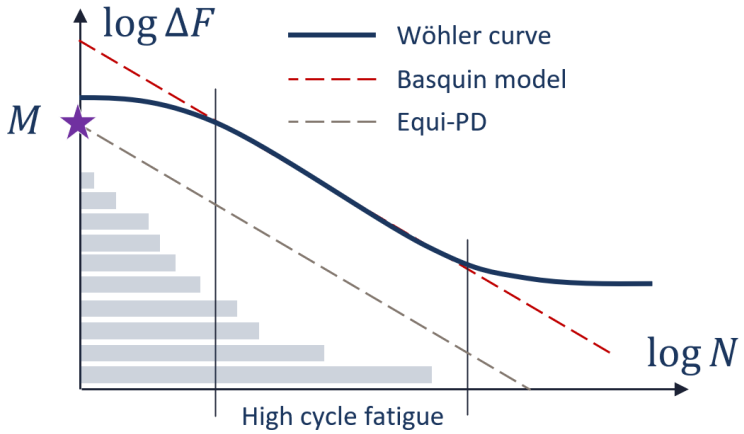

Fig. III.8: Equivalent cyclic loads are located on a line in the high cycle domain. Equivalent magnitude is defined as their amplitude. The EMI is the intercept with the ordinate of the graph

$$M(\gamma,\vec{\mathbf{F}}) = \sqrt[m]{\sum_{i}^{n_{\text{bin}}} n_i \left(\widetilde{\alpha}\cdot\vec{\mathbf{F}}\right)\cdot(\Delta F)_i^m} \tag{III.7.2}$$

The Equivalent Magnitude at Intercept (EMI) M, further simply called magnitude, denotes the amplitude of a single cycle in unidimensional load conditions given by $\widetilde{\alpha}$, that would yield the same pseudo-damage as $\vec{\mathbf{F}}$ on the local context γ, if we artificially extrapolated the Basquin fatigue model of corresponding assemblies to non-fatigue loads.

In the case of large Basquin exponents (larger than 8), we consider that the magnitude is mostly determined by the marginal damages associated with the largest Rainflow ranges. This corroborates the idea that different kinds of components have different sensibility to rare and large versus frequent and low solicitations, as explained in §III.7.1.

For a given global loading history $\vec{\mathbf{F}}$, for any load case determined by $\widetilde{\alpha}\cdot\vec{\mathbf{F}}$ and analyzed through Rainflow counting, the equivalent magnitude at intercept converges towards the maximum Rainflow range of the count (see Fig. III.9).

Nota bene: If the Rainflow count is classed, *i.e.* ranges are sorted in boxes of set sizes (see Eq. II.5.8), the convergence may be altered by the number of cycles in the highest non-zero class. In most cases, the maximum range of the signal (connecting the minimum and maximum of the signal) is associated with a count of 1.

III.7.3 Magnitude radars

Our vectors of interest have $\kappa = 26$ components (see Table III.5). In this paragraph, we introduce a tool for efficient visualization of such vectors.

A radar is a polar histogram. Each variable can be drawn as a point or an arc on its

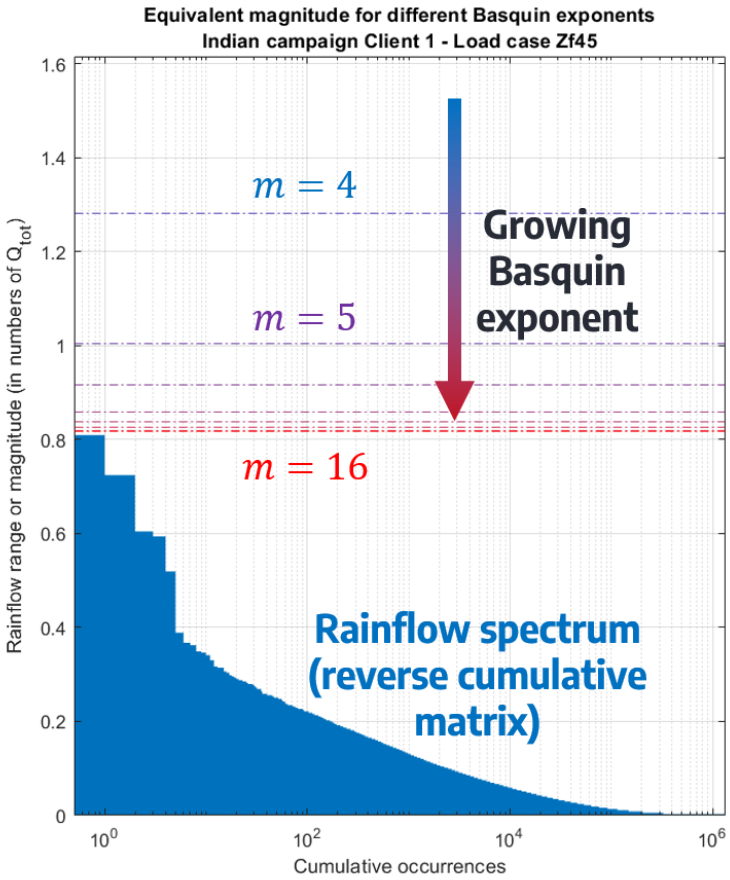

Fig. III.9: Convergence of the equivalent magnitude for increasing Basquin. The blue histogram is the Rainflow matrix of the load case of interest: symmetrical vertical loads on the front axle. The global loading history associated with this Rainflow matrix stems from the Indian measurement campaign introduced in §IV.3.2.

associated radius. Points can be connected to one another: it may be used to hint at continuity between the variables of adjacent radii.

A basic bar histogram could have been chosen to plot a fatigue vector. However, later in the next chapters, magnitude radars will be understood as shapes, and the polar format will give fatigue characterization more readability than the bar one.

Let $\vec{\mathbf{F}}$ be a global loading history corresponding to a mission in service, a sample of the experimental plan presented in Section V.3. An example of calculation of the 26 equivalent magnitudes for a driver of a measurement campaign presented afterwards is displayed in Fig. III.10.

Here, each radius has the same limits. This shape will be typical because of the lingering heterogeneity of magnitude vectors, despite the transformation of pseudo-damage to magnitudes. Indeed, global load cases, as we defined them from Eq. III.6.1, are not normalized. Global loading histories have heterogeneous components and load case variations will be heterogeneous according to what component do they combine. Vertical efforts have higher variations than acceleration solicitations, which in turn have higher variations than lateral

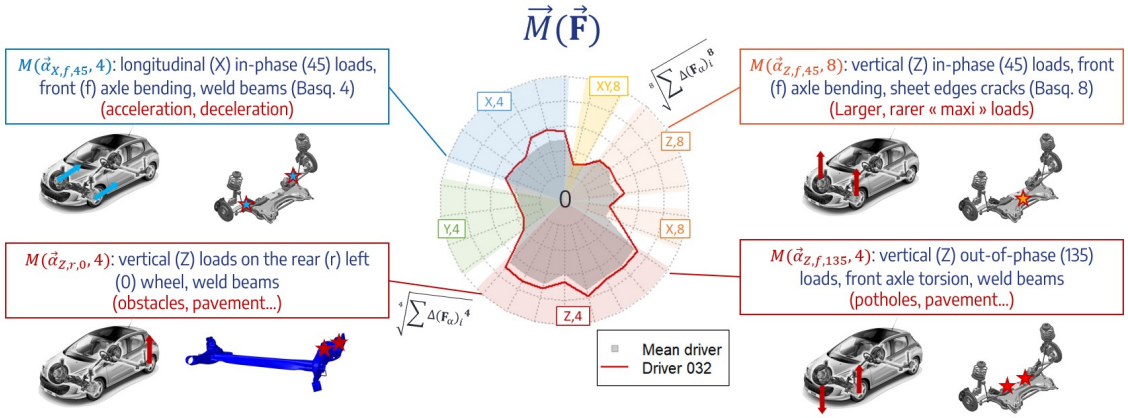

(a) Examples for 4 radii

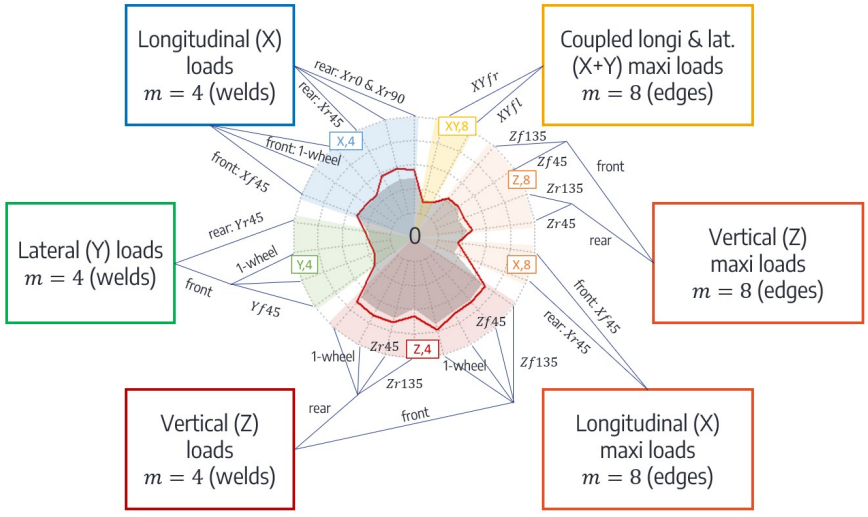

(b) Radius breakdown

Fig. III.10: Absolute magnitude radar for driver 032 on trip US-DT1 compared to mean driver. Each radius is a magnitude component. Radii are gathered in arbitrary sectors of color. All radii have the same minimum (0) and maximum (a confidential factor times the total charge of the vehicle in Newton)

solicitations.

We call radars thus drawn "absolute" radars, because the plotted vector was not transformed and the radius limits are trivial. Thanks to this radar, we can attest that the driver 032 is more damaging than the mean driver of the dataset on local contexts that are sensible to rear (r) longitudinal (X) and vertical (Z) load cases, for both weld beads ($m = 4$) and the edges of laminated metal sheets ($m = 8$).

We gather magnitude components in color sectors as per apparent homogeneity for the sake of readability. Load combinations using different global load component directions (X,Y,Z) are separated for the lower Basquin exponent $m = 4$.

A first radar normalization method, adapted to the analysis of a service measurement campaign, is introduced in Section V.3.2. A second radar normalization method, adapted to

the comparison of proving ground tracks, is introduced in Section VII.3.

III.8 Chapter conclusion

III.8.1 Synthesis

This chapter introduced two changes of perspective.

In a first movement, we have switched the object of interest from a material zone submitted to a local Cauchy stress history, to a part with several zones submitted to a variable population of global loading histories. Said structure might fail at a variety of locations for different global loading histories; these locations of interest are called sensible zones. Thus, in order to describe the fatigue induced on the structure, we need to handle the fatigue models of all these locations.

In a second movement, the system is no longer associated with a locally defined geometry and material characterization; rather to a function, a global geometry and the loads that the system may encounter while performing such a function.

Our objective then becomes to define a sufficient characterization of the fatigue that a mission would induce on a structure once designed. Sufficient here means allowing us to compare and to map missions, and allowing us to translate fatigue characterization to a Stress-Strength interference problem for a design part.

The key to summarize and handle the fatigue at locations that have real-time load correlations in the structure is the definition of local contexts. They are the combinations of distinct structural load cases and the partial fatigue models of associated stress concentration zones for each one. Each local context determines the relation between global loads and the damage of a different set of zones. And the damage of all sensible zones can be determined from fatigue characterization on one or a few local contexts.

The knowledge of each unit combination vector $\widetilde{\alpha}$ and the Basquin exponent of a fatigue model m for one local context allows separating the formula for damage into design-dependent and load-dependent terms. The load-dependent term is called pseudo-damage. This mathematical object has low structural dependency, which means that its formula is constant over all plausible design of a system with a given function.

The chosen characterization of fatigue induced by multi-input global loading histories on the sensible zones of vehicle suspension and body takes the form of equivalent magnitude vectors, a transformation of these pseudo-damages, inspired from 1D fatigue equivalents, with better mathematical properties.

An adequate set of local contexts stems from industrial and/or scientific experience on relevant load cases for the design of different zones of the structure as well as from a discussion of future threats on the design of future vehicles. The reference set that we have chosen in §III.6.2 is therefore adapted to the framework of Stellantis.

Technological innovation means that the sufficient local contexts may change in time in

load combination or fatigue behavior of sensible zones in the vehicle. New materials justify checking for adequate fatigue models to add in the decomposition. The definition of a fatigue vector is always limited to a set of technologies and architectures for the system to design. In the following statistical analyses of service pseudo-fatigue, adding a new variable of interest would only be relevant if it brought about a new, complementary information on the way a mission may damage the parts of a vehicle.

III.8.2 Transition: Stress or severity?

Historical analyses of service loads commonly began with the definition of a scalar (1D) Stress variable φ, the first ingredient of Stress-Strength Interference (SSI) methods. In such a unidimensional framework, Stress can be the damage of a component. This variable can also be a pseudo-damage associated with a set of components. The scope of design is therefore restricted to these zones, not to the entire part. Stress can even be defined as the unique parameter of a loading history: a number of repetitions of a standard loading, the amplitude of a sinus, etc. Either way, Stress will be monotonous with respect to one or several inner damage variables.

Because Stress is scalar in that case, it is already equipped with a total order relation. A loading history $\vec{\mathbf{F}}_A$ dominates a loading history $\vec{\mathbf{F}}_B$ if $\varphi_A > \varphi_B$. This domination usually denotes a difference in severity, denoted S and defined quantitatively as $S = \varphi$: $\vec{\mathbf{F}}_A$ is more severe than $\vec{\mathbf{F}}_B$, or A is more severe than B.

However, Stress is monotonous with respect to inner damage variables. Therefore, for any zone z the fatigue of which is characterized by S, we know directly that if $\varphi_A > \varphi_B$, then $D\left(z,\vec{\mathbf{F}}_A\right) > D\left(z,\vec{\mathbf{F}}_B\right)$ and the risk of failure of a component submitted to $\vec{\mathbf{F}}_A$ will be higher than if it was submitted to $\vec{\mathbf{F}}_B$.

In a multivariate setting with several local contexts and associated fatigue characterizations, we lose both the ability to transform damage into any increasing quantity suitable for load description and a total order between vectors of pseudo-fatigue. When raising a problem to an upper dimension, we need to check that the definitions of our words fit with the rise in dimension. Let us therefore make a distinction between Stress and severity.

Stress, again not to be mixed up with Cauchy stress, is the first ingredient of Stress-Strength interference methods. It is a variable calculated on a mission and that increases with the risk of failure of the system to design.

Pseudo-damage is proportional to the damage of a set of zones. It increases with the risk of failure of components within its associated local context. Therefore, it is a suitable Stress variable for application of Stress-Strength interference methods. Likewise, cyclic or variable amplitude loads that would be used to test the resistance of such components, using a local fatigue criterion, can be translated to pseudo-damage as per Eq. II.5.16. Therefore, a point in the criterion can be translated to pseudo-damage, and Resistance can be defined using pseudo-damage. We are on the right track to discussing the reliability of zones of our system. The application of pseudo-damage in a full Stress-Strength interference method will be the discussion of Chapter VI. However, we lack a definition for severity to compare two missions.

In the general, vernacular language, "severity" is an intensive attribute used for comparison. One is severe when compared to another: The comparison is determined by a given attribute, severity, regardless of the duration of the bases for comparison. Mining rock with a pickaxe is deemed more severe than with a hammer, no matter how many hits one marks with each tool.

In the next chapter, we will investigate the dimension, the attributes and the variability of severity over a population of missions for the system. From there, we may be able pinpoint and describe severe missions. These severe missions will be anchor points of service, plausible references for the future evaluation of the performance of a system. Yet, not until chapter VI will we quantitatively make sense of these severe clients in terms of risk of failure of a system, *i.e.* in terms of Stress.

Our strategy is to find the best transformations of our base variables - magnitudes - to define such a severity as a quantitative variable. We will show how these transformations actually track the profiles of the drivers in terms of behavior and of their missions in terms of encountered structural load cases.

Chapter IV

Exploratory analysis of pseudo-fatigue in service

IV.1 Chapter introduction

In order to establish necessary conditions for the reliable design of automotive components, a primordial ingredient is sufficient knowledge on the variability of solicitations in real-life and of their effect on the system. The information of interest in these solicitations is the fatigue they induce. We will make use of the variables of pseudo-fatigue defined in the previous chapter, vectors of equivalent magnitudes, to gather it.

Pseudo-fatigue denotes here the consequences of the realization of a mission on the system. Service was first defined in §III.2.2 as a restriction of the loads of interest on the structure to loads that regular use of a vehicle may induce, in the absence of abuse. The population of service pseudo-fatigue covers all plausible values of the fatigue variables of the system in service.

A mission is a combination of different factors: the driver, the trip and the payload of the vehicle. These mission factors will be defined more precisely later. The joint information of these factors determines a global loading history on the vehicle, from which we can calculate pseudo-fatigue.

Drivers, trips and payloads are diverse and their diversity induce variability in pseudo-fatigue. What causes drivers to induce different values of pseudo-fatigue? The answer to this question lies both in the situations they have to face during the trip and in their behavior. A multidimensional description of these behavioral traits will be called an intrinsic severity.

When investigating the variability of pseudo-fatigue in a population of missions, the latter is sampled: a number of random drivers may be selected, a few segments of road in the region of interest may also be selected. From this sampling, our objective is to justify the variability of pseudo-fatigue from the diversity of severity profiles.

In this exploratory chapter, we seek to learn, explain and track the causes for variability and non-homogeneity of service pseudo-fatigue over available samples of missions. These

causes for variability will correspond to a first definition of intrinsic severity.

Mission factors are detailed in §IV.2.1. They are our starting point towards understanding the physical sense of the latent factors - severity - that underlie the variability of our quantities of interest. We will add more details on one of these mission factors, trip, in §IV.2.2 and §IV.2.3, introducing respectively road events and road environments.

The presentation and definition of available data, and what we can learn from them, is detailed in Section IV.3. We will make use of this introduction to discuss the representativeness of these datasets and justify our strategy for the analysis of pseudo-fatigue.

In this chapter, we will focus on a measurement campaign involving a number of drivers asked to drive on several road environments. The structure of the dataset will be illustrated in Fig. IV.3. In Section IV.4, the observation of variables and implementation of Multiple Factor Analysis (MFA) serve as an introduction to multivariate statistical analyses. This allows us to analyze the variability in induced fatigue in service through the lens of both driver behaviors and road environments.

The post-treatment algorithm for available data is introduced in Appendix C.

We will see that the sampling of missions lacks diversity in terms of payload. As a perspective, we will discuss the effect of this factor in Appendix E.

The knowledge that we can gather from the exploratory analysis of available data will feed our modeling strategy of service pseudo-fatigue in Chapter V.

IV.2 Missions for personal vehicles

IV.2.1 Mission factors: Driver, Trip and Payload

A mission denotes one application of the function of the vehicle by its user. For the study of the fatigue induced by heavy duty vehicle loads, having a similar variety of use conditions and situations as personal vehicles, [Karlsson 2007], Chap. 1 and [Johannesson and Speckert 2014], Chap. 7 advise to determine several sources of variability between service loads. This leads to factor models. The sources of variability are expressed in terms of use-case descriptors, or mission factors, such as what the truck is carrying, what terrain it is operating on, etc.

Using such a causal framework, the exploration plan of the population of missions amounts to a few labelled measurement campaigns to pinpoint the effect and convolution of each use case variable, that is, to associate to each use case the populations of damages.

From the point of view of fatigue loads on chassis and body parts of a personal vehicle, an episode can be summarized by the following proposition: a client - the Driver - drove their vehicle on a set path - the Trip - with given passengers and luggage - Payload. The mission of a vehicle can be an episode or a concatenation of episodes of different duration.

The knowledge of a mission and of the dynamical properties of the vehicle model determine

the global loading history on the system, and therefore the value of all pseudo-fatigue variables predicted for the end of the mission (see Fig. IV.1).

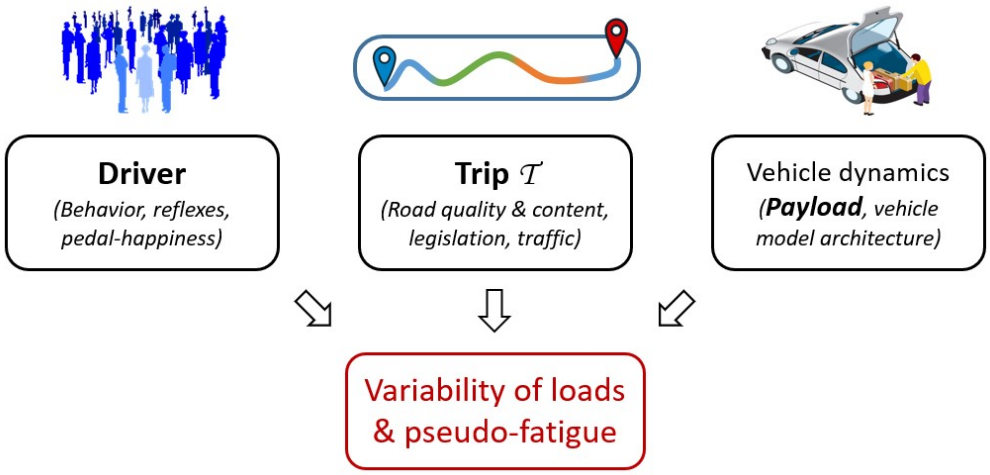

Fig. IV.1: A factor model of the missions of a vehicle model, using three factors.

The exploration of service pseudo-fatigue requires determining an adequate sampling of missions in service by tapping strategically into combinations of these three mission factors:

- The first factor, the Driver, corresponds to the agent taken as a real time decision maker. It contains the information of its personal driving habits: When confronted with a situation, an obstacle or an instruction, the Driver is described by all the traits that determine their next move [Tang *et al.* 2014]. It is an intensive factor, defined independently of the situations that the driver will effectively have to manage during the trip;

- The second factor, the Trip, is associated with the most basic function of a personal vehicle: to go from a point A to a point B. The Trip will report road state, traffic conditions and regulations over said paths. It is an extensive factor: it also carries the information of the length of the mission. Note, however, that weather and traffic conditions may modify the agent's decision-making, making these first two factors interdependent;

- The last factor, Payload, characterizes both the extra mass borne by a vehicle and its distribution over the seats and the trunk, as the latter also modifies vehicle inertia. It is roughly near-constant over a driving episode, ignoring the depletion of eventual fuel. It is an intensive, aggravating mission factor, because it has a tendency to increase the loads and their variations on wheel axles.

Nota bene: The trip is not the same thing as the trajectory of the vehicle. For instance, the trip determines whether or not there is a pothole on the way, but the driver may decide to take it head-on or to evade it, determining the true spatial position and speed of the vehicle.

Pseudo-damages and magnitudes, being continuous variables, can be used to express correlations and distances between two kinds of pseudo-fatigue associated with different

missions. Similarity between drivers and fully defined missions will have slightly different mathematical expressions. Two missions will be similar if they induce similar magnitudes on the local contexts of the vehicle. Two drivers are similar if they induce similar pseudo-damages each kilometer.

Let us generalize the definition of service to describe not only loads (as in §III.2.2), but also missions that yield service loads and associated pseudo-fatigue. In order to evaluate pseudo-fatigue of a large population of lifelong missions in service from limited samples, we need a clever sampling strategy. We need to have an idea of the bias of our sample. We need to analyze our previously defined mission factors through one or several distinct samplings, otherwise restrict them to a given value (as we will see in Chap. V).

The effect of the third factor, Payload, will not be evaluated quantitatively in this thesis. Indeed, available data on service loads lacks diversity in the sampling of this factor. The expected influence of Payload, as well as a preliminary analysis of its effect on pseudo-fatigue are presented in Appendix E. In practice, as explained in the last section of this appendix, measurements, analyses and validation procedures are all conducted at a large setting of payload.

IV.2.2 Road events

Until now, we have considered global loads on the wheel axles of the vehicle to be the input of the system. In order to investigate the mission factor Trip, we need to shed some light on the direct cause of variation in these global loads: the road.

High load variations on the wheel axles of a vehicle are mostly caused by what we will call road events: maneuvers such as braking or cornering and obstacles such as potholes or pavement.

The precise values of the global loads, and therefore the induced damage on sensible zones of car chassis and body, depend on the trajectory of the vehicle (including its speed), on its dynamics (including its mass), and on the geometry of the obstacles (see for instance [Frinkle *et al.* 2004]). Fatigue results from the accumulation of such events, it is therefore important to determine how often and with what intensity they might occur.

Unfortunately, the enumeration of events on service load signals does not allow firsthand to evaluate the amount of fatigue induced by a mission. Indeed, the mechanical response of a vehicle when encountering a pothole may vary wildly according on speed, actual trajectory and the geometry of the obstacle.

A quantitative identification requires formulas for pseudo-fatigue. This further shows that a fatigue characterization remains a necessary arbiter to evaluate and compare missions, events and road environments.

Segmentation and quantitative exploitation of road load data in terms of maneuvers, road rugosity and obstacles are proposed in [Bellec *et al.* 2023]. The arbitrative variables of this segmentation are integrated in a full fatigue characterization by the authors. The fatigue induced by high frequency loads is evaluated using spectral fatigue theories. Low frequency variations of variables are analyzed through similar tools as ours: local combination

vectors, Rainflow counting and Miner law. These new variables represent alternatives and extensions to the magnitudes that we use in this thesis. We will comment on the use of alternative variables for evaluation of pseudo-fatigue severity in the conclusion of this chapter, as perspectives.

IV.2.3 Road environments

We may justify a good share of induced pseudo-fatigue per kilometer by talking in terms of road environments, such as city, highway or country roads (Fig. IV.2). Indeed, obstacles like potholes will be more frequent in damaged roads, while the many crossroads and dense traffic of city roads increase the number of braking and cornering maneuvers.

This segmentation of the trip into road environments is already performed for motor pseudo-fatigue and is also rather easily surveyed. Indeed, people can describe the usual road they drive on using such a description. Moreover, speed limitations are very different between urban, highway and country environments. Large databases like OpenStreetMaps may contain road data segmented using similar attributes [Burger *et al.* 2021].

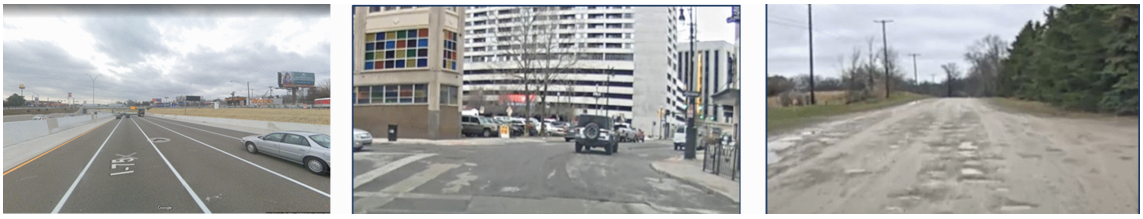

Fig. IV.2: Road environments labeled as (from left to right): Highway, City and Dirt

Over the life of a vehicle, users will drive on these different road environments with different frequency and for different distances, depending on where they live and where they want to go. The distance driven on each road environment is a manageable method to map the population of trips in a market. We will come back on this sampling of trip compositions in §V.2.2.

IV.3 Service load data

IV.3.1 Direct service sampling: vehicle loans, connected vehicles

A sample of a population is a smaller group of individuals over which relevant data is measured. Properties on the population are inferred from observed properties of the sample [Thompson 2012]. The assessment or determination of a so-called "representative" sample from a nebulous population such as pseudo-fatigue for commonplace systems such as personal vehicles can be tricky, as explained in [Kruskal and Mosteller 1979a,b,c, 1980].

In order to assess driving habits, past measurement campaigns involved lending a sensor vehicle to drivers in a population. These drivers may have been volunteers or acquirers of new vehicles. Note the possible bias of this mission sampling method: such populations

are determined respectively by their availability at the time of the campaign, or by their purchasing power.

Moreover, during such vehicle loans, the processing system or some sensors may malfunction without the driver noticing, in the absence of a campaign technician. This would lead to failed acquisition of data.

Campaign cost, duration and risk of sensor mishap therefore encouraged the company to move on to stratified sampling methods, *i.e.* measurement campaigns on set trips, as presented in §IV.3.2.

However, direct sampling may make a comeback with the possible advent of the connected vehicle. This prospect may be economically sound if the extra sensors, processing bus and acquisition system have a reasonable marginal price in mass production, balanced by the improvement in terms of generic analysis of service. In a connected vehicle perspective, the bias of the sample of missions would most likely not be a question.

The legal considerations surrounding the acquisition, transmission and evaluation of driving habits - driver behavior and trips - fall into the scope of privacy laws. Even the descriptors of pseudo-fatigue that we may elaborate in this chapter could very pessimistically be used by some actors against the interest of the users. The literature on the legal difficulties for the implementation of such connected vehicle solutions were not explored in this thesis.

For the sole concern of service pseudo-fatigue analysis for the reliable design of suspension and body subsystems, data acquisition should allow two simultaneous evaluations:

- the characterization of pseudo-fatigue, through an equivalent evaluation of pseudo-damage per kilometer;
- and a segmentation of the mission: trip description in terms of events or environments, number of passengers and luggage and sociological traits of the driver.

If these mission factors and pseudo-fatigue can be evaluated simultaneously (*i.e.* if loads are measured and exploited live), correlations and the latent structure of pseudo-fatigue may be analyzed efficiently using the statistical methods proposed further in this thesis.

IV.3.2 Measurement campaigns on aggregated trips

Recent measurement campaigns involved a number of drivers of the region of interest, tasked to drive a sensor vehicle on a set trip. The trip is divided in several segments corresponding to different road environments (as introduced in §IV.2.3). Even if such measurements are made on a single aggregated trip, rich in events from each environment, the segments can be recombined to work out relevant results for any trip, as we will see in Chapter V.

Measurement campaigns on a given segmented trip with a number of drivers and a fixed payload reduce the number of mission factors to handle and disambiguate, mitigating the curse of high dimensionality. Segmented trips with labeled road environments allow the analysis of the coupled effects of Driver and Trip on induced pseudo-fatigue.

IV.3.2.1 The Indian campaign

A diesel mid-size vehicle, model Peugeot 508 I, was driven for thousands of kilometers in the vicinity of Mumbai in 2011. A large fraction of this distance corresponds to what we will refer to as the Indian campaign IN11, corresponding to a dozen Indian drivers asked to drive this vehicle over a 225km urban and peri-urban trip.

This small sample was a first experiment of measurement campaign on an aggregated trip, following previous vehicle loan campaigns. In this thesis, this campaign served as a proof-of-concept for the pseudo-fatigue analysis strategy developed in the next section [Baroux *et al.* 2022]. A few practical conclusions were drawn from this analysis to have a better approach of the US campaign.

IV.3.2.2 The US campaign

The campaign US18-DTconducted in the USA in 2018 by Stellantis aimed to evaluate service conditions in this country to compare them to existing reference missions used in other regions. A gasoline SUV, model Peugeot 3008 II, was driven for thousands of kilometers corresponding to a variety of samples performed over the country. Several aggregated trips were determined to try different driving conditions in different states. For some of these trips, a sampling of US drivers was performed. This was the case three times in the region of Detroit (DT), Michigan.

We will be interested in the first campaigns US18-DT1 and US18-DT2. In these campaigns, a trip was determined with a requirement on the fractions of four pre-defined road environments: highway (H), city/urban (C), back road (B) and damaged roads (D). Respectively n = 44 and 40 US drivers, solicited by an intermediary partner company, were invited to drive the vehicle on the pre-determined trip. The sub-populations of drivers do not overlap between the two campaigns. The trips were respectively l =245 and 420km long. The second trip US18-DT2 contained a much larger fraction of highway than US18-DT1.

IV.4 Statistical analysis of Driver-Trip interactions on segments of a trip

The first dataset of interest stems from the measurement campaign US18-DT1 introduced previously. The dataset, denoted $\mathcal{C}$, is composed of n individuals (drivers) who drove on the whole trip $\mathcal{T}_1$, which is l kilometers long in theory. It is composed of $r = 6$ road segments: two highway (H1 and H2), one urban (C), two back road (B1 and B2) and one damaged road (D) segments. The associated composition is given by $(l_e)_{e\in[\![1,r]\!]}$.

For each driver c, for each road segment e, κ magnitudes $\left(M\left(\gamma_k,\vec{\overline{\mathbf{F}}}_e^c\right)\right)_{k\in[\![1,\kappa]\!]}$ were calculated from Eq. III.7.2. The procedures for efficient acquisition, pre-treatment and post-treatment of these variables of pseudo-fatigue are detailed in Appendix C.

In this section, we investigate the coupled effects of driver behavior and road environment on the fatigue induced on suspension and body structures. Different evaluations of pseudo-fatigue variables for different drivers and different road environments aim to analyze the latent structure of the connections between different variables of pseudo-fatigue in service.

The complete dataset is presented in Fig. IV.3. Fatigue characterizations are calculated for each driver on each segment of the trip, as well as supplementary variables that we will present later. These supplementary variables describe the speeds and accelerations practiced by the drivers on each segment. They will help us interpret the results of the upcoming statistical analysis. In the following paragraph, we will first define a new variable, the load intensity, that characterizes the fatigue induced per kilometer by each driver on each segment of the trip.

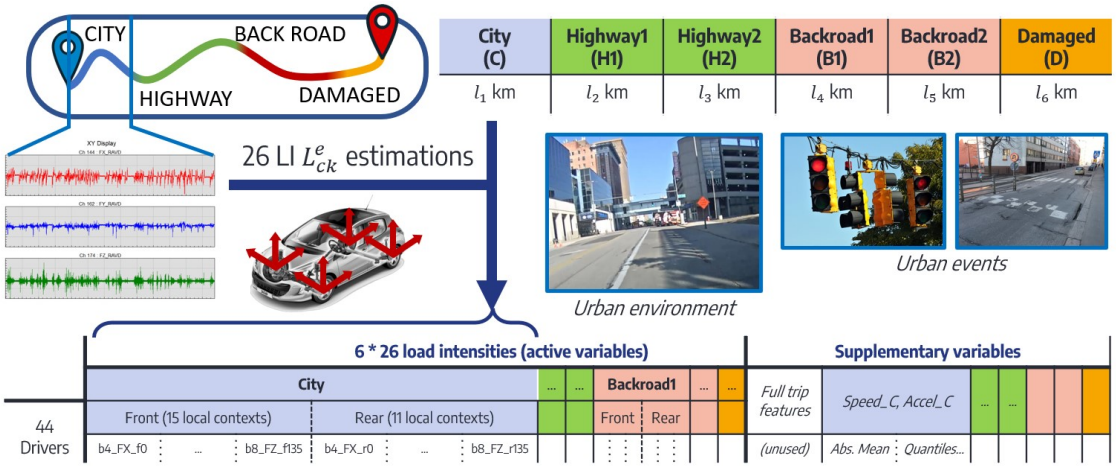

Fig. IV.3: Dataset analyzed in this chapter. Load intensities (*i.e.* magnitude per kilometer) and speed and acceleration quantities are calculated for each driver on each segment of the trip.

An exploratory data analysis on this multi-factorial dataset has three objectives:

- Interpret the correlations between the different covariates in each separate subset;
- Observe the similarities and dissimilarities in the dataset between variables calculated on different segments to interpret the role of the road environment;
- Analyze the shape of the population and how the drivers distinguish themselves, both globally over all segments and locally on each road environment

IV.4.1 Separate road environment analyses

Let us consider each segment $e \in [\![1,r]\!]$ of the campaign US18-DT1 individually for each driver. The evaluation of a driver on a road segment is considered to be an evaluation of the driver's "manner of use", on the corresponding road environment. Each segment has a different length and density of road events. In order to compare them, we need a variable that measures a quantity of pseudo-fatigue per kilometer.

IV.4.1.1 Load intensity

For each driver c, for each road segment e inducing a global loading history $\vec{\mathbf{F}}_e^c$, we define the load intensity $L\left(\gamma,\vec{\mathbf{F}}_e^c\right)$ corresponding to the m-root of the pseudo-damage per kilometer:

$$L\left(\gamma,\vec{\mathbf{F}}_e^c\right) = \sqrt[m]{\frac{1}{l_e}\breve{D}\left(\gamma,\vec{\mathbf{F}}_e^c\right)} = \sqrt[m]{\frac{1}{l_e}}M\left(\gamma,\vec{\mathbf{F}}_e^c\right) \tag{IV.4.1}$$

denoting $\breve{D}\left(\gamma,\vec{\mathbf{F}}_e^c\right)$ and $M\left(\gamma,\vec{\mathbf{F}}_e^c\right)$ respectively the pseudo-damage and equivalent magnitude at intercept induced by the global loading history $\vec{\mathbf{F}}_e^c$ on the local context γ, from Eqs. III.5.8 and III.7.2.

Nota bene: We recall from Section III.7 that the equivalent magnitude at intercept schematically represents the amplitude of a single load cycle, that would theoretically deal the same amount of fatigue damage as the loading history of interest on the structure. In a similar sense, load intensity represents the amplitude of a load cycle to apply once every kilometer to amount to the same amount of fatigue damage as the full loading history. That is, of course, if the Basquin logarithmic model was valid in the non-fatigue domain of the Wöhler curve.

Load intensity might need to be estimated rather than calculated directly. In a stricter sense, a hypothesis of ergodicity is required to argue that the load intensity does summarize the amount of pseudo-damage induced at each kilometer. Ergodicity means that the statistical properties (for instance the load intensity) of different fractions of the segment should remain similar.

The goal of a windowed analysis of each segment can be the determination of a typical kilometer that summarizes the segment. If ergodicity is not verified, fractions of the segment drawn at different timestamps may be biased by the *ad hoc* events of the road. In that case, we could imagine recombining the road events met over a segment to achieve relative ergodicity. However, the Rainflow algorithm would have to be performed again after this recombination, because of the reordering of the extrema of the loading histories.

The vector of dimension κ containing load intensities for all contexts for a driver $c \in [\![1,n]\!]$ on a road segment $e \in [\![1,r]\!]$ is denoted:

$$\vec{L}_{c\bullet}^{e} = \left(L_{ck}^{e}\right)_{k\in[\![1,\kappa]\!]} \tag{IV.4.2}$$

The data subset containing all measured load intensities on the population over a single road segment e is denoted $\mathcal{C}_e$. We define for each local context k and for each road segment e the scaled load intensity with respect to the data subset $\mathcal{C}_e$:

$$Z_{ck}^{L,e} = \frac{L_{ck} - \overline{L}_k}{s_{L_k}} \tag{IV.4.3}$$

denoting $\overline{L}_k$ and s_{L_k} respectively the empirical mean and the standard deviation of the

load intensity on the data subset $\mathcal{C}_e$. The vector of all scaled load intensities for an individual c on a road segment e is denoted $Z_{c\bullet}^{L,e}$. The vector contained all observations of a single load intensity k over all drivers is denoted $Z_{\bullet k}^{L,e}$.

IV.4.1.2 Preliminary observation of the covariates per segment

Prior to analyzing the structure of the dataset, an observation of the empirical means and dispersion for each covariate on each segment is a first step toward understanding how the content of each road segment has an influence on the trends in load intensity vectors.

Fig. IV.4a shows the box plot of absolute load intensity vectors for the urban segment of the trip, in the form of a radar as in §III.7.3. Box plots allow us to check for the existence of heavy outliers in one of the covariates: values that stretch far from the interquartile range, as well as to observe differences in deviation from one marginal variable to another.

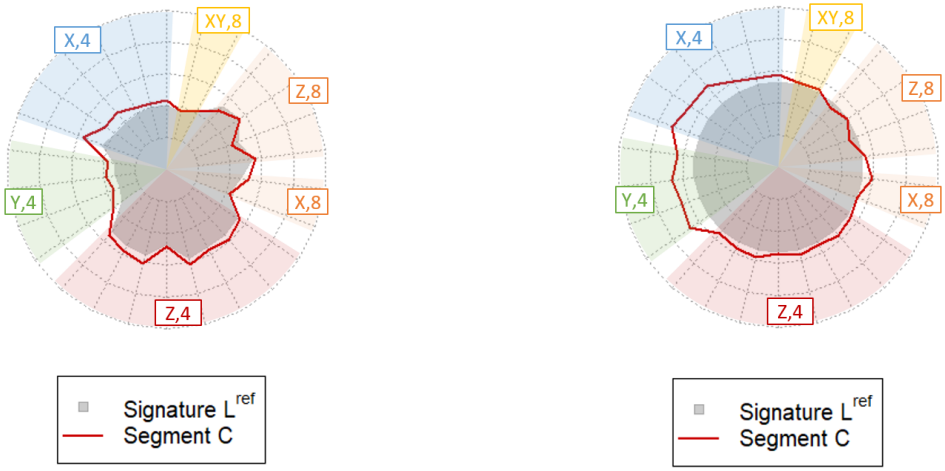

(a) Absolute radar, all radii have the same limits 0 and a confidential fraction of Q_{tot}

(b) Normalized radar, each radius has a different range chosen so that all observations over all road segments fit in the same scale.

Fig. IV.4: Radars of empirical means for each load intensity on the urban segment (C) of US18-DT1. The chosen signature vector is the load intensities calculated on the whole aggregated trip. Q_{tot} denotes the total mass of the vehicle.

The absolute radar appears to be heterogeneous. Each load intensity or each magnitude performs a measure on load cases that are built from different global load components. Different measures are also made with different Basquin exponents. Longitudinal, lateral and vertical global load components have an inherent heterogeneity in their values and ranges that will show on the load intensities.

Let us review the definition of pseudo-damage, in §III.5.2. Analytically, pseudo-damage is one of two parameters of the damage of a zone, the other containing a localization norm term and a parameter of the fatigue criterion of the zone. For a given Basquin exponent, pseudo-damages calculated on combinations of vertical (Z) load components will have much larger quantitative values than pseudo-damages calculated from longitudinal (X) load components.

However, the set of zones of interest in the structure may also be generally sturdier, *i.e.* these zones will not necessarily be more damaged than zones associated with local contexts combining longitudinal load components.

In other words, the quantitative differences in load intensity between contexts combining longitudinal, lateral or vertical load components, or between contexts with different Basquin exponents, is not relevant for the exploration of the variability of pseudo-fatigue in service nor directly for the determination of adequate design conditions. Moreover, reading an absolute radar may be tedious. Therefore, the observation of pseudo-fatigue for the sake of comparison between drivers and trips requires normalization.

Later on, to implement statistical analysis tools to explore the correlations between variables and the latent structure of pseudo-fatigue, we will standardize the dataset, *i.e.* all variables will be centered and reduced. However, for the sake of visualization, differences in standard deviation from one context to another are also an interesting piece of information. Reducing load intensities would hide this information.

Instead, we propose a different method to adapt the visualization of load intensity vectors. The grey zone in Fig. IV.4a corresponds to what we will call a signature: a reference vector for comparison. Here this signature is denoted $\overrightarrow{L}^{\text{ref}}$. For each context $k \in [\![1,\kappa]\!]$, it is calculated as the mean, over all drivers $c \in [\![1,n]\!]$, of all aggregated load intensities L_{ck} over the whole trip:

$$L_k^{\text{ref}} = \frac{1}{n_c} \sum_{c=1}^{n_c} L_{ck} \ \forall k \in [\![1,\kappa]\!] \tag{IV.4.4}$$

This aggregated load intensity $L_{ck} = L\left(\gamma_k, \overrightarrow{\mathbf{F}}_c\right)$ is calculated for each driver c as the m-root of the pseudo-damage per kilometer evaluated over the whole trip:

$$L_{ck} = L\left(\gamma_k, \overrightarrow{\mathbf{F}}_c\right) = \sqrt[m_k]{\frac{1}{l} \sum_{e=1}^{r} \left(M\left(\gamma_k, \overrightarrow{\mathbf{F}}_c^e\right)^{m_k} \right)} \ \forall c \in [\![1,n]\!], \ \forall k \in [\![1,\kappa]\!] \tag{IV.4.5}$$

denoting $\overrightarrow{\mathbf{F}}_c^e$ the global loading history measured on road segment e for driver c; $\overrightarrow{\mathbf{F}}_c$ the global loading history measured associated to the whole trip; l the distance of the whole aggregated trip and m_k the basquin exponent contained in the local context γ_k.

Different signatures may be defined further in the manuscript to illustrate comparisons between episodes from different sources (new trips, proving grounds...). When plotting a normalized radar, the signature will be shown as a reference.

The deviations of each load intensity are retained in a normalized form following normalization by a signature vector. That way, we can visualize differences in deviation indirectly from the sizes of the interquartile ranges and of the inter-extremum zones in the box plot.

Normalized load intensity for the dataset $\mathcal{C}$ is calculated for each driver c, for each road segment e and for each local context γ_k using the following formula:

$$\breve{L}\left(\gamma_k,\vec{\mathbf{F}}_c^e\right) = \frac{L\left(\gamma_k,\vec{\mathbf{F}}_c^e\right)}{L_k^{\text{ref}}} \quad \forall c \in [\![1,n]\!],\ \forall e \in [\![1,r]\!],\ \forall k \in [\![1,\kappa]\!] \tag{IV.4.6}$$

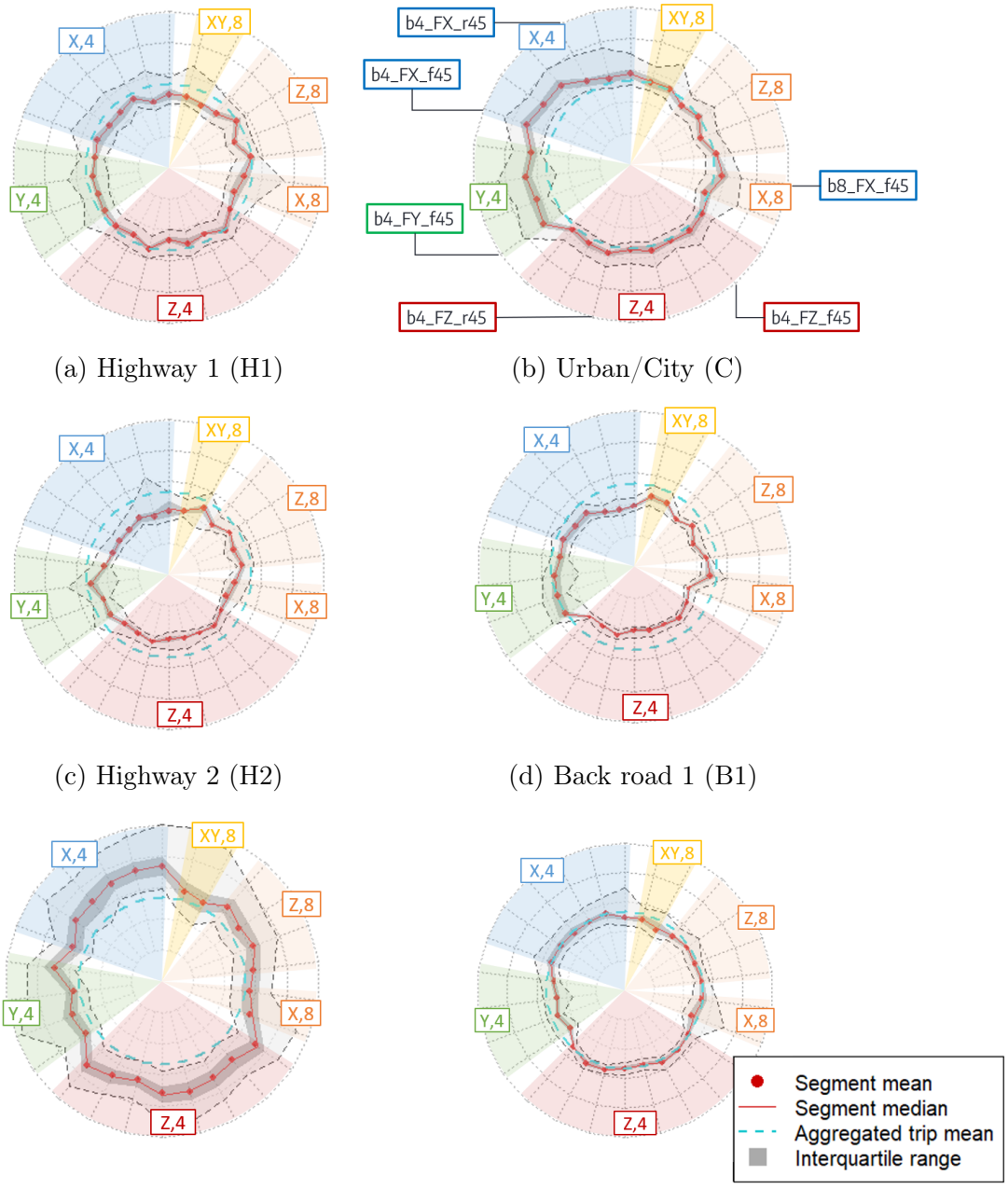

(a) Highway 1 (H1)

(b) Urban/City (C)

(c) Highway 2 (H2)

(d) Back road 1 (B1)

(e) Damaged road (D)

(f) Back road 2 (B2)

Fig. IV.5: Normalized load intensity box plots for each of the 6 segments of campaign US18-DT1. The dashed green line is the mean load intensity over all clients over all segments. It is the base for normalization of all data subsets. The red dots are the empirical mean of each load intensity. The continuous red line is their median. The dark grey zone with blue limits is the interquartile range. The dotted limit of the light grey zones are the extrema of the subset. The light blue dashed line is the signature vector (a circle)

The sole purpose of this normalization is to improve the readability of the radar, to keep only what matters to the eye of an observer. Fig. IV.4 show side-to-side the box plots of absolute resp. normalized load intensities for the urban road segment of US18-DT1. The circle shape of the reference allows for easier interpretation of the shape of the vectors at stake. We can see on this radar that a kilometer of city is significantly more damaging on local contexts associated with longitudinal (X) and lateral (Y) load cases on the front axle that a mean kilometer of the whole trip, and slightly more damaging on all other contexts.

The normalized radars for all road segments of the trip are shown in Fig. IV.5. The damaged road shows, over all components, the largest levels and deviations of load intensities (Fig. IV.5e). A difference in behavior among drivers on this damaged segment causes a large difference in resulting pseudo-damage. Load intensities in City also show higher levels of load intensity than the rest of the segments Fig. IV.5b).

We also begin to observe significant differences between the two segments labelled as highway and those labelled as backroad. The first backroad segment (B1) is much less damaging on vertical load cases than the second one (B2), which is also more dispersive on longitudinal load cases. The first highway segment (H1) yields larger load intensities in average but is more balanced (closer to a circle) than the second highway segment (H2).

The more maneuvers there are in an environment, the more the recurrent behavior of a driver in these maneuvers has an importance on the load intensity evaluated in this environment. The urban (C) segment is dense in crossroads, stops and sharp turns. Hence, its radar of normalized load intensities in Fig. IV.5b will show larger deviations on load intensities that are associated with this kind of events: b4_FX_f45, b8_FX_f45 for acceleration and deceleration and b4_FY_f45, b8_FY_f45 for cornering. Note from the edges of the light grey zone on top of the radar that a few drivers were observed to have very large load intensities on rear longitudinal load cases such as b4_FX_r45. However, the interquartile range for these contexts is as slightly above the signature as on the radii associated with vertical load cases: these high values of b4_FX_r45 only represent a little fraction of the drivers.

The data subsets for each road segments contain 44 observations of 26 load intensities. At first sight, this seems like a dimensionality problem: too many features for too little data. However, some variables may have similar variations over the dataset. Let us first observe, as a preliminary observation of these connections, pair correlations in each data subset. The correlation between two load intensities of the same data subset $\mathcal{C}_e$ is given by the following formula:

$$\text{corr}\ \left(L^e_{\bullet h}, L^e_{\bullet k}\right) = \frac{\text{covar}\ \left(L^e_{\bullet h}, L^e_{\bullet k}\right)}{\text{Var}\ \left(L^e_{\bullet h}\right) \cdot \text{Var}\ \left(L^e_{\bullet k}\right)} = \text{corr}\ \left(Z^{L,e}_{k\bullet}, Z^{L,e}_{k\bullet}\right) = \text{covar}\ \left(Z^{L,e}_{k\bullet}, Z^{L,e}_{k\bullet}\right) \qquad \text{(IV.4.7)}$$

denoting covar and var respectively the covariance and variance operators:

$$\text{covar}\ (L^e_{\bullet h}, L^e_{\bullet k}) = \sum_{c=1}^{n} \left(L_{ck} - \overline{L}_k\right) p \left(L_{ch} - \overline{L}_h\right) \tag{IV.4.8}$$

$$\text{Var}\ (L^e_{\bullet h}) = \sum_{c=1}^{n} \left(L_{ck} - \overline{L}_k\right)^2 \tag{IV.4.9}$$

Two covariates that have a high positive (≈ 1) linear correlation are either both low, both moderate or both large for the same individual. Contrariwise, two covariates that have a high negative ($\approx$ -1) linear correlation are usually at odds with respect to their respective means for each individual. Let us observe the matrices of pair correlations for selected covariates on the first highway, second highway and damaged road segments, in Fig. IV.6. Not all variables are displayed for each data subset. The selection of variables in these graphs is actually justified later on in §V.3.2.

Note that a few load intensities are consistently positively correlated over these three road segments, such as those calculated with a Basquin exponent of 4 on the load cases $Xr45$ (symmetrical rear longitudinal loads), $Zr45$ (symmetrical rear vertical loads) and $Zf45$ (symmetrical front vertical loads), in the first line, fifth and sixth column of each graph (red boxes). All these global load cases are ignited on the same road events, namely obstacles *i.e.* events that either only induce vertical loads (such as speed bumps) or load the wheel axles in all directions (such as potholes and pavements).

Load intensities calculated on the load case $Xf45$ (symmetrical front longitudinal loads, associated with braking and accelerating) for both Basquin exponents 4 and 8 also have a large positive correlation, in the second line, seventh column of each graph (green boxes).

These two groups of variables are two-by-two uncorrelated in the highway segments: indeed the correlation coefficient has a low value in the first line, second column as well as in the second line, fifth and sixth columns. Such relations of correlation and non-correlation between groups of variables are exactly what factor analysis methods such as the one developed further in this section will help us build and interpret.

We can observe on the penultimate column of Figs. IV.6a and IV.6b that the mean of non-zero speed measured on segments Highway1 and Highway2 has a significant negative correlation with some load intensities. A negative correlation between average speed and longitudinal load intensities can be interpreted as an effect of traffic. A driver encountering dense traffic will drive slower and brake and accelerate more often, and vice-versa. The positive correlation between the mean of absolute non-zero correlation and magnitudes calculated on the in-phase (45) combination of longitudinal (X) loads on the front axle corroborates this interpretation.

The correlation matrix for selected components on the damaged road (D) shows a lot more significant positive pair correlation than the other graphs. This homogeneous map of correlations hint at a lower number of degrees of freedom for driver severity on the damage road. We will confirm and interpret this low effective dimensionality of the data subset in the following paragraph.

To understand the negative correlation between speed average and vertical load intensity on Highway2, we have to account for the road conditions on the right-hand side of the road in

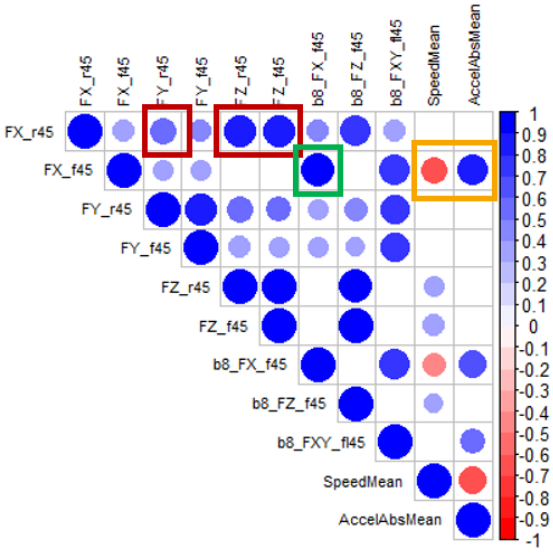

(a) Highway1

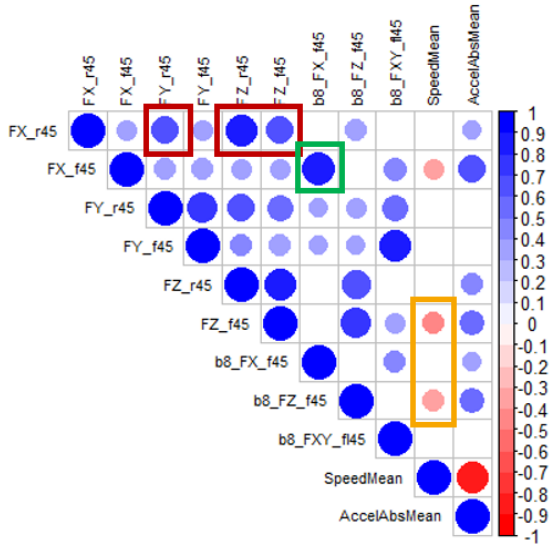

(b) Highway2

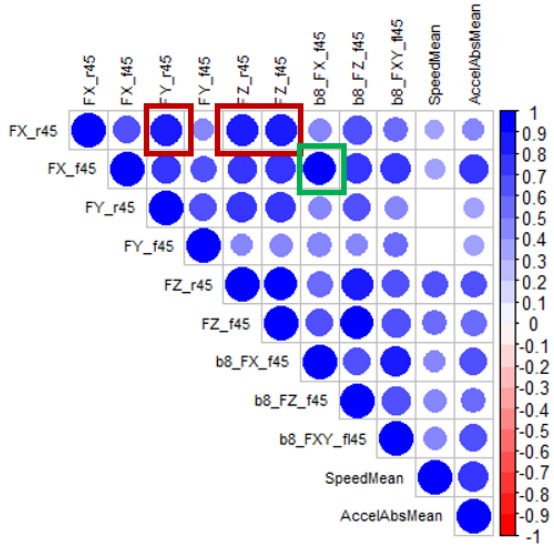

(c) Damaged road

Fig. IV.6: Pair correlations between selected variables for three segments from campaign US18-DT1. Selected variables are in order: symmetrical Y loads $m = 4$ rear and front; symmetrical Z loads $m = 4$ rear and front; symmetrical X and Z loads $m = 8$ front; average of non-zero speed; average of absolute non-zero acceleration

this segment. Fig. IV.7 shows a sample of the video feed during operation on the Highway1, Highway2 and Damaged segments in Detroit. Repetitively on Highway2, the right-hand side of the road contains ditches and road repairs that do not show up in the other lanes. On a highway, faster drivers may drive preferably or at least more often on the middle and left-hand, whereas slower and more cautious drivers may prefer sticking to the right lane and avoiding passing other vehicles. Unexpectedly, this seems to induce more pseudo-damage on some contexts.

While Highway1 roads correspond to urban freeways with even qualities and absence

(a) Highway1

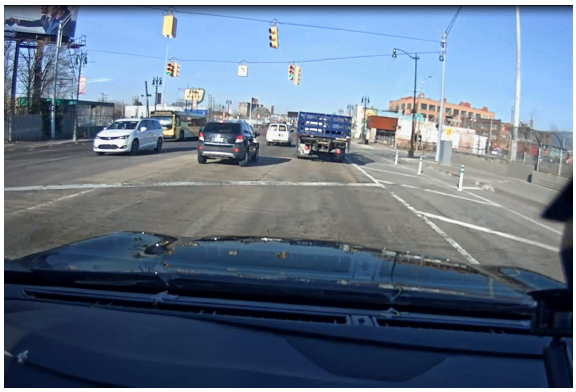

(b) Highway2

(c) Damaged road

Fig. IV.7: Video sample of three different road segments from US18-DT1

of crossroads, Highway2 involves crossroads, with its associated deceleration and the other vehicles turning, as well as a damaged slow lane. This variation between two segments associated with the same road environment is a first limitation of the definition of the segments of the trips.

IV.4.1.3 Separate PC analysis on each segment

As a reminder, $\mathcal{C}_e = \vec{L}^e_{\bullet\bullet}$ denotes the dataset given by all absolute load intensities calculated for all drivers on the e-th segment of the trip. $\mathcal{C}'_e = Z^{L,e}_{\bullet\bullet}$ denotes the scaled dataset or the dataset of all scaled load intensities on the segment.

A Principal Component Analysis (PCA) [Husson *et al.* 2011; Jolliffe and Cadima 2002, 2016] is performed on the scaled data subset $\mathcal{C}'_e$ associated with each road segment $e \in [\![1,r]\!]$. Each data subset is a cloud of observations in the space $\mathbb{R}^\kappa$. The main objective of PCA is to find the natural directions of the cloud, *i.e.* the variables over which the variance is maximum. These new variables are linear combinations of the covariates. Taken all together, they represent an appropriate rotation of the space $\mathbb{R}^\kappa$, so that the first two or three dimensions allow for visualizing the data efficiently. A development of the equations underlying PCA is available in Appendix D.

Let us denote $\left(\lambda^e_h\right)_{h\in[\![1,\kappa]\!]}$ the eigenvalues of the correlation matrix $A_{\mathcal{C}'_e}$ associated with each

dataset, solving the following problem (same eigenvalue problem as the one developed in Eq. D.3.2 and further in the appendix):

$$A_{\mathcal{C}'_e} = \left(\text{corr } \left(Z^{L,e}_{\bullet k}, Z^{L,e}_{\bullet h}\right)\right)_{(k,h)\in[\![1,\kappa]\!]^2} \tag{IV.4.10}$$

$$A_{\mathcal{C}'_e} \cdot \overrightarrow{b}^{\,e}_h = \lambda^e_h \cdot \overrightarrow{b}^{\,e}_h \tag{IV.4.11}$$

$$\overrightarrow{b}^{\,e}_h = \sum_{k=1}^{\kappa} x^e_{hk} \cdot Z^{L,e}_{\bullet k} \forall e \in [\![1,r]\!],\ \forall h \in [\![1,\kappa]\!] \tag{IV.4.12}$$

denoting $A_{\mathcal{C}'_e}$ the correlation matrix associated with the scaled data subset $\mathcal{C}'_e$; $\overrightarrow{b}^{\,e}_h$ the unit eigenvector, or Principal Component (PC), associated with the eigenvalue λ^e_h and x^e_{hk} its k-th coordinate in the space of the base variables.

PCA is an efficient way to understand the structure of each data subset. The first PCs usually carry a significant fraction of the variance of the dataset. This means that they suffice to explain the same fraction of the variability among the individuals. An efficient dimension reduction method for the description of the individuals is to select enough first PCs to recover a large fraction of the variance of the subset. This reduction of the dimension of the dataset can be used to improve the performances of further learning algorithms, such as the partition algorithms that we will develop further in this section. The scree plot of each separate analysis is shown in Fig. IV.8. For each road environment e, the number of PCs sufficient to explain 70% of the variance of the data subset $\mathcal{C}'_e$ is between two and three, except for Highway2, for which we have already identified non-trivial sources of variability from the observation of the correlation matrix in the previous paragraph.

The number of first PCs needed to summarize a large fraction of cloud variance is an indication of the number of degrees of freedom for the behavior of the driver with respect to how they can induce damage on the structure. We can begin to interpret the reasons behind driver variability through the analysis of correlations between the quantities of interest and the PCs.

The coordinate or observation of an individual c on the h-th PC of the e-th data subset is denoted S^e_{ch}. The correlation between the observations on a PC $S^e_{\bullet h}$ and a load intensity $L^e_{\bullet k}$ of the same subset $\mathcal{C}_e$ is given by:

$$\text{corr } \left(S^e_{\bullet h}, \overrightarrow{L}^{\,e}_{k\bullet}\right) = \frac{\text{covar } \left(S^e_{\bullet h}, \overrightarrow{L}^{\,e}_{k\bullet}\right)}{\text{Var } \left(S^e_{\bullet h}\right) \cdot \text{Var } \left(L^e_{\bullet k}\right)} = \text{corr } \left(S^e_{\bullet h}, Z^{L,e}_{k\bullet}\right) = \sqrt{\lambda^e_h} \cdot x^e_{hk} \tag{IV.4.13}$$

Fig. IV.9 shows the correlation circle for the quantities of interest plotted in the first ($\overrightarrow{b}^{\,e}_1 \otimes \overrightarrow{b}^{\,e}_2$) and second ($\overrightarrow{b}^{\,e}_1 \otimes \overrightarrow{b}^{\,e}_3$) principal planes, for the separate analysis of load intensities in the City environment.

All quantities of interest for this data subset are positively correlated to the first PC. This could be expected for datasets with variables that all observe similar aspects of the individual: here fatigue per kilometer. This is called a size effect. The predominance of this first PC

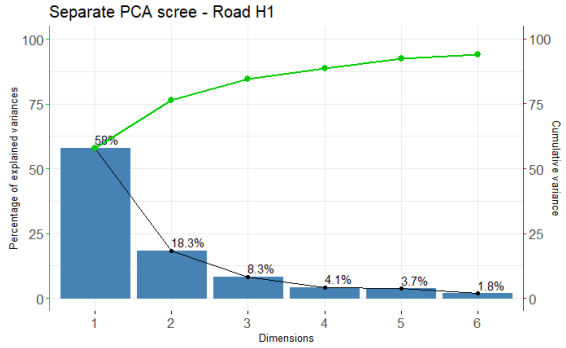

(a) Highway1

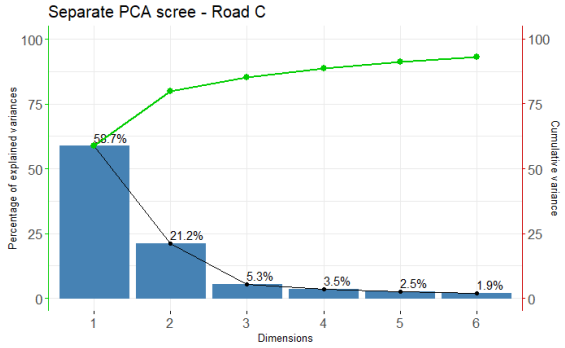

(b) City

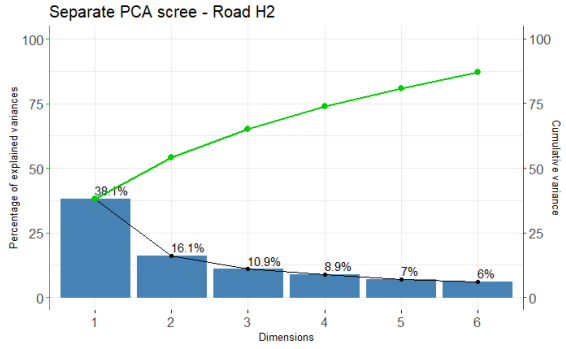

(c) Highway2

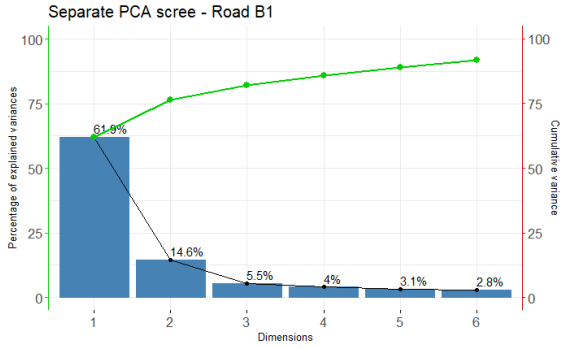

(d) Backroad1

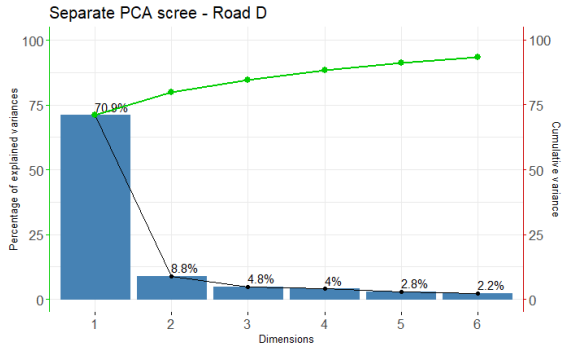

(e) Damaged road

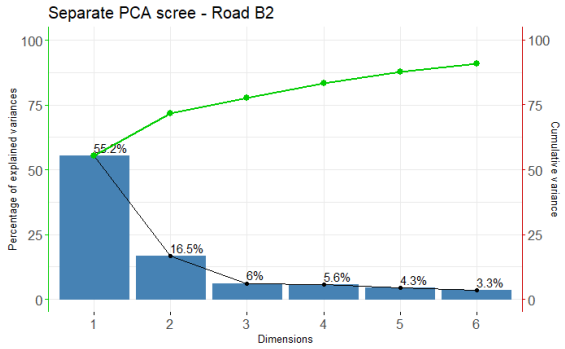

(f) Backroad2

Fig. IV.8: Variance scree plot, in percentage of total data subset variance, following PCA on each road environment. For each subset, the green curve shows the cumulative variance captured by the first PCs

is observed on all road environments. In terms of load intensity, individuals with a large positive coordinate on this axis are more damaging over all contexts than the average driver. This overall damaging pattern, present on all or most trip segments, will be denoted global severity.

The second and the eventual third PCs on each road environment add complementary information to the differences between drivers. They are akin to shape factors [Jolliffe and Cadima 2016]. We will investigate the correlations between quantities of interest and these extra PCs by plotting the most correlated (in absolute) ones in a bar plot. Fig. IV.10 shows the 5 to 6 most positively and 5 to 6 most negatively correlated quantities of interest to the second and third PCs of the separate analysis on the first highway segment.

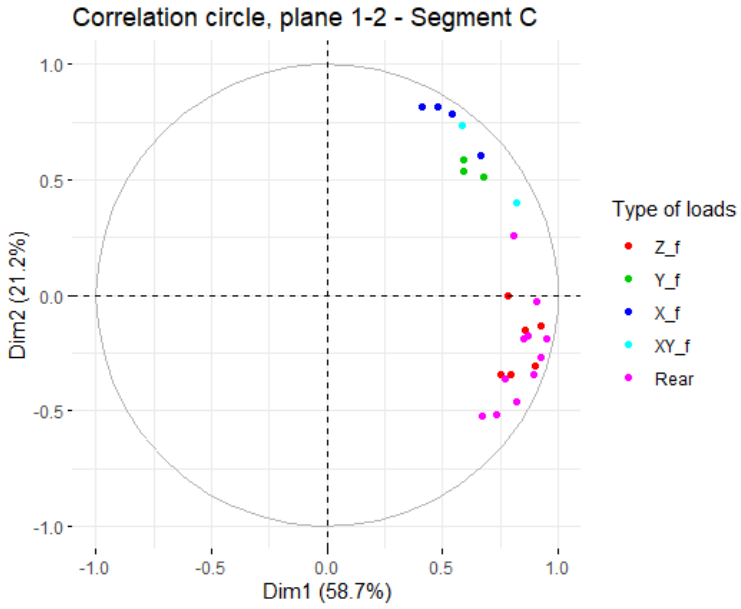

(a) First principal plane

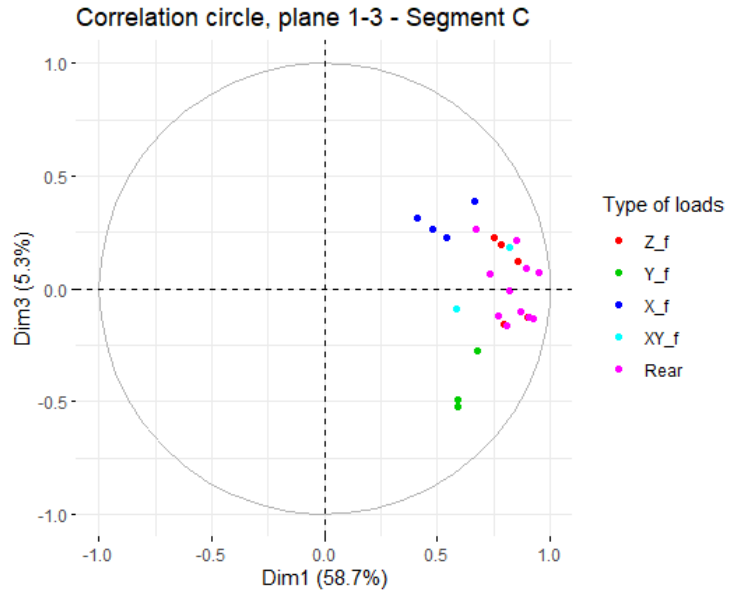

(b) Second principal plane

Fig. IV.9: Correlation circle over the first and second principal planes of the separate PC analysis on segment City. Each variable is colored according to the global load components of interest (X, Y, Z and front/rear) in the local context

On all road environments, the second PC is positively correlated to load intensities associated with contexts involving front (f) longitudinal (X) and/or lateral (Y) global load components. It is often negatively correlated to load intensities associated with contexts involving front (f) vertical (Z) and/or rear (r) global load components.

For a given evaluation in terms of global severity (the first PC), a driver showing a positive coordinate on this second PC is interpreted as inducing more damage per kilometer on the maneuvers (braking and cornering) than on the vertical obstacles met on the road environment

of interest. A driver showing a negative coordinate would have a reverse comparison. When relevant for the analysis of a trip segment, this aspect of driver severity will be called sportiness, as it measures how much a driver brakes/accelerates or dodges in the vicinity of obstacles.

The third PC does not have a set composition on all road environments. On the first segment of highway, this component mostly opposes lateral (Y) to longitudinal (X) solicitations. This may measure the absence or presence of a habit of slowing down before a turn. When relevant for the analysis of a trip segment, we will refer to this aspect of driver severity as a tendency toward quick turns, or simply quick turning.

Fig. IV.11 shows the same kind of selection of most relevant correlations for the second PC on the separate analyses of back road and damage road. The importance of this second PC in the variability of drivers dwindles as the fraction of borne variance diminishes. This means that the drivers have fewer or smaller occasions to show how differently severe they are along this kind of severity. Indeed, the more remote the road, the fewer maneuvers are expected on the segment and sporty drivers may not display their sportiness.

Global severity, sportiness and quick turning are three traits that define the conditional severity of drivers on one segment. These quantities are conditioned to each segment. In the next section, we are looking for traits of severity that characterize the variability induced by drivers over all situations.

Nota bene: The global severity of a driver is a combination of several aspects of driver behavior. A driver that is severe everywhere is altogether severe in maneuvers, on obstacles, on rough roads, etc. They are severe on several degrees of freedom at once.

Indeed, PC analysis searches for uncorrelated PCs that complete each other to reconstruct the variance of the cloud, solving Eqs. IV.4.11 and IV.4.12. This procedure does not seek actual singular degrees of freedom in terms of driver severity. While the number of PCs does inform on the number of degrees of freedom of driver severity, PCs are not individual degrees of freedom.

Another technique to unveil different profiling variables is to alleviate the constraint of uncorrelated PCs. This leads to a different problem definition and a different strategy to investigate latent linear models, as explained in [Murphy 2012] Chap. 12. Still, the property of non-correlation between PCs will be useful to simplify the construction of a distribution of pseudo-fatigue in Chapter V.

IV.4.2 Multiple Factor Analysis

In order to investigate the latent heterogeneity underlying pseudo-fatigue per kilometer from the variability of drivers and the effect of trip environment, we perform a Multiple Factor Analysis (MFA) [Escofier and Pagès 1998; Pagès 2014] on the full scaled dataset. As proposed in the literature, the variables associated with the evaluation of a driver on all road environments are normalized as per the first eigenvalue of their separate analyses, hence the application of PCA in the previous paragraph. The dataset, displayed earlier in Fig. IV.3, is rewritten as the horizontal concatenation of each normalized data subset:

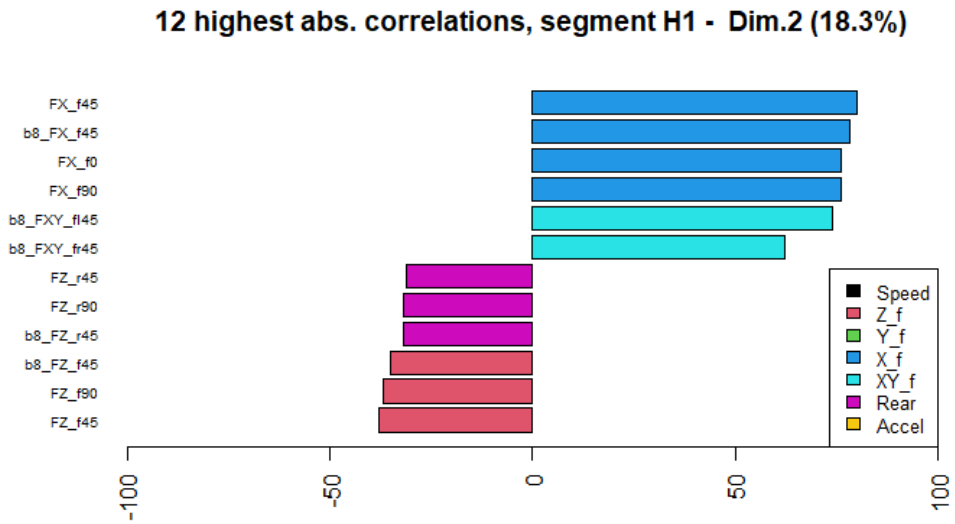

(a) Second PC

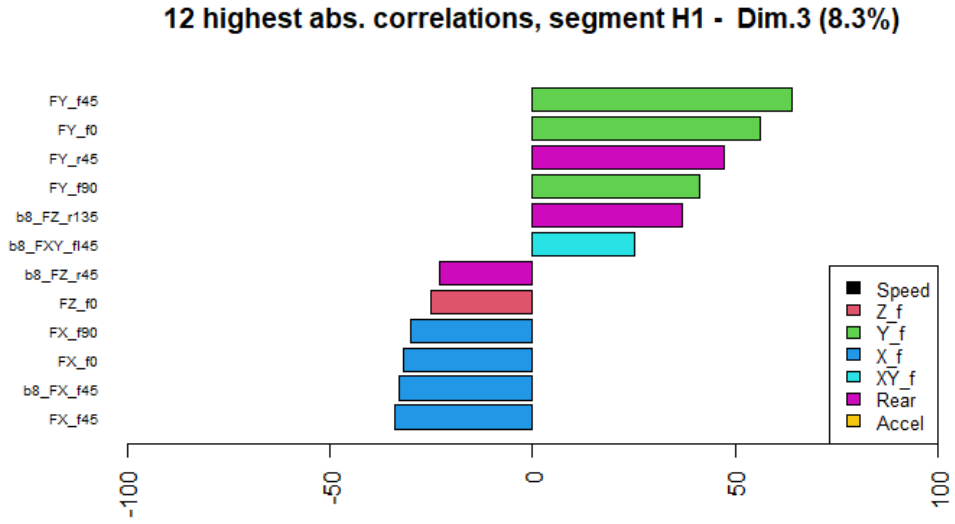

(b) Third PC

Fig. IV.10: Most significant correlations with the first PCs, following the separate analysis of the first highway segment. Local contexts are associated with a Basquin exponent of 4 unless prompted (as in b8_FX_f45). Each variable is colored according to the global load components of interest (X, Y, Z and front/rear) in the local context

$$\mathcal{C} = \left(\left(\frac{Z_{\bullet k}^{L,\mathcal{C}_1}}{\sqrt{\lambda_1^1}} \right)_{k \in [\![1,\kappa]\!]}, \dots, \left(\frac{Z_{\bullet k}^{L,\mathcal{C}_r}}{\sqrt{\lambda_1^r}} \right)_{k \in [\![1,\kappa]\!]} \right) \tag{IV.4.14}$$

denoting $\mathcal{C}_e$ the data subset corresponding to the evaluation of κ load intensities on the

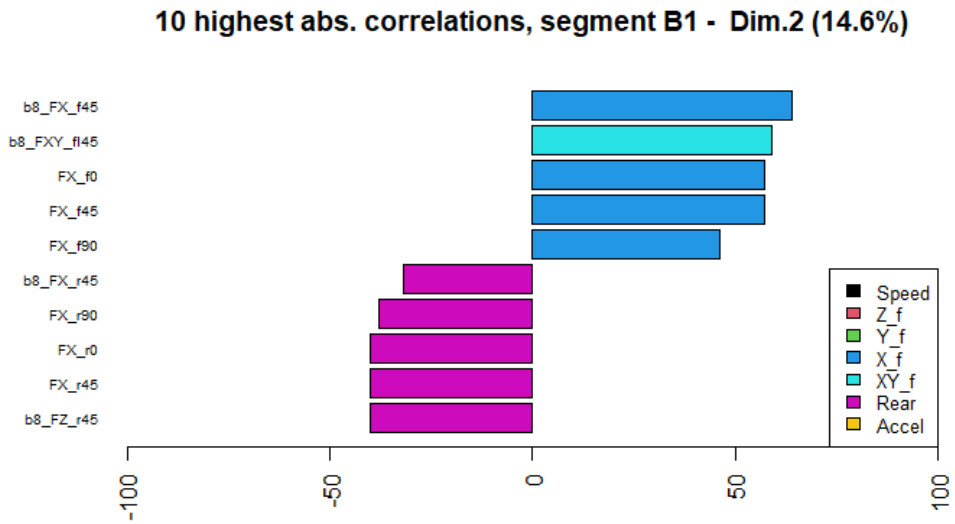

(a) Second PC, Backroad1

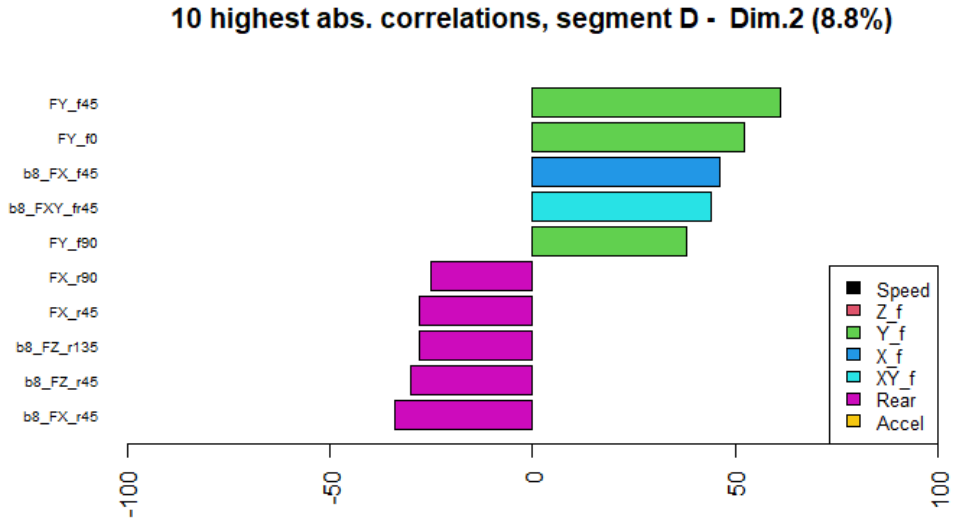

(b) Second PC, damaged road

Fig. IV.11: Most significant correlations with the second PC, following the separate analyses of the first back road and of the damaged road segments. Local contexts are associated with a Basquin exponent of 4 unless prompted (as in b8_FX_f45). Each variable is colored according to the global load components of interest (X, Y, Z and front/rear) in the local context

e-th road segment on n drivers and λ_1^e the first eigenvalue of the correlation matrix calculated on the subset $\mathcal{C}_e$ from Eq. IV.4.11.

The procedure yields PCs $\left(\vec{S}_h\right)_{h\in[\![1,\kappa\cdot r]\!]}$ associated with eigenvalues $(\lambda_h)_{h\in[\![1,\kappa]\!]}$ of the full correlation matrix $A_{\mathcal{C}}$ of the scaled and normalized dataset, solving the following problem:

$$A_{\mathcal{C}} \bullet \overrightarrow{b}_h = \lambda_h \cdot \overrightarrow{b}_h \tag{IV.4.15}$$

$$\overrightarrow{b}_h^e \approx \sum_{k=1}^{(\kappa \cdot r)} x_k^h \cdot Z_{\bullet k}^{L,\mathcal{C}} \forall h \in [\![1, n_b]\!] \tag{IV.4.16}$$

MFA as presented in [Escofier and Pagès 1998; Pagès 2014] yields uncorrelated PCs in a fashion similar to a weighted PCA.

Fig. IV.12 shows the variance scree plot of the 14 first PCs of the analysis. It takes 8 PCs to recover 75.9% of the total variance of the dataset over 156 variables; 16 PCs to recover 89.9%; and 23 PCs to recover 95%. Reducing the number of PCs in this method serves to diminish the "noise" in the data: the individual discrepancies that do not represent trends over the whole population.

The average inertia (average of all scaled individual vector norms) brought by one scaled individual is given by $1/n_c$, here 2.3%. Therefore, only 9 PCs bring more information than the average marginal inertia of a driver.

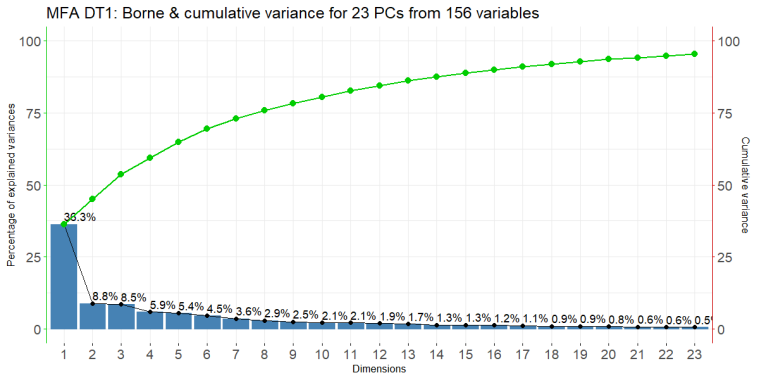

Fig. IV.12: Variance scree plot, in percentage of total dataset variance, following MFA on the measurement campaign US18-DT1. The blue curve shows the cumulative variance captured by the first PCs.

The first PC turns out to be a size effect, positively correlated to all quantities of interest, as shown in the correlation circle for the first principal plane in Fig. IV.13. Drivers with a positive coordinate on this first component induce more pseudo-damage per kilometer over all contexts and over all road environments. This first component denotes intrinsic global severity, as opposed to the conditional global severity previously observed in the separate analysis of each segment.

The variance borne by the following PCs slowly decreases. The PCs beyond the size effect are sometimes called shape factors: they add to the explanation of the observations on an individual. Let us find an interpretation for the four next PCs (each bearing more than 5% of the total variance).

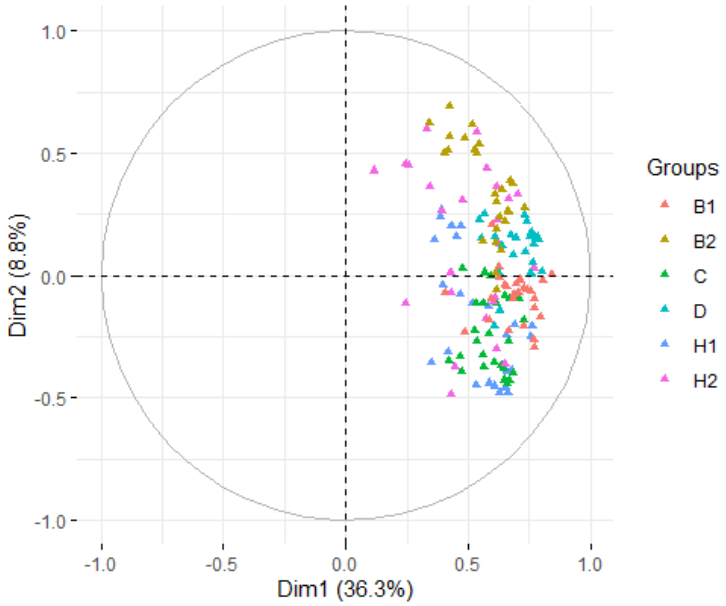

Fig. IV.13: Correlation circle for the first principal plane (first and second PC) following the multiple factor analysis on US18-DT1. Each load intensity is colored according to the road segment over which it was evaluated

IV.4.2.1 Second PC (8.8% of variance)

Let us add speed and acceleration quantities as supplementary variables to the analysis. Indeed, making a turn resp. encountering an obstacle with a larger speed increase the centrifugal resp. impact forces at the wheel axles, and therefore induce larger pseudo-damages per kilometer on lateral resp. vertical load cases. Likewise, accelerating or braking more frequently and/or more swiftly induce larger longitudinal loads and faster mass transfers (therefore also larger vertical loads on the front axle).

These speed and acceleration quantities do not partake in the correlation matrix of the analysis, and therefore on the construction of PCs. The speed and acceleration quantities and the method to work them out are described in Appendix C.3. An example for the characterization of driver style from the analysis of acceleration quantities is shown in [Tang *et al.* 2014].

Fig. IV.14 shows the 8 most positively and 8 most negatively correlated observation variables or speed quantities with respect to the second PC.

From 44 observed individuals, the critical correlation to pass a Pearson test with a test level of 90% is approximately 24% [Niño-Zarazúa 2012]. This value corresponds to the minimal absolute correlation above which a Pearson test would consider the hypothesis of non-zero correlation to be significant compared to the alternative. Note that a correlation coefficient can be positive or negative.

33 load intensities out of 156 have a positive correlation of more than 24% with the second PC. The highest positive correlations correspond to load intensities calculated on the second back road (B2) and second highway (H2) segments, on local contexts associated

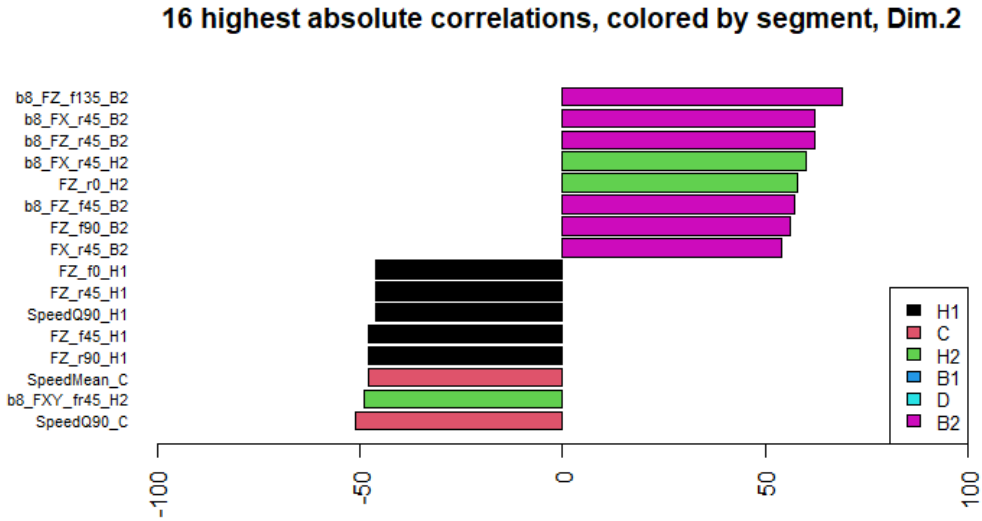

Fig. IV.14: Sixteen most significant correlations with the second PC, following MFA on dataset $\mathcal{C}'$ from the measurement campaign US18-DT1.. Local contexts are associated with a Basquin exponent of 4 unless prompted (as in b8_FX_f45). Each variable is colored according to the road segment it was calculated on

with a Basquin exponent of 8 instead of 4. For a given global severity, drivers with a positive coordinate on this second PC will have higher load intensities calculated with a larger Basquin exponent.

The differences in load intensities for large Basquin exponents can be understood as larger or more frequent peaks per kilometer, as explained in §III.7.1. Therefore, we can understand differences in load intensities for larger Basquin exponents as larger or more frequent high values of Rainflow ranges per kilometer. These drivers are either more "brutal" on rare obstacles like potholes or other isolated obstacles, or they are more prone to meet them than other drivers.

33 load intensities out of 156 have a negative correlation of less than -24% with the second PC. The highest negative correlations correspond to load intensities on the first highway (H1) segment and on the urban (C) environment, on local contexts associated with a Basquin exponent of 4 and on vertical (Z) load cases. Their behavior is also characterized by larger high quantiles of non-zero (SpeedQ90) speed on these two segments. For a given global severity, drivers with a negative coordinate on this second PC would be more damaging through their encounter of frequent and medium vertical solicitations, such as city obstacles or road rugosity.

One interesting aspect of this second PC is that it opposes two kinds of driver severity that depend on the road environment. For a given intrinsic global severity (first PC of the MFA), drivers that are more severe and driving faster in urban environments (black and red bars in Fig. IV.14) do not appear to be the most damaging on more damaged roads (purple and green bars). Another piece of information to gather is that one population is more damaging to local contexts associated with spot weld and weld beads (Basquin exponent of 4), and the other population is more dangerous to metal sheet edges (higher Basquin exponents).

A larger description of the driver behavioral characteristic measured by the second PC could be achieved by looking at more significant correlations beyond these sixteen variables, but we will stick to this partial explanation of the variable.

IV.4.2.2 Third PC (8.5% of variance)

Fig. IV.15 shows the 8 most positively and 8 most negatively correlated observation variables or speed quantities with respect to the third PC. The first graph colors each variable according to the road segment it was evaluated on. The second graph colors each variable according to its type, in terms of speed or effort, and in the latter case of the global load components of interest for its calculation.

Correlations with variables from a given road segment, like City (in red in Fig. IV.15 a)), may be significantly positive or negative. There is also no clear discrimination between load intensities calculated with different Basquin exponents. While the previous PC made a clear distinction in terms of severity between two driving environments, this third PC is better visualized according to load cases of interest.

36 load intensities out of 156 have a positive correlation of more than 24% with the third PC. The highest positive correlations correspond to load intensities calculated from load cases involving longitudinal (X) and lateral (Y) load components. Indeed we can visualize the positive correlations with some lateral load cases in Fig. IV.16, in green. The corresponding behavior is accompanied with a high quantile (Q95) of non-zero acceleration in the urban environment (C) and to a high mean absolute acceleration (AccelAbsMean) on the first highway (H1) segment.

29 load intensities out of 156 have a negative correlation of less than -24% with the third PC. The highest negative correlations correspond to load intensities calculated on front vertical ($Zf\bullet$) load cases and on all rear ($Zr\bullet$) load cases.

Nota bene: As explained in A.2, modern vehicles are often designed with a front-engine, front-wheel-drive (FF) layout, meaning that both the motor and the driving roadwheels are at the front of the car. The cornering wheels are exclusively on the front axle except for four-wheel drives. Therefore, the acceleration and cornering efforts are mainly input to the front axle. Braking commands are generally input to all wheels in a normal configuration, however braking may shift a fraction of vehicle mass up front and increase front loads. Effort from obstacles are common for front and rear wheels, and obstacles like potholes and pavement always induce solicitations in all directions. For these reasons, all rear load cases are here gathered under the same color in graphs like Fig. IV.15b and interpreted as originating from the encounter of obstacles.

For a given intrinsic global severity, drivers with a positive coordinate on the third PC are generally more damaging following acceleration events and more generally maneuvers, while drivers with a negative coordinate are generally more damaging around obstacles. This comparison is a reminiscence of sportiness from the separate analyses in §IV.4.1.3. It holds for all road environments and positive sportiness can be explained by patterns of acceleration.

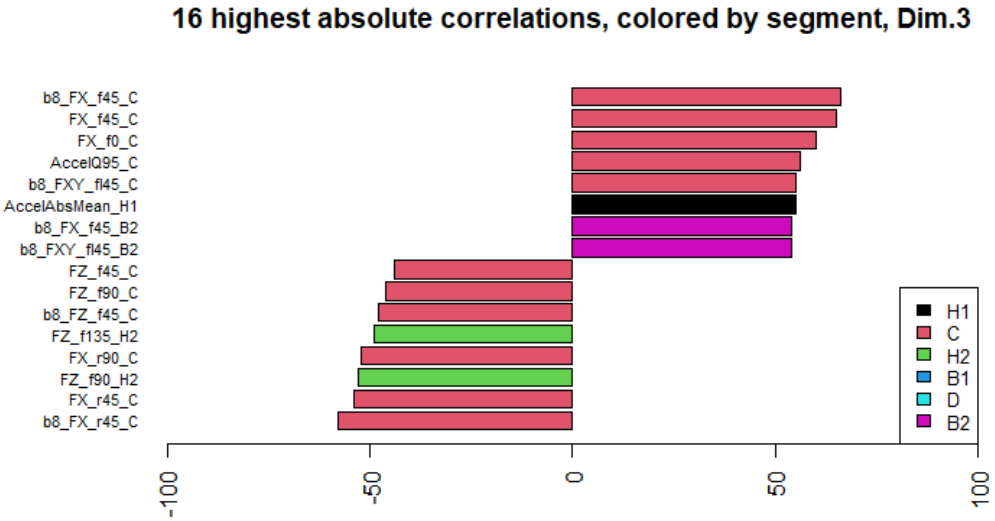

(a) Contexts colored per road segment

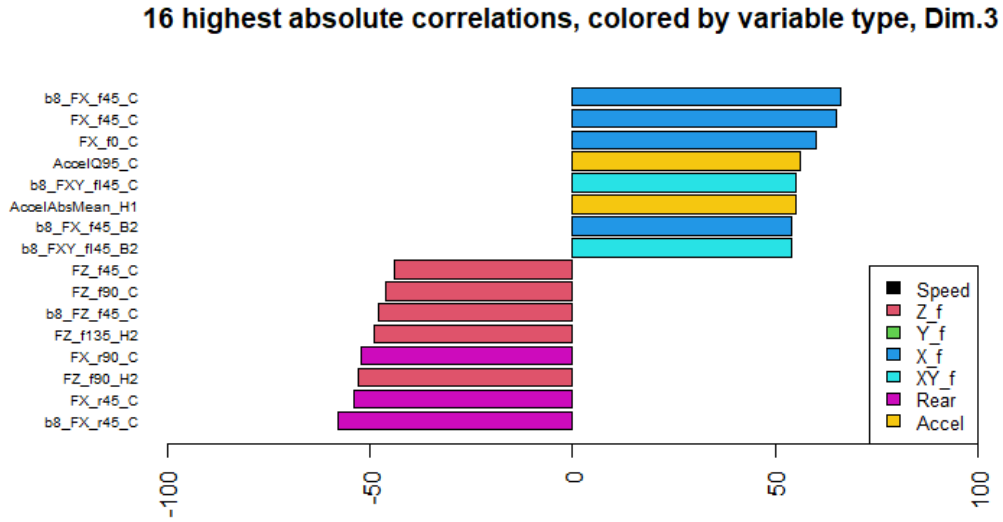

(b) Contexts colored per load case

Fig. IV.15: Sixteen most significant correlations with the third PC, following MFA on dataset $\mathcal{C}'$ from the measurement campaign US18-DT1.

IV.4.2.3 Fourth and fifth components (5.9 and 5.4% of variance)

Fig. IV.17 shows the 8 most positively and 8 most negatively correlated observation variables or speed quantities with respect to the fourth PC, colored as per segment.

This fourth PC opposes load intensities calculated on the first highway (H1) segment to the second (H2) one. There are not a lot of significant correlations with speed or acceleration quantities, even as we increase the number of bars to 60 in Fig. IV.17 b): no significant color

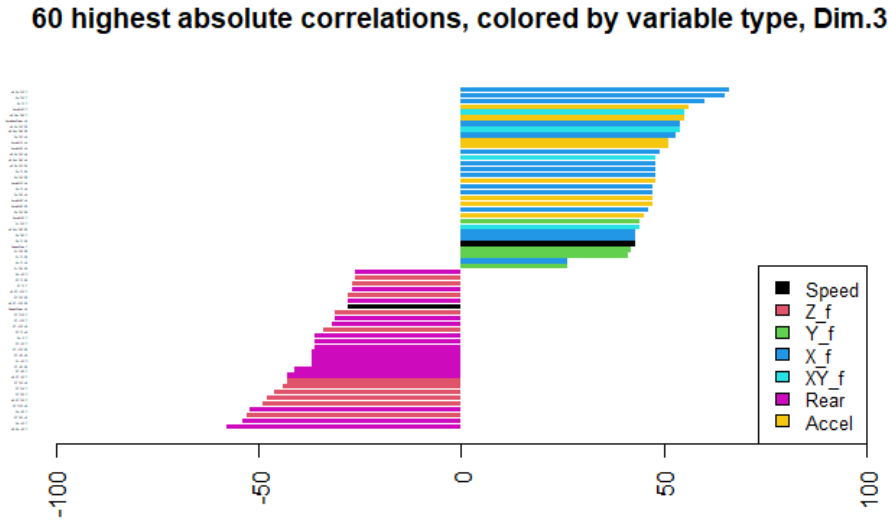

Fig. IV.16: For the sake of illustration, sixty most significant correlations with the third PC, following MFA on dataset $\mathcal{C}'$ from the measurement campaign US18-DT1. Variables are colored as per associated load case.

seems to dominate this histogram. We may consider this difference in behavior to be an effect of confidence with respect to the state of the road.

Remark: the number of load intensities with a significantly non-zero correlation (more than 24% in absolute value) with the fourth PC is 57, but some speed or acceleration quantities do verify this criterion, hence our arbitrary limit of 60 bars in this graph.

Fig. IV.18 shows the 8 most positively and 8 most negatively correlated observation variables or speed quantities with respect to the fifth PC, colored either as per road segment or as per load case.

The first graph shows that this fifth PC informs on the severity of drivers strictly on rear load cases. Just like the previous dimension, it compares them on mostly two road segments: the second back road segment (B2) and the damaged road (D). This fifth PC may inform indirectly on the driver's confidence on the damaged road segment.

IV.4.2.4 Synthesis of the interpretation of PCs

The first PC, intrinsic global severity, is a new variable calculated from the separately standardized and mutually normalized load intensities, calculated on each road segments. It is a size effect, positively correlated to all load intensities and denotes drivers that are generally more severe, on all road environments, for all local contexts of the structure.

The following PCs add complementary information on the complexity of driver severity. Some PCs compare the behavior of clients on different road segments. Others compare them on different kinds of road events. Others perform both comparisons at once. These profiling

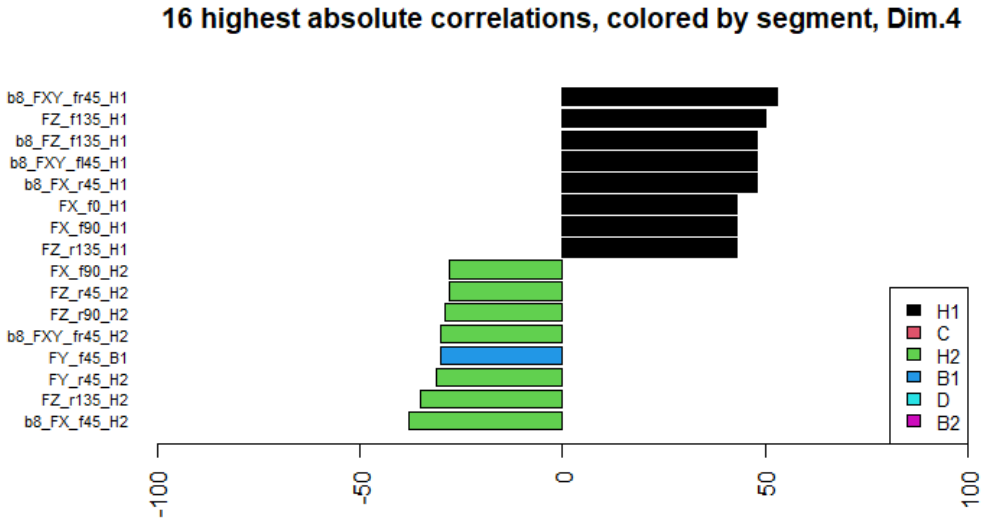

(a) Contexts colored per road segment

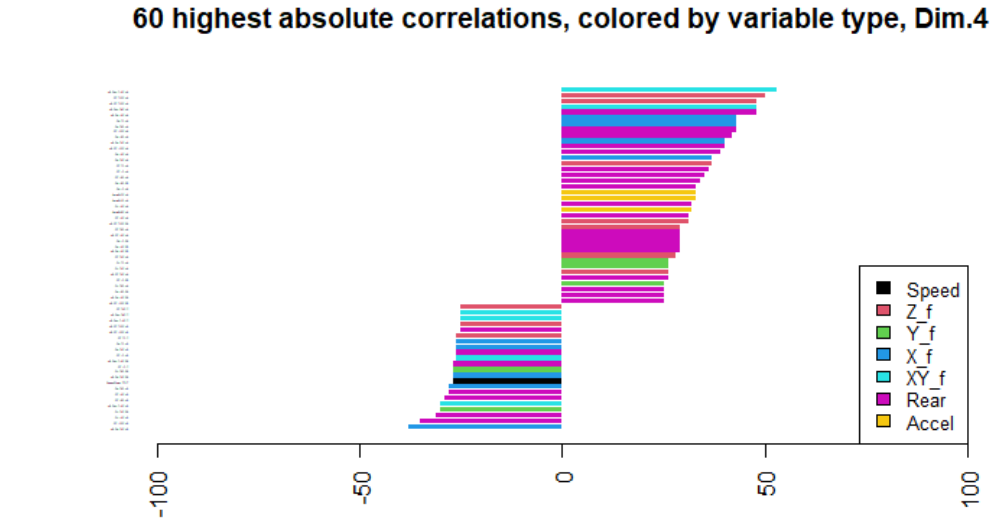

(b) Fifty-two contexts, colored per load case, for the sake of illustration

Fig. IV.17: Most significant correlations with the fourth PC, following MFA on dataset $\mathcal{C}'$ from the measurement campaign US18-DT1.

variables, associated with explanatory variables such as speed and acceleration quantities, help understand what kind of situations and what kind of decisions made each driver unique in terms of induced fatigue on the vehicle.

Further PCs may add more comparisons between road segments and load cases in terms of privileged local contexts.

The contribution of each road segment to the inertia of the PCs informs us on the amount

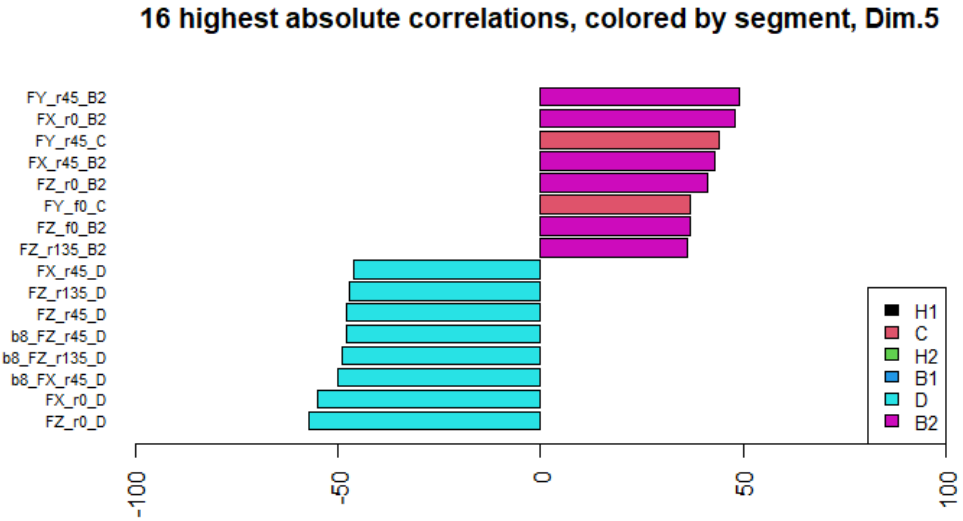

(a) Contexts colored per road segment

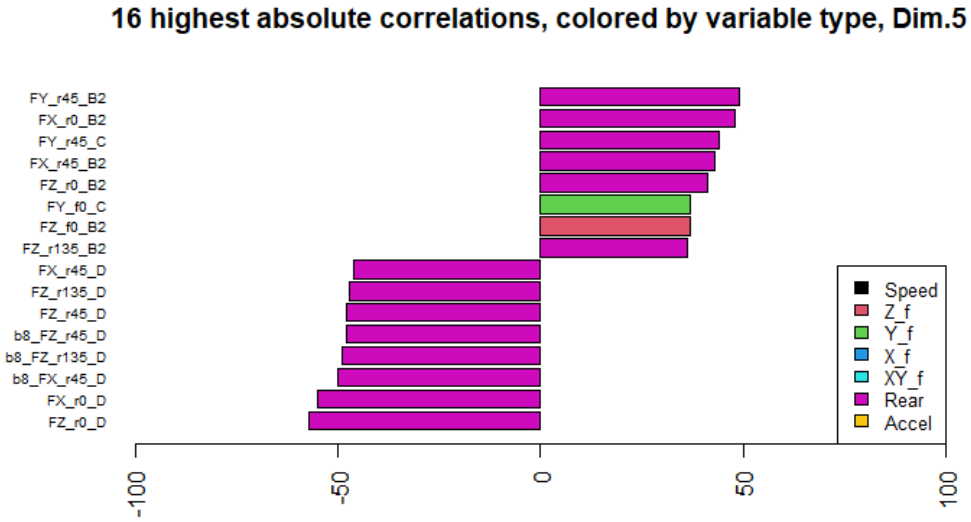

(b) Contexts colored per load case

Fig. IV.18: Sixteen most significant correlations with the fifth PC, following MFA on dataset $\mathcal{C}'$ from the measurement campaign US18-DT1.

of information they add to the complexity of driver severity. Fig. IV.19 shows, for each PC, the origin of its inertia in terms of road segments. The oppositions between road segments are supported by the higher contribution of the belligerents, like second back road versus second highway segments in the second PC, or between the two segments of highway in the fourth PCs. The relevance of adding more road segments to evaluate the severity of drivers can be measured by the amount of specific information that they would bring on the PCs.

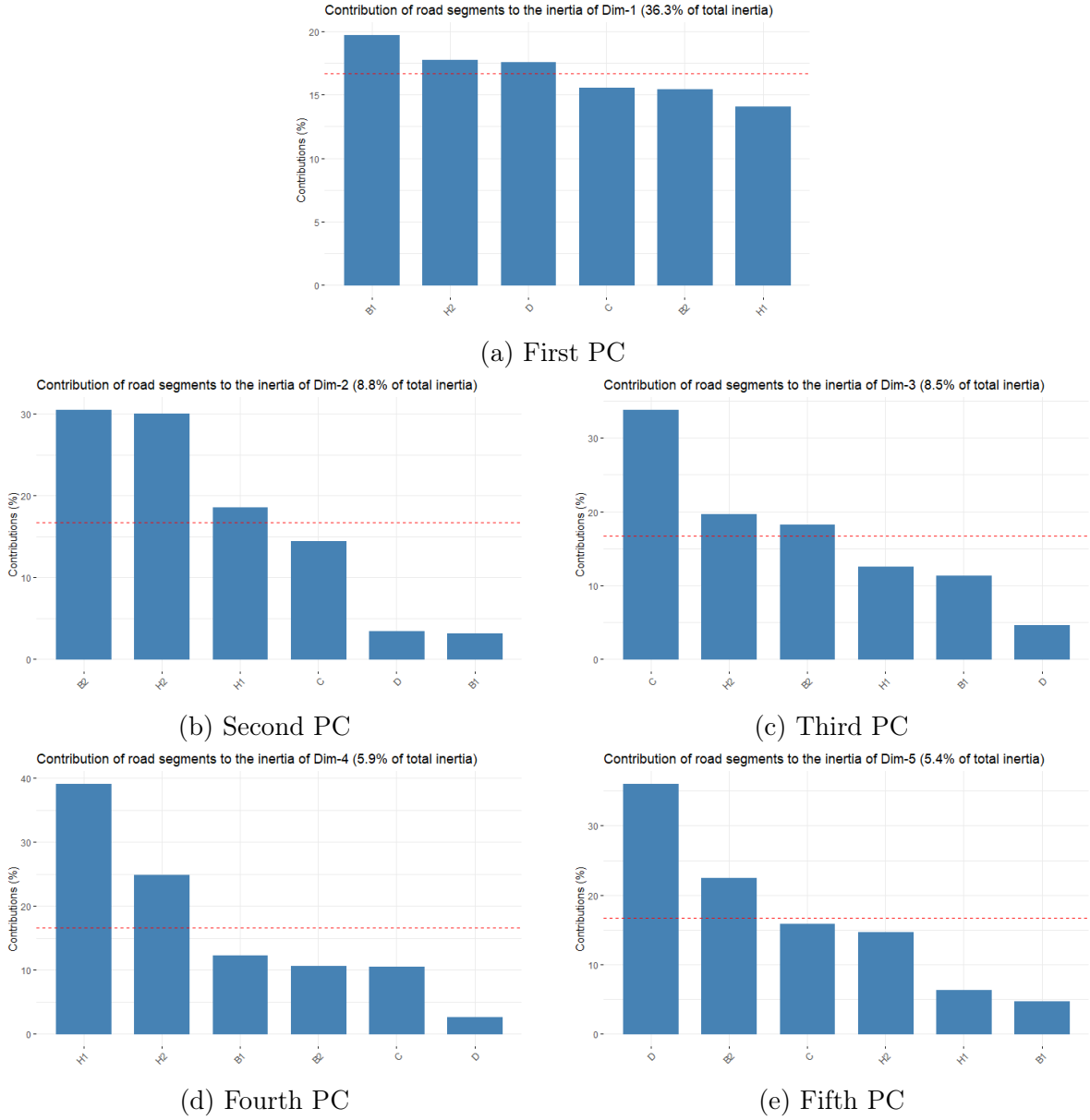

(a) First PC

(b) Second PC

(c) Third PC

(d) Fourth PC

(e) Fifth PC

Fig. IV.19: Contribution of each road segment, in percentage, to the inertia of the first to the fifth PCs. The dashed red line is a reference corresponding to the case where all road environments have equivalent importance for the PC.

IV.4.3 Population analysis

Throughout the analysis of the individuals, we will look for outliers and homogeneous sub-populations in our population of drivers. We will also analyze the shape of the population from the scope of the different road segments.

IV.4.3.1 Driver clusters

A population partitioning algorithm will help us discuss the presence of sub-populations of drivers, and may identify outliers as being distant observations from the outskirts of such sub-populations.

A first proposed strategy to determine an appropriate partition of the dataset is called Hierarchical Clustering on Principal Components (HCPC) [Husson *et al.* 2010]. Following a decomposition in PCs (here the implementation of MFA), an agglomerative hierarchical clustering is performed and a criterion like the Ward method is used to determine an adequate number of clusters. Finally, a k-means algorithm is implemented to determine the final partition of the dataset.

The distances between individuals are here calculated from their coordinates on the 23 first PCs, enough to capture 95% of dataset variance, instead of their 156 scaled load intensities. This restriction help cover a fraction of uninterpretable data noise.

Agglomerative hierarchical clustering incrementally decreases the number of clusters. At each decrement, the algorithm seeks the pairing that represents the smallest increase in the total sum of all intra-cluster inertia. Therefore, the clustering is nested from one step to the next. Fig. IV.20 shows the dendogram following the hierarchical clustering of dataset $\mathcal{C}$ on 23 PCs. The y-axis of this graph corresponds to the gain in total intra-cluster inertia following a reduction of the number of clusters. It denotes simultaneously a loss in inter-cluster variance.

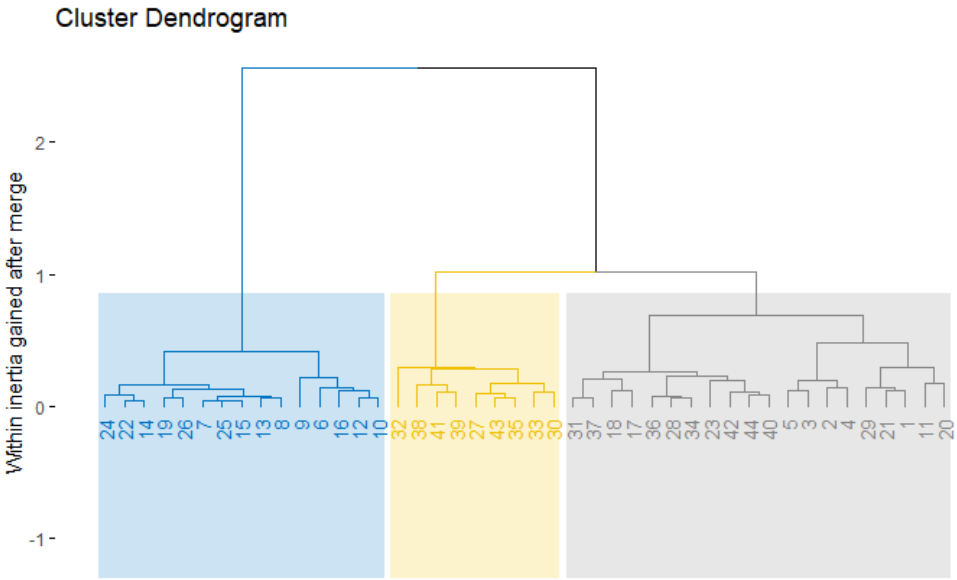

Fig. IV.20: Cluster dendogram following hierarchical clustering on dataset $\mathcal{C}$ from campaign US18-DT1. The indices at each branch of the first floor are driver indices. The top of the colored zones correspond to the advocated cut, preceding the maximum value of a Lance-Williams dissimilarity.

The Ward method consists in finding the number of clusters that maximizes a dissimilarity (a combination of inter-cluster distances and intra-cluster inertias) between two steps of hierarchical clustering. The Ward method is implemented by taking specific values for the

parameters of a Lance-Williams formula for the update of dissimilarity [Murtagh and Legendre 2014; Wishart 1969]. The proposed number of clusters is represented in Fig. IV.20 as the upper end of the colored rectangles. For this analysis, the algorithm yields an optimal number of three clusters.

The k-means algorithm is a well-known clustering method. This incremental algorithm looks for sub-populations that have spherical to ellipsoidal shapes. Indeed, each observation is associated with the cluster with the closest center. However, it requires prior information on the adequate number of clusters in the dataset (k in the name, n_s in this thesis).

The algorithm begins from a random configuration, with k random points taken as initial centers. The result depends on this starting point. However, several attempts are made by the program, with 10 different starting configurations, to ensure proximity with the globally optimal solution. Performing the k-means algorithm on increments of this parameter k does not yield nested clusters.

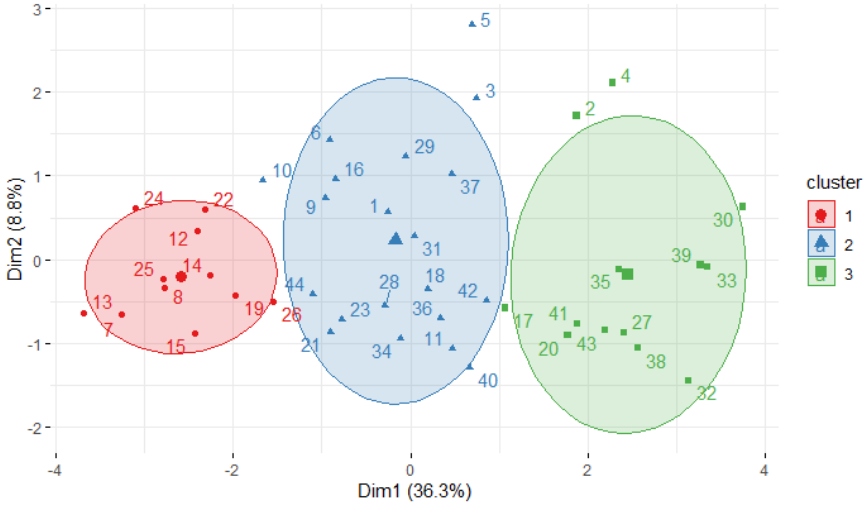

(a) First plane (second PC on y-axis)

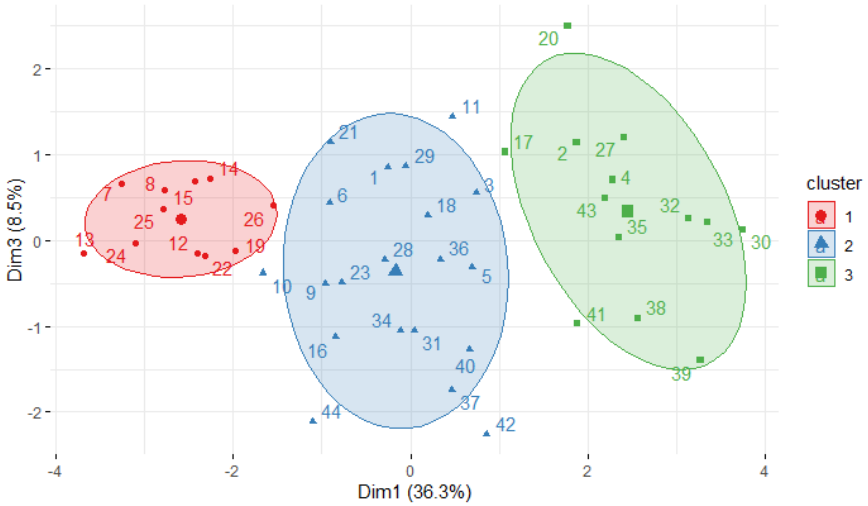

(b) Second plane (third PC on y-axis)

Fig. IV.21: Cloud of individuals observed in the first and second principal planes of the MFA on dataset $\mathcal{C}$.

Let us observe the shape of the population following this partitioning through the application of k-means with a number of clusters n_s = 3. The first PCs correspond to optimal sub-spaces of observation for the data, as they are the ones allowing us to recover the most variance in the dataset. Fig. IV.21 shows the cloud of individuals in the first and second principal planes of the MFA. Individuals are identified as per their clusters.

Note that the partition proposed through the implementation of k-means is different from the proposed partition of the hierarchical clustering. The right-end cluster (in green) contains 13 individuals following k-means whereas it was predicted to contain 9 (in yellow) following hierarchical clustering.

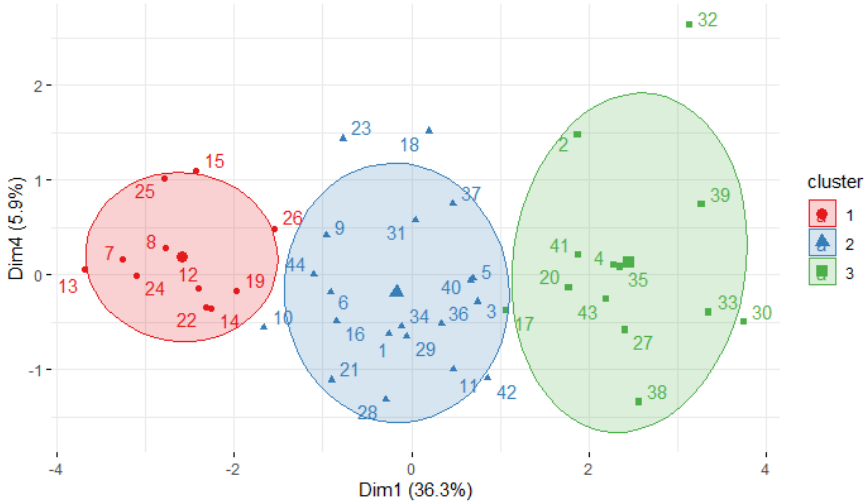

(a) Third plane (fourth PC on y-axis)

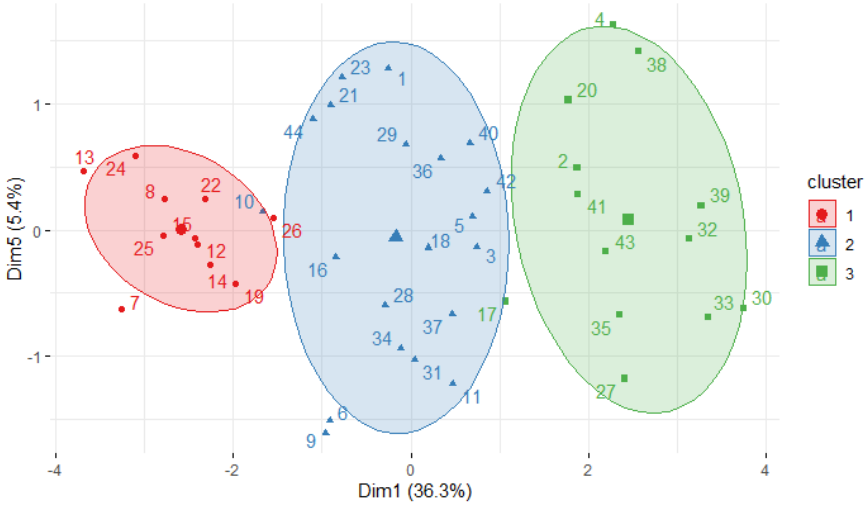

(b) Fourth plane (fifth PC on y-axis)

Fig. IV.22: Cloud of individuals observed in the third and fourth principal planes of the MFA on US18-DT1.

On all principal spaces, we observe that the clusters mostly distinguish themselves from each other as per their global severity (see also Fig. IV.22 for the third and fourth principal planes). Each cluster may have different marginal dispersion when projected on each following

PC, the first one being the most concentrated. The third cluster therefore consists of drivers that are first of all globally severe, and may then display supplementary variability over the next first PCs.

The ellipses allude to multivariate Gaussian approximations of the sub-population associated with each cluster. The colored zone corresponds to a centered range of 75% of the integral of the marginal Gaussian distribution obtained through projection of the cluster on any direction.

On the first principal plane, we observe that two individuals from the severe cluster are vertically very distant from the center of the cluster. In the other principal planes, their behavior appears to be much more similar to the rest of the cluster. These individuals and their "neighbors" associated with the second cluster display unusual dissimilarity on this second PC, compared to the rest of the dataset. This may hint at an important source of heterogeneity that a distribution of the population may be designed to include.

IV.4.3.2 Cluster normality tests

We can evaluate the relevance of modeling each subset of driver severities per kilometer as the issues of a multivariate Gaussian law, by submitting each cluster as a subset of data to a statistical normality test.

A generalization of the unidimensional Quantile-Quantile (QQ) plots is achieved by plotting the Mahalanobis distances calculated for each observation of the dataset against the quantiles of a Chi-squared law with n_b degrees of freedom, n_b being the number of dimensions of the dataset [Mahalanobis 1930; G. J. McLachlan 1999]. However, the number of observations of the severe cluster (13) is insufficient to test for a multivariate Gaussian law of more than 12 dimensions. We will test for the normality of their intrinsic severity restricted to the five first PCs.

The Mahalanobis distance J is calculated between a point of coordinates $\vec{S} = (S_h)_{h\in[\![1,n_b]\!]}$ and the mean of a multivariate variable Q with given center $\vec{\mu}_0 = (\mu_h)_{h\in[\![1,n_b]\!]}$ and covariance matrix Σ by the formula:

$$J(\vec{S},Q) = \sqrt{{}^T\left(\vec{S} - \vec{\mu}_0\right) \cdot \Sigma \cdot \left(\vec{S} - \vec{\mu}_0\right)} \tag{IV.4.17}$$

Fig. IV.23 displays such a multi-normal QQ plot with Mahalanobis distances calculated from the five first principal coordinates of each individual of the third cluster.

The Henze-Zirkler multivariate normality tests evaluates a functional distance, *i.e.* a distance between the distribution of the data and the expected distribution in the hypothesis of a multivariate Gaussian law [Henze and Zirkler 1990]. If the data follows a multivariate Gaussian law, then the statistic of the test follow a log-normal distribution. For the 13 observations of the third cluster of US18-DT1, the description of which is restricted to the five first PCs, the p-value of the test is 0.12, superior to 0.05 for a test level of 90%. Therefore, we cannot reject the hypothesis of normality of this third sub-population.

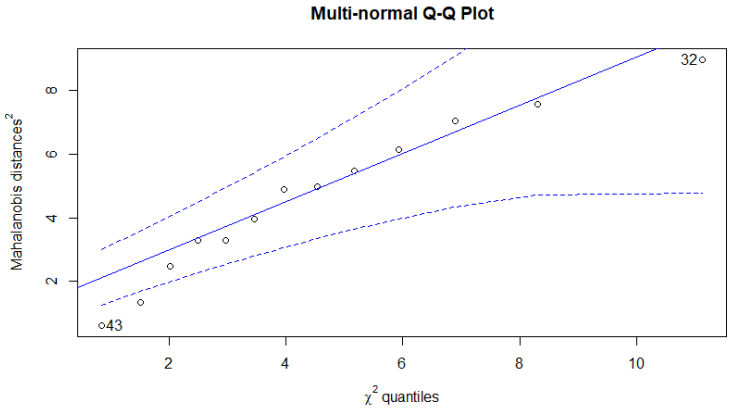

Fig. IV.23: Multivariate QQ-plot for the 13 individuals of the third cluster of driver pseudo-fatigue per kilometer for US18-DT1, described only by their 5 first principal coordinates

The Mardia multivariate normality test evaluates the skewness and kurtosis for each dimension of the dataset and compares them to the expected values for multivariate Gaussian laws [Mardia 1974]. For the 13 observations of the third cluster of US18-DT1, the description of which is restricted to the five first PCs, the p-value of the test on distribution skewness is 0.22, superior to 0.05. The p-value of the test on distribution kurtosis is 0.45, also superior to 0.05. Therefore, the data subset passes the Mardia test and the hypothesis of normality still cannot be rejected.

IV.4.3.3 Cluster characterization through the lens of speed

Fig. IV.24 shows the box plots per cluster of the third quartile of non-zero speed, calculated for each individual on each road segment. Fig. IV.25 shows the box plots per cluster of the mean of absolute non-zero acceleration and the 5% quantile of non-zero acceleration, calculated for each individual on each road segment. The 5% quantile of absolute non-zero acceleration (AccelQ05) evaluates the level of the most negatives values of acceleration, therefore measuring the violence of braking events.

The medians and third quartile of these box plots are logically arranged in some of the road segments, like city, damaged roads and the first highway segment. This supports the importance of driver decisions and habits in maneuvers and cruise control with respect to the amount of fatigue induced on the vehicle. However, for mildly damaged roads such as back roads and the second highway segment, speed and acceleration quantities are insufficient to evaluate the severity of driver behaviors.

IV.4.3.4 Partial individuals: driver severity as a function of road environment

Each separate analysis conducted in §IV.4.1.3 yields an evaluation of driver severity restricted to the road segment of interest. For each road segment, each driver can be described by their coordinates on the separate principal space associated with each segment. We have seen that

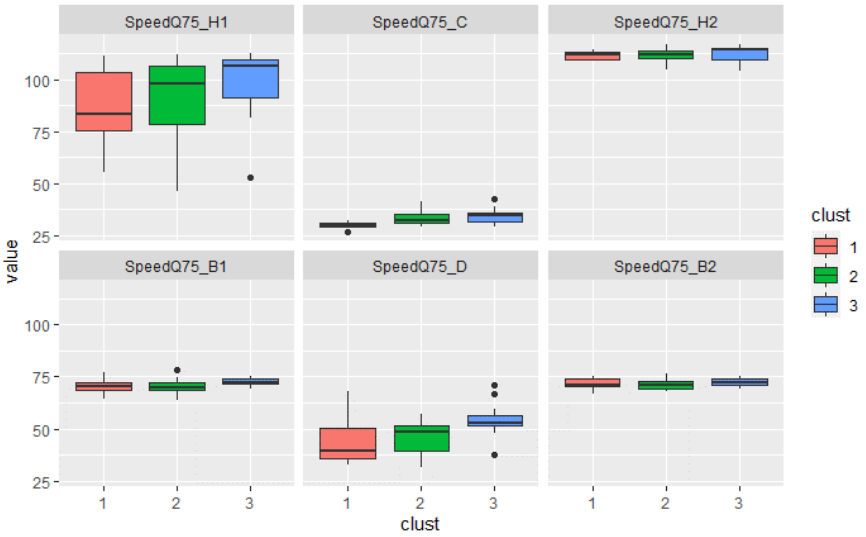

Fig. IV.24: Box plot for each cluster on each road segment of campaign US18-DT1 of the third quartile of non-zero speed, first calculated for each individual

the first PC always denotes global severity in the separate analyses. The second PC usually denotes sportiness, but its relevance is diminished on some road segments. Comparing the coordinates of drivers on the first PC of each separate analysis determines whether some drivers can be considered as severe on all road environments or only on some of them.

Fig. IV.26 shows the partial individuals for three drivers on the right end of the cloud (the most globally severe). The graph of partial individuals plots the different positions of the individual in each separate principal space. The center of each "star" is the actual coordinates of the individual in the principal space of the MFA.

For instance, the global severity associated with driver 042 is reasonably large (2) in the principal space of the MFA. However, the global severity of the driver is below average on the first back road segment (B1) and very large on the second one (B2). Driver 034 is evaluated as more globally severe on the second highway segment (H2) than on the city segment (C), and driver 031 is evaluated as more globally severe on the first back road (B1) and second highway (H2) segments than on urban (C and H1) environments.

Fig. IV.27 shows the inertia associated with the "star" of each individual projected on the first PC of each plane. In other words, it is the sum of all differences between the individuals' global severity at the end of the MFA, and their partial coordinates on the first PC in each separate analyses. This denotes how much the global severity of the driver seems to change from one road type to another. Some globally severe drivers, like the 39th (driver 040), have similar global severity on all road segments. Others, like the 4th (driver 005) or the 32th (driver 033) are evaluated very differently over all road segments.

The observation of partial individuals indicates that even the most severe drivers are not necessarily the most severe on all road environments. Therefore, in the following analysis of aggregated trips in Section V.3, we may expect that some new trip compositions putting the emphasis on specific road environments, may rearrange the drivers in terms of global severity for the vehicle.

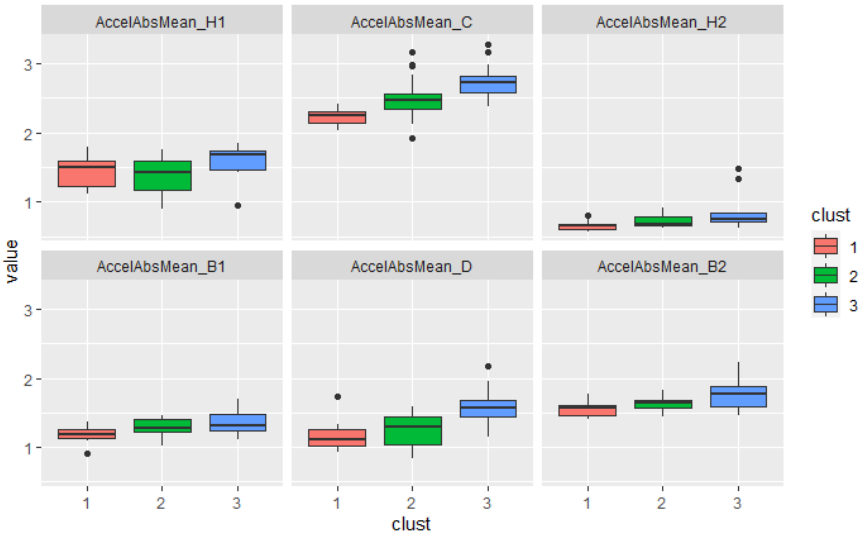

(a) Mean of absolute non-zero acceleration

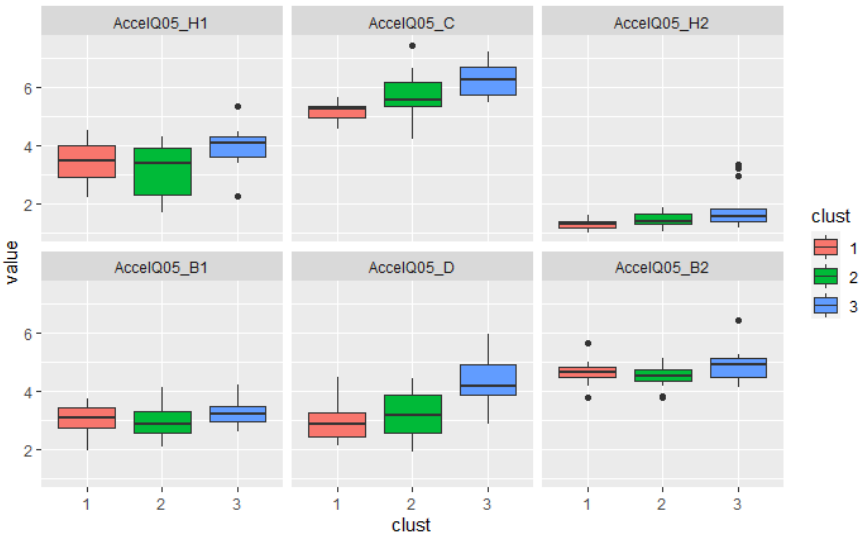

(b) 5% quantile of non-zero acceleration (strong deceleration)

Fig. IV.25: Box plot for each cluster on each road segment of campaign US18-DT1 of two different acceleration quantities calculated for each driver.

IV.4.4 Discussion: the sampling of road environments

In this section, we address the representativeness of the road segments of the total trip. As mentioned previously, the 6 road segments of US18-DT1 are identified using 4 road environments: city, highway, back road and damaged road. The 5 segments of campaign US18-DT2 are identified using the same categorization.

IV.4.4.1 Road segment similarity through the RV measure

The 44 drivers of US18-DT1 all have driven on the road segments B1, B2, H1 and so on. The RV-coefficient (Rhô-Vectoriel) [Escoufier 1973; Robert and Escoufier 1976] serves as a

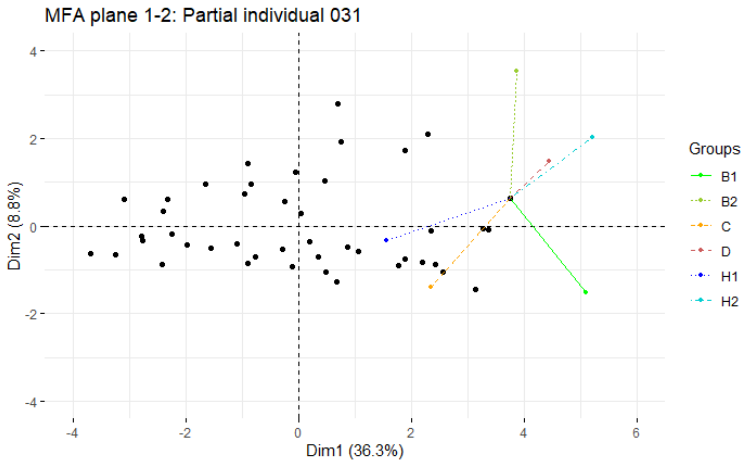

(a) Driver 031

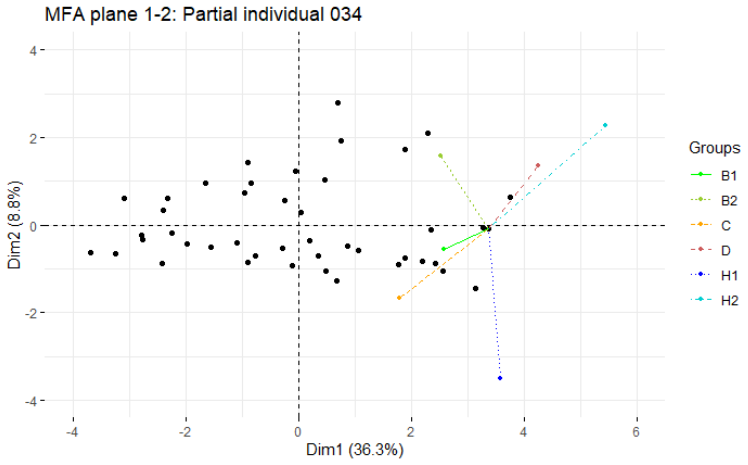

(b) Driver 034

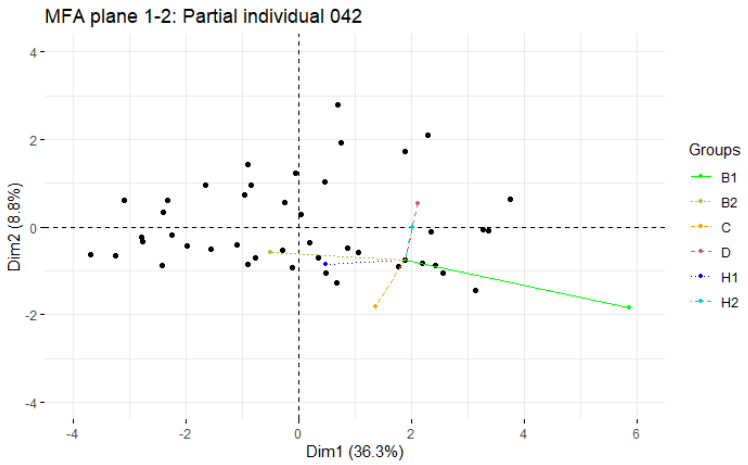

(c) Driver 042

Fig. IV.26: Observation of three partial individuals on the principal space obtained from an MFA on US18-DT1

measure of similarity between two subsets of data obtained from the same individuals. It is calculated between two datasets, *f.i.* $\mathcal{C}_1$ and $\mathcal{C}_2$, with the formula:

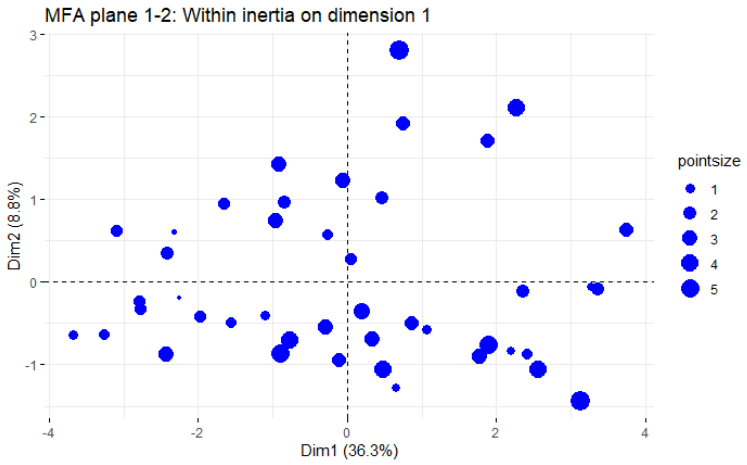

Fig. IV.27: Observation of the partial inertia of the different evaluations of each driver's global severity (first PC) on each separate analysis

$$RV\left(\mathcal{C}_1,\mathcal{C}_2\right) = \frac{\sum_{k=1}^{\kappa}\sum_{j=1}^{\kappa}\operatorname{cov}\left(\frac{Z_{\bullet k}^{L,\mathcal{C}_1}}{\lambda_1^1},\frac{Z_{\bullet j}^{L,\mathcal{C}_2}}{\lambda_1^2}\right)}{\sqrt{\sum_{k=1}^{\kappa}\operatorname{var}\left(\frac{Z_{\bullet k}^{L,\mathcal{C}_1}}{\lambda_1^1}\right)}\cdot\sqrt{\sum_{j=1}^{\kappa}\operatorname{var}\left(\frac{Z_{\bullet j}^{L,\mathcal{C}_2}}{\lambda_1^2}\right)}} \tag{IV.4.18}$$

assuming that both data subsets $\mathcal{C}_1$ and $\mathcal{C}_2$ have the same number of variables κ (not necessary in general); denoting var the variance operator and cov the covariance operator. The RV-coefficient lies between 0 and 1. If close to 1, it means that the cloud of observations is homothetic from one data subset to the other.

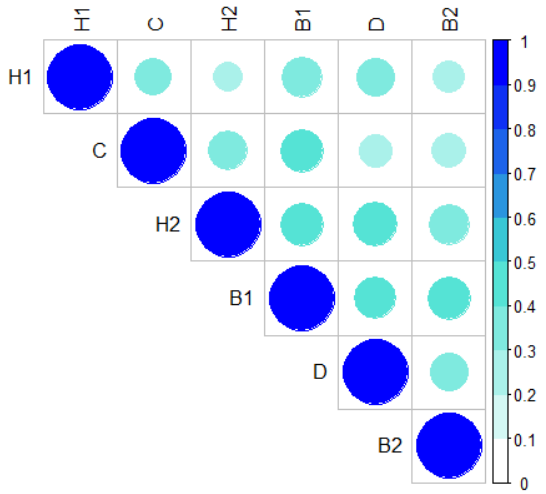

Fig. IV.28: RV-coefficients calculated between all data subsets of load intensities $(\mathcal{C}_e)_{e\in[\![1,6]\!]}$.

Fig IV.28 shows the values of the matrix of RV between all active groups of load intensities in the analysis. It is notable that segments H1 and H2 (line 1 column 3) or B1 and B2 (line 4 column 6) do not have similar structures as their RV coefficient lies low, despite being associated with the same road environments. This dissimilarity questions the classification of each road segment of the campaign to their associated road environment.

IV.4.4.2 The time of the day and the effect of traffic

In order to evaluate the robustness of our results obtained from the measurement campaign US18-DT1, we wanted to develop the same method on the campaign US18-DT2. At a bird's eye view, this campaign was built in a similar way to the first, albeit containing a much larger fraction of highway roads.

Let us take a look at the time of the day at which each sample was obtained in both measurement campaigns. A new driver was tried each day on the vehicle and the preset trip for both US18-DT1 and US18-DT2. No measurements were made on Saturdays and Sundays. Most measurements of US18-DT1 were performed in the morning. Some recordings occurred in the early afternoon. The traffic conditions can be expected to have been somewhat similar among all drivers of this first campaign. Contrariwise, half the measurements of US18-DT2 started at 4am local time while another half started in the middle of the afternoon at 3pm local time. Some drivers also unpredictably had to drive in the rain.

(a) Driver 012, location 1 (H1)

(b) Driver 011, location 1 (H1)

(c) Driver 014, location 2 (H1)

Fig. IV.29: Samples of the first highway segment of measurement campaign US18-DT2 for three different drivers.

Figs. IV.29a and IV.29b show a sample of the video feed of the first highway segment of US18-DT2 at the same geographical location for two drivers. One had rain during their run and the other had none. Fig. IV.29c shows a sample for another driver at another location that seems prone to high traffic. All captures were taken from the first highway segment of the trip.

The observation of pair correlations in the segments of US18-DT2 hints at the importance of these effects of time of the day and therefore traffic conditions. Fig IV.30b shows the correlations on a selection of contexts for the Highway and Damaged road segments of this second measurement campaign.

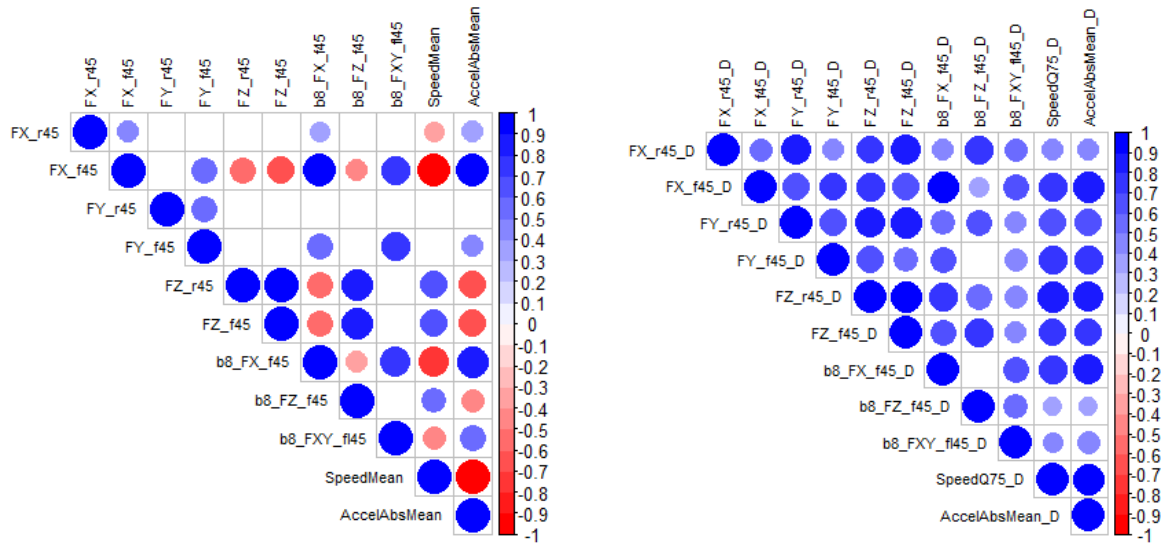

(a) Highway 1 (H1) (b) Damaged road (D)

Fig. IV.30: Pair correlations for a selection of variables for segments of campaign US18-DT2. Selected variables are in order: symmetrical Y loads $m = 4$ rear and front; symmetrical Z loads $m = 4$ rear and front; symmetrical X and Z loads $m = 8$ front; average of non-zero speed; average of absolute non-zero acceleration

Fig IV.30b shows pair correlations for the damaged road segment as a reminiscence of the previous damaged segment in US18-DT1 (Fig. IV.6). Being a segment with little decision-making associated with maneuvers and a lot of obstacles, the two damaged road segments are very similar in terms of correlations from one campaign to another.

This bias in terms of traffic conditions for highway segments questions the hypothesis of independent and identically distributed variables underlying the observations of load intensities. A forced implementation of MFA on the second dataset did not yield the same results in terms of PC correlations. The size effect of the analysis developed previously, dubbed the intrinsic global severity of drivers per kilometer, does not appear in this analysis of the second campaign.

Indeed, the normalization parameter of the analysis is represented by the first eigenvalue of a PCA on each road segment. The highway segments of US18-DT2 are much longer, richer and prone to the effects of traffic than in US18-DT1. Therefore, the first eigenvalue of a separate analysis on these segments will be low and MFA will give more importance to the variance borne by highway segments.

Note that this *de facto* prioritization of highway segments on the characterization of intrinsic driver severity is coincidentally legitimate, because highway segments make up for more than half of this second trip. The angular points of this second analysis would be the

relevance of calculating load intensity on the whole segment, the eventual necessity to cut the segment further and of course the differences in times of the day.

In order to manage the variability caused by traffic and time of the day, an identification of a difference in traffic and in weather conditions should be added as a qualitative active variable to the observed variables. This identification of traffic and weather conditions was not conducted in the thesis.

IV.4.5 Synthesis of the multiple factor analysis

The analysis of load intensities of drivers on several segments of a full trip in the region of Detroit unveils differences in pseudo-fatigue per kilometer that can be interpreted as differences in driver behavior. The conclusive traits that distinguish drivers from each other define an intrinsic severity of drivers.

For each road environment, the conditional severity per kilometer for a driver can be discussed in terms of global severity, sportiness and quick turning. In a mixed trip, the behavior or specificity of each driver may change from one road environment to the next. The investigation of driver severity per kilometer driven on any road environment may allow for the selection of drivers with a specific profile toward mission simulation as in [Dreßler *et al.* 2009].

A sensitivity analysis could be conducted on the implementation of MFA on campaign US18-DT1: we may consider removing a few drivers from the dataset prior to the analysis, and check that the first PCs still have the similar correlations and interpretations. We may also try the robustness of the partition, by implementating HCPC on this reduced number of individuals, then checking that the ones left out are still associated with the "correct" clusters.

Developing the same method on a similar dataset, US18-DT2, led to large changes in the result of the MFA, because of the bias of the dataset. Indeed drivers were not all sampled at similar times of the day. However, this latter dataset may help determine what road environments are the most prone to the effects of visibility and traffic.

IV.5 Chapter conclusion

In this chapter, we have introduced mission factors as preliminary and surveyable sources of variability for the loads and therefore the pseudo-fatigue induced on a vehicle. Driver behavior, trip duration and composition, and payload setting are the three factors defining one episode of the life a vehicle for the sake of its characterization of fatigue.

These three mission factors are inter-dependent because of their connection to the function of a vehicle. Their sampling over the population of mission must allow to disambiguate or separate the effect of each factor.

In order to make sense of the differences in loads and pseudo-fatigue induced by different

trips, we propose a description of the variable Trip using a classification of the road into road environments. Each environment, being visually identifiable by a user, modifies the number and level of road events, obstacles and maneuvers, met each kilometer.

From an introduction of available data, we have identified an appropriate dataset for the exploration of Driver-Trip interactions. Load intensities, being equivalent variables to pseudo-damage per kilometer, were calculated on all local contexts for a number of drivers on several segments of a reference trip. Implementation of MFA on the dataset $\mathcal{C}$ associated with campaign US18-DT1 revealed a manageable number of traits of driver behavior - dimensions of intrinsic severity - that are best suited to explain the variability amongst drivers in the pseudo-fatigue that they may induce on their vehicle each kilometer.

The dimensions of intrinsic severity allow us to identify, on the one hand, differences in driver behavior with respect to an increased frequency of maneuvers or of obstacles in a road environment. On the other hand, the conditional global severity, sportiness and propension to quick turning of drivers may also change from one road environment to the other, and some principal components of the MFA are able to track these empirical oppositions between road environments.

The first principal component, the intrinsic global severity of drivers per kilometer, explains a significant fraction of driver variance over normalized variables on the dataset $\mathcal{C}$ (36%). It allows us to identify in this measurement campaign a few homogeneous sub-populations. This first partition over the intrinsic global severity gives us a first relevant basis for the identification of so-called "globally severe" drivers over all road environments. This characterization of drivers per kilometer is yet to be performed again after including additional knowledge on the population of trips that they would drive for a lifetime.

Moreover, different road environments determine different trends (radar shapes w.r.t. the average intensity) and levels in terms of pseudo-fatigue. Some environments are generally more damaging and dispersive each kilometer, such as urban and heavily damaged roads. Urban environments put an emphasis on maneuvers, and this shows on their average load intensity radars over the population of drivers.

This separate analysis of the load intensity for each road environment is a first step towards handling the variety of trips for a new vehicle model. For instance, for a given duration, we can expect that trips containing a larger fraction of urban roads will induce more pseudo-damage on contexts of the front axle associated with combinations of longitudinal and lateral loads. Therefore, vehicle models designed for urban environments will endure more pseudo-fatigue associated with these contexts over their life.

The remaining mission factor, Payload, was observed in Appendix E to have a non-trivial influence on the magnitudes induced by separate road events. More observations would be required to establish proper prediction models for the magnitudes induced by given Driver and Trip for different payload settings or for new vehicle models. In order to alleviate this lack of knowledge on the effect of payload, the common practice is to perform all measures, calculations and design at a large payload setting.

In the next chapter, further restricting the population of missions toward the evaluation of their pseudo-fatigue will prove to be a manageable strategy to model conservatively the pseudo-fatigue induced by a variety of inter-dependent drivers and trips.

Chapter V

Modeling the pseudo-fatigue induced by missions in service

V.1 Chapter introduction

As we have announced in the general introduction, the reliable design of safety parts and their validation in the automotive industry can be achieved through the implementation of Stress-Strength Interference. The generic design and validation problems and their resolution in a simple case, using this new distribution, will be detailed in Chapters VI and VII.

In such a framework, the relevant variable associated with Stress is or should be evaluated as a distribution of the pseudo-fatigue induced over the market of the vehicle. Such a distribution must be elaborated from the analysis of available data on service.

In this chapter, we make use of the new decomposition of mission factors and adapt the definition of intrinsic severity, introduced in §IV.4.2, to elaborate a distribution of pseudo-fatigue on a restriction of the population of missions.

One mission or episode in the life of a vehicle is defined as the meeting of a driver, a trip of reasonable duration and payload (passengers and luggage). These three mission factors were defined in §IV.2.1.

A lifelong mission is a concatenation of all such episodes in the life of a vehicle. The reliability of the safety parts of the vehicle is defined as a maximum admissible risk of failure over the whole population of service missions of the vehicle model lasting exactly a lifetime objective. These lifelong missions are the population of interest.

Elaborating a market-wide distribution of pseudo-fatigue over these lifelong missions would require an indiscriminately large sampling of mission factors. This would be extremely costly, to achieve little improvement on the objectives for the design and validation of the components of interest. Instead, Section V.2.1 introduces the idea of a conservative restriction of the population of missions, to reduce the complexity of service sampling and still achieve a distribution of pseudo-fatigue that is suitable toward the reliable design of automotive components (see Fig. V.1).

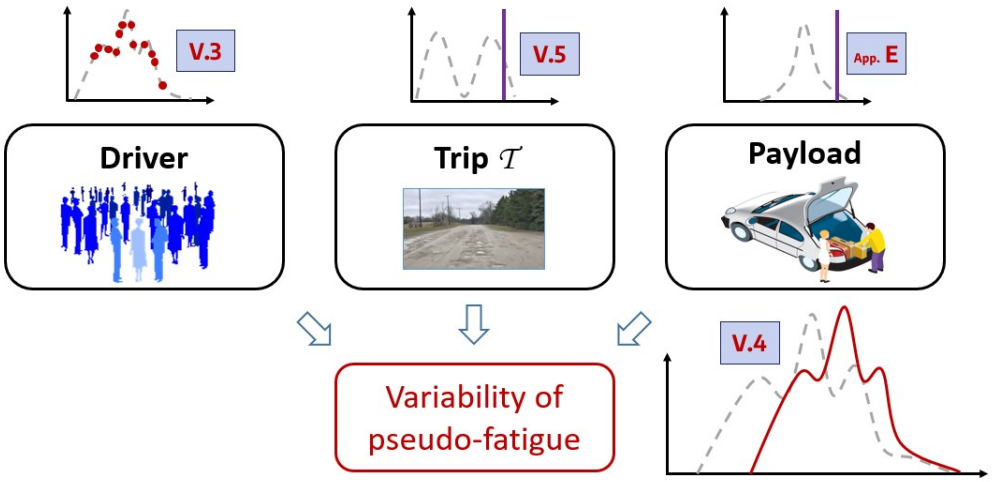

Fig. V.1: In this chapter, we restrict the population of missions to achieve a conservative distribution of our variables of pseudo-fatigue.

We must also be cautious with regard to the extrapolation from a kilometer of driving or from an episode with set duration l_0 to the objective lifetime of the system $l_f \gg l_0$. In the previous chapter, the load intensity was defined as the averaged equivalent magnitude for each kilometer of driving on a road segment. The measurement campaign of interest consisted of a set trip lasting 245km. Is the life of a vehicle a repetition of one random mission or a series of random experiments? §V.2.3 discusses the characteristic duration of a mission and introduces missions of reference as an elementary brick toward the evaluation of missions of any duration.

The rest of the chapter outline is as follows: in §V.3.1, we define aggregated trips as combinations of road environments that represents the composition of the life of a vehicle. The new statistical analysis of pseudo-fatigue on an aggregated trip is presented in Section V.3. This leads to the evaluation and distribution of the conditional severity of a driver in Section V.4. Finally, we compare the results in terms of pseudo-fatigue for different choices of aggregated trip in §V.5.2. The extrapolation from an aggregated trip with manageable duration to the objective lifetime of the system is tackled in Section V.6.

V.2 How to elaborate a model on a large population of lifelong missions?

V.2.1 Restriction on the market and conservative pseudo-fatigue models

For a given vehicle model, the population of missions with their complete descriptions and associated pseudo-fatigue is full of ramifications, such as:

- How many passengers are in the car?

- Does the number of passenger affect the driver's behavior?
- Is Payload correlated with the type of trips?
- How many users live in specific environments like non-urban areas or islands, displaying only some sorts of road environments?
- Does this regional aspect come with a specific sociology of driver behaviors?
- How often do urban users commute? How often do rural users commute?
- Are there cultural or regulatory changes caused by or related to climate change?
- Etc.

All these questions have a consequence on the interdependence between mission factors and therefore on the complexity of severity and the resulting distribution of pseudo-fatigue. Taking these considerations into account and gathering/exploiting the necessary data to conclude, raises the complexity of both sampling and analysis. It should aim at improving an already existing distribution of pseudo-fatigue.

In this thesis, we focus on providing a firsthand improvable solution to robustly evaluate and distribute severity and pseudo-fatigue whilst making use of currently available data. Afterwards, making the effort to improve a first proven model will be justified by further industrial needs and available means.

Moreover, the risk of failure of such a system, having independence between pseudo-fatigue and resistance, is mostly determined by the probabilities that the most severe clients may lead it to fail. The determination of severe, extreme or conservative references of pseudo-fatigue is hardly impacted by the precision of the modeling of average users.

For these reasons, making conservative assumptions on the missions, *i.e.* that overestimate the induced pseudo-damage of missions, helps to reduce the amount of required data to conclude on satisfying reference missions for further use. For instance, if the most pseudo-damage is induced on urban or damaged roads, then we should focus on the trips that contain a large fraction of these road environments.

V.2.2 Trip composition, trip sampling

The life environment of the customer will determine whether they need to drive for a long time on city roads, highways or country roads. Since each of these road environments may contain different amounts and kinds of obstacles and driving situations, their levels of pseudo-damage per kilometer will be different and very variable. The company needs to evaluate the variability of the composition of service missions for the vehicle model of interest.

Let l denote the distance of a mission. The composition of a trip can be expressed as a mix of segments of a given distance, or as the proportion of each road environment:

$$\sum_{e=1}^{r} l_e = l \tag{V.2.1}$$

$$\sum_{e=1}^{r} \frac{l_e}{l} = 1 \tag{V.2.2}$$

Information on the composition of trips can be derived from regional knowledge on traffic volume (vehicle-miles) [Leduc *et al.* 2008]. We may cite for instance:

- In the UK, [UK-DfT 2020, 2022] separating the traffic volume for different road environments and vehicles that are personal and non-personal (bus, trucks);
- In France, [Hubert *et al.* 2016] where road environments are segmented as per the population of the surrounding (eventually) urban area;
- In the US, [MU-CSS 2021] taking into account non-personal vehicles in the figures of transportation but mentioning the average number of passengers; and data banks like [Davis and Boundy 2021] in general and [FHWA 2019] (sections 5 and 6) for highway traffic.

In this thesis, knowledge on the composition of trips in the region of interest stems from available data at Stellantis. It is first considered to be integrated in the definition of some trips of the measurement campaigns performed in different regions of the world such as US18-DT1. We will develop more on the necessity of a larger sampling of trips toward the verification of the conservativeness of a choice of aggregated trip in Section V.5.

V.2.3 Vehicle life, aggregated trips

The life of a vehicle corresponds to the concatenation of all the episodes that it encounters in service before it is decommissioned. The "life" of a vehicle should not be mixed up with lifetime, which corresponds to the duration of said life. Nor with lifetime objective which is defined as the duration or distance of reference for the specification of requirements in reliability. These three terms are expressed in kilometers in this work.

For the sake of requirements in reliability, we are interested in evaluating the level and dispersion of fatigue characterizations on a vehicle at the end of a life that would last exactly up to the lifetime objective. Driver and payload aside, this still represents a very large population of trips.

One episode of the life of the vehicle serves a given purpose: going to work, to the groceries, on holidays... These trips will have different road compositions for a given customer, because of these different purposes but also because of the environment they live in. A customer living in an urban environment may be led to drive more on urban roads.

One method to map the population of trips would be to take into account and concatenate randomly different trips with different duration and composition. This analysis would require including further data on the composition of trips in the method.

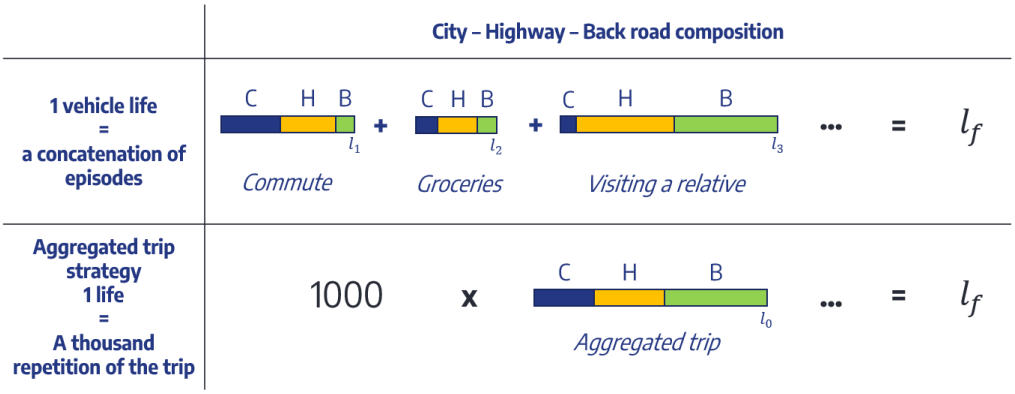

Fig. V.2: A mission is a concatenation of episodes. An aggregated trip is a summary of all episodes.

Instead, we will consider an aggregate of all these episodes, in the form of an aggregated trip with a manageable duration l_0 (see Fig. V.2). An aggregated trip is a mixture of different road environments designed to represent a reference trip driven by a vehicle over its life. This typical trip serves as a summary for the different purposes and for the different origins of the customers. The pseudo-fatigue induced throughout a lifelong mission on the vehicle will be considered to be calculated from an extrapolation on the values calculated on this aggregated trip.

An aggregated trip carries the information of an average or conservative composition of road environments, with diversity in terms of events and perhaps traffic conditions. The joint knowledge of a population of drivers, of an aggregated trip and of a conservative payload setting denote a restriction on the whole market of the vehicle model. If trip and payload are fixed, then the only remaining variability in the restriction is brought by driver behavior.

We first consider that said random driver needs only be drawn once for a whole vehicle lifetime for a conservative evaluation of lifelong magnitudes. In reality, several drivers may take turns or pass on to each other over the life of a vehicle, as it is shared within a group or resold. Such practice has an observed slight tendency to standardize pseudo-fatigue, as was shown in an internal study conducted by Stellantis [Pagnoux 2010]: it regroups the values of pseudo-fatigue around their mean and curbs their variance. Ignoring these second-hand effects is considered to yield conservative results. Indeed, this means that a vehicle sold to a severe driver would endure this severity for its whole lifetime, instead of having a chance at being owned by a second, less severe driver.

The use of an aggregated trip instead of the whole population of trips is a strong preconception on the market of the vehicle model. Results from the following analysis should be updated regularly with new trip compositions to ensure the conservativeness of the analysis.

Moreover, there is no total order on vectors of magnitudes induced by a single driver on different trips. We have observed from the separate observations of road segments in §IV.4.1.2 that urban environments induce in general more pseudo-damage per kilometer on contexts associated with longitudinal (X) and lateral (Y) solicitations than the average kilometer, because of their density of maneuvers. Likewise, damaged roads contain more obstacles per kilometer and will be more dangerous to other contexts. Indeed different road environments

do not contain the same population of road events. Therefore, an aggregated trip considered conservative for the design of one subset of contexts may be non-conservative for another subset.

In Section V.5, we will show how modifying the reference trip has an influence on the outer reaches of the distribution of pseudo-fatigue. The relatively short duration of an aggregated trip also poses the question of extrapolation to a lifetime objective. This will be the discussion of Section V.6.

V.3 Statistical analysis of driver severity for an aggregated trip

Let us analyze the variability of pseudo-fatigue induced by different drivers on an aggregated trip through the lens of driver behavior. This section is another exploratory analysis, much like the previous chapter in which the dataset was segmented as per the segments of the trip. We will see in Section V.4 how the results of this new analysis will be of use to justify our strategy for the distribution of magnitudes over a restriction of the population of missions of the vehicle.

V.3.1 Problem definition for an aggregated trip

The measurement campaign US18-DT1 tried several drivers on a short trip, lasting 245 kilometers. From there, the goal is to find an adequate prediction of the pseudo-fatigue induced by similar missions lasting exactly a lifetime objective. A first proposition for an aggregated trip for the analysis of pseudo-fatigue from the measurement campaign US18-DT1 is the original composition of the measure, denoted $\mathcal{T}_1$.

V.3.1.1 Trip distance homogenization

Individuals of measurement campaigns on a pre-specified trip may end up with a distance different from the theoretical distance of the trip. Small deviations from the trip cause by lane changes, obstacle dodges or parking maneuvers may add up to justify such distances.

However, some client exhibited different itineraries altogether. In Fig. V.3, we observe two phenomena. First, in the middle of the drive, one of the two drivers had to skip a turn, probably because of a clogged street that day, and performed a different trip. Second, the processing system seems to shut down way earlier in the case of driver 032, missing out on the long straight branch that led to the next segment of the run. The main consequence is a difference in kilometers driven: while the objective was l_2 km, driver 032 registered $0.66 \cdot l_2$ km in City.

While these discrepancies might be interpreted artificially as day-by-day variation on the trip, they question the hypothesis of a trip of reference for the lifetime of a vehicle, introduced

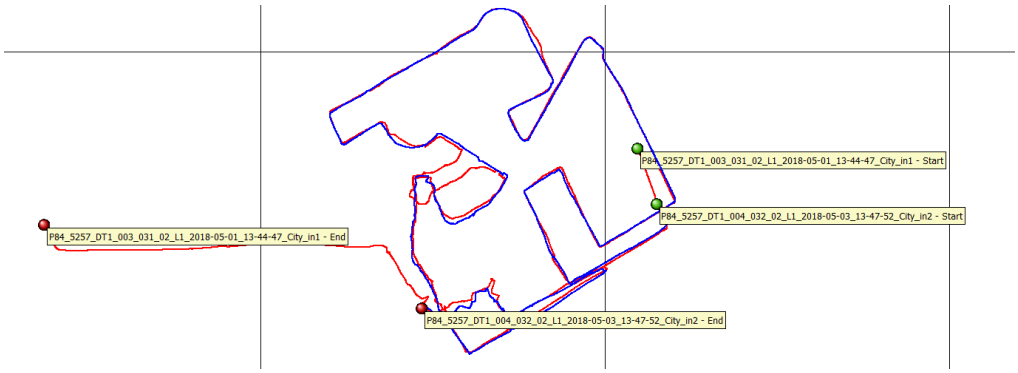

Fig. V.3: GPS trajectories of drivers 031 (red) and 032 (blue) of campaign US-DT1 in the segment City (of Detroit).

in §V.2.1. Arguably, day-by-day variability should be considered to be included in the mission of reference, and not persist in the samples.

Moreover, the drop in kilometers for driver 032 represents a lack of City sampled for this driver. If the composition of the measured trip is extrapolated "as is" to a vehicle lifetime, this driver's fraction of urban driving would still be reduced compared to other individuals.

For the analysis of an aggregated trip, we have made the choice to simulate all pseudo-damages induced by a driver on an artificial trip composition $\mathcal{T} = (l_e)_{e\in[\![1,r]\!]}$ (see Eq. V.2.1) using the following formula:

$$M\left(\gamma,\vec{\mathbf{F}}^c_{\mathcal{T}}\right) = \sqrt[m]{\sum_{e=1}^{r} l_e \cdot L\left(\gamma,\vec{\mathbf{F}}^c_e\right)^m} \tag{V.3.1}$$

denoting $L\left(\gamma,\vec{\mathbf{F}}^c_e\right)$ the load intensity as defined in Eq. IV.4.1, associated with the local context γ, calculated for driver c on the e-th road segment; and l_e the distance drive on the e-th segment of the trip.

This simulation method has a few limitations in the estimation of a driver's load intensity over a segment. Driver 032, having skipped a straight line at the end of the City segment, may have encountered more crossroads *per kilometer* than other drivers. Thus, the chosen simulation method in Eq. V.3.1 might overestimate the amount and level of maneuvers met by the driver in l_2 actual kilometers.

A middle ground solution would be to evaluate the number of events expected for each kilometer of this city segment. The missing pseudo-damage, induced by driver 032 on the missing part of the segment, could be predicted from the difference in measured events between them and the rest of the drivers. This method would increase the number of assumptions and require a model to count, identify and sort chronologically events on a segment. Hence our sticking with the simulation of pseudo-damage based on the normalization of driven kilometers.

V.3.1.2 Magnitude dataset for the analysis on an aggregated trip

The aggregated trip $\mathcal{T}_1$ associated with campaign US18-DT1 lasts l kilometers. Its composition is confidential. The dataset $\mathcal{C}_{\mathcal{T}_1}$ for this analysis is composed of $\kappa = 26$ variables (equivalent magnitudes) observed over $n = 44$ individual drivers.

$$\mathcal{C}_{\mathcal{T}_1} = \left(M\left(\gamma_k, c\right)\right)_{c\in[\![1,n]\!],\ k\in[\![1,\kappa]\!]} \tag{V.3.2}$$

The aggregated trip $\mathcal{T}_1$ is considered by the company to be a plausible and synthetic trip with respect to the market of missions that the vehicle is associated with. It means that this trip contains *a priori* a reasonable fraction of each road environment with respect to the (unknown) population of plausible trips. The evaluation of pseudo-fatigue on this aggregated trip is hypothesized to be conservative, *i.e.* the resulting distribution overestimates the pseudo-damage induced by the true most severe missions. We will discuss the evaluation of this hypothesis after this analysis, in Section V.5.2.

We are looking for a new description of driver severity, suitable for the comparison of pseudo-fatigue between similar missions. We then seek knowledge on the shape of the population and the existence of outliers, and an adequate model for the distribution of pseudo-fatigue variables.

V.3.2 Prior observation of the magnitudes

The random variable corresponding to the observation over all drivers of a magnitude component $M\left(\gamma_k, \bullet\right)$ is denoted $M_{\bullet k}$. The joint information of all magnitude measurements for an individual c is grouped in an observation vector $\overrightarrow{M}_{c\bullet}$. Similarly, the dataset $\mathcal{C}_{\mathcal{T}_1}$ can be rewritten as a matrix $M_{\bullet\bullet}$

Fig. V.4 shows the box plots of each magnitude $M_{\bullet k}$ over the campaign in a single radar. It allows us to check for the existence of heavy outliers in one of the covariates: values that stretch far from the interquartile range. These box plots also display differences in standard deviation from one marginal variable to another.

Like a vector of absolute load intensities (see Fig. IV.4 a)), a vector of absolute values of equivalent magnitude displays heterogeneity over different local contexts. Longitudinal, lateral and vertical global load components have an inherent heterogeneity in their values and ranges that will show on the magnitudes (hence the colored sectors in the radar). Therefore, the analysis of pseudo-fatigue on the aggregated trip will require standardizing the variables.

Let us define a different signature vector - a reference vector for normalization - in order to establish a normalized visualization of vectors of magnitude over the dataset $\mathcal{C}_{\mathcal{T}_1}$. We define, for all $k \in [\![1,\kappa]\!]$, the empirical mean $\overline{M}_k$, the standard deviation $\overline{M}_k$, the variation coefficient v_k and the dataset signature vector $\overrightarrow{M}^{\text{ref}}$ by:

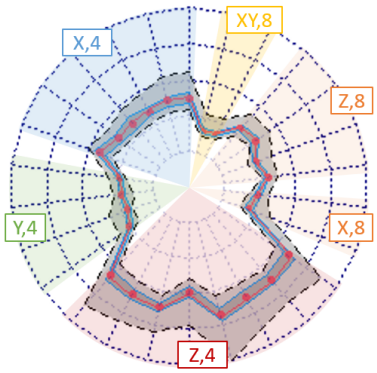

Fig. V.4: Absolute magnitude box plots for US18-DT1. The red line is the empirical mean. The red dots are the median magnitudes. The dark grey zone with blue limits is the interquartile range. The dotted limit of the light grey zones are the extrema of the population. All radii have the same limit between 0 and a confidential factor times the total charge of the vehicle in Newton

$$\overline{M}_k = \frac{1}{n}\sum_{c=1}^{n} M_{ck} \tag{V.3.3}$$

$$\left(s_{M_k}\right)^2 = \frac{1}{n}\sum_{c=1}^{n}\left(M_{ck} - \overline{M}_k\right)^2 \tag{V.3.4}$$

$$v_k = \frac{s_{M_k}}{\overline{M}_k} \tag{V.3.5}$$

$$M_k^{\text{ref}} = \overline{M}_k \ \forall k \in [\![1,\kappa]\!] \tag{V.3.6}$$

In order to illustrate the comparison between individual drivers and their mean values of pseudo-fatigue over the population, let us plot the values of normalized variables of pseudo-fatigue for a few drivers in Fig. V.5b. On this second graph, it is easier to observe for instance that the magnitudes calculated on lateral load cases are larger for driver 039, while driver 037 is consistently more damaging on most local contexts.

The pair correlation between two variables on the dataset is given by the same formula as Eq. IV.4.7:

$$\text{corr}\ \left(M_{\bullet h}, M_{\bullet k}\right) = \frac{\text{covar}\ \left(M_{\bullet h}, M_{\bullet k}\right)}{\text{Var}\ \left(M_{\bullet h}\right) \cdot \text{Var}\ \left(M_{\bullet k}\right)} = \text{corr}\ \left(Z_{k\bullet}^{M,1}, Z_{k\bullet}^{M,1}\right) = \text{covar}\ \left(Z_{k\bullet}^{M,1}, Z_{k\bullet}^{M,1}\right) \tag{V.3.7}$$

Let us observe pair correlations on a first selection of the variables. Fig. V.6 shows pair correlations between magnitudes for which the load case includes only global load components on the front axle of the vehicle. Pairs of covariates that are heavily correlated most likely bear the same information in terms of population variability. We can see on the figure that magnitudes built from similar global load components (X, Y or Z) and with the same Basquin exponent form groups of significantly correlated pairs.

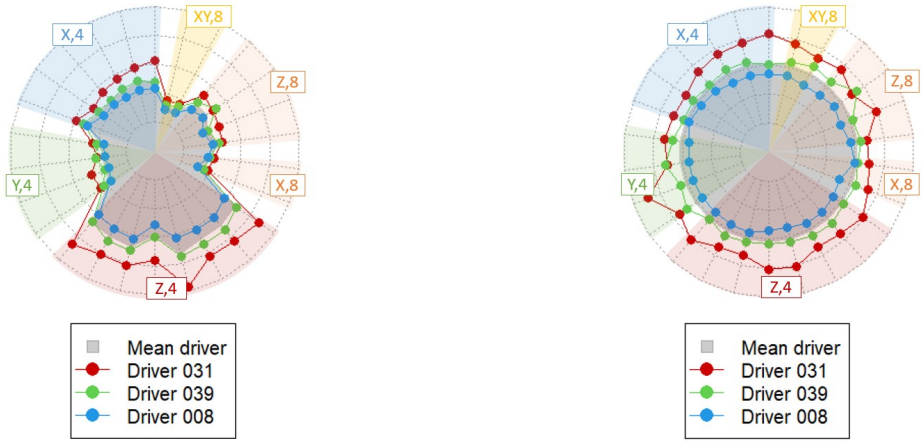

(a) Absolute magnitudes. Radar limits are the same for all radii.

(b) Normalized magnitudes. Radar limits are 0 and $1 + \eta \cdot q_k$ for each radius k.

Fig. V.5: Magnitude radars for three drivers on dataset $\mathcal{C}_{\mathcal{T}_1}$. Q_{tot} is the total charge of the vehicle in Newtons; η is a common scalar coefficient chosen once and for all so that all drivers fit in the radar; v_k denotes the variation coefficient of the k-th magnitude.

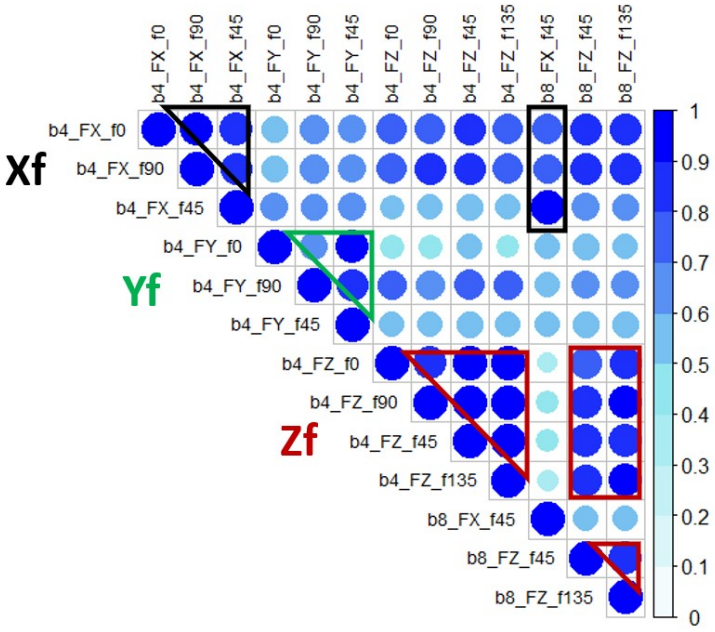

Fig. V.6: Pair correlations between pseudo-fatigue variables associated with 13 local contexts of the front suspension for the dataset $\mathcal{C}_{\mathcal{T}_1}$. A Pearson correlation coefficient close to 1 means that a driver exhibiting a high resp. low value on the first variable will exhibit a high resp. low value on the second one.

As a reminder, we distinguished these local contexts in §III.6 with respect to the different sets of sensible zones that they each encompass. However, the degrees of freedom of magnitude vectors over an aggregated trip are determined by the latent factors of driver severity. We need to have enough different contexts to unveil all degrees of freedom of interest, but the

sheer number of contexts does not increase the quantity of information to seek.

Knowing that magnitudes built from similar load components and with the same Basquin exponent will be heavily correlated, we can restrict our visualization of pair correlations to one representative variable per load direction (X, Y or Z) and Basquin exponent (4 or 8). Fig. V.7 shows the values of correlations of a selection of individual magnitudes for campaign US-DT1.

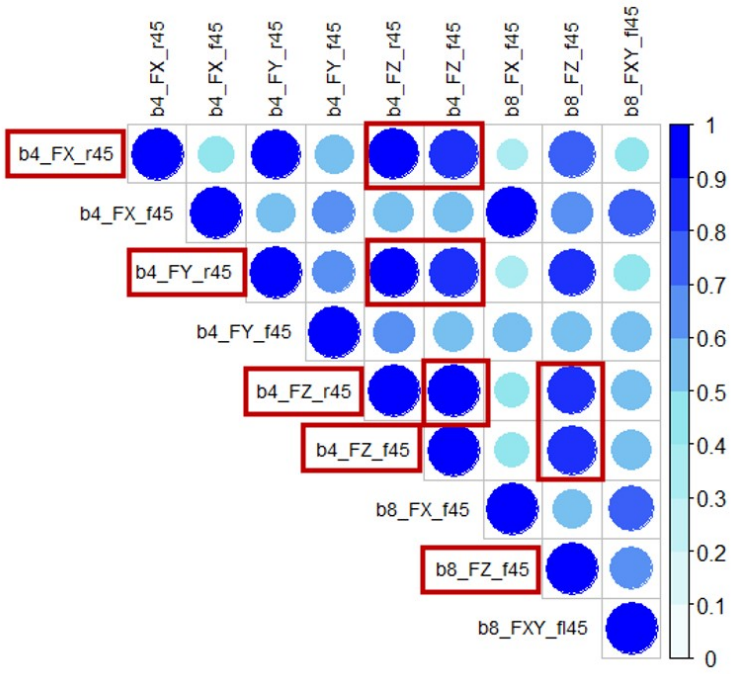

Fig. V.7: Pair correlations between selected variables for the campaign US18-DT1. Selected variables are, in order: symmetrical X and Y loads $m = 4$ rear and front; symmetrical Z loads $m = 4$ rear and front; symmetrical X and Z loads $m = 8$ front; third quartile of non-zero speed; average of absolute non-zero acceleration.

The correlation plot shows high values of pair correlations between magnitudes calculated from symmetrical (45) rear (r) global load components, those calculated from front (f) vertical (Z) solicitations (column 6), and all other variables around which a red box is drawn. These magnitudes track the presence of larger load variations on road obstacles, like speed bumps or ditches. They are determined by the trip composition, and are expected to bring the same kind of information on driver behavior.

Magnitudes associated with front (f) longitudinal (X) or lateral (Y) solicitations have lower correlation with this former group of variables. Load cases associated with these other contexts are prevalent during maneuvers. Low values of correlation between obstacle-related and maneuver-related magnitudes hint at the existence of extra degrees of freedom in terms of driver behavior: higher values for magnitudes related to obstacles for a driver does not necessarily mean higher values for those related to maneuvers.

Fig. V.8 shows, in the upper triangle of the table, a visualization of each plane associated with pairs of selected variables. Pairs of covariates with a large absolute correlation will display

a linear relationship on their projected plane. This comforts our previous observation on the similarity between what we simply call "rear" magnitudes and "front vertical" magnitudes.

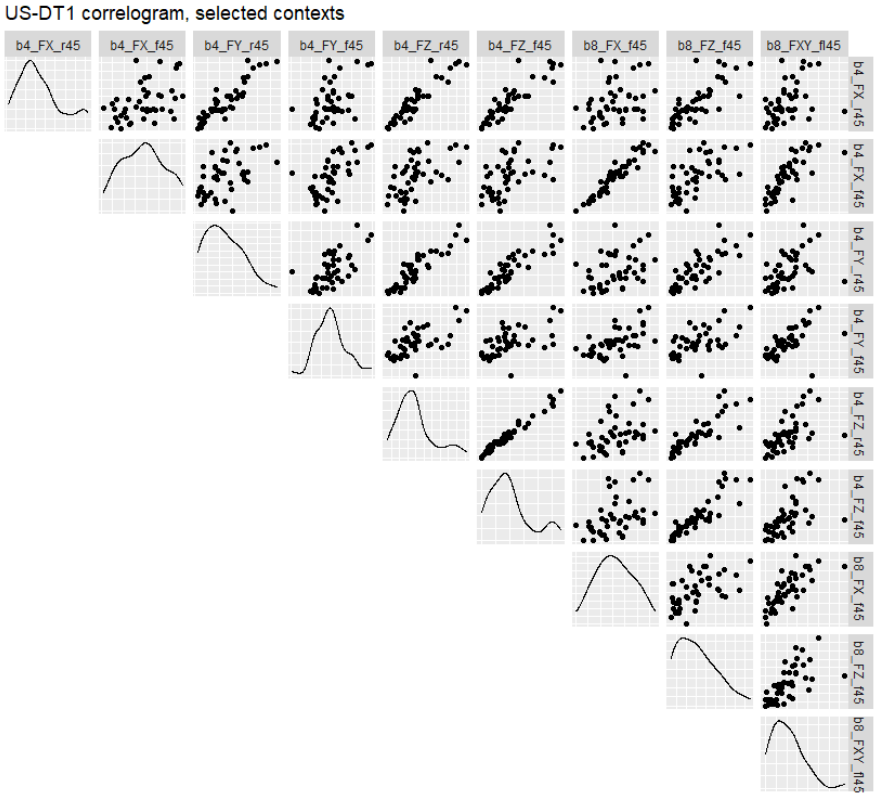

Fig. V.8: Correlogram on selected magnitudes for the dataset $\mathcal{C}_{\mathcal{T}_1}$. Graphs on the diagonal display a kernel density estimation for each marginal magnitude. Graphs in the upper triangle show the projection of all individuals on the plane corresponding to one pair of covariates.

The diagonal of Fig. V.8 shows a kernel density estimation for each magnitude over the selected contexts. We can observe that magnitudes associated with maneuvers, *i.e.* $\left(\widetilde{\alpha}_{f,X,45},4\right)$, $\left(\widetilde{\alpha}_{f,Y,45},4\right)$ and $\left(\widetilde{\alpha}_{f,X,45},8\right)$ have little skewness. Contrariwise, magnitudes associated with obstacles, *i.e.* calculated from global load components on the rear (r) axle and vertical (Z) solicitations on the front (f) axle, have a positive skewness, with a significant core of individuals on values below average, and a small fraction of the population above average.

The shape of the correlation plots and of the population when projected onto each marginal variable encourage the application of multivariate analysis methods. Their goals will be to find adequate interpretations for the relations between base variables, and to determine a better representation and analysis strategy for the shape, and later the distribution, of the population.

V.3.3 Principal Component Analysis

V.3.3.1 Principal component definitions

As a reminder, Principal Component Analysis (PCA) is a tool for the multivariate analysis on datasets of quantitative variables. It determines uncorrelated linear combinations of the covariates, denoted Principal Component (PC), that best explain the variability between different individuals and the connection between different base variables. The equations and hypotheses used for the application of PCA are described in more detail in Appendix D.3 and in [Husson *et al.* 2011].

In §IV.4.1, PCA was a preliminary step to the implementation of MFA on a multiple factor dataset. Indeed the variance λ_1^e borne by the first PC of each separate analysis was used as a normalization term prior to the analysis of the whole dataset in Eq. IV.4.14. Here, the results of PCA will allow us to analyze *de facto* relations between magnitudes induced by different drivers on the aggregated trip.

The observation of the vectors of absolute magnitudes over the population encouraged their standardization prior to their analysis. Standardized values of pseudo-fatigue are given for all individual $c \in [\![1,n]\!]$ by:

$$Z_{ck}^{M,1} = \frac{M_{ck} - \overline{M}_k}{s_{M_k}} \ \forall c \in [\![1,n]\!], \ \forall k \in [\![1,\kappa]\!] \tag{V.3.8}$$

The scaled dataset, containing all scaled observations for all individuals, is denoted $\mathcal{C}'_{\mathcal{T}_1}$ or $Z_{\bullet\bullet}^{M,1}$.

Let us denote $(\lambda_h)_{h\in[\![1,\kappa]\!]}$ the eigenvalues of the correlation matrix A^1 associated with the scaled dataset $\mathcal{C}'_{\mathcal{T}_1}$, solving the following problem:

$$A^1 \cdot \overrightarrow{b}_h = \lambda_h \cdot \overrightarrow{b}_h \tag{V.3.9}$$

$$\overrightarrow{b}_h = \sum_{k=1}^{\kappa} x_{hk} \cdot Z_{\bullet k}^{M,1} \ \forall h \in [\![1,\kappa]\!] \tag{V.3.10}$$

denoting A^1 the correlation matrix associated with the scaled dataset $Z_{\bullet\bullet}^{M,1} = \left(Z_{\bullet k}^{M,1}\right)_{k\in[\![1,\kappa]\!]}$; $\overrightarrow{b}_h$ the unit eigenvector associated with the eigenvalue λ_h; and x_{hk} its k-th coordinate in the space of the base variables.

The goal of PCA is to elaborate new variables that are best suited to explain the variability of the dataset and to observe it in an adequate space. Each Principal Component (PC) is canonically defined as the product:

$$\overrightarrow{S}_h = \sqrt{\lambda_h} \cdot \overrightarrow{b}_h \ \forall h \in [\![1,\kappa]\!] \tag{V.3.11}$$

Thus each PC carries a fraction of the variance of the original scaled dataset $\mathcal{C}'$. Fig. V.9 displays the scree plot of the eigenvectors following PCA on the dataset $\mathcal{C}_{\mathcal{T}_1}$. Three PCs

explain more than 90% of driver variance. Past the fifth one, the variance borne by following components is less than the average contribution of a single driver (2.3%).

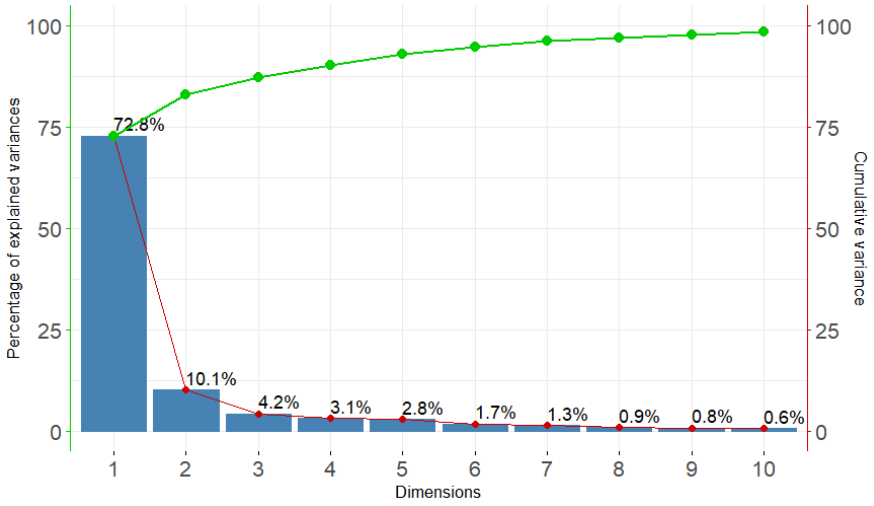

Fig. V.9: Variance scree plot, in percentage of total dataset variance, following PCA on dataset $\mathcal{C}_{\mathcal{T}_1}$. The green curve shows the cumulative variance captured by the first PCs

The dataset of scaled magnitudes $\mathcal{C}'_{\mathcal{T}_1}$ on the aggregated trip $\mathcal{T}_1$ contains less information on the variability of drivers than the segmented dataset of load intensities $\mathcal{C}$ in the previous multiple factor analysis. Therefore, the variance of the cloud is easier to reconstruct efficiently (for instance more than 90%) with a small number of post-PCA PCs, whereas previously 16 post-MFA PCs were required.

V.3.3.2 Principal component correlations with the original variables

Fig. V.10 shows the correlation circles plotted on the first and second principal planes following PCA on the dataset $\mathcal{C}'_{\mathcal{T}_1}$. The symbol for each magnitude was colored according to the global load components included in its associated local context.

V.3.3.2.1 First PC: conditional global severity

All magnitudes are significantly and positively correlated to the first PC. It is, again, a size effect, that we refer to as the global severity of the drivers **for this aggregated trip** *i.e.* a **conditional** global severity. The projection of drivers onto this variable captures 72.8% of the cloud variance. Conditional severity is defined as a dimension of severity that is associated with the restriction on the population of missions that we have performed, as opposed to intrinsic severity, which was defined for the driver regardless of the environment they drive on.

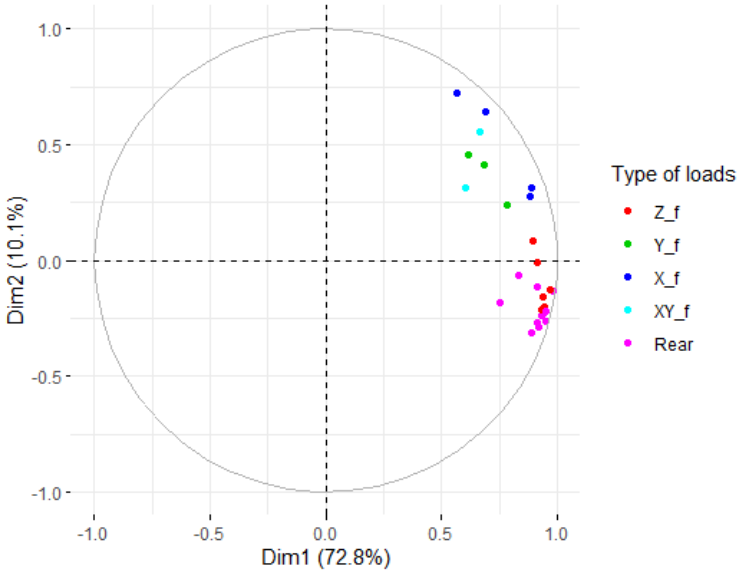

(a) First plane (second PC on y-axis)

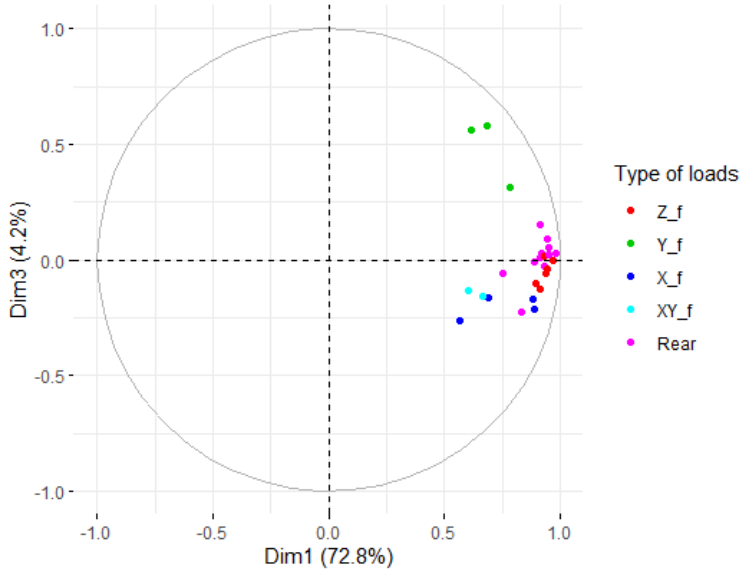

(b) Second plane (third PC on y-axis)

Fig. V.10: Correlation circle over the first and second principal planes following PCA on dataset $\mathcal{C}_{\mathcal{T}_1}$. Each magnitude is colored according to the global load components involved in the unit combination vector of the associated local context.

V.3.3.2.2 Second PC: conditional sportiness

The second PC bears 10% of the cloud variance. 8 and 4 magnitudes out of 26 have a significant positive resp. negative correlation to it. It is positively correlated to magnitudes involving combinations of front (f) longitudinal (X) and lateral (Y) global load components. It is poorly correlated to magnitudes calculated from front (f) vertical (Z) loads and slightly and negatively correlated to all rear (r) components.

For a given global severity, drivers with a positive coordinate on this second principal

direction induce more pseudo-damage than the rest of the population on local contexts associated with longitudinal braking, acceleration and cornering events. Drivers with a negative coordinate on this direction induce more pseudo-damage on components of the rear suspension.

Fig. V.11 shows the 5 resp. 4 most positively and 5 resp. 6 most negatively correlated quantities of interest to the second resp. third PCs. On the first graph, we can see that the highest correlations to the second PC are more specifically associated with the front (f) symmetrical (45) longitudinal (X) load case, regardless of the Basquin exponent. This difference in pseudo-fatigue between drivers is most likely associated with larger variations of effort in braking and acceleration events. We will discuss this interpretation in the following paragraph, §V.3.3.3.

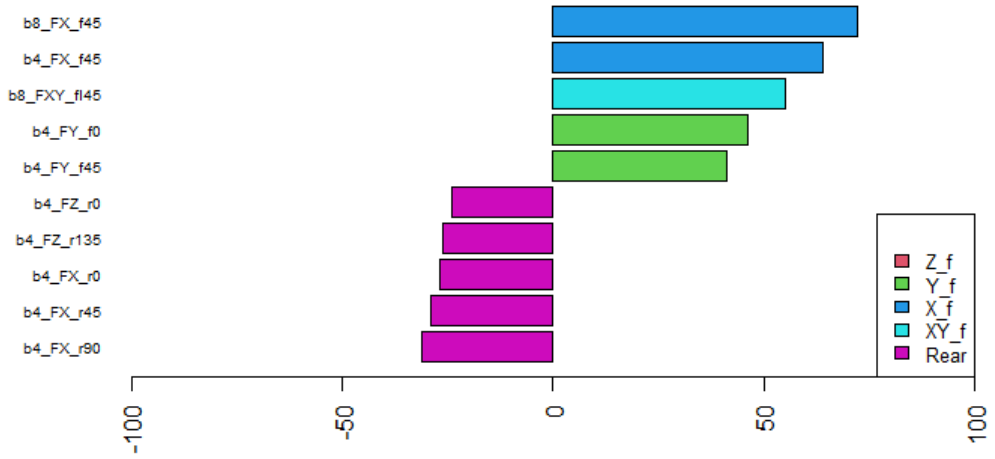

(a) Second PC (sportiness)

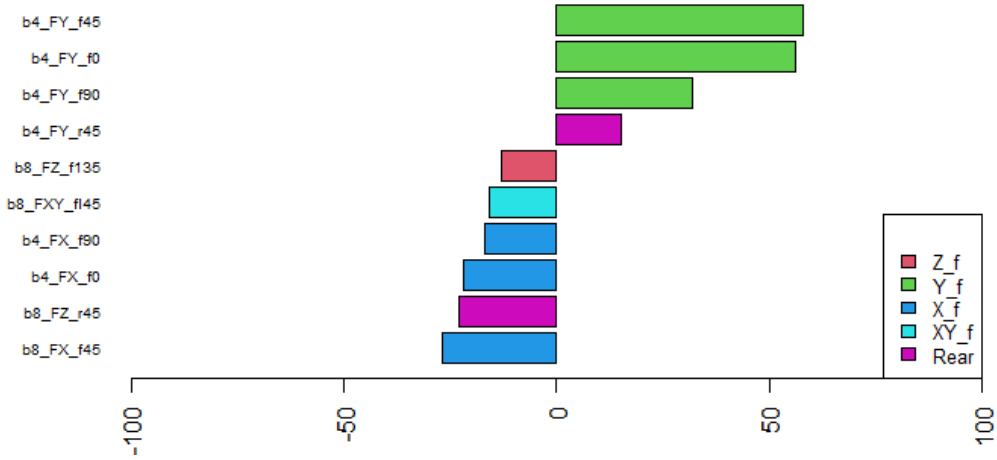

(b) Third PC (quick turning)

Fig. V.11: Ten most significant correlations with the second resp. third PC, following PCA on scaled dataset $\mathcal{C}'_{\mathcal{T}_1}$. Each variable is colored according to the global load components of interest (X, Y, Z and front/rear) in the local context

V.3.3.2.3 Third PC: conditional quick turning

The third PC bears 4.2% of cloud variance. 3 resp. 1 magnitudes out of 26 have a significant positive resp. negative correlation to it. It is positively correlated to magnitudes involving combinations of front (f) lateral (Y) global load components. It bears a slight negative correlation to magnitudes involving combinations of front (f) longitudinal (X) global load components. From Fig. V.11 b), we can see that the negative correlation is slightly lower for magnitudes calculated with a Basquin exponent of 8 instead of 4.

For a given global severity, a driver with a positive coordinate on this third PC induced more pseudo-damage on contexts associated with lateral events than other drivers in the population. This variability may be caused by different speeds practice among drivers during cornering events.

V.3.3.3 Principal component correlations with speed

Following the application of PCA on the scaled dataset $\mathcal{C}'_{\mathcal{T}_1}$, we have identified positive correlations between the second or third PCs and magnitudes associated with maneuvers. We have proposed to interpret them as differences in acceleration and speed behaviors among drivers. Let us support these interpretations from the observation of correlations between acceleration and speed quantiles on the different road segments of the trip $\mathcal{T}_1$.

Nota bene: "Aggregated" speed and acceleration indicators for the whole aggregated trip were approximated from a weighted average on speed and acceleration quantiles and means from each segment of the trip. However, while aggregated pseudo-damages on a reference trip are our variables of interest for the evaluation of service pseudo-fatigue, the aggregation of all road environments blurs together specific situations that would otherwise allow for observing specific driver behavior. Besides, these weighted averages of speed and acceleration quantiles do not represent quantiles of the total aggregated trip. Therefore, such aggregated quantities lose their power for interpretation. We will not exploit them for the interpretation of driver severity.

Fig. V.12 shows the correlation of the three first PCs with some speed and acceleration quantities calculated on each segment of the trip of US18-DT1 and integrated in the MFA in Section IV.4.2. The 5% (AccelQ05) and 95% (AccelQ95) quantiles of non-zero acceleration correspond to the driver's habits in terms of most drastic deceleration resp. acceleration maneuvers. The 75% (SpeedQ75) and 90% (SpeedQ90) quantiles of non-zero speed correspond to their habits in terms of cruising speed.

Note that acceleration is negative when the vehicle decelerates, hence the sign of correlations between the first and second PCs and the variable AccelQ05. Hence, in Fig. V.12, we plot the opposite (-AccelQ05) of this variable to improve readability.

Correlation between acceleration or speed quantities and the first PC is significant in most cases, especially on the City (C) and Dirt (D) segments (correlation coefficients of approximately 50% for all variables, the threshold for significance according to the correlation test being 24% as in §IV.4.2). Indeed, the global severity per kilometer of drivers on both

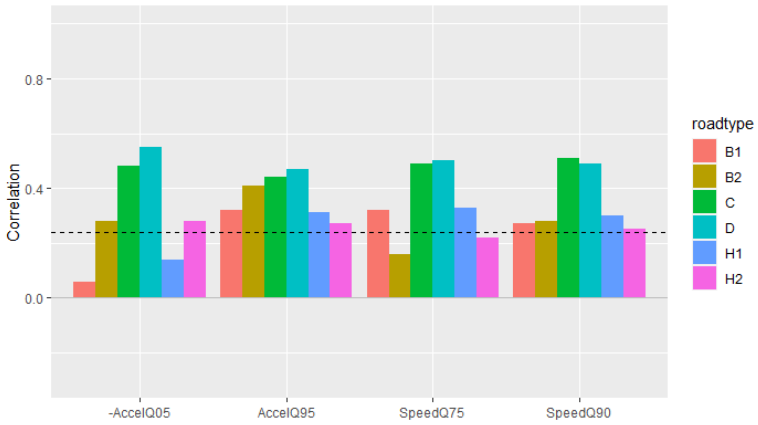

(a) Correlations with Dim.1 (global severity)

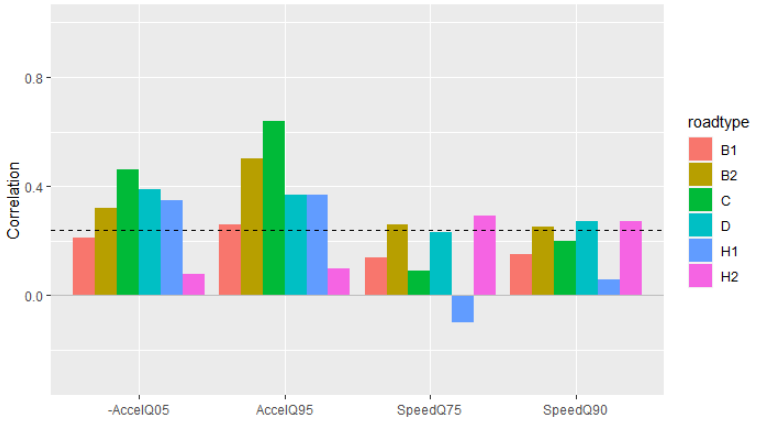

(b) Correlations with Dim.2 (sportiness)

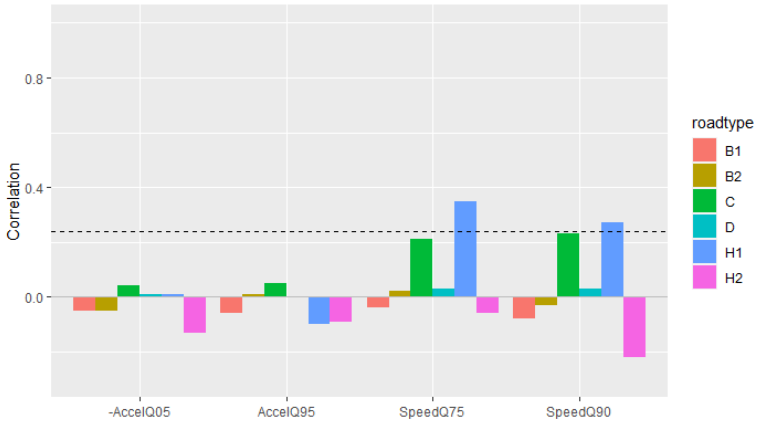

(c) Correlations with Dim.3 (quick cornering)

Fig. V.12: Correlations between acceleration or speed quantiles calculated on each road segment of the trip $\mathcal{T}_1$ for drivers of US18-DT1, and the three first PCs following PCA on the scaled dataset $\mathcal{C}'_{\mathcal{T}_1}$. The dotted line represents the limit for significant positive correlation with a 90% test level

segments increases with speed and acceleration habits, as was already observed at the end of the MFA on the dataset $\mathcal{C}$ in §IV.4.3.3.

The second PC bears higher absolute values of correlation coefficients with acceleration

quantiles, especially on City (C) and the second back road segment (B2), than with speed quantiles. Strong and sudden deceleration and acceleration preceding or following road events denotes the sportiness of drivers. It follows that the second PC brings additional information on the sportiness of the drivers for this aggregated trip.

Correlations between the third PC and speed quantiles on City and Highway segments are roughly significant. In order to confirm the interpretation of positive coordinates on this PC as a tendency towards high cornering speed or quick turning, a supplementary variable should be elaborated to evaluate speed habits only during cornering events.

Speed is an aggravating variable for most road events. It increases wheel axle accelerations and therefore the loads on the vehicle during maneuvers and obstacles. It is indirectly linked to the command of the driver, unlike vehicle acceleration and deceleration. Hence, acceleration quantiles are more efficient as explanatory variables for the sportiness and propensity to quick turning of drivers.

However, the severity of a driver on road obstacles also corresponds to their propensity to avoid them or hit them differently. Speed quantities in themselves do not inform us on the acceleration and braking habits of the driver either, unlike acceleration quantities, which in turn do not inform us on the cruising speed practiced by the driver.

V.3.4 Population analysis

Like in the previous statistical analysis, in §IV.4.3, the analysis of individual aims to identify the existence of homogeneous sub-populations and of outliers in the population of interest.

V.3.4.1 Driver clusters

Let us denote B the rotation matrix allowing transfer between the base of the original scaled variables and the base built by the PCs:

$$B = (x_{hk})_{(h,k)\in[\![1,\kappa]\!]^2} \tag{V.3.12}$$

The coordinates of each individual c in the base built by the PCs is given by:

$$\overrightarrow{S}_c = \sqrt{\Lambda} \cdot B \cdot^T \left(\overrightarrow{M}_c\right) \tag{V.3.13}$$

denoting $\sqrt{\Lambda} = \text{Diag}\left(\sqrt{\lambda_h}\right)_{h\in[\![1,\kappa]\!]}$ the diagonal matrix containing all square roots of the eigenvalues.

Let us determine an adequate number of sub-populations to partition the dataset through HCPC. The distances between individuals are calculated in the principal space restricted to the 5 first PCs out of 26, enough to capture 93% of the total dataset variance.

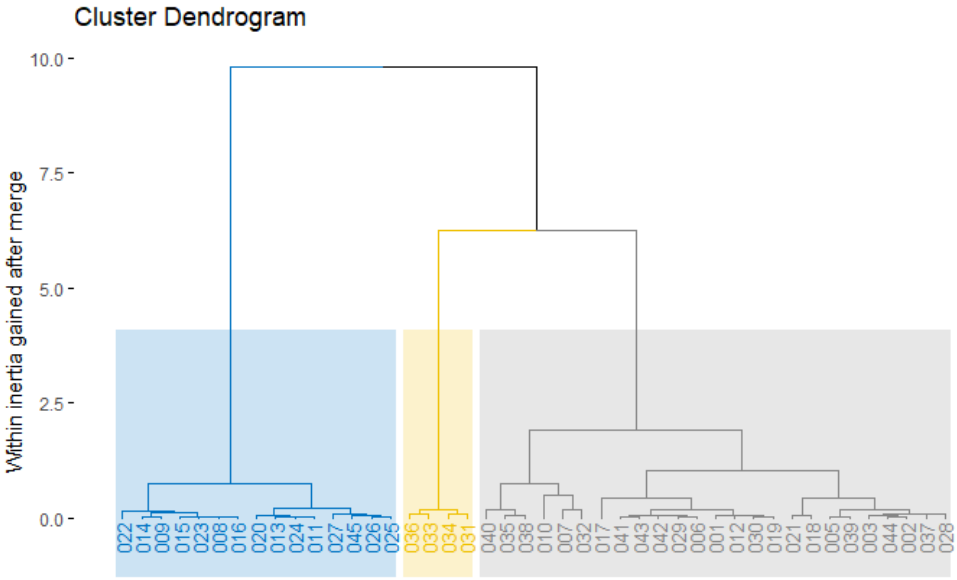

Fig. V.13: Cluster dendogram following hierarchical clustering on dataset $\mathcal{C}'_{\mathcal{T}_1}$ on campaign US18-DT1. The indices at each branch of the first floor are driver indices. The top of the colored zones correspond to the advocated cut, preceding the maximum value of a Lance-Williams dissimilarity (Ward criterion, see §V.3.4.1).

Fig. V.13 shows the dendogram of intra-cluster inertia gain at merge for different numbers of cuts in the agglomerative hierarchical clustering. Following the Ward method, a number of clusters of $n_s = 3$ is proposed.

The final clustering is performed through the application of k-means with a parameter k=3. Fig. V.14 shows the observation cloud on the two first principal planes. The coordinates of each driver are calculated using Eq. V.3.13. Each driver is associated with their cluster. We observe again that the clusters mostly distinguish themselves from each other as per their global severity.

The third cluster on the right corresponds to drivers that are more globally severe than the rest of the population. They seem to represent a small fraction of the sample (18%), smaller than the fraction of the third cluster following MFA on the full dataset $\mathcal{C}$ (30%). Indeed, the chosen trip may have given some drivers more occasions to be more severe than the rest of the population.

V.3.4.2 Cluster normality test

Similarly to the analysis of driver severity per kilometer in §IV.4.3.2, let us consider each cluster separately and check for their normality, *i.e.* whether it is a good hypothesis to associate the conditional severity of drivers in a cluster to a multivariate Gaussian variable.

Fig. V.15 displays the multi-normal QQ plot with Mahalanobis distances calculated from the three first principal coordinates of each individual of the second and third cluster. Two individuals out of 8 fall out of the confidence interval bounds. These two individuals, driver

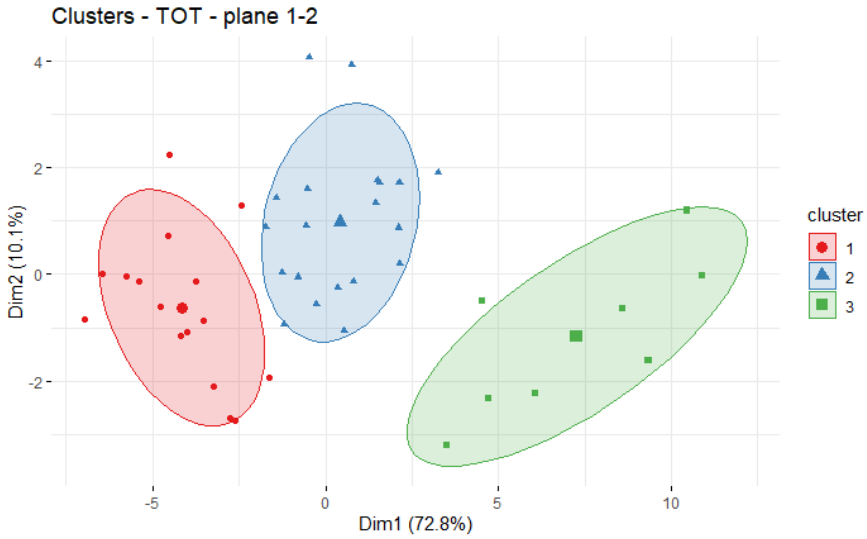

(a) First plane (second PC on y-axis)

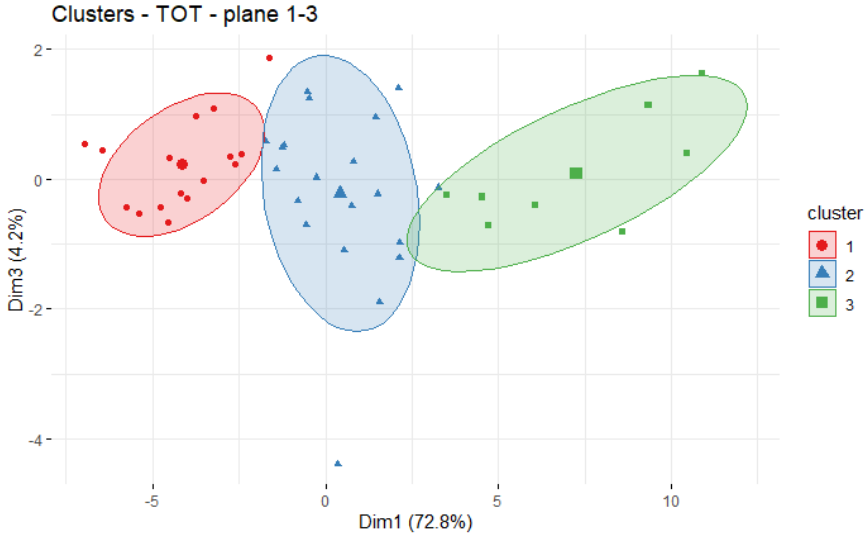

(b) Second plane (third PC on y-axis)

Fig. V.14: Cloud of individuals observed in the first and second principal planes of the PCA on dataset $\mathcal{C}'_{\mathcal{T}_1}$.

035 and 038 (only the latter is displayed in Fig. V.15b), lie somewhere between the center of the second and the third cluster in the first principal planes.

These two outliers of the third cluster question the artificial frontier that we propose here between both sub-populations. More samples would be required to ensure or root out the existence of distinct sub-populations for aggregated trips. However, in the next section, we will implement a statistical procedure that is robust to these in-between individuals to determine an appropriate distribution of the population and a good estimation of the proportion of each sub-population.

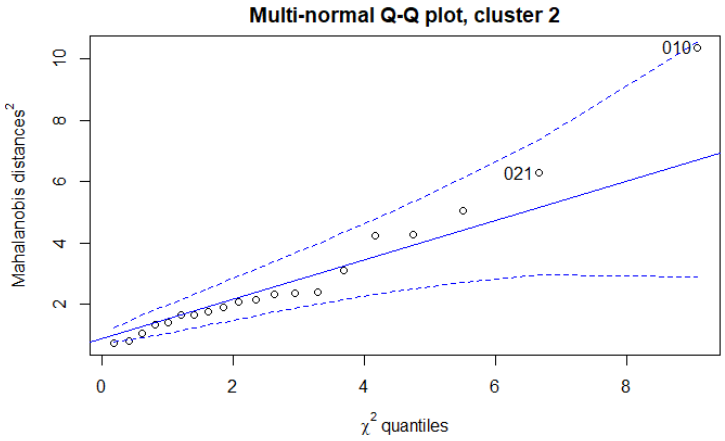

(a) 16 individuals of the second cluster

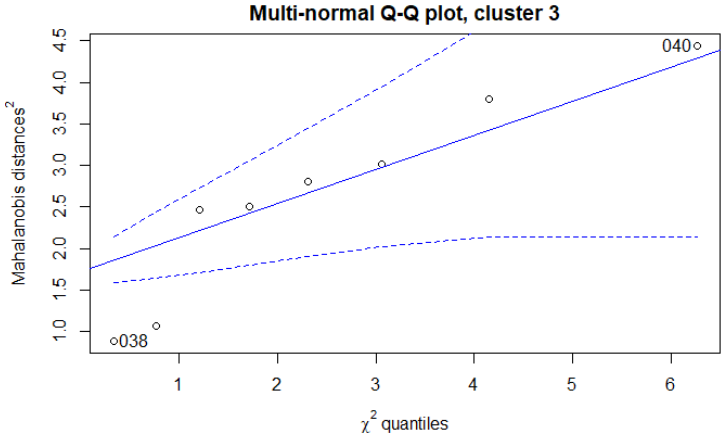

(b) 8 individuals of the third cluster

Fig. V.15: Multivariate QQ-plot for the individuals of the second and third cluster of driver pseudo-fatigue for dataset $\mathcal{C}'_{\mathcal{T}_1}$, described only by their coordinates on the 3 first PCs

V.4 Population distribution

V.4.1 Intrinsic versus conditional severity

In order to elaborate a distribution of our variables of interest over the restricted population of missions of the vehicle, we have to determine an adequate random experiment with respect to the inherent variability of the population.

This step marks the separation between exploratory analyses and building a distribution for the population of interest. Different choices for a model lie before us, as well as different paradigms in terms of random experiments. Let us enumerate five different modeling strategies. Each has its own mathematical relevance, feasibility and physical meaning.

The state-of-the-art of the distribution of pseudo-fatigue consists in observing the values of each variable individually and build as many univariate distributions as there are local

contexts. These distributions would not be connected by any mean. Instead, we want to elaborate a random experiment in which a mission is drawn from the population and directly determines the full vector of magnitudes that it induces.

The second strategy follows the elaboration of the full dataset on load intensities on the segmented trip of US18-DT1. The random experiment consists in drawing random vectors of load intensities. The model of the population is given by the three clusters determined in §IV.4.3: the distribution would be a multivariate Gaussian mixture with 3 cores in $\kappa \cdot r$ dimensions. However, the covariance matrix for each core needs to represent adequately the empirical correlations between load intensities, and this constraint must be input to the resolution.

Third, the variability of drivers is given by their intrinsic severity, defined as the first PCs following MFA on the whole dataset. Therefore, we can choose to draw random intrinsic severities instead of load intensities, *i.e.* elaborate a distribution of intrinsic severity as a Gaussian mixture with three cores. The load intensity vector for each drawn driver can be determined by transposing the rotation matrix, containing the coordinates of each PC following MFA. The mathematical formulation of this transposition will indirectly be apparent from the development of the fifth proposition in this section.

However, the distribution of each magnitude would have to be determined through a non-linear transformation of the Gaussian mixture on intrinsic severity. Such calculations were not conducted to their end. They would also impede us from finding an analytical solution to the 1D Stress-Strength Interference problem in the next chapter, because the resulting distribution would not be a Gaussian mixture.

A fourth strategy is to consider the observations of the magnitudes induced by each driver at the end of an aggregated trip to be the result of a random experiment. After building the dataset $\mathcal{C}_{\mathcal{T}_1}$ for the aggregated trip, a model for the random variable corresponding to the magnitude vector $\overrightarrow{M}$ is sought as a Gaussian mixture of 3 cores in κ dimensions. Again the empirical correlations between all magnitudes should be compatible with the coefficients of the covariance matrix of each core.

The fifth and final strategy will be the one implemented in this section and guarantees that these correlations will be maintained in the resulting distribution. The previous Section V.3 led to the definition of a conditional driver severity for a given aggregated trip. This is considered to be the main random element underlying pseudo-fatigue over our restriction of missions. In the next paragraph, we will build a distribution of this conditional driver severity

V.4.2 Model determination

Let us determine a distribution of the conditional severity of drivers of the base population - drivers of the state of Michigan - from the observations obtained on the 44 drivers of $\mathcal{C}'_{\mathcal{T}_1}$.

We make the hypothesis that the probability distribution underlying conditional severity for the aggregated trip $\mathcal{T}_1$ is best modeled by a multivariate Gaussian mixture with $n_s = 3$ cores (for three clusters). We have chosen to describe the conditional severity of a driver on $n_b = 5$ PCs, as it covers 94% of the variance of the dataset $\mathcal{C}_{\mathcal{T}_1}$. Therefore we seek a

density function defined over the space $\mathbb{R}^{n_b}$. Instead of relying on the conclusion of HCPC with respect to the number n_s of sub-populations to consider, this parameter could also be determined by minimizing an information criterion (Akaike (AIC) or Bayesian (BIC)) [Burnham and Anderson 2004]. We have not conducted this optimization.

The sought parameters of such a distribution are the proportion associated with each core $\vec{\pi} = (\pi_y \in [0,1])_{y\in[\![1,3]\!]}$, the coordinates of each core center (or mean vector) $U = (\vec{\mu}_y \in \mathbb{R}^5)_{y\in[\![1,3]\!]}$ and the covariance matrix associated with each core $\vec{\Sigma} = \left(\Sigma_y \in \mathbb{R}^{5^2}\right)_{y\in[\![1,3]\!]}$. The density function is given by:

$$f_1\left(\vec{S}\right) = \sum_{y=1}^{3} \pi_y \cdot f\left(\vec{S} \mid \vec{\mu}_y, \Sigma_y\right) \quad \forall \vec{S} \in \mathbb{R}^5 \tag{V.4.1}$$

$$= \sum_{y=1}^{3} \frac{\pi_y}{\sqrt{(2\cdot\pi)^5 \cdot |\Sigma_y|}} \cdot \exp\left(-\frac{1}{2} \cdot {}^T\left(\vec{S} - \vec{\mu}_y\right) \cdot \Sigma_y^{-1} \cdot \left(\vec{S} - \vec{\mu}_y\right)\right) \tag{V.4.2}$$

denoting $\vec{S}$ a vector in the space of conditional severity; $|\Sigma_y|$ the determinant of the covariance matrix Σ_y; f the generic density function associated with a multivariate Gaussian random variable and π the number pi. Note that the symbol for a fraction π_y, used in the formula for a Gaussian mixture, always has an index in this manuscript, or an arrow for the vector of all fractions $\vec{\pi}$.

The best fit for the parameters $\left(\vec{\pi}, U, \vec{\Sigma}\right)$ of the models is sought by maximizing a log-likelihood function, trying different values of model parameters against the observed values.

In our case, the labelling of the observations is unknown: it is a latent variable. In order to solve this maximization problem, we implement the Expectation-Maximization (EM) algorithm [Dempster *et al.* 1977; G. McLachlan and Peel 2000]. In this iterative procedure, a conditional formula for the log-likelihood is determined at each step from the temporary values of the parameters (proportion, center and covariance).

For each step w of the algorithm, let us denote C_w the random variable of dimension 1 associated with drawing one of the 3 sub-populations with probabilities $\vec{\pi}_w$:

$$P\left(C_w = y\right) = \pi_{w,y} \tag{V.4.3}$$

This probability is conditional to the values of the parameters of the model at the step w.

Let us denote $\mathbb{I}_w^C$ the binary random variable of dimension 3 such that each observation c is associated with a vector $\mathbb{I}_{w,c}^C$ containing zeros save for the y-th coordinate if the observation belongs to the y-th sub-population:

$$P\left(\mathbb{I}_{w,y}^C = 1\right) = \pi_{w,y} \tag{V.4.4}$$

$$P\left(\mathbb{I}_{w,y}^C = 0\right) = 1 - \pi_{w,y} \tag{V.4.5}$$

At each step w, the likelihood and log-likelihood for a set of parameters $\left(\vec{\pi}_w, U_w, \vec{\Sigma}_w\right)$, calculated over dataset $\mathcal{C}'_{\mathcal{T}_1}$ and labelling $\mathbb{I}^C_{w,\bullet}$, are given by:

$$\mathcal{L}\left(M_{\bullet\bullet}, \mathbb{I}^C_w \mid \vec{\pi}_w, U_w, \vec{\Sigma}_w\right) = \prod_{c=1}^{n_c} \prod_{y=1}^{3} \left(\pi_{w,y} \cdot f\left(\vec{S}_c \mid \vec{\mu}_{w,y}, \Sigma_{w,y}\right)\right)^{\mathbb{I}^C_{w,c}} \tag{V.4.6}$$

$$\log \mathcal{L}\left(M_{\bullet\bullet}, \mathbb{I}^C_w \mid \vec{\pi}_w, U_w, \vec{\Sigma}_w\right) = \sum_{c=1}^{n_c} \sum_{y=1}^{3} \mathbb{I}^C_{w,c} \cdot \left(\log\, \pi_{w,y} + \log\, f\left(\vec{S}_c \mid \vec{\mu}_{w,y}, \Sigma_{w,y}\right)\right) \tag{V.4.7}$$

Let us denote $\epsilon_y\left(\vec{S}\right)$ the responsibility of the core y on the observation $\vec{S}$. It is the posterior probability that this given observation stems from the y-th sub-population;

$$\epsilon_{w,y}\left(\vec{S}\right) = P\left(C_w(x) = y \mid x = \vec{S}\right) = \frac{\pi_{w,y} \cdot f\left(\vec{S} \mid \vec{\mu}_y, \Sigma_y\right)}{\sum_{i=1}^{3} \pi_{w,i} \cdot f\left(\vec{S} \mid \vec{\mu}_i, \Sigma_i\right)} \tag{V.4.8}$$

The "E" step of the EM-algorithm stands for expectation. It consists in writing the conditional expectation for the log-likelihood given the parameters at the step w.

$$\begin{aligned} \log \mathcal{L}\left(M_{\bullet\bullet}, \mathbb{I}^C_{w+1} \mid \vec{\pi}_w, U_w, \vec{\Sigma}_w\right) &= E_{\mathbb{I}^C_w}\left[\log \mathcal{L}\left(M_{\bullet\bullet}, \mathbb{I}^C_w \mid \vec{\pi}_w, U_w, \vec{\Sigma}_w\right)\right] \\ &= \sum_{c=1}^{n} \sum_{y=1}^{3} \epsilon_{w,y}\left(\vec{S}_c\right) \cdot \left(\log\, \pi_{w,y} + \log\, f\left(\vec{S}_c \mid \vec{\mu}_{w,y}, \Sigma_{w,y}\right)\right) \end{aligned} \tag{V.4.9}$$

The "M" step stands for maximization and consists in finding the new parameters that maximize Eq. V.4.9. They are given by:

$$n_y = \sum_{c=1}^{n} \epsilon_{w,y}\left(\vec{S}_c\right) \quad \forall y \in [1,3] \tag{V.4.10}$$

$$\pi_{w+1,y} = \frac{n_y}{n} \tag{V.4.11}$$

$$\vec{\mu}_{w+1,y} = \frac{1}{n_y} \cdot \sum_{c=1}^{n} \epsilon_{w,y}\left(\vec{S}_c\right) \cdot \vec{S}_c \tag{V.4.12}$$

$$\Sigma_{w+1,y} = \frac{1}{n_y} \cdot \sum_{c=1}^{n} \epsilon_{w,y}\left(\vec{S}_c\right) \cdot \left(\vec{S}_c - \vec{\mu}_{w+1,y}\right) \cdot {}^T\left(\vec{S}_c - \vec{\mu}_{w+1,y}\right) \tag{V.4.13}$$

denoting n_y the expected number of individuals from the original dataset (n_y out of n) to be associated with the y-th sub-population.

The initialization of the algorithm is taken as the mean estimator of both proportions, centers and covariance matrices of all clusters from observed variables from the dataset $\mathcal{C}'_{\mathcal{T}_1}$, determined through the implementation of HCPC in §V.3.4.1:

$$\pi_{0,y} = \frac{\text{Card}\,(C_y)}{n} \quad \forall y \in [1,3] \tag{V.4.14}$$

$$\mu_{0,y,k} = \frac{1}{\text{Card}\,(C_y)} \sum_{c \in C_y} S_{c,k} \quad \forall y \in [1,3],\ \forall k \in [\![1,\kappa]\!] \tag{V.4.15}$$

$$\Sigma_{0,y,k,h} = \frac{1}{\text{Card}\,(C_y)} \sum_{c \in C_y} (S_{c,k} - \mu_{0,y,k}) \cdot (S_{c,h} - \mu_{0,y,k}) \quad \forall y \in [1,3],\ \forall\,(k,h) \in [\![1,\kappa]\!]^2 \tag{V.4.16}$$

denoting C_y the set of individuals in the y-th cluster; Card (C_y) the number of observations associated with the y-th cluster by the k-means algorithm; n the total number of individuals in the dataset; $S_{c,k}$ the k-th component of severity for the c-th driver.

Note that the k-means associated a cluster to each observation, while in the EM algorithm we are interested in the probabilities that each observation has to stem from the underlying sub-populations. This explains the different formulas between the expected number of individuals in each sub-population at each step (Eq. V.4.10) (n_y) and the observed number of individuals following a clustering algorithm (Eq. V.4.14) (Card (C_y)).

The series of estimations for the parameters converges towards the maximum likelihood as explained in [Dempster *et al.* 1977]. The algorithm checks for convergence of the parameters at the end of the "M" step, with a criterion of 10^{-8} on the Euclidian difference in parameters between two iterations. For our example, the algorithm converged in 42 steps.

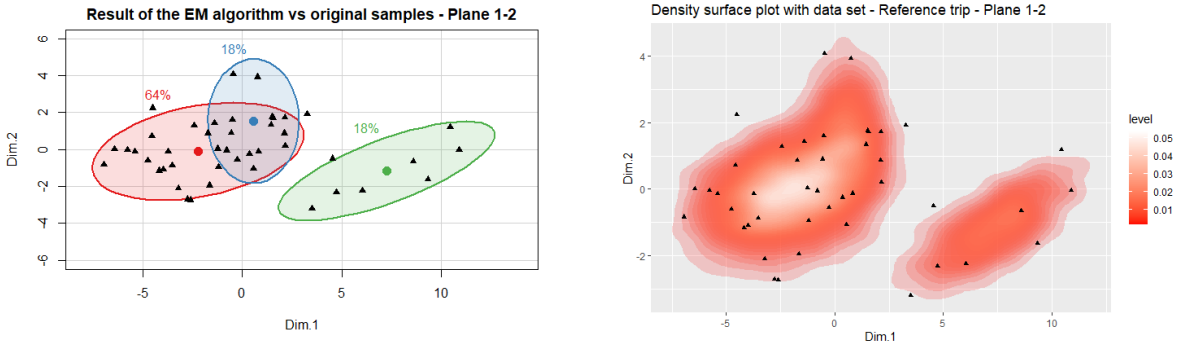

(a) Ellipses associated with each core of the mixture

(b) Mixture density

Fig. V.16: Mixture model, visualized on the first principal plane, obtained after application of the EM algorithm to determine an optimal distribution of driver severity over 5 principal axes on dataset $\mathcal{C}'_{\mathcal{T}_1}$. The projections of the three Gaussian cores of the mixture on the first principal plane are here represented as ellipses. The numbers correspond to the proportion of each core in the mixture.

The result of the EM-algorithm is displayed in Fig. V.16 on the first principal plane and in Fig. V.17 on the second principal plane. The first graph shows the ellipses built from the statistical moments associated with each core. The second graph shows the total density function f_1 associated with the Gaussian mixture, projected onto each principal plane.

Note that unlike the k-means algorithm, the new tripartite partition at the end of the EM algorithm allows the two first sub-populations to overlap each other (this is the case on

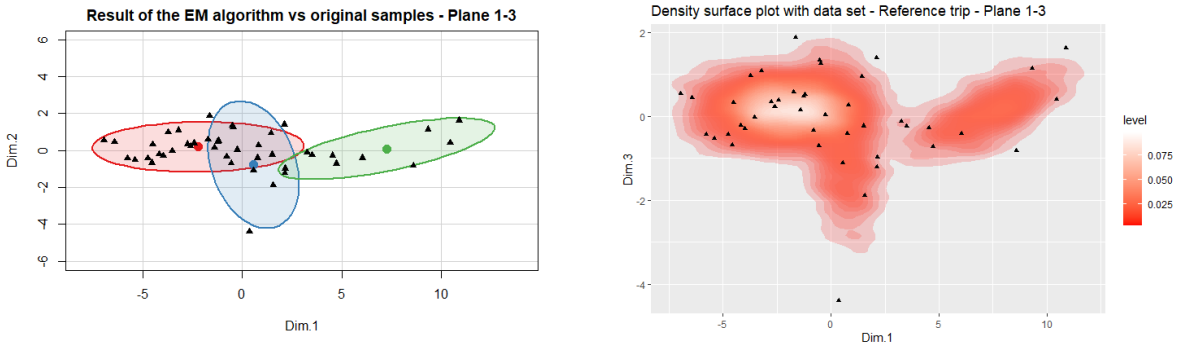

(a) Ellipses associated with each core of the mixture

(b) Mixture density

Fig. V.17: Mixture model, visualized on the second principal plane, obtained after application of the EM algorithm to determine an optimal distribution of driver severity over 5 principal axes on dataset $\mathcal{C}'_{\mathcal{T}_1}$. The projections of the three Gaussian cores of the mixture on the second principal plane are here represented as ellipses. The numbers correspond to the proportion of each core in the mixture.

all principal planes). This may seem daunting at first in terms of population segmentation. Yet it simply means that each driver of the original dataset has a nonzero probability to be associated with either cluster.

As per its construction, the k-means algorithm always establishes a partition into sub-populations that do not overlap. Indeed, each observation is always associated with the cluster with the nearest center. In light of our hypothesis that there are three homogeneous sub-populations of drivers, nothing forces these sub-populations to be separated in terms of conditional severity. Anyhow, neither algorithm can help us conclude whether the sub-populations of drivers are truly separated or not in the space of conditional severity.

V.4.3 Distribution of variables of pseudo-fatigue

We have determined a distribution of conditional severity on the five first principal axes of the PCA. At last, in this section, we explain how to translate this distribution of severity back into a distribution of the variables of pseudo-fatigue, for later use in Chapter VI.

Let us recall the link between the observation of the scaled variables $Z_{\bullet c}^{M,1}$ and of conditional severity $\overrightarrow{S}_c$ from Eq. V.3.13 through the transfer matrix B from Eq. V.3.12.

B is a rotation matrix. Its determinant is one and its columns are orthogonal. It is therefore invertible and its transposed matrix ${}^T(B)$ is also its inverse. For a given severity $\overrightarrow{S}$, the associated description in the space of scaled equivalent magnitudes is given by:

$$Z_{\bullet}^{M,1} = \Lambda^{-1/2} \cdot {}^T(B) \cdot \overrightarrow{S} \tag{V.4.17}$$

denoting $\Lambda^{-1/2}$ the diagonal matrix containing all coefficients $\lambda_h^{-1/2}$. The conditional severity of a driver is described only by the first five PCs. This corresponds to approximating

its coordinates on all other PCs by 0 for all drivers. In that case, the coordinates of the driver in the space of scaled equivalent magnitudes is approximately:

$$\begin{aligned} Z_{\bullet}^{M,1} &\approx \Lambda_5^{-1/2} \cdot {}^T(B_5) \cdot (S_h)_{h\in[1,5]} + {}^T\left(B_{(\kappa-5)}\right) \cdot \vec{0}_{(\kappa-5)} \\ &\approx {}^T(B_5) \cdot (S_h)_{h\in[1,5]} \end{aligned} \tag{V.4.18}$$

denoting B_5 the 5 by κ matrix containing the coordinates of the five first PCs in the space of base variables $\mathbb{R}^{\kappa}$; $\Lambda_5^{-1/2}$ a $5 \otimes 5$ diagonal matrix containing the 5 first eigenvalues of A_1; $B_{(\kappa-5)}$ the coordinates of the $\kappa - 5$ following PCs and B the square matrix $\begin{pmatrix} B_5 \\ B_{(\kappa-5)} \end{pmatrix}$.

Therefore, the knowledge of the coordinates of the first five PCs is sufficient to rebuild the vector of equivalent magnitude of any point in the space of conditional severity.

Let $\overrightarrow{M}_*$ be a unit magnitude vector corresponding to a projection direction in the space of absolute magnitudes. Let us determine the corresponding direction in the space of severity.

The vectors $\vec{0}$ and $\overrightarrow{M}_*$ in the space of absolute magnitudes are both scaled into $Z_{0\bullet}^{M,1}$ and $Z_{*\bullet}^{M,1}$ respectively, belonging to the space of scaled magnitudes. They both have a location, respectively $\overrightarrow{S}_0$ and $\overrightarrow{S}_*$ in the space of severity in 5 dimensions, given by:

$$\overrightarrow{S}_0 = \sqrt{\Lambda_5} \cdot B_5 \cdot Z_{0\bullet}^{M,1} \tag{V.4.19}$$

$$\overrightarrow{S}_* = \sqrt{\Lambda_5} \cdot B_5 \cdot Z_{*\bullet}^{M,1} \tag{V.4.20}$$

denoting $Z_{0\bullet}^{M,1}$ and $Z_{*\bullet}^{M,1}$ the scaled observations associated respectively to $\vec{0}$ and $\overrightarrow{M}_*$.

Let us define the unit vector $\delta\overrightarrow{S}$. It denotes a **severization** direction in the space of conditional severity. It is equal to the projection of the vector $\overrightarrow{M}^*$ onto the principal space restricted to the first five components:

$$\delta\overrightarrow{S} = \frac{1}{\left|\overrightarrow{S}^* - \overrightarrow{S}_0\right|} \cdot \left(\overrightarrow{S}^* - \overrightarrow{S}_0\right) \tag{V.4.21}$$

$$\delta\overrightarrow{Z} = \left(Z_{\bullet *}^{M,1} - Z_{\bullet 0}^{M,1}\right) \tag{V.4.22}$$

The projection of a multivariate Gaussian mixture on a single direction of the space $\mathbb{R}^{\kappa}$ is a Gaussian mixture. The means and variances of the cores of the univariate mixture are given by:

$$\forall y \in [1,3],\ \ \overrightarrow{\mu}_y|_{\delta\overrightarrow{S}} = {}^T(\delta S) \cdot \overrightarrow{\mu}_y \tag{V.4.23}$$

$$\forall y \in [1,3],\ \ \Sigma_y|_{\delta\overrightarrow{S}} = {}^T(\delta S) \cdot \Sigma_y \cdot \delta S \tag{V.4.24}$$

Let $k \in [\![1,\kappa]\!]$ be the index of a local context. Let $\overrightarrow{M}^*$, defined previously, now be an elementary vector $\overrightarrow{M}^* = \overrightarrow{e}_k$. We are therefore interested in the marginal law and distribution of the k-th magnitude over the population.

The density of the scaled magnitude $Z_{\bullet k}^{M,1}$ is given by:

$$\forall z \in \mathbb{R},\ \ f_1|_{\delta\overrightarrow{Z}}(z) = \sum_{y=1}^{3} \frac{\pi_y}{\sqrt{2 \cdot \pi \cdot \Sigma_y|_{\delta\overrightarrow{S}}}} \cdot \exp\left(\frac{\left(z - \overrightarrow{\mu}_y|_{\delta\overrightarrow{S}}\right)^2}{2 \cdot \Sigma_y^{-1}\big|_{\delta\overrightarrow{S}}}\right) \tag{V.4.25}$$

For all probability $P_{n,k} \in]0,1[$, any quantile of this magnitude can be obtained numerically, finding an approximation of the (unique) solution to the equation:

$$\text{We're looking for } q_{n,k} \ \text{ such that } \int_{z=-\infty}^{q_{n,k}} f_1|_{\delta\overrightarrow{Z}}(z)dz - P_{n,k} = 0 \tag{V.4.26}$$

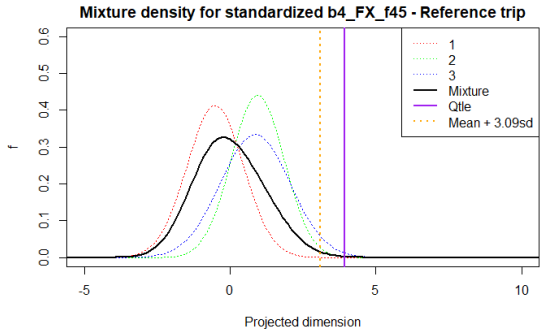

(a) Symmetrical longitudinal loads on the front axle

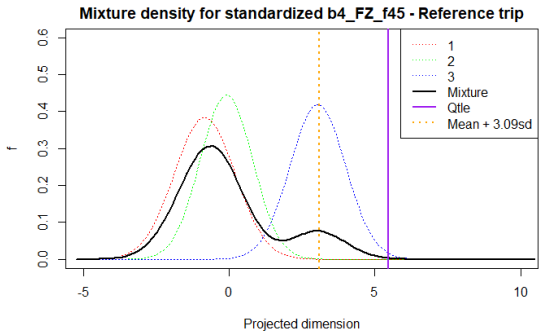

(b) Symmetrical vertical loads on the front axle, exponent of 4

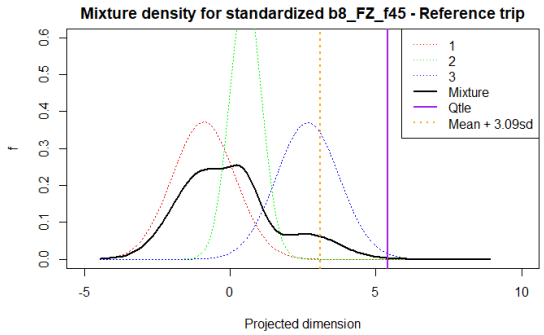

(c) Symmetrical vertical loads on the front axle, exponent of 8

Fig. V.18: Density associated with the marginal law of standardized magnitude following projection of the distribution of conditional severity over dataset $\mathcal{C}'_{\mathcal{T}_1}$ onto three local contexts. The colored Gaussian curves show the marginal density of each cluster once projected. The quantile is calculated on the mixture with a probability $P_{n,k} = 99.9\%$

Fig. V.18 shows the projected distributions for three local contexts: symmetrical braking with a Basquin $m = 4$ and symmetrical vertical loads on the front axle with Basquin exponents

$m = 4$ and 8. The densities are drawn both for each cluster and for the mixture. The quantile associated with a probability $P_{n,k} = 99.9\%$ is shown as a purple vertical line.

Note that for a Gaussian law, such a 99.9% quantile would be given by the empirical mean of the dataset plus 3.09 empirical standard deviations. The value is shown with an orange line on the graph. Assuming an estimation of the law's mean and standard deviation from the mean estimator on the observations, the comparison between the orange and the purple line determines which strategy leads to the most conservative quantile.

Another method to evaluate the relevance of a Gaussian approximation to obtain such a quantile is to calculate its confidence interval based on the number of observations of the dataset, following the method described in [Meeker *et al.* 2017] Appendix E. The calculation of such a confidence interval was not conducted in this thesis.

The cores of the projected mixture are well separated for magnitudes calculated from vertical (Z) load cases (Figs. V.19b and V.19c). Contrariwise, they are seemingly merged in the distribution of the magnitude calculated on the context $\gamma = \left(\widetilde{\alpha}_{Xf45}, 4\right)$, *i.e.* the magnitude induced on weld beads and spot welds by braking and acceleration events (Fig. V.19a).

Let us recall that different Basquin exponents attribute different weights to frequent, moderate loads versus rare, large load variations. The slight difference between the results on the same load case $Zf45$ between the Basquin exponents 4 and 8 may be interpreted as a general absence of large (maxi) loads in the least globally severe sub-population, while drivers in the second sub-population of the mixture consistently induce a reasonable level of infrequent large loads, albeit lower than the maxi loads of the third, most globally severe sub-population of drivers.

The transformation from standardized to absolute variable is given by inverting Eq. V.3.8. The density of the absolute variable M_k is given by:

$$\forall M \in \mathbb{R},\ \ f_1|_{\vec{e}_k}(M) = \frac{1}{\int_{-\infty}^{\infty} f_1|_{\delta\vec{Z}}\left(\frac{u-\overline{M}_k}{s_{M_k}}\right)} \cdot f_1|_{\delta\vec{Z}}\left(\frac{M-\overline{M}_k}{s_{M_k}}\right) \tag{V.4.27}$$

The $P_{n,k}$-quantile of the absolute magnitude can be calculated simply from descaling $q_{n,k}$:

$$q'_{n,k} = \overline{M}_k + s_{M_k} \cdot q_{n,k} \tag{V.4.28}$$

Fig. V.19 shows the distribution of the magnitude M_k after anonymization by the total charge of the vehicle, Q_{tot}. The comments that were made on the previous graphs still hold, because descaling these magnitudes is a linear operation.

The determination of the parameters for a distribution of each magnitude, from the observations of the dataset $\mathcal{C}'_{\mathcal{T}_1}$, and the calculation of any quantile of such a distribution will be useful to the determination of design and validation objectives for the design of single local contexts in Chapter VI.

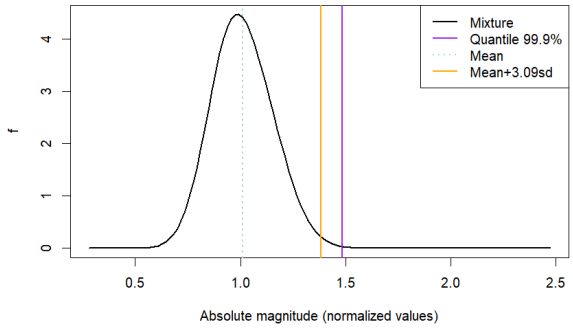

(a) Symmetrical longitudinal loads on the front axle

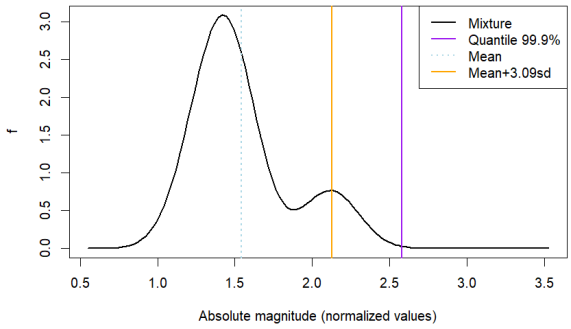

(b) Symmetrical vertical loads on the front axle, exponent of 4

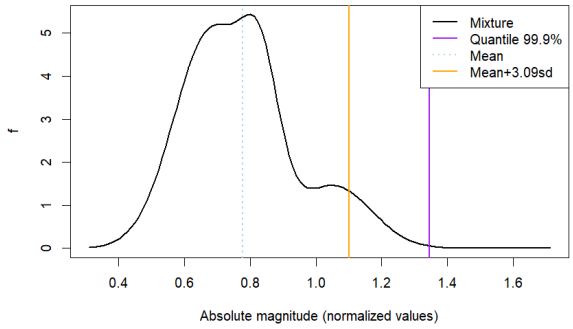

(c) Symmetrical vertical loads on the front axle, exponent of 8

Fig. V.19: Density associated with the marginal law of absolute magnitude following projection of the distribution of conditional severity over dataset $\mathcal{C}'_{\mathcal{T}_1}$ onto three local contexts. The quantile is calculated on the mixture with a probability $P_{n,k} = 99.9\%$

V.5 The choice of an aggregated trip

By defining an aggregated trip in §V.3.1, we have introduced a restriction on the population of trips of the vehicle models. In order to use the new distribution of pseudo-fatigue to determine necessary conditions for the respect of requirements in reliability, we must ensure that such a restriction yields conservative results.

We need to shed some lights on criteria that may determine whether the results of an analysis are indeed conservative for the sake of reliable design. Eventually, in the next chapter, adequate validation objectives are defined in terms of pseudo-fatigue to induce on a prototype in a trial. One very important family of attributes needed to determine such objectives is the values of very large quantiles of each magnitude.

Therefore, in this section, we will compare such large quantiles of magnitudes on all contexts for different choices of aggregated trips. If the distribution of these magnitudes is alleged to be Gaussian, such quantiles can be determined from the knowledge of magnitude mean and standard deviation, or mean and variation coefficient. If this distribution is not Gaussian, as is our case, we will need to find each quantile numerically on an appropriately projected scalar distribution.

V.5.1 Alternative trip

We do not have access to a survey of trip composition for whole vehicle lives. Let us make assumptions on alternative plausible aggregated trips.

Allegedly, the original composition of the aggregated trip $\mathcal{T}_1$ used in the measurement campaign US18-DT1 corresponds to a representative trip in the life of a vehicle in the region of Detroit.

However, it may have been designed to satisfy a broader range of requirements. One of them is the representativeness of road environments: did we drive long enough on damaged roads to have a proper evaluation of damaged road conditions in the region or even country of interest? Indeed, as observed in the separate analyses of each segment in Fig. IV.5, urban (C) and damaged (D) segments brought more dispersion among drivers. A longer observation on these segments would be needed to converge on an adequate dispersion. Likewise, as discussed in §IV.4.4.1, the dissimilarity between the two back road (B1 and B2) and highway (H1 and H2) segments observed in Fig. IV.28 question the acquisition of an average characterization of these two road environments.

Instead of being, as hypothesized, a representative trip, the measured trip of campaign US18-DT1 may actually be a compromise between the severity of the trip composition and an adequate sampling of the chosen road environments.

Once our objective becomes achieving a conservative evaluation of pseudo-fatigue from a single aggregated trip, a different mix of the measured road environments may be sought. The drivers sampled from the population may be judged on their simulated magnitudes on this alternative trip instead of the original measurement.

Let us consider two alternative trips for the following study. The first trip, denoted ALT, is a remixing of the original trip with more City and Damaged roads. Its distance in kilometers l_0 is the same as the original trip.

We may also want to design a vehicle model for a very specific market, like purely urban usage. In this case, the second trip, denoted URB contains a larger fraction of City and a low percentage of surrounding environments: freeway (H1) and suburbs (H2, B2). Fig. V.20 compares the composition of both alternative trips to the reference trip REF.

Let us discuss the duration of the alternative trip URB. Until now, we have always considered the lifetime objective to be expressed as a number of kilometers. However, in practice, the lifetime objective of a vehicle is the minimum value between a number of years and a driven distance. The requirement in reliability does not include missions that last more than the objective duration in years in the calculation of the risk of failure.

One should note that reaching the lifetime objective in a purely urban environment may take more years than the usual lifetime of a personal vehicle, except for taxis. Let us artificially decrease the lifetime objective for purely urban uses. We arbitrarily consider that:

$$l_f^C = 0.6 \cdot l_f \tag{V.5.1}$$

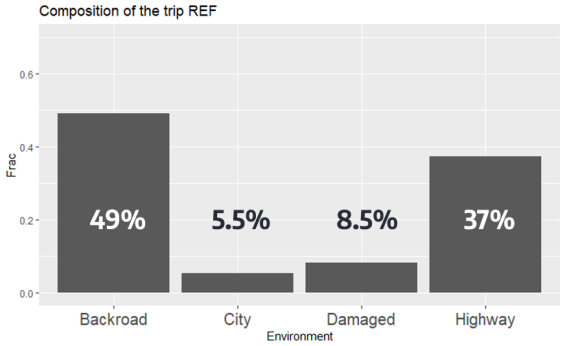

(a) Reference trip (245km)

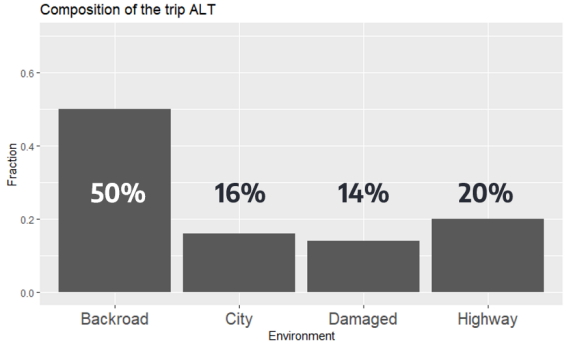

(b) Alternative trip (245km)

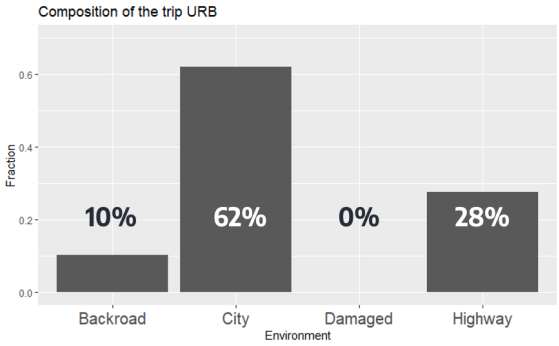

(c) Urban trip (145km)

Fig. V.20: Trip composition in terms of road environments for the reference trip of campaign US18-DT1 and for two alternative trips.

denoting l_f^C the adapted lifetime objective for vehicles destined to purely urban usage. In order to make sound comparisons between all trips, we consider the urban aggregated trip to be $l_0^C = 0.6 \cdot l_0$ kilometers long.

V.5.2 Comparison of pseudo-fatigue for different aggregated trips

The objective in this section is to illustrate the elaboration of a conservative restriction of the population to a single trip, by remixing the segments of the original measured trip.

The reference (REF), alternative (ALT) and urban (URB) trips are denoted $\mathcal{T}_1$, $\mathcal{T}_2$ and $\mathcal{T}_3$, each associated with composition vectors in kilometers $(l_e^{\mathcal{T}})_{e\in[\![1,r]\!]}$. Their composition vectors in percentage of total trip distance l_0 were shown in Fig. V.20.

The magnitudes induced at the end of each trip are simulated for each driver c following the method described in §V.3.1.1, using Eq. V.3.1:

$$\forall k \in [\![1,\kappa]\!],\ M\left(\gamma_k, \vec{\mathbf{F}}_{\mathcal{T}}^c\right) = \sqrt[m_k]{\sum_{e=1}^{r} l_r^{\mathcal{T}} L\left(\gamma_k, \vec{\mathbf{F}}_e^c\right)^{m_k}}$$

V.5.2.1 Comparison of empirical mean magnitudes

The average magnitudes $(s_{M_k})_{k\in[\![1,\kappa]\!]}$ predicted for each aggregated trip $\mathcal{T}$ are shown in Fig. V.21, in a normalized graph. The signature/reference, being a gray circle in this graph, was taken as the empirical mean of each magnitude on the original trip, here denoted REF. This signature vector was given by Eq. V.3.6.

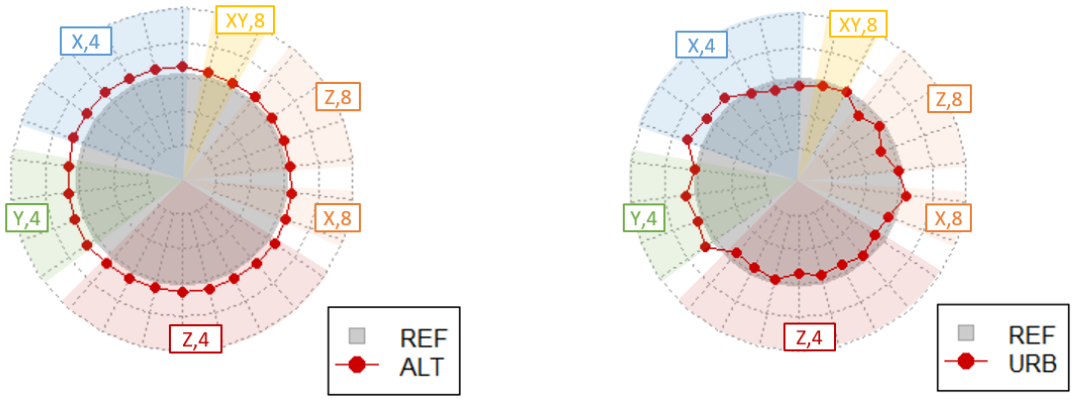

(a) REF vs ALT (b) REF versus URB

Fig. V.21: Comparison between the reference trip REF and two alternative trips in terms of empirical mean magnitudes over all drivers. Variables were normalized using the empirical mean vector from trip REF as denominators.

Note that despite being a shorter trip, the urban aggregated trip URB deals a reasonable amount of damage compared to our reference REF, as shown in Fig. V.21a. Indeed, urban environments contain more events per kilometer and are expected to induce considerably larger damage than mixed trips at equivalent distances, hence our caution with respect to its associated lifetime objective l_f^C for the aggregated trip in Eq. V.5.1.

The alternative trip ALT leads to a higher evaluation of the empirical mean magnitude on all contexts. This was expected from the increase of the fractions of urban and damaged road environments compared to the original mix (as seen in the trip composition histograms Fig. V.20).

Let us recall from §III.7.3 that four contexts out of the 26 here represented are associated with longitudinal loads (X) on each axle (front and rear): three with a Basquin exponent of 4 and one with an exponent of 8. The urban trip URB is only more damaging on the four contexts associated with longitudinal (X) loads on the front (f) axle, as well as on the contexts associated with lateral loads (Y). This result was expected as per the higher density of maneuvers in an urban environment.

V.5.2.2 Comparison of variation coefficients

Let us discuss the variability of magnitude vectors among our population of drivers for each aggregated trip. For each aggregated trip $\mathcal{T}$, for each component of magnitude vectors, the variation coefficient is defined as the ratio between standard deviation and empirical average:

$$v_k = \frac{\overline{M}_k}{s_{M_k}} \ \forall k \in [\![1,\kappa]\!] \tag{V.5.2}$$

Fig. V.22 shows the variation coefficients $(v_k)_{k\in[\![1,\kappa]\!]}$ for each aggregated trip.

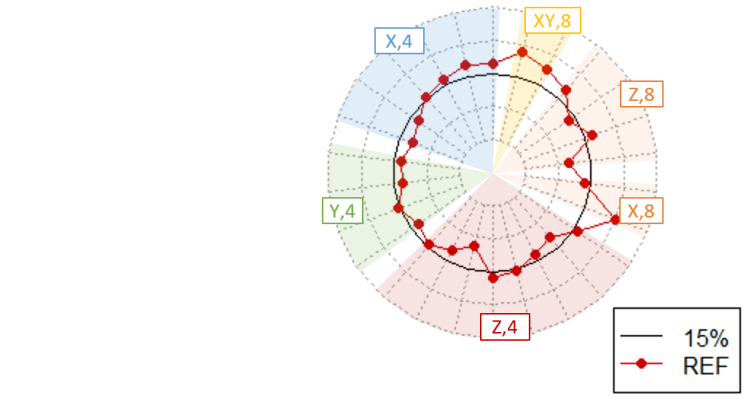

(a) Trip REF

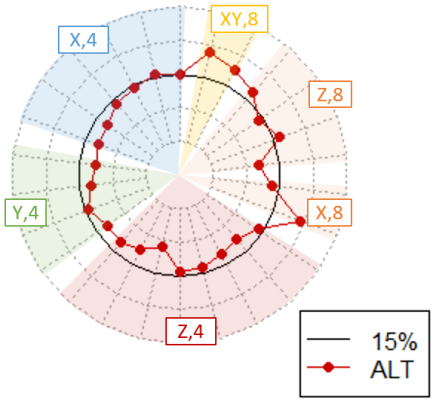

(b) Trip ALT

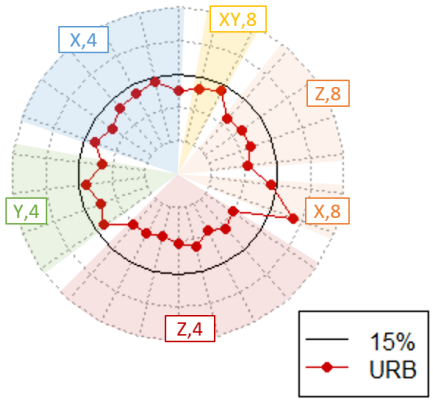

(c) Trip URB

Fig. V.22: Comparison between the reference trip REF and two alternative trips in terms of variation coefficient over all drivers. All radii have the same minimum and maximum limits: 0% and 30%.

The variation coefficient is a normalized measure of the variability of each marginal variable. It appears that the variability amongst drivers is slightly lower on all magnitudes on the alternative trip ALT than on the original trip REF (Figs. V.22b resp. V.22a). For instance, the variation coefficients calculated on contexts involving vertical (Z) load components on the front (f) axle and associated with a Basquin exponent of 4 show approximately 13% for the trip ALT, against 15% for the trip REF.

The variability on magnitudes is lower on the urban trip URB compared to the two other trips (Fig. V.22c), for instance 7.5% on most contexts associated with vertical loads and a Basquin exponent of 4. Indeed, this urban trip gives less importance to road sections with lower road quality. Therefore drivers may not distinguish themselves on their behavior against the kind of obstacles one meets on damaged roads. It is however interesting to note that the

variation coefficient on some of the contexts associated with maneuvers (X, Y on the front axle) stuck to values close to 13%.

If the market of a vehicle model is explicitly targeted toward urban uses, these variation coefficients show that the variability of the fatigue induced on local contexts that are sensible to vertical obstacles is largely diminished. However, this variability is maintained on the magnitudes associated with load cases that occur during maneuvers. Indeed the decisions of the drivers in terms of maneuver management will have a large impact on their loads in such an environment, whereas their specific behavior when encountering obstacles will not be challenged as often as a market targeted toward all kinds of trips.

V.5.2.3 Comparison of high quantiles of magnitudes

In a magnitude-per-magnitude unidimensional analysis, we are interested in high values of quantiles for each magnitude. If and only if the distribution of each magnitude is considered to be Gaussian, such quantiles would be acquired by combining the knowledge of empirical mean and variation coefficient using the following formula:

$$q\left(P_n,k\right)^{\mathcal{N}} = \overline{M}_k + \alpha_{P_n} \cdot s_{M_k} \quad \forall k \in [\![1,\kappa]\!] \tag{V.5.3}$$

denoting $\alpha_{P_n} = q\left(P_n\right)^{\mathcal{N}^0}$ the quantile of the standard normal distribution associated with the probability P_n.

In the general case, we need to determine a distribution of each magnitudes and find our quantile of interest numerically. Let us conduct the same modeling strategy as previously to determine the new stochastic model for driver severity on the alternative trips. We will then be able to project it back onto each magnitude.

The calculation of magnitudes induced by the observed drivers of campaign US18-DT1 on the aggregated trips REF, ALT and URB yields different datasets $\mathcal{C}_{\mathcal{T}_1}$, $\mathcal{C}_{\mathcal{T}_2}$ and $\mathcal{C}_{\mathcal{T}_3}$, each composed of $n = 44$ individuals for $\kappa = 26$ active variables. Each variable for each dataset is scaled accordingly and the scaled datasets may be analyzed through the application of PCA as in §V.3.3. The results of each separate analysis will be discussed in the next paragraph, §V.5.2.4.

Following the same procedure as previously, we determine an adequate number of sub-populations and an initial Gaussian mixture from the application of HCPC as in §V.3.4.1. The proposed partition still consists of 3 clusters. For each aggregated trip, we propose a multivariate Gaussian mixture with 3 cores over 5 dimensions as a model of the distribution of magnitudes over our population of drivers. The optimal distribution is obtained from the maximization of a log-likelihood just as in Eq. V.4.7, through application of the EM algorithm as presented in §V.4.2.

The three cores of the Gaussian mixture determined through the application of the EM algorithm for each aggregated trip are shown in Fig. V.23 on the first and second principal plane of each analysis.

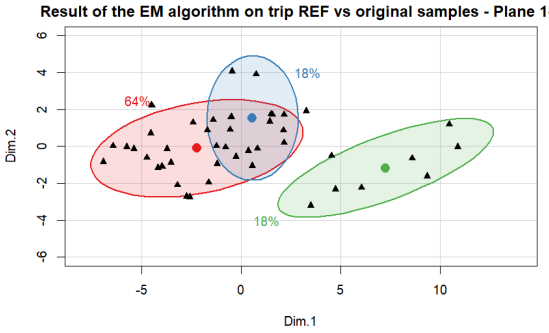

(a) Trip REF

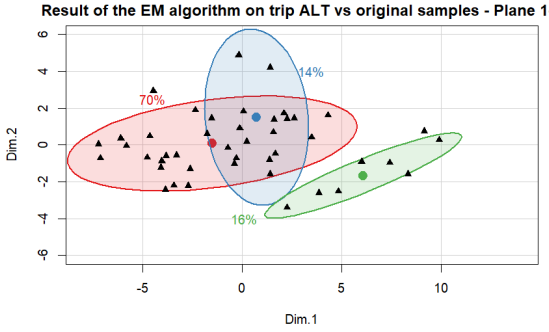

(b) Trip ALT

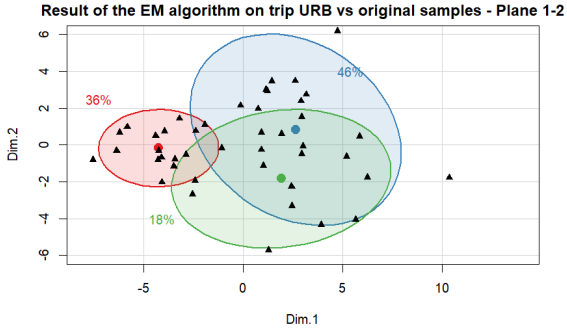

(c) Trip URB

Fig. V.23: Representation of the three cores of the Gaussian mixture associated with conditional severity, dimension 5, determined by application of an EM-algorithm for three different choices of an aggregated trip. Each mixture is shown in the first principal plane of the corresponding analysis. The black triangles represent the two first dimensions of the conditional severity of the drivers following simulation of their induced magnitudes on each aggregated trip.

The resulting distribution of conditional severity shown in Fig. V.23 for each alternative trip can be projected onto each magnitude following the method detailed in §V.4.3.

In a similar fashion as Fig. V.18, Fig. V.24 shows the comparison between the 99.9% quantile of the resulting distribution of one magnitude (solid line in purple) and the same quantile predicted from a Gaussian hypothesis on the total distribution (dotted line in orange).

The gap between the Gaussian prediction and the quantile calculated numerically from a Gaussian mixture model can be explained by the positive skewness of the distribution: its tail on the right-hand (severe) side is more elongated in the case of the reference trip REF as shown in Fig. V.24a. The third core of the mixture is apparent. On the alternative trip ALT, Fig. V.24b, the third core seems to be nearly merged with the two other cores. The skewness is reduced and so is the gap between both quantile prediction methods. The comparison between the two methods (Gaussian approximation and numerical computation) can be improved by calculating the confidence interval for these quantiles as explained in [Meeker *et al.* 2017].

The absolute values of the quantiles of each magnitude for all three aggregated trips are compared on a single absolute graph in Fig. V.25. The difference between these solid lines

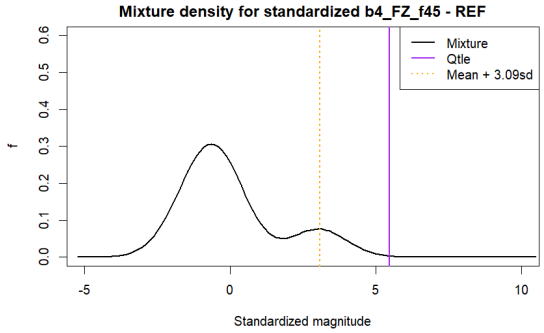

(a) Trip REF

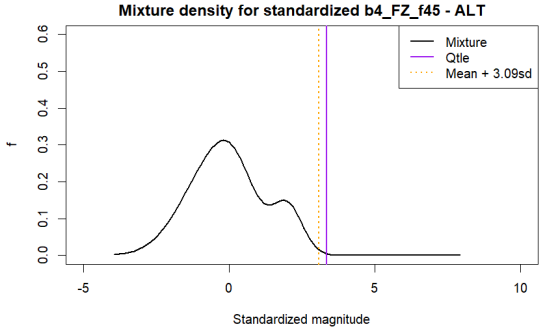

(b) Trip ALT

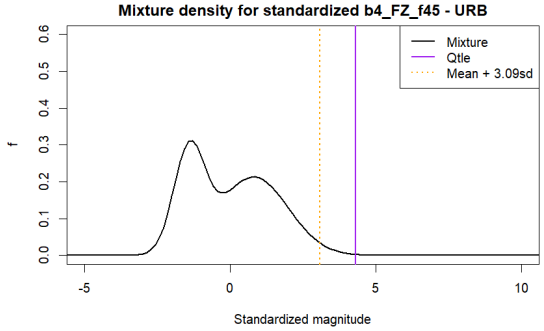

(c) Trip URB

Fig. V.24: 99.9% quantile of standardized magnitude obtained from the analysis on each aggregated trip on the magnitude calculated from in-phase (45) combination of vertical (Z) loads on the front (f) axle with a Basquin exponent of 4. The dotted line in orange represents the prediction of the same quantile following the hypothesis that the distribution of the magnitude would be Gaussian.

represent the effect of the choice of an aggregated trip on the prediction of a large quantile of the distribution for each magnitude.

We can see in Fig. V.25a that for the magnitude associated with in-phase (45) vertical (Z) loads on the front (f) axle calculated with a Basquin exponent of 4, the reference trip REF yields a more **conservative** quantile than the two alternative trips. Even if the alternative trip ALT corresponded to larger average magnitudes as per Fig. V.21, their magnitudes displayed reduced variability among all drivers, as shown in Fig. V.22. Therefore, the outskirts of the distribution of these magnitudes could be expected to lie closer to their mean, and a large quantile calculated on the alternative trip ALT may land below the quantile calculated on the reference trip REF. Both trips REF and ALT yield equivalent quantiles for the same magnitude calculated with a Basquin exponent of 8.

For magnitudes associated with longitudinal loads (X) on the front axle (f) calculated with an exponent of 4, however, the alternative ALT and urban URB trips yield a larger quantile than the reference trip. As a consequence, if those alternative trips are plausible, then the reference trip may be **non-conservative** for the reliable design of weld beads (exponent of 4) most sensible to decelerations and accelerations.

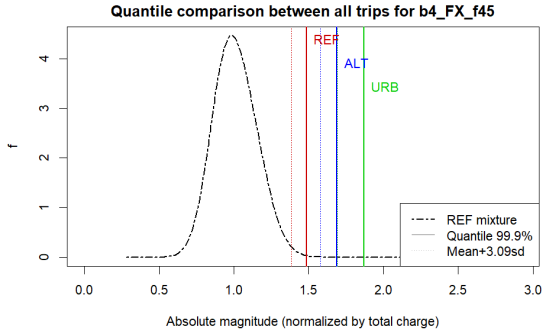

(a) In-phase longitudinal loads on the front axle, exponent of 4

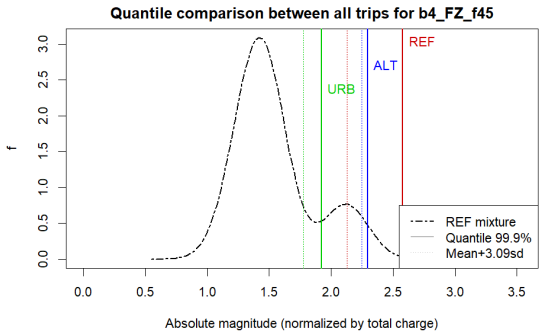

(b) In-phase vertical loads on the front axle, exponent of 4

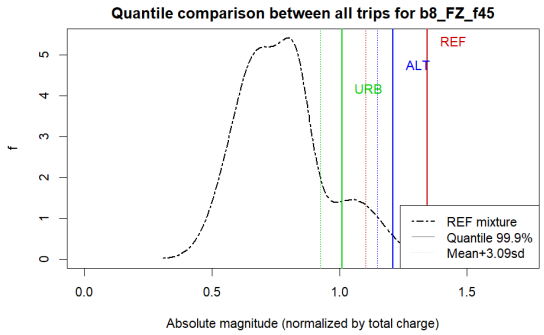

(c) In-phase vertical loads on the front axle, exponent of 8

Fig. V.25: Comparison of the 99.9% quantile of absolute magnitude calculated from the simulation of magnitudes induced by three different aggregated trips. The dotted lines represent the associated predictions of said quantiles under a Gaussian hypothesis. The absolute magnitudes were anonymized by the total charge of the vehicle, Q_{tot}

V.5.2.4 Most conditionally severe observed drivers

Let us discuss the shape of the population of drivers for each new aggregated trip. In this paragraph, we will be interested in the answer to these two questions:

- Who is the most severe driver for each choice of an aggregated trip?
- Could we predict a hierarchy between drivers on each aggregated trip, from the exploratory analysis of their load intensities and the definition of their intrinsic severity?

Fig. V.26 shows the correlation circle associated with the first principal plane for all aggregated trips REF, ALT and URB, following application of PCA on their associated scaled datasets $\mathcal{C}'_{\mathcal{T}_1}$, $\mathcal{C}'_{\mathcal{T}_2}$ and $\mathcal{C}'_{\mathcal{T}_3}$. Equivalent magnitudes calculated on the same load cases have similar correlations with the first and second PCs on all datasets. Thus the two first principal components can still be interpreted as conditional global severity and conditional sportiness following PCA for each new aggregated trip. Indeed the first principal component is a size effect in both datasets $\mathcal{C}'_{\mathcal{T}_2}$ and $\mathcal{C}'_{\mathcal{T}_3}$. The second principal component is positively correlated

to magnitudes associated with braking and cornering maneuvers, and negatively correlated to magnitudes associated with obstacles.

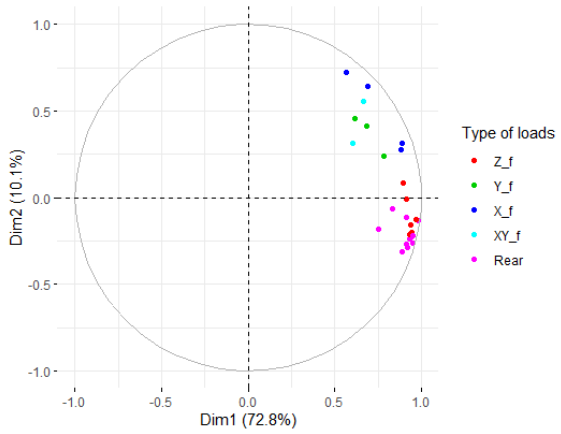

(a) First plane - Trip REF

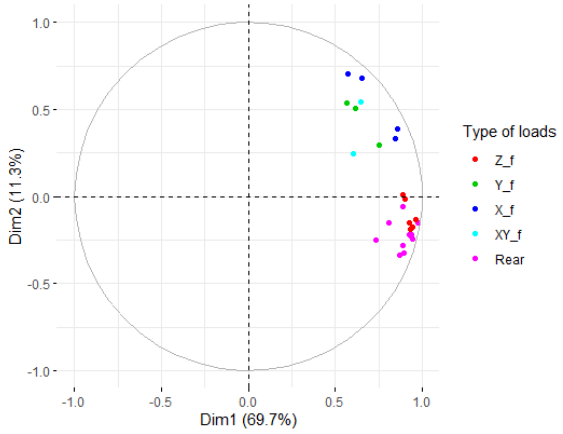

(b) First plane - Trip ALT

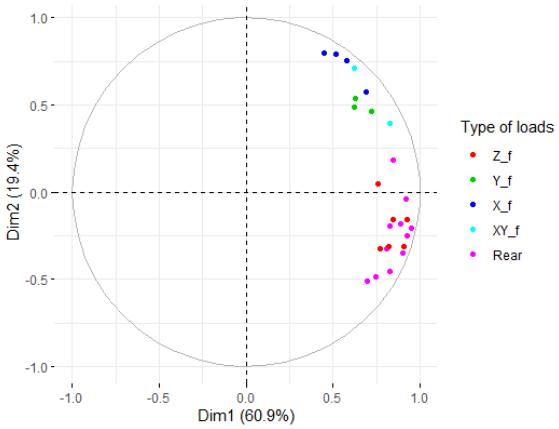

(c) First plane - Trip URB

Fig. V.26: Correlation circle over the first principal plane following PCA applied individually on the dataset associated with three different aggregated trips. Each magnitude is colored according to the global load components involved in the unit combination vector of the associated local context.

Fig. V.27 shows the correlation circles for each trip on the second principal plane. Note that the third principal component was inverted during the determination of the eigenvalues of the correlation matrix for the urban trip URB. However, this third component, associated with quick turning, remains significantly correlated, in absolute values, to contexts associated with lateral (Y) loads on the front (f) axle, *i.e.* trackers of more severe cornering events.

Differences in variance borne by each of these three first principal components mean that these driver traits have varying importance according to the actual composition of the trip. This conclusion is similar to what was observed on the separate analyses on each road segment of US18-DT1 in §IV.4.1.3: Drivers distinguish themselves in terms of pseudo-fatigue if and as many times as they have the opportunity (maneuvers, obstacles, traffic) to behave differently.

Let us compare the composition of the clusters on the first principal plane for each application of HCPC following the analysis of the datasets $\mathcal{C}_{\mathcal{T}_2}$ and $\mathcal{C}_{\mathcal{T}_3}$. Fig. V.28c shows the

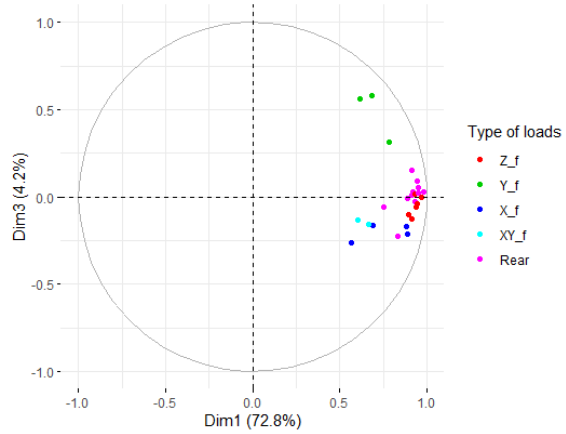

(a) Second plane - Trip REF

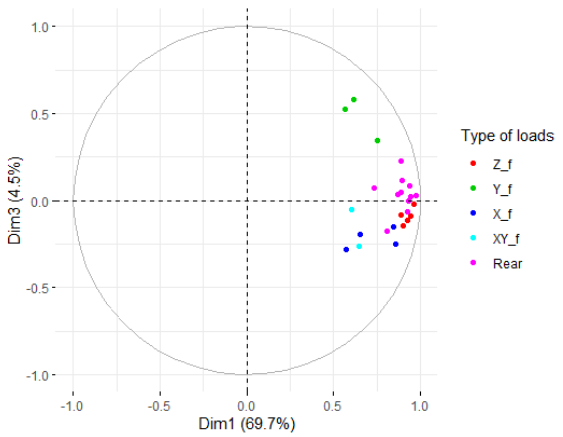

(b) Second plane - Trip ALT

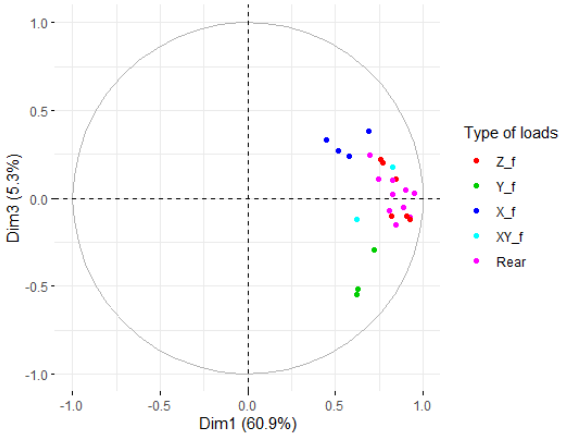

(c) Second plane - Trip URB

Fig. V.27: Correlation circle over the first principal plane following PCA applied individually on the dataset associated with three different aggregated trips. Each magnitude is colored according to the global load components involved in the unit combination vector of the associated local context.

resulting clusters and their associated classification of each driver. Let us display the labels of all drivers of the (green) cluster that has its centroid on the largest coordinate of global severity (Dim.1).

Note that when building each principal space, each dataset was scaled with different empirical average magnitudes and standard deviations. The numerical values of conditional severity do not mean the same thing from one graph to the other. Note also, as was observed following the application of the EM-algorithm in §V.4.2, that the cores of the distributions of conditional severity shown in Fig. V.23 will not match those given here by the implementation of HCPC.

The composition of the green cluster in terms of drivers did not change much from the reference trip REF to the alternative trip ALT. Driver 031 is the most globally severe driver. Its contender, Driver 034, displays a slightly larger positive difference on conditional sportiness (the second principal component) on the trip ALT than Driver 031.

However, the most globally severe driver on the alternative trip URB is Driver 039. Drivers

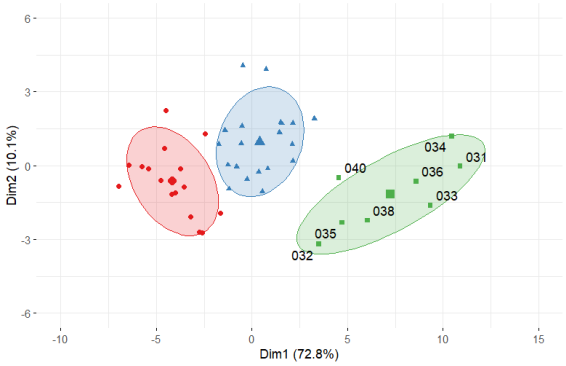

(a) First plane - Trip REF

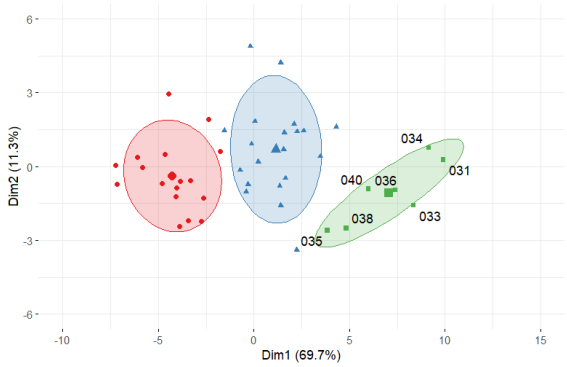

(b) First plane - Trip ALT

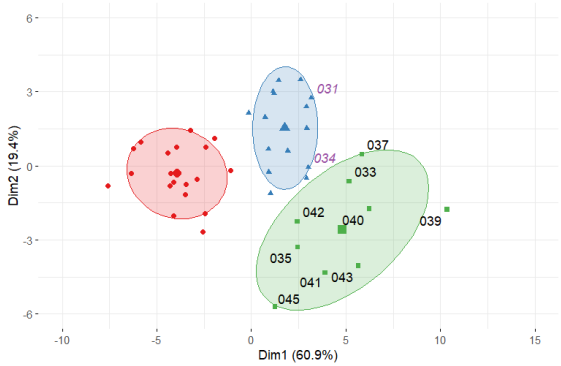

(c) First plane - Trip URB

Fig. V.28: Result of the application of HCPC on the dataset built from simulation of the magnitudes induced by all drivers of campaign US18-DT1 on each aggregated trip. Black labels are added to the drivers of the cluster that has the largest average conditional global severity (the first principal component). The labels of drivers 031 and 034 were added on the last graph for information

031 and 034 have much lower conditional global severities on this aggregated trip. The whole composition of this cluster is modified. While the green cluster is still associated with the most globally severe drivers, namely Driver 039, the blue and green clusters are no longer clearly separated on the dimension of global severity alone.

Therefore, the partition proposed in the exploratory analysis of driver load intensities on all road segments, in §IV.4.3, is not robust to the choice of an aggregated trip. This could be expected from the analysis of partial individuals in §IV.4.3.4. Driver behavior and road environments are interdependent. The most globally severe drivers on urban road environments are not necessarily the most globally severe on back roads and damaged roads.

V.5.3 Section perspective: including a sampling of trips to the model

We have defined a few different aggregated trips with arbitrary compositions: a reference trip corresponding to the original measurement, an alternative trip with more kilometers of the most damaging segments and an urban-exclusive trip. We have shown in this section that

this choice of an aggregated trip as a restriction of the population of trips leads to different models of the pseudo-fatigue induced by a population of drivers.

The determination of a most severe driver among a population (§V.5.2.4) or of an artificial quantile of each magnitude (§V.5.2.3) are both heavily impacted by this choice of an aggregated trip. Just as drivers have different global severity and sportiness on different road environments, the most severe quantiles of the population will not correspond to the same drivers from one choice of an aggregated trip to the next.

Aggregated trips may still yield lower absolute values of magnitude quantiles, if drivers induce more pseudo-damage in average but are not as spread out, as shown from the comparison of aggregated trips REF and ALT in §V.5.2.3.

We have also compared the determination of a quantile for each magnitude to its approximation in the hypothesis of a Gaussian distribution. The distribution of conditional severity determined once and for all for each aggregated trip can be projected onto each variable of interest and a quantile can be determined numerically at the desired probability. The choice of this probability for the sake of reliable design will be discussed in section VI.4.

An aggregated trip is, by definition, an aggregate of life situations that corresponds to the average composition of a vehicle life. These trips are random over the market of a vehicle model. Their variability and the extent of plausible trips should be included in the choice of an aggregated trip toward a conservative evaluation of the pseudo-fatigue induced in service.

Indeed, we could have imagined aggregated trips that are non-plausible for our vehicles, such as trips only composed of highway roads or damaged roads. Indeed four-wheel drives and other offroad vehicles fall out of the scope of our method, as they have a different design procedure and description of service than usual personal vehicles [Pinto Filho *et al.* 2003]. Perhaps even the three aggregated trips that we have proposed in this section were non-plausible.

From a model of the random composition of trips in the market of a vehicle model, the previous comparative analysis can be performed repetitively for a larger sample of trip compositions. Thus one will be able to find one or several adequate aggregated trips, yielding conservative models of pseudo-fatigue toward the reliable design of suspension and body components.

Note that drivers simulated on the urban trip URB were more damaging to local contexts that are sensible to braking and accelerating situations, and the reference trip REF was more damaging on other contexts. There might not be one single plausible trip composition that yields conservative results for all contexts.

V.6 Extrapolating trips to an objective lifetime

V.6.1 The issue: aggregated trips are short

Aggregated trip used in this method do not last a lifetime objective, denoted l_f in kilometers. Let us denote $l_0 = \sum_{e=1}^{r} l_e$ the total duration of the aggregated trip, $l_0 << l_f$.

The most usual extrapolation method to predict the pseudo-damage induced over a lifetime from a smaller measurement is direct extrapolation or simply cross-multiplication. This direct formula is written:

$$\breve{D}\left(\gamma_k, \vec{\overline{\mathbf{F}}}_c^{l_f}\right) = \frac{l_f}{l_0} \cdot \breve{D}\left(\gamma_k, \vec{\overline{\mathbf{F}}}_c^{l_0}\right) \quad \forall k \in [\![1,\kappa]\!] \tag{V.6.1}$$

denoting $\vec{\overline{\mathbf{F}}}_c^{l_0}$ the measured or simulated loading history on the aggregated trip, and $\vec{\overline{\mathbf{F}}}_c^{l_f}$ the alleged loading history for the whole life of the vehicle.

A first idea included in this direct extrapolation is that $\vec{\overline{\mathbf{F}}}_c^{l_f}$ is a replication of the measured loading history $\vec{\overline{\mathbf{F}}}_c^{l_f}$ for an adequate number of repetitions given by $\frac{l_f}{l_0}$ (not necessary an integer).

In Appendix B, we put forward arguments and a formula for an exact calculation of the pseudo-damage induced by a concatenation of loads. The deviation brought by the direct sum was observed to be important for the concatenation of proving ground tracks, not for the concatenation of service loads. We will not replace the direct formula of Eq. V.6.1 by the exact formula, Eq. B.7.6.

The second idea suggested by direct extrapolation is that the pseudo-damages induced by a driver will be the same for each repetition of the preset trip. This is similar to choosing aggregated trips that directly last a lifetime objective. This amounts to replicating the measured loads several times and is equivalent to using Eq. V.6.1 from a shorter trip. This hypothesis of invariant loads for each repetition of a trip should give us pause.

Let us take the example of potholes met repetitively throughout the life of a vehicle. The loads measured in service on a real pothole will vary from one repetition to the next, even if the driver constantly makes the same decision around it. In proving grounds, potholes are built with specific geometries to be reproducible. Even then, several runs are necessary to determine the true loads on a pothole.

One may object that the load variations (Rainflow ranges) induced by a pothole may vary homogeneously around a mean value. Therefore the deviation from the average encounter of a pothole may be curbed by the repetition of the aggregated trip. However, pseudo-damage is not a linear function of said range. A variation of δF in a Rainflow range leads to a variation in marginal pseudo-damage (Eq. II.5.10) of δF^m, m being the Basquin exponent. Small discrepancies above an average Rainflow range may cause large differences in predicted pseudo-damage and magnitude.

We propose a first approach to the extrapolation of induced pseudo-fatigue. We consider

the Rainflow matrix of an aggregated trip for each local context. These ranges are used to identify parameters of a spectrum model in §V.6.2. Then, the Rainflow matrix following repetitions of a trip are obtained using this spectrum model in §V.6.3.

The hypothesis of invariant loads for each repetition of a trip also questions the effect of random traffic, weather and the mood shifts of the driver. The effects of traffic and weather were already discussed in §IV.4.4.2. We have made the hypothesis that the aggregated trip corresponded to a specific restriction on the population of trips, and therefore contained its own constraints in terms of traffic and weather.

As for driver mood, we have discussed in §V.3.3 differences between drivers in terms of sportiness or propensity to quick turning. In practice, these traits may be variable over the life of a driver. This idea leads to a second proposition in §V.6.4, introducing another hypothesis on the variability in conditional severity for a given driver on a given aggregated trip.

V.6.2 Rainflow spectrum model identification

This preliminary section introduces the modeling of reverse cumulative range-only Rainflow matrices a.k.a. Rainflow spectra or fatigue load spectra for the characterization of automotive loads [Facchinetti 2018].

The use of Rainflow spectra in the literature for the durable and reliable design of automotive components is discussed further in §VI.2.1. We are here most interested in the idea that service loading histories may be expected to follow a typical distribution in terms of cumulative Rainflow ranges.

Let us focus on one local context $\gamma = \left(\widetilde{\overline{\alpha}},m\right)$ in the structure. In order to evaluate the pseudo-damage induced on that context, a Rainflow counting algorithm is applied on the scalar loading history $\widetilde{\overline{\alpha}} \cdot \vec{\mathbf{F}}$. The Rainflow algorithm was introduced in §II.5.1 and the definition of pseudo-damage in §III.5.2. The occurrences of Rainflow ranges are counted by class. The classed range-only Rainflow count following closure of the residual is given by Eq. II.5.3, that we recall here:

$$Rf\left(\widetilde{\overline{\alpha}} \cdot \vec{\mathbf{F}}\right) = \left(\Delta F_i, n_i(\widetilde{\overline{\alpha}} \cdot \vec{\mathbf{F}})\right)_{i \in [\![1,n_{\text{bin}}]\!]}$$

The load spectrum of $\widetilde{\overline{\alpha}} \cdot \vec{\mathbf{F}}$ is its reverse cumulative range-only Rainflow matrix:

$$Sp\left(\widetilde{\overline{\alpha}} \cdot \vec{\mathbf{F}}\right) = \left(\Delta F_i, H_i(\widetilde{\overline{\alpha}} \cdot \vec{\mathbf{F}})\right)_{i \in [\![1,n_{\text{bin}}]\!]} \tag{V.6.2}$$

$$H_i(\widetilde{\overline{\alpha}} \cdot \vec{\mathbf{F}}) = \sum_{u=i}^{n_{\text{bin}}} n_u(\widetilde{\overline{\alpha}} \cdot \vec{\mathbf{F}}) \ \forall i \in [\![1,n_{\text{bin}}]\!] \tag{V.6.3}$$

denoting H_i the reverse cumulative occurrences associated with the i-th class of Rainflow ranges.

The relation between class range ΔF and cumulative number of occurrences H can be modeled from the observation of one scalar loading history. The modeling of Rainflow spectra was tackled in [Bellec *et al.* 2021; Heuler and Klätschke 2005; Klemenc and Fajdiga 2008; Nagode and Klemenc 2021].

As an illustration, let us implement a magnitude-per-magnitude identification of a model for the Rainflow spectrum associated with in-phase (45) vertical (Z) loads on the front (f) axle from the observation of one driver, Driver 001, on the urban (C) segment of the measurement campaign US18-DT1. The associated range-only Rainflow matrix is shown on the left-hand graph of Fig. V.29. The ranges were anonymized by the total charge of the vehicle Q_{tot}

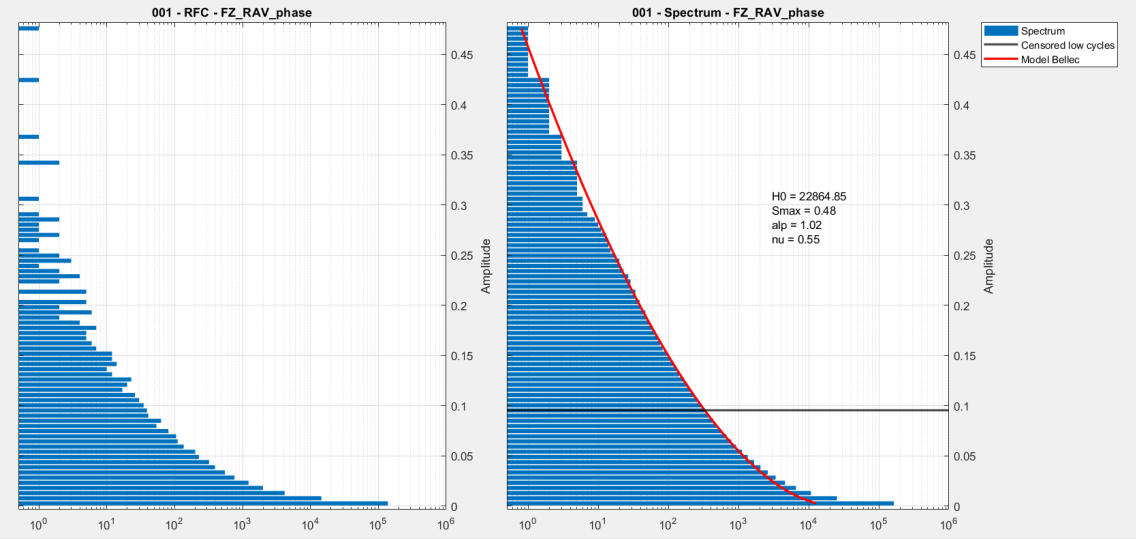

Fig. V.29: Range-only Rainflow matrix (left) and spectrum (right) counted on the load case built from in-phase (45) combination of vertical (Z) load components on the front (f) axle for Driver 001 driving on the urban (C) segment of measurement campaign US18-DT1. The values of the parameters of the Modified Heuler (Bellec) model that minimize the sum of square differences with the dataset on the uncensored cycles are displayed. The amplitudes in Newton were anonymized by the total charge of the vehicle Q_{tot}.

The distance driven by the driver on this segment is shown as a comment. Note that the Rainflow matrix may be sparse: classes between the maximum range (on top) and the mild ranges may have null counts. This is caused by the relatively small duration of the recording. The highest Rainflow ranges are hard to sample, because they are rare.

The load spectrum associated with this recording is denoted:

$$Sp\left(\widetilde{\alpha}\cdot\vec{\mathbf{F}}\right) = Sp\left(\mathbf{F}^{C}_{001,k}\right) = \left(\Delta F_i, H_i\left(\mathbf{F}^{C}_{001,k}\right)\right)_{i\in[\![1,n_{\text{bin}}]\!]} \tag{V.6.4}$$

denoting $\mathbf{F}^{C}_{001,k}$ the history of the global load case of interest measured for Driver 001 on the urban segment.

The chosen formula for the model of the load spectrum is the Modified Heuler model introduced by [Bellec *et al.* 2021]:

$$\frac{\log \widehat{H}(\Delta F)}{\log H^0} = 1 - \alpha \cdot \left(\frac{\Delta F}{S_{\max}}\right)^{\nu} \quad \forall \Delta F < \frac{S_{\max}}{\alpha^{\frac{1}{\nu}}} \qquad \text{(V.6.5)}$$
$$\widehat{H} = 0 \text{ otherwise}$$

The parameters of the model are the total number of cycles H^0, the predicted maximum range $S_{\max}$ and two shape factors α and ν. Let us determine the optimal values of these parameters by implement the least square method [Levenberg 1944].

The cycles at the bottom of the matrix have very low significance in the computation of equivalent magnitude: they are not expected to induce fatigue on our components of interest. However, their evaluation is very dependent on the sampling rate of our measurement of efforts.

If we include these low cycles in the identification of the Modified Heuler model, the model would strike a compromise between the cumulative number of occurrences H on high ranges and on low ranges. However, our evaluation of pseudo-fatigue is very dependent on such high ranges.

Likewise, we will arbitrarily censor a fraction of the spectrum that corresponds to low cycles, in a similar fashion to the implementation of a gate in [Bellec *et al.* 2021]. The threshold for this censorship was set arbitrarily to 20% of the maximum range of the spectrum.

In the quoted document [Bellec *et al.* 2021], the parameters H^0 and $S_{\max}$ are determined on a censored version of the spectrum. In this section, we include them in the optimization of the sum of square differences. The sum of square differences to minimize is given by the following formula:

$$\mathrm{SSD}\left(\mathbf{F}^{C}_{001,k} \mid H^0,\alpha,\nu,S_{\max}\right) = \sum_{i=i_0}^{n_{\text{bin}}} \left(\widehat{H}(\Delta F_i) - H_i\right)^2 \qquad \text{(V.6.6)}$$

denoting i_0 the first index of the classed Rainflow matrix such that $\Delta F_i > 0.2 \cdot \Delta F_{\max}$, the latter factor denoting the maximum range of the spectrum $\Delta F_{\max} = \max_i (\Delta F_i \mid n_i > 0)$.

The algorithm used to determine the optimal parameters of the Modified Heuler model is the "NonLinearLeastSquare" method of the MATLAB function `fit` with an initial state $(H^0,\alpha,\nu,S_{\max}) = (H_1,1,2,\Delta F_{\max})$.

The result of the model identification is shown in Fig. V.29 on the right-hand graph. The R-squared coefficient of determination is 0.9999. It denotes high correlation in the sense of Pearson between the model predictions and the actual measurement, meaning that the model fits the spectrum well.

A spectrum model is a reduced description of the contents of the spectrum. Instead of managing as many variables as there are Rainflow classes for each scalar loading history, sufficient knowledge on the content of the Rainflow spectrum is summarized in four parameters.

V.6.3 Per magnitude spectral extrapolation by inverse transform sampling

Let us see how spectrum models can be used to extrapolate Rainflow ranges and therefore pseudo-damage at a lifetime objective.

The Rainflow cycles counted on the global load case $Zf45$ for Driver 001 on the urban (C) segment of the measurement campaign US18-DT1 correspond to pairs of extrema in the signal obtained from the sum of both vertical global load components on the front axle. Significant extrema, associated with cycles that were not censored in the identification of a Modified Heuler spectrum model, are considered to be caused by the encounters of road events. Let us denote $\Delta F_{\min}$ the minimum Rainflow range (class) that is not censored.

This urban segment is l^C kilometers long. We are looking for the magnitude induced by Driver 001 after driving a distance of l_f^C on this urban segment, $l_f^C >> l^C$. The first major hypothesis in this section is that the driver will encounter the same road events at each repetition of the segment. However, the precise trajectory of the vehicle may be different at each repetition, meaning the loads (and the extrema) induced by each road event will be variable.

Let us first ignore the temporal correlations that exist between different load components on each event. We consider that we can extrapolate the Rainflow matrix associated with the above mentioned scalar global load case independently from the other load cases.

The extrapolation of Rainflow matrices was tackled in [Augustins 2007; Dewa and Kepka 2019; Johannesson and Thomas 2001; Socie 2001]. In these works, the goal was to achieve a robust and significant description of the contents of the loading history. Most importantly, these methods are able to simulate altogether Rainflow ranges and means.

In this thesis, we are interested in the difference in magnitude between direct extrapolation and a method that relieves the hypothesis of exact same loads. The above mentioned methods are suited to perform this extrapolation. As per our fatigue model presented in Chapter III, we need only extrapolate the counts of Rainflow ranges at an objective lifetime.

In this section, we propose an additional method based on the identification of load spectrum models. This method was developed alongside the work of [Bellec *et al.* 2021] and inserts itself in the framework of load spectrum analysis. The spectrum model $\widehat{H} : \Delta F$ identified in the previous paragraph on the measurement (see Fig. V.29) is considered to be the expected shape of the spectrum induced by driving a distance of l^C on the urban segment. This model is suitable for all uncensored cycles.

Let us split the extrapolation of the observed Rainflow spectrum in two parts. The uncensored cycles are considered to be associated with road events. The censored cycles are considered to be induced by the sampling rate of the measures of loads. Their occurrences depend on the number of kilometers that are driven. These cycles induce little marginal pseudo-damage, therefore approximating their extrapolation does not yield a large approximation of resulting pseudo-damage.

The extrapolated number of occurrences of Rainflow ranges in the censored zone are obtained from direct extrapolation, as in Eq. V.6.1. We need to define the frontier between

censored and uncensored classes:

$$n_{\min} = \max\left[i \mid \Delta F_i < \Delta F_{\min}\right] \tag{V.6.7}$$

$$n_i\left(\mathbf{F}^{C,f}_{001,Z,f,45}\right) = \frac{l_f^C}{l^C} \cdot n_i\left(\mathbf{F}^{C}_{001,Z,f,45}\right) \quad \forall i \in [\![1, n_{\min}]\!] \tag{V.6.8}$$

denoting $n_{\min}$ the index of the censored Rainflow class associated with the highest range $\Delta F_{\min}$; $n_i\left(\mathbf{F}_{001,Z,f,45}\right)$ the number of occurrences counted on the global load case $Zf45$ for Driver 001 on the urban (C) segment of the measurement campaign US18-DT1; $n_i\left(\mathbf{F}_{001,Z,f,45}\right)$ the number of occurrences predicted on the same global load case at the extrapolation duration l_f^C.

The extrapolation of the higher part of the Rainflow spectrum is considered to be a re-sampling procedure of the censored spectrum. The associated random experiment consists in drawing random Rainflow ranges in the range $[\Delta F_{\min}, +\infty[$ such that the reverse cumulative matrix of ranges is expected to fit the spectrum model. Coincidentally, the function $\widehat{H}$ is proportional to the reverse cumulative distribution $(1 - \mathcal{F})$ associated with a random variable ΔF that generates such random Rainflow ranges:

$$P\left(\Delta F \leq x\right) = \mathcal{F}\left(x\right) \quad \forall x \in [\Delta F_{\min}, +\infty[\tag{V.6.9}$$

$$P\left(\Delta F \geq x\right) = 1 - \mathcal{F}\left(x\right) = K \cdot \widehat{H}\left(x\right) \quad \forall x \in [\Delta F_{\min}, +\infty[\tag{V.6.10}$$

$$P\left(\Delta F \geq \Delta F_{\min}\right) = 1 \tag{V.6.11}$$

$$\text{with } K = \frac{H^0}{\widehat{H}\left(\Delta F_{\min}\right)} \tag{V.6.12}$$

denoting K a scalar necessary to ensure that the probability that a drawn range falls in the interval $[\Delta F_{\min}, +\infty[$ is one, *i.e.* $P\left(\Delta F \geq \Delta F_{\min}\right) = 1$.

The function $\widehat{H}$ is continuous and strictly decreasing on the interval $[\Delta F_{\min}, +\infty[$. Therefore the function $\mathcal{F}$ is continuous and strictly increasing on this interval. Its inverse function $\mathcal{F}^{-1}$ is well defined on the interval $[0,1[$ and is given by:

$$\mathcal{F}^{-1}\left(u\right) = S_{\max} \cdot \left(\frac{-\log\ \left(1-u\right)}{\alpha \cdot \log\ H^0}\right)^{\frac{1}{\nu}} \quad \forall u \in [0,1[\tag{V.6.13}$$

The knowledge of the cumulative distribution $\mathcal{F}\left(x\right)$ of this random variable ΔF is sufficient to apply the inversion method, or inverse transform sampling, as per [Devroye 2006] chap. 2. The availability of an analytical formula for the function $\mathcal{F}^{-1}$ makes the method easy to compute. Let $U \sim \mathbb{U}[0,1[$ be a random variable following a uniform distribution on the open interval $[0,1[$. Let us define the inverse of $\mathcal{F}$ over the space $[0,1[$ by:

$$\mathcal{F}^{-1}\left(u\right) = \inf\left\{x \mid F(x) \leq u\right\} \quad \forall u \in [0,1[\tag{V.6.14}$$

As per theorem 2.1 from [Devroye 2006], the random variable given by the combination $\mathcal{F}^{-1}oU$ is well defined and follows the same law as ΔF.

The number N_0 of uncensored Rainflow cycles in the original measurement is given by:

$$N_0 = \sum_{i=n_{\min}+1}^{n_{\text{bin}}} n_i \left(\mathbf{F}^C_{001,Z,f,45}\right) \tag{V.6.15}$$

Following the hypothesis that these cycles are induced by road events and that each repetition of the trip repeats the same road events, the number of uncensored cycles in the extrapolated Rainflow matrix is given by $N_f = N_0 \cdot l^C_f / l^C$ (rounded to the next integer).

Therefore the uncensored part of the extrapolated Rainflow matrix is given by a re-sampling of size N_F of the random experiment associated with the random variable $\mathcal{F}^{-1}oU$.

Thus written, the two-step extrapolation of the original spectrum can be implemented in a code. The Rainflow matrices obtained from the direct extrapolation and the inverse transform sampling method are shown in Fig. V.30. The ratio between the distance for extrapolation and the original distance for Driver 001 on the urban segment and an objective duration on urban roads of l^C_f km is approximately $1/77$.

Note that the top of the new matrix stops at the intersection between the model and the abscissa $n = 10^0$. On this global load case, its top is lower than the maximum cycle counted on the original signal. This is often the case on other global load cases. Indeed, the spectrum model was not forced to yield a number of cumulative occurrences $\widehat{H} > 1$ at the maximum observed range. Therefore, this method alone does not predict efficiently the occurrences of larger maximum ranges following several repetitions of a trip.

On this context (in-phase (45) vertical (Z) loads on the front (f) axle, Basquin exponent of 4), on two other contexts and on another road segment, the magnitudes were compared to the ones obtained by direct extrapolation and stored in Table V.1. Even for higher Basquin exponents, our method yields inferior or equal magnitudes. Note that this re-sampling was only performed once, as an illustration.

The choice of inverse transform sampling for the extrapolation of a Rainflow matrix yields a new matrix that is more even than the original sample, with no unexplained holes in the matrix. However, from what we have gathered here, direct extrapolation seems to be a more conservative approach to calculate the pseudo-damage of extrapolated Rainflow matrices measured in service.

We can improve the prediction of occurrences of large Rainflow ranges (at the top of the spectrum) by implementing a further model on the upper tail of the distribution of Rainflow ranges, such as Pareto distributions [Geng *et al.* 2019] or extreme value distributions. Indeed, the maximum range of the Rainflow matrix at each realization of a given trip falls in the domain of extreme value statistics [Coles *et al.* 2001].

Another limitation to the extrapolation method presented here is its unidimensionality. Any road event takes part in several global load components at a time. The temporal correlation between load components should be included in the random evaluation of new Rainflow cycles at each repetition of said road event. The best way to achieve this inclusion

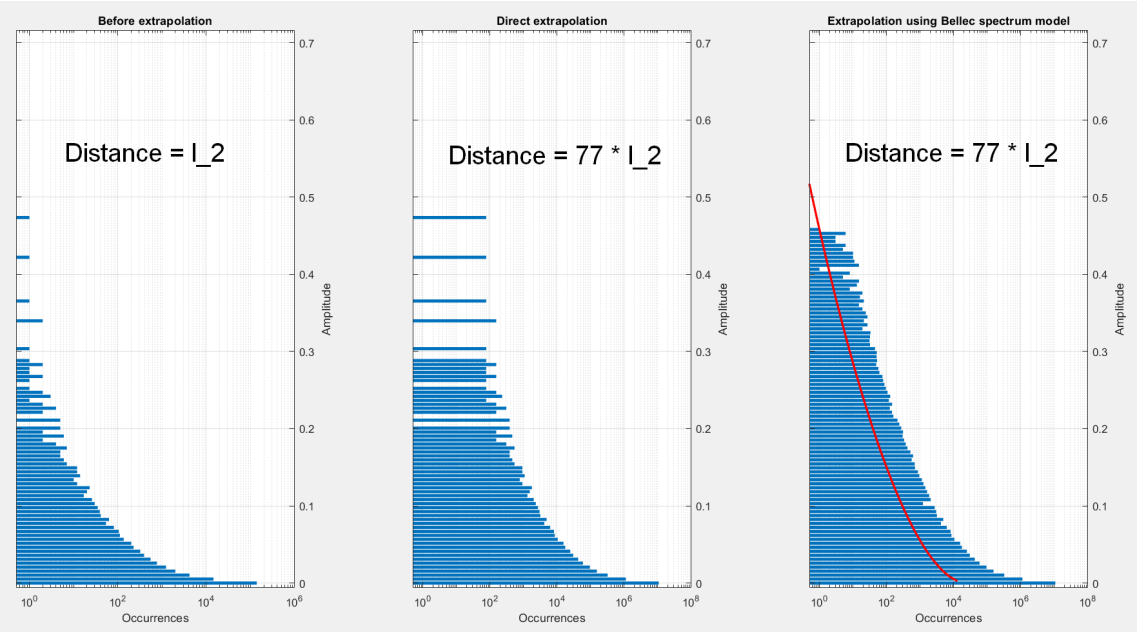

Fig. V.30: Comparison between the Rainflow matrices obtained by direct extrapolation, of the original Rainflow matrix and by inverse transform sampling using a Modified Heuler spectrum model, identified on the original Rainflow spectrum. The loading history of interest corresponds to the recording of in-phase (45) vertical (Z) loads on the front (f) axle from the observation of one driver, Driver 001, on the urban (C) segment of the measurement campaign US18-DT1.

Recording	Method	Distance ratio	FZ_f45 $m = 4$	FZ_f135 $m = 4$	FZ_f45 $m = 8$
Urban road	Direct extrapolation	77	2.31	2.01	0.89
	Inverse transform	77	2.25 (-3%)	1.99 (-1%)	0.83 (-7%)
Damaged road	Direct extrapolation	50	2.64	2.79	0.92
	Inverse transform	50	2.58 (-2%)	2.74 (-2%)	0.87 (-6%)

Table V.1: Magnitudes obtained from the direct extrapolation or inverse transform sampling of the Rainflow matrix measured on Driver 001 on two segments of measurement campaign US18-DT1. Magnitudes were anonymized by the total charge of the vehicle, Q_{tot}

is to determine a distribution for the multivariate random variable associated with the whole magnitude vector.

Note that said temporal correlation between loading histories should not be mixed up with pair correlation between load intensities or magnitudes at the end of a driver's run. The latter denotes the effect of driver behavior on an accumulation of events. Examples of

analyses of temporal correlations between different load or acceleration components for the case of automotive structures can be found in [Bellec *et al.* 2021; Grubisic and Fischer 1997].

V.6.4 Perspective: modeling the variability in severity for one driver

In this section, we no longer consider that the behavior of the driver is constant from one repetition of a trip to the other. This calls for an extra hypothesis on the variability of conditional driver severity. We will not propose examples of this second strategy for extrapolation, rather discuss its feasibility and relevance with respect to available data.

Let c be a driver surveyed during the measurement campaign US18-DT1. Their conditional severity on an aggregated trip is a random variable. Each time the driver is asked to drive once on the segments that built this aggregated trip, a new observation of their severity is achieved.

The principle of this proposed method for extrapolation to a lifetime is presented in Fig. V.31. A multivariate Gaussian distribution is used to simulate the conditional severity of the driver on each repetition of the aggregated trip. Each simulated severity is then translated back to reduced variables and to absolute magnitudes. The total absolute pseudo-damage of the concatenation of all these random runs would here be approximated by the sum of all simulated pseudo-damages.

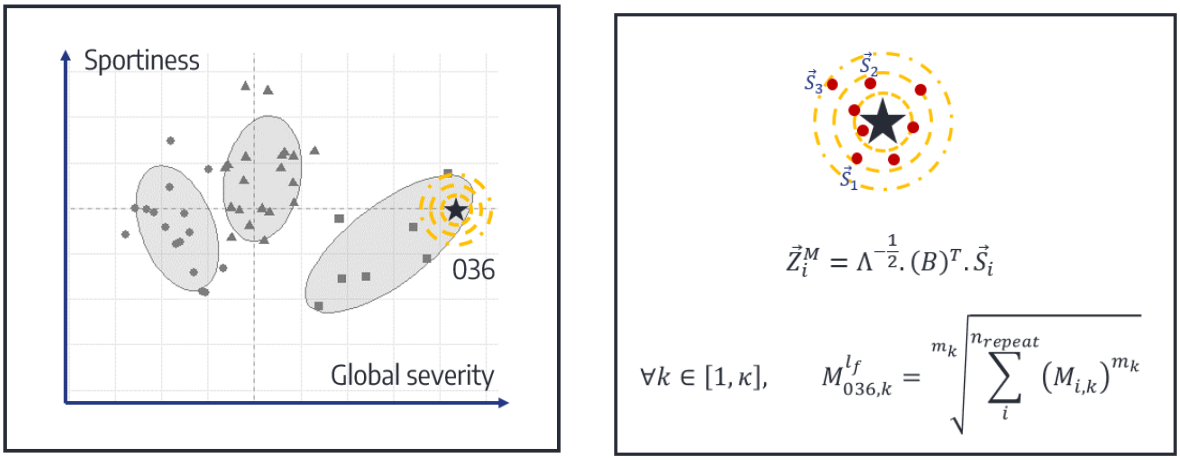

(a) Driver severity stochastic modeling (b) Re-simulation of severity

Fig. V.31: Extrapolation method in the hypothesis of variable driver severity, example with driver 036 from the dataset $\mathcal{C}_{\mathcal{T}_1}$.

Note that we only have one observation of conditional severity per driver. This is not enough to evaluate the variability of driver severity. In other words, we cannot ascertain that the observed behavior on that day was the average behavior of the driver over the life of their vehicle.

Modeling the variability of driver severity is only relevant if drivers with different severity profiles - general locations in the space of severity - are observed to be more or less constant in their behavior. If all drivers experience the same importance in term of mood shift, then a

proper model of this phenomenon would not induce significant modification of the distribution of induced pseudo-fatigue.

In other words, one may still choose a representative mission from the distribution of conditional severity on the short reference trip. However, in the hypothesis of variable driver severity over the life of a vehicle, a model for the variability of driver severity would still be required to achieve extrapolation of this representative mission to an objective lifetime.

Relevant strategies for the sampling of multivariate random variables are:

- In the case of multivariate Gaussian variables, a Cholesky decomposition of the variable can be used to obtain several independent intermediary scalar variables. Each can then be sampled individually using a scalar re-sampling technique (see [Williams and Rasmussen 2006] Appendix A.2 or [Gentle 2010] Chap. 7);
- Correlation between successive samples can also be achieved by implementing the Metropolis-Hastings method (see [Chib and Greenberg 1995]).

V.7 Chapter conclusion

V.7.1 Synthesis

The statistical analysis of the pseudo-fatigue induced in service aims at evaluating the level and severity over the population of missions of a vehicle model. Through the exploration and stochastic modeling of a population of drivers, we have developed a new method to elaborate a unique distribution of vectors of pseudo-fatigue. We have also proposed tools such as simulation (using a new trip composition) or extrapolation (to adapt the duration of the trip to the objective) to achieve such a distribution over any market of interest. Most importantly, we have shown how to achieve a distribution fit for the evaluation of the respect of the requirement in reliability for our subsystems of interest, *i.e.* for missions that last exactly a lifetime objective.

Instead of modeling our variables of interest over the whole population of missions, we have first defined aggregated trips as a restriction on the population of mission trips. These trips of reference correspond to the aggregation of all life situations that the vehicle model may encounter in service, independently of who drives it. The simulation of our sample of drivers onto this aggregated trip was considered to be an adequate sample of all missions, although it is obviously a huge preconception.

This preconception on the population of trips is a valid strategy if the results of the analysis are known to be conservative, *i.e.* to overestimate the fatigue induced by the real population of missions of the vehicle. The conservativeness of the results for a given aggregated trip can be verified *a posteriori*, by comparing it to a different plausible aggregated trip.

The exploratory analysis of the pseudo-fatigue induced by our sample of drivers on the aggregated trip led to new best-suited variables to explain the variability of drivers: condi-

tional severity. The physical sense of the PCs acquired through the application of PCA are interpreted according to their correlations with different families of local contexts.

For instance, larger magnitudes on contexts associated with heavy deceleration and acceleration are associated with drivers that push their braking and accelerating pedals harder and/or more often than the rest of the population. Speed and acceleration quantities that are significantly correlated to these PCs further confirm our interpretation of driver behaviors on maneuvers and obstacles.

The most important traits to describe the conditional severity of drivers are, in order, global severity, sportiness and quick turning. We can identify sporty drivers from their large positive coordinates on the first and second dimensions of severity. We can now also comment that these drivers will be more damaging for zones that are sensible to braking, acceleration and cornering events, while clumsy (*i.e.* non-sporty) drivers may be more damaging to zones that are sensible to vertical solicitations.

We have chosen to make a hypothesis that the conditional severities were distributed according to a Gaussian mixture. The number of cores of the mixtures, *i.e.* of homogeneous (Gaussian) sub-populations of drivers, corresponds to the optimal partition proposed by HCPC. The likeliest distribution of conditional severity was achieved through the implementation of an EM-algorithm. Thanks to the orthogonality of the factor matrix (B), we were able to translate this distribution of severity to one of magnitudes, fulfilling our objective for this chapter.

Drivers distinguish themselves on the aggregated trip with respect to the amount and type of situations that they meet on the trip. This observation already was the main result of Chapter IV, as we defined road events and analyzed the variability of driver load intensities on several road environments. In this chapter, we reveal a consequence of this observation: the moments and shape of the distribution of conditional driver severity and therefore of the distributions of our variables of interest are very dependent on the composition of the aggregated trip.

Service measurements are short. A cautious way to define aggregated trips is to choose their duration to correspond to the sampled distance of the campaign. In the last section, we have proposed two starting points for future methods to extrapolate results of a multidimensional analysis from such a short aggregated trip to an objective lifetime: the Rainflow counts for each global load case, or conditional severity for each driver. Both strategies are associated with different hypotheses on how variable event encounters and driver behavior may be over repetitions of the same trip.

V.7.2 Adapting the method to new markets

The whole procedure of exploration and modeling unveils the major ingredients to the modeling of pseudo-fatigue in service and the main origin of their variability:

- The dynamics and payload population for a new vehicle model will have non-trivial effects on the loads input to the vehicle throughout its life. The latter factor can be

restricted conservatively to a large payload setting. The effect of the former effect on the loas needs to be determined for each new model;

- The chosen aggregated trip or more generally the population of aggregated trips determine the average value for each magnitude. Indeed, different road environments display different road quality and event density. More maneuvers or larger obstacles systematically mean higher mean magnitudes;

- The variability of all magnitudes, characterized by their variation coefficients, is also linked to the trips of interest. Indeed, drivers have as many opportunities to be different from one another as there are situations to which their conditional severity is a parameter;

- Finally, the global severity of drivers on the situations of the trip determines whether the mission induces higher than usual values of pseudo-fatigue. The supplementary traits of driver conditional severity help us determine if different sets of local contexts may be unequally loaded over the population of globally severe drivers;

- We must also recall from the previous chapter the effect of traffic and weather on driver behavior and trip characteristics. As developed here, the aggregated trip strategy enacts a set traffic and weather as a lifelong reference for all drivers. This is why this restriction was adapted to the campaign US18-DT1 in which both aspects had low variability. Managing traffic and weather conditions on a population of trips was not tackled further in this thesis.

These ingredients will change from one vehicle model or from one region to another. The effect of a change in target market for a vehicle model can be passed on to the construction of the unique distribution of conditional severity and to the ingredients (mean, standard deviation) for magnitude descaling. Thus our method allows dynamical updates from new available data of the knowledge of the company on the level and variability of magnitudes in service. The thorough development of the statistical methods and hypotheses throughout these two chapters ensure that this procedure will scale robustly to an increasing amount of service data.

V.7.3 Adapting the method to new variables

This analysis was conducted from the variables of interest that our mechanical theory had determined in Chapter III. This method does not permit the evaluation of the mechanical *relevance* of our variables, nor does it ensure that their distribution will allow us to define adequate conditions for the reliable design of suspension and body parts. These two concerns are handled respectively in the previous and in the following chapters.

Consequently, the method could be adapted to the use of other methods for fatigue characterization, *i.e.* other variables of pseudo-fatigue. It is likely that adding variables representing different physical phenomena may unveil new characteristics of drivers and trips alike that partake to the variability of service pseudo-fatigue.

We have made extensive use of the property that pseudo-damages can be cumulated additively from the concatenation of several driving episodes. If the variables of interest do not have this extensive property, some steps of the analysis may prove more difficult to translate, such as the simulation of variables of interest on aggregated trips or their extrapolation to a lifetime objective.

An example of alternative variables to implement in this method is the decomposition of the pseudo-damage induced on each local context into two terms - one for the quasi-static contribution of low frequencies and a term of spectral fatigue associated with the contribution of road asperity - as presented in [Bellec *et al.* 2023]. Both these variables can be cumulated additively for the evaluation of concatenated loading episodes.

Chapter VI

Design and validation objectives for the reliability of automotive components

VI.1 Chapter introduction

The two previous chapters led to a distribution of a conditional severity in service on a conservative aggregated trip. This distribution can be projected to distribute the variables of interest - variables of pseudo-fatigue - which were defined and justified in Chapters II and III.

In this chapter, we provide insights to exploit the resulting model towards the reliable design and validation of suspension and body subsystems. The existing method for the reliability of simple components is developed and adapted to the shape of our distribution of severity.

As introduced in Section I.2 and Fig. I.1, a system requirement puts an upper bound (control) on the risk of failure of the system. An allocation of risk then defines requirements for each subsystem - parts, components - according to their sensible zones and associated failure modes in service. Each part has a specific set of sensible zones and specific load conditions, *i.e.* local contexts (§III.6). Each such local context may contextually be called a component, *i.e.* a subset of the structure for which failure can be predicted by a single scalar variable of pseudo-fatigue.

Nota bene: In this context, "Controlling" the risk of failure of a subsystem may be associated with the meaning of regulating. "Determining an upper bound" for a probability of failure would be translated in the French verb "majorer". Indeed, the French word "contrôler" rather means "to check" or "to verify".

The project team in charge of designing a new vehicle model has access to a variety of design parameters - part shape, joint geometry, weld dimensions, definition of articulations - that they can modify to create a new design for the subsystem at stake, be it a joint, a part or the whole organ. The reliable design of a subsystem means finding a setting of these parameters that ensure the respect of its associated requirement in reliability. The meeting of a requirement is verified by a validation procedure.

The question of part design includes managing unknown mechanical response. Although joints and assemblies are predefined functionally, reinforcing a weakness in the structure will modify its stiffness. Therefore, stress localization factors associated with each global load component (see Section III.4) are unknown, increasing the complexity of the problem. In this thesis, we do not completely solve the question of design, we will merely determine necessary theoretical conditions for appropriate design.

Our main focus is the determination of adequate validation procedures in the presence of a proposed design. Validation procedures for the fatigue resistance of automotive components take the form of load procedures. For each load procedure, a pass criterion determines whether or not the prototype passes. For instance, the prototype may fail the procedure if it breaks under reasonable load conditions, or pass the procedure if a sufficient number of its issues live through a severized loading history [Beaumont 2013; Palin-Luc *et al.* 2006].

The fact that a procedure actually serves to validate needs to be justified with respect to the requirement in reliability at stake. We therefore separate the elaboration of validation procedures in two: objectives and loads. In this chapter, we focus on the determination of adequate validation objectives, in terms of severity or vectors of pseudo-fatigue, so that they adequately inform us on the reliability of the prototype (see Fig. VI.1, last column). In Chapter VII, we will explain how to determine validation loads that reproduce the desired validation objectives.

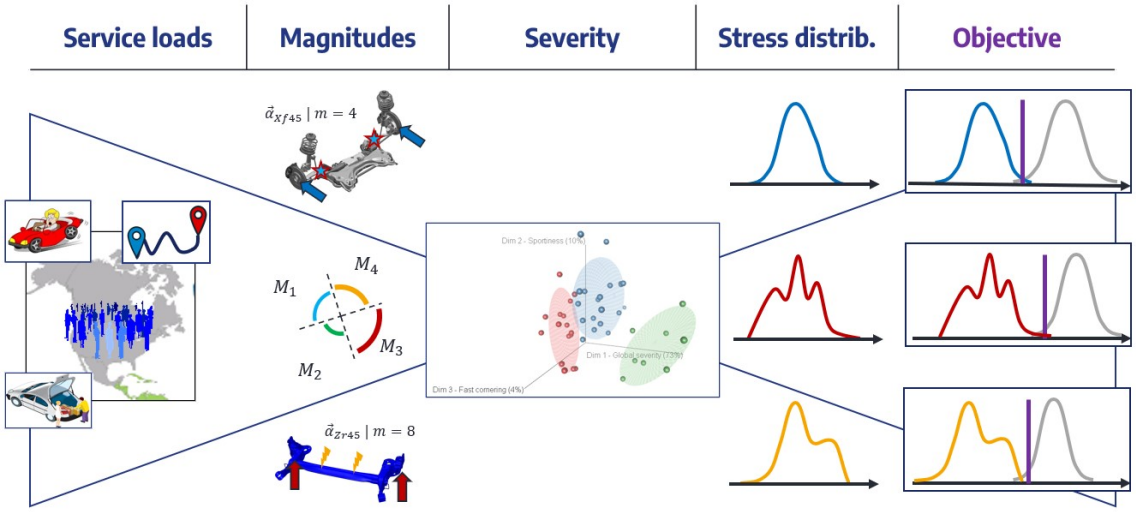

Fig. VI.1: Strategy for the determination of validation objectives for the design of each local context

The outline of the chapter is as follows: Section VI.2 reviews the current paradigms of reliability analysis and reliable design of mechanical systems in the literature and the industry, with an emphasis on methods used in the automotive industry.

The design and validation problems for subsystems associated with risk-based requirements of reliability are defined in the general case in sections VI.3.4 and VI.3.5. However, following a discussion on current limitations in §VI.3.6, we will only grant a solution to these problems in the unidimensional case, in Section VI.4.

Examples of synthetic severe missions, handpicked from our distribution of condition sever-

ity built in Section V.4, are worked out in §VI.5 and compared to existing multidimensional references for the elaboration of validation objectives.

VI.2 The ingredients of reliable design

VI.2.1 Standard loading histories and spectra

In order to design a new version of a system, engineers need to evaluate the mechanical response of the system to service and trial loads. They also need to know the trials that it will have to pass to be validated.

The analysis of the mechanical response of prototypes is more and more conducted through numerical simulation. It is historically done by submitting the prototype or its parts to loads corresponding to a run on proving grounds. Physical measurements still serve nowadays to improve the performance of numerical models and to fit digital twins for further simulations.

Either way, a learning base of loads for the evaluation of mechanical response is welcome. It is also usually desired that this learning base and the validation loads stem from a single set of loads, such as proving grounds. We will introduce proving grounds more extensively in the next chapter.

Standard loading histories and proving ground schedules for the reliable design of automotive subsystems have the ambition to propose a small number of **exhaustive** - all manners of degradation are represented - and **conservative** - a car withstanding a lifetime of this history is expected to withstand any other service conditions - multi-input loading histories.

From these historical and/or standard histories, the interface loads on each subsystem are determined using multi-body models and transfer functions. The use of standard loading histories is developed in [Heuler and Klätschke 2005]. This practice originated from the aerospace industry, much like Stress-Strength interference [Lipson *et al.* 1967].

Such load references may be obtained from the statistical analysis on the real-life loads measured over a measurement campaign in a significant region. It is the case for the Car Loading Standard (CarLoS) (see [Schütz *et al.* 1990] and Fig. VI.2). A number of driving episodes were evaluated, road conditions identified and re-mixed into a summary. These load references may also be determined from driving or simulating a prototype on a predetermined schedule of proving ground events or load cases.

Picking a quantile on the number and/or presumably unidimensional "severity" of events allows this summary to be interpreted as representative of a percentage of missions. However, these quantiles are scarcely gathered from the distribution of a pseudo-fatigue variable directly associated with the risk of failure of the system.

For instance, to determine the first iterations of the design schedule used at Stellantis, the number of obstacles (braking, potholes, bumps, turns etc.) was evaluated on each kind of road environment (highway, country, city) [Frey and Demaimay 1991]. The objective schedule settled on a representative mix of these road environments with a conservative number of

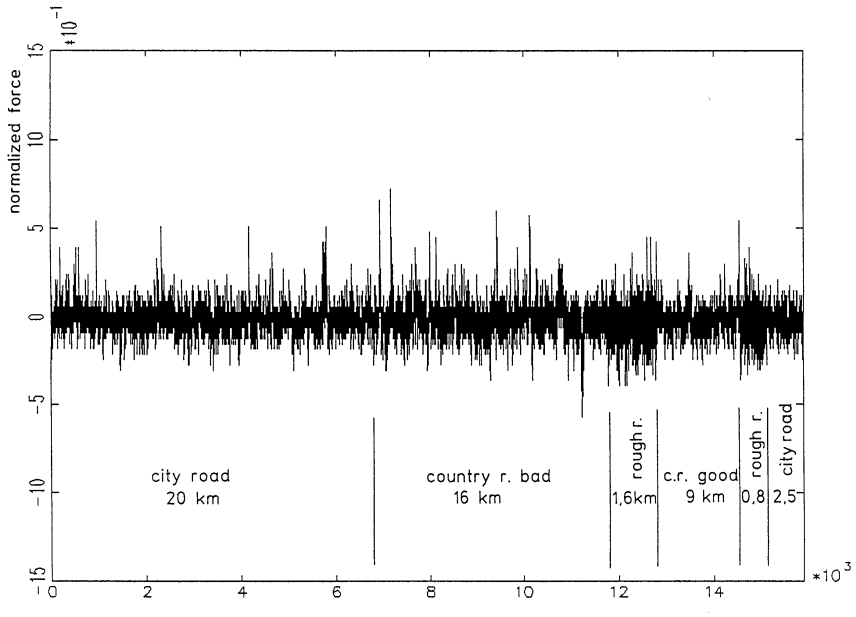

Fig. VI.2: Fraction of the vertical load sequence from CarLoS [Schütz *et al.* 1990]

events per environment. Severe and reproducible counterparts of these events were reproduced in proving grounds, and the resulting loading history was considered to be a reference for the severity of validation trials.

Following the discussions on driver and trip segmentation in the last chapter (see Section V.5), the weights associated with different driving situations when building such standard missions can be adapted to the classification and survey of personal vehicle missions.

Characterization of a mission through road events and road rugosity is also the backbone of standard and/or historical so-called load spectra vastly used in the automotive industry [Facchinetti 2018]. The use of such load spectra became so renowned (especially in Germany [Berger *et al.* 2002]) that they are now a widespread currency toward the design of vehicle structures, often casting a shadow on the statistical analysis of road environments and events that determined them in the first place.

As introduced in Fig. II.15, a load spectrum is the reverse cumulative matrix of the Rainflow ranges of a scalar loading history. It may then be reproduced numerically or on test benches with a chaotic order to avoid sequence effects on component fatigue (see §II.5.1).

Note that the term "spectrum" does not refer here to frequential fatigue analysis methods. This latter family of methods is sometimes used nonetheless for reliable design purposes [Pitoiset *et al.* 2001] and most importantly in the case of vibratory fatigue [Dirlik and Benasciutti 2021].

Gassner [Gassner 1939; Grubisic and Fischer 1997; Heuler and Klätschke 2005] adapted the Wöhler method to represent the fatigue behavior of an assembly when subjected to a given load spectrum shape with a parametric maximum range. The resulting curve, in a $F_{\max} - N$ diagram, is called a Gassner curve (see Fig. VI.3). The parameterization of the maximum cycle of a load spectrum is propagated to the whole spectrum, and serves as a decision-maker for a test severization procedure.

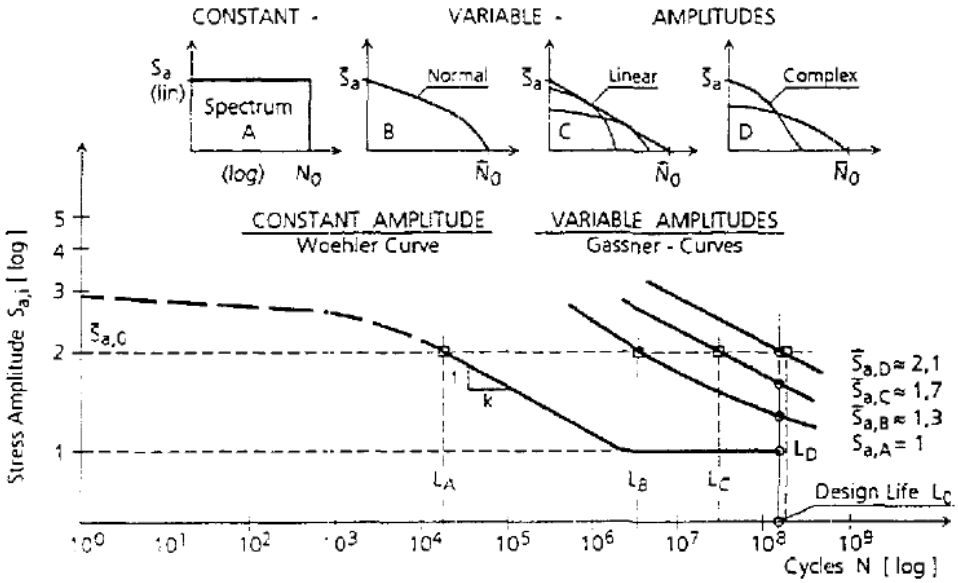

Fig. VI.3: Gassner curves for four different spectrum shapes [Gassner 1939]

Coming back to our investigation of different profiles of drivers and content of road environments in terms of events in Chapters IV and V, observing differences in spectrum shapes between different drivers or trips can lead to the definition of new spectrum references to represent different kinds of missions. Such a characterization of service loads can also take advantage of the multiplicity of the global load cases, that are handled in parallel in our method.

It is important to note that the ordinate of Gassner curves points to the amplitude of the maximum cycle of said spectrum. The number of cycles N in usual Gassner plot configurations contains all cycles of a required repetition of the base spectrum with a corresponding maximum cycle to lead the component to failure. With that formalism, a Wöhler curve is the Gassner curve of the rectangle ("constant") load spectrum in Fig. VI.3 - N cycles with a single amplitude. A Gassner curve maps the lifetime prediction of the system when submitted to spectra of different amplitude (or equivalent description). It is best suited to improve the durability of a structure.

The parameterization of the maximum range of a load spectrum comes after the determination of a mix of road events by use surveys and industrial experience. Moreover, combinations of load spectra are treated as new specific load spectra and their fatigue characterization is technically always based on the Wöhler curve associated with a component.

These one-size-fits-all loading histories have the advantage of representing a natural reference for the design, resistance and comparison of different vehicle models. They are realistic in the sense that they are built from a description of road events and are therefore understandable in terms of service conditions.

Finally, the description of a standard from a schedule of road events is a promise of robustness. It allows to capitalize on the experience and physical sense of industrial test

engineers, as well as on physical trial to fill in the gaps of a method. Therefore, at the procedural level, validation conditions and levels are best expressed in terms of road events than of damage or loads at the theoretical level.

However, using a single parameter - for instance the maximum of the spectrum - to compare load spectra that have the same shape is not suitable for the analysis of service loading histories. We will rather resort to the variables of pseudo-fatigue that we have introduced in Chapter III.

VI.2.2 Customer correlation

In order to implement SSI to determine adequate validation condition for reliability validation, the moments of the distribution of pseudo-fatigue evaluated from service data must be known and included in a full design procedure [Svensson and Johannesson 2013]. Their importance in the expression for the risk of failure of a subsystem will be apparent in Section VI.4.

The current method at Stellantis [Bignonnet and Thomas 2001; Thomas *et al.* 1999] allows quantification and statistical analysis of a single pseudo-damage quantity on any unidimensional global load case $\mathbf{F}_j$. The spirit of the method is to discuss severity in terms of equivalent analytical loads, by enacting a reference variable $\varphi = \Delta F_{eq}$, called the endurance equivalent load (EEL) amplitude. This parameter sets the amplitude of a sinus cyclic loading history lasting a number N_{ref} of cycles.

Said differently, an equivalent cyclic loading history lasting N_{ref} cycles with an amplitude ΔF_{eq} is supposed to deal the same pseudo-damage as a projection of a global loading history to a single scalar loading history $\mathbf{F}_j$.

A scalar variable being always ordered, any loading $\overrightarrow{\mathbf{F}}'$ is more severe than a loading $\overrightarrow{\mathbf{F}}$ if $\Delta F_{eq}(\overrightarrow{\mathbf{F}}') > \Delta F_{eq}(\overrightarrow{\mathbf{F}})$, as it deals a larger pseudo-damage and therefore damage. Thus, pseudo-fatigue description $\varphi = \Delta F_{eq}$ is equated to severity.

The resistance or Strength to loads homogeneous to $\mathbf{F}_j$ for a specimen is given by the level r_j such that the structure fails under any loading characterized by $\Delta F_{eq} = r_j$. This resistance is a random variable over a vehicle design, homogeneous to 1D pseudo-fatigue, homogeneous to 1D severity. Its distribution is considered to be known by industrial experience: it is usually modeled by a Gaussian law $\mathcal{N}\left(\mu_{r_j},\sigma_{r_j}\right)$ with a fixed variation coefficient $v = \sigma_{r_j}/\mu_{r_j}$.

The distribution of historically unidimensional severity for each unidimensional load case is considered to be Gaussian, with parameters $\mathcal{N}\left(\mu_{\varphi_j},\sigma_{\varphi_j}\right)$, and its moments are determined from statistical analyses on samples of endurance equivalent loads on a reference service trip.

From the knowledge of these two distributions, an adequate position for the nominal resistance μ_{r_j} can be determined and sought as a design objective [Echard *et al.* 2016], see Fig. VI.4.

In the hypothesis of appropriate design, the risk of failure of an issue of the subsystem submitted to a given mission severity $\varphi_{j,n}$ is known from the cumulative distribution of r_j. Trying the subsystem under such a validation objective $\varphi_j = \varphi_{j,n}$ allows to conclude on its

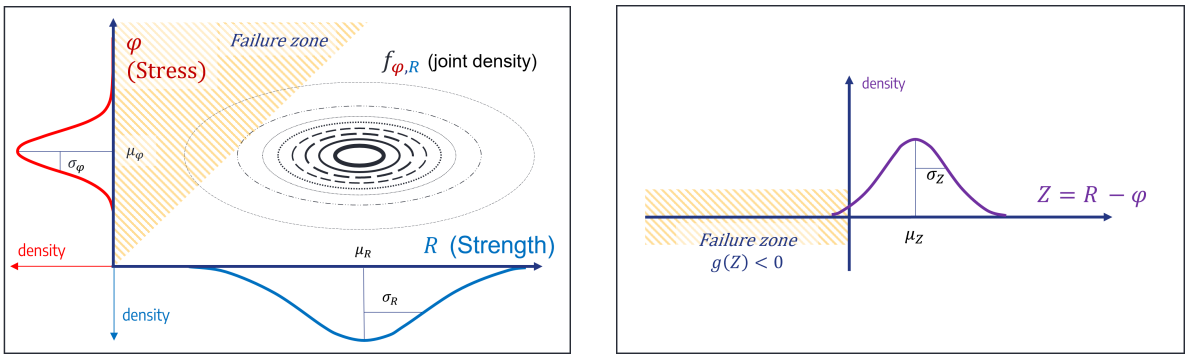

(a) View of the joint distribution (b) View of the associated base variable

Fig. VI.4: 1D Stress-Strength interference with Gaussian distributions for Stress φ and Strength r. Iso-densities of the joint density of tuples (φ,r) is shown in black. The determination of system state in this framework is given by defining the random variable $Z = R - \Phi$ and comparing it to 0.

reliability, see Fig. VI.5. The mathematical development of these design and validation objectives will be written in Section VI.4.

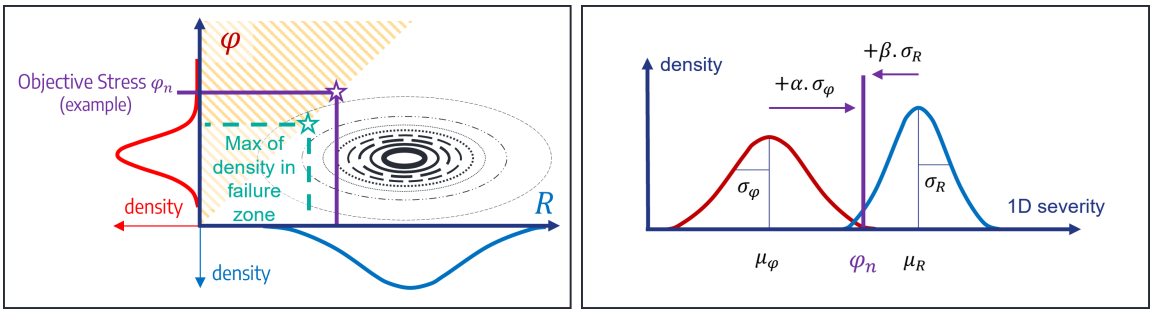

Fig. VI.5: Objective Stress in the Stress-Strength paradigm. The objective to reproduce is a known quantile of the distribution of Stress. If an ideal distribution of Strength is known (ideal design), then the objective is also a known quantile of the distribution of Strength.

Thus, the reference for validation is a known quantile of the severity of pseudo-fatigue for each load case of interest. This denotes customer correlation for the determination of design and validation loads [Dreßler *et al.* 2009]. A standard loading history is sought to achieve the simultaneous realization of all these validation objectives.

The historical reference, used at Stellantis and introduced in the previous section, is stored as a proving ground schedule. While the first version originated from a statistical analysis of events met in service, it is regularly updated to fit new load conditions and different distributions of unidimensional severity in new regions of interest, following the method presented in this section.

VI.2.3 Reliability analyses, state functions

Let us take a step back and consider the problem of probabilistic reliable design for any kind of system. The concern of this chapter - designing or validating a system according to a

maximum admissible risk of failure in service - is the inverse problem of the determination of its risk of failure.

Let us denote base variables $\vec{\chi} = (\chi_k)_{k\in[1,n_d]}$ [Hasofer and Lind 1974] the variables necessary to predict a risk of failure of the system, *i.e.* a change in the state of the system between absence of failure and failure. $\vec{\chi}$ must be considered to be the joint knowledge of pseudo-fatigue and resistance variables corresponding to one meeting between a system issue and a mission.

For instance, in a unidimensional paradigm prone to the application of Stress-Strength Interference methods, [Echard *et al.* 2016] introduce a random variable $Z = R - \Phi$ corresponding to the difference between resistance and pseudo-fatigue. The failure of the system before the end of the mission associated with φ can be predicted from this base variable.

Let us define the state (or performance) function $g_{\mathcal{V}}$, the input of which is a scalar χ or a vector of base variables $\vec{\chi}$. The state of the system may be modified when failure occurs. In the more general case, systems with redundant components may still have a viable, degraded function when non-catastrophic failure occurs [Yingkui and Jing 2012].

In this thesis, we consider the safety parts of personal vehicles, for which a failure is always considered catastrophic: the macroscopic apparition of a crack in any of these safety parts denotes functional failure.

Let us therefore considered that the state of the system, much like the state of any of its safety parts, is either strictly positive or negative. This defines respectively the safety and the failure domains in the space of base variables (see Fig. VI.6):

$$\begin{cases} g_{\mathcal{V}}(\vec{\chi}) > 0 & \text{safety domain} \\ g_{\mathcal{V}}(\vec{\chi}) \leq 0 & \text{failure domain} \end{cases} \tag{VI.2.1}$$

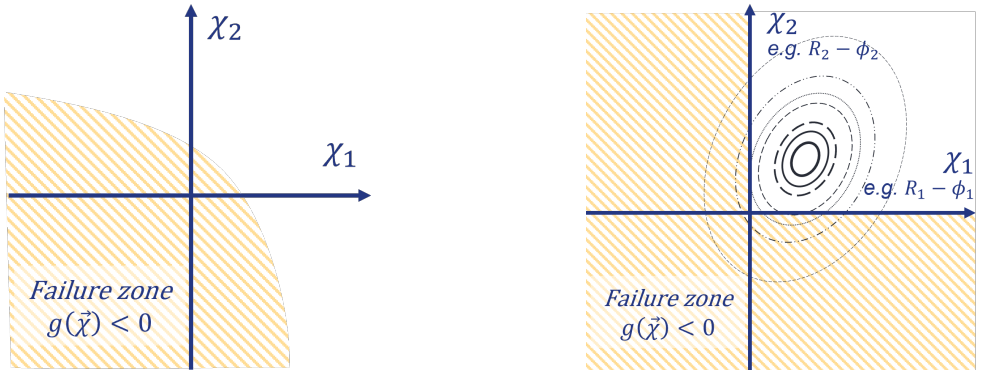

(a) Differentiable state function

(b) Example with classical base variables from SSI

Fig. VI.6: Failure zone in a bi-dimensional case. In the second case, the underlying distributions for both pseudo-fatigue and resistance variables are both Gaussian.

The purpose of reliability analyses is to estimate the risk of failure of a designed system, with known distribution of resistance submitted to a known population of pseudo-fatigue (see [Gayton 2012] chap. 1). This corresponds to evaluating the probability to fall in the failure domain.

The probability that the system is led to failure over a population of pseudo-fatigue can be estimated in a most basic sense using a Monte Carlo algorithm [Raeside 1976], sampling the space of base variables. While Monte Carlo methods slowly converge to the solution in theory, they require an enormous amount of computation resources and/or prior information for a low precision on overall risk determination [Svensson and Johannesson 2013]. Re-sampling methods adapting the experimental plan (the sampling of pseudo-fatigue and resistance) to focus on subsets of the sample space more prone to lead to failure may increase the convergence rate of the algorithm (see [Gayton 2012] Chap. 1).

An upper bound (control) of the risk of failure P_f of a system can be determined from the evaluation of a single tuple of base variables $\vec{\chi}^*$, determining both pseudo-fatigue objective and expected resistance. It is the purpose of the well-known First Order Reliability and Second Order Reliability methods (FORM/SORM) [Hasofer and Lind 1974]. The name of both methods corresponds to the chosen approximation of a state or performance function $g_{\mathcal{V}}$, determining the state of the system, around a variable ι, the reliability index, akin to $\vec{\chi}^*$, solving the following problem:

$$\vec{u} = \Gamma(\vec{\chi}) \ \forall \vec{\chi} \tag{VI.2.2}$$

$$\iota = \min_{\vec{u} \mid g_{\mathcal{V}}(\vec{\chi}) \leq 0} \sqrt{\vec{u} \cdot^T (\vec{u})} \tag{VI.2.3}$$

$$\iota = T\left(\vec{\chi}^*\right) \tag{VI.2.4}$$

where $\vec{u}$ is the image of $\vec{\chi}$ through an isoprobabilistic transformation Γ, like the Rosenblatt transformation [Lebrun and Dutfoy 2009a,b,c], such that all components of $\vec{u}$ are uncorrelated and follow a standard Gaussian law (see Fig. VI.7).

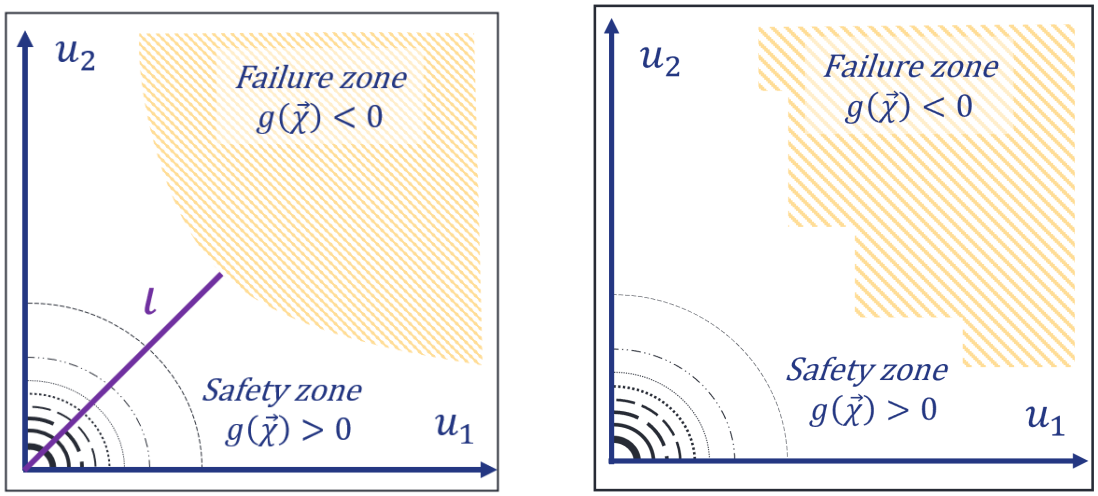

(a) Differentiable state function (b) Non-differentiable state function

Fig. VI.7: Failure zone after the isoprobabilist transformation of the base variables. In (a) the length of the purple segment denotes a reliability index. In (b), a reliability index can be defined, but FORM/SORM methods cannot be directly applied as long as the state function is not differentiable.

We may consider developing the design problem using this paradigm, considering the state function to be unknown. In practice, not all investigations of Stress-Strength interference are conducted through an isoprobabilistic transformation of the partially known base variables and an approximation of the performance function $g_{\mathcal{V}}$ in the vectorial case.

However, the idea to seek a reference tuple $\vec{\chi}^*$ and to control from there the risk of failure of the system is well installed in industrial practice, and serves as a good theoretical basis for the determination of validation conditions in the general case.

VI.2.4 Synthesis

On the one hand, methods for the elaboration of design objectives in the automotive industry are confined to unidimensional sub-problems. The definition of the base variable $Z = R - \Phi$ is made simple by the use of a single variable of pseudo-fatigue, making the definition of severity and the evaluation of Stress a mere topological transformation in $\mathbb{R}$.

In a multidimensional framework, we will see in the next section that, unless a few critical hypotheses are established, the variables of pseudo-fatigue (underlying Stress) and the parameters of resistance (underlying Strength) do not necessarily fit in the same space. They do not necessarily have the same topology.

Methods for reliability analysis are fit for the determination of the risk of failure of complex systems with a large dimension in terms of base variables, but the inverse problem with a maximum admissible risk of failure is not yet written for our matter. We will use this formalism to write down the problem of reliable design and validation in the multidimensional case.

VI.3 Definition of the design and validation problems for complex systems

VI.3.1 Complex systems

For the sake of its reliable design, a system is deemed complex if it exhibits several failure scenarios that are not always equally probable for a given mission in service. In other words, a part is complex if one of its sensible zones may fail before the end of a mission and not another zone, or vice-versa. This idea was already the anchor point of our definition of local contexts in Chapter III.

The reliability of a complex system is given by a combination of all its plausible scenarios of failure in service. These scenarios, while associated with modes of failure that are not equally probable - say, different sensible zones of the structure, different local contexts - are not independent. Therefore the reliability of the system is not simply the sum of the reliability of all its components. This trivial difficulty theoretically makes controlling the risk of failure of a complex system more complicated than merely controlling the risk of failure of each of its components.

This knot lies in the propagation of requirements in reliability: Lower-level requirements associated with single joints, to local contexts or to a part ideally ensure the respect of requirements at the organic or functional levels. Therefore, the associated risk of failure for each subsystem must ensure that the risk of the higher-level subsystem is well controlled. Fault tree analyses serve such a purpose, but the components of the tree and the correlation of their failure modes need to be known to allow risk propagation.

In this section,we investigate necessary mathematical conditions for the determination of design and validation objectives for the reliability of complex systems when mission characterization and design parameters are separated (as in independent Stress and Strength).

The separation of the design and validation problems is important, because the necessary hypotheses and parameter definitions to be able to solve either will differ from one to the other.

VI.3.2 Towards multidimensional Stress and Strength

As a reminder, design parameters - part shape, joint geometry, weld dimensions, definition of articulations - are considered to have an influence on the resistance of the system at stake, not on the pseudo-fatigue induced by a mission. Mission characterization and the resistance of designed components are independent variables. Let us also consider that the pseudo-fatigue of a mission and the resistance of a system can be described using a finite number of dimensions. We may then rewrite the base variables (χ_k) as a mapping of tuples of mission and resistance descriptors $\overrightarrow{\varphi}$ and $\overrightarrow{r}$:

$$\forall\,(\overrightarrow{\varphi},\overrightarrow{r}) \in \mathbb{D}\otimes\mathbb{V},\ (\overrightarrow{\varphi},\overrightarrow{r}) \to (\chi_k)_{k\in[1,n_d]} \tag{VI.3.1}$$

denoting $\overrightarrow{\varphi}$ the fatigue characterization (*i.e.* pseudo-fatigue) of a mission of the system; $\overrightarrow{\Phi}$ the associated random variable of pseudo-fatigue; $\mathbb{D}$ the space of service pseudo-fatigue induced by admissible missions (the notation $\mathbb{A}$, previously used, denoted admissible loading histories); $\overrightarrow{R}$ a random vector containing factors determining the resistance of sensible zones of the system; $\overrightarrow{r}$ one of its realizations; $\mathbb{V}$ the space of the resistances of issues of the system $\mathcal{V}$. $\overrightarrow{\Phi}$ and $\overrightarrow{R}$ are independent variables.

When pseudo-fatigue and resistance variables are not scalar, the integral definition of risk of failure is harder to obtain. We must properly define a probability triple (sample space, set of events and probability function associated with events) prior to defining the random experiment yielding the state of an issue of the system following a mission. The sample space is the set of all plausible couples $(\overrightarrow{\varphi},\overrightarrow{r}) \in \mathbb{D}\otimes\mathbb{V}$. In short, we have to prove that the spaces of pseudo-fatigue and of resistance are measurable (see Fig. VI.8).

VI.3.2.1 Measurability of pseudo-fatigue

In our case, $\mathbb{D}$ maps sets of magnitudes in $\mathbb{R}^\kappa$ with a fixed size κ, it is therefore continuous and measurable. A first definition of a mathematical measure on any subset $W \subset \mathbb{D}$ may

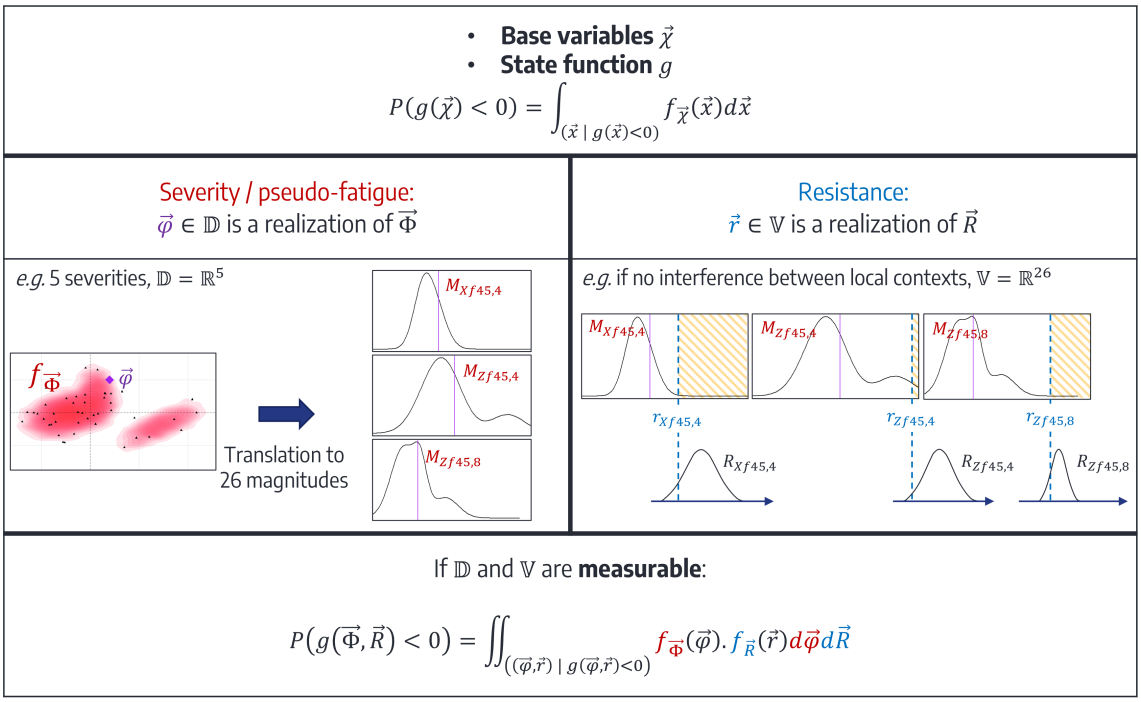

Fig. VI.8: Decomposition of the base variables into pseudo-fatigue and resistance. An example is given with the magnitudes and the conditional severity defined previously, under the hypothesis of no influence in the resistance of sensible zones between two local contexts. If the now separated terms lie in measurable spaces $\mathbb{D}$ and $\mathbb{V}$, their distribution can be defined and used to rewrite the integral formula for the risk of failure.

be $dW^* = \prod_{k=1}^{\kappa} \int_{W_k} dM_k$; denoting $W = \prod_{k=1}^{\kappa} W_k$; W_k being the projection of the elementary volume W onto the direction corresponding to the k-th magnitude.

However, as we have established in Section V.4, pseudo-fatigue can be mapped as per its conditional severity on an aggregated trip. In that case, another measure of interest is $dW = W_0 \cdot \prod_{h=1}^{5} \int_{B_h} dS_h$; denoting B_h the projection of the elementary volume W onto the h-th dimension of conditional severity, and dS_h the associated measure for this dimension. In that case, W_0 is considered to be a constant for all elementary volumes selected on the space of conditional severity.

VI.3.2.2 Measurability of resistance

At first sight, the vector $\vec{r}$ may contain the information of geometry, material parameters and fatigue properties of all components of the system, being a finite vector of unknown dimension. We need to find a transformation of these design parameters into a variable that is easily compared to pseudo-fatigue.

We have made a hypothesis of non-interdependence between different local contexts of the systems. Indeed, we consider that the propagation of a crack in a given local context does not modify the propagation of a crack in other local contexts, see §III.5.1. Therefore, the resistance of components of the system can also be defined in terms of a vector of each minimum pseudo-damage that the system may withstand or not. In that case, $\vec{r}$ is equivalent

to a vector of κ maximum admissible pseudo-damages for an issue of the system. $\mathbb{V}$ is therefore also continuous and measurable.

If the resistance of the system $\overrightarrow{r}$ is defined from the vector of minimum values of pseudo-fatigue $\overrightarrow{\varphi}$ that lead the system to failure, then the state function is determined by the first local context over which pseudo-damage surpasses associated resistance:

$$\overrightarrow{\varphi} \in \mathbb{R}^{\kappa},\ \overrightarrow{r} \in \mathbb{R}^{\kappa},\ g_{\mathcal{V}}\left(\overrightarrow{\varphi},\overrightarrow{r}\right) < 0 \Leftrightarrow \overrightarrow{\varphi} \triangleright \overrightarrow{r} \tag{VI.3.2}$$

denoting $\triangleright$ a homogeneous relation (endorelation) such that for any vectors $\vec{a}$ and $\vec{b}$ of $\mathbb{R}^{\kappa}$:

$$\vec{a} \triangleright \vec{b} \Leftrightarrow \exists k \in [\![1,\kappa]\!],\ a_k > b_k \tag{VI.3.3}$$

Note that this binary relation between vectors of the same dimension is neither symmetrical nor antisymmetrical.

An example of state function achieving this relation is $g_{\mathcal{V}} : \left(\overrightarrow{\varphi},\overrightarrow{r}\right) = \min_{k\in[\![1,\kappa]\!]}\left(r_k - \varphi_k\right)$. In that case, one may consider the design variables to be mapped (Eq. VI.3.1) as the differences $\chi_k = \left(r_k - \varphi_k\right)$ for each failure mode of the system. However, this example of a state function is only partially differentiable (see Fig. VI.7b). Other more regular functions can be chosen.

The question of a convenient mathematical measure for $\overrightarrow{R}$ is however left open in the general case.

Nota Bene: In the case of interdependent failure modes, the dependence of failure over different local contexts must be explored, searching for orthogonal latent factors of resistance for instance. Only then can one establish an adequate measure of the resistance of the system. Otherwise the space of resistance defined as an aggregation of each failure mode is *a priori* non-measurable, as the measure of a union of subsets of $\overrightarrow{R}$ with null intersections will not be the sum of the measures of subsets.

If both spaces of pseudo-fatigue and resistance are measurable, then the random variable that yields tuples $\left(\overrightarrow{\varphi},\overrightarrow{r}\right)$ is well defined over the probability space $(\mathbb{D}\otimes\mathbb{V})$, with adequate measures for each space $\mathbb{D}$ and $\mathbb{V}$.

VI.3.3 Risk of failure of a system

The risk of failure of the system (the vehicle) $\mathcal{V}$ is given by the probability of the event $\left(g_{\mathcal{V}}\left(\vec{\chi}\right) \leq 0\right)$. If the sample set is associated with a probability measure $d\vec{\chi}$ and a distribution $f_{\vec{\chi}}$ of the base variables exist, the risk can be written in an integrable form:

$$P\left(g_{\mathcal{V}}\left(\vec{\chi}\right) \leq 0\right) = \int\limits_{g_{\mathcal{V}}(\vec{x})\leq 0} f_{\vec{x}}\, d\vec{x} \tag{VI.3.4}$$

Following the mapping of base variables from separate descriptions of pseudo-fatigue and

resistance in Eq. VI.3.1, and the definition of the binary relation $\vec{\varphi} \triangleright \vec{r}$ in Eq. VI.3.2, this integral can be written:

$$P\left(g_{\mathcal{V}}\left(\vec{\chi}\right) \leq 0\right) = P\left(\vec{\varphi} \triangleright \vec{r}\right) = \iint\limits_{\vec{\varphi} \triangleright \vec{r}} f_{\vec{\varphi},\vec{R}}\left(\vec{\varphi},\vec{r}\right) d\vec{\varphi} d\vec{r} \tag{VI.3.5}$$

We make the further hypothesis that pseudo-fatigue and resistance are independent variables, and that measures $d\vec{\varphi}$ and $d\vec{r}$ exist. The density $f_{\vec{\varphi},\vec{R}}$ can be replaced by the product of the distributions of each variable, and the integral can be written using either form:

$$P\left(\vec{\varphi} \triangleright \vec{r}\right) = \int\limits_{\vec{\varphi} \in \vec{\Phi}} \left(\int\limits_{\vec{r} | \vec{\varphi} \triangleright \vec{r}} f_{\vec{R}}\left(\vec{r}\right) d\vec{r} \right) \cdot f_{\vec{\Phi}}\left(\vec{\varphi}\right) d\vec{\varphi} \tag{VI.3.6}$$

$$P\left(\vec{\varphi} \triangleright \vec{r}\right) = \int\limits_{\vec{r} \in \mathbb{V}} \left(\int\limits_{\vec{\varphi} | \vec{\varphi} \triangleright \vec{r}} f_{\vec{\Phi}}\left(\vec{\varphi}\right) d\vec{\varphi} \right) \cdot f_{\vec{R}}\left(\vec{r}\right) d\vec{r} \tag{VI.3.7}$$

Eq. VI.3.7 is a particular form of the equation (1) of [Eryilmaz 2008], from which the author investigates the evaluation of the risk of failure of a system with multiple components and separable multivariate Stress and Strength. In this article, the formalism allows the analysis of subsystems with multiple states and non-trivial state functions (different from a minimum of all states).

As we have pointed out in §VI.2.3, we can consider the direct problem of reliability to be the determination of the risk of failure of a designed system with known distributions of the components of the resistance $\vec{R}$ and known service conditions. In the following section, we will elaborate a definition for the inverse problem: to determine an appropriate design for a given maximum admissible risk of failure.

VI.3.4 The design problem

We have established conditions for the redaction of the direct problem of the evaluation of the risk of failure of a system. In this section, an upper boundary on said risk is established by a requirement in reliability.

The requirement on the reliability of the system $\mathcal{V}$ is written using the state function of the system:

$$\left(\mathcal{R}_{\mathcal{V}}\right) \ : \ \mathcal{P}_{\mathcal{V}} = P\left(g\left(\vec{\chi}\right) \leq 0\right) < P_f \tag{VI.3.8}$$

The objective of the design problem is to determine an appropriate setting of the random variables $\vec{R}$ such that the system is reliable enough.

The design problem is propagated from the vehicle (system) level to the level of its component. Let $\mathcal{Y}$ denote a subsystem of the system. It may be an organ, a part, a component *i.e.* a local context, even sometimes a single zone.

Let us consider $\vec{\varphi}$ to be the input of the problem for the design of $\mathcal{Y}$. Indeed, the state function $g_{\mathcal{Y}}$ of the subsystem will be able to censor the dimensions of $\vec{\varphi}$ that are not relevant to its design.

$\mathcal{Y}$ is designed once we have access to the joint knowledge of a geometrical set of material (sensible) zones prone to failure, their associated fatigue law and a set of localization factors defining the mechanical response of the subsystem to global loading histories.

Note that these three sets of parameters correspond to variables that were left unknown in Chapter III. The set of sensible zones is stored in local contexts as of Eq. III.5.7. The fatigue law of these zones is given in Eq. III.5.1 by the tensor H used to calculate appropriate fatigue variable τ as well as a reference point (τ_0,N_0) of the Wöhler curve of the zone. The localization factors $\left(\underline{\underline{K}}_j\right)_{j\in[1,n_F]}$ correspond to our hypothesis of linear mechanical response of the structure in Eq. III.4.2

The requirement in reliability for the subsystem $\mathcal{Y}$ is written using its terms of pseudo-fatigue and resistance:

$$(\mathcal{R}_{\mathcal{Y}})\ \ \mathcal{P}_{\mathcal{Y}} = P\left(g_{\mathcal{Y}}\left(\vec{\chi}\right) \leq 0\right) < P_{f,\mathcal{Y}} \tag{VI.3.9}$$

denoting $P_{f,\mathcal{Y}}$ the propagated maximum admissible risk of failure for the subsystem $\mathcal{Y}$, determined from a propagation of risks on the system $\mathcal{V}$; and $g_{\mathcal{Y}}$ the state function associated with $\mathcal{Y}$. The probability $P\left(g_{\mathcal{Y}}\left(\vec{\chi}\right) \leq 0\right)$ can be developed for known distributions of $\vec{\Phi}$ and $\vec{R}$ using Eq. VI.3.5, replacing g by $g_{\mathcal{Y}}$.

Given a population of missions $\mathbb{C}$ for a vehicle model to design and a description of pseudo-fatigue $\vec{\varphi}(c) \in \mathbb{R}^{\kappa}\ \forall c \in \mathbb{C}$, the **design problem** consists in determining a random variable $\vec{R}_{\mathcal{Y}}$ following:

$$\text{We're looking for } \vec{R}^{*}_{\mathcal{Y}} \text{ such that } P\left(\vec{\Phi} \triangleright \vec{R}_{\mathcal{Y}} \mid \vec{R}_{\mathcal{Y}} = \vec{R}^{*}_{\mathcal{Y}}\right) < P_{f,\mathcal{Y}} \tag{VI.3.10}$$

In order to allow the comparison $\vec{\Phi} \triangleright \vec{R}_{\mathcal{Y}}$ despite the lower dimension of the resistance of $\mathcal{Y}$, we may consider that all local contexts that are not relevant to the design of $\mathcal{Y}$ have infinite resistance.

As explained previously, this random variable $\vec{R}_{\mathcal{Y}}$ is parametric, *i.e.* engineers only have indirect access to a few parameters of a predetermined law for resistance. For instance, the manufacturing chain is already decided, or the locations of the weld beads and spot welds were already determined by other conditions. The parameters of the weld procedure or the distance between spot welds are examples of parameters to determine.

Therefore, in practice, the problem takes the form of finding the appropriate values of parameters that determine the distribution of $\vec{R}_{\mathcal{Y}}$.

For a given value of pseudo-fatigue $\vec{\varphi}^{*}$, the following conditional probability may be manageable to evaluate:

$$P\left(\overrightarrow{\Phi} \triangleright \overrightarrow{R}_{\mathcal{Y}} \mid \overrightarrow{\Phi} = \overrightarrow{\varphi}^*,\ \overrightarrow{R}_{\mathcal{Y}} = \overrightarrow{R}^*_{\mathcal{Y}}\right) = P\left(\bigcup_{k=1}^{\kappa|_{\mathcal{Y}}} \left(R^*_k \leq \Phi^*_k\right)\right) \tag{VI.3.11}$$

denoting $\kappa|_{\mathcal{Y}}$ the number of pseudo-fatigue variables of interest for the subsystem $\mathcal{Y}$. Note that the elementary events of the union are not disjoint, *i.e.* there may exist missions that may be predicted to provoke failure on all local contexts of the subsystem.

However, the formulation of the probability in a more general sense, based on our available model of $\overrightarrow{\Phi}$ and on simple hypotheses on $\overrightarrow{R}$, was not investigated. Later on, in Section VI.4, we will solve this design problem in a simple case.

VI.3.5 The validation problem

The objective of the validation problem is to determine whether the designed subsystem $\mathcal{Y}$ has the required resistance to withstand service. An important difference with the design problem is that any design can be tested for validation: under-designed, adequate or over-designed versions. The design is not the unknown and the geometry, stiffness and quality of the parts of the system are no longer unknown parameters.

The main principle that summarizes practices in validation is a reminiscence of maximalist design: if the proposed subsystem holds with a satisfying probability when submitted to loads that represent a "very severe" mission, then it should hold to a satisfying extent over all service missions. For instance, such a very severe mission can be taken as one of the most severe observed mission, plus a margin - a safety factor - according to the confidence one has on the knowledge of this outskirt of the distribution of missions [Speckert *et al.* 2009].

Our goal is to provide a similar definition of the validation problem in a probabilistic framework. The solution to the validation problem aims to ascertain that the risk of failure of the proposed design over the population of mission is indeed below the maximum admissible risk of failure.

The validation problem therefore seeks an upper bound to the actual risk of failure of the subsystem based on its response to validation trials. An upper bound is found by evaluating the risk of failure under a set of validation conditions and levels.

Let us also propose a broad definition of the validation problem that includes validation procedures conducted through a series of different load conditions and associated pass criteria.

VI.3.5.1 Procedures

We define a procedure as the joint information of load conditions and levels $\left(\overrightarrow{\varphi}_t\right)_{t\in[\![1,n_v]\!]}$ and criteria, *e.g.* trial failure probability $\left(P_{0,t}\right)_{t\in[\![1,n_v]\!]}$, verifying:

$$\left(V_{\mathcal{Y}}\left(\Phi_t\right)\right) \ :\ \forall \overrightarrow{\varphi}_t \in \Phi_t,\ P\left(\overrightarrow{\Phi} \triangleright \overrightarrow{R} \mid \overrightarrow{\Phi} = \overrightarrow{\varphi}_t\right) \leq P_{0,t} \tag{VI.3.12}$$

denoting $\Phi_t \in \Phi_{\mathcal{Y}}$ a (finite) subset of the population of pseudo-fatigue variables for the subsystem to validate; n_v denotes the number of trials included in the procedure. We can understand the load conditions and level of a procedure respectively as the direction (unit vector) and norm of $\overrightarrow{\varphi}_t$.

A procedure is a richer definition of a loading history used for a trial. Indeed, it also determines the variables of interest for the analysis of the trial and the threshold below which the subsystem is said to pass. Moreover, we do not rout out the possibility of a procedure consisting of two or more distinct trials, with corresponding loads, metrology and pass criteria.

Note that the probabilities $P\left(\overrightarrow{\Phi} \triangleright \overrightarrow{R} \mid \overrightarrow{\Phi} = \overrightarrow{\varphi}_t\right)$ need to be evaluated, estimated or controlled sufficiently to be compared to $P_{0,t}$. For instance, in the case of physical trials, a sufficiently narrow confidence interval should be determined after evaluation of several issues of the same prototype (*i.e.* several outcomes of the random law $\overrightarrow{R}$).

Note also that procedures with very permissive pass criteria or very light load levels are easy to pass. They will not bring any information on the reliability of the subsystem. The goal of the validation problem is to determine conditions that define the most relevant procedures to assess the respect of the requirement.

VI.3.5.2 Total validation

Let us consider the opposite of a permissive procedure with respect to assessing the adequacy of a design. A procedure $V(\Phi_{\mathcal{Y}})$ performs the total validation of subsystem reliability if passing this procedure is strictly equivalent to the respect of the requirement for the subsystem:

$$(\mathcal{R}_{\mathcal{Y}}) \ : \ (V(\Phi_{\mathcal{Y}})) \tag{VI.3.13}$$

denoting $(\mathcal{R}_{\mathcal{Y}})$ the requirement for the reliability of subsystem $\mathcal{Y}$ written in Eq. VI.3.9.

An example of total validation for a subsystem with two non-interdependent components would be a procedure with two distinct load configurations. These two configurations can be chosen so as to disambiguate the risk of failure of each component as well as the probability of the union of their failures. Thus the risk of failure of the system can be determined from the results of the procedures thanks to Eq. VI.3.11.

VI.3.5.3 Validation procedures

An adequate procedure for the total validation of subsystems with a large number of non-interdependent components would require a very large number of distinct trials, with a clever sampling of the most globally severe missions of the system.

Instead of looking for sufficient and necessary conditions for the verification of the requirement, the main strategy for the validation of complex subsystems is to find a simple procedure, one with one or a small number of trials, that distinguishes best between bad and

good designs. It should be hard to pass but fair. A validation procedure is a procedure that brings a satisfying prediction of whether or not a design verifies the requirement.

A failed procedure needs to imply that the proposed design does not verify the requirement: it needs to be absolutely specific. Otherwise, the failed procedure would lead the project to conduct an extra design loop. Passing an ideal validation procedure with a limited number of trials (say $n_v = 1$) should predict the adequacy of the design with an optimal probability: the sensitivity of the procedure is the criterion of the procedure to maximize.

This search for an optimal prediction of design adequacy naturally leads to the simulation of "very severe" or "worse-case" but plausible missions. In §V.2.1, we have introduced the concept of a conservative evaluation of pseudo-fatigue in service. The assessment of this conservativeness conducted in §V.5.2 leads naturally to the choice of such "very severe" missions. It is the combination of a large setting of payload, a damaging and dispersive trip and of a globally severe driver.

In the absence of total validation procedures, the arguments to prefer one validation procedure or the other have a part of arbitrariness. A harder validation procedure brings more confidence in the verification of the requirement, but may lead to costly over-design. A lighter validation procedure puts less stress on the design, but confidence associated with the whole method may be revised. The cost of a validation procedure is a major ingredient to the optimisation of its definition.

VI.3.6 Current limitations

An analytical formula for the distribution of conditional severity is available from the distribution of pseudo-fatigue performed in Section V.4, in the form of a Gaussian mixture.

An analytical formula for the distribution of resistance is usually available for each component of the structure. However, there is no known distribution of resistance in a configuration with a variety of failure modes that are not always equally probable. As of now, there is no guarantee that a parametric form for such a complex distribution may be established prior to a design proposition.

The theoretical framework established in this section serves as a starting point towards the elaboration of design and validation objectives for complex subsystems with a variety of failure modes. A more in-depth analysis of the reliability of a given organ of the suspension could not be conducted in the duration of the thesis.

In the next section, we will settle on the existing framework for the design and validation of subsystems with a single independent mode of failure. However, we will adapt it to the shape of the distribution of pseudo-fatigue determined in the previous chapter.

VI.4 Determination of design and validation objectives in a unidimensional framework

VI.4.1 Risk of failure and severe clusters

In section V.3.4, for the aggregated trip of the measurement campaign US18-DT1, we have identified a number of clusters $(\mathbb{C}_y)_{\in[\![1,3]\!]}$ separated by their drivers' global severity. Drivers in the most severe cluster, representing roughly a quarter of the samples, induce higher pseudo-damages on the vehicle on all local contexts.

It is safe to assume that if a vehicle model is designed in a way so that only a very little fraction of the most severe cluster may lead weak issues of the vehicle to fail, then the model would not be led to failure by any driver of the other clusters.

We can split the integral in Eq. VI.3.6 over the three sub-populations of missions with no further hypotheses on the dimension and shape of pseudo-fatigue and resistance.

Let us denote $\left(\overrightarrow{\Phi}_y\right)_{\in[\![1,3]\!]}$ the random variable associated with variables of pseudo-fatigue for each sub-population $(\mathbb{C}_y)_{\in[\![1,3]\!]}$.

Let us propose the hypothesis that the risk of failure of a well-designed subsystem for given drivers of the clusters associated with lower global severity $y \in [\![1,2]\!]$ (number of clusters minus one) is negligible, hence:

$$P\left(\overrightarrow{\Phi} \triangleright \overrightarrow{R} \mid \overrightarrow{\Phi} = \overrightarrow{\Phi}_3\right) \gg P\left(\overrightarrow{\Phi} \triangleright \overrightarrow{R} \mid \overrightarrow{\Phi} = \overrightarrow{\Phi}_y\right) \quad \forall y \in [\![1,2]\!] \tag{VI.4.1}$$

$$P\left(\overrightarrow{\Phi} \triangleright \overrightarrow{R}\right) = \sum_{y=1}^{3} \pi_y \cdot \int_{\overrightarrow{\varphi} \in \mathbb{D}_y} \left(\int_{\overrightarrow{r} \mid \overrightarrow{\varphi} \triangleright \overrightarrow{r}} f_{\overrightarrow{R}}(\overrightarrow{r})\, d\overrightarrow{r} \cdot f_{\overrightarrow{\Phi},y}(\overrightarrow{\varphi})\, d\overrightarrow{\varphi} \right) \tag{VI.4.2}$$

$$\approx \pi_3 \cdot \int_{\overrightarrow{\varphi} \in \mathbb{D}_3} \left(\int_{\overrightarrow{r} \mid \overrightarrow{\varphi} \triangleright \overrightarrow{r}} f_{\overrightarrow{R}}(\overrightarrow{r})\, d\overrightarrow{r} \right) \cdot f_{\overrightarrow{\Phi},3}(\overrightarrow{\varphi})\, d\overrightarrow{\varphi} = \pi_3 \cdot P\left(\overrightarrow{\Phi} \triangleright \overrightarrow{R} \mid \overrightarrow{\Phi} = \overrightarrow{\Phi}_3\right) \tag{VI.4.3}$$

In that case, the largest modeling efforts should be focused on the distribution $f_{\overrightarrow{\Phi},3}$ of the most severe sub-population of pseudo-fatigue. The proportion π_3 must also be estimated from available data.

Let us recall the results in terms of extreme quantiles of magnitudes and population shapes observed in §V.4.3 and §V.5.2.3.

The negligibility of different sub-populations of drivers in the calculation of the risk of failure can be questioned and verified by evaluating the ratio between their contribution and the contribution of the third sub-population.

Let us take an example in one dimension. Let q_k be the quantile associated with a probability $P_{n,k} \in [0.9,1[$ calculated on the total distribution of equivalent magnitudes on the

k-th local context of the analysis performed in §V.4.3. The lower bound 0.9 is arbitrary. We calculate for each sub-population the probability:

$$P\left(\Phi_k > q_k \mid \Phi_k = \Phi_{y,k}\right) = 1 - F_{\mathcal{N}_0}\left(\frac{q_k - \mu_{y,k}}{s_{y,k}}\right) \tag{VI.4.4}$$

denoting $F_{\mathcal{N}_0} : y \to P(x \leq y)$ the cumulative distribution associated with the standard Gaussian law; $\mu_{y,k}$ and $s_{y,k}$ respectively the projected mean and deviation for the y-th sub-population on the k-th magnitude.

The probability for a mission to induce more magnitude than the quantile can be written using the law of total probability, *i.e.* the sum of the contributions of each sub-population:

$$P\left(\Phi_k > q_k\right) = 1 - P_{n,k} \tag{VI.4.5}$$

$$= \sum_{y=1}^{3} P\left(\Phi_k = \Phi_{y,k}\right) \cdot P\left(\Phi_k > q_k \mid \Phi_k = \Phi_{y,k}\right) \tag{VI.4.6}$$

$$= \sum_{y=1}^{3} \pi_y \cdot P\left(\Phi_k > q_k \mid \Phi_k = \Phi_{y,k}\right) = \sum_{y=1}^{3} P_y \tag{VI.4.7}$$

The probabilities P_y associated with each sub-population $y \in [\![1,3]\!]$ for the contexts presented in §V.4.3 and the quantiles calculated in the same section are presented in Tab. VI.1.

Context	Quantile value	P_1	P_2	P_3	Sum
		$\pi_1 = 64\%$	$\pi_2 = 18\%$	$\pi_3 = 18\%$	100%
$\gamma_1 = \left(\widetilde{\alpha}_{X,f,45}, 4\right)$	$1.79 \cdot Q_{\text{tot}}$	1.3E-6	8.5E-5	9.1E-4	1.0E-3
$\gamma_2 = \left(\widetilde{\alpha}_{Z,f,45}, 4\right)$	$3.52 \cdot Q_{\text{tot}}$	4.4E-10	5.2E-11	1.0E-3	1.0E-3
$\gamma_3 = \left(\widetilde{\alpha}_{Z,f,135}, 4\right)$	$3.52 \cdot Q_{\text{tot}}$	4.8E-10	7.9E-8	1.0E-3	1.0E-3
$\gamma_4 = \left(\widetilde{\alpha}_{Z,f,45}, 8\right)$	$2.05 \cdot Q_{\text{tot}}$	1.3E-9	0	1.0E-3	1.0E-3

Table VI.1: Contributions of each sub-population of drivers, as modeled in Section V.4 over the aggregated trip REF, to the probability that a mission has a higher magnitude that the 99.9% quantile of the marginal population of magnitude for four local contexts. This probability is known to be 0.1% as per the definition of a quantile.

Note that the values stored in Tab. VI.1 were obtained from the analysis on the aggregated trip REF, over which the globally severe sub-population of drivers is well separated to the other sub-populations. If we were to choose the aggregated trip URB, the sub-populations of drivers would not be well separated for some magnitudes. This means that there is not always a significant sub-population of severe drivers.

VI.4.2 1D design objective

Let us consider a subsystem $\mathcal{Y}$ that can be summarized to one local context γ^* such that $\mathcal{Y} = (z \in \mathcal{V}, \gamma_z = \gamma^*)$, its resistance can be described using one single random variable R, and so can its pseudo-fatigue Φ. For instance, this last variable can result from a projection of the distribution of conditional severity. The conditions for the exploitation of Stress-Strength Interference methods are met.

From the decomposition of pseudo-fatigue into Gaussian sub-populations in section V.3.4, the translation of the failure domain in the case of separate and independent Stress and Strength variables in Eq. VI.3.6 and the approximation of risk of failure from the most severe cluster of pseudo-fatigue in Eq. VI.4.3, we can adapt the requirement on the reliability of the subsystem $\mathcal{Y}$:

$$\mathcal{P}_{\mathcal{Y}} \approx \pi_3 \cdot P\left(\Phi \geq R \mid \Phi = \Phi_3\right) < P_{f,\mathcal{Y}} \tag{VI.4.8}$$

We will provide an analytical solution for the appropriate parameters of R in the case of Gaussian Stress and Strength distributions. The Stress variable Φ is considered to follow a Gaussian law $\mathcal{N}(\mu_{\Phi,3}, s_{\Phi,3})$ with known mean and deviation $\mu_{\Phi,3}$ and $s_{\Phi,3}$. The Resistance variable R is considered to follow a Gaussian law $\mathcal{N}(\mu_R, s_R)$ with unknown mean and deviation μ_R and s_R.

The support of both Gaussian laws spans $\mathbb{R}$. Negative values of Stress and Strength do not represent realistic pseudo-fatigue and resistance conditions. We consider that events $\Phi \leq 0$ and R have negligible probabilities, as usual in typical implementations of SSI.

Let us define the design variable $Z = R - \Phi$. It follows a Gaussian law with mean $\mu_R - \mu_{\Phi,3}$ and deviation $\sqrt{s_R^2 + s_{\Phi,3}^2}$. The requirement Eq. VI.4.8 becomes:

$$\mathcal{P}_{\mathcal{Y}} = \pi_3 \cdot P\left(Z \leq 0\right) < P_{f,\mathcal{Y}} \tag{VI.4.9}$$

$$\Leftrightarrow \pi_3 \cdot F_{\mathcal{N}_0}\left(-\frac{\mu_R - \mu_{\Phi,3}}{\sqrt{s_R^2 + s_{\Phi,3}^2}}\right) < P_{f,\mathcal{Y}} \tag{VI.4.10}$$

denoting $F_{\mathcal{N}_0} : y \to P(x \leq y)$ the cumulative distribution associated with the standard Gaussian law.

Most of the time in the industry, the variation coefficient of R, $v_R = s_R/\mu_R$ is set in advance for the organ of interest as it corresponds to process variability inherent to the infrastructure in place in the factory. Let us replace s_R by $v_R \cdot \mu_R$ and consider μ_R as the unknown of the problem.

Let us write $T = F_{\mathcal{N}_0}^{-1}\left(\frac{P_{f,\mathcal{Y}}}{\pi_3}\right)$ denoting $F_{\mathcal{N}_0}^{-1}$ the quantile function associated with the standard Gaussian law. We also define $v_{\Phi,3} = s_{\Phi,3}/\mu_{\Phi,3}$ the variation coefficient associated with the variable of pseudo-fatigue for subsystem $\mathcal{Y}$. The quantile function being an increasing function, Eq. VI.4.10 becomes:

$$T > -\frac{\mu_R - \mu_{\Phi,3}}{\sqrt{\left(v_R \cdot \mu_R\right)^2 + \left(v_{\Phi,3} \cdot \mu_{\Phi,3}\right)^2}} \tag{VI.4.11}$$

$$\Leftrightarrow \mu_R > \mu_{\Phi,3} \cdot \frac{1 + \sqrt{1 - \left(1 - v_R^2 T^2\right) \cdot \left(1 - v_{\Phi,3}^2 T^2\right)}}{1 - v_R^2 T^2} = \mu_R^* \tag{VI.4.12}$$

Therefore, a well-designed version of the subsystem $\mathcal{Y}$ must display a resistance of at least μ_R^* given by Eq. VI.4.12, the so-called 1D design objective.

VI.4.3 1D validation objective

We make the hypothesis that the subsystem $\mathcal{Y}$ is well designed. This leads to a contradiction if a consequence of the requirement in reliability is not met.

The variation coefficient v_R is evaluated from samples of the production lines. We do not need to ascertain this coefficient in our validation strategy.

Therefore, the minimum admissible value μ_R^* is known following Eq. VI.4.12. Let us look for a validation procedure $(V_{\mathcal{Y}}\{\varphi_n\})$ with a single trial φ_n and associated pass criterion P_0, able to test whether:

$$\mu_R \leq \mu_R^* \tag{VI.4.13}$$

Let M_n be a magnitude in $\mathbb{R}^+$. It can be associated arbitrarily to the magnitude induced by a severe mission of the subsystem $\mathcal{Y}$, the projected pseudo-fatigue of which is $\varphi_n = M_n$. It can also be associated with the resistance $r_n = M_n$ of an issue of the subsystem, defined as the minimum magnitude necessary to lead such an issue to failure. In other words, there exist scalar coefficients $\alpha_3 \in \mathbb{R}$ and $\beta \in \mathbb{R}$ such that:

$$M_n = \varphi_n = \mu_{\Phi,3} \cdot \left(1 + \alpha_3 \cdot v_{\Phi,3}\right) \tag{VI.4.14}$$

$$M_n = r_n = \mu_R \cdot \left(1 - \beta \cdot v_R\right) \tag{VI.4.15}$$

M_n can therefore be considered as a quantile of both the known law of pseudo-fatigue Φ_3 and of the law of resistance R (see Fig. VI.9). These quantiles are associated respectively to the probabilities $\mathcal{F}_{\mathcal{N}_0}(\alpha)$ and $\mathcal{F}_{\mathcal{N}_0}(-\beta)$, calculated from the cumulative distribution of the standard Gaussian law. We denote these probabilities respectively P_n and P_0:

$$P\left(\Phi_3 \leq \varphi_n\right) = \mathcal{F}_0\left(\alpha_3\right) = P_{n,3} \tag{VI.4.16}$$

$$P\left(R \leq r_n\right) = \mathcal{F}_0\left(-\beta\right) = P_0 \tag{VI.4.17}$$

Eqs. VI.4.14 and VI.4.15 denote the same variable. $P_{n,3}$ represents the probability that a mission induces a magnitude lower than M_n on the local context γ^* of the subsystem of

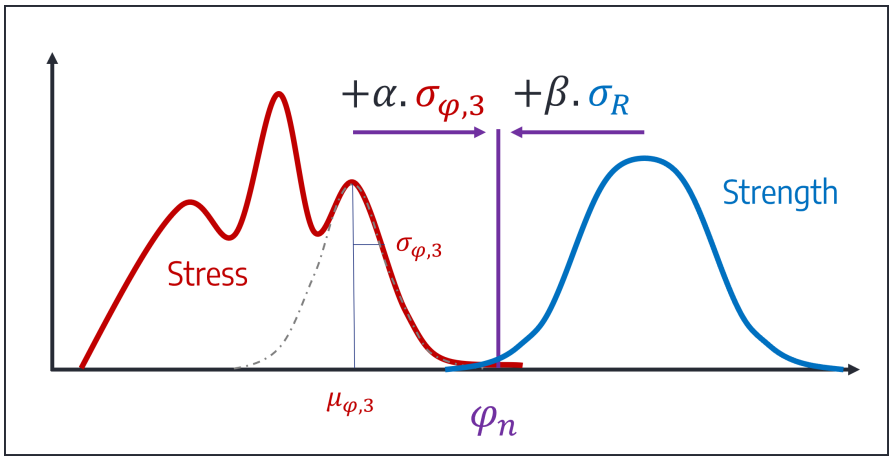

Fig. VI.9: Location of the objective as a quantile of both Stress and Strength, in the case of a mixture with negligible contributions of the two lower cores to the risk of failure of the component

interest. P_0 is the rate of failure of the subsystem under a mission that induces a magnitude of exactly M_n. We can write a condition between α and β:

$$\mu_{\Phi,3} \cdot (1 + \alpha_3 \cdot v_{\Phi,3}) = \mu_R \cdot (1 - \beta \cdot v_R) \tag{VI.4.18}$$

Let us inject Eqs. VI.4.14 and VI.4.15 into the condition to verify on the nominal resistance μ_R of the subsystem, Eq. VI.4.13, and use the formula for μ_R^* as given by Eq. VI.4.12:

$$\begin{aligned} & \mu_R \leq \mu_R^* \\ \Leftrightarrow \quad & \frac{\mu_{\Phi,3} \cdot (1 + \alpha_3 \cdot v_{\Phi,3})}{1 - \beta \cdot v_R} \leq \mu_{\Phi,3} \cdot \frac{1 + \sqrt{1 - (1 - v_R^2 T^2) \cdot \left(1 - v_{\Phi,3}^2 T^2\right)}}{1 - v_R^2 T^2} \end{aligned} \tag{VI.4.19}$$

Let us first consider that the magnitude objective φ_n was chosen as a quantile of the whole population of pseudo-fatigue, associated with a probability P_n, for instance $P_n = 99.9\%$. If the population was Gaussian, this quantile would correspond to the mean of the population plus approximately 3.09 deviations.

However, our population of pseudo-fatigue is modeled by a Gaussian mixture. We have proposed in §VI.4.1 to restrict the formula for the risk of failure to the contribution of the last sub-population when the contributions of the other cores are negligible.

Following the same approximation, the quantile of the Gaussian mixture associated with the probability P_n can be approximated by a quantile on the third sub-population associated with a probability $P_{n,3} = P_n * \pi_3$ (Conditional probability). The third sub-population follows a Gaussian law with parameters $\mu = \mu_{\Phi,3}$ and $\sigma = v_{\Phi,3} \cdot \mu_{\Phi,3}$, therefore this quantile is adequately given by Eq. VI.4.16.

We can solve Eq. VI.4.19 with β as the unknown. The adequate number β of standard

deviations of the law of resistance for the validation of the subsystem $\mathcal{Y}$ at the objective φ is given by:

$$\beta^* = \frac{1}{v_R} \cdot \left(1 - \frac{(1 - v_R^2 \cdot T^2) \cdot (1 + \alpha \cdot v_{\Phi,3})}{1 + \sqrt{1 - (1 - v_R^2 \cdot T^2) \cdot \left(1 - v_{\Phi,3}^2 \cdot T^2\right)}} \right) \tag{VI.4.20}$$

As a reminder, $T = F_{\mathcal{N}_0}^{-1}\left(\frac{P_{f,\mathcal{Y}}}{\pi_3}\right)$, denoting $F_{\mathcal{N}_0}^{-1}$ the quantile function associated with the standard Gaussian law.

If the probability of failure associated with the validation procedure is required to be a set probability P_0, then the coefficient β is fixed. The previous formula can be inverted to determine an adequate coefficient α^*:

$$\alpha^* = \frac{1}{v_{\Phi,3}} \cdot \left((1 - \beta \cdot v_R) \cdot \frac{1 + \sqrt{1 - (1 - v_R^2 \cdot T^2) \cdot \left(1 - v_{\Phi,3}^2 \cdot T^2\right)}}{1 - v_R^2 \cdot T^2} - 1 \right) \tag{VI.4.21}$$

In other words, the 1D validation objective φ_n is determined either as a quantile of the variable Φ_3 by Eqs. VI.4.14 and VI.4.21 or as a quantile of the variable R by Eqs. VI.4.15 and VI.4.20.

VI.4.4 Consequences for the elaboration of validation objectives

The probability P_n is associated with the choice of a quantile φ of pseudo-fatigue. The probability P_0 is associated with the conditional risk of failure of the subsystem when submitted to a trial inducing φ. If the probability P_n is chosen arbitrarily, then P_0 is not arbitrary, and vice-versa. This is true for the reliable design of each (simple) component of the system that has a single independent mode of failure.

Let us consider a validation strategy corresponding to the reliable design of a variety of simple components with different associated moments of pseudo-fatigue and resistance. For instance, each of these components may be all the zones associated with a local context $(\gamma_k)_{k \in [\![1,\kappa]\!]}$ in a system.

One may want to set a single quantile probability over pseudo-fatigue P_n for all components, indexed by $k \in [\![1,\kappa]\!]$. This strategy yields a variety of validation criteria $P_{0,k}^*$ for each component. Likewise, one may want to set arbitrarily a single quantile probability over resistance P_0 for all components. This forces using different quantile probabilities $P_{n,\kappa}^*$ (different values of α) for each variable of pseudo-fatigue.

Setting the validation objective to be a quantile of either pseudo-fatigue or resistance has different practical consequences:

- If the validation objective is set as a quantile of pseudo-fatigue, then, in a numerical simulation, (see section II.6) the material criterion used to evaluate the proposition

would need to be adapted to verify different thresholds ($X\%$ stochastic fatigue criteria see section II.4.4);

- In a physical trial, the hypothesis $P(\Phi > R \mid \Phi = \varphi^*) < P_0^*$ would require different numbers of samples to be verified with sufficient confidence. Low probabilities of failure are harder to control with a limited number of trials than probabilities closer to 50%;
- If the validation objective is set as a quantile of resistance, the tail of the distribution of pseudo-fatigue must be known to recalculate the appropriate quantile, and associated validation loads must be computed anew, hence the discussion of the following chapter VII to compute new validation loads.

A specific situation that allows couples of probabilities (P_n,P_0) or number of deviations (α,β) to be equal from one context to another is when the variation coefficients for both pseudo-fatigue and resistance are constant from one context to another. However, a slight variation on the reference coefficient of 15% can be expected over a population of driver as we have seen in §V.5.2.2, Fig. V.22a.

VI.5 Application to previous models

VI.5.1 Objective magnitude per simple component

In this section, we consider that the pass criterion P_0 used in validation procedures of simple components is set to 0.1% for all contexts. In practice, following the discussion of Section II.6 on the fatigue analysis in the industry, this corresponds to using material criteria that predict whether the probability of failure of the component is below or above 0.1%.

We also consider that the variation coefficient v_R is known and set to 10% for all components and that R follows a Gaussian law. A quantile calculated for the probability $P_0 = 0.1\%$ corresponds to a number of deviations $\beta = 3$ from the nominal resistance μ_R.

In the hypothesis of a well designed subsystem, we are looking for the location of the 0.1% quantile of R on the distribution of Φ for each local context. The maximum admissible risk of failure is set to $P_f = 10^{-6}$.

We have chosen the aggregated trip REF to model our population of pseudo-fatigue. Following the strategy developed in §VI.4.1, only the third sub-population is considered to contribute to the risk of failure of each component. For each local context, the three major ingredients needed to solve this problem are the fraction π_3, the mean magnitude and variation coefficient associated with the third core following projection on each magnitude as in §V.4.3. We are looking for the number α_3^* of standard deviations from the mean of the third Gaussian core that correspond to the location (see Fig. VI.9). The formula is given by VI.4.21.

Tab. VI.2 summarizes the results following the evaluation of these three ingredients on the model and the determination of a minimum value for α as per Eq. VI.4.18 for a few contexts. The objective magnitude is then determined from the results in all other columns of the table:

$$M_n = \mu_{3,k} \cdot (1 + \alpha_3 \cdot v_{3,k}) \tag{VI.5.1}$$

Context	Fraction π_3	Mean $\mu_{3,k}$	Coefficient $v_{3,k}$	α_3	Obj. magnitude M_n
$\gamma_1 = \left(\widetilde{\overline{\alpha}}_{X,f,45},4\right)$	18%	$1.30 \cdot Q_{\text{tot}}$	6.8%	3.26	$1.58 \cdot Q_{\text{tot}}$
$\gamma_2 = \left(\widetilde{\overline{\alpha}}_{Z,f,45},4\right)$	18%	$2.40 \cdot Q_{\text{tot}}$	4.1%	3.49	$2.75 \cdot Q_{\text{tot}}$
$\gamma_3 = \left(\widetilde{\overline{\alpha}}_{Z,f,135},4\right)$	18%	$2.56 \cdot Q_{\text{tot}}$	4.5%	3.53	$2.97 \cdot Q_{\text{tot}}$
$\gamma_4 = \left(\widetilde{\overline{\alpha}}_{Z,f,45},8\right)$	18%	$1.23 \cdot Q_{\text{tot}}$	5.0%	3.29	$1.43 \cdot Q_{\text{tot}}$

Table VI.2: Determination of objective magnitudes in a 1D context-per-context strategy for procedures with set pass criterion $P_0 = 0.1\%$ and known resistance dispersion.

Note that the variation coefficient $v_{3,k}$ shown in this table is calculated only on the third sub-population of drivers. It does not refer to the variability of the full population. The variability of a magnitude over the measurement campaign US18-DT1 simulated on the aggregated trip REF was investigated using the empirical variation coefficient calculated over all drivers, v_k, in §V.5.2.2.

For instance, let $\mathcal{Y}$ be a component of a subsystem of the suspension, consisting of a set of weld beads (Basquin exponent $m = 4$ of the front (f) axle that are located in zones that are sensible to symmetrical vertical road loads ($\widetilde{\overline{\alpha}}_{Z,f,45}$). A validation procedure for the reliability of $\mathcal{Y}$ consists in testing the hypothesis:

$$P\left(M\left(\gamma_2,\bullet\right) > R_{\mathcal{Y}} \mid M = 2.75 \cdot Q_{\text{tot}}\right) \leq 0.1\% \tag{VI.5.2}$$

against:

$$P\left(M\left(\gamma_2,\bullet\right) > R_{\mathcal{Y}} \mid M = 2.75 \cdot Q_{\text{tot}}\right) > 0.1\% \tag{VI.5.3}$$

Note that these calculations were performed with a "short" reference trip, lasting $l_0 << l_f$ kilometers. Following the discussion on the extrapolation of vehicle lives up to a lifetime objective l_f in Section V.6, we make the hypothesis that the quantile of pseudo-fatigue corresponding to a distribution of lifelong missions is equal to the extrapolation of the quantile determined above.

In the case of direct extrapolation, *i.e.* replicating the reference trip N times is expected to induce exactly N times the pseudo-damage, the objective of the trial is given by $M_n^{l_f} = 15.4 \cdot Q_{\text{tot}}$.

Fig. VI.10 follows up on the illustration of the quantiles calculated with a single probability of 99.9% of several magnitudes in Fig. V.19. The new quantiles are added in red for each context. The quantile in purple is determined with a set probability of 99.9% from the distribution of magnitude. The probability associated with the red quantile is determined from the parameters of the variable of Resistance in Eq. VI.4.21. Note that with such parameters, the objectives take different values ($P_{\mathcal{N}_0}\left(\alpha^*\right) \neq 99.9\%$).

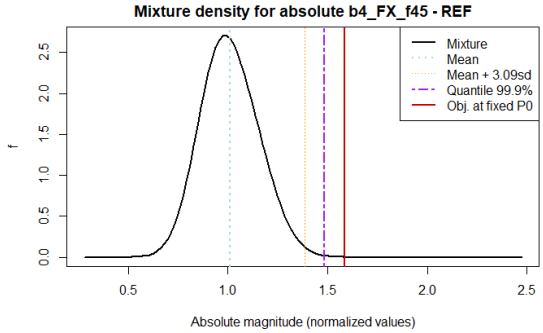

(a) Symmetrical longitudinal loads on the front axle

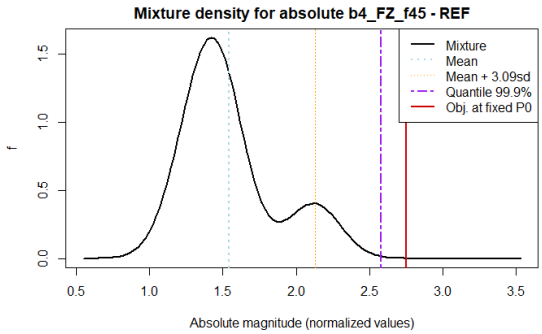

(b) Symmetrical vertical loads on the front axle, exponent of 4

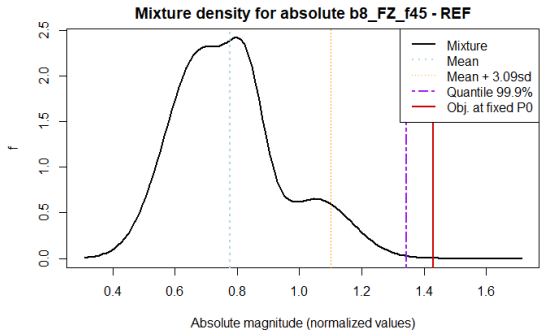

(c) Symmetrical vertical loads on the front axle, exponent of 8

Fig. VI.10: Following up on Fig. V.19, density associated with the marginal law of absolute magnitude following projection of the distribution of conditional severity over dataset $\mathcal{C}'_{\mathcal{T}_1}$ onto three local contexts. The purple quantile is calculated on the mixture with a probability $P_{n,k} = 99.9\%$. The red quantile is the minimum necessary validation objective for a trial with a pass criterion $P_0 = 0.1\%$ (β=3), a known variation coefficient of Strength $v_R = 10\%$ and a maximum admissible risk of failure $P_f = 10^{-6}$, calculated from Eqs. VI.4.21 and VI.4.14.

In [Dreßler and Speckert 2022], the authors judiciously warn against looking for large quantiles of the distribution of pseudo-fatigue. The tails of the distribution are scarcely known: the number of samples is insufficient to determine an adequate model of the tails of the distribution. Large values of α make the quantile fall in the population of large outliers. A sensitivity analysis on the evaluation of the center and covariance coefficients of the third core of the Gaussian mixture should be conducted to establish a confidence interval on the parameters $\mu_{\Phi,3}$ and $v_{\Phi,3}$.

However, because of the condition between α and β as per Eq. VI.4.18, picking a more reasonable quantile of pseudo-fatigue to validate such a high level of reliability ($P_f = 10^{-6}$) means having to check for very low probabilities of failure P_0^*. In numerical trials, the tails of the stochastic criteria are also very scarcely known with confidence. In physical trials, such very low probabilities would only be checked by severizing the objective: picking an alternative objective, further on the Stress distribution, to increase the probability of failure of the prototype. This reduces the number of samples necessary to estimate appropriately

the rate of failure, and therefore the cost of the procedure (see [Beaumont 2013] Chap. 5).

In order to improve the evaluation of the tails of the distribution of pseudo-fatigue, the method would require more data. At Stellantis, the confidence on the variation coefficient of the distribution of pseudo-fatigue was increased on the very long run by feedback (with a Gaussian hypothesis on said distribution): merging and normalizing the results on several datasets to increase the number of samples used to evaluate a general variation coefficient. Connected vehicle solutions may also be future solutions to increase the confidence on the model of pseudo-fatigue (see §IV.3.1).

VI.5.2 Synthetic severe mission

The previous paragraph presented the adaption of current design paradigms exploiting a scalar variable for severity. In the automotive industry, this paradigm is adapted to requirements in reliability written for sets of sensible zones in a subsystem that have redundant failure modes.

This framework is adapted to validation by numerical simulation on the subsystem, as introduced in Section II.6 and discussed further in the next chapter. A series of simple loads on the subsystem, designed to inflict the right amount of magnitude to each context, allows for the verification of their marginal reliability.

We have not conducted the determination of adequate validation objectives for complex subsystems with several non-interdependent failure modes to an end, as discussed in §VI.3.6. Schematically, this problem would consist in finding an adequate "quantile" for a vector of magnitudes of interest for the design of a complex subsystem. The input of the problem would consist of known parameters of the distribution(s) of variables of Strength associated with each local context of the subsystem.

Note that there is no conventional definition of "quantiles" for multivariate random variables. For a given probability P_n, we can find an infinity of partitions of the multidimensional space of pseudo-fatigue $\mathbb{D}$ so that the probability to fall in either subspace is either P_n or $1 - P_n$.

However, as we have introduced in §VI.2.1, a reference mission is often sought to store the knowledge of validation objectives for future projects. This mission is required to be synthetic and "severe", *i.e.* to try all or most components of the system at a large but plausible level.

In the next paragraphs, we introduce several propositions for a severe synthetic mission. We evaluate for each proposition a vector of magnitudes induced by the mission and we will compare them in §VI.5.3.2. Each vector has a translation in the space of conditional severities associated with the dataset $\mathcal{C}_{\mathcal{T}_1}$, and we will discuss their interpretation with respect to the conditional severity of the drivers of US18-DT1 in in §VI.5.3.1.

VI.5.2.1 The objective collection

A first idea of a covering reference for the validation of all components would be a validation objective built as the vector of all validation objectives of all simple components, calculated

in the previous paragraph. Let us consider a vector of coefficients α_k for each local contexts. These coefficients can have the same value or not, as discussed in §VI.4.4. We denote this "objective collection" $\overrightarrow{M}^o$:

$$\overrightarrow{M}_o = (M_{k,n})_{k\in[\![1,\kappa]\!]} \quad \text{with} \quad M_{k,n} = \mu_{\Phi_k,3} \cdot (1 + \alpha_{k,3} \cdot v_{k,3}) \tag{VI.5.4}$$

Note, however, that the vector of all magnitude quantiles is not a "quantile" of driver conditional severity. In fact, it is very unlikely to represent a plausible mission. Indeed, nothing forces the magnitude quantiles determined previously (Tab. VI.2) to stem from the same mission (the same driver).

We may work out the conditional severity of this objective collection by scaling this vector and projecting it onto the space of conditional severities:

$$Z_{o\bullet}^{M,1} = \left(\frac{M_{o,k} - \overline{M}_k}{s_{M_k}} \right)_{k\in[\![1,\kappa]\!]} \tag{VI.5.5}$$

$$\overrightarrow{S}_o = \sqrt{\Lambda_5} \cdot B_5 \cdot Z_{o\bullet}^{M,1} \tag{VI.5.6}$$

This transformation will allow us to discuss the kind of driver that would be represented by the objective collection if we were to choose it as a reference mission, in §VI.5.3.1.

The objective collection stores the 1D validation objectives for all local contexts of the system. However, it hardly defines an appropriate procedure to validate them all at once. Indeed, this single multidimensional objective is significantly severe to all local contexts. In a physical trial, such a procedure could virtually lead any location to failure. This indetermination of the zones that are most sensible to the procedure makes locating design faults much more difficult.

VI.5.2.2 A reference mission representing a specific severity

A second idea to identify a reference mission is to pinpoint a mission with desired "severity". This means selecting an aggregated trip for the stochastic modeling of service pseudo-fatigue, and choosing a driver behavior with desired conditional severity.

We have not defined a transformation of the variables of Strength of a complex subsystem into counterparts to our variables of conditional severity in §VI.3.2. We are here considering the selection of a desired conditional severity to be an arbitrary selection based on the physical understanding of mission severity.

Following the analysis of conditional driver severity in Section V.3, the three principal components that best explain the variability of drivers were interpreted as global severity, sportiness and quick turning. Drivers with a positive coordinate on the first principal component induced larger magnitudes on all local contexts than the average driver.

VI.5.2.2.1 Globally severe synthetic mission

A first proposition of a synthetic mission is to consider a balanced but globally severe driver, *i.e.* associated with a conditional severity given by:

$$\overrightarrow{S} = S_1^* \cdot (1,0,0,...) = S_1^* \cdot \delta\overrightarrow{S}_1 \tag{VI.5.7}$$

with a coefficient S_1^* to determine. The subspace $\left\{\overrightarrow{S} \in \mathbb{R}^5 \mid \exists S \in \mathbb{R},\ \overrightarrow{S} = S \cdot \delta\overrightarrow{S}_1\right\}$ containing all drivers corresponding to this description is a line in the space of conditional severity. The direction of this line is a **severization** direction given by $\delta\overrightarrow{S}_1 = (1,0,0,...)$. We consider that the mean driver, given by the vector $(0,0,0,...)$, belongs to this subspace. We may project the distribution of conditional severity onto this subspace and look for an arbitrary quantile of this distribution (see Fig. VI.11c).

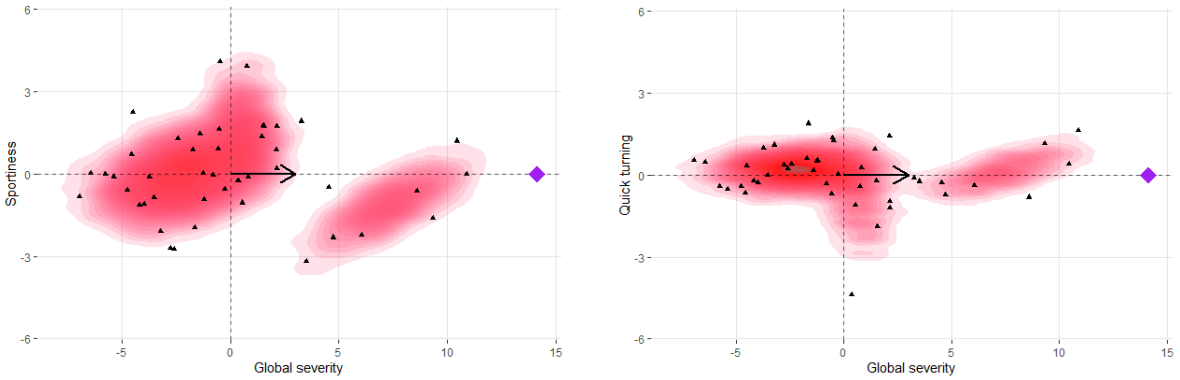

(a) First principal plane (b) Second principal plane

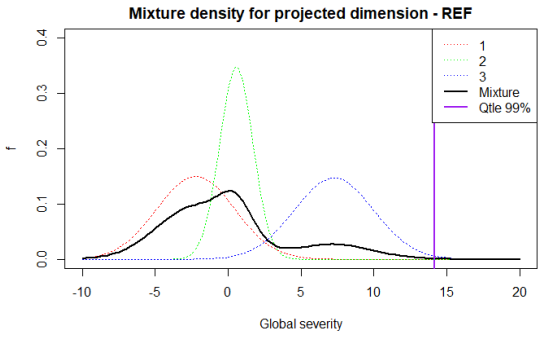

(c) Projected distribution of global severity

Fig. VI.11: Projection of the distribution of conditional severity onto the first principal component and determination of a 99.9% quantile of this projected distribution.

In a fashion similar to the method developed in §V.4.3, the distribution of global severity is obtained from projecting the distribution of conditional severity onto the vector $\overrightarrow{S}_1$. The projection of a multivariate Gaussian mixture with three cores is a univariate Gaussian mixtures with proportions, centers and variances given by:

$$\pi_y|_{\delta\overrightarrow{S}_1} = \pi_y \ \forall y \in [\![1,3]\!] \tag{VI.5.8}$$

$$\mu_y|_{\delta\overrightarrow{S}_1} = \delta\overrightarrow{S}_1 \bullet \overrightarrow{\mu}_y = \sum_{h=1}^{5} S_{1,h} \cdot \mu_{y,h} \tag{VI.5.9}$$

$$\Sigma_y|_{\delta S_1} = \delta\overrightarrow{S}_1 \bullet \Sigma_y \bullet \delta\overrightarrow{S}_1 = \sum_{h=1}^{5}\sum_{k=1}^{5} S_{1,h} \cdot \Sigma_{y,k,h} \cdot S_{1,k} \tag{VI.5.10}$$

denoting $\Sigma_{y,k,h}$ the coefficient of the matrix Σ_y located at the k-th row and the h-th column.

The distribution of this new univariate Gaussian mixture is given by:

$$f|_{\delta\overrightarrow{S}_1}(x) = \sum_{y=1}^{3} \frac{\pi_y}{\sqrt{2 \cdot \pi \cdot \Sigma_y|_{\delta\overrightarrow{S}_1}}} \cdot \exp\left(-\frac{\left(x - \mu_y|_{\delta\overrightarrow{S}_1}\right)^2}{2 \cdot \Sigma_y|_{\delta\overrightarrow{S}_1}}\right) \ \forall x \in \mathbb{R} \tag{VI.5.11}$$

The 99.9% quantile S_1^* of this new distribution is computed numerically. This procedure yields an objective severity $\overrightarrow{S}_1$, associated with a synthetic severe mission. This conditional severity can be translated back into a vector of scaled magnitudes following Eq. V.4.17 and descaled into a vector of absolute magnitudes by adapting Eq. V.4.28:

$$Z_{1*\bullet}^{M,1} = \Lambda_5^{-1/2} \bullet {}^T(B_5) \bullet \left(S_1^* \cdot \delta\overrightarrow{S}_1\right) \tag{VI.5.12}$$

$$\overrightarrow{M}_1^* = \left(s_{M_k}\right)_{k\in[\![1,\kappa]\!]} \bullet Z_{1*\bullet}^{M,1} + \left(\overline{M}_k\right)_{k\in[\![1,\kappa]\!]} \tag{VI.5.13}$$

denoting B_5 the 5 by κ matrix containing the coordinates of the five first principal components in the space of scaled magnitudes following the analysis of the drivers of the measurement campaign US18-DT1 on the aggregated trip REF a.k.a. $\mathcal{T}_1$; $\overline{M}_k$ resp. s_{M_k} the empirical mean resp. standard deviation of the k-th magnitude in the associated dataset.

The magnitude vector associated with this proposition of a synthetic severe mission will be compared to other propositions and references in the following paragraph.

VI.5.2.2.2 Sporty synthetic mission

The synthetic mission can also be arbitrarily chosen to represent a certain type of driving. This selection can be influenced by two considerations:

- Extreme patterns of sporty or clumsy behaviors can be considered as abuse. The selection of a severization direction that excludes too clumsy drivers for instance, will indirectly censor the outskirt of the distribution in the negative domain of the second principal component;

- For a given global severity, sporty drivers are known to induce larger magnitudes on local contexts associated with longitudinal loads on the front axle. If the reliable design of the sensible zones associated with these contexts is expected to be tough or to require extra vigilance, then a sporty synthetic mission might be preferred.

A second proposition for a synthetic severe mission is therefore sought on the subspace of drivers that have the following conditional severity:

$$\overrightarrow{S}_2 = S_2 \cdot (+4, +0.8, +0.5, ...) = S_2 \cdot \delta\overrightarrow{S}_2 \tag{VI.5.14}$$

This "sporty" severization direction $\delta\overrightarrow{S}_2$ defines a new unidimensional subspace Span $\left(\delta\overrightarrow{S}_2\right)$ containing the mean driver (the intersection of the axes in the graph of conditional severity). These coefficients were chosen arbitrarily. They correspond to a search for a globally severe driver that is sporty and has a tendency to turn at higher speed than the average driver.

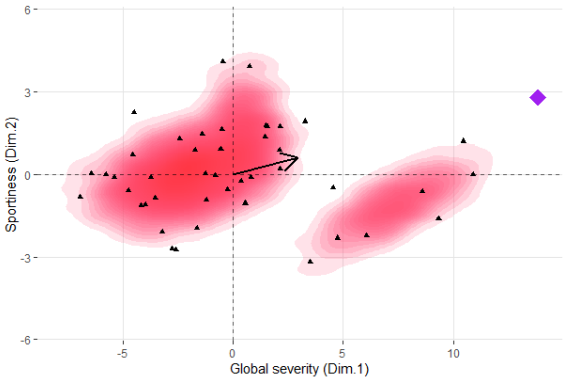

(a) First principal plane

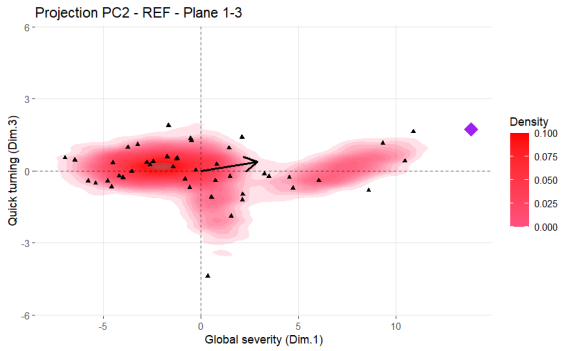

(b) Second principal plane

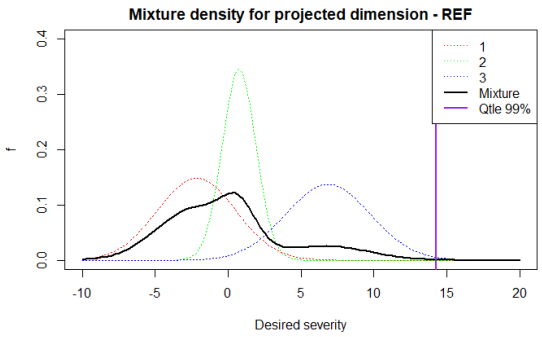

(c) Projected distribution of global severity

Fig. VI.12: Projection of the distribution of conditional severity onto an arbitrary severization direction and determination of a 99.9% quantile of this projected distribution.

We can perform the same procedure as before, replacing δS_1 by $\delta\overrightarrow{S}_2$. A new 99.9% quantile S_2^* is sought on the projected distribution onto $\delta\overrightarrow{S}_2$. The magnitude vector associated with this sporty synthetic mission is given by:

$$Z_{2*\bullet}^{M,1} = \Lambda_5^{-1/2} \bullet {}^T(B_5) \bullet \left(S_2^* \cdot \delta \overrightarrow{S}_2\right) \tag{VI.5.15}$$

$$\overrightarrow{M}_2^* = \left(s_{M_k}\right)_{k\in[\![1,\kappa]\!]} \bullet Z_{2*\bullet}^{M,1} + \left(\overline{M}_k\right)_{k\in[\![1,\kappa]\!]} \tag{VI.5.16}$$

The obtention of the quantile S_2^* is shown in Fig. VI.12c. The location of the desired severe mission in the space of conditional severity is shown in the rest of Fig. VI.12.

VI.5.2.2.3 Severe synthetic mission drawn from a relevant sub-population

The most globally severe drivers stem from the third core of the Gaussian mixture. A synthetic severe mission can be expected to stem from the outskirts of the associated ellipsoid.

Following this principle, the third proposition for a synthetic mission is a projection of the model onto the principal axis of the third ellipsoid. The direction vector of this principal axis is given by the first eigenvector of the covariance matrix of the ellipsoid, denoted $\overrightarrow{b}_3^1$. A known point on this axis is the center of the ellipsoid, $\overrightarrow{\mu}_3$. The subspace of severities over which we are looking for a severe mission is given by:

$$\left(\overrightarrow{S} \in \mathbb{R}^5 \mid \exists S_3 \in \mathbb{R},\ \overrightarrow{S} = \overrightarrow{\mu}_3 + S_3 \cdot \overrightarrow{b}_3^1\right) \tag{VI.5.17}$$

Following the same procedure as before, a 99.9% quantile S_3^* on the distribution projected onto $\overrightarrow{b}_3^1$ is determined and the vector of magnitudes associated with this synthetic mission is given by:

$$Z_{3*\bullet}^{M,1} = \Lambda_5^{-1/2} \bullet {}^T(B_5) \bullet \left(\overrightarrow{\mu}_3 + S_3^* \cdot \overrightarrow{b}_3^1\right) \tag{VI.5.18}$$

$$\overrightarrow{M}_3^* = \left(s_{M_k}\right)_{k\in[\![1,\kappa]\!]} \bullet Z_{3*\bullet}^{M,1} + \left(\overline{M}_k\right)_{k\in[\![1,\kappa]\!]} \tag{VI.5.19}$$

The obtention of the quantile S_3^* is shown in Fig. VI.13c. The location of the desired severe mission in the space of conditional severity is shown in the rest of Fig. VI.13.

VI.5.2.3 Existing proving ground schedules

In the following paragraph, we will compare these so-called synthetic severe missions to a reference that is currently used in the company. As explained in §VI.2.1, the values of objective variables of pseudo-fatigue used for the validation of the reliability of suspension and body components are stored in a proving ground schedule.

The company has access to a variety of proving grounds in several regions of the world following recent acquisitions and merges. As introduced in section IV.2.2, they contain severe but reproducible replications of real-life road events used to rebuild a schedule of events. Such a schedule makes for a fatigue-equivalent summary of the loads that the vehicle may

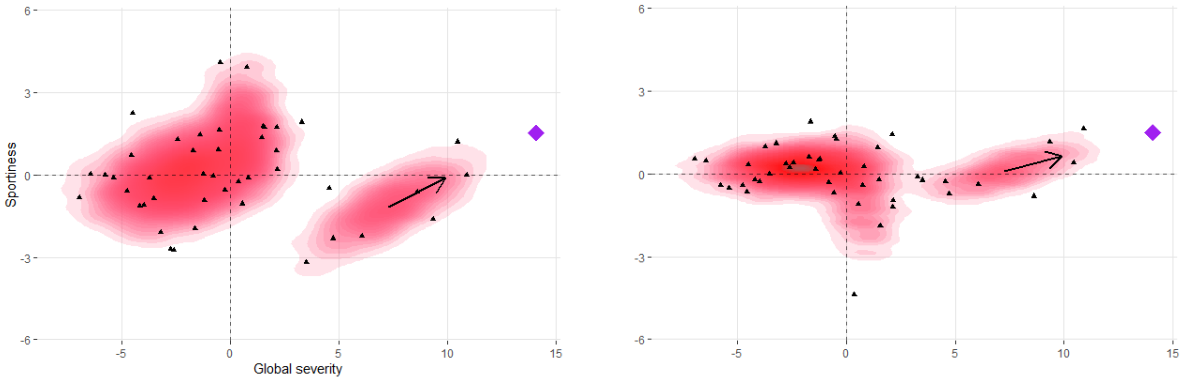

(a) First principal plane (b) Second principal plane

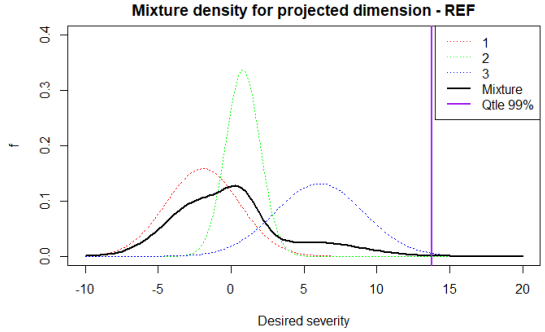

(c) Projected distribution of global severity

Fig. VI.13: Projection of the distribution of conditional severity onto the principal axis of its third Gaussian core and determination of a 99.9% quantile of this projected distribution.

meet in service. It has other design purposes such as NVH (noise, vibration, harshness) and powertrain.

A more in-depth description of the tracks composing this reference is provided in the next chapter, in Section VII.3. Here we consider this reference mission to be provided as is by the company.

Being a concatenation of track loads individually characterized, the pseudo-damage induced by the schedule depends on the order of the concatenation, as explained in section II.5.1, Appendix B and embodied by Eqs. II.5.4 and II.5.5. §B.8 discusses methods to determine this method for large concatenations of loading histories. Since the direct sum of pseudo-damages may be conservative for some global load cases (result of Appendix B.8), we will take the vector of the direct sums of pseudo-damages as the corresponding reference vector.

$$\overrightarrow{M}_p^{l_f} = \left(\sqrt[m_k]{\sum_{e=1}^{g} n_e \cdot \breve{D}(\gamma_k, \overrightarrow{\overline{\mathbf{F}}}_e)} \right)_{k\in[1,\kappa]} \tag{VI.5.20}$$

The proving ground schedule represents an artificial, accelerated, lifelong mission alleged to account for the most damaging situations that the vehicle model may encounter in service. When it comes to the repetition of a series of proving ground tracks, the loads on each event of

the tracks can be expected to be roughly the same. If the proving ground schedule consists in a number N of repetitions of an elementary combination $\vec{n}_0$ of tracks, its total pseudo-damage is given by N times the pseudo-damage of the elementary combination. We can invert this extrapolation and consider that the magnitude induced by a distance $l_0 << l_f$ of this schedule is given as a fraction of the total magnitude:

$$\overrightarrow{M}_p = \left(M_{p,k}^{l_f} \cdot \sqrt[m_k]{\frac{l_0}{l_f}} \right)_{k \in [\![1,\kappa]\!]} \tag{VI.5.21}$$

Thus the vector $\overrightarrow{M}_p$ corresponds to a reference synthetic mission that can be compared with ease to the dataset US18-DT1.

We can also compare this reference mission to the synthetic missions proposed in the two previous paragraphs. However, the proving ground schedule is considered to be associated with a confidential quantile of the population of missions, without the trip restriction that was implemented in Chapter V.

The space of absolute magnitudes is the most relevant space for the comparison of this schedule with the dataset and with the previous propositions for a severe synthetic mission. This comparison will be the goal of §VI.5.3.2.

However, we can translate the magnitude vector associated with the proving ground schedule into conditional severity to interpret the kind of driver that this schedule may represent when compared to the severity of drivers in service. This transformation is achieved by translating this vector in the space of scaled magnitudes associated with the dataset $\mathcal{C}_{\mathcal{T}_1}$ and by projecting it onto the space of conditional severities:

$$Z_{p\bullet}^{M,1} = \left(\frac{M_{p,k} - \overline{M}_k}{s_{M_k}} \right)_{k \in [\![1,\kappa]\!]} \tag{VI.5.22}$$

$$\overrightarrow{S}_p = \sqrt{\Lambda_5} \cdot B_5 \cdot Z_{p\bullet}^{M,1} \tag{VI.5.23}$$

VI.5.3 Comparison of synthetic severe missions

VI.5.3.1 In the space of severity

Three propositions for magnitudes associated with synthetic severe missions were proposed in the previous paragraph. Associated conditional severities with respect to the aggregated trip REF a.k.a. $\mathcal{T}_1$ were calculated for the objective collection $\overrightarrow{S}_o$, for the three propositions $\left(\overrightarrow{S}_c\right)_{c \in [\![1,3]\!]}$ based on the choice of a severization direction and for the proving ground schedule $\overrightarrow{S}_p$.

The first three coordinates of conditional severity associated with each proposition are displayed in Fig. VI.14 alongside the dataset $\mathcal{C}_{\mathcal{T}_1}$ built from the simulation of the drivers of the measurement campaign US18-DT1 on the aggregated trip $\mathcal{T}_1$.

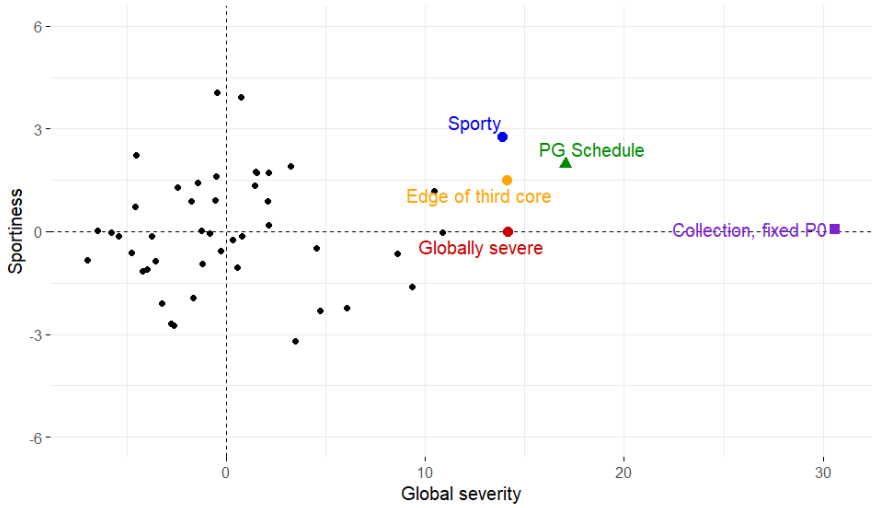

(a) First principal plane

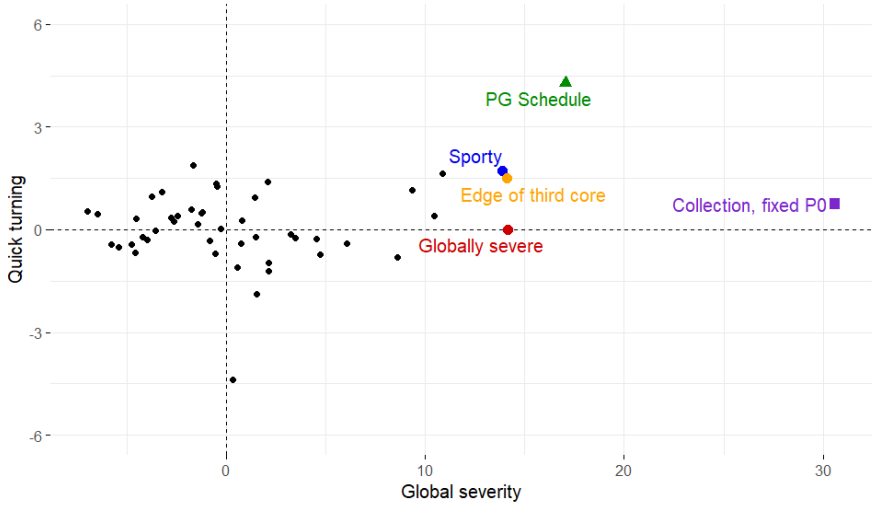

(b) Second principal plane

Fig. VI.14: Conditional severity with respect to the dataset $\mathcal{C}_{\mathcal{T}_1}$, calculated on the five propositions for a synthetic severe mission. Only the circles were determined from the outskirts of the distribution. Note that each objective was not designed to represent the same quantile of the population.

From these graphs, we can comment on the behavior represented by the proving ground schedule. Compared to the drivers of US18-DT1 simulated on the aggregated trip REF, the mission represented by the proving ground schedule is sportier than the whole sample of drivers. This means that the vehicle was submitted to very heavy longitudinal and lateral loads on its front axle. The maneuvers reproduced in this schedule were particularly damaging to this model.

The collection is projected onto a vector with a very high conditional severity. This is caused by two aspects of its creation. First, this collection was determined using a set expected probability of failure P_0. Because of the very low value of the maximum admissible risk of failure, the number of standard deviations from the center $\mu_{\Phi,3}$ of the third core of the population was high: α_k is more than 3 (more than 99.9% of the third core) on all components.

Second, the collection of all objective quantiles is an artificial vector that does not represent a mission or the severization of a mission, as explained in §VI.5.2.1.

VI.5.3.2 In terms of magnitudes

The magnitudes associated with each proposition of a synthetic mission are compared to the magnitude vector of the proving ground schedule in Fig. VI.15

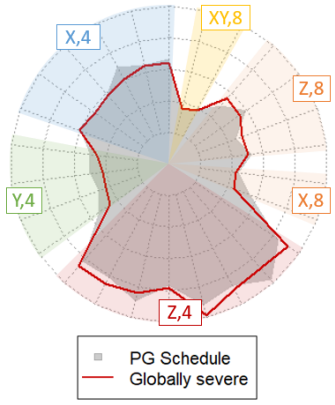

(a) Globally severe mission

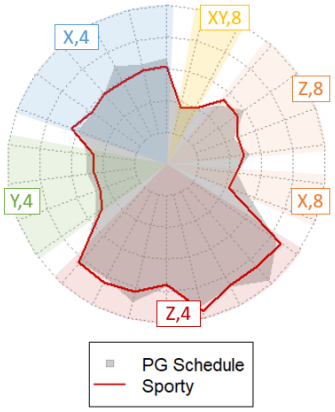

(b) Sporty mission

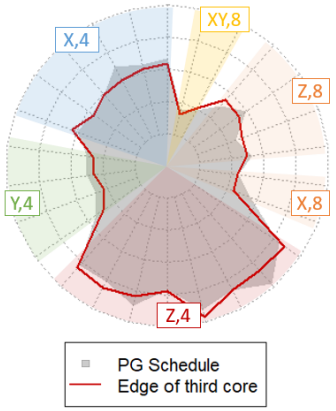

(c) Edge of third core

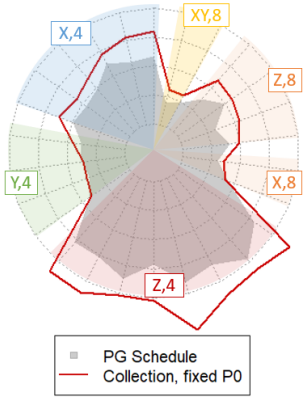

(d) Collection with fixed P_0

Fig. VI.15: Absolute magnitude radars for each proposition of a synthetic mission, compared to the proving ground schedule. All radii have the same range between 0 and a confidential factor times the total charge of the vehicle in Newton

In order to better visualize the difference between each proposition and the reference, we may look for a normalization of these vectors. We could use the same normalization as the one used in V.3.2 to observe the magnitude vectors of the drivers of the dataset $\mathcal{C}_{\mathcal{T}_1}$. The signature used for normalization was the magnitude vector associated with the mean driver of the dataset.

Instead, let us simply compare each vector to the values induced by the proving ground schedule. Fig. VI.16 shows the magnitudes of each proposition relatively to their associated magnitude on the proving ground schedule.

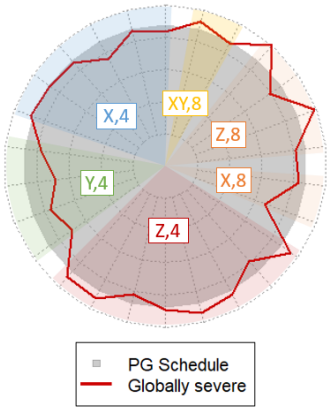

(a) Globally severe mission

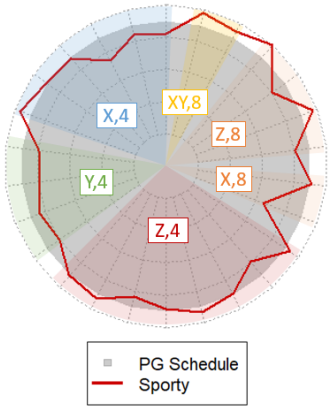

(b) Sporty mission

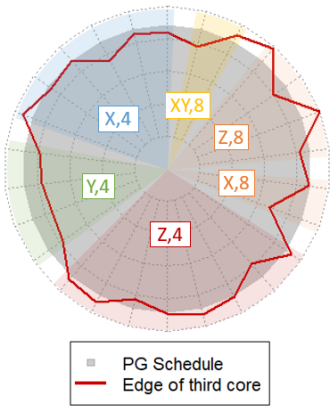

(c) Edge of third core

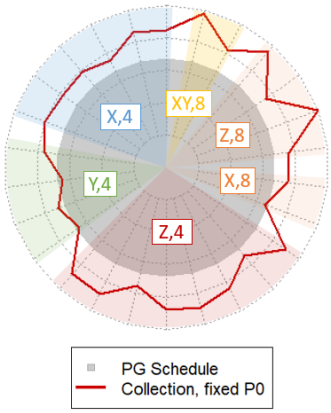

(d) Collection with fixed P_0

Fig. VI.16: Magnitude radars for each proposition of a synthetic mission, when divided by the values associated with the proving ground schedule. All radii have dissimilar ranges starting from 0.

Figs. VI.15d and VI.16d, displaying the magnitude vector associated with the collection of objectives, further show the relevance of normalization for the visualization of magnitude vectors. Comparatively to the magnitudes induced by the proving ground schedule, we can see on this graph that all objective magnitudes from a 1D context-per-context strategy are higher with a similar ratio except on contexts associated with lateral (Y) loads and contexts associated with large and rare (Basquin exponent $m = 8$) longitudinal (X) loads.

We may observe from Figs. VI.16a and VI.16b that the choice of a sporty synthetic mission indeed corresponds to higher values of magnitude on longitudinal (X) and lateral (Y) loads on the front (f) axle calculated with a Basquin exponent of both 4 and 8. Compared to the globally severe mission, this sporty mission represents more pseudo-damage induced by repetitive ($m = 4$) and emergency ($m = 8$) maneuvers, and slightly less pseudo-damage induced by frequent and mild obstacles ($m = 4$).

VI.6 Chapter conclusion

The evaluation and distribution of variables of pseudo-fatigue conducted in the previous Chapter V were used in this chapter as an entry point to develop adequate design references and validation objectives for the reliability of suspension and body components.

The conditions for an integral expression for the risk of failure of the system or any of its subsystems were written and used to define the design and the validation problem for requirements of reliability setting an upper boundary to such risks of failure.

The design and validation problems were written in a general case for (complex) subsystems that exhibit several failure scenarios that are are not always equally probable for a given mission. We have then adapted the Stress-Strength Interference paradigm to our own model for the distribution of pseudo-fatigue.

Thus the design and validation problems were solved for subsystems with a set of failures modes that can be described using a single variable of pseudo-fatigue (components). To solve them, we have made use of the hypothesis that the random variable underlying pseudo-fatigue followed a Gaussian mixture and that the associated resistance for the subsystem of interest followed a univariate Gaussian law.

The definition of the design and validation problems in a general case did not lead to the proposition of a generic method to find adequate design references and validation objectives for the reliability of more complex subsystems. In order to delve further into this issue, the propagation of risk from the point of view of the subsystem to each of its failure scenarios must be performed thoroughly. Such an allocation will be dependent on the vehicle model, its architecture and the technologies that were used to create it. An example should first be conducted on a given vehicle model.

However, we have shown how the definition of conditional driver severity for a given trip may be used to determine synthetic severe missions that make sense with respect to the driver behaviors observed on a given dataset.

The unified model of conditional severity developed in Chapter V therefore displayed its versatility with respect to the determination of magnitude objectives in a unidimensional framework and toward an informed selection of synthetic missions that may be used as design references and replicated as trials in a test environment. Moreover, the dimensions of severity are linked to specific local contexts. Hence sportiness informs us that the magnitude vector of the associated mission will be relatively tougher on contexts of the front (f) axle highlighted by longitudinal (X) and lateral (Y) loads. The existing standards in the company can now be directly compared to the conditional severity of drivers, to better interpret what kind of mission said standards represent in the region of interest.

The determination of objective magnitudes in a unidimensional case and the comparison of these results to the existing reference at Stellantis must be observed critically for two reasons. First, the conservative restriction of trips performed in Section V.2.1 did not include managing the plausibility of the chosen aggregated trip. Indeed, information on trip compositions in service was not included in this thesis. Second, the tails of our Gaussian mixture were not refined because of a lack of knowledge on the representativeness of the sample of drivers in

terms of the most globally severe ones in a region. Moreover, at such extremes, we would need to determine a steadfast criterion to define a frontier between service and abuse on the basis of extreme pseudo-damages induced by the mission as a whole.

Analytical formulas may be available for a minimal condition on the mean resistance of such components even when laws of pseudo-fatigue and resistance are not Gaussian, as long as such laws still have analytical formulas for their distributions and numerically manageable quantile functions. We have not implemented non-parametric distributions such as Gaussian kernels to elaborate our distribution of pseudo-fatigue because these methods have a larger risk of overfitting the dataset.

Chapter VII

Equivalent test loads for the validation of reliability

VII.1 Chapter introduction

VII.1.1 From objectives to loads

The previous chapters led to several propositions for vectors of magnitude and/or mission severity, to reproduce in a validation procedure for the reliability of suspension and body subsystems. Validation procedures are ultimately defined as load procedures, alongside a criterion to determine whether the validation passed or failed. These loads must be reproducible in a protected (industrial) environment, in a time scale compatible with project schedules.

As presented in §VI.2.1, standard loading histories have the ambition of determining, on the one hand, design and validation objectives for new vehicle projects, and on the other hand loads that fulfill these objectives. For instance, the car loading standard CarLoS is both an assumed quantile of the severity of missions of a personal vehicle and the loading procedure able to reproduce this severity.

Thanks to the paradigm of Gassner curves, standard loading spectra can be severized to verify the reliability of vehicle subsystems with an accelerated test. This is similar to deciding to choose a larger maximum required risk of failure P_0 for a given validation objective for practical reasons (see Eq. VI.4.18 and §VI.4.4).

Following the discussions of §VI.4.4 on updating either the objective mission/pseudo-fatigue (adapting the probability P_n associated to the quantile of pseudo-fatigue $\vec{\varphi}_n$) or validation criteria in terms of risk of failure P_0, each new validation objective must, in this paradigm, be translated from the space of severity to new loading conditions.

Fatigue equivalence [Genet (Le Corre) 2006; Raoult and Delattre 2020; Roux *et al.* 2013] aims to find the values of parameters that describe loading histories reproducing a desired vector of induced variables of fatigue or pseudo-fatigue. These parameters may correspond to

load amplitudes, duration of different cyclic load sequences or number of repetitions of given variable amplitude load sequences. A loading history built from a choice of such parameters will be called parametric.

Different conditions in terms of metrology and computation resources often lead to different choices in terms of parametric loads between numerical simulation and physical trials. The restrictions associated to protected environments and associated metrology are discussed in §VII.1.2.

The difference between strong and weak fatigue/damage equivalence is tackled in §VII.1.3. The use of parametric analytical loads for the resolution of strong damage equivalence is then presented in Section VII.2.

Proving Ground(s) (PG) are the available test elements that are closest to real-life road events for new vehicle model projects. Section VII.3 introduces their definition and the different sets of PG tracks available in the company. This presentation of PG tracks will allow us to review some of the effects and concepts discussed previously, such as the the differences in fatigue induced by maneuvers and obstacles and the effects of payload and architecture on the values of global loads.

The definition of weak equivalence problems for large numbers of local contexts is given in Section VII.4. In this thesis, we focus on parametric loads built from concatenations of proving ground tracks concatenations (schedules) of proving grounds. These concatenations are defined in their simple form in §VII.3.3 and discussed further in Appendix B.7.1. The method to determine an optimal pseudo-damage equivalent PG schedule is written and solved as a quadratic optimization problem in §VII.4.4.

Examples of equivalent schedules for different severe missions identified in §VI.5.3 are presented in Section VII.5.

VII.1.2 Testable loads, numerical and physical trials

Let us recall a distinction that we have made in the different spaces of global loading histories of a vehicle. A plausible loading history $\vec{\mathbf{F}} \in \mathbb{A}$ is one to which a vehicle may be submitted throughout its life in service. A testable loading history $\vec{\mathbf{F}} \in \mathbb{F}$ is one that the company can simulate or reproduce in a protected environment (as opposed to real roads).

Note that the set of testable loading histories $\mathbb{F}$ is not equivalent to the set of service loading histories $\mathbb{A}$. Moreover, one is neither a subset nor a superset of the other. For instance, lifelong missions cannot be considered testable because they would be too expensive, and test bench loads are not service loads because the vehicle is not being used *per se*.

Let us qualify the missions and loads that we have been working with until now. A synthetic severe mission is determined, arbitrarily or not, from an analysis of service loads. It may be chosen among the drivers that were sampled in the measurement campaign US18-DT1. Its associated loading history belongs to $\mathbb{A}$. This synthetic mission may also be drawn from reasonable outskirts of a distribution of driver severity on a reference trip as in §VI.5.2.2. If so, then this mission belongs to service. Its associated loading history is unknown: it is not

what was drawn. Both loading histories are non-testable.

These examples of synthetic severe missions yield vectors of pseudo-fatigue. In order to replicate the same fatigue in a protected environment, we must determine an equivalent loading history that can be input with available means. This history will be shorter to implement than an actual life and the loads will be predictable. Both these conditions mean the test loads will fall out of $\mathbb{A}$.

Let us make an extra distinction between loads that can reasonably be input in numerical simulations and loads that can reasonably be input in physical trials. On the one hand, rich numerical models with few hypotheses and submitted to complex loads may be too long to compute. Improvements in computation mean longer and more complex loading histories can be input to a numerical model, up to the possibility of simulating complete PG schedules on a multi-body model with little physical imprecision. Test benches, on the other hand, are limited by the frequential response of both the loading system and of the prototype.

Numerical and physical trials are also different in terms of available metrology: a numerical calculation gives access to inner mechanical variables such as Cauchy stress, however it only represents phenomena that are implemented in the model. On the other hand, measuring inner variables in situ during a physical trial is more expensive and adds a lot of constraints on the procedure, but no mechanical phenomenon will be ruled out.

VII.1.3 Strong or weak fatigue equivalents

Let us consider a vehicle submitted to a global loading history $\vec{\vec{\mathbf{F}}}$ inducing pseudo-fatigue $\overrightarrow{M}_{\text{obj}}$ and a space of parametric loads $\mathbb{F}_{eq}$ with parameters denoted λ_1, λ_2, etc. Strong damage equivalence means seeking an equivalent loading history in $\mathbb{F}_{eq}$ that deals exactly the same damages on the structure (and therefore pseudo-damage and magnitude).

We have already mentioned analytical strong fatigue-equivalent unidimensional loads for a single component with a single failure mode in §II.5.5, or to a single local context when defining equivalent magnitudes in Section III.7. Strong damage equivalence is manageable for low numbers of local contexts of interest and/or for large numbers of available parameters with distinct influences on the fatigue induced by the procedure.

However, complete automotive organs, such as the front suspension, may have several modes of failures that do not necessarily co-occur, *i.e.* several local contexts (see Section VI.3.1). In the case of validation objectives taking this complexity in account, there is no certainty that a strong fatigue-equivalent loading history exists in a parametric set of testable loads.

In most cases, we can only minimize the distance between the vector of pseudo-fatigue to replicate and an optimal equivalent loading history, solving a weak form of pseudo-fatigue equivalence. We have to define such a distance between two loading histories in terms of pseudo-damage or magnitude. This will be tackled in §VII.4.2.

VII.2 Analytical parametric loads: a literature review

VII.2.1 1D formulation

Let $\vec{\mathbf{F}}$ be a global loading history of a vehicle. We want to reproduce the pseudo-damage induced by $\vec{\mathbf{F}}$ on a given local context γ of the structure $\breve{D}_{\text{obj}}$ using parametric loads. The inputs of the sought loading history will be those of the global load case associated with this context.

For instance, if the sensible zone of interest is a lower edge of the metal sheet that forms the cross member of the rear axle, then the load case of interest is assymetrical vertical loads on the rear axle ($Zr135$ in Tab. III.3), as shown in Fig. III.4d, and the Basquin exponent m lies in the range 10 to 20:

$$\breve{D}_{\text{obj}} = \breve{D}\left(\gamma, \vec{\mathbf{F}}\right) = \sum_{i=1}^{n_{\text{bin}}} n_i\left(\mathbf{F}_{Zr135}\right) \cdot \Delta F_i^m \tag{VII.2.1}$$

denoting $\mathbf{F}_{Zr135} = \widetilde{\vec{\alpha}}_{Zr135} \bullet \vec{\mathbf{F}}$. Equivalent loading histories $\left\{\vec{\mathbf{F}}_0 \in \mathbb{F} \mid \breve{D}\left(\gamma, \vec{\mathbf{F}}_0\right) = \breve{D}_{\text{obj}}\right\}$ are sought in a given set of parametric loading histories. Let us take some examples of such sets.

In the case of 1D equivalents, we can define manifolds (fr. *variétés*) of loads consisting of cyclic sinus loads having a set angular frequency ω_0, a fixed number of cycles N_0, a variable amplitude λ (Fig. VII.1a) and a null mean effort. As a reminder, our method ignores the effect of cycle mean as explained in §II.5.4. The search for a strong 1D damage-equivalent is therefore given by the following problem:

$$\begin{aligned} &\text{We're looking for } \lambda_{eq} \in \left\{\lambda \in \mathbb{R} \mid F_{Zr135,0}(t) = \left[\lambda \cdot \sin\ (\omega_0 \cdot t)\ \ \forall t < \frac{2 \cdot \pi \cdot N_0}{\omega_0}\right]\right\} \\ &\text{such that } \breve{D}\left(\gamma, \vec{\mathbf{F}}_0\right) = N_0 \cdot \lambda_{eq}^m = \breve{D}_{\text{obj}} \end{aligned} \tag{VII.2.2}$$

These loading histories may also have a set amplitude ΔF_0 and some freedom in terms of number of cycles λ (Fig. VII.1b):

$$\begin{aligned} &\text{We're looking for } \lambda_{eq} \in \left\{\lambda \in \mathbb{R} \mid F_{Zr135,0}(t) = \left[\Delta F_0 \cdot \sin\ (\omega_0 \cdot t)\ \ \forall t < \frac{2 \cdot \pi \cdot \lambda}{\omega_0}\right]\right\} \\ &\text{such that } \breve{D}\left(\gamma, \vec{\mathbf{F}}_0\right) = \lambda_{eq} \cdot \Delta F_0^m = \breve{D}_{\text{obj}} \end{aligned} \tag{VII.2.3}$$

In another case, both their amplitude and duration may be parameters (Fig. VII.1c). In that case, there is only one scalar condition for two unknowns and the number of solutions is infinite:

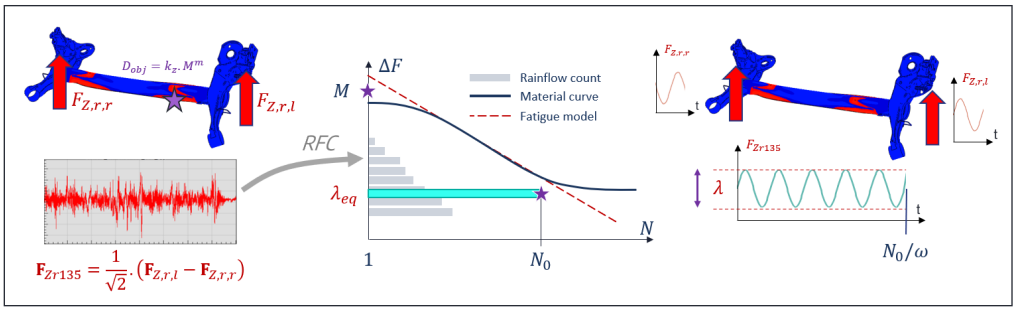

(a) Cycle range as parameter

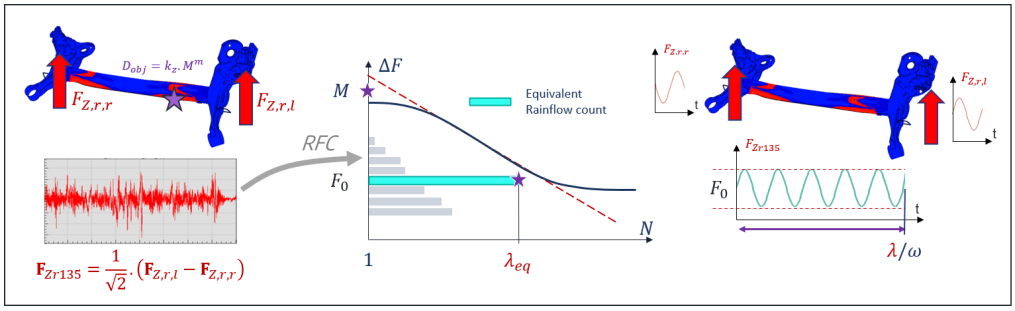

(b) Number of cycles as parameter

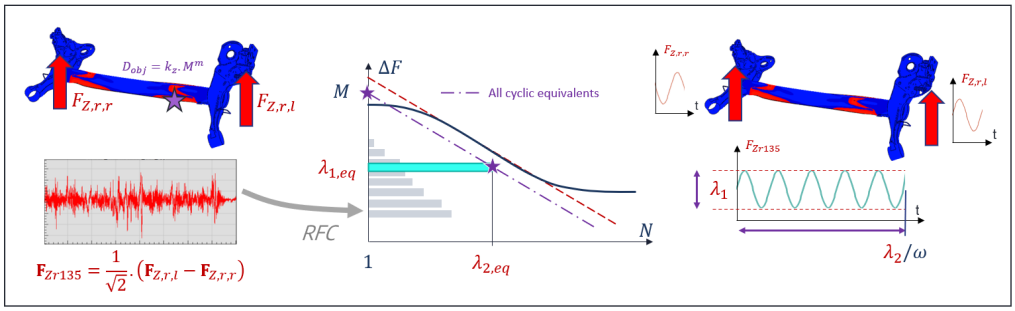

(c) Both range and duration are parameters (infinity of solutions)

Fig. VII.1: Different formulations for the search of a damage-equivalent unidimensional cyclic loading history representing asymmetrical vertical loads on the rear axle.

$$\text{We're looking for } (\lambda_{1,eq},\lambda_{2,eq}) \in \left\{ \vec{\lambda} \in \mathbb{R}^2 \mid F_{Zr135,0}(t) = \left[\lambda_1 \cdot \sin\ (\omega_0 \cdot t)\ \ \forall t < \frac{2 \cdot \pi \cdot \lambda_2}{\omega_0} \right] \right\} \tag{VII.2.4}$$

$$\text{such that } \breve{D}\left(\gamma,\vec{\mathbf{F}}_0\right) = \lambda_{2,eq} \cdot \lambda_{1,eq}^m = \breve{D}_{\text{obj}}$$

Looking for **cyclic** loading histories that are fatigue-equivalent to a variable amplitude loading history is a first strategy to replicate simple validation objectives. The industry may conclude on the resistance of components of interest from their behavior following one cycle of the equivalent load. A fatigue model like a Wöhler curve would then be used to analyze the result at each sensible zone. The fatigue model must be valid in the domain of the number of cycles N_0 (or λ in Eq. VII.2.3 or λ_2 in Eq. VII.2.4). For instance, the Basquin model is valid between low cycle fatigue ($N_0 \approx 10^3$) and the endurance domain $N_0 \approx 10^6$).

If the equivalent cyclic loading history has a number of cycles that falls at the assumed

frontier of the endurance domain, then the fatigue induced can also be discussed through the use of a fatigue criterion (see §II.4.3 for theory and Section II.6 for industrial application; see [Coudray 2022; Coudray *et al.* 2020, 2021] for further aspects of this question). As explained in §II.4.3, a fatigue criterion is usually built from the endurance limit of the assembly measured at two or more baseline trials ([Weber 1999] Chap. 1): these characterization procedures using StairCase, Locati or mixed methods are usually more affordable than the characterization of the Wöhler curve of the assembly.

VII.2.2 Multidimensional perspectives

However, to be able to fit several values of damage or pseudo-damage at once, the number of parameters for the search space of loads may need to be larger than one. In [Genet (Le Corre) 2006] Chap. 7, 8, 9 and in [Genet (Le Corre) *et al.* 2009], manifolds of more complex analytical loads were used, for instance multi-input sinus loads with parametric amplitudes and phases, or cyclic loads that are not sinuses but Gaussian processes.

Let us take the example of a global load case associated to two local contexts with different Basquin exponents m_1 and m_2, *i.e.* two kinds of material assemblies like weld beads and metal sheet edges.

The third formulation in the previous paragraph with two parameters can be adapted to this new issue. With two parameters and two pseudo-damages to replicate, a single solution exists. The strong pseudo-damage equivalence problem is written:

$$\begin{aligned} &\text{We're looking for } (\lambda_{1,eq},\lambda_{2,eq}) \in \mathbb{R}^2, \\ &\text{such that } \breve{D}(\gamma_1,\mathbf{F}) = \lambda_{1,eq} \cdot \lambda_{2,eq}^{m_1} = \breve{D}_{\gamma_1,\text{obj}} \\ &\text{and } \breve{D}(\gamma_2,\mathbf{F}) = \lambda_{1,eq} \cdot \lambda_{2,eq}^{m_2} = \breve{D}_{\gamma_2,\text{obj}} \end{aligned} \tag{VII.2.5}$$

The solution is illustrated in Fig. VII.2 for Basquin exponents of 4 and 15. A third magnitude with a different Basquin exponent 8 can be calculated on the same load case. Note that the equivalent cyclic loading history found for Basquin exponents 4 and 15 will not necessarily induce the same magnitude if calculated with a Basquin exponent of 8. In order to fit this new magnitude in a strong equivalence problem, more degrees of freedom are necessary.

An equivalent scalar 2-block uni-input loading history $\mathbf{F}_0$ can be sought, for instance with set duration (N_1,N_2) in cycles for each block, and a null mean effort. The amplitudes of each block can be tuned to fit the objective pseudo-damage for both local contexts γ_1 and γ_2. These amplitudes are sought in the following space:

$$\mathbb{L}_{\text{block}} = \left\{ \vec{\lambda} = (\lambda_1,\lambda_2) \in \mathbb{R}^2 \mid F_0(t) = \begin{cases} \lambda_1 \cdot \sin\ (\omega_0 \cdot t)\ \text{ if } t < \frac{2 \cdot \pi \cdot N_1}{\omega_0} \\ \lambda_2 \cdot \sin\ (\omega_0 \cdot t)\ \text{ if } t < \frac{2 \cdot \pi \cdot N_2}{\omega_0} \end{cases} \right\} \tag{VII.2.6}$$

The strong pseudo-damage equivalence problem is written:

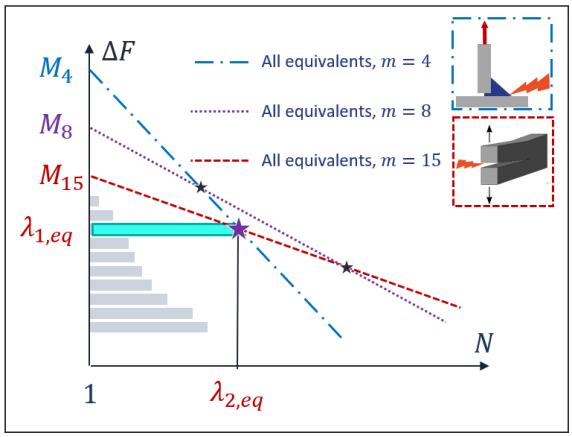

Fig. VII.2: Cyclic fatigue equivalents between pairs of Basquin exponents calculated on the same load case. Three Basquin exponents are considered. A Basquin exponent of 4 corresponds to the fatigue behavior of weld beads. A Basquin exponent of 15 corresponds to the fatigue behavior of metal sheet edges.

$$\begin{aligned} &\text{We're looking for } (\lambda_{1,eq},\lambda_{2,eq}) \in \mathbb{L}_{\text{block}}, \\ &\text{such that } \breve{D}(\gamma_1,\mathbf{F}) = N_1 \cdot \lambda_1^{m_1} + N_2 \cdot \lambda_2^{m_1} = \breve{D}_{\gamma_{1,\text{obj}}} \\ &\text{and } \breve{D}(\gamma_2,\mathbf{F}) = N_1 \cdot \lambda_1^{m_2} + N_2 \cdot \lambda_2^{m_2} = \breve{D}_{\gamma_{2,\text{obj}}} \end{aligned} \tag{VII.2.7}$$

A rise in problem dimension can also be caused by an increase in number of load inputs for the subsystem at stake. Independent load inputs may lead the part to a variety of deformation cases throughout the loading history of interest, hence our strategy in Chapter III. An analytical equivalent loading history should replicate all these load/deformation cases of the part. The resolution of multi-input fatigue equivalence using analytical loads allows creating simplified loading procedures for test benches as in [Schrank 2022].

An example of resolution of a strong form of the damage equivalence problem for the sensible zone of a laminated suspension arm submitted to two load inputs is developed in [Genet (Le Corre) 2006] Chap. 11 (see also Fig. VII.3a). The sought equivalent is a two-block bi-sinusoidal loading history. Each bi-input block loading has null means, is considered to last exactly 500 cycles and is fully determined by 3 degrees of freedom (parameters): the cycle range at each input and the phase between both inputs.

Different triangle technologies manufactured with different processes will have their weakness at a different location (see for instance [Nadot and Denier 2004], Fig. VII.3b for a cast arm and [Grubisic and Fischer 1997], Fig. VII.3c for a welded arm).

The use of block signals for the validation or for the replication of the damage induced by a variable amplitude load is discussed in [Pierron *et al.* 2020] Chap. 1 and in Appendix B.3.1: One should keep in mind the limitations of the Miner Law for trivial concatenations of loads with very different ranges. High load variations concentrated at the beginning or at the end of a signal may break the hypothesis of linear damage cumulation brought with the Miner Law.

(a) Laminated suspension arm [Genet (Le Corre) 2006] Chap. 11

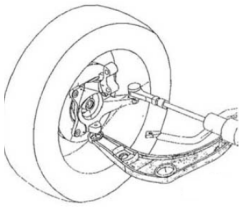

(b) Cast arm [Nadot and Denier 2004]

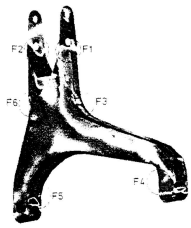

(c) Welded arm [Grubisic and Fischer 1997]

Fig. VII.3: Different suspension triangle technologies (all for a pseudo-McPherson suspension, see Appendix A.2.1.3)

All problems formulated in this section until now are strong damage or pseudo-damage equivalence problems, as an exact match for the objective vector of damages can be found analytically. A caution proposing a high dimensionality of the vector of pseudo-fatigue to replicate is formulated in §VII.4.1, while the switch to weak damage equivalence problems was justified in §VII.1.3 in such cases of high dimensionality.

An example of resolution of a weak form of the damage equivalence problem for a structure submitted to a bi-input variable amplitude loading history and with a large number of local contexts is shown in [Raoult and Delattre 2020] Section 3. Unlike in this thesis, the effect of cycle mean on the fatigue behavior of all sensible zones was taken into account. The sought equivalent loading history is a bi-sinusoidal multi-block signal. Each bi-input block loading is described by 6 parameters: the number of cycles, the mean and range of each input, and the phase between both inputs. The program iterates on the number of blocks until damage equivalence is achieved, with a given threshold, on all local contexts.

An implementation and illustration of fatigue equivalence for a rear suspension member are presented in [Roux *et al.* 2013]. The authors show how the equivalent loading history managed to replicate the values of a fatigue variable at sensible zones of interest, and how other locations of the part ended up being loaded differently from the original loading history.

VII.3 Proving grounds (PG)

In this chapter, our ambition is to adapt the framework of fatigue equivalence to the creation of schedules of road events that are able to replicate multidimensional objectives that are suited to the reliability validation of automotive parts. These building bricks will be Proving Ground(s) (PG) tracks.

By using road events as a building brick for the replication of pre-determined validation objectives (Chapter VI), we expect to create new reference loading histories that are closest to the situations that we want to simulate on the vehicle.

A certain measure of robustness with respect to the vehicle model was also expected, in the sense that an adequate objective for two different models could be described uniquely through

(a) PG facility

(b) Speed bump (fr. *Gendarme couché*)

(c) Speed hump (fr. *Ralentisseur*)

(d) Pothole (fr. *Nid-de-poule*)

Fig. VII.4: Examples of tracks

the definition of a PG schedule. However, in Appendix E, we have made the observation that predicting the loads, the pseudo-damages and therefore the distribution of pseudo-fatigue for another vehicle model was not a trivial task.

VII.3.1 Tracks

Tracks are relatively short road segments built in a protected environment and containing one or a variety of matched road event(s). The definition of the event, be it the geometry of the obstacle or the instruction for the trajectory of a maneuver, are carefully set and practiced by PG technicians, as well as the instructed speed of encounter. That way, the loads induced on a vehicle are as deterministic as possible.

A prototype of a new vehicle model can be driven on PG tracks long before the project gets on the market. Vehicles are instrumented with all necessary sensors to evaluate quantities of interest during the run, such as global loads. Tracks are used to learn the mechanical behavior of the vehicle: the relationship between road and wheel axle loads (for a given wheel), and the relationship between wheel axle loads and interface loads in the system. They are also more and more reproduced numerically to perform this operation on numerical prototypes.

Fig. VII.4 shows some examples of tracks used historically by Stellantis. The set of tracks associated to this PG facility (Fig. VII.4a) in France is our reference for the elaboration of equivalent PG schedules in this chapter.

An inherent variability remains for the loads induced on a vehicle, especially for complex

obstacles such as pavement. Therefore, in the case of PGs at Stellantis, vehicles are driven a few runs on each track to seek an appropriate signal based on load signal post-analyses and engineer experience.

The geometry of track obstacles was chosen from observations and sometimes statistical analyses of the geometry of samples of obstacles met in service. The geometry of turns, uphills, downhills as well as the speed for the braking track were determined from service measurements in locations prone to maneuvers like braking, cornering and climbing. Each automotive company has its own historical version of these PG. For example, Stellantis presents at least five PG facilities from different previously competing companies that merged into the corporation.

A few components of the loading histories associated to three tracks are illustrated in Fig. VII.5. A small event-free (*i.e.* non-damaging) distance before and after the road event is considered part of the track, as it serves as time for the vehicle loads to stabilize around their static values.

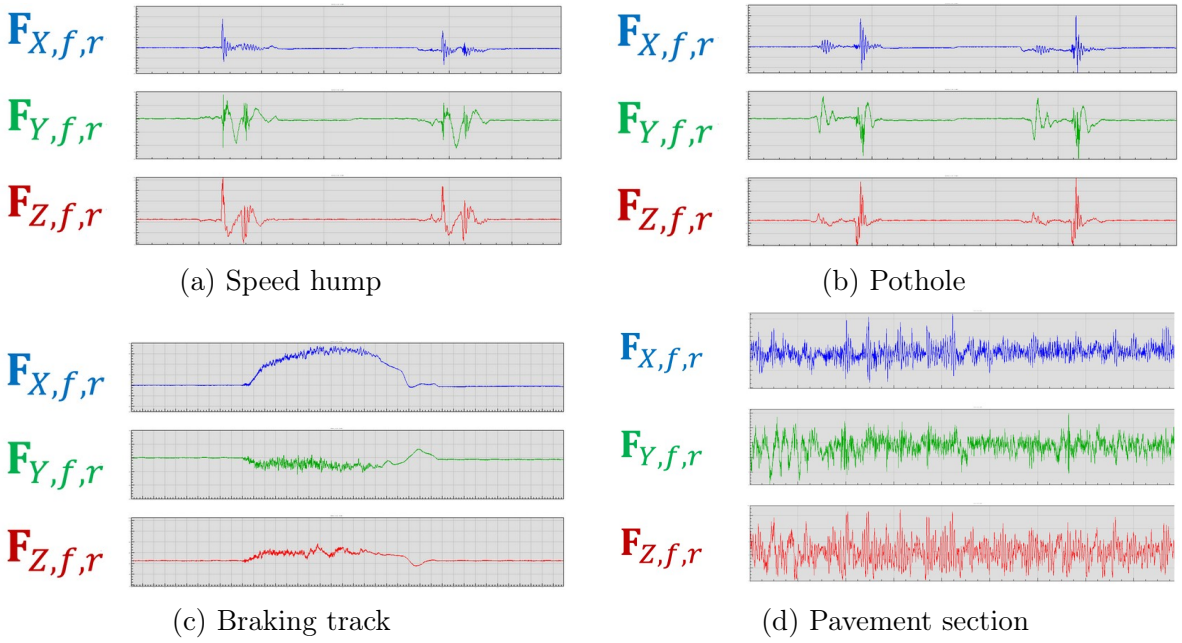

(a) Speed hump (b) Pothole

(c) Braking track (d) Pavement section

Fig. VII.5: Examples of track loading histories on the front right-hand wheel axle. The vehicle is the same as the US campaign in Chapter IV

Being severized obstacles as per their geometry or the speed of their encounter, tracks might induce on some structures loads strong enough to cross limitations in terms of macroscopic plastic deformation or frequential content. If these situations occur on PG, the hypotheses of linear structure and linear damage should be challenged. This means that the damage model defined in III.5.1 and used for the definition of magnitude vectors and the analysis of pseudo-fatigue could be no longer valid. Tracks that are too severe for the hypotheses of our characterization of pseudo-fatigue should not be used as building blocks for validation procedures for the reliability of automotive subsystems (they can be useful for other RAMS requirements).

Proving ground facilities in different regions of the world will contain different sets of

tracks, motivated by road event analyses from different regions of the world as well as different historical theories and practice in terms of RAMS design. Fig. VII.6 shows examples of tracks and associated loading histories in another proving ground facility of the group Stellantis in Germany.

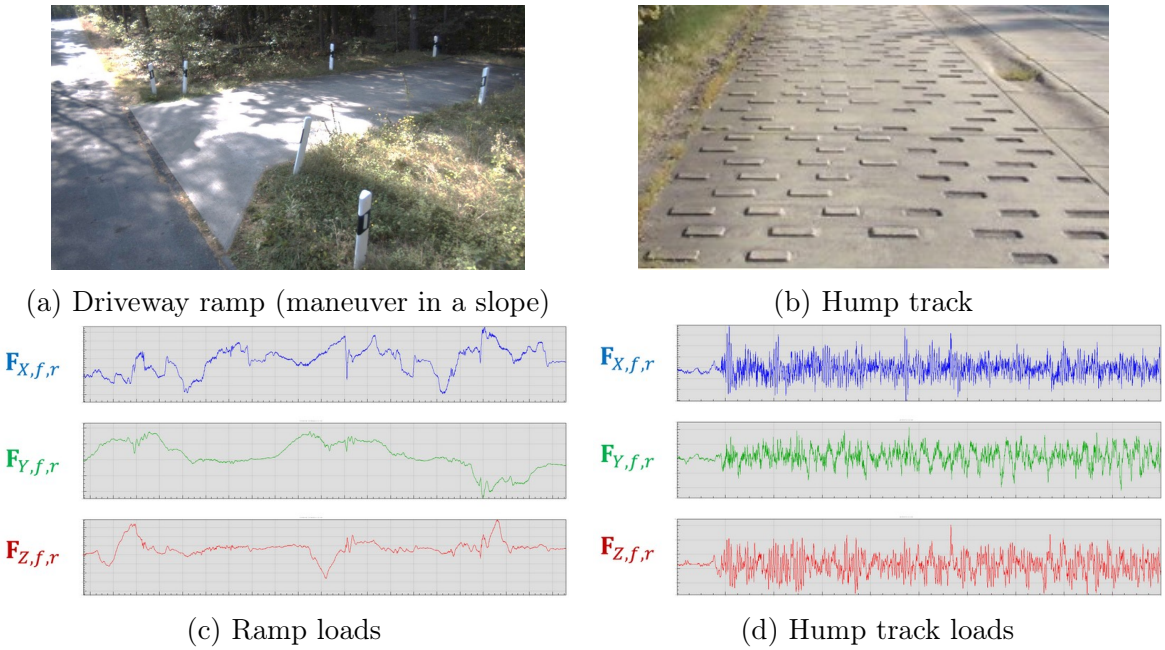

(a) Driveway ramp (maneuver in a slope)

(b) Hump track

(c) Ramp loads

(d) Hump track loads

Fig. VII.6: Examples of tracks and associated loading histories from another PG facility, measured with the same vehicle as previously

VII.3.2 Track absolute magnitudes

For a given vehicle model, tracks yield predictable loads that can be used as a learning base for its mechanical response to road events. In fact, when we interpreted differences in magnitude between different clients or different road environments in chapter IV, the interpretation in terms of behavior and road events was supported by the observation of the global loads and magnitude radars measured on different track events with the measurement campaign's vehicle.

Let us consider some examples. Fig. VII.7 shows the absolute magnitude radars of some tracks of the reference set.

The circuit called in these graphs "Common Driving" is a track associated with common driving. It contains several regular obstacles (speed bump, road asperities) and maneuvers (changes in speed, turns, slopes) in balanced proportions and induces reasonable pseudo-damage per kilometer. We use this track as a reference for the values of magnitudes.

The vector of magnitudes induced by this circuit could also be used as a signature vector: a vector used to normalize other track vectors when visualizing them. However, we will stick to absolute radars in this section, for the sake of simplicity.

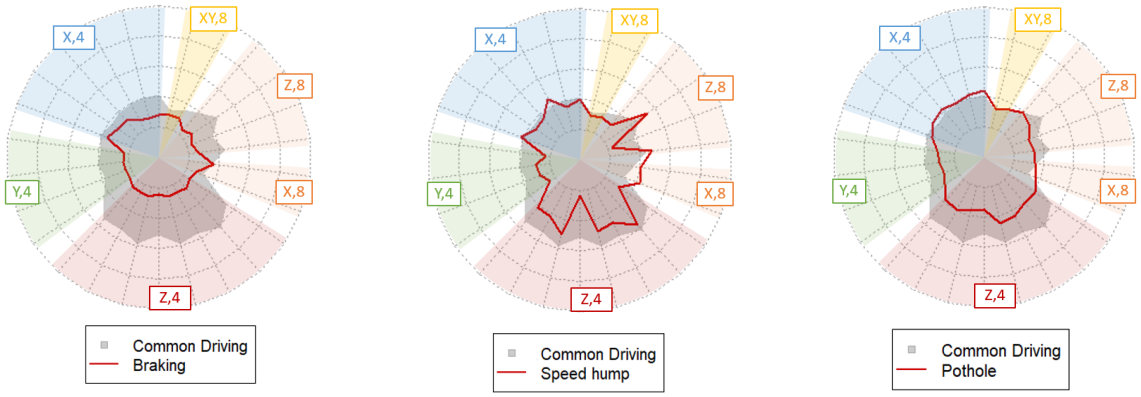

(a) Braking (b) Speed hump (c) Pothole

Fig. VII.7: Absolute magnitude radars for three PG tracks.

Braking (Fig. VII.7a) and cornering (Fig. VII.8b) respectively induce larger variations on their longitudinal and lateral load cases of the front axle. Urban vertical obstacles such as speed humps (Fig. VII.7b) highlight single-wheeled and in-phase (45) vertical load cases. However, pothole (Fig. VII.7c) and pavement tracks (Fig. VII.8a), just like potholes and pavement in real life, are significant on all load cases.

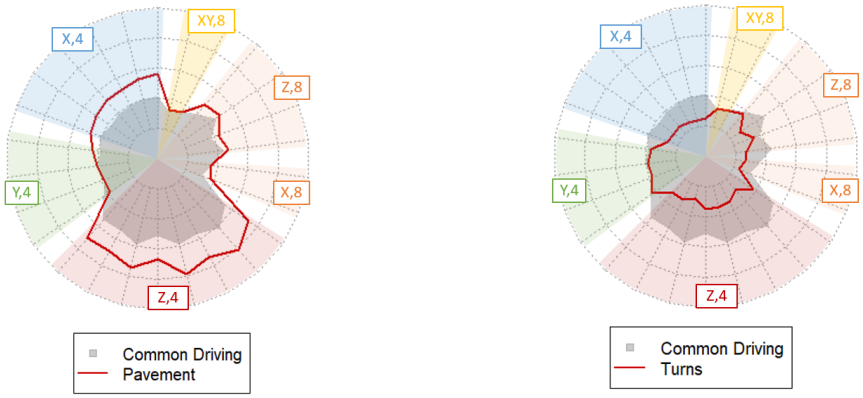

(a) Pavement section (b) Cornering section

Fig. VII.8: Absolute magnitude radars for two more PG tracks.

VII.3.3 PG schedules

Tracks are the building blocks of proving ground schedules as introduced in Section VI.2.1, which are in turn often used as validation objectives as illustrated in §VI.5.2.3.

The distance associated to a schedule is not necessarily representative of the lifetime objective for requirements of reliability. The events, however, are representative either of a number and severity of road events met in service, or of the pseudo-damage induced by service missions as worked out in chapter VI.

Let us consider a set of global loading histories associated to a selection of g PG tracks $\left(\vec{\mathbf{F}}_e\right)_{e\in[\![1,g]\!]}$ with:

$$\overrightarrow{M}\left(\vec{\mathbf{F}}_e\right) = \left(\sqrt[m_k]{\breve{D}\left(\gamma_k, \vec{\mathbf{F}}_e\right)} \right)_{k\in[\![1,\kappa]\!]} \quad \forall e \in [\![1,g]\!] \tag{VII.3.1}$$

A combination of repetitions of these tracks is denoted by the vector of repetitions $\vec{n}$. A PG schedule is a random, or at least non-trivial (chaotic, see Appendix B.7.1), concatenation of all these repetitions. Its associated loading history is denoted $\vec{\vec{\mathbf{F}}}_{\vec{n}}$:

$$\vec{\vec{\mathbf{F}}}_{\vec{n}} = \mathop{\Big\|}_{i=1}^{N} \psi\left(\underbrace{\vec{\mathbf{F}}_1, \ldots, \vec{\mathbf{F}}_1}_{n_1}, \ldots, \underbrace{\vec{\mathbf{F}}_e, \ldots, \vec{\mathbf{F}}_e}_{n_e} \ldots \right) \tag{VII.3.2}$$

denoting ψ a random permutation on vectors of $N = \sum_{e=1}^{g}$ components (repetitions) and $\|$ the concatenation operator such that:

$$\vec{\vec{\mathbf{F}}}_1 \| \vec{\vec{\mathbf{F}}}_2 = \begin{bmatrix} \vec{F}_1(t) \text{ if } 0 < t < T_1 \\ \vec{F}_2(t) \text{ if } T_1 < t < T_2 \end{bmatrix} \tag{VII.3.3}$$

We will be interested in the pseudo-damages and magnitudes induced by a PG schedule $\vec{\vec{\mathbf{F}}}_{\vec{n}}$. The calculation of the pseudo-damage of a concatenation of loading histories is discussed in Appendix B.8. While the exact formula for the pseudo-damage of a load concatenation was written in Eqs. II.5.4 and II.5.5, we will stick to the usual linear method - the sum of individual pseudo-damage vectors - for the sake of simplicity:

$$\overrightarrow{\breve{D}}\left(\vec{\vec{\mathbf{F}}}_{\vec{n}}\right) = \sum_{e\in[\![1,g]\!]} n_e \cdot \overrightarrow{\breve{D}}\left(\vec{\vec{\mathbf{F}}}_e\right) = \vec{n} \bullet G \tag{VII.3.4}$$

Using this direct sum, all permutations ψ of a vector of repetitions of our PG track loading histories are predicted to yield the same pseudo-damage vector. The matrix G contains all pseudo-damage vectors for our set of tracks:

$$G = \left(\overrightarrow{\breve{D}}\left(\vec{\vec{\mathbf{F}}}_e\right)\right)_{e\in[\![1,g]\!]} = \begin{pmatrix} \breve{D}\left(\gamma_1, \vec{\vec{\mathbf{F}}}_1\right) & \ldots & \breve{D}\left(\gamma_1, \vec{\vec{\mathbf{F}}}_g\right) \\ \ldots & & \ldots \\ \breve{D}\left(\gamma_\kappa, \vec{\vec{\mathbf{F}}}_1\right) & \ldots & \breve{D}\left(\gamma_\kappa, \vec{\vec{\mathbf{F}}}_g\right) \end{pmatrix} \tag{VII.3.5}$$

Note this direct sum should not be confused with the "direct extrapolation" of Section V.6. The proposed strategy to predict the pseudo-damage induced by a lifelong mission was, at that time, to predict the new content of the total Rainflow matrix. No matter the hypotheses established for the constant or inconstant behavior of the driver, the pseudo-damage induced by two repetitions of a mission is not exactly the sum of the pseudo-damages induced by each repetition. Approximating the pseudo-damage of a concatenation of repetitions of a mission

did not represent a large imprecision on the predicted pseudo-damage, because the reference missions were long enough.

Tracks, however, can be very short. Using a direct sum to predict the pseudo-damage induced by a schedule of proving grounds may lead to large discrepancies with the exact formula. The comparison between direct sum and exact formula for the concatenation of tracks in Section B.8 shows that the direct sum may underestimate or overestimate the induced magnitude of a pair by up to 10%.

VII.4 Pseudo-fatigue equivalence

VII.4.1 Restrictions of inputs, restrictions of contexts

A small set of design references (standards) for the pre-project phase of a new vehicle model is preferred by the company. First and foremost, the purpose of this constraint to reduce the number of design references needed for the whole range of vehicle models to develop.

Validation procedures, however, can be adapted, in load condition and level, to the specific behavior and weaknesses of the vehicle model at hand. We could indeed imagine adapting the validation procedure for each organ. The associated objectives would be made to represent the worst kind of missions for the part of interest.

For instance, a part like the suspension arm on a front axle is well characterized by pseudo-damages calculated from combinations of longitudinal and lateral loads on the front axle (*e.g.* $Xf0$ or $XYfl$ in Tabs. III.2 and III.4 for the left-hand arm). It could be validated robustly with a sporty driver in an urban environment. A part like the cross member, more sensible to rare and heavy vertical loads, would be validated on a mission that represents clumsier drivers or more damaged roads.

In this paragraph, we ponder the strategy to write the equivalence of this mission only for the variables of pseudo-fatigue that were assumed to be of interest for the validation of the part at hand. For instance, we may look for an equivalent loading history that precisely replicates the magnitudes induced by braking and cornering events on the section minimum of a suspension arm. Such contexts of interest would be $\gamma_1 = \left(\widetilde{\alpha}_{Xf0},8\right)$, $\gamma_2 = \left(\widetilde{\alpha}_{Yf0},8\right)$, $\gamma_3 = \left(\widetilde{\alpha}_{XYfl},8\right)$ for a left-hand suspension arm on the front axle.

However, should any assembly of the subsystem be unrepresented by the kept variables, a relevant variable for said assembly could take whatever value. Perhaps the found partial equivalent largely overestimates the damage of this assembly and would rather break the arm at an irrelevant location. The suspension arm, for instance, may fail in fatigue at the aforementioned location, but is also found to fail by bending under exceptional (non-fatigue and non-service) vertical loads. This situation should not be replicated in a physical trial.

Nota bene: The difference between usual load conditions for the triangle and this partial equivalent, potentially overestimating vertical loads, lies in the number of inputs. The fatigue trial of a triangle is nowadays a 1-poster trial in a bent X+Y direction, a configuration that will not induce significant damage on assemblies concerned by vertical solicitations.

Overestimating pseudo-damage on an ignored or unexpected context can be avoided by a cautious preparation of the equivalence problem. It must be ensured that all sensible zones have been accounted for in the subsystem, and that they are submitted to similar load configurations in the base loading history and in the bricks used for the equivalence. Another important step to consider for the implementation of an equivalent loading history built from a restriction of contexts is to restrict the number of inputs in accordance with the load cases that were accounted for.

VII.4.2 Pseudo-damage and magnitude distances

A population of missions $\mathbb{C}$ yields a distribution of stochastic pseudo-damages, determined previously in section V.4. Any mission c chosen from this distribution can be translated into a vector of pseudo-damages:

$$\forall c \in \mathbb{C},\ \overrightarrow{\breve{D}}_c = \left(\breve{D}_{c,k}\right)_{k\in[\![1,\kappa]\!]} \tag{VII.4.1}$$

Pseudo-damages are translated into equivalent magnitudes at intercept for matters of consistency (see Section III.7):

$$\forall c \in \mathbb{C},\ \overrightarrow{M}_c = \left(\sqrt[m_k]{\breve{D}_{c,k}}\right)_{k\in[\![1,\kappa]\!]} \tag{VII.4.2}$$

The pseudo-damage distance between two missions is evaluated by a norm on the vector of differences between pseudo-damages. The canonical 2-norm on vectors of $\mathbb{R}^\kappa$ is given by:

$$\left\|\overrightarrow{\breve{D}}_1 - \overrightarrow{\breve{D}}_2\right\| = \sqrt{\sum_{k=1}^{\kappa}\left(\breve{D}_{1,k} - \breve{D}_{2,k}\right)^2} \tag{VII.4.3}$$

Let $\vec{v}$ be a vector of $\mathbb{R}^\kappa$ with strictly positive coefficients. Let us define the $\vec{v}$-weighted 2-norm:

$$\left\|\overrightarrow{\breve{D}}_1 - \overrightarrow{\breve{D}}_2\right\|_{\vec{v}} = \sqrt{\sum_{k=1}^{\kappa} v_k^2 \cdot \left(\breve{D}_{1,k} - \breve{D}_{2,k}\right)^2} \tag{VII.4.4}$$

This operator defines a norm on $\mathbb{R}^\kappa$. It can be used in a minimization problem to achieve a better optimization on some dimensions (on some local contexts) at the expense of others.

The magnitude distance is evaluated by any of these norms on the vector of differences between magnitude vectors:

$$\left\|\overrightarrow{M}_1 - \overrightarrow{M}_2\right\|_{\vec{v}} = \sqrt{\sum_{k=1}^{\kappa} v_k^2 \cdot \left(\sqrt[m_k]{\breve{D}_{1,k}} - \sqrt[m_k]{\breve{D}_{2,k}}\right)^2} \tag{VII.4.5}$$

As explained in III.7, distance between magnitudes is a preferred tool for comparisons of clients. However, only pseudo-damage can be linearly accumulation under some hypotheses in the case of concatenated loading histories (see Appendix B.7.1).

VII.4.3 Magnitude homogenization versus weighting

Magnitudes over different local contexts are heterogeneous by construction: for instance, variations of vertical load combinations will be larger than in other directions. However, because the associated resistance (the denominator of damage) is also heterogeneous over contexts (i.e. assemblies historically sensible to vertical loads are also inherently stronger), this heterogeneity should not have an influence on the quality of design of different assemblies.

Some local contexts are still more important than others to control the risk of failure of the vehicle. Contexts that will be preponderant for a small set of assemblies in the system should be given lower importance than the most "critical" contexts.

This is true both for the determination of objectives and of equivalent loads. For instance, when selecting a synthetic severe mission (Section VI.5.2), local contexts associated to vertical load cases may be given a larger priority, as they will be harder to design. When it comes to equivalent loads, we will retain some distance between the solution of a weak pseudo-fatigue equivalence and the objective to replicate. The same contexts may also be given a larger priority in the search for an optimal equivalent.

Given a ponderation vector $\vec{v} = \overrightarrow{M}_{\text{wei}}$, normalized or weighted magnitudes are calculated from absolute magnitudes following the formula:

$$\frac{\overrightarrow{M}}{\overrightarrow{M}_{\text{wei}}} = \left(\frac{M_k}{M_{\text{wei},k}}\right)_{k\in[\![1,\kappa]\!]} \tag{VII.4.6}$$

Weighted pseudo-damage vectors follow the same principle, with $\overrightarrow{\breve{D}}_{\text{wei}} = \left(M_{k,\text{ref}}^{m_k}\right)_{k\in[\![1,\kappa]\!]}$.

VII.4.4 Optimization problem definition

Let $\overrightarrow{M}_{\text{obj}}$ and $\overrightarrow{\breve{D}}_{\text{obj}}$ be a magnitude resp. pseudo-damage vector to replicate using a PG schedule built from the set $\left(\vec{\mathbf{F}}_e\right)_{e\in[\![1,g]\!]}$. The unconstrained weak pseudo-damage equivalent problem is written:

$$\vec{n}_{\text{eq}} = (n_e)_{e\in[\![1,g]\!]} = \underset{\vec{n}}{\text{argmin}} \left\| \overrightarrow{\breve{D}}_{\text{obj}} - \overrightarrow{\breve{D}}\left(\vec{\vec{\mathbf{F}}}_{\vec{n}}\right) \right\|_{\vec{v}}^2 \tag{VII.4.7}$$

denoting $\vec{v}$ a weight vector used in the $\vec{v}$-weighted 2-norm and $\vec{\vec{\mathbf{F}}}_{\vec{n}}$ the loading history of a concatenation built from the combination vector $\vec{n}$ in a random (chaotic) order. The

norm becomes the Euclidian norm if $\vec{v} = \vec{1}$. The constrained weak pseudo-damage equivalent problem is written:

$$\begin{cases} \vec{n}_{\text{eq}} & = \underset{\vec{n}}{\text{argmin}} \left\| \frac{\vec{D}_{\text{obj}}}{\vec{v}} - \frac{\vec{D}\left(\vec{\mathbf{F}}_{\vec{n}}\right)}{\vec{v}} \right\|^2 \\ n_e & \geq 0 \quad \forall e \in [\![1,g]\!] \end{cases} \tag{VII.4.8}$$

A more realistic search for equivalent schedules would force $\vec{n}$ to be a vector of integers. We will relieve this constraint, as it would suppress the continuity of the search space. It is anyway conservative to round a number of repetitions of a track to the next integer.

Following the approximation of the pseudo-damage induced by a concatenation of proving ground tracks in Eq. VII.3.4, let us denote:

$$\vec{a} = \frac{\vec{1}}{\vec{v}} \cdot G \tag{VII.4.9}$$

$$\frac{\vec{D}\left(\vec{\mathbf{F}}_{\vec{n}}\right)}{\vec{v}} = \vec{a} \cdot \vec{n} \tag{VII.4.10}$$

The problem can be translated to a quadratic optimization problem by developing the squared norm:

$$\begin{cases} \vec{n}_{\text{eq}} & = \underset{\vec{n}}{\text{argmin}} \left(-2 \cdot {}^{T}\left(\vec{D}_{\text{obj}}\right) \cdot \vec{a} \cdot \vec{n} + {}^{T}(\vec{n}) \cdot {}^{T}(\vec{a}) \cdot \vec{a} \cdot \vec{n} \right) \\ n_e & \geq 0 \quad \forall e \in [\![1,g]\!] \end{cases} \tag{VII.4.11}$$

$$\Leftrightarrow \begin{cases} \vec{n}_{\text{eq}} & = \underset{\vec{n}}{\text{argmin}} \left(-\langle {}^{T}(\vec{a}) \cdot \vec{D}_{\text{obj}} \mid \vec{n} \rangle + \langle {}^{T}(\vec{a}) \cdot \vec{a} \cdot \vec{n} \mid \vec{n} \rangle \right) \\ \left(I_d^g \cdot \vec{n}\right) & \geq 0 \quad \forall e \in [\![1,g]\!], \end{cases} \tag{VII.4.12}$$

denoting I_d^g the identity matrix of size g. The method used to solve the problem defined in Eq. VII.4.11 is detailed in [Goldfarb and Idnani 1983].

VII.5 Equivalent PG schedules for synthetic severe missions

VII.5.1 Replicating measured or simulated missions

Let us first consider the mean driver of the reference trip REF. The magnitude vector associated with this mission is shown in grey in Figs. VII.9b (absolute values) and VII.9c

(normalized radar). The optimal combination that best replicates this magnitude vector is shown in Fig. VII.9a. It is the solution of the quadratic optimization problem defined previously in Eq. VII.4.11. Magnitudes induced by the resulting schedule are shown in red in both radars.

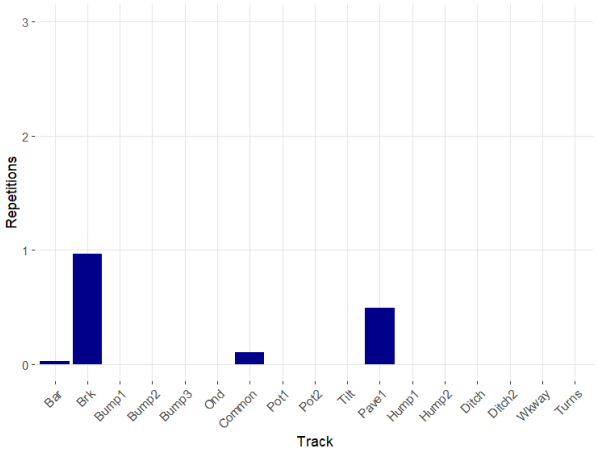

(a) Optimal schedule

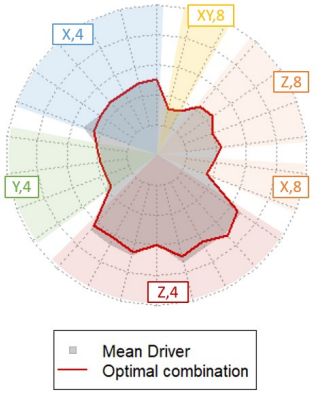

(b) Absolute magnitude radar

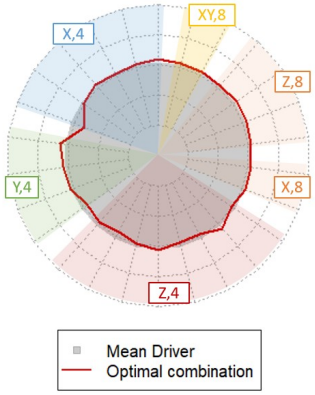

(c) Normalized magnitude radar

Fig. VII.9: Determination of a pseudo-damage equivalent schedule for the mean driver on trip REF. Reminder: the vector of magnitudes associated with this driver is the one used to normalize other vectors of magnitude prior to their normalized visualization.

The radars can be used to visualize how close the equivalent is to replicating the pseudo-damages induced by the mean driver, and which magnitude components were difficult to replicate. The radar also informs us whether the magnitudes of the schedule are superior to the objectives, denoting conservativeness of the equivalent. The magnitude that prove to be the most difficult to replicate, without degrading the solution on all other components, is the one associated with in-phase (45) longitudinal (X) loads on the front (f) axle and calculated with an exponent of 4 (weld beads, spot welds). It is the magnitude that corresponds to larger repetitive acceleration and deceleration episodes.

The combination obtained for this average driver does not include all tracks of the set. Let us calculate the condition number of the matrix G, being the ratio of its first eigenvalue on its last one. It is very high ($29 \cdot 10^{-6}$), meaning that at least one of its lowest eigenvalues is negligible. This bad conditioning of the matrix can be interpreted as redundancy between

two or several tracks of the set in terms of pseudo-damages: tracks that are colinear to each other or the pseudo-damage vector of which can be rebuilt from a linear combination of other tracks. This redundancy does not mean that some tracks are to be ignored, as we will discuss further in §VII.5.3.

Let us consider three drivers with different profiles in the space of conditional severity associated with the reference trip REF. The conditional severity of these drivers, n°021, 031 and 035, is shown in Figs. VII.10a and VII.10b respectively in the first and second principal planes of the analysis developed in Section V.3.

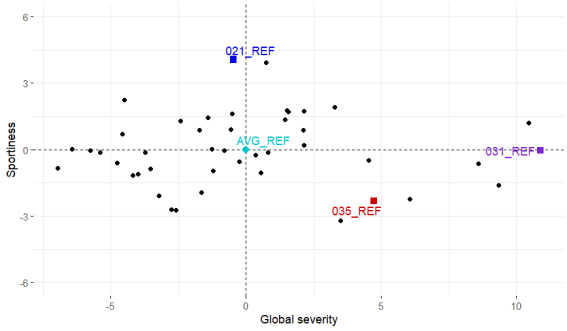

(a) Trip REF - First plane

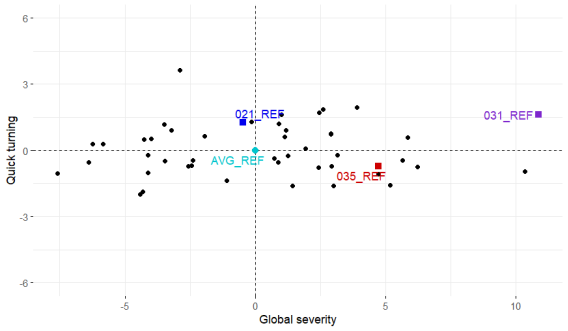

(b) Trip REF - Second plane

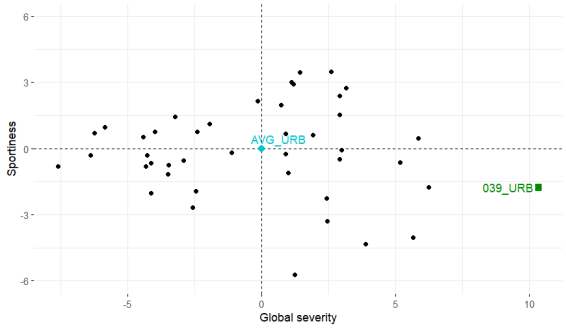

(c) Trip URB - First plane

Fig. VII.10: Select drivers for the elaboration of equivalent schedules

Let us also consider a globally severe driver n°039 on the alternative trip URB built mostly from urban environments. The driver of interest is shown in Fig. VII.10c in the first plane of conditional severity for the trip URB.

The optimal combination vectors for drivers 021, 031 and 035 on the trip REF are shown respectively in Figs. VII.11a, VII.13a and VII.12a. The magnitudes induced by the schedules built from these combination vectors are shown in Figs. VII.11b, VII.13b and VII.12b.

Being a sporty but average driver, the optimal combination found for the driver 021 in Fig. VII.11a contains a fraction of the common driving circuit and a smaller fraction of the pavement track to begin with, and a larger number of repetitions of the braking track compared to the other drivers of interest. The large sportiness of driver 021 was interpreted as an increased value of the magnitudes associated with longitudinal and lateral load cases on the front axle, and this naturally results in an emphasis on braking events in the equivalent schedule.

Driver 035 is a somewhat globally severe but most importantly non-sporty driver. Negative

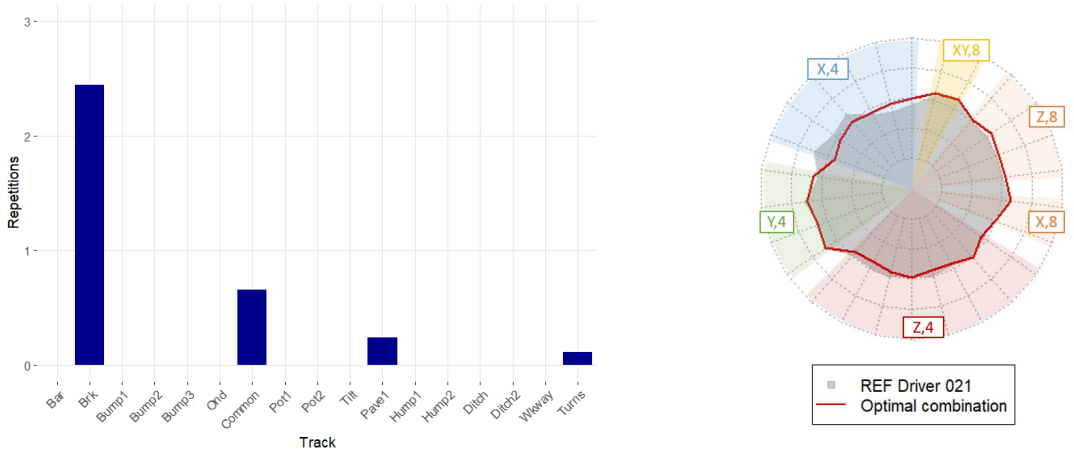

(a) Optimal schedule

(b) Normalized magnitude radar

Fig. VII.11: Determination of a pseudo-damage equivalent schedule for the driver 021 (sporty and average) simulated on trip REF.

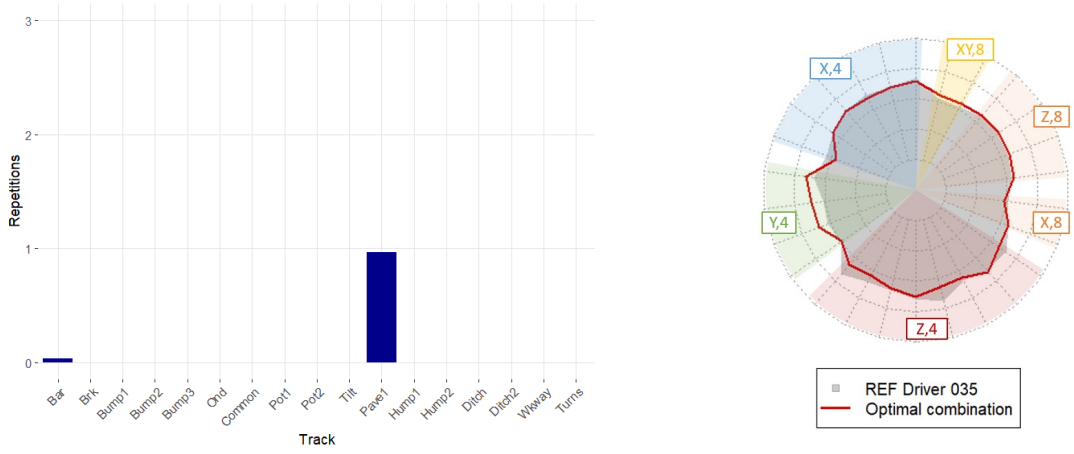

(a) Optimal schedule

(b) Normalized magnitude radar

Fig. VII.12: Determination of a pseudo-damage equivalent schedule for the driver 035 (low sportiness but high global severity) simulated on trip REF.

coordinates in this second dimension are associated with larger magnitudes on vertical (Z) load cases on the front (f) axle and on all load cases on the rear (r) axle. The optimal schedule to replicate this driver in Fig. VII.12a is composed solely of the pavement section. It is the most damaging track of the set, but it contains no maneuver whatsoever. Pavements ignite all local contexts at the same time.

The driver 031 is globally severe but shows no tendency towards sportiness or clumsiness, and a slight tendency towards quick turning. They are a somewhat balanced severe driver, severe on both maneuvers and obstacles. The global severity of the equivalent schedule is brought by the repetitions of the pavement track (Fig. VII.13a), while braking and cornering tracks bring the schedule closer to the events that are met during the trip REF.

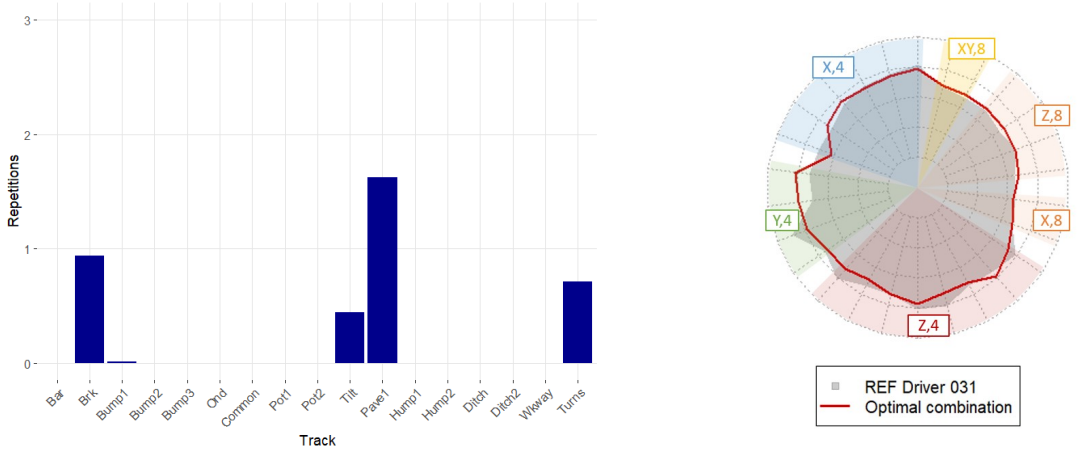

(a) Optimal schedule

(b) Normalized magnitude radar

Fig. VII.13: Determination of a pseudo-damage equivalent schedule for the driver 031 (globally severe) simulated on trip REF.

For this trip REF, the magnitudes induced by driver 031 are between 20 and 50% larger than those that correspond to the mean driver. Inducing a 20% to 50% larger magnitude on a context built with a Basquin exponent of 4 means inducing 2 (1.2^4) to 5 (1.2^8) times more pseudo-damage, hence we can expect that order of difference between the combination vector for the mean driver and the one for driver 031. The pavement section, being the most damaging track of the set over all local contexts, is replicated half a time in the schedule equivalent to the driver mean (Fig. VII.9a), and one time and a half for driver 031 (Fig. VII.13a): three times more.

These equivalent schedules were calculated for a trip that last roughly l_0 = 245km. If we consider that the extrapolation of a mission to a lifetime objective can be achieved by direct extrapolation (each repetition of the mission induces the same pseudo-damages), then the equivalent schedule able to replicate the extrapolated mission is determined by multiplying each number of repetitions of a track by l_f/l_0.

The optimal combination vector for driver 039 on the trip URB is shown in Fig. VII.14a. The magnitudes induced by the schedule built from this combination vector is shown in Figs. VII.14b.

The trip URB was less damaging for all drivers on all contexts except those associated with braking, accelerating (X on the front axle) and cornering (Y on the front axle). This can be understood from the specific shape of the "normalized" radar. Indeed, in Fig. VII.14b, the vector of magnitudes induced by the driver 039 was normalized by the vector induced by the mean driver on the reference trip REF. The radar for the driver 039 on trip URB is therefore deformed towards the blue and green sectors, whereas the mean driver of trip REF would show as a circle.

The driver 039 is the balanced and most globally severe driver from the sample of drivers of the measurement campaign US18-DT1 on trip URB. Just like driver 031 on the reference trip REF, their equivalent schedule combines the pavement track with cornering and braking

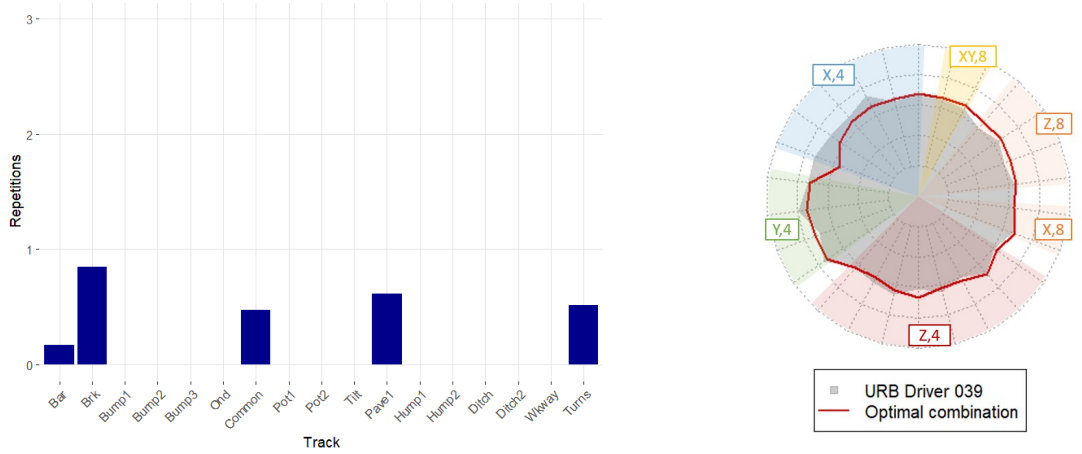

(a) Optimal schedule

(b) Normalized magnitude radar

Fig. VII.14: Determination of a pseudo-damage equivalent schedule for the driver 039 (globally severe) simulated on trip URB. The normalization of the radar was achieved with the magnitude vector induced by the mean driver on the trip REF.

tracks. However, a fraction of the pavement track for driver 031 on trip REF was switched to repetitions of the common driving track, including more turns. The fraction of braking events remains the same to maintain the level of the associated magnitudes.

VII.5.2 Replicating objective clients

VII.5.2.1 Non-weighted resolution

Let us now consider the globally severe synthetic mission and the synthetic severe mission determined from the principal axis of the third sub-population of the mixture of drivers, proposed from the analysis of trip REF in §VI.5.2.2. Their magnitude vectors are denoted respectively $\overrightarrow{M}_G$ and $\overrightarrow{M}_E$ (for "globally" and for "edge"). Their conditional severity was displayed in Fig. VI.14a. The latter synthesis, the edge of the third core, has a positive sportiness and is roughly as globally severe as the former proposition.

The optimal combination vectors for these synthetic severe missions are shown respectively in Figs. VII.15a and VII.16a. The magnitudes induced by the schedules built from these combination vectors are shown in Figs. VII.15b and VII.16b.

As can be expected from the positive sportiness associated with the second proposition, the optimal schedule to replicate the associated magnitudes includes more braking and turns than the schedule for the globally severe mission, at the expense of a tiny fraction of the repetitions of the pavement section and of the sway track (denoted "Tilt" in Fig. VII.15a).

We can observe on both radars that the schedule proposed for the globally severe synthetic mission fits the magnitudes well on all contexts built from a Basquin exponent of 8 and on some contexts rear in-phase. The optimal equivalent shows larger discrepancies on other

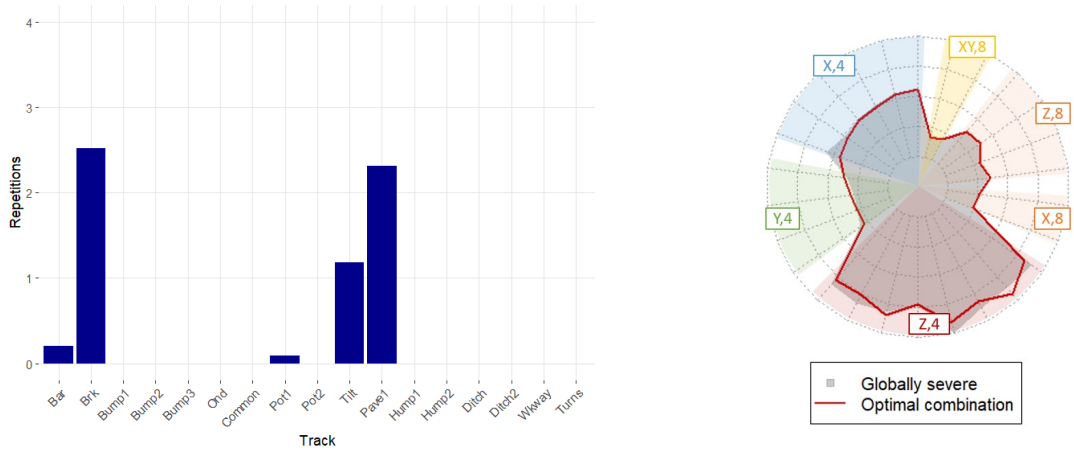

(a) Optimal schedule (b) Absolute magnitude radar

Fig. VII.15: Determination of a pseudo-damage equivalent schedule for the globally severe synthetic mission determined from trip REF.

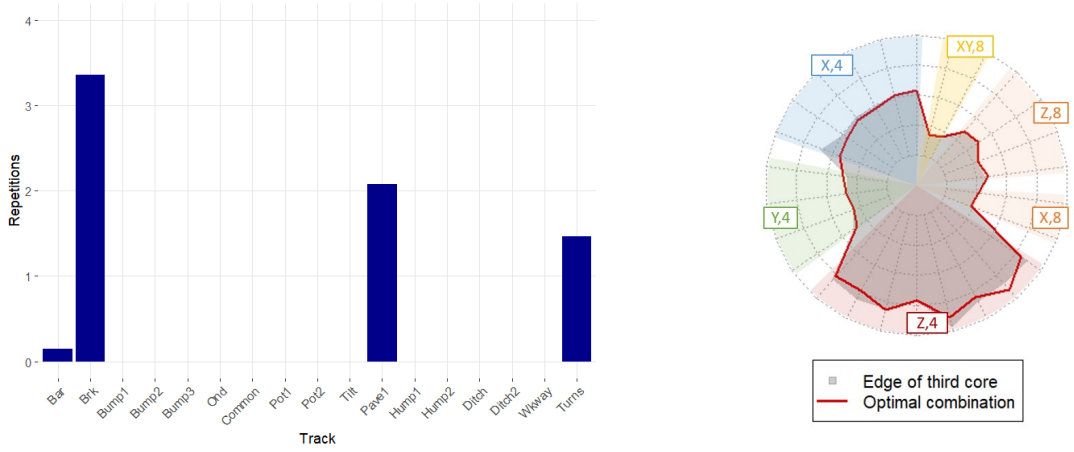

(a) Optimal schedule (b) Absolute magnitude radar

Fig. VII.16: Determination of a pseudo-damage equivalent schedule for the synthetic severe mission determined from the principal axis of the third sub-population of drivers on trip REF.

contexts associated with vertical load cases calculated with a Basquin exponent of 4 and on the braking context with the same exponent.

VII.5.2.2 Weighted optimization

Until now, all pseudo-damage components had the same importance in the function ot minimize, Eq. VII.4.8. However, because of the effect of the Basquin exponent, this naturally gives more importance to the replication of the pseudo-damages calculated with a Basquin exponent of 8. In order to prioritize some of the contexts built from a Basquin exponent of 4, we propose to tweak the equivalence by minimizing a weighted 2-norm (Eq. VII.4.4) instead of a regular 2-norm (Eq. VII.4.1) on the vectors of pseudo-damage.

The proposed weight vector was built arbitrarily. Local contexts that are built from unidimensional load cases and a Basquin exponent of 4 are given a weight of 0.2. Local contexts that are built from in-phase and out-of-phase combinations of global load components and an exponent of 4 are given a weight of 1. The local context built from the in-phase (45) combination of longitudinal (X) loads on the front (f) axle is given a weight of 1.5. All local contexts built from a Basquin exponent of 8 are given weights below 0.2.

In the least square formula that forms the backbone of the equivalent problem in Eq. VII.4.8, these weights are applied to the square differences calculated between the objective pseudo-damage to replicate and the pseudo-damage. Differences calculated on the contexts with a larger weight are given a little boost to encourage their reduction.

These weights do not suppress the effect of large discrepancies on pseudo-damages calculated with high Basquin exponents. To do so, the equivalent problem would need to be written using differences of magnitudes. However, the problem could not be rewritten into a quadratic optimization in that case. Thus we would lose critical properties (such as convexity) of the function to minimize.

The optimal combination vector calculated with a weighted 2-norm for the globally severe synthetic mission is shown in Fig. VII.17a. The magnitudes induced by the schedule built from this combination vector is shown in Fig. VII.17b.

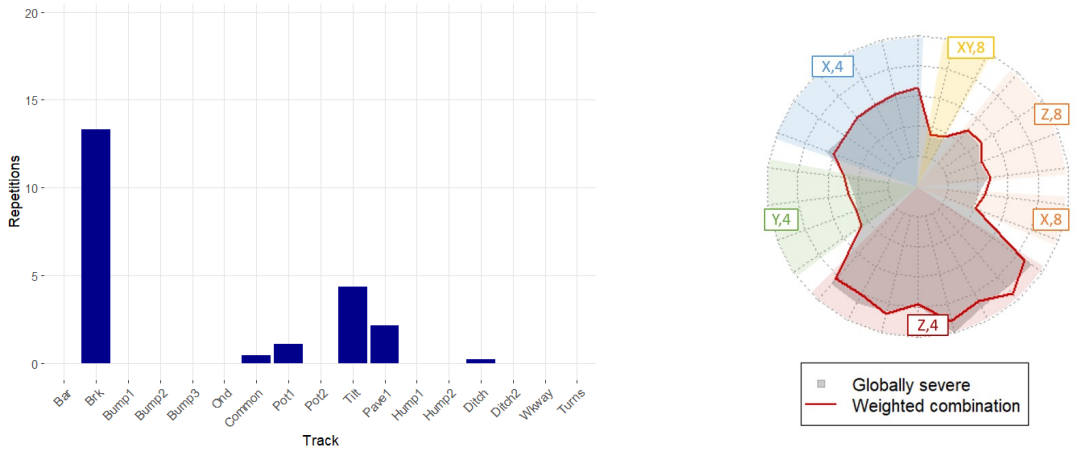

(a) Optimal schedule (b) Absolute magnitude radar

Fig. VII.17: Determination of a pseudo-damage equivalent schedule with a weighted 2-norm, prioritizing 2D load cases and Basquin exponent of 4, for the globally severe synthetic mission determined from trip REF.

By reducing the importance of pseudo-damages calculated with a Basquin exponent of 8 in the search of an equivalent schedule, the new combination vectors include a lot more repetitions of the braking track.

Fig. VII.18 shows the relative differences in magnitudes between each optimal equivalent schedule and the objective to replicate: the magnitudes induced by the globally severe synthetic mission. The relative differences are given by:

$$r_k = \frac{M\left(\gamma_k, \vec{\vec{\mathbf{F}}}_{\vec{n}}\right) - M_{\text{obj},k}}{M_{\text{obj}}} \quad \forall k \in [\![1,\kappa]\!] \tag{VII.5.1}$$

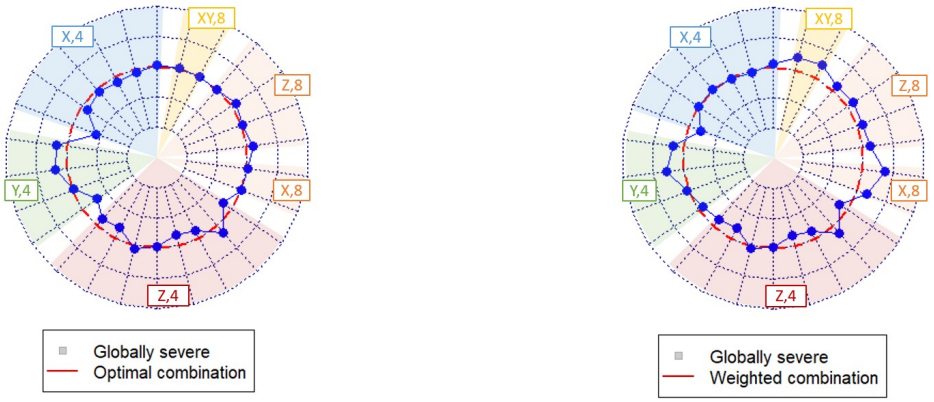

(a) Unweighted optimization (b) Weighted optimization

Fig. VII.18: Determination of a pseudo-damage equivalent schedule with a weighted 2-norm, prioritizing 2D load cases and Basquin exponent of 4, for the globally severe synthetic mission determined from trip REF. All radii on both graphs range from -50% to +50%, *i.e.* each concentric sector has a range of 25%.

We can see that the weights applied to the vectors of pseudo-damages in the equivalent problem have caused the new optimal schedule to allow more distance between the schedule and the objective magnitudes calculated with a Basquin exponent of 8. However, the relative difference on the "difficult" context to replicate - in-phase longitudinal loads on the front axle with an exponent of 4 - was increased from roughly -25% in the unweighted case to -12% in the weighted case. Applying the aforementioned weights did not improve at all the replication of magnitudes associated with vertical (Z) load cases and a Basquin exponent of 4 (the red radii).

VII.5.3 Balanced PG schedules

The optimal combinations found in the previous paragraphs only involved a fraction of the available tracks. The conditioning of the matrix T containing all track pseudo-damages indicates that this set of tracks has a certain redundancy for our local contexts of interest.

A large variety of tracks represents a large variety of events and associated loads. Despite their similarity in terms of pseudo-damages, including several variations of typical road events helps to better understand or model the mechanical behavior of the vehicle. An obstacle driven on at two or three different speeds also shows. Moreover, these tracks may have very different frequential contents. Our fatigue characterization does not take these dynamical effects in account, but

As discussed in §VI.2.1, standard PG schedules have a variety of purposes that go beyond the replication of the pseudo-damage induced by a reference mission.

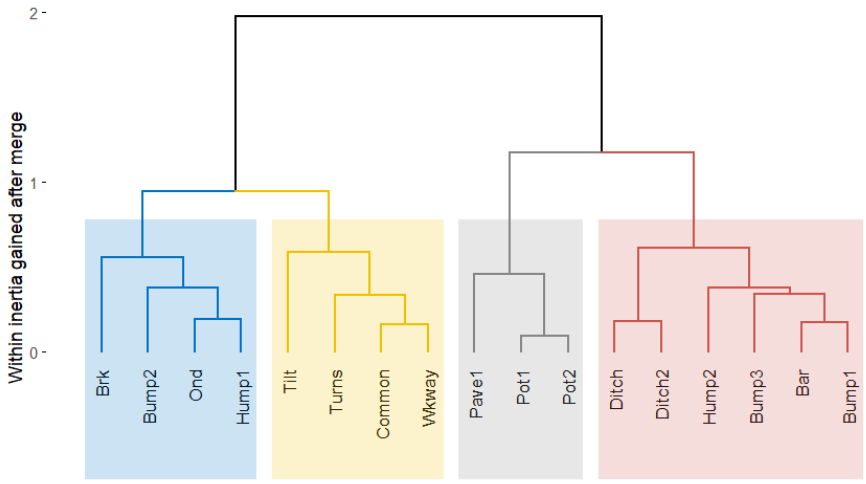

Fig. VII.19: Dendogram

VII.5.3.1 Groups of similarly damaging tracks

Given that global loads will be measured at the wheel axles of the prototype on all these tracks anyhow, we may look for a combination of tracks that displays more diversity. This can be achieved by grouping tracks based on one of two criteria:

- We can regroup tracks that induce the same kinds of pseudo-damage, *i.e.* have similar unit vectors of pseudo-damage or magnitudes;
- Events that are considered to belong to the same environment, such as urban or back road obstacles.

The magnitude vectors associated to all tracks included in T were divided by their Euclidian norm to compare their direction in the space $\mathbb{R}^k$. A hierarchical clustering algorithm based on their Euclidian distances was conducted to determine a relevant number of similar subsets of tracks.

The dendogram of the hierarchical clustering is shown in Fig. VII.19. We arbitrarily propose to partition this set of tracks into four subsets, based on the composition of the clusters at this level, and on their low within inertia.

Tracks that represent urban speed reducing installation - such as speed bumps, humps and tables - and urban obstacles - ditches - induce similar vectors of pseudo-fatigue and are stored in the first and fourth groups, respectively in blue and red. Tracks and circuits that include a lot of turns or other lateral solicitations are together and form a third group, in yellow (the walkway "Wkway" obstacle is oblique). Tracks that correspond to damaged roads - pavement and potholes - induced pseudo-damage on all contexts form a third group in black.

Note that all tracks containing maneuvers were contained in the two first clusters. They would have been grouped if we had chosen to partition the set of tracks in three subsets.

VII.5.3.2 Track ratios within groups and new formulation for equivalence

We have proposed a partition of our PG tracks into subsets of tracks that induce similar magnitudes on a vehicle. However, this clustering was done on the unit vectors of magnitudes associated with each track. The tracks within a group may be very damaging, or not, based on their geometry and their encounter speed.

The repetitions of each track within a group will be proportional to the number of repetitions of the group. However, inside a group, we can determine a fixed ratio between the repetitions of two similar but unequal events. This is already the case in the reference schedules used by the company: a severe variation of an event will have a lower number of repetitions than its more moderate variation. For instance, in our previous set, the two potholes have different depths, and therefore induce different levels of loads.

To each track, identified by its index e, we associate a group index $w \in [\![1,4]\!]$ that determines the track group it belongs to; and a repetition rate u that corresponds to its relative number of repetitions compared to the rest of the group. These parameters are shown in Tab. VII.1. They are arbitrary and not representative of the ratios applied by Stellantis.

Group $w = 1$	Braking u=4	Bump 2 2	Ond. 1	Hump 1 1		
Group $w = 2$	Sway (Tilt) 4	Turns 2	Common 4	Ob. Wkway 1		
Group $w = 3$	Pavement 3	Pot 1 1	Pot 2 2			
Group $w = 4$	Ditch 1	Ditch 2 2	Hump 2 3	Hump3 3	Metal bar 1	Bump 1 2

Table VII.1: Repetition rate for each track in their respective subset

The equations developed in Section VII.4 need to be adapted to this grouping of tracks. Eq. VII.3.2 is transformed into a new definition of a schedule with a modified vector $\vec{n}|_4$ with only 4 components:

$$\vec{\mathbf{F}}_{\vec{n}|_4} = \mathop{\Big\|}_{i=1}^{N} \psi \left(\underbrace{\vec{\mathbf{F}}_1, \ ..., \ \vec{\mathbf{F}}_1}_{n_{w_1} \cdot u_1} , \ ... \ , \underbrace{\vec{\mathbf{F}}_e, \ ..., \ \vec{\mathbf{F}}_e}_{n_{w_e} \cdot u_e} \ ... \right) \tag{VII.5.2}$$

denoting w_e and u_e respectively the group index and repetition rate of the e-th track of the set.

The κ-by-g pseudo-damage matrix G, defined in Eq. VII.3.5, used to rebuild the pseudo-damage of a schedule, must be rebuilt into a κ-by-4 matrix using the repetition rates and the new definition of the combination vector:

$$G = \left(\sum_{e|w_e=w} u_e \cdot \vec{\vec{D}}\left(\vec{\vec{\mathbf{F}}}_e\right) \right)_{w\in[\![1,4]\!]} \tag{VII.5.3}$$

From there, all other equations of §VII.4.4 are the same with $g = 4$.

The real combination vector $\vec{n}$ can be rebuilt from the modified vector $\vec{n}|_4$ by the following formula:

$$n_e = \left(n|_4\right)_{w_e} \cdot u_e \tag{VII.5.4}$$

VII.5.3.3 Results

The optimal reconstructed combination vector $\vec{n}$ calculated with a weighted 2-norm with grouped tracks for the two synthetic severe missions proposed above are shown respectively in Figs. VII.20a and VII.21a. The magnitudes induced by the schedules built from these combination vectors are shown in Figs. VII.20b and VII.21b.

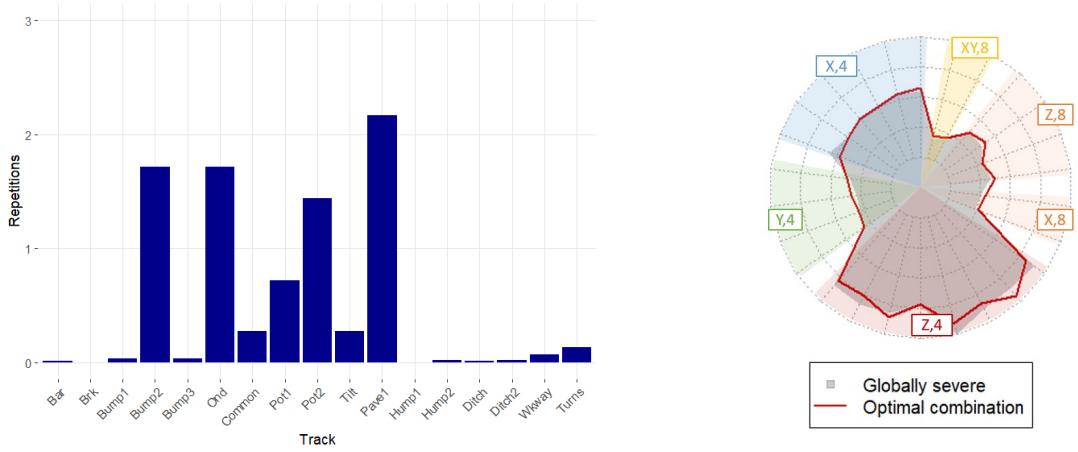

(a) Optimal schedule

(b) Absolute magnitude radar

Fig. VII.20: Determination of a pseudo-damage equivalent schedule using a weighted 2-norm and grouped tracks for the globally severe synthetic mission determined from trip REF.

These schedules have better diversity in terms of tracks with no significant loss in precision of the replication of magnitudes. Some tracks are still not represented in the resulting schedules. The group of tracks including the braking track was shunned by both optimizations. The optimization was also conducted with the braking track solo in a specific group, and it was still absent from the resulting optimal schedules.

VII.6 Chapter conclusion

The fatigue induced by measured service loading histories or determined by reliable design references and validation objectives needs to be replicated by adequate testable loads in a

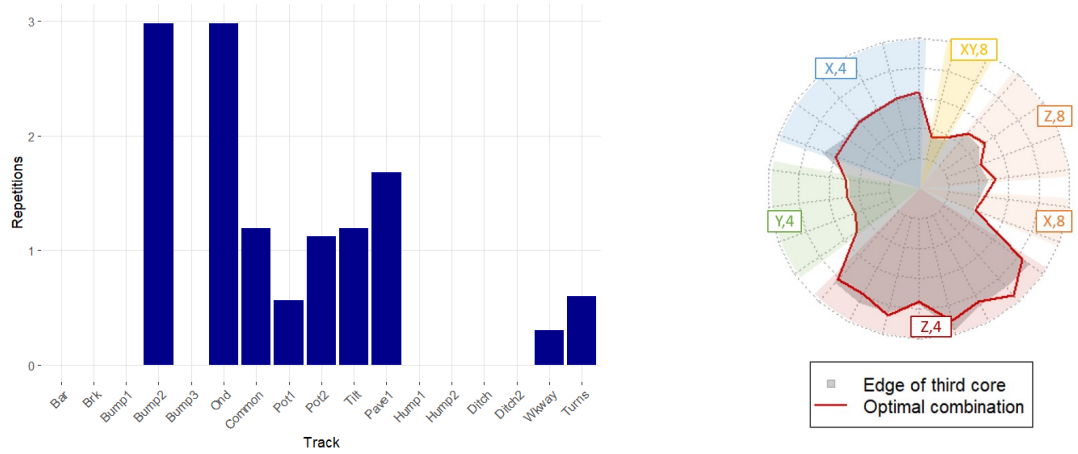

(a) Optimal schedule (b) Absolute magnitude radar

Fig. VII.21: Determination of a pseudo-damage equivalent schedule using a weighted 2-norm and grouped tracks for the synthetic severe mission determined from the principal axis of the third sub-population of drivers on trip REF.

protected environment to be exploited by the company. The determination of such loads is achieved by the resolution of a fatigue equivalence.

Equivalent loading histories are sought in different sets of testable loads that correspond to the available means of loading at the relevant stage of the development project.

Different parts of the system will be impacted by different sets or combinations of global load components, or by different interface loads. Each part may have a specific number of input load directions and of local contexts. Just like each part can be given specific validation objectives that correspond to its specific most severe missions in service, each part can be submitted to a specific validation loading history that is equivalent to these objectives. In this chapter, we have recalled works conducted on this matter in which analytical equivalent loading histories are determined to design trials for automotive subsystems.

The major ambition of this chapter was the adaptation of the framework to the creation of equivalent PG schedules that best replicate the fatigue induced on all local contexts of the structure by service loading histories or synthetic objectives of interest. We have presented a set of PG tracks from which we can build schedules that represent artificial and reproducible missions.

Different sets of tracks star different events and different driving instructions. These selected events often stem from an analysis of similar events in the region at stake. However, international prospects may prompt sharing these events among colleagues or partners and allow the definition of schedules for the design of vehicles aimed at markets located on the other side of the world. Thus engineers may modify their building blocks for the determination of a schedule for any vehicle project.

Several strategies for the optimization of a weak pseudo-fatigue equivalent were proposed. The search for an equivalent that minimizes the differences between pseudo-damages leads to the elaboration of a quadratic optimization that allows simple resolution of the equivalence. When writing the equivalence problem as a minimization of the differences in equivalent

magnitudes, the problem cannot be translated into quadratic optimization anymore. The strategy would need to be adapted to include the better mathematical properties of equivalent magnitudes while ensuring the performance of an adapted optimization algorithm.

In Chapter V, we have studied the different profiles of conditional driver severity for a few aggregated trips. From the observation of their apparent prioritization of different magnitudes associated with different global load cases, we had managed to interpret the conditional severity of these drivers from their behaviors on maneuvers or obstacles. When determining equivalent schedules to the simulation of specific drivers on aggregated trips of interest, the composition of the equivalent schedule confirms our previous interpretation of the dimensions of severity. Thus each reference mission or vector objective, such as those already in place in a company expertise, can be translated and interpreted as combinations of historical PG elements that said company already uses extensively.

The equivalent schedules determined from the resolution of a pseudo-fatigue equivalence are only optimized with respect to this constraint. The reality of building proving ground schedules brings together several requirements and constraints that go beyond the replication of the fatigue induced on suspension and body components. Another strategy for the elaboration of proving ground schedules is to focus on the optimal replication of a specific vector of Rainflow matrices or Rainflow spectra, in order to reproduce satisfyingly the actual load variations that are met in service or in the synthetic severe mission of interest.

Actually, at the beginning of the thesis, the main ambition that led us to determining equivalent schedules was to determine an alternative form of validation objectives that are robust to a change in vehicle models. The current limitation to implementing this strategy is the unknown effect of a change in vehicle model in the importance of driver severity and in the loads induced by road events. The distribution of driver severities and the projected distributions of equivalent magnitudes may have very different shapes from one vehicle model to another, even if the market for both models is the same.

However, an equivalent PG schedule can be made more robust to a change in vehicle models by including several vehicle models with the same market and mission definition into the equivalence. If the objectives for two different vehicle models have the same mission definition, then an equivalent PG schedule would replicate the magnitude vectors induced by each mission on the corresponding vehicle model.

A translation of the continuous distribution of driver severity into a distribution of repetitions was imagined but not conducted. To ensure continuity of the equivalent schedules from one driver to another, the first necessary ingredient is a well conditioned set of groups of tracks. In that case, this continuity is ensured as long as the equivalence is written into a quadratic optimization. In the case of the minimization of magnitude distances, the probable existence of local optima may cause discontinuity in the transformed space of equivalent schedules.

Chapter VIII

General conclusion

Requirements enforcing the reliability of suspension and body parts ensure the safety of the users of personal vehicles in service. Rich and appropriate validation procedures at early stages of the development of a new vehicle aim at reducing the number of late adjustments and design loops to achieve vehicle models that are sufficiently resistant to the loads of the road. These procedures are most efficient when they are adapted to the sensible zones of the subsystem - component, part, organ - at stake. That is, when they are representative of the most damaging situations that it may encounter in service.

The definition of these validation procedures more and more needs to be adapted to the specific market of the vehicle model to design. Cultural and regulatory differences have an influence on the driver behavior profiles in a population. The quality and content of roads are conditioned by a large range of factors, from road maintenance means to the topology and climate in the region. The social organization of the society as well as ecological incentives, such as carpooling or minimal commuting, also have a growing influence on the purpose and payload of each trip. Finally, different vehicle market segments and brands are aimed at different fractions of the population.

Our contribution to the determination of adequate validation loads is the complete decomposition of all steps that lead to their derivation from wheel axle load measurements in the region of interest. We have expressed most hypotheses that need to be made throughout the method with respect to computational cost and partial knowledge or data, either to model the mechanical and fatigue behavior of the structure, to achieve a distribution of the population of pseudo-fatigue or to determine objectives to replicate in validation procedures.

We have presented mechanical phenomena at stake in the initiation and propagation of defects under service loads in Chapter II. Methods to predict the failure of a single component by high cycle fatigue were presented in the hypothesis of a known local loading history at the location of interest, and of a known material characterization of the fatigue of said location under said load configuration. When all these conditions are met, the fatigue analysis of the component submitted to variable amplitude local loads leads to the determination of a damage.

Thanks to this formula for component damage under a given load configuration and to hypotheses on the mechanical behavior of the structure, we have presented a method to

determine an exhaustive, low structural dependent fatigue characterization for the structure in Chapter III. Any global loading history at the wheel axles of a vehicle is derived into several global load cases, individual and composite. These new scalar loading histories are associated with repetitive concentrations of Cauchy stress at given sets of sensible zones. From them, we calculate several pseudo-damages, a quantity proportional to the damage of all sensible zones in each set - in each local context. Furthermore, we have proposed a generic formula for equivalent magnitudes, that carry the same information as the pseudo-damage but have better mathematical properties.

The resulting multidimensional fatigue characterization is a first step toward the generalization of the concept of damage to the structure. We have also proposed a graphical way to visualize these magnitudes in the form of a polar histogram - a radar. Throughout the manuscript, we have shown how these graphs could be tweaked to transform a comparison of magnitude vectors between two clients into a comparison of radar shapes.

The different surveyable mission factors - Driver, Trip and Payload - that have an expected influence on the loads induced on a vehicle are introduced in Chapter IV. We have presented the sampling strategy associated with this factor model and the potential of the datasets that we have analyzed. The coupled effect of the first two factors are studied through the implementation of MFA to reveal the latent structure justifying the variability among drivers. Relevant new variables that best explain this variability describe, in several dimensions, the intrinsic severity of drivers. This new strategy to analyze service loads relies on our characterization of the fatigue induced on the vehicle, whereas a more classical approach would be conducted on the contents (level crossings, Rainflow cycles) of each component of the global loading history.

The composition of the trip, decomposed into different road environments, modifies the density and type of road events that a driver may encounter. We managed to interpret these differences from the analysis of correlations between load intensities - a.k.a. magnitude per kilometer - calculated on different load cases with different material parameters. We reinforced these interpretation with further correlations between load intensity and quantities calculated on the histories of speed and acceleration practiced by each driver.

We needed to elaborate an initial sampling and further a model of the magnitudes induced by a population of missions, in the absence of knowledge on the variety and distribution of trip compositions. To achieve that, we have proposed the definition of an aggregated trip in the beginning of Chapter V. In order to ensure that all drivers of the measurement campaign are tried on this same trip, the magnitudes that they would induce on said trip were simulated from the evaluation of their load intensity on each road environment. The new dataset of magnitudes was analyzed through the implementation of PCA and of HCPC. We have thus determined new variables denoting the conditional severity of driver on this aggregated trip, and that are best suited to visualize and describe the shape of the population of driver severity.

Despite the variety of local contexts and associated magnitudes to consider over the structure, five dimensions of conditional severity were sufficient to explain 94% of the variance of the dataset calculated with our first choice of aggregated trip. The first dimension, global severity, is an optimal choice for a scalar definition of severity. In our dataset, it manages to gather 73% of the variance of the dataset. These percentages show the difference in explanation power between defining severity as a scalar or as a vector.

For our dataset of interest, a Gaussian mixture model was proposed to achieve a distribution of the conditional severities of drivers. We have determined the likeliest parameters for such a mixture through the implementation of an EM-algorithm, and we have shown how this mixture could be projected back onto each of the initial variables of pseudo-fatigue.

The major influence of the choice of an aggregated trip was shown in terms of population shape and extreme values of magnitudes in Section V.5. Finally, we have tackled the question of extrapolation from a plausible aggregated trip to a vehicle lifetime in Section V.6 and proposed a few ways to implemented this extrapolation, both in the literature and from the tools that it provides.

The main takeaway of these two Chapters IV and V, dedicated to the analysis of service loads, is that the distribution of variables of pseudo-fatigue can be understood from the point of view of driver behavior and trip composition. This analysis encourages a further exploration of the circumstances that make drivers behave differently. From there, the company will be able to manage differences between targeted sub-populations (for different vehicle segments and brands) or between regions, and to re-evaluate service conditions for each new vehicle model.

In Chapter VI, we have recalled existing tools in the literature to include the probabilistic definition of requirements in reliability into the method for the determination of the adequate design of a subsystem and of validation procedures that ensures this adequacy. We have provided reasons and mathematical conditions for the redaction of reliable design and validation problems for subsystems containing several distinct local contexts and therefore requiring a multidimensional fatigue characterization.

We did not have the time conduct the analysis to the elaboration of a solution for such complex subsystems. Instead, we have adapted the existing univariate implementation of Stress-Strength Interference (SSI) methods to the specific shape of our distributions of magnitudes.

However, we have shown how the previously determined distribution of conditional driver severity could be used to select synthetic severe missions, representing specific driver profiles and therefore specific threats for different local contexts in the vehicle. Our method is compatible with the expression of historical industrial choices that underlie the determination of their referential missions or standard loads. Furthermore, we are able to compare these references with respect to service situations and driver behaviors witnessed on our dataset.

This Chapter VI also highlighted the important distinction between validation *objectives* and the *loads* that replicate them. The objectives are written in terms of mission severity or fatigue characterization, and they correspond to the formulation of a control on the risk of failure of the subsystem.

In Chapter VII, we adapt the existing framework of fatigue-equivalent loads to the creation of PG schedules that are able to replicate or synthesize such objectives in a protected environment: a numerical simulation, a test bench or the proving grounds themselves.

The choice of a search space in which fatigue equivalents are sought is determined by the available means of physical trials and numerical simulations. Only our variables of interest were optimized in this search for equivalent loads, whereas several supplementary aspects are

considered by the company to settle on a reference schedule, such as spectral content for the vibratory behavior of the structure, or load levels to try non-linear parts (such as rubber joints) in different conditions.

In the automotive industry, reference loads are the focal point both for the elaboration of a digital twin of the new vehicle model and for the definition of its appropriate validation procedures. The analysis of service loads is performed through the definition of intermediary variables (characterization) that are both measurable from mission samples, interpretable and compatible with the theory of reliable design. Ultimately, the analysis leads back to the definition of adequate test loads. Thus have we managed to anchor our work altogether to available data, theory and practice surrounding the reliable design of personal vehicle suspension and body parts.

VIII.1 Perspectives on fatigue characterization

VIII.1.1 Mechanical hypotheses

By defining equivalent magnitudes as our fatigue characterization in Section III.7, we have ensured continuity with existing numerical validation processes in Stellantis.

Most importantly, these variables are compatible with existing material fatigue criteria that are used in the numerical validation of suspension and body parts. Indeed, an equivalent magnitude is but a proportional quantity to the range of a cyclic unidimensional loading history that induces the same pseudo-damage on the local context of interest. The same kind of loads is used in baseline tests for the fatigue characterization of a component. Unidimensional load cases are currently the definition of partial validation procedures that manage each local context separately. Thus, the parameters of these validation loads can easily be modified to fit an objective magnitude.

However, the mechanical hypotheses that underlie the definition of pseudo-damage were strong. In this thesis, confidence in their validity stems from the historicity of the method, not from their experimental nor numerical validation.

The quasi-static and elastic behavior of the structure is not ensured when it encounters obstacles such as a pothole. Indeed the structure may filter out a fraction of the spectral (frequency) content of such an event, and rubber stops will filter out the highest load variations, preventing their transmission to inner parts of the structure.

We have considered the existence of a fatigue criterion based on a variable (projected shear stress) that is a linear form on Cauchy stress. This choice was made for computational reasons as well as to ensure the additivity of the fatigue characterization. Relieving this constraint of linearity may give access to a larger variety of characterizations that better predict the fatigue of the various components of the structure. However, this gain should not be cancelled by later complications to evaluate the pseudo-fatigue induced by a mission on a partially known structure.

The set of sensible zones for each global load case was observed on a few load cases

but never mapped for a given, known vehicle model. When submitting a part such as a front suspension member to each load case of interest (say braking, cornering, symmetrical vertical loads, asymmetrical vertical loads, one-wheel loads...), we can identify separately sets of Cauchy stress concentrations. However, each location may be damaged separately by different load cases, on the same fatigue mode (same REV, same mesoscopic slip plane) or not (different slip plane). We have made the hypothesis that it was the latter case for all zones.

VIII.1.2 Alternative fatigue characterization

Let us consider two alternatives to the sole use of pseudo-damage calculated on a global load case, for the implementation of the whole reliable design method and the derivation of validation loads. Both following propositions are compatible with the fatigue characterization of a concatenation of loading histories, as is the case in the simulation of an aggregated trip and in the construction of a proving ground schedule.

In Section III.5.2, we have transformed the Rainflow range-only matrix calculated on each global load case into one or several pseudo-damages. Instead, an equivalent loading history could aim at replicating the very Rainflow matrices on all load cases. At first sight, there would naively be as many dimensions to the characterization as there are Rainflow classes. However, Rainflow matrices can themselves be characterized by an equivalent Rainflow matrix with only a few classes having non-zero occurrences. This reduced matrix yields equivalent pseudo-damages for a selected number of Basquin exponents. The number of exponents determines the minimum number of classes to achieve equivalence on all associated local contexts.

The characterization of a multi-input global loading history would have a very large dimension. However, statistical analyses and dimension reduction methods can reveal similar or richer dimensions of intrinsic or conditional severity than the ones that we have defined in this thesis. Most importantly, solving an equivalence on these Rainflow parameters would lead to schedules that are more representative of the actual loads of the objective mission.

A second alternative is the use of the decomposition of road-induced pseudo-damage into spectral fatigue induced by the rugosity of the road (the so-called Random Road), the quasi-static pseudo-damage induced by maneuvers (so-called Driven Road) and the pseudo-damage induced by obstacles, as proposed in [Bellec *et al.* 2023]. Three quantities would be calculated for each local context. The mechanical justification of these variables was thoroughly conducted. Thanks to the strict distinction between road rugosity, maneuvers and obstacles, the interpretation of variations and correlations between drivers and trips would be richer.

Note that the endpoint of the analysis of service loads is the determination of equivalent loads that best replicate the situations encountered in a synthetic severe mission, of interest for the validation of a subsystem. Once a complete testable validation procedure is determined, the resistance of the subsystem can be evaluated through the lens of a different mechanical model.

VIII.2 Perspective on the statistical analysis of service loads

VIII.2.1 Improving the sampling of Trip

The Driver-Trip-Payload mission factor model introduced in Chapter IV is a practical starting point for the strategic elaboration of an adequate sampling of the missions of the vehicle.

If a factor, like Trip, is considered to have a large effect on the required validation objectives for the design of a vehicle model, then the efforts to model and sample this specific factor can be increased, through the inclusion of a survey of trips in the method for instance. Contrariwise, if a deeper sampling of Payload is not expected to yield large improvement on the outskirts of the distribution of severity, then the analysis of service can restrict this factor in a conservative manner, as is already the case (see Appendix E).

The analyses developed in this thesis have shown the marginal effect of driver behavior and the effect of a change in road environments on this behavior. Knowledge on the population of trips in a market is the main required ingredient to improve the selection of an appropriate aggregated trip, or to achieve a coupled distribution of both Driver and Trip in a market.

Trip samples would be characterized by their composition in each road environment. This leads us to the second difficulty, for which we have only scratched the surface: the classification of roads into road environments.

VIII.2.2 Improving the characterization of Trip

We have compared two different sets of road segments associated with the highway and back road environments in §IV.4.4. From differences in correlations between load intensities and speed quantities, we have concluded that the situations that drivers had to face and the events of the roads were consistently different from one segment to another. Despite being labeled as the same road environment, different segments would contain different events, and different times of the day revealed the influence of traffic and visibility.

Moreover, the estimation of the load intensity of a driver on a road segment was performed very quickly. A windowed analysis should be conducted on the global loading history of each driver. Results on a population of drivers can be gathered if the windows coincide from a driver to another: two windows on two different drivers characterize the same location if the GPS coordinates match.

Note that this windowed analysis must be implemented during the calculation of pseudo-damage and not in the post-treatment of the results (see Appendix C on the data treatment process in this thesis). It requires a different management of the dataset. Our workflow was not prepared to conduct this study.

The windowed analysis load intensities on each segment of one or several measurement campaigns can help to determine formally a relevant partition of the road into road environ-

ments for the sake of pseudo-fatigue characterization. In other words, a new implementation of a clustering method on these segmented data may reveal different trip patterns.

An adequate classification of the trip into different road environments serves two purposes. First, any trip selected from a map should be describable as a concatenation of such road environments. They must be identifiable from the interpretation of a map or observation of the surroundings (such as crossroads, damaged roads, highways, highway entry lanes...).

Second, a sample of trips obtained from a survey or from service measurements in a large population must be translatable into a sample of trip compositions. In the case of a survey, it is likely that a customer will be asked the percentage of kilometers that they in a city or on highway in general, instead of the complete description of their path. This is why the prior labeling of road environments in our study was made of environments that a person can identify qualitatively (urban, highway, back road, damaged road).

Let us consider an alternative decomposition of road environments, for instance one identifying crossroads, highway entry lanes, parking lots and so on. To achieve this second purpose, we need to model the density of such alternative environments in the surveyed decomposition. The density of highway entry lanes can be estimated by the average distance driven on a highway by a customer; the number of crossroads per kilometer in a city can be estimated from a map, etc. The connection between road quality, road environment and the variety of service loads was further investigated in [Burger *et al.* 2021].

VIII.2.3 Refined model of the outskirts of the population

The distribution of driver severity was elaborated on a limited number of samples. We have justified the choice of a Gaussian mixture from an analysis of the population of drivers *at hand*.

The particular shape of this population in aggregated trips containing all kinds of road environments may be specific to the region of Detroit. It may also be justified by the unknown bias of the sample. In order to confirm this population shape, more samples or a sociological/psychological model explaining the behavior of different drivers would be required.

Moreover, this first model does not include the variability of trips in its construction. Perhaps the severe drivers are all customers that drive in specific road environments. Perhaps the intrinsic severity of a driver and the place where they live are completely independent. We have not conducted a literature review to determine whether this question was tackled. However, the characterization of driver behavior from a social or psychological point of view is a research field, for instance in [Pérez-Diaz 2000; Simons-Morton *et al.* 2005].

Enacting a conservative restriction on the population of missions ensures the safety of the vehicles developed by a company. However, the risk is to vastly overestimate the severity of the outskirts of the population, leading to validation objectives that are very and unnecessarily hard to withstand.

In this thesis, we have not calculated confidence intervals for the objectives calculated in a unidimensional SSI framework. Neither have we included the elaboration of safety margins

that coincide with the confidence that we have on our hypotheses, models and data [Speckert *et al.* 2009]. Still, the values of the distribution of severity at the outskirts of the population are very dependent on the hypothesis of a Gaussian mixture.

The post-analysis of loads acquired during a measurement campaign determines from a quantitative criterion whether they correspond to regular driving or to abuse/incident. Thus is it determined that our samples belong to service. However, this frontier becomes blurry once we elaborate a distribution of the severity of drivers.

The most globally severe driver of the campaign US18-DT1, driver 031, must be considered regular if no abuse was observed. But what about a larger quantile of global severity? How really plausible is it to find driver behaviors in these outskirts? This reflection is redirected toward the shape of the distribution at the edge as well as the acceptability of severity.

A larger sample of drivers would help improve the model of the population of drivers at such outskirts. Connected vehicle solutions (§IV.3.1) can lead to such an increase in driver (and trip) sampling.

VIII.2.4 Quantitative identification of road events

Finally, the quantitative identification of road events and maneuvers is made possible by the evaluation of pseudo-damage. Instead of merely detecting an event (qualitative), we can carry along the information of how much pseudo-damages it inflicted on the vehicle.

The identification of events can be conducted by a windowed or precise segmented analysis of the loading histories measured on each road environment. Specific kinds of effort variations as well as road load frequency content would help identify the beginning and end of an event. The vector of magnitudes of the event can then be used as its measure as well as to determine its class.

The identification of road events can supplant or complement a clustering of road environments. The main difference between both analyses is the size of the window. Once events are identified, their higher density in a location can be interpreted as an effect of the road environment.

Available tracks in a proving ground facility may then be compared to the population of road events identified in a region or aggregated trip of interest. After all, these tracks were often historically selected as a severe and reproducible version of events observed in the region of the facility.

VIII.3 Perspectives on the reliable design of complex parts

In Chapter VI, we have laid several tracks for improvement with respect to the reliable design of parts that have several local contexts. We have tied these ends to propositions in the literature for frameworks that handle this plurality of failure modes. We have not

investigated eventual relationships between the Strength of different local contexts over an automotive structure. Thus we could not progress on the proposition of a method to solve the design and validation problem in a general case.

Theoretical bases for the reliable design of such complex parts may exist, but one or more examples should be conducted on a given part, to aid in implementing these bases in an application.

We have contemplated conducting the reliable design of a suspension arm with respect to our available load data. Thus could we tether our analysis to the determination of equivalent loads on such a part already conducted in [Genet (Le Corre) 2006; Raoult and Delattre 2020]. However, the part had too few local contexts, all associated with the same sensible zone.

A rear suspension member, connecting both rear wheels and containing a variety of different contexts was the second considered option. This case study could also serve as a proof-of-concept for the decomposition of a global loading history into several global load cases and their relevance for the factorization of the damages induced on several sets of sensible zones. Unfortunately, we could not include such a sizeable analysis in the timeline of the project.

The location of the existing PG schedule in the space of severity reveals methods to tweak its content to modify the synthetic severe mission that it represents. Indeed, on the one hand, traveling in a space of conditional severity modifies the magnitudes induced by the mission. On the other hand, adding a repetition of a track in the schedule also modifies the overall magnitudes and the diagnosed severity of the mission thus represented. Therefore, it is possible to increase or decrease the sportiness of the mission represented by the schedule by determining an appropriate severization direction in the space of severity.

Bibliography

[1] AFNOR, *Fatigue sous sollicitations - méthode rainflow de comptage des cycles d'amplitude variable*, Nov. 1993 (cit. on p. 308).

[2] C. Amzallag, J. P. Gerey, J. L. Robert, and J. Bahuaud, "Standardization of the rainflow counting method for fatigue analysis," *International journal of fatigue*, vol. 16, no. 4, pp. 287–293, 1994 (cit. on pp. 308, 309).

[3] ASTM, "Standard practices for cycle counting in fatigue analysis," ASTM International, West Conshohocken, PA, Standard, 2017 (cit. on p. 306).

[4] L. Augustins, "Représentation des courbes iso-durée de vie dans le diagramme de dang van," PSA Peugeot Citroën, Tech. Rep., 2007 (cit. on pp. 46, 176).

[5] J. Axsen and Z. Long, "Sport utility vehicles and willingness-to-downsize: a mixed-method exploration of functional, symbolic, and societal consumer perceptions in canada," *Energy Research & Social Science*, vol. 92, p. 102 776, 2022 (cit. on p. 295).

[6] E. Baroux, B. Delattre, A. Constantinescu, P. Pamphile, and I. Raoult, "Analysis of real-life multi-input loading histories for the reliable design of vehicle chassis," *Procedia Structural Integrity*, vol. 38, pp. 497–506, 2022, Fatigue Design 2021, International Conference Proceedings, 9th Edition (cit. on p. 91).

[7] B. Bayart, J. Despujols, and P. Madelpech, "Fatigue crack growth approach for fleet monitoring," in *3rd International Conference on Material and Component Performance under Variable Amplitude Loading*, Mar. 2015, pp. 4–12 (cit. on p. 289).

[8] P. Beaumont, "Optimisation des plans d'essais accélérés application à la tenue en fatigue de pièces métalliques de liaison au sol," Ph.D. dissertation, Université d'Angers, 2013 (cit. on pp. 14, 16, 38, 43, 47, 186, 212, 292).

[9] E. Bellec, M. L. Facchinetti, C. Doudard, S. Calloch, and S. Moyne, "Loading classification proposal for fatigue design of automotive chassis-parts: a relevant process for variable amplitude and multi-input load cases," *International Journal of Fatigue*, vol. 166, p. 107 284, 2023 (cit. on pp. 70, 88, 184, 259).

[10] E. Bellec, M. L. Facchinetti, C. Doudard, S. Calloch, S. Moyne, and M. P. Silvestri, "Modelling and identification of fatigue load spectra: application in the automotive industry," *International Journal of Fatigue*, vol. 149, p. 106 222, 2021 (cit. on pp. 174–176, 180).

[11] A. Benaouda, R. Hauteville, A. Juin, P. Amuzuga, and F. Lefebvre, "State of the art of fatigue strength of materials & structures from additive manufacturing – the pivot, a cetim development.," *Procedia Structural Integrity*, vol. 38, pp. 116–131, 2022, Fatigue Design 2021, International Conference Proceedings, 9th Edition (cit. on p. 47).

[12] C. Berger *et al.*, "Betriebsfestigkeit in germany - an overview," *International Journal of Fatigue*, vol. 24, pp. 603–625, 2002 (cit. on p. 188).

[13] A. Bignonnet and J. J. Thomas, "Fatigue assessment and reliability in automotive design," SAE Technical Paper, Tech. Rep., 2001 (cit. on pp. 17, 190).

[14] A. Bignonnet and J. J. Thomas, "Approche fiabiliste en conception automobile," *SF2M-Journées de Printemps*, 2004 (cit. on p. 16).

[15] L. Binda, "Advanced creep damage and deformation assessment of materials subject to steady and cyclic loading conditions at high temperatures," Ph.D. dissertation, ETH Zurich, 2010 (cit. on p. 16).

[16] S. Bosia and A. Constantinescu, "Fast time-scale average for a mesoscopic high cycle fatigue criterion," *International journal of fatigue*, vol. 45, pp. 39–47, 2012 (cit. on p. 301).

[17] S. S. T. Brown H. C. Robertson A. J., *Motor Vehicle Structures: Concepts and Fundamentals*. Butterworth-Heinemann, 2002 (cit. on pp. 68, 291).

[18] M. Burger, K. Dreßler, and M. Speckert, "Load assumption process for durability design using new data sources and data analytics," *International Journal of Fatigue*, vol. 145, p. 106 116, 2021 (cit. on pp. 89, 261).

[19] K. P. Burnham and D. R. Anderson, "Multimodel inference: understanding aic and bic in model selection," *Sociological methods & research*, vol. 33, no. 2, pp. 261–304, 2004 (cit. on p. 152).

[20] E. Castillo and A. Fernández-Canteli, *A unified statistical methodology for modeling fatigue damage*. Springer Science & Business Media, 2009 (cit. on p. 42).

[21] E. Charkaluk, A. Constantinescu, F. Szmytka, and S. Tabibian, "Probability density functions: from porosities to fatigue lifetime," *International Journal of Fatigue*, vol. 63, pp. 127–136, 2014 (cit. on p. 41).

[22] P. Cheney, "Minivans are perfect. why do we hate them?," Sep. 27, 2011. [Online]. Available: https://www.theglobeandmail.com/globe-drive/culture/commuting/minivans-are-perfect-why-do-we-hate-them/article4256886/ (cit. on p. 295).

[23] S. Chib and E. Greenberg, "Understanding the metropolis-hastings algorithm," *The American Statistician*, vol. 49, no. 4, pp. 327–335, 1995 (cit. on p. 181).

[24] V. Chmelko and M. Margetin, "The performance of selected multiaxial criteria under tension/torsion loading conditions," *International Journal of Fatigue*, vol. 135, p. 105 532, 2020 (cit. on p. 75).

[25] F. D. C. Coelho, "Maîtrise de la tenue en fatigue des cordons de soudure," Ph.D. dissertation, ISAE-ENSMA Ecole Nationale Supérieure de Mécanique et d'Aérotechique-Poitiers, 2014 (cit. on p. 56).

[26] S. Coles, J. Bawa, L. Trenner, and P. Dorazio, *An introduction to statistical modeling of extreme values*. Springer, 2001, vol. 208 (cit. on p. 178).

[27] O. Coudray, "A statistical point of view on fatigue criteria : from supervised classification to positive-unlabeled learning," Ph.D. dissertation, Dec. 2022 (cit. on p. 230).

[28] O. Coudray, P. Bristiel, M. Dinis, C. Keribin, and P. Pamphile, "Caractérisation de zones critiques pour le dimensionnement en fatigue d'une pièce mécanique," in *22e Congrès de Maîtrise des Risques et Sûreté de Fonctionnement λ-μ22*, 2020 (cit. on pp. 47, 230).

[29] O. Coudray, P. Bristiel, M. Dinis, C. Keribin, and P. Pamphile, "Fatigue data-based design: statistical methods for the identification of critical zones," in *SIA Simulation Numérique*, 2021 (cit. on p. 230).

[30] C. Cristia, "Le processus doctoral: entre souffrances et vulnérabilités," *Essais. Revue interdisciplinaire d'Humanités*, no. Hors-série 7, 2022 (cit. on p. 6).

[31] MU-CSS, "Personal transportation factsheet," University of Michigan - Center for Sustainable Systems, Tech. Rep. CSS01-07, 2021 (cit. on p. 132).

[32] K. Dang-Van, B. Griveau, and O. Message, "On a new multiaxial fatigue limit criterion-theory and application," *Biaxial and multiaxial fatigue*, pp. 479–496, 1989 (cit. on p. 44).

[33] G. Darling, *Dossier: les principaux types de suspension automobile*, https://www.guillaumedarding.fr/dossier-les-principaux-types-de-suspension-automobile-2883821.html, Jan. 26, 2015 (cit. on p. 294).

[34] S. C. Davis and R. G. Boundy, "Transportation energy data book: edition 39," Oak Ridge National Lab.(ORNL), Oak Ridge, TN (United States), Tech. Rep., 2021 (cit. on p. 132).

[35] A. Débarbouillé, F. Renaud, Z. Dimitrijevic, D. Chojnacki, L. Rota, and J. L. Dion, "Wheel forces estimation with an augmented and constrained extended kalman filter applied on a nonlinear multi-body model of a half vehicle," *Procedia Structural Integrity*, vol. 38, pp. 342–351, 2022 (cit. on p. 317).

[36] A. P. Dempster, N. M. Laird, and D. B. Rubin, "Maximum likelihood from incomplete data via the em algorithm," *Journal of the royal statistical society: series B (methodological)*, vol. 39, no. 1, pp. 1–22, 1977 (cit. on pp. 152, 154).

[37] L. Devroye, "Nonuniform random variate generation," *Handbooks in operations research and management science*, vol. 13, pp. 83–121, 2006 (cit. on pp. 177, 178).

[38] R. T. Dewa and M. Kepka, "Statistical approaches on the design of fatigue stress spectra for bus structures," *SN Applied Sciences*, vol. 1, p. 1360, 2019 (cit. on p. 176).

[39] UK-DfT, "Road traffic estimates: great britain 2019," Government of the United Kingdom - Department for Transport, Tech. Rep., 2020 (cit. on p. 132).

[40] UK-DfT, "Road traffic estimates: great britain 2021," Government of the United Kingdom - Department for Transport, Tech. Rep., 2022 (cit. on p. 132).

[41] T. Dirlik and D. Benasciutti, "Dirlik and tovo-benasciutti spectral methods in vibration fatigue: a review with a historical perspective," *Metals*, vol. 11, no. 9, 2021 (cit. on p. 188).

[42] P. Dong, "A structural stress definition and numerical implementation for fatigue analysis of welded joints," *International Journal of Fatigue*, vol. 23, no. 10, pp. 865–876, 2001 (cit. on p. 57).

[43] P. Dong, Z. Wei, and J. K. Hong, "A path-dependent cycle counting method for variable-amplitude multi-axial loading," *International Journal of Fatigue*, vol. 32, no. 4, pp. 720–734, 2010 (cit. on pp. 44, 46, 302, 303).

[44] K. Dreßler and M. Speckert, "Durability validation for variable customer usage," SAE Technical Paper, Tech. Rep., 2022 (cit. on p. 211).

[45] K. Dreßler, M. Speckert, R. Müller, and C. Weber, "Customer loads correlation in truck engineering," Fraunhofer (ITWM), Tech. Rep. 151, 2009 (cit. on pp. 127, 191).

[46] P. Du Bois *et al.*, *Vehicle crashworthiness and occupant protection*, P. Prasad and J. E. Belwafa, Eds. American Iron and Steel Institute, 2004 (cit. on p. 288).

[47] B. Echard *et al.*, "Guide d'aide à l'estimation et à la validation de la fiabilité automobile," *Congrès Lambda Mu 20 de Maîtrise des Risques et de Sûreté de Fonctionnement, 11-13 Octobre 2016, Saint Malo, France*, 2016 (cit. on pp. 190, 192).

[48] D. El Khoukhi, "Etude de l'effet des hétérogénéités microstructurales sur la dispersion detenue en fatigue à grand nombre de cycles d'alliages d'aluminium de fonderie: passage de l'élément de volume à la structure," Ph.D. dissertation, HESAM Université, 2020 (cit. on p. 41).

[49] Electropedia, *Dependability*, in *Electropedia: The World's Online Electrotechnical Vocabulary*, Feb. 2015. [Online]. Available: https://www.electropedia.org/iev/iev.nsf/display?openform&ievref=192-01-22 (cit. on p. 287).

[50] T. Endo, M. Matsuishi, K. Mitsunaga, K. Kobayashi, and K. Takahashi, "Rain flow method, the proposal and the applications," *Memoirs of Kyusyu Institute of Technology*, vol. 28, pp. 33–62, 1974 (cit. on p. 308).

[51] S. Eryilmaz, "Multivariate stress-strength reliability model and its evaluation for coherent structures," *Journal of Multivariate Analysis*, vol. 99, pp. 1878–1887, Oct. 2008 (cit. on p. 198).

[52] B. Escofier and J. Pagès, "Analyses factorielles simples et multiples," *Dunod, Paris*, vol. 284, 1998 (cit. on pp. 104, 107).

[53] Y. Escoufier, "Le traitement des variables vectorielles," *Biometrics*, pp. 751–760, 1973 (cit. on p. 122).

[54] M. L. Facchinetti, "Fatigue damage of materials and structures assessed by wöhler and gassner frameworks: recent insights about load spectra for the automotive," *Procedia Engineering*, vol. 213, pp. 117–125, 2018, 7th International Conference on Fatigue Design, Fatigue Design 2017, 29-30 November 2017, Senlis, France (cit. on pp. 173, 188).

[55] A. Fatemi and L. Yang, "Cumulative fatigue damage and life prediction theories: a survey of the state of the art for homogeneous materials," *International Journal of Fatigue*, vol. 20, no. 1, pp. 9–34, 1998 (cit. on p. 52).

[56] F. Fauvin, J. C. Roux, P. Monnet, and E. Feulvarch, "Fast estimation of the shear stress amplitude for fatigue life analysis of metals," *European Journal of Mechanics-A/Solids*, vol. 80, p. 103 928, 2020 (cit. on p. 44).

[57] J. L. Fayard, "Dimensionnement à la fatigue polycyclique de structures soudées," Ph.D. dissertation, Ecole Polytechnique, 1996 (cit. on pp. 56, 57).

[58] A. Fernández-Canteli, E. Castillo, and S. Blasón, "A methodology for phenomenological analysis of cumulative damage processes. application to fatigue and fracture phenomena," *International Journal of Fatigue*, vol. 150, p. 106 311, Sep. 2021 (cit. on p. 41).

[59] FHWA, "Highway statistics 2019," Federal Highway Administration, Tech. Rep., 2019 (cit. on p. 132).

[60] A. Fissolo, C. Gourdin, Y. Chen, G. Perez, and J. M. Stelmaszyk, "Investigations into the cumulative fatigue life of an aisi 304l austenitic stainless steel used for pressure water reactors: application of a double linear damage rule," *International Journal of Fatigue*, vol. 77, pp. 199–215, 2015 (cit. on p. 304).

[61] S. Forest, M. Amestoy, S. Cantournet, G. Damamme, and S. Kruch, Eds., *Mécanique des milieux continus*. École des Mines de Paris, 2006 (cit. on p. 34).

[62] R. Fouchereau, G. Celeux, and P. Pamphile, "Probabilistic modeling of S-N curves," *International Journal of Fatigue*, Apr. 2014 (cit. on pp. 41, 47).

[63] F. Fremy *et al.*, "Load path effect on fatigue crack propagation in i+ ii+ iii mixed mode conditions–part 1: experimental investigations," *International Journal of Fatigue*, vol. 62, pp. 104–112, 2014 (cit. on p. 302).

[64] D. Frey and J. M. Demaimay, "Etalonnage de l'endommagement des trains et de la structure," Automobiles Citroën, Tech. Rep., 1991 (cit. on p. 187).

[65] W. Fricke, "Iiw guideline for the assessment of weld root fatigue," *Welding in the World*, vol. 57, no. 6, pp. 753–791, 2013 (cit. on p. 37).

[66] M. Frinkle, R. Weir, and J. B. Ferris, "A graphical representation of road profile characteristics," SAE Technical Paper, Tech. Rep., 2004 (cit. on p. 88).

[67] D. Garvin, "Competing on the eight dimensions of quality," *Harvard Business Review*, 1987 (cit. on pp. 14, 289, 290).

[68] E. Gassner, "Festigkeitsversuche mit wiederholter beanspruchung im flugzeugbau," in *Luftwissen*, vol. 6, 1939, pp. 61–64 (cit. on pp. 188, 189).

[69] N. Gayton, "Méthodes probabilistes pour la conception mécanique," Habilitation à diriger des recherches, 2012 (cit. on pp. 192, 193).

[70] G. Genet (Le Corre), "A statistical approach to multi-input equivalent fatigue loads for the durability of automotive structures," Ph.D. dissertation, Chalmers University of Technology and Göteborg University, 2006 (cit. on pp. 22, 35, 225, 230–232, 263, 303).

[71] G. Genet (Le Corre), P. Johannesson, D. Gualandris, J. de Maré, *et al.*, "Multi-input markov chain equivalent fatigue loadings," *Metallurgical Research & Technology*, vol. 106, no. 5, pp. 220–224, 2009 (cit. on p. 230).

[72] S. Geng, X. Liu, X. Yang, Z. Meng, X. Wang, and Y. Wang, "Load spectrum for automotive wheels hub based on mixed probability distribution model," *Proceedings of the Institution of Mechanical Engineers, Part D: Journal of Automobile Engineering*, vol. 233, no. 14, pp. 3707–3720, 2019 (cit. on p. 178).

[73] J. E. Gentle, *Computational statistics*. Springer, 2010 (cit. on p. 181).

[74] R. Glon, "Fwd vs. rwd vs. awd: drivetrain layouts and what they mean," *Digitaltrends*, Mar. 11, 2021. [Online]. Available: https://www.digitaltrends.com/cars/fwd-vs-awd-vs-rwd/ (cit. on p. 293).

[75] D. Goldfarb and A. Idnani, "A numerically stable dual method for solving strictly convex quadratic programs," *Mathematical Programming*, vol. 27, pp. 1–33, 1983 (cit. on p. 241).

[76] V. V. Grubisic and G. Fischer, "Methodology for effective design evaluation and durability approval of car suspension components," *SAE Transactions*, pp. 21–33, 1997 (cit. on pp. 180, 188, 231, 232).

[77] M. Guarascio, M. Lombardi, G. Rossi, and G. Sciarra, "Risk analysis and acceptability criteria," *WIT Transactions on the Built Environment*, vol. 94, 2007 (cit. on p. 16).

[78] J. Happian-Smith, Ed., *An Introduction to Modern Vehicle Design*. Butterworth Heinemann, 2002 (cit. on p. 68).

[79] C. Haskins and K. Forsberg, "Systems engineering handbook: a guide for system life cycle processes and activities," International Council on Systems Engineering, 2007 (cit. on pp. 13, 296).

[80] A. M. Hasofer and N. Lind, "Exact and invariant second-moment code format," *Journal of Engineering Mechanics*, vol. 100, pp. 111–121, 1974 (cit. on pp. 192, 193).

[81] N. Henze and B. Zirkler, "A class of invariant consistent tests for multivariate normality," *Communications in statistics-Theory and Methods*, vol. 19, no. 10, pp. 3595–3617, 1990 (cit. on p. 119).

[82] P. Heuler and H. Klätschke, "Generation and use of standardised load spectra and load-time histories," *International Journal of Fatigue*, vol. 27, pp. 976–990, 2005 (cit. on pp. 174, 187, 188).

[83] A. Hobbacher *et al.*, *Recommendations for fatigue design of welded joints and components*. Springer, 2016, vol. 47 (cit. on pp. 37, 43).

[84] J. P. Hubert, P. Pistre, and J. L. Madre, "L'utilisation de l'automobile par les ménages dans les territoires peu denses: analyse croisée par les enquêtes sur la mobilité et le recensement de la population," *Economie et Statistique/Economics and Statistics*, no. 483-484-485, pp–179, 2016 (cit. on p. 132).

[85] F. Husson, J. Josse, and J. Pagès, "Principal component methods-hierarchical clustering-partitional clustering: why would we need to choose for visualizing data," Applied Mathematics Department, Tech. Rep., 2010 (cit. on p. 116).

[86] F. Husson, S. Lê, and J. Pagès, *Exploratory multivariate analysis by example using R*. CRC press Boca Raton, 2011, vol. 15 (cit. on pp. 100, 141, 321, 323).

[87] G. R. Irwin, "Analysis of stresses and strains near the end of a crack traversing a plate," 1957 (cit. on p. 36).

[88] ISO26262, "Road vehicles – functional safety," International Organization for Standardization, Geneva, CH, Standard ISO 26262:2018, Dec. 2018 (cit. on p. 287).

[89] M. Jabbado, "Fatigue polycyclique des structures métalliques: durée de vie sous chargements variables.," Ph.D. dissertation, Ecole Polytechnique, 2006 (cit. on p. 302).

[90] P. Johannesson and M. Speckert, Eds., *Guide to load analysis for durability in vehicle engineering*. John Wiley & Sons, Ltd, 2014 (cit. on pp. 67, 86).

[91] P. Johannesson and J. J. Thomas, "Extrapolation of rainflow matrices," *Extremes*, vol. 4, pp. 241–262, 2001 (cit. on p. 176).

[92] I. T. Jolliffe and J. Cadima, "Principal component analysis for special types of data," in *Principal Component Analysis*. New York, NY: Springer New York, 2002, pp. 338–372, ISBN: 978-0-387-22440-4 (cit. on p. 100).

[93] I. T. Jolliffe and J. Cadima, "Principal component analysis: a review and recent developments," *Philosophical transactions of the royal society A: Mathematical, Physical and Engineering Sciences*, vol. 374, no. 2065, p. 20 150 202, 2016 (cit. on pp. 100, 102).

[94] K. Kanazawa, K. J. Miller, and M. W. Brown, "Cyclic deformation of 1% cr-mo-v steel under out-of-phase loads," *Fatigue & Fracture of Engineering Materials & Structures*, vol. 2, no. 2, pp. 217–228, 1979 (cit. on p. 302).

[95] M. K. Karlsson, "Load modelling for fatigue assessment of vehicles - a statistical approach," Ph.D. dissertation, Chalmers University of Technology and Göteborg University, 2007 (cit. on p. 86).

[96] D. Kim, S. Hwang, and H. Kim, "Vehicle stability enhancement of four-wheel-drive hybrid electric vehicle using rear motor control," *IEEE Transactions on Vehicular technology*, vol. 57, no. 2, pp. 727–735, 2008 (cit. on p. 293).

[97] J. Klemenc and M. Fajdiga, "Improved modelling of the loading spectra using a mixture model approach," *International Journal of Fatigue*, vol. 30, no. 7, pp. 1298–1313, 2008 (cit. on p. 174).

[98] W. Krüger, M. Scheutzow, A. Beste, and J. Petersen, "Markov- und rainflow-rekonstruktionen stochastischer beanspruchungszeitfunktionen," 1985. [Online]. Available: http : / / nbn - resolving . de / urn : nbn : de : hbz : 386 - kluedo - 6967 (cit. on p. 305).

[99] W. Kruskal and F. Mosteller, "Representative sampling, i: non-scientific literature," *International Statistical Review/Revue Internationale de Statistique*, pp. 13–24, 1979 (cit. on p. 89).

[100] W. Kruskal and F. Mosteller, "Representative sampling, ii: scientific literature, excluding statistics," *International Statistical Review/Revue Internationale de Statistique*, pp. 111–127, 1979 (cit. on p. 89).

[101] W. Kruskal and F. Mosteller, "Representative sampling, iii: the current statistical literature," *International Statistical Review/Revue Internationale de Statistique*, pp. 245–265, 1979 (cit. on p. 89).

[102] W. Kruskal and F. Mosteller, "Representative sampling, iv: the history of the concept in statistics, 1895-1939," *International Statistical Review/Revue Internationale de Statistique*, pp. 169–195, 1980 (cit. on p. 89).

[103] A. Kullgren, A. Lie, and C. Tingvall, "Comparison between euro ncap test results and real-world crash data," *Traffic Injury Prevention*, vol. 11, no. 6, pp. 587–593, 2010 (cit. on p. 288).

[104] L. I. Kumajas, N. F. Wuryaningrat, and H. S. Lembong, "Profitability in the automotive and component industry," *Asia Pacific Journal of Management and Education (APJME)*, vol. 4, no. 3, pp. 115–129, 2021 (cit. on p. 290).

[105] S. Lajqi, S. Pehan, N. Lajqi, A. Gjelaj, J. Psenicnik, and S. Emin, "Design of independent suspension mechanism for a terrain vehicle with four wheels drive and four wheels steering," *Annals of the Faculty of Engineering Hunedoara*, vol. 11, no. 1, p. 101, 2013 (cit. on p. 294).

[106] R. Lebrun and A. Dutfoy, "A generalization of the nataf transformation to distributions with elliptical copula," *Probabilistic Engineering Mechanics*, vol. 24, no. 2, pp. 172–178, 2009 (cit. on p. 193).

[107] R. Lebrun and A. Dutfoy, "An innovating analysis of the nataf transformation from the copula viewpoint," *Probabilistic Engineering Mechanics*, vol. 24, no. 3, pp. 312–320, 2009 (cit. on p. 193).

[108] R. Lebrun and A. Dutfoy, "Do rosenblatt and nataf isoprobabilistic transformations really differ?" *Probabilistic Engineering Mechanics*, vol. 24, no. 4, pp. 577–584, 2009 (cit. on p. 193).

[109] G. Leduc *et al.*, "Road traffic data: collection methods and applications," *Working Papers on Energy, Transport and Climate Change*, vol. 1, no. 55, pp. 1–55, 2008 (cit. on p. 132).

[110] B. D. Lévai, "Damage and equivalent load definition for durability of vehicle," Ph.D. dissertation, Linköping University, Aug. 2018 (cit. on pp. 55, 64).

[111] K. Levenberg, "A method for the solution of certain non-linear problems in least squares," *Quarterly of applied mathematics*, vol. 2, no. 2, pp. 164–168, 1944 (cit. on p. 175).

[112] C. Lipson, N. J. Sheth, and R. L. Disney, "Reliability prediction - mechanical stress/strength interference," University of Michigan, Tech. Rep., 1967 (cit. on pp. 17, 187).

[113] P. C. Mahalanobis, "On tests and measures of group divergence," *J. Asiat. Soc. Bengal*, vol. 26, pp. 541–588, 1930 (cit. on p. 119).

[114] F. Mainnemare, "Modélisation du point de soudure électrique pour la tenue en service des structures automobiles," Ph.D. dissertation, Université Paris-Saclay, 2021 (cit. on p. 56).

[115] F. Mainnemare, B. Delattre, I. Raoult, O. Villars, P. A. Boucard, and P. A. Guidault, "A numerical analysis to investigate the spot weld local influence," in *MATEC Web of Conferences*, EDP Sciences, vol. 165, 2018, p. 21 006 (cit. on p. 57).

[116] F. Mainnemare, B. Delattre, I. Raoult, O. Villars, P. A. Boucard, and P. A. Guidault, "Éléments préalables à l'élaboration d'un modèle de connecteur pour le point de soudure électrique," in *CSMA 2019-14ème colloque national en calcul de structures*, 2019 (cit. on p. 57).

[117] H. Maïtournam, *Matériaux et structures anélastiques*. École Polytechnique, 2017 (cit. on pp. 34, 300–302).

[118] E. N. Mamiya, J. A. Araújo, and F. C. Castro, "Prismatic hull: a new measure of shear stress amplitude in multiaxial high cycle fatigue," *International Journal of Fatigue*, vol. 31, no. 7, pp. 1144–1153, 2009 (cit. on p. 44).

[119] S. S. Manson, J. C. Freche, and C. R. Ensign, *Application of a double linear damage rule to cumulative fatigue*. National Aeronautics and Space Administration, 1967, vol. 3839 (cit. on p. 304).

[120] S. S. Manson and G. R. Halford, "Re-examination of cumulative fatigue damage analysis—an engineering perspective," *Engineering Fracture Mechanics*, vol. 25, no. 5-6, pp. 539–571, 1986 (cit. on p. 304).

[121] K. V. Mardia, "Applications of some measures of multivariate skewness and kurtosis in testing normality and robustness studies," *Sankhyā: The Indian Journal of Statistics, Series B*, pp. 115–128, 1974 (cit. on p. 120).

[122] G. Marsh *et al.*, "Review and application of rainflow residue processing techniques for accurate fatigue damage estimation," *International Journal of Fatigue*, vol. 82, pp. 757–765, 2016 (cit. on pp. 49, 306, 308, 309).

[123] M. Matsuishi and T. Endo, "Fatigue of metals subject to varying stresses," *Japan Society of Mechanical Engineers*, Mar. 1968 (cit. on p. 308).

[124] C. Mattrand, "Approche probabiliste de la tolérance aux dommages," Ph.D. dissertation, Université Blaise Pascal - Clermont-Ferrand II, 2011 (cit. on p. 37).

[125] H. Mayer, C. Ede, and J. E. Allison, "Influence of cyclic loads below endurance limit or threshold stress intensity on fatigue damage in cast aluminium alloy 319-t7," *International Journal of Fatigue*, vol. 27, no. 2, pp. 129–141, 2005 (cit. on p. 43).

[126] C. H. McInnes and P. A. Meehan, "Equivalence of four-point and three-point rainflow cycle counting algorithms," *International Journal of Fatigue*, vol. 30, no. 3, pp. 547–559, 2008 (cit. on pp. 48, 307, 308).

[127] G. McLachlan and D. Peel, "Multivariate normal mixtures," in *Finite Mixture Models*. John Wiley & Sons, Ltd, 2000, ch. 3, pp. 81–116, ISBN: 9780471721185 (cit. on p. 152).

[128] G. J. McLachlan, "Mahalanobis distance," *Resonance*, vol. 4, no. 6, pp. 20–26, 1999 (cit. on p. 119).

[129] W. Q. Meeker, G. J. Hahn, and L. A. Escobar, *Statistical intervals: a guide for practitioners and researchers*. John Wiley & Sons, 2017, vol. 541 (cit. on pp. 158, 165).

[130] M. A. Meggiolaro, J. T. P. de Castro, and H. Wu, "Non-linear incremental fatigue damage calculation for multiaxial non-proportional histories," *International Journal of Fatigue*, vol. 100, pp. 502–511, 2017 (cit. on pp. 302, 303).

[131] M. A. Meggiolaro and J. T. P. de Castro, "An improved multiaxial rainflow algorithm for non-proportional stress or strain histories – part ii: the modified wang–brown method," *International Journal of Fatigue*, vol. 42, pp. 194–206, 2012 (cit. on p. 53).

[132] E. Merhy, N. T. Niane, B. Weber, and P. Bristiel, "Process induced residual stress effect on fatigue lifetime of automotive steel components," in *Advanced Materials Research*, Trans Tech Publ, vol. 996, 2014, pp. 808–813 (cit. on p. 40).

[133] K. J. Miller and K. P. Zachariah, "Cumulative damage laws for fatigue crack initiation and stage i propagation," *The journal of strain analysis for engineering design*, vol. 12, no. 4, pp. 262–270, 1977 (cit. on p. 304).

[134] M. A. Miner, "Cumulative damage in fatigue," *Journal of Applied Mechanics*, vol. 3, pp. 159–164, 1945 (cit. on p. 51).

[135] A. Morel, A. Bignonnet, G. Germain, and F. Morel, "Teaching durability in automotive applications using a reliability approach," *International Journal on Interactive Design and Manufacturing (IJIDeM)*, vol. 4, pp. 281–287, 2010 (cit. on p. 16).

[136] Y. Mortureux, "La sûreté de fonctionnement : méthodes pour maîtriser les risques," *Techniques de l'ingénieur Conception et Production*, vol. TIP083WEB. No. ag4670, 2001 (cit. on p. 287).

[137] P. Može, *Lecture 12.1: basic introduction to fatigue*, http://fgg-web.fgg.uni-lj.si/~/pmoze/ESDEP/master/wg12/l0100.htm, 2015 (cit. on p. 42).

[138] K. Murphy, *Machine learning: a probabilistic perspective*. MIT press, 2012 (cit. on p. 104).

[139] F. Murtagh and P. Legendre, "Ward's hierarchical agglomerative clustering method: which algorithms implement ward's criterion?" *Journal of classification*, vol. 31, pp. 274–295, 2014 (cit. on p. 117).

[140] N. Nadjitonon, "Contribution à la modélisation de l'endommagement par fatigue," Ph.D. dissertation, Université Blaise Pascal-Clermont-Ferrand II, 2010 (cit. on p. 52).

[141] Y. Nadot and V. Denier, "Fatigue failure of suspension arm: experimental analysis and multiaxial criterion," *Engineering Failure Analysis*, vol. 11, no. 4, pp. 485–499, 2004 (cit. on pp. 231, 232).

[142] M. Nagode and J. Klemenc, "Modelling of load spectra containing clusters of less probable load cycles," *International Journal of Fatigue*, vol. 143, p. 106 006, 2021 (cit. on p. 174).

[143] N. T. Niane, N. Garsot, and P. Bristiel, "Intégration de l'historique du procédé de soudage dans les calculs de tenue en fatigue," *Matériaux & Techniques*, vol. 100, no. 4, pp. 299–308, 2012 (cit. on p. 40).

[144] M. Niño-Zarazúa, "Quantitative analysis in social sciences: an brief introduction for non-economists," *SSRN Electronic Journal*, May 2012 (cit. on p. 108).

[145] P. J. O'Keefe, *Mechanical power transmission – the centrifugal clutch and metal fatigue*, http://www.engineeringexpert.net/Engineering-Expert-Witness-Blog/tag/atomic-structure, May 13, 2012 (cit. on p. 37).

[146] J. Pagès, *Multiple Factor Analysis by Example Using R*. Nov. 2014, pp. 1–253, ISBN: 9780429171086 (cit. on pp. 104, 107).

[147] G. Pagnoux, "Influence de la durée de vie effective des véhicules et des changements de mains sur la moyenne des résistances," PSA Peugeot Citroën, Tech. Rep., 2010 (cit. on p. 133).

[148] T. Palin-Luc, A. Banvillet, and J. F. Vittori, "How to reduce the duration of multiaxial fatigue tests under proportional service loadings," *International journal of fatigue*, vol. 28, no. 5-6, pp. 554–563, 2006 (cit. on p. 186).

[149] T. Palin-Luc, S. Lasserre, C. Froustey, and J. Y. Berard, "Experimental approach of damage cumulation in high cycle fatigue with random loadings in blocks," *ECF 11. Mechanisms and Mechanics of Damage and Failure.*, vol. 2, p. 1996, 1996 (cit. on p. 304).

[150] M. Palmonella, M. Friswell, J. Mottershead, and A. Lees, "Finite element models of spot welds in structural dynamics: review and updating," *Computers & Structures - COMPUT STRUCT*, vol. 83, Feb. 2005 (cit. on p. 56).

[151] J. Papuga and M. Růžička, "Two new multiaxial criteria for high cycle fatigue computation," *International Journal of Fatigue*, vol. 30, no. 1, pp. 58–66, 2008 (cit. on p. 44).

[152] P. Paris and F. Erdogan, "A critical analysis of crack propagation laws," 1963 (cit. on p. 37).

[153] D. G. Pavlou, "A phenomenological fatigue damage accumulation rule based on hardness increasing, for the 2024-t42 aluminum," *Engineering Structures*, vol. 24, no. 11, pp. 1363–1368, 2002 (cit. on p. 304).

[154] C. Pérez-Diaz, "Comportements des conducteurs et modèles du risque," *Déviance et société*, vol. 24, no. 2, pp. 187–208, 2000 (cit. on p. 261).

[155] C. Perkins, "Why is double-wishbone suspension the best?" *Road and Track*, Jan. 6, 2023. [Online]. Available: https://www.roadandtrack.com/car-culture/a42417679/double-wishbone-vs-macpherson-strut-suspension/ (cit. on p. 294).

[156] G. Perroud, "Le dimensionnement par le risque," Groupe PSA, Tech. Rep., 2009 (cit. on p. 16).

[157] Q. Pierron, "Caractérisation de la fatigue des assemblages soudés soumis à des chargements à amplitude variable," Ph.D. dissertation, Université Paris-Saclay, 2018 (cit. on pp. 38, 304, 305).

[158] Q. Pierron, H. Maitournam, and I. Raoult, "Thermographic approach for high cycle fatigue of seam welded steel joints under variable amplitude loadings," *Fatigue & Fracture of Engineering Materials & Structures*, vol. 43, no. 12, pp. 2966–2983, 2020 (cit. on pp. 58, 231).

[159] R. R. Pinto Filho, J. C. C. Rezende, M. De Freitas Leal, and J. A. F. Borges, "Automotive frame optimization," SAE Technical Paper, Tech. Rep., 2003 (cit. on p. 171).

[160] X. Pitoiset, I. Rychlik, and A. Preumont, "Spectral methods to estimate local multiaxial fatigue failure for structures undergoing random vibrations," *Fatigue & Fracture of Engineering Materials & Structures*, vol. 24, no. 11, pp. 715–727, 2001 (cit. on p. 188).

[161] K. Przybysz, S. Dygnatowski, and N. Grzesik, "An analysis of reliability of military vehicles," *Journal of KONBiN*, vol. 49, no. 3, pp. 527–546, 2019 (cit. on p. 289).

[162] D. E. Raeside, "Monte carlo principles and applications," *Physics in Medicine & Biology*, vol. 21, no. 2, p. 181, 1976 (cit. on p. 193).

[163] R. K. Rajput, *A textbook of automobile engineering*. Firewall Media, 2008 (cit. on p. 291).

[164] I. Raoult, "Structures élastomères sous chargement cyclique: comportement, fatigue, durée de vie," Ph.D. dissertation, Ecole Polytechnique X, 2005 (cit. on p. 65).

[165] I. Raoult and B. Delattre, "Equivalent fatigue load approach for fatigue design of uncertain structures," *International Journal of Fatigue*, vol. 135, p. 105 516, 2020 (cit. on pp. 22, 55, 225, 232, 263).

[166] H. Remes, P. Gallo, J. Jelovica, J. Romanoff, and P. Lehto, "Fatigue strength modelling of high-performing welded joints," *International Journal of fatigue*, vol. 135, p. 105 555, 2020 (cit. on p. 75).

[167] B. Reynier, *Métallurgie structurale*. ENSTA ParisTech, 2013 (cit. on p. 35).

[168] M. A. Richard, "Nouveau phénomène de mode, ces voiturettes cartonnent chez les 14-18 ans à trouville et deauville," *Ouest France*, Jan. 25, 2022. [Online]. Available: https://www.ouest-france.fr/normandie/deauville-14800/a-deauville-et-trouville-les-voiturettes-ami-cartonnent-a-la-sortie-des-ecoles-a000d3d6-7de4-11ec-92fb-6689e2d2ee1b (cit. on p. 296).

[169] P. Robert and Y. Escoufier, "A unifying tool for linear multivariate statistical methods: the rv-coefficient," *Journal of the Royal Statistical Society Series C: Applied Statistics*, vol. 25, no. 3, pp. 257–265, 1976 (cit. on p. 122).

[170] C. Roux, X. Lorang, H. Maitournam, M. L. Nguyen-Tajan, and B. Quesson, "Multi-parameter fatigue equivalence loadings for specification applications," *Procedia Engineering*, vol. 66, pp. 393–402, 2013, Fatigue Design 2013, International Conference Proceedings (cit. on pp. 225, 232).

[171] I. Rychlik, "A new definition of the rainflow cycle counting method," *International Journal of Fatigue*, vol. 9, no. 2, pp. 119–121, 1987 (cit. on pp. 48, 306).

[172] S. Sano, Y. Furukawa, and S. Shiraishi, "Four wheel steering system with rear wheel steer angle controlled as a function of sterring wheel angle," *SAE Transactions*, pp. 880–893, 1986 (cit. on p. 293).

[173] J. Schijve, "The significance of flight-simulation fatigue tests," Delft University of Technology, Department of Aerospace Engineering, Tech. Rep. LR-466, 1985 (cit. on p. 289).

[174] R. Schrank, "Definition of simplified fatigue tests using numerical optimization," *Procedia Structural Integrity*, vol. 38, pp. 30–39, 2022 (cit. on p. 231).

[175] D. Schütz, H. Klätschke, H. Steinhilber, P. Heuler, and W. Schuetz, "Standardized load sequences for car wheel suspension components. car loading standard - carlos. final report," Fraunhofer-Institut für Betriebsfestigkeit, Tech. Rep., 1990 (cit. on pp. 187, 188).

[176] G. P. Sendeckyj, "Constant life diagrams—a historical review," *International journal of fatigue*, vol. 23, no. 4, pp. 347–353, 2001 (cit. on p. 54).

[177] E. Shams and M. Vormwald, "Schwingfestigkeit von nahtenden msg-geschweißter feinbleche aus stahl unter schubbeanspruchung," *Forschungsvereinigung Automobiltechnik eV (FAT)*, 2013 (cit. on p. 56).

[178] H. Shen, J. Lin, and E. Mu, "Probabilistic model on stochastic fatigue damage," *International Journal of Fatigue*, vol. 22, no. 7, pp. 569–572, 2000 (cit. on p. 41).

[179] J. C. Simo, "Numerical analysis and simulation of plasticity," *Handbook of numerical analysis*, vol. 6, pp. 183–499, 1998 (cit. on p. 304).

[180] J. C. Simo and R. L. Taylor, "A return mapping algorithm for plane stress elastoplasticity," *International Journal for Numerical Methods in Engineering*, vol. 22, no. 3, pp. 649–670, 1986 (cit. on p. 304).

[181] B. Simons-Morton, N. Lerner, and J. Singer, "The observed effects of teenage passengers on the risky driving behavior of teenage drivers," *Accident Analysis & Prevention*, vol. 37, no. 6, pp. 973–982, 2005 (cit. on pp. 261, 335).

[182] A. P. Singulani, "Advanced methods for mechanical analysis and simulation of through silicon vias," Ph.D. dissertation, Ph. D. thesis, Technischen Universität Wien, 2014 (cit. on p. 37).

[183] R. Skjong, "Social indicators and risk acceptance," in *Offshore mechanics and arctic engineering conference, 1998*, OMAE, 1998 (cit. on p. 288).

[184] D. Socie, "Modelling expected service usage from short-term loading measurements," *International Journal of Materials and Product Technology*, vol. 16, no. 4-5, pp. 295–303, 2001 (cit. on p. 176).

[185] C. M. Sonsino, "Principles of variable amplitude fatigue design and testing," in *Fatigue Testing and Analysis Under Variable Amplitude Loading Conditions*, P. McKeighan and N. Ranganathan, Eds., West Conshohocken, PA: ASTM International, 2005, pp. 3–23 (cit. on p. 16).

[186] C. M. Sonsino, "Course of sn-curves especially in the high-cycle fatigue regime with regard to component design and safety," *International Journal of Fatigue*, vol. 29, no. 12, pp. 2246–2258, 2007 (cit. on p. 43).

[187] M. Speckert, N. Ruf, K. Dreßler, R. Müller, C. Weber, and S. Weihe, "Ein neuer ansatz zur ermittlung von erprobungslasten für sicherheitsrelevante bauteile," Fraunhofer (ITWM), Tech. Rep. 177, 2009. [Online]. Available: http://nbn-resolving.de/urn:nbn:de:hbz:386-kluedo-16429 (cit. on pp. 200, 262).

[188] C. Starr, "Risk management, assessment, and acceptability," *Risk Analysis; (United States)*, vol. 5, no. 2, 1985 (cit. on p. 16).

[189] Y. Sun and B. Goh, "In china, global automakers seek clarity from a more ambitious regulator," *Reuters*, Nov. 16, 2021. [Online]. Available: https://www.reuters.com/business/autos-transportation/china-global-automakers-seek-clarity-more-ambitious-regulator-2021-11-11/ (cit. on p. 291).

[190] L. Susmel and P. Lazzarin, "A bi-parametric wöhler curve for high cycle multiaxial fatigue assessment," *Fatigue and Fracture of Engineering Materials and Structures*, vol. 25, pp. 63–78, 2002 (cit. on pp. 24, 42, 53, 66).

[191] L. Susmel and D. Taylor, "The theory of critical distances to estimate lifetime of notched components subjected to variable amplitude uniaxial fatigue loading," *International Journal of Fatigue*, vol. 33, no. 7, pp. 900–911, 2011 (cit. on pp. 44, 46, 53–55, 57).

[192] T. Svensson and P. Johannesson, "Reliable fatigue design, by rigid rules, by magic or by enlightened engineering," *Procedia Engineering*, vol. 66, pp. 12–25, 2013 (cit. on pp. 15, 190, 193).

[193] F. Szmytka, E. Charkaluk, A. Constantinescu, and P. Osmond, "Probabilistic low cycle fatigue criterion for nodular cast-irons," *International Journal of Fatigue*, vol. 139, pp. 105–701, 2020 (cit. on p. 41).

[194] X. Z. Tang, S. J. Yang, and H. C. Xia, "Control strategy of hybrid electric vehicles based on driving style identification," in *Advanced Materials Research*, Trans Tech Publ, vol. 945, 2014, pp. 1587–1596 (cit. on pp. 87, 108).

[195] J. J. Thomas, G. Perroud, A. Bignonnet, and D. Monnet, "Fatigue design and reliability in the automotive industry," in *Fatigue Design and Reliability*, ser. European Structural Integrity Society, G. Marquis and J. Solin, Eds., vol. 23, Elsevier, 1999, pp. 1–11 (cit. on p. 190).

[196] S. K. Thompson, *Sampling*. John Wiley & Sons, 2012, vol. 755 (cit. on p. 89).

[197] D. Turlier *et al.*, "Seam weld shell element model for thin walled structure fe fatigue design," in *MATEC Web of Conferences*, EDP Sciences, vol. 165, 2018, p. 21 007 (cit. on pp. 56, 57).

[198] A. Vatanen, *Loopholes in the registration of cars in europe/jiangling landwind*, Parliamentary question, Oct. 6, 2005. [Online]. Available: https://www.europarl.europa.eu/doceo/document/P-6-2005-3751_EN.html (visited on 04/02/2023) (cit. on p. 15).

[199] B. Weber, "Fatigue multiaxiale des structures industrielles sous chargement quelconque," Ph.D. dissertation, Institut National des Sciences Appliquées de Lyon, 1999 (cit. on pp. 44, 230).

[200] C. K. Williams and C. E. Rasmussen, *Gaussian processes for machine learning*. MIT press Cambridge, MA, 2006, vol. 2 (cit. on p. 181).

[201] D. Wishart, "An algorithm for hierarchical classifications," *Biometrics*, pp. 165–170, 1969 (cit. on p. 117).

[202] A. Wöhler, "Versuche zur ermittlung der auf die eisenbahnwagenachsen einwirkenden kräfte und die widerstandsfähigkeit der wagen-achsen," *Zeitschrift für Bauwesen*, vol. 10, no. 1860, pp. 583–614, 1860 (cit. on p. 41).

[203] G. Yingkui and L. Jing, "Multi-state system reliability: a new and systematic review," *Procedia engineering*, vol. 29, pp. 531–536, 2012 (cit. on p. 192).

[204] J. Zarka and J. Casier, "Elastic-plastic response of a structure to cyclic loading: practical rules," in *Mechanics today*, Elsevier, 1981, pp. 93–198 (cit. on pp. 302, 303).

[205] U. Zerbst *et al.*, "Safe life and damage tolerance aspects of railway axles–a review," *Engineering Fracture Mechanics*, vol. 98, pp. 214–271, 2013 (cit. on p. 38).

[206] O. C. Zienkiewicz, R. L. Taylor, and J. Z. Zhu, *The finite element method: its basis and fundamentals*. Elsevier, 2005 (cit. on p. 56).

[207] V. Živković, B. Nedić, and S. Đurić, "Manufacturing specificity of vehicle's independent suspension system parts," *Mobility & Vehicle Mechanics*, vol. 46, no. 1, pp. 31–41, 2020 (cit. on p. 294).

Glossaries

RAMS

Specification A specification denotes an expected property of a system. The act of specification corresponds to defining adequate properties of the system to satisfy its functions (fr. *Spécification*, de. *Spezifikation*) 13, 296

Allocation Allocation is the act of decomposing higher-level requirements and assigning them to lower-level functions. For instance, the mass window of an organ or the external loads applied to an organ must be translated into mass windows and inner loads for its parts (fr. *Allocation*, de. *Zuteilung*) 13, 296

Lifetime The duration of a mission or loading history that led, leads or will lead a specimen to failure (fr. *Durée de vie*, de. *Lebensdauer*). 132, 279, 282

Lifetime objective The reference duration of loading histories over the population of which a requirement in reliability is written. 15, 129, 132, 134, 160, 172, 181, 279

Reliability The ability of a system to pursue its function in regular conditions for a given lifetime objective (fr. *Fiabilité*, de. *Zuverlässigkeit*). 14, 15, 132, 289

Durability The performance of a system in terms of lifetime as long as it is used in regular conditions (fr. *Durabilité*, de. *Betriebsfestigkeit*) 40, 189, 289

System A combination of elements that function together to produce the capability required to meet a need. 13, 30, 85

Subsystem Any functional or geometrical subset of a system. 13, 30, 198, 200

Part A part ("as in portion, one of the pieces from which something is designed to be assembled, *e.g.* the model car came in several small parts that had to be put together" - Merriam-Webster) is a manufactured - non assembled - subsystem with a given mechanical function (fr. *Pièce*, de. *Bauteil*). 13, 30

Component A component ("as in element: one of the parts that make up a whole, *e.g.* each set is composed of several distinct components" - Merriam-Webster) may refer to a single or a set of assemblies, joints or zones with a single characterization of pseudo-fatigue

(fr. *Constituant*, de. *Teil*). Not to be mixed up with the components of a vector (as in dimensions). 15, 24, 30, 185, 189, 198, 229

Material mechanics

REV A mesoscopic volume of granular material such that the fatigue behavior of the volume is isotropic. At the macroscopic level, an REV is considered as a point. 53, 55

Trivial damage models A cumulative damage variable that is not linearly associated with the evolution of a measurable mechanical property, rather arises from an empirical fatigue model. 66

Stress concentration The vicinity of a local optimum of the Cauchy stress field in a structure submitted to a given load configuration. 36, 69

Stress concentration zone A location of a structure that is susceptible to be a stress concentration in service. 36, 295

Critical zone A stress concentration zone that fails to check an associated fatigue criterion, in a structure submitted to cyclic loads. 44, 63

Rainflow

Classed Rainflow counts Classed Rainflow or matrices counts are Rainflow counts or matrices defined with a set number of Rainflow range bins of set sizes. A classed Rainflow count does not memorize individual cycles, rather number of cycles counted for each bin or class. 50, 68

Closure A Rainflow count is unclosed if it consists only of the counted Rainflow cycles and not of any information on the residual. A Rainflow count is closed if the residual was translated to an additional Rainflow count using a residual closure method. 26, 49, 308

Rainflow range Histogram representation of the closed or unclosed Rainflow count of a signal. A Rainflow range matrix only contains counts in terms of ranges, all cycle means being ignored. 68

Structural mechanics

Sensible zone A stress concentration zone in a structure, that may be predicted to be critical in service. 20, 63, 66, 68, 69, 138, 194, 196, 199, 228, 256

Local context The partial knowledge of localization terms and fatigue model parameters for one or a set of sensible zones in a structure. 68, 83, 128, 138, 194, 208, 228, 256

Fatigue characterization An indirect or partial evaluation of the fatigue induced on a number of sensible zones of a partially known structure. 20, 63, 183, 256

Pseudo-damage Low structural-dependent variable proportional to the damages of a set of zones in a system (fr. *Pseudo-endommagement*, de. *Pseudo-Schädigung*) 20, 87, 94, 228, 256

Fatigue-equivalent magnitude A fatigue characterization for a global loading history on a vehicle. Effort range of a cyclic loading history with a limited number of cycles N_{ref} that deals the same pseudo-damage as the characterized loading history. The Equivalent Magnitude at Intercept is the value of magnitude when the number of cycles N_{ref} is arbitrarily set to 1 87, 256

Personal vehicle service

Mission A realization or sequence of realizations of a system's function by its customer to serve their needs and goals. 85, 192

Service Missions and associated loads that are plausible and acceptable in the scope of regular use for the market of interest (fr. *Service/Usage normal*, de. *Lebensdauer*). 14, 16, 27, 63, 84, 85, 88, 129, 171, 173, 181, 185, 200, 226, 255, 280, 332, 335

Dataset A dataset is one collection of data, corresponding to a number of measurements obtained from a number of individuals. The expression "data set" is also accepted by some English dictionaries, but trends are in favor of "dataset" in one word. 101, 141

Road event A situation during a driving episode that is typically identifiable by the user or an exterior observation using vernacular terms, and that induces specific loads on the vehicle. Examples: an emergency braking, cornering, a paved section, a pothole, a stop at a crossroads... 86, 88, 128, 134, 147, 176, 182, 256, 332, 335

Road environment A surveyable type of road describing the topology of a segment of the vehicle trip. A road environment is associated with a specific rough distribution of road events. Examples: urban, highway, damaged road... 21, 86, 89, 92, 127, 128, 160, 182, 256

Road segment A fraction of a trip. Not to be mixed up with vehicle segment, being a classification of vehicles with different sizes and uses. 92

Maneuver A road event during which the solicitations on the vehicle are directly caused by the driver's command. Examples: an emergency braking, cornering, a stop at a crossroads... 21, 88, 89, 104, 126, 128, 133, 139, 145, 162, 182, 226, 233, 331

Road obstacle A road event during which the solicitations on the vehicle are directly caused by the road's geometry. Obstacle solicitations are only indirectly caused by previous driver decisions. Examples: a paved section, a pothole, a speed bump... 21, 88, 89, 126, 128, 133, 139, 182, 226, 233, 296, 332

Global severity A trait of severity associated with a driver that induces more damage over all kinds of road events. 102, 104, 107, 126, 127, 128, 142, 167, 182, 213

Sportiness A trait of severity associated with a driver that evades obstacles and/or brakes and accelerates strongly and quickly before and after road events 104, 127, 128, 147, 167, 173, 182, 213, 223, 263

Quick turning A trait of severity associated with a driver that practices higher speed than the average population during cornering. 104, 127, 128, 147, 168, 173, 182, 213

Severity A descriptive variable suitable for comparison of the pseudo-fatigue that different missions may induce on a system (fr. *Sévérité*, de. *Schwere/Schärfe*). 83, 84, 104, 185

Intrinsic driver severity A descriptive variable suitable for comparison of the pseudo-fatigue that different drivers may induce on a system per kilometer. 28, 85, 127, 128, 129, 142, 151, 167, 256

Conditional severity A descriptive variable suitable for comparison of the pseudo-fatigue that a population of drivers may induce on a system for a given restriction of trips. 29, 104, 130, 142, 181, 213, 243, 256

Aggregated trip A synthetic trip composed of an aggregate of different situations that may occur in the whole population of trips. Built from the concatenation of different real-life driving situations. 22, 130, 133, 159, 172, 173, 181, 204, 256

Reliability

Pseudo-fatigue The description of quantities that arise from a mission and are relevant for the design of the system. For instance, the damage or the pseudo-damage induced by a mission on a sensible zone of the vehicle is a fatigue characterization and a variable of pseudo-fatigue. 21, 85, 86, 88, 95, 127, 128, 129, 134, 151, 159, 168, 171, 181, 183, 185, 202, 203, 227, 279, 282, 290, 331, 332, 335

Stress An ordered description of the severity of the missions of a system, that increases with its risk of failure (fr. *Contrainte*, de. *Beanspruchung/Kundenbeanspruchung*). Also called Severity (fr. *Sévérité*, de. *Schwere/Schärfe*), Load (fr. *Chargement*, de. *Belastung*) or Duty/Demand (fr. *Service*, de. *Betrieb*) in other contexts. Not to be mixed up with the Cauchy stress. 17, 83, 282

Resistance An equivalent description to the lifetime of a system that describes the lowest value of stress that leads a specimen of the system to failure (fr. *Résistance*, de. *Festigkeit*). Also called Strength (fr. *Force*, de. *Stärke/Festigkeit*) or Capacity (fr. *Potentiel*, de. *Belastbarkeit*) in other contexts. 18, 190, 200

Risk of failure Probability of failure of a system submitted to one or a population of loading histories (fr. *Risque*, de. *Ausfallwahrscheinlichkeit*). 15, 129, 131, 185, 194, 195, 196, 197, 200

Conservative This term qualifies a strategy for the analysis of variables of interest that ultimately leads to overestimation of the fatigue induced in service, and therefore overestimation of the necessary conditions for adequate design (fr. *Conservateur*, de. *Vorsichtig*) 22, 129, 131, 133, 159, 181, 185, 202, 260, 335

Procedure The joint information of load conditions, of levels for a trial or a set of trials of a subsystem, of the outcomes/variables to observe and of a criterion determining whether or not a prototype passes the procedure. 21, 257

Automotive terms

Personal vehicle Personal vehicle or passenger car (fr. *Véhicule particulier*, de. *Personenkraftwagen (PKW)*) as opposed to heavy duty vehicle (fr. *Poids lourd*, de. *Lastkraftwagen (LKW)*). 279

Bushing Soft (rubber) part used to absorb shocks at interfaces between suspension parts and car body or other chassis parts (fr. *Silentbloc*) 65, 279

Gusset Plate used to reinforce angles in shaped parts, such as the extremities of the suspension cross member. Gussets can also be found in parts of the body such as the screen pillars at the sides of the windshield (fr. *Gousset*) 74, 279

Wheel mount Static connector between wheel and suspension in deformable suspension technologies (fr. *Montant de roue*) 57, 74, 279

Suspension Static organ maintaining wheel contact with the road and filtering road loads. 14, 279, 291

Body/frame Static metallic organ connecting front and rear suspension, carrying and protecting the cabin and other organs of the vehicle (fr. *caisse*). 14, 279, 291

Ground link Joint assembly of the organs of suspension, direction and braking (fr. *Liaison au sol (LAS)* 279, 291

Driveshaft System of cogs and belts ensuring the mechanical transmission and reduction of motor speed to each driving wheel of the vehicle (fr. *Arbre de transmission*) 279, 291

Powertrain Organ containing the engine and all parts that transfer its power to the wheels. 16, 279, 291

Suspension arm/triangle Mobile connector between wheel and suspension in McPherson or double wishbone suspension technologies. Flat with respect to the road. Transmits longitudinal and lateral road efforts to the structure. Replaces wheel posts. 70, 74, 279

Ball joint A ball joint is generally a mechanical link that allows full rotation between two parts around the center of the joint. A ball joint is present at the connection between the suspension arm and the spindle. 279

Cup Connector between the suspension member and the springs in McPherson suspension technologies (fr. *Coupelle*) 279

Suspension spring Guided coiled assembly designed to absorb vertical road loads in McPherson and double wishbone suspension technologies. Has a significant camber angle to absorb loads in the case of coupled longitudinal, lateral and vertical loads (fr. *Amortisseur*). 279

Timing belt Rubber part ensuring transmission of rotational efforts between two or more parallel axes. Locally replaces cogs in a driveshaft (fr. *Courroie de distribution*) 279

Differential Mechanical system that balances the mechanical efforts transmitted to each wheel in the case of cornering (fr. *Différentiel*) 279, 291

Motor cradle Static part carrying and protecting the motor while filtering motor loads (fr. *Berceau moteur*) 279, 291

Acronyms

SSI Stress-Strength Interference 17, 19, 83, 190, 192, 205, 257, 261

REV Representative Element of Volume 24, 259

S-N Strength versus Number of cycles 24, 41, 42, 47, 53, 55

PCA Principal Component Analysis 22, 29, 100, 102, 104, 107, 126, 141, 142, 143, 144, 145, 146, 149, 155, 164, 167, 168, 169, 182, 256, 326

PC Principal Component 101, 116, 141, 147, 155, 156, 182

MFA Multiple Factor Analysis 21, 28, 86, 104, 107, 116, 117, 118, 121, 123, 126, 127, 128, 141, 145, 146, 148, 151, 256

HCPC Hierarchical Clustering on Principal Components 116, 127, 147, 164, 168, 169, 170, 182, 256

FORM First Order Reliability Method 30

SORM Second Order Reliability Method 30

CarLoS Car Loading Standard 187, 188

RAMS Reliability, Availability, Maintainability and Safety 14, 234, 287

EM Expectation-Maximization 22, 152

EMI Equivalent Magnitude at Intercept 79

PG Proving Ground(s) 226, 227, 232, 240, 253, 257

SUV Sport Utility Vehicle 91, 295

ASIL Automotive Safety Integrity Level 287

Appendix A

Elements of vehicle design in the field of RAMS

In this appendix, we provide further elements to understand more aspects of the safe and reliable design of suspension parts in personal vehicles.

Section A.1 introduces the framework of Reliability, Availability, Maintainability and Safety (RAMS) to a larger extent than reliability alone or the automotive industry alone. A few examples of associated applications and methods in the automotive industry and beyond are added alongside each dimension of RAMS to compare with our own topic.

Section A.2 presents the architecture and the function of parts of interest for our study, especially those composing vehicle suspension. We present different technologies of vehicle suspension and their expected incidence on the behavior of vehicle structures.

A.1 RAMS functions and design

RAMS is important both for electronic systems and for systems submitted to mechanical loads. In the former case, it is sometimes associated to the word dependability [Electropedia 2015]. In France, the domain encompassed by RAMS is generally known as "*Sûreté de fonctionnement*" [Mortureux 2001]. Requirements associated to RAMS aim to ensure that a system to design will be able to perform its function as required and when required.

A.1.1 Safety

Safety is a dimension that partakes to every function of the system. For instance, the behavior or protective characteristics of the system following failure, incident, abuse or attacks on the vehicle or its passengers are all regulated by required levels of safety.

The safe design of personal vehicles is regulated by the norm ISO 26262 [ISO26262 2018]. The norm provides a risk-based approach for all RAMS requirements as well as the classification called Automotive Safety Integrity Level (ASIL). The ASILs are risk classes

for different scenarios having different gravity with respect to the safety of the user. The associated risks are coherent with the acceptability of risk [Skjong 1998].

A main principle of safe design is that using the vehicle should not increase the general risk for the life of the user. Safety covers all plausible scenarios that would put the users in danger, including the catastrophic failure of the system in service (unreliability, *i.e.* the concern of the thesis) or crash. ASILs are included in the definition of requirements in reliability. We will tackle this dimension in the following paragraphs.

In the rest of this paragraph, let us mention the safe design of vehicle in the case of accidents. Countermeasures such as emergency braking systems, driver fatigue monitoring and other driving assistance features are developed to reduce the eventuality of an accident. When an accident occurs, safety requirements in crash ensure the survivability of the passengers [Du Bois *et al.* 2004].

These crash requirements are associated to norms and standards. Norms determine whether a vehicle model can be sold in the region of application or not. Standards are bases - ratings - for the comparison of different vehicle models with respect to safety.

New vehicle models are tested by independent vehicle safety rating programs such as the European New Car Assessment Program (Euro NCAP) or the New Car Assesment Program of the National Highway Traffic Safety Administration (NHTSA NCAP) in the USA [Du Bois *et al.* 2004; Kullgren *et al.* 2010].

Norms and standards in the domain of crash evolve with respect to new traffic situations and to the concerns of the public. New ratings may be added such as, in 2016, vulnerable road user protection for pedestrians or cyclists. For instance, new concerns associated to autonomous driving functions of the vehicles may lead to the definition of new trials for such vehicles.

A.1.2 Availability and maintainability

Availability evaluates the degree at which a system and each of its subsystems is able to operate when required. Maintainability measures the capacity to repair the system or to replace subsystems that may have failed, at a low cost for the customer and for the manufacturer. Both dimensions are important to the design of replaceable parts in the system. They lead to compromises between component price, longevity, cumbersomeness of maintenance and of replacement.

A.1.2.1 Availability and maintainability in defense and aircraft

Military and civilian aircraft, as well as ground defense vehicles, are sold for contractual amounts, frequency and severity of uses, along with thorough maintenance procedures or services.

For civilian aircraft landing gears, the damaging operational events are take-offs, landings and system retraction. Landing gears are designed to withstand an expected number of them

overall and are investigated before each flight. Loads on military aircraft structures during flight are more unpredictable because of the variety of missions undertaken [Schijve 1985].

There exists standard loading sequences for the trial of aircraft structures, following the same paradigm as the standard loading histories presented in Section VI.2.1. In order to monitor the need for maintenance, these aircrafts are equipped with in-service load sensors for post-service analysis [Bayart *et al.* 2015]. This tracking of the product's state allows to monitor damage and performances during its life and to repair any observed degradation.

Armored ground vehicles are also regularly submitted to maintenance, adapted to their operation conditions [Przybysz *et al.* 2019].

A.1.2.2 Availability and maintainability of personal vehicle subsystems

A personal vehicle is not sold with a use plan for the customer. Their vehicles may be used at virtually any time for any duration with no contractual monitoring.

In France, personal vehicles are legally needed to attend controls on a regular basis, and more frequently when the vehicle is old. This procedure aims to determine required maintenance operations to ensure the proper function and adequacy to norms of the vehicle.

Most replaceable parts may be subject to replacement schedules: filters, brake discs, timing belts, batteries (for thermal and electric vehicles) and tires are changed on a regular basis. Some components like gears, steering wheel and shock absorbers can also be replaced if needed.

However, car motors and chassis are very difficult to replace, and car body can not be replaced. Moreover, there are no simple, widespread and efficient procedures to control their damage status. Fatigue ruin of car chassis, motors and frames can only be observed and quantified when it actually occurs. Therefore, most components of car powertrain and chassis are designed to hold with sufficient probability for the objective lifetime of the system. This objective is one of durability and reliability.

A.1.3 Durability and reliability

Durability denotes the expected lifetime of a system. The distribution of the lifetime of the system is the measure of interest to ensure that the systems are durable enough with respect to the expectations of the market.

Reliability denotes the capacity of the system to be functional within a specified time period [Garvin 1987]. This dimension informs on the degree at which a system is likely to fail during its life in the absence of abuse or incident. When the failure of a subsystem is not final, *i.e.* if the system can be repaired or the subsystem replaced, the expected duration to the next failure is an indirect measure of reliability. Otherwise, if the failure of a set of components is unacceptable, as is the case for automotive safety parts, then the reliability of associated subsystems is characterized by the probability that the system does not fail before its objective lifetime. For the sake of simplicity, the measure of interest for the characterization

of reliability is often its complement: unreliability, or the probability that the system fails before its objective lifetime.

As explained in [Garvin 1987], durability and reliability have close definitions. If the distribution of the lifetime of a system has the same shape from one model to another, then the most reliable model is also the most durable.

For a system subject to variable loads and variety in strengths, the frontier between the two dimensions is even blurrier. The most relevant way to manage the difference between the two problems is to consider the associated population of missions over which the induced pseudo-fatigue must be evaluated and model to implement relevant design methods. The maximum admissible risk of failure associated to requirements on reliability holds for all missions that last up to an objective lifetime. Contrariwise, in order to predict the expectancy of vehicle lifetime in service, we must be able to handle a population of missions with varying duration.

There are no norms on the structural reliability of a vehicle. The requirements in reliability are set and checked by the car manufacturer. For each new vehicle project, it is evaluated neither by rating agencies nor by customer reviews, despite the existence of standard loading histories although we have discussed their relevance in Section VI.2.1.

A.1.4 Explicit and implicit performances, what the customer buys

Let us denote performances or ratings the attributes that allow customers to have an opinion on the model. When a new vehicle model is released on a market, these ratings are important to encourage the sales of the model and to justify higher net profit margins.

The most prominent factors of a car's performance are related to the main explicit functions of the structure: driving performances, comfort, room for luggage, software services, style, etc. The words "performance" and "feature" are usually associated strictly to those attributes. These are the explicit attributes people and specialized press look at when comparing cars, along with price, as long as they trust them to be safe and reliable.

Performances in the fields of reliability and safety are not measured by the public *per se*. They are implicit. A lower risk of failure of a new vehicle model does not bring the company short-term flair on the market. However, when systems delivered by a given manufacturer show to be unreliable or unsafe, the whole range of vehicles may suffer from having the spotlights on them. Contrariwise, being known for selling robust and reliable cars is a huge asset for keeping a long-term grasp on a market.

As the sales of personal vehicles are receding in occidental countries, the economical strategies for automotive companies in these regions are to expand to new regions of the world and/or to increase their net profit margins on the sales of new vehicles [Kumajas *et al.* 2021].

Increasing the explicit performances of a car is a traditional lever to increase the margin on a vehicle sale. Implementing new features such as driving assistance or in-built trip planners are further examples that

Increasing the margin on a vehicle while maintaining its reliability or increasing its durability are competing objectives. Strict safety requirements require a thorough validation and integration process. A difficult or incoherent validation procedure may lead to extra design loops and associated trials. Increasing the duration of project development reduces the profit of the manufacturer on the end product without justifying for larger margins.

Likewise, ensuring the reliability of a vehicle onto new kinds of roads and legislation may require further service load measurements and analyses, as well as agile updates on the validation objectives to adapt to the expectations or standards in the new regions [Sun and Goh 2021].

A.2 Car subsystems and development

A generic presentation of automotive engineering is available in [Rajput 2008]. Fundamental concepts for the design of motor vehicles are documented in [Brown H. C. 2002]. In Section A.2.1, we recall some technical aspects of suspension and body architecture that are of importance to the structural mechanical concepts invoked in Chapter III.

A generic overview of the development process in an automotive company is presented in Section A.2.2. In this paragraph, we highlight the timeline of the project and the availability of resources for the design and validation of its subsystems.

A.2.1 Architecture of the rolling chassis of a vehicle

A.2.1.1 Organ definitions

The rolling chassis of a vehicle denotes all organs that are necessary for the object to drive: ground link (or running gear in [Rajput 2008] chap. 6) and powertrain (or power plant).

Three major organs of the chassis carry the rest of the system and filter out most loads from the road and the motor. These carrier subsystems are the suspension (Fig. A.1), the body or frame (Fig. A.2) and the cradle of the vehicle.

The term ground link (fr. *liaison au sol*) covers altogether the suspension, steering and braking subsystems of the vehicle, as well as the wheels.

Powertrain corresponds to all parts that take part to the longitudinal movement of the vehicle: motor, transmission, driveshaft and differential. These two last elements ensure proper motorization during cornering.

With respect to driving efficiency, the second main function of the suspension organ is to maintain vehicle control and effort transmission despite the shocks induced by the road. This means ensuring contact between the wheel and the road as well as the stability of all components of the powertrain.

The car body also contains active and passive safety components that are necessary for the respect of requirements in the event of a crash.

(a) Suspension 3D view (Peugeot RCZ)

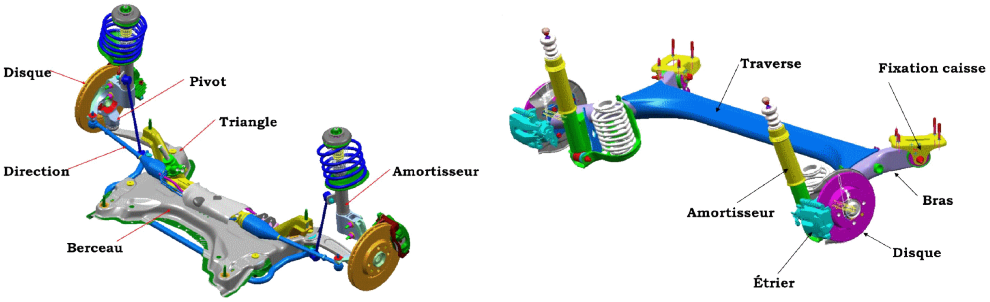

(b) Part breakdown (front and rear) [Beaumont 2013]

Fig. A.1: Suspension, example for a compact car

Fig. A.2: Car body (Peugeot 308 II)

The reliable design of the motor cradle needs to take in account the load configurations and frequencies associated with motor usage. The suspension is in charge of filtering road loads with respect to the cradle.

A.2.1.2 Acceleration, deceleration, direction

Vehicle acceleration is generated by the motor and transmitted to driving wheels. Vehicle deceleration is created by the brakes on all wheels. Vehicle steering allows changing the

direction of the vehicle. Note that the term "steering wheel" (fr. *volant directionnel*) corresponds to the control wheel at the hands of the driver.

Most modern cars have two driving wheels on the same axle. Front-wheel drivetrains are preferred on casual modern vehicles for their proximity with the motor, built in the front of the vehicle, leaving room in the trunk. Rear-wheel drivetrains have higher performances in terms of acceleration and direction, but are more expensive and are harder to drive [Glon 2021].

Some cars are built either with dual motorization (one motor for both axles) or an extra transmission interface. The first layout (dual-motor, four-wheel-drive) is popular for some battery electric vehicles. Indeed electric motors have smaller sizes than thermal motors and can be added to the rear of a vehicle with little loss in usable volume. The second layout is popular for off-road vehicles, which may temporarily lose friction with the ground on either axle, as well as for most hybrid vehicles [Kim *et al.* 2008].

The braking pedal of the driver controls simultaneously brakes on all four wheels of the vehicle. However, the front brakes are designed to induce a larger braking torque than the rear brakes. This imbalance is explained by the charge transfer to the front axle of the vehicle during braking: a lower vertical charge on the rear axle induces less friction between the road and the wheel and therefore less available braking efficiency.

It is necessary to conduct vehicle steering using the front wheels, otherwise the vehicle is oversteering and may lose stability during cornering. The direction in most personal vehicles is controlled by the front wheels. In that case, cornering induces larger lateral loads on the front axle of the vehicle. Some models, especially cross-road vehicles, may be built with a four-wheel steering system. In that case, the lateral forces associated with cornering are shared over all wheels [Sano *et al.* 1986].

Note that understeering cars have increased stability during cornering but are, naturally, harder to steer. Front-wheel drivetrains are the usual cause for a vehicle being understeering, as opposed to rear-wheel or four-wheel drivetrains.

The location (front, rear) of the load transfers that allow controlling the vehicle may modify the sets of global load cases that are highly dependent on driver behavior. For instance, the vehicle used for the evaluation of the pseudo-fatigue induced in service in Chapters IV and V had a front-wheel drivetrain and a two-wheel (front) steering system. Therefore, differences in acceleration and cornering habits on the side of the driver had a larger impact on the global load components on the front axle of the vehicle.

A.2.1.3 Different suspension technologies

The suspension of a vehicle consists of a front and a rear axle. Both axles may be built with different technologies, as they connect different other organs of the vehicle and have different allocated volumes.

Suspension technologies are separated into dependent, semi-dependent and independent suspensions. Different technologies of dependent and independent suspensions are presented

(a) Pseudo-McPherson, independent

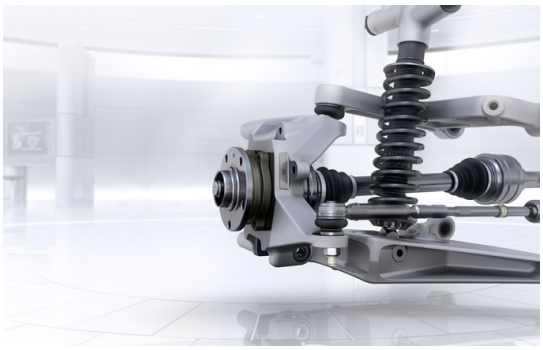

(b) Double wishbone, independent

(c) Deformable rear suspension, semi-dependent

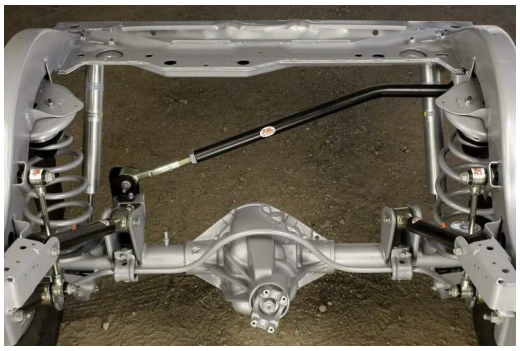

(d) Panhard, dependent

Fig. A.3: Examples of suspension technologies [Darling 2015]

in [Darling 2015; Lajqi *et al.* 2013; Živković *et al.* 2020]. Selected examples are shown in Fig. A.3.

Independent suspensions are the most common technology used in casual modern cars. They correspond to axles that allow each wheel to move vertically independently from the other.

McPherson or more usually pseudo-McPherson suspensions (Fig. A.3a) are mounted with a strut containing a coil able to absorb vertical loads on each wheel. Longitudinal and lateral loads are transferred by a single suspension arm. This widespread technology requires a large vertical space for the coils. It is a common choice for the front suspension of thermal vehicles. Indeed, engine size already determines the available volume in the front of the car.

In double wishbone suspensions (Fig. A.3b), the coil is included between two control arms mounted on each wheel. Double wishbone suspensions bring better driving performances that pseudo-McPherson suspensions (see [Perkins 2023] for further comparison of the two technologies).

Deformable suspensions (Fig. A.3c) are semi-dependent suspension systems devoid of coils and suspension arms. This system is favored for the rear suspension of casual compact cars because it takes little volume at a low price. The independence between the wheels when submitted to asymmetrical road events is permitted by the torsion of the axle. Note that a deformable suspension is a single part while double wishbone and pseudo-McPherson suspensions are assemblies of several parts.

Well-known dependent rear suspension systems are the de Dion and the Panhard (Fig. A.3d) suspensions. In the latter case, the axle is rigid and an oblique connection - the Panhard rod - permits the system to filter vertical loads.

The choice of a suspension technology modifies the locations and geometrical properties of the stress concentration zones over the structure. Two different technologies will have different axial and torsional rigidity and therefore transfer road loads differently. The dynamical response of the structure will differ, therefore the global loads over known road events will not be trivial to predict.

For instance, dependent suspension systems built with a Panhard rod may have an asymmetrical response to road obstacles as well as an asymmetrical sensitivity to each global load case. Wheel axle loads on the side of the lower connection of the Panhard rod will lead to deformation of this part and transfer of loads toward its upper connection, while wheel axle loads on the other side will not.

A.2.2 The development of a new vehicle

A.2.2.1 Automotive market segments

Vehicle models are separated into several market segments that may then be associated with differences in regulations and associated use. The European classification uses letters for each category. The segments are divided as per their wheelbase (the distance between both axles) and the size of their engine.

Segments may be associated with typical customer bases. Urban commuters are well served by small and efficient vehicles such as minicompacts and subcompacts (A and B). Families may require affordable compact (C) or mid-size (D) cars. Taxi drivers and executives are the main targets of higher segment vehicles (E and F).

Sport cars and utility vehicles such as SUVs have different expectations in terms of driving performances and are associated with their own segments, S and J/SUV. Multi-purpose vehicles such as minivans are even larger vehicles and are associated with segment M.

A.2.2.2 Specification for a new vehicle project

A new vehicle model inserts itself in an automotive segment and a region of the world. A specific fraction of the population can be targeted as a marketing strategy. The vehicle can also be targeted to specific environments, such as urban or cross-country roads.

Note that the idea of a target population exists mainly for marketing reasons and may evolve as the vehicle model hits the market. Two examples of this situation are the SUVs and microcars. SUVs were designed as smaller alternatives to the minivan [Cheney 2011] with satisfying (sport) driving performances. They are now widespread due to the feeling of extra safety, flair and ergonomy that they inspire [Axsen and Long 2022]. Battery-powered microcars such as the Citroën Ami were designed to be practical low-autonomy vehicles for

urban use. However, their low price and separate regulation system became of interest to younger populations in rural areas [Richard 2022].

For a new vehicle project, innovations to implement and shifts in priorities for cost allocation justify modifications to previous specification and allocation plans. This means new mass distributions over the structure, new joint methods or different jointing strategies, and therefore new weak point locations.

Requirements need to be clearly stated - necessary, verifiable and attainable ([Haskins and Forsberg 2007] chap. 7) - for each step of the V-cycle. System requirements in reliability may limit the risk of failure of the vehicle. They still need to be propagated into requirements stated for each subsystem, and further on to parts and to the materials and manufacturing processes that are used.

For a new vehicle project, the first quantification of the conditions in service, for instance in terms of loads, is given by its association to a design group. Design groups correspond to references in terms of expected service conditions according to the segment and the region of the world. In order to create and qualify these design bases, the properties (constraints) of service in all regions of the world are evaluated and a classification is determined. Such properties include a description of the climate, driving regulation, fuel quality and the quality of the road or density of obstacles. The number of design groups number in the company is limited to reduce the number of references to maintain. This constraint justifies looking for a single typical mission for the design of all suspension components in Section VI.5.2.

These design references help the design department to finalize the specification and allocation of requirements for the system. Then, thanks to internal initiatives and/or reverse engineering on external solutions, the project team proposes designs - solutions - first at the part level, trying to solve the requirements at this level.

A.2.2.3 Validation procedures throughout the project

First prototypes of the part undergo validation procedures to determine their performances and the respect of their associated requirements. If the part passes, it is integrated to the upper level, which is then tested for upper level requirements, and so on.

Numerical prototypes are created at each step of validation. Numerical tests are much cheaper than physical trials and the models are much faster to produce and modify than prototypes, abundantly reducing the duration and cost of most design loops. Numerical calculations allow measurements of variables that would otherwise be very expensive or complicated to measure using sensors on a prototype. However, models are very dependent on hypotheses made, sometimes leading to bad surprises when moving on to physical prototypes.

Physical prototypes can be submitted to design load conditions specific to their service usage on test benches. Said load conditions must be defined in terms of subsystem inputs, in contrast to global car loads, being described as input wheel forces or simply requested driven paths. Note that the validation procedures implemented by the test teams may be different from the initial reference stored in the previously mentioned design groups: loading procedures may be truncated or adapted to the load configuration of the subsystem of interest.

All car prototypes are submitted to synthesis trials on proving grounds. The loads measured at wheel axles and organ interfaces become the learning base to a new updated multi-body model for the vehicle model. These loads allow posterior correction of the validation objectives and associated load definitions used for the validation of the system.

The main takeaway of this presentation is that the knowledge of the response of the new vehicle model evolves with the project. Therefore, the validation procedures must be updated throughout the project with respect to the specific properties of the model and of its market.

Appendix B

Loading concatenation

Cycle counting is a major brick used in the industry to characterize the fatigue induced by service and artificial loads. Why is this signal treatment method mechanically relevant? What phenomenon does it help describe?

Secondly, addition or concatenation of single events into test schedules is the main application of proving grounds for physical fatigue testing. In the thesis, we want to elaborate a robust fatigue equivalency method, to replicate the fatigue induced by complex real-life loading histories on car chassis and structures, using single controlled and repeatable track loads.

In this appendix, we provide the conceptual tools to understand the underlying mechanical ideas and issues for the Rainflow cycle counting algorithm and load concatenation operations.

B.1 Fatigue, variations and sequences - mechanical point of view

Local load variations provoke coalescence and propagation of defects/micro-cracks in the granular material. This physical phenomenon is modeled precisely through the Paris Law (crack growth speed) or stress concentration factors (Relation between macroscopic stress and crack tip stress), both requiring rich knowledge of local loading histories and geometry at the location of the defect (Fig. II.1).

Crack growth from varying loads can also be understood through elastoplastic models. Plasticity, being the non-linear behavior observed both macroscopically and microscopically in metallic materials, stems from the increase in size of micro-cracks in the material.

At the macroscopic scale, the material seems to behave purely elastically when submitted to loads below its elastic limit. When dealing with thousands to millions of variations, even seemingly elastic loads may induce plasticity at the microscopic level, eventually leading to fatigue failure (Fig. B.1)[1].

[1]The following images were drawn from an internal course at Stellantis

Mechanical work induced by load variations is either stored as elastic energy or dissipated as plastic energy. This plastic energy amounts to the cracking energy dissipated by the propagation and coalescence of cracks in the material.

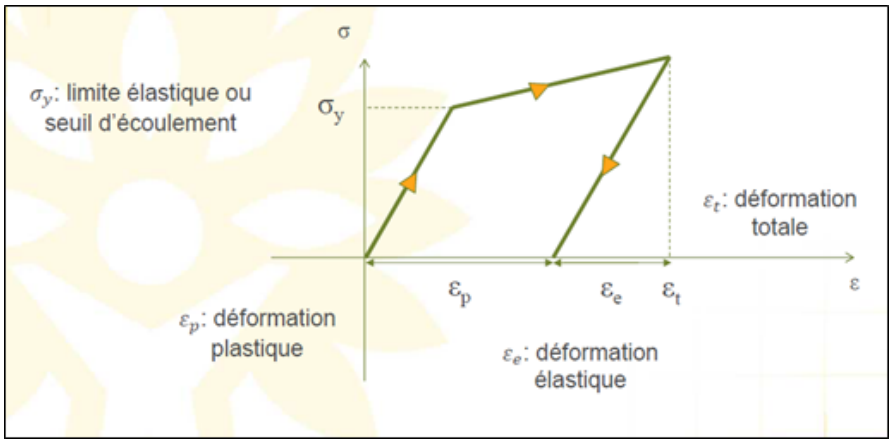

Fig. B.1: Elastoplasticity [Maïtournam 2017]

Under multiaxial loads, the elastic domain (defined by $f(\underline{\underline{\sigma}}) < 0$) of isotropic materials can be modeled by an elasticity criterion such as Tresca or Mises (k is a material constant) (Fig. B.2:

$$f_{Mises}(\underline{\underline{\sigma}}) = \sqrt{\frac{1}{2}\left[(\sigma_I - \sigma_{II})^2 + (\sigma_{II} - \sigma_{III})^2 + (\sigma_{III} - \sigma_I)^2\right]} - k = \sqrt{3 \cdot J_2} - k \qquad \text{(B.1.1)}$$

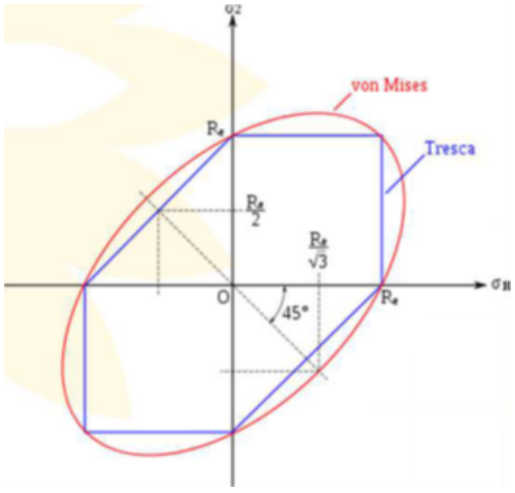

Fig. B.2: Mises and Tresca criteria in plane stress state [Maïtournam 2017]

Plasticity shifts the load domains over which the material behaves elastically. Under cyclic loads, this phenomenon is called hardening. There are two basic models for hardening of a material point under cyclic loadings. Kinematic hardening (Eq. B.1.2) represents a translation of the elastic domain. Isotropic hardening (Eq. B.1.3) represents its dilatation. Whether either or both of them are relevant to characterize the behavior of the point depends on its material properties and geometrical context B.3.

$$f\left(\underline{\underline{\sigma}} - \underline{\underline{\sigma}}_p\right) = \sqrt{3 \cdot J_2} - k \tag{B.1.2}$$

$$f\left(\underline{\underline{\sigma}}\right) = \sqrt{3 \cdot J_2} - (k + k_p) \tag{B.1.3}$$

denoting $\underline{\underline{\sigma}}_p$ a plastic shift in the location of the center of the yield domain; k_p a plastic shift in the radius of the yield domain.

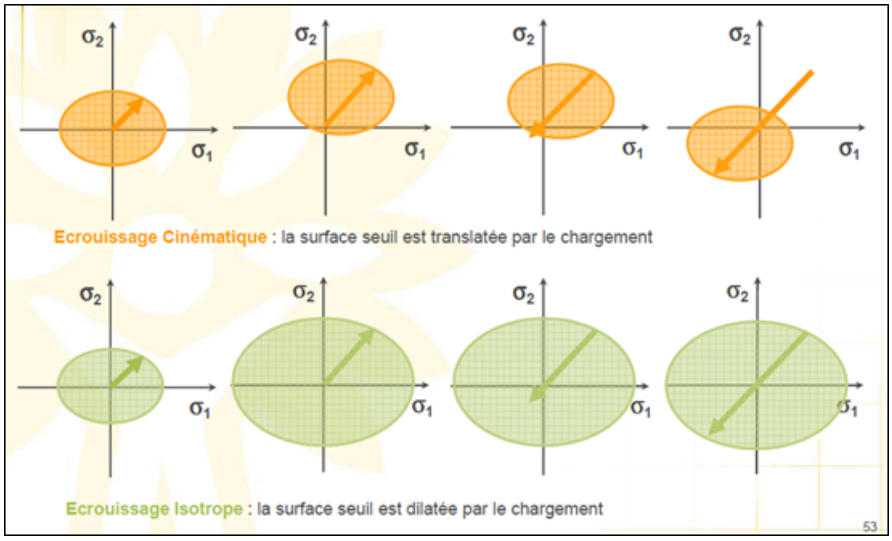

Fig. B.3: Two hardening models [Maïtournam 2017]

Isotropic hardening can be considered the first kind of hardening at play when a part begins its service life. The second phase, the saturation phase, lasts much longer than the other two. During this phase, we can consider that the material hardens cinematically. Phases are described schematically in B.4

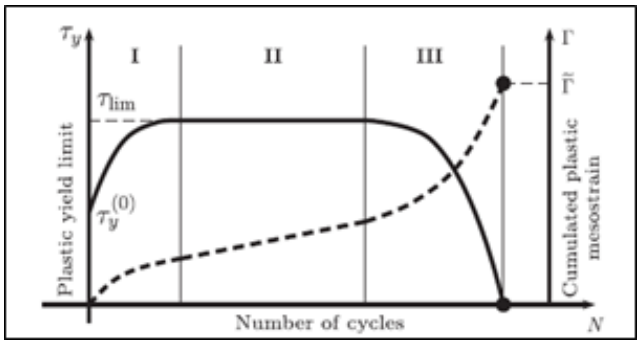

Fig. B.4: Typical life cycle of a component [Bosia and Constantinescu 2012]

A shift in the elastic domain is linked to plastic flow in the material. Therefore, any movement of the elastic domain is akin to plastic damage. While Wöhler curves are experimental curves - they are obtained empirically - their mechanical interpretation says no less than that for elastoplastic materials: The unlimited endurance zone ($\sigma < \sigma_\infty$) corresponds to cyclic loads that don't modify the elastic domain beyond the first life phase (the hardening phase) (Fig. B.5).

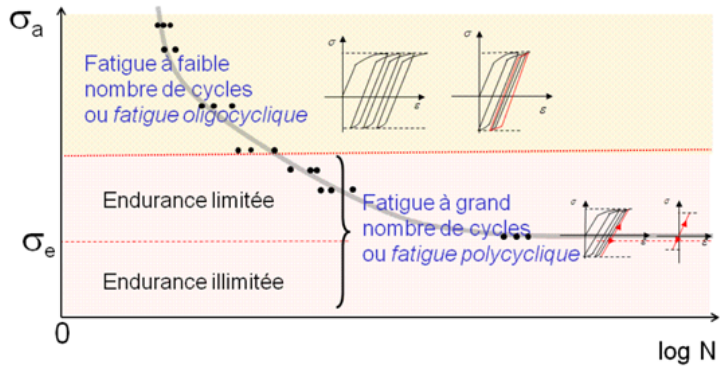

Fig. B.5: Fatigue domains seen through the lens of elastoplasticity [Maïtournam 2017]

In the next sections, we will seek the most relevant order of concatenation of loads, to create artificial fatigue design loads. From this paragraph, the main mechanical certitude we have is that, under variable amplitude loads, translations of the elastic domain during the load are related to plastic damage. Therefore, the concatenation order that yields the most shift in elastic domain is expected to be the most damaging.

In the next paragraphs, we will see in the literature how other works tackled the question of load order.

B.2 Path effect in fatigue prediction

A framework is set up in [Zarka and Casier 1981], see also [Jabbado 2006] chap. 1.6, to predict the lifetime of components submitted to cyclic loads by identifying a stabilized hardening cycle and counting the amount of damage induced by this stabilized cycle (Fig. B.6). The damage induced by the three-point bi-axial local load cycle is quantified by the plastic flow given by trajectory y_1, y_2, y_3, y_4.

Under multiaxial loads and more generally, we can model and quantify fatigue damage under cyclic loads using shear stress and hydrostatic pressure. For uni-input sinusoidal loads, the result is a V-cycle (Fig. B.7a). For bi-sinusoidal loads with a given phase, the result is an ellipse in the Tau-P diagram (Fig. B.7b).

The Dang Van criterion considers the shear stress range and maximum hydrostatic pressure over a cycle to be sufficient to determine whether or not a cyclic loading history leads to failure or not. Its results are satisfying under uni-input sinusoidal loads / in-phase bi-sinusoidal loads. [Dong *et al.* 2010] showed that the criticity of a cyclic bi-sinusoidal load depends on the phase between the two sinusoidal inputs.

In the bi-sinusoidal case, a larger fraction of the loading path leads to microscopic plasticity. This observation explains the result of [Kanazawa *et al.* 1979]. Further investigation of the effect on fatigue prediction of different paths of local shear versus hydrostatic pressure is given in [Fremy *et al.* 2014; Meggiolaro *et al.* 2017] (see Fig. B.8)

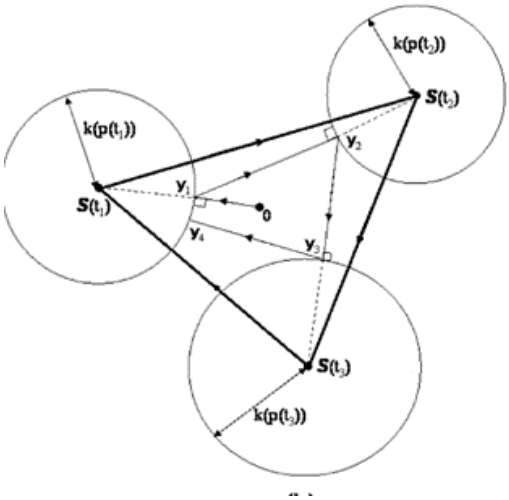

Fig. B.6: Three-point stabilized cycle in a stress-stress space with drawn elastic domain [Zarka and Casier 1981]

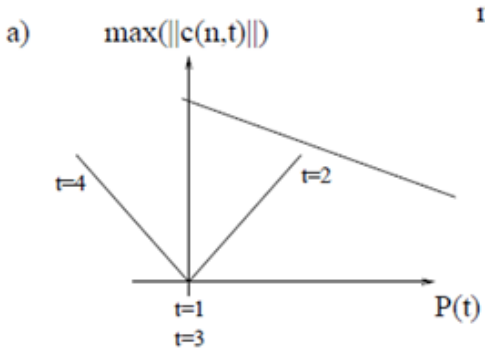

(a) Unidimensional sinus loads [Genet (Le Corre) 2006] Chap. 4

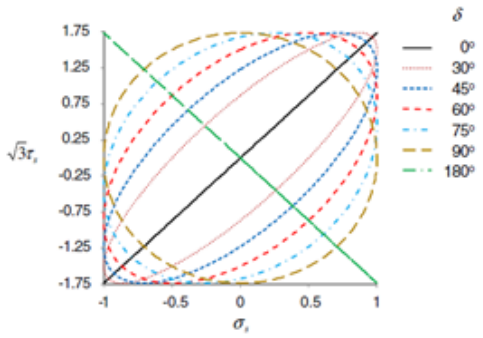

(b) Bi-sinusoidal loads with different phases [Dong *et al.* 2010]

Fig. B.7: Load paths in a shear-pressure diagram for uni-input versus bi-input analytical loads

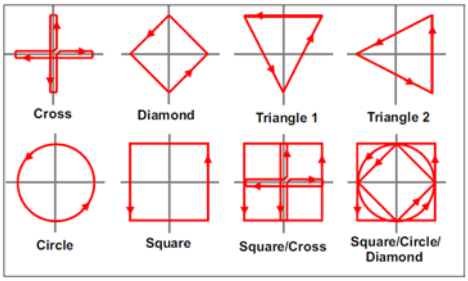

(a) Load paths compared

Table 2
Predicted and observed lives, in number of blocks, for each applied path.

Tension-torsion path	Predicted	Observed	Error (%)
Cross	1314	1535	−14
Diamond	1436	976	+47
Triangle 1	1135	842	+35
Triangle 2	1180	840	+40
Circle	996	837	+19
Square	751	772	−3
Square/Cross	482	342	+41
Square/circle/diamond	327	288	+14

(b) Fatigue life prediction for each path

Fig. B.8: Fatigue analysis of a component submitted to different bi-axial load paths [Meggiolaro *et al.* 2017]

B.3 Sequences of loads

B.3.1 Block loads versus the randomness of events

Let us compare the amount of plastic energy dissipated by a material point submitted to a 2-block bi-input sinusoidal load sequence with that under a mixed load sequence (Figs. B.9 and B.10).

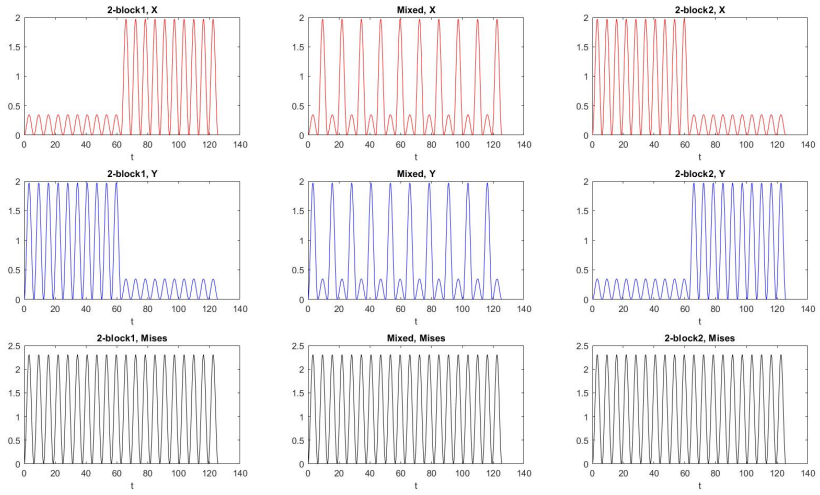

Fig. B.9: Definition of three different multi-input block loads: Block1, Mixed and Block2

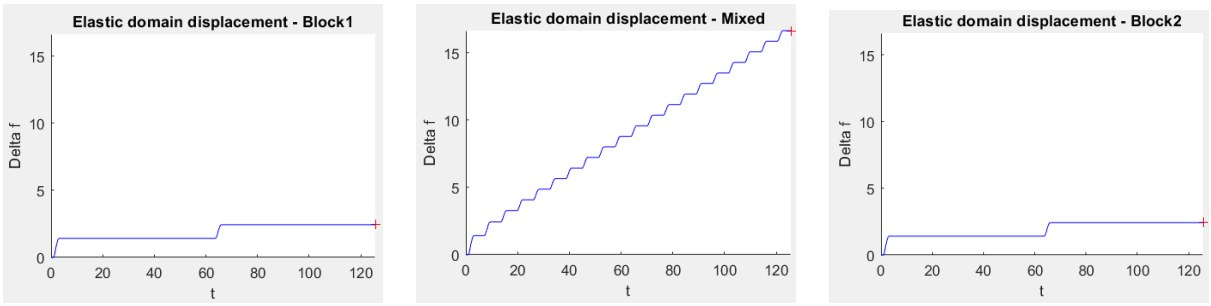

(a) Block1: high Y then high X

(b) Mixed large X and Y cycles

(c) Block1: high X then high Y

Fig. B.10: Comparison of the progression of pseudo-damage between the three block loading histories

A more exact algorithm for plastic flow is available in [Simo 1998], chap 3.4, or [Simo and R. L. Taylor 1986]. Studies of the accumulation of damage for block loads are available in [Fissolo *et al.* 2015; Manson *et al.* 1967; Manson and Halford 1986; Miller and Zachariah 1977; Palin-Luc *et al.* 1996; Pavlou 2002]. A result of [Pierron 2018] Chap. 1 is displayed in Fig. B.11

Do these non-mixed (two-block) loads appear in the case of real-life car loads? We may wonder whether loads are always “mixed”:

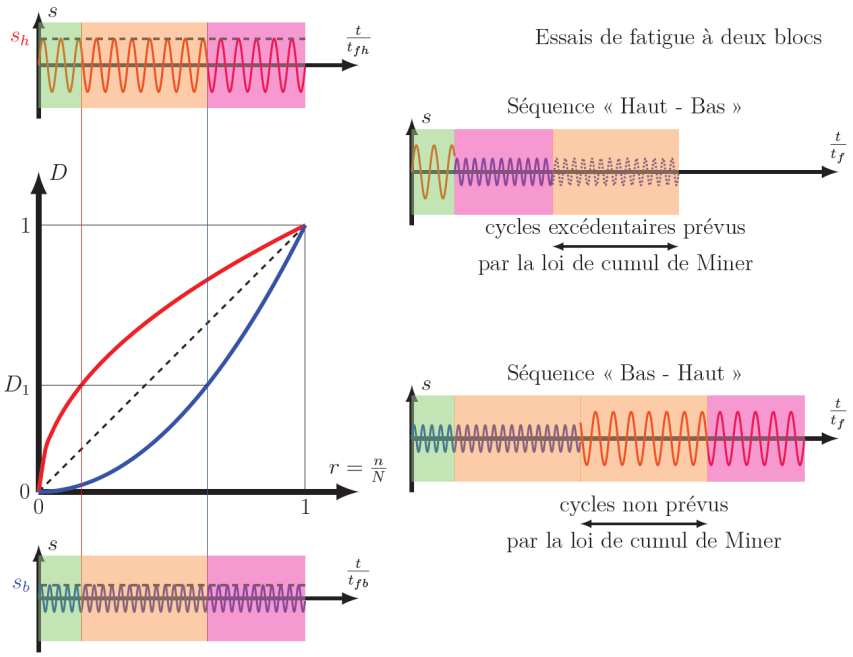

Fig. B.11: Number of cycles withstood under different orders for two-block loading histories [Pierron 2018] Chap. 1

- Braking is usually followed by acceleration.
- A turn on one side begets a turn on the other side.
- As for vertical loads (potholes, pavements, speed bumps), their loads are usually symmetrical (a high peak then a low valley)

Specifically, we can expect real-life loading histories obtained from measurement campaigns to be "chaotic" enough to be akin to mixed loads. Therefore, the damage of the concatenation of measured samples can be assimilated to the sum of each sample's damage, as it is already the "worst case scenario". However, when creating an artificial, experimental load for track purposes, we need to keep in mind that repeating the same load, while easier in practice, may yield lower damage than mixing them up.

However, when creating an artificial, experimental load for track purposes, we need to keep in mind that repeating the same load, while easier in practice, may yield lower damage than mixing them up.

A general method for reconstruction of a Rainflow matrix (unidimensional loading history) considering the order of cycles to be random is presented in [Krüger *et al.* 1985], using stochastic processes.

B.4 Rainflow counting algorithm

When analyzing variable amplitude loading histories for fatigue calculations, the ASTM recommends picking between Level Crossing counting and Rainflow cycles counting methods,

as they have showed the most reliable results for fatigue prediction in most usual applications [ASTM 2017].

Rainflow counting algorithms identify closed hysteresis loops in the stress-strain space under a variable amplitude loading history (Fig. B.12). These loops are called Rainflow cycles, as they are quantified as though they were cycles in an equivalent cyclic load [Rychlik 1987].

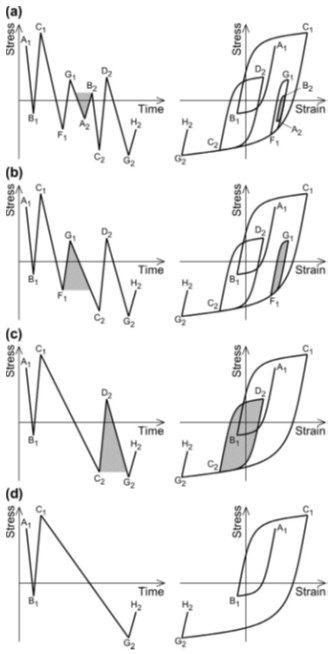

(a) Algorithm on a Stress-Time graph [Marsh *et al.* 2016]

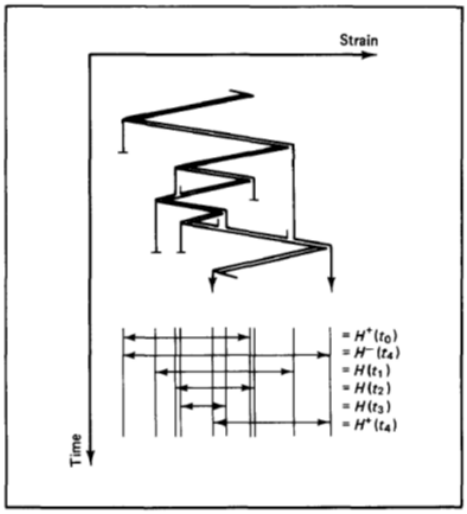

(b) Pagoda view [Rychlik 1987]

Fig. B.12: Principle of the Rainflow counting algorithm

Because of the way Rainflow cycles are calculated, non-extremal (in-between) points in the temporal signal do not matter in the calculation. Therefore, Rainflow counting algorithms are applied on sequences of peaks and valleys, measured on the signal. Their sequence matters, but not their instants.

Under very brutal load variations, the elastoplastic model may become imprecise because of viscosity effects. However, in our applications, the elastoplastic model is a satisfying hypothesis, and not taking viscosity in account is a relevant move. Therefore, the shape of the variations also does not matter.

We define the sequence of turning points from a scalar loading history $\mathbf{F}$:

$$\mathrm{TP}\ (\mathbf{F}) = \mathbf{s} = (s_j)_{j\in[\![1,n_{tp}]\!]} = \{\mathbf{F}(n)\ \forall n \in [\![1,n_{tp}]\!]\} = \{..., M_0, m_1, M_2, m_3,...\} \tag{B.4.1}$$

denoting n_{tp} the number of turning points of signal $\mathbf{F}$. A sequence of turning points always alternates between a local maximum $s_j = M_j$ and a local minimum $s_j = m_{j+1}$ (see Fig. B.13.

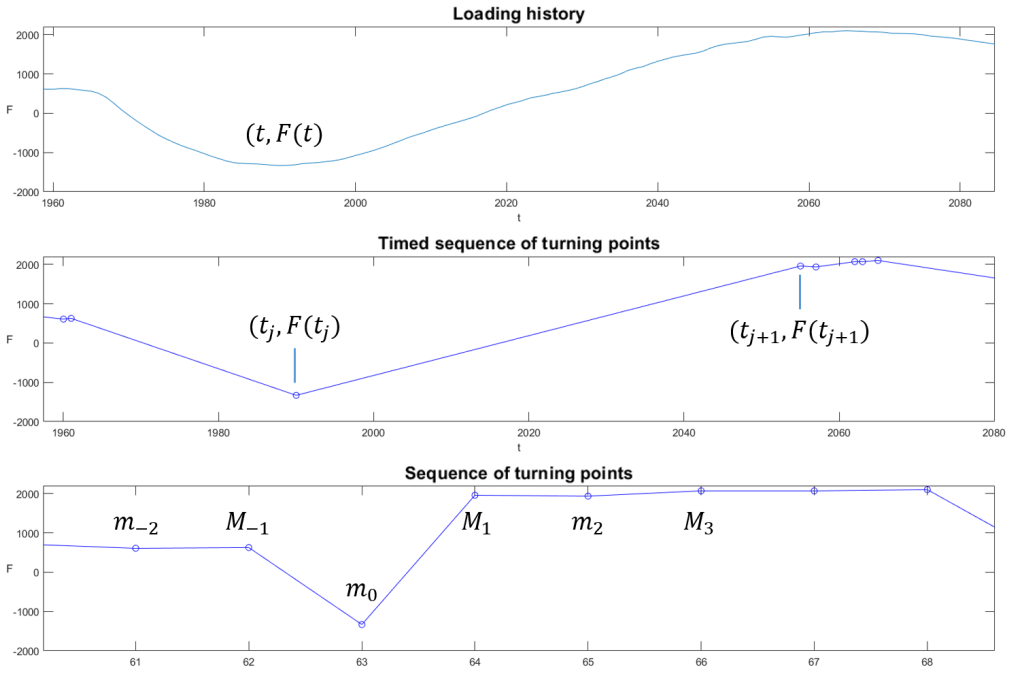

Fig. B.13: A scalar loading history, a timed sequence of turning points, and an indexed sequence of turning points

The result of a Rainflow counting (see also Fig. II.14) is the couple of a count of cycles in a loading history and the residual, being a sequence of the remaining extrema that could not be paired using the previous algorithm:

$$\mathrm{Rf}^0\ (\mathbf{F}) = \mathrm{Rf}^0\ (\mathbf{s}) = \left(C^0, R^0\right) \tag{B.4.2}$$

$$C^0 = \left\{\left(m_{j_i}, M_{J_i}\right), i \in [\![1, n^0_{\mathrm{cyc}}]\!]\right\} \tag{B.4.3}$$

$$R^0 = \left(s_j\right)_{j \in [\![1, n_r]\!]} \tag{B.4.4}$$

denoting (j_i, J_i) the indices of respectively the local minimum and maximum paired in the i-th cycle, and n_r the number of extrema that could not be paired.

Rainflow cycles can be described either by their extremal points $(m_j, M_J)_i$ or by their amplitude and mean $\left(M_J - m_j, \frac{m_j + M_J}{2}\right)_i$.

B.5 Rainflow residual, properties and treatment

The Rainflow residual always contains the minimum and the maximum of a scalar loading history. The Rainflow residual obtained from a four-point Rainflow algorithm is always an increasing-decreasing sequence (see Fig. B.14) [McInnes and Meehan 2008]. Note, on the figure, that the elastic domain seems to have shifted between the increasing part (culminating at point A) and the decreasing one (starting at point B).

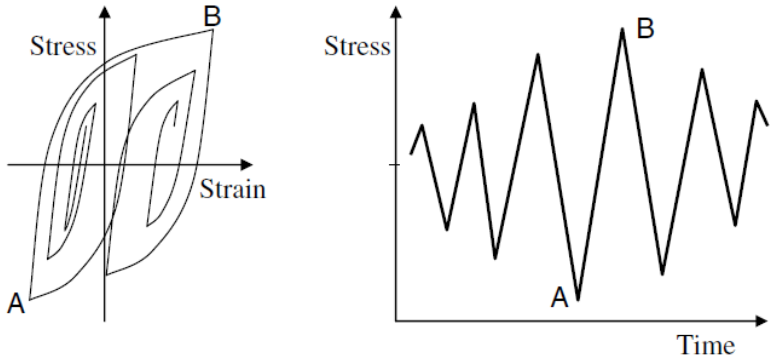

Fig. B.14: A residual, as seen in the Stress-Strain diagram or in a Stress-time graph, is over time an increasing-decreasing sequence of points [McInnes and Meehan 2008]

We can separate the residual of a Rainflow count in three parts:

$$R^0 = \begin{pmatrix} R^{\nearrow} & = \{...,M_{-4},m_{-3},M_{-2},m_{-1}\}, \\ & (M_0,m_1), \\ R^{\searrow} & = \{M_2,m_3,M_4,m_5,...\} \end{pmatrix} \tag{B.5.1}$$

$$\text{Or} \quad \begin{pmatrix} R^{\nearrow} & = \{...,m_{-2},M_{-1}\}, \\ & (m_0,M_1), \\ R^{\searrow} & = \{m_2,M_3,...\} \end{pmatrix} \tag{B.5.2}$$

If the treated signal starts and ends with negligible variations, we can artificially add any number of minima or maxima at very low values without tampering with the damage done by the signal. If we really want to, we can make all equilibrium-starting turning point sequences begin with a local minimum and end with a local maximum. Therefore, we can make all residuals have the same number of maxima and minima and therefore an even number of turning points.

The Miner Law predicts the damage induced by cycles counted by the Rainflow algorithm. Damage or pseudo-damage can also be associated with the sequence of turning points corresponding to the residual. Two residual damage counting methods were recalled in [Marsh *et al.* 2016]: half-cycle counting and residual closure.

Half-cycle counting is presented in the original introduction of Rainflow counting by Matsuishi and Endo [Endo *et al.* 1974; Matsuishi and Endo 1968]. Residual turning points are paired in-order and the associated marginal damage is given by half the marginal damage obtained from the range between the two points.

Residual closure or "Simple Rainflow counting" is presented in [Amzallag *et al.* 1994] and is the advised method according to AFNOR recommandations [AFNOR 1993]. Closed residual corresponds to the following formula:

$$R^{\bullet} = \frac{C^0\left(R^0 \| R^0\right)}{2} \tag{B.5.3}$$

denoting $R^0||R^0$ the concatenation (see Eq. B.7.1) of the residual with itself and $C^0(...)$ the cycles counted by application of the Rainflow algorithm $RF(...)$. The division by two is applied on the cycle counts.

Extrema of the increasing sequence are paired with extrema of the decreasing sequence, and the last pair is simply the minimum and the maximum of the signal. This last cycle, being the one of largest amplitude, can have a large effect on damage cumulation, depending on the material exponent used to calculate marginal damage and on the distribution of counted Rainflow ranges below this maximum one.

These two residual processing methods were compared by Marsh [Marsh *et al.* 2016] on a full offshore wind plant loading history with the sum of counts performed on small fraction of the history. The authors used Basquin exponents of 3 and 5, and tested subsets of either 10 or 180 minutes. They compared the damage of the full sequence to the sum of each subset's damage. They always find that the sum of each subset's damage yields lower damage than the damage calculated over the whole signal.

The closed residual method yields closer results to the reference than the half-cycle counting method. But the error increases as the Basquin exponent m increases and as the sampling size decreases.

B.6 Intermediary conclusion and the problem of concatenated loads

Despite the application of the recommended residual processing algorithm, an error perdures. When concatenating short loads in a schedule, for the creation of proving groud schedules for instance, this error may create a large discrepancy between the damage we want to model and the one we actually calculate.

The missing information that residual processing tries to replace is the displacement in elastic domain between the beginning and the end of each individual track (see section B.1).

The Rainflow algorithm has a complexity of $O(n^2)$, n being the number of turning points in the sequence to process. Applying the algorithm on the whole concatenated loading history may overload the amount of memory and time necessary to achieve a result. In the following paragraph, we justify a very simple formula for the calculation of the exact Rainflow count of a concatenation of loads without processing the whole concatenation in a single Rainflow algorithm application.

B.7 Rainflow counting on concatenations of loads

[Marsh *et al.* 2016] also proposed a method to calculate the Rainflow cycle of a concatenated load, based on [Amzallag *et al.* 1994] pages 292-293. The idea is to reapply Rainflow counting on the concatenation of each base signal's residual, and post-treatment of the ultimate residual rather than on each individual residual.

Let us define the signal concatenation operator:

$$\mathbf{F}_1 \| \mathbf{F}_2 = \begin{bmatrix} F_1(t) \ \forall t \leq T_1 \\ F_Z(t) \ \forall T_1 < t \leq T_2 \end{bmatrix} \tag{B.7.1}$$

$$\mathop{\Big\|}_{e=1}^{g} \mathbf{F}_e = \mathbf{F}_1 \| ... \| \mathbf{F}_g \tag{B.7.2}$$

The cycles of the concatenation are obtained from the sum of the cycles of each individual signal plus the cycles found in the concatenation of each residual.

$$C^0 \left(\mathop{\Big\|}_{e=1}^{g} \mathbf{F}_e \right) = C^0 \left(\mathop{\Big\|}_{e=1}^{g} R_e^0 \right) + \sum_{e=1}^{g} C^0 \left(\mathbf{F}_e \right) \tag{B.7.3}$$

The residual of the concatenation is calculated on $(\|_{e=1}^{g} R_e^0)$ and can be closed using Eq. B.5.3

$$R^\bullet \left(\mathop{\Big\|}_{e=1}^{g} R_e^0 \right) = \frac{C^0 \left((\|_{e=1}^{g} R_e^0) \, \| \, (\|_{e=1}^{g} R_e^0) \right)}{2} \tag{B.7.4}$$

The damage or pseudo-damage obtained by linear cumulation of all marginal damages counted on $C^\bullet = (C^0, R^\bullet)$ is equal to the damage obtained by applying Rainflow counting directly on the concatenation and closing the obtained residual. To summarize, by denoting $\breve{D}(\mathbf{F})$ the total pseudo-damage cumulated from any loading history $\mathbf{F}$:

$$\breve{D}(\mathbf{F}) = \breve{D} \left(C^0 \left(\mathbf{F} \right) \right) + \breve{D} \left(R^\bullet \left(\mathbf{F} \right) \right) \tag{B.7.5}$$

$$\breve{D} \left(\mathop{\Big\|}_{e=1}^{g} \mathbf{F}_e \right) = \sum_{e=1}^{g} \left(\breve{D} \left(C^0 \left(\mathbf{F}_e \right) \right) - \breve{D} \left(R^\bullet \left(\mathbf{F}_e \right) \right) \right) + \breve{D} \left(\mathop{\Big\|}_{e=1}^{g} R_e^0 \right) \tag{B.7.6}$$

Equation B.7.5 stems from previous equations B.4.3 and B.5.3.

Nota bene: The difference between damage and pseudo-damage lies in the (mechanical) definition of the marginal damage associated with each counted cycle. A marginal damage is a fraction of a cyclic trial that would lead the component to failure. A marginal pseudo-damage is the numerator of such a marginal damage.

B.7.1 Definition of naive and chaotic schedules

Let us consider a set of g reference loading histories, say of loading histories associated with proving ground tracks, defined by $\left(\vec{\mathbf{F}}_e \right)_{e \in [\![1,g]\!]}$ with:

$$\overrightarrow{M} \left(\vec{\mathbf{F}}_e \right) = \left(\sqrt[m_k]{\breve{D} \left(\gamma_k, \vec{\mathbf{F}}_e \right)} \right)_{k \in [\![1,\kappa]\!]} \quad \forall e \in [\![1,g]\!] \tag{B.7.7}$$

A naive proving ground schedule, corresponding to a global loading denoted $\vec{\vec{\mathbf{F}}}^{\star}_{\vec{n}}$ is a trivial concatenation of tracks, directed by a vector of repetitions of each tracks $\vec{n} = (n_e)_{e\in[\![1,g]\!]}$:

$$\vec{\vec{\mathbf{F}}}^{\star}_{\vec{n}} = \Big\Vert_{e=1}^{g} \left(\Big\Vert_{i=1}^{n_e} \vec{\vec{\mathbf{F}}}_e \right) = \left(\Big\Vert_{i=1}^{n_1} \vec{\vec{\mathbf{F}}}_1 \right) \Vert \ ... \ \Vert \left(\Big\Vert_{i=1}^{n_g} \vec{\vec{\mathbf{F}}}_g \right) \tag{B.7.8}$$

A chaotic proving ground schedule is a random permutation $\psi \in \Psi^N$ on the repetitions of tracks in a naive proving ground schedule, denoting $N = \sum_e n_e$ and Ψ^N the space of permutations on vectors of dimension N. Using a sequence notation for load concatenations, we can write the global loading history of a chaotic proving ground schedule as:

$$\text{If } \vec{\vec{\mathbf{F}}}^{\star}_{\vec{n}} = \left(\left(\vec{\vec{\mathbf{F}}}_1 \right)_{i\in[\![1,n_1]\!]}, ..., \left(\vec{\vec{\mathbf{F}}}_g \right)_{i\in[\![1,n_g]\!]} \right) \text{ Then } \vec{\vec{\mathbf{F}}}^{\psi}_{\vec{n}} = \psi\left(\vec{\vec{\mathbf{F}}}^{\star}_{\vec{n}} \right) \tag{B.7.9}$$

The difference in predicted damage between a naive proving ground schedule and its associated chaotic schedules lies in the model used to predict the pseudo-damage of a concatenation of loads. In most previous works, the pseudo-damage of a concatenation of loads is considered to be the sum of all individual loading histories' pseudo-damages, following for instance closure of the Rainflow matrix.

However, this is an inexact approximation of the pseudo-damage of a concatenation, and can lead to large relative gaps between truth and model, as we will show in the following paragraph. This is comprehensible both numerically - the Rainflow algorithm is not linear - and physically - sequence effects matter in fatigue.

A random permutation on a naive sequence is called chaotic because the variety of events contained in the schedule is shuffled through the new sequence. Service loads over a vehicle life are considered chaotic in that sense. The choice of a chaotic schedule for the replication of mission severity is a quest for authenticity, to avoid the limitations of implemented fatigue models.

In practice, the construction of proving grounds and the elaboration of proving ground test procedures enforce a few sets of permutations of proving ground tracks. A circuit, containing several events, will be driven from beginning to end or vice-versa. Keeping this set sequence of events during the exploitation of proving ground trials may question the hypothesis of chaotic schedule.

For instance, a half-built speed bump driven upwards in one direction of the circuit and downwards in the other one direction of the circuit does not necessarily induce the same damage as a full speed bump, depending on the other events contained in the circuit.

Nota bene: The differences in concatenated damage between several orders of concatenation are caused by asymmetry in the residual of events. An event the residual of which contains a positive peak before stabilization, will be associated with more pseudo-damage when followed by an event starting with a negative peak, than when followed by one starting with another positive peak. For instance, two braking events following each other will not induce as much damage as braking-acceleration alternations with similar individual pseudo-damages.

B.8 Effect of concatenation order on the pseudo-damages induced by a schedule

Proving ground schedules are used extensively in the automotive industry to store historical knowledge on design references for new vehicles. They are built from repetitions of individual proving ground tracks, being either single obstacles (potholes) or sequences of events (cornering, slopes...).

Proving ground schedules can be positioned on a distribution of Stress used in an S-R paradigm for the design of a component or subsystem, as explained in the reliable design state-of-the-art in §VI.2.2. We may also compare them generally to the severity of drivers like in §VI.5.3. In either case, these concatenations must be translated to pseudo-damages.

As shown in this appendix, the order of concatenation is expected to have an effect on the total pseudo-damage. Thanks to the previous paragraph, we have access to the exact calculation of concatenated pseudo-damage from the individual counts and the knowledge of each signal residual.

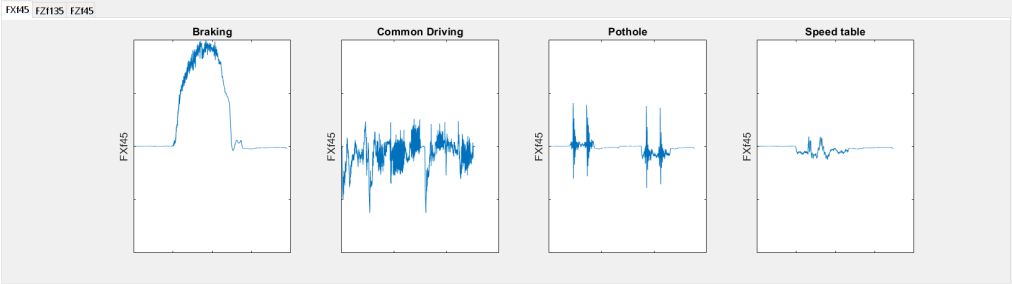

(a) Symmetrical longitudinal loads on the front axle $Xf45$

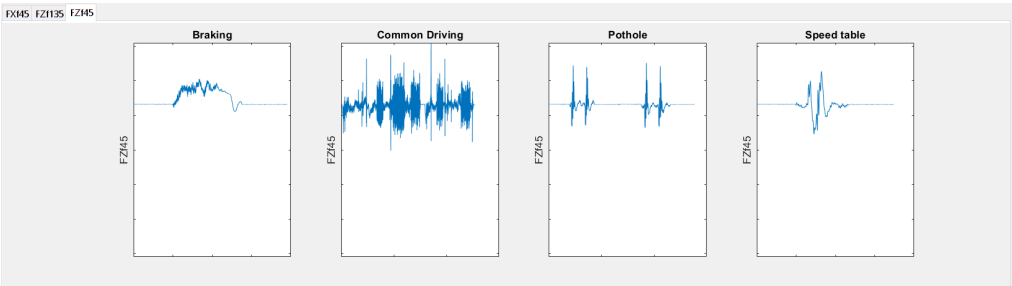

(b) Symmetrical vertical loads on the front axle $Zf45$

Fig. B.15: Comparison of two global load cases calculated on each track using formula III.6.1

Let us consider four tracks $\left(\vec{\mathbf{F}}_e\right)_{e\in[\![1,4]\!]}$ and their 4! = 24 possible orders of concatenation $(\psi_{ijkl})_{i,j,k,l\in[\![1,4]\!]^4}$. The loading histories induced by the selected tracks are illustrated in Fig. B.15. The common driving circuit includes accelerations, maneuvers and reasonable obstacles. The braking circuit is much more asymmetrical in terms of loads. The pothole induces large variations on all global load components while the speed hump (table)

A permutation on the vector $\left(\vec{\mathbf{F}}_e\right)$ yields a schedule. Its loading history is denoted $\vec{\mathbf{F}}_{\psi_{ijkl}}$

These tracks correspond to an emergency braking, a pothole, a series of and a speed table (or speed hump).

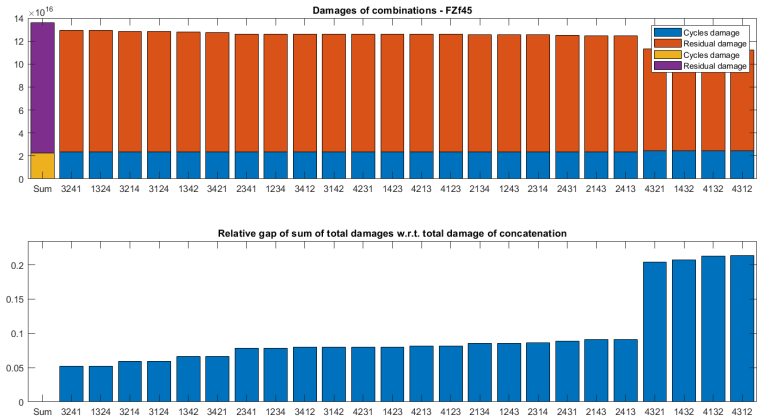

(a) Symmetrical vertical loads on the front axle $Zf45$

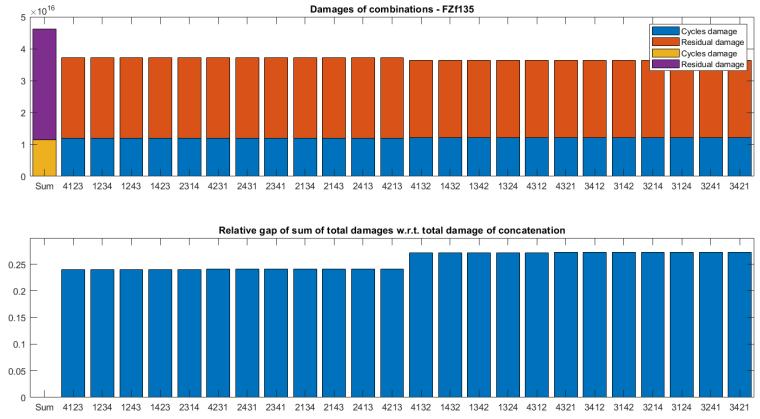

(b) Asymmetrical vertical loads on the front axle $Zf135$

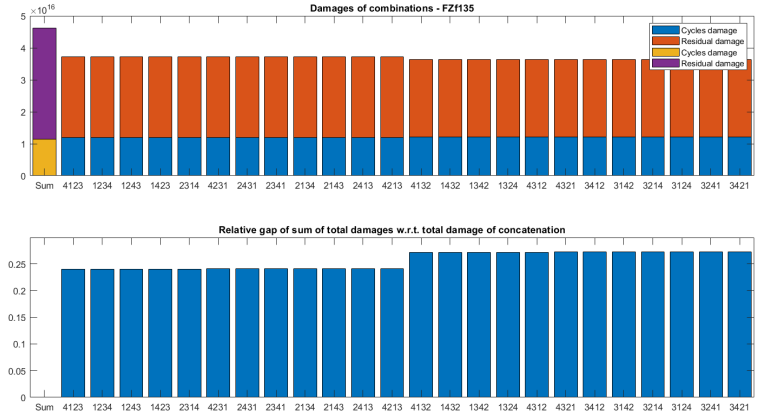

(c) Symmetrical longitudinal loads on the front axle $Xf45$

Fig. B.16: Pseudo-damage at Basquin $m = 4$ for 3 local contexts for different permutations of a schedule containing one repetition of 4 tracks: braking, common driving, pothole and speed table. The first bar corresponds to the direct sum of the pseudo-damage of each track. All other columns are the pseudo-damage of concatenations of the tracks calculated using the exact formula.

The pseudo-damages calculated at a Basquin exponent of 4 for three load cases are presented in Fig. B.16, first from the direct sum of the pseudo-damage induced by each track, then for each of the 24 combinations of the tracks. Since the concatenated formula is the exact one, relative gaps were calculated on the direct sum using formula:

$$\frac{\sum_e^4 \breve{D}(\gamma,\vec{\overline{\mathbf{F}}}_e) - \breve{D}(\gamma,\vec{\overline{\mathbf{F}}}_{\psi_{ijkl}})}{\breve{D}(\gamma,\vec{\overline{\mathbf{F}}}_{\psi_{ijkl}})}$$

While the first graphs show that the direct sum of pseudo-damages overestimates the pseudo-damage of the track for vertical load cases, but underestimates it for longitudinal load cases.

This may be caused by the asymmetry of the braking event in terms of load direction: longitudinal load components go high positive (braking) but are not followed by acceleration, as we can see in Fig. B.15.

Note, however, that comparisons in pseudo-damages are impacted by the Basquin exponent. A relative gap of -60% in pseudo-damage corresponds to a relative gap of $\sqrt[4]{0.4} - 1 \approx -20\%$ in magnitude. Fig. B.17 shows the comparisons in magnitudes instead.

$$\frac{\sum_e^4 M(\gamma,\vec{\overline{\mathbf{F}}}_e) - M(\gamma,\vec{\overline{\mathbf{F}}}_{\psi_{ijkl}})}{M(\gamma,\vec{\overline{\mathbf{F}}}_{\psi_{ijkl}})}$$

As a consequence of this difference between the exact formula and the direct sum of the pseudo-damages induced by each track, an extra step is required to avoid carrying such a difference over in the method.

A proposed strategy is to evaluate a matrix of all concatenated residuals for all pairs of tracks $\left(\vec{\overline{\mathbf{F}}}_{e_1} || \vec{\overline{\mathbf{F}}}_{e_2}\right) \forall\, (e_1,e_2) \in [\![1,g]\!]^2$. That way, depending on the concatenation order established by proving ground technicians and engineers, the terms of the exact concatenation formula B.7.6 are known and the exact pseudo-damage of the proving ground schedule can be determined.

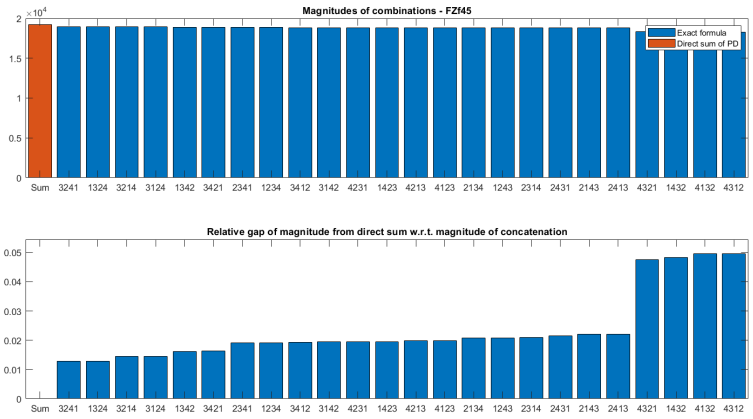

(a) Symmetrical longitudinal loads on the front axle $Xf45$

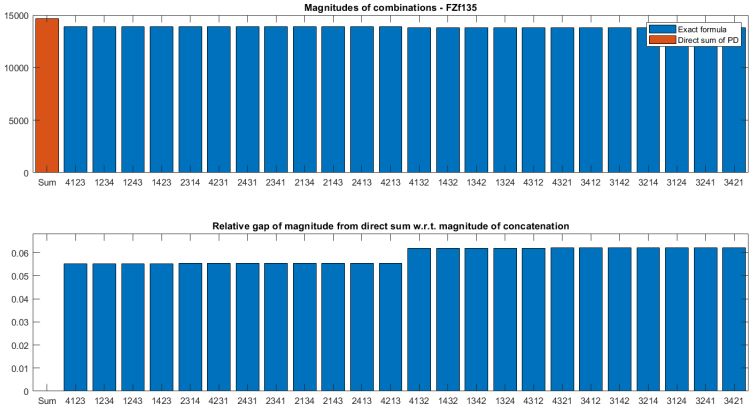

(b) Symmetrical longitudinal loads on the front axle $Xf45$

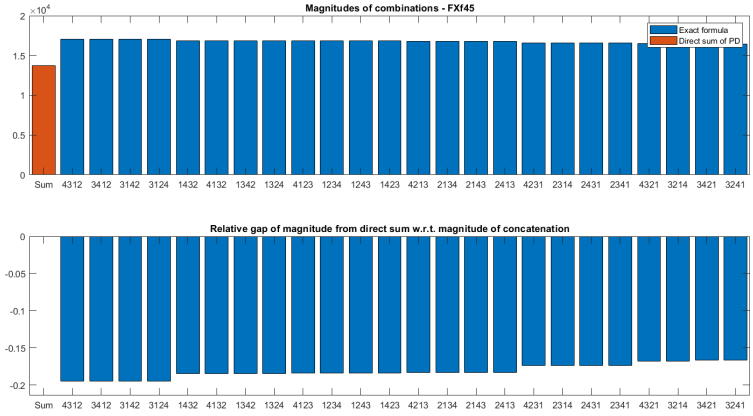

(c) Symmetrical longitudinal loads on the front axle $Xf45$

Fig. B.17: Equivalent magnitude at Basquin $m = 4$ for 3 local contexts for different permutations of a schedule containing one repetition of 4 tracks: braking, common driving, pothole and speed table. The first bar corresponds to the direct sum of the pseudo-damage of each track. All other columns are the pseudo-damage of concatenations of the tracks calculated using the exact formula.

Appendix C

Data preparation

The purpose of this section is to give an overview of the computational process used to access kilometric or non-kilometric magnitudes, and other quantities of interest for the evaluation of usage severity on a fixed trip (section V.3), or for the evaluation of Driver-Trip relationships on road environments, section IV.4.

C.1 Origin and structure of road load data

For our variables of interest, raw data is acquired between the start and stop of the vehicle's engine. Note that a halt in the mission may lead to a cut in data flow and a restart of the onboard processing system.

Wheel axle acceleration signals are measured using accelerometers and sampled with a frequency of 1000Hz. Speed signals are sampled with a speedometer at a frequency of 50Hz.

The company performs a set chain of automatic and manual operations on raw data to filter out sensor malfunction (drift or zero detection), sensor noise (frequency filter).

Service loads are predicted from accelerations and speed signals using a learning model, a neural network with a confidential structure. The model was learned for the specific vehicle at stake on proving ground tracks. Indeed the sensor vehicle was equipped with wheel load cells on the proving grounds, but not in service measurement campaigns such as US18-DT. Parallel studies are underway to increase the robustness and the relevance of this prediction [Débarbouillé *et al.* 2022].

Load variations that exceed the threshold for service loads (associated with a requirement of absence of local plasticity, see Eq. III.2.2) are branded as incidents and corresponding time sections are removed from the signals.

Global loading histories are segmented by driver and by road segment, unless they were separated once or twice by the existence of a halt, as commented previously.

C.2 Origin and elaboration of (reference) proving ground schedules

We must also mention the origin of proving ground load data used for the comparison of results with existing references in §VI.5.2.3. Proving ground schedules are combinations of repetitions of different proving ground tracks. They represent artificial synthetic missions of interest for the reliable design of all subsystems of a vehicle. Proving ground tracks were briefly introduced in section IV.2.2 and their use in reliable design will be further developed in chapter VII.

The sensor vehicle is driven by a technician on a series of tracks. At Stellantis, each track circuit is driven on three times. Most tracks containing cornering events are either driven on three times clockwise and three times anticlockwise or are combined clockwise and anticlockwise in adequate circuits.

The engineer's experience as well as the use of statistical moments on all three runs on a track yield a selected version of the run for use in schedule building.

C.3 Computing pseudo-damage and speed quantities

In the case of a halt/split in a road segment, both signals were appended to each other to rebuild the road segment, despite a possible re-initialization of the processing system. This was performed automatically, so unexpected or repetitive halts could lead to the exclusion of an individual. Still, we managed to salvage all available samples of the US campaign.

A few missions of the US campaign had missing road segments caused by processing system shutdown or continued sensor malfunction. They were detected automatically and completely ignored for our analysis, hence eventual discrepancy between driver indexing and labeling.

The computation of pseudo-damage on relevant and unmentioned extra local contexts, the computation of speed quantities and the sorting and gathering of all obtained data per mission, per road segment and per local context were conducted using nCode GlyphWorks.

The charge (payload) associated with each wheel was known in advance, thanks to an extra measurement on a flat surface in the region of interest, and input to the analysis in a parameter file. Changes in payload caused by the depletion of fuel or the refueling of the vehicle are ignored.

Each multi-input loading history was processed individually before moving on to another file, performing the following calculations:

- Identification of the vehicle name, driver index, region of interest, payload setting, road segment index, processing system configuration, from the parameter file or from the name of the loading history's file;
- Construction of the extra time series corresponding to global load cases *i.e.* arithmetic

combinations of global load components. The duration in seconds of all global load components is previously set to the minimum available duration;

- A charge (in Newtons) is associated with each global load case as the static value of the vertical load for the structure subset of interest. For instance, global load cases calculated using a single global load component on a wheel are associated with said wheel's borne static charge on a flat surface.

- The duration of the run in kilometers is calculated through the numerical integration of speed over time;

- Speed and acceleration moments or quantiles were calculated on the non-null sections of speed (vehicle not at a stop) for use in the exploratory analysis of driver behavior. The threshold for speed was set to 1km/h. The threshold for acceleration was set to $1km/h^2$;

- The chosen quantiles for speed were 75%, 90% and 100% (max), the latter being considered unstable because very sensible to isolated peaks. The average non-zero speed was also computed;

- The chosen quantiles for acceleration were 5%, 10% (heavy decelerations), 90% and 95% (heavy acceleration). The absolute average of non-zero acceleration was also computed;

- Statistical moments are retrieved from load signals, most importantly minimum, mean and maximum effort values;

- The size of all Rainflow classes is calculated using a pre-processing script, so that all Rainflow matrices of all global load cases of one multi-input loading history have the same class size and edges;

- A Rainflow algorithm is applied to each global load case;

- The speed signal as well as the closed Rainflow matrix and cumulative closed Rainflow matrix (spectrum) of all global load are stored for extra manual analyses;

- The pseudo-damage associated with each global load case is calculated using a fatigue life glyph (*i.e.* computational element) containing the parameters of a Basquin model of a Wöhler curve. In practice, this glyph caps pseudo-damages at $10^{35}N^m$. In order to circumvent this saturation, each Rainflow range in Newton was divided by 50000 before calculation of marginal damage. The resulting pseudo-damage is then multiplied by 50000^m and the resulting equivalent magnitude by 50000, denoting m the Basquin exponent associated with the local context of interest. This allows pseudo-damage values to reach powers of 10 of more than 35, which is expected for high Basquin exponent such as $m = 15$.

- In the result table, we store both the pseudo-damage of the closed Rainflow count and the pseudo-damage associated with an unclosed Rainflow count on the residual of (see the next paragraph).

Computing the Rainflow matrix of the whole mission through signal concatenation of its road segments would be very costly in computation time but most importantly in memory. The program would make use of swap memory to manage the overflow, inducing lengthy communication of data packets between ROM and RAM.

Thanks to the equations II.5.4 and II.5.5 for the Rainflow matrix of a concatenation of loading histories presented in section II.5.1 and justified in Appendix B, we can add an extra calculation step to efficiently retrieve the difference between individual characterizations and concatenated results, and compute exact values of pseudo-damage post-concatenation.

The residuals of each structural load case for all road segments are retrieved and concatenated. Once individual characterization of all road segments is completed, the program performs a different analysis on the concatenation of residuals. The pseudo-damage and magnitude calculated on this new signal are stored in an extra table.

A sampled mission of a duration of 240km is processed in roughly 25 minutes, with an i7-6820HQ (quad-core) and 32Go of installed RAM. Raw data was stored in the company's cloud and downloaded at a speed of 3 megabytes per second. Missions were analyzed one after the other through a background process (batch). A larger calculation capacity, making use of a laboratory or a company's computing cluster for instance, was not deemed necessary because a complete measurement campaign data set could already be achieved in the background in a day or two.

The analysis of a set of missions yields two tables, one for the individual characterization of each structural load case of each road segment for each driver and one for the fatigue characterization of the concatenation of residuals for each structural load case for each driver.

C.4 Building the data tables

Each row of the first table contains the fatigue characterizations (one for each Basquin exponent) for one structural load case of one road segment driven by one driver. Each row of the second table contains the fatigue characterizations of the concatenation of the residuals of one structural load case for the whole mission of one driver.

The same calculation is performed on proving ground tracks for the elaboration of proving ground schedules and yields two similar tables.

For each driver, the pseudo-damage and equivalent magnitude of each local context induced by the whole concatenated mission are calculated using equations II.5.4 and II.5.5. They are then gathered in a row vector.

For each driver, the row vectors associated with each road segment, containing all identifiers, speed moments, signal moments, pseudo-damages and equivalent magnitudes are established and gathered in a new table, along with the previously calculated concatenated characterization. Load intensities are also calculated using formula IV.4.1 as they are the new basis for trip re-simulation and will be the covariates for the Driver-Trip multiple factor analysis.

Appendix D

Multivariate statistics

We consider vectors of random variables $(V_{\bullet k})_{k\in[1,\kappa]}$. Their values span a linear space $\mathbb{R}^\kappa$ (see Fig. D.1).

Let $\mathcal{C}$ be a population over which these variables were measured. Let $\vec{V}_{c\bullet} = (V_{ck})_{k\in[\![1,\kappa]\!]}$ be the joint information of all measurements $V_{\bullet k}$ on a single individual, identified by c.

We denote $V_{\bullet\bullet}$ the $n \otimes \kappa$ matrix of all observations of all variables over population $\mathcal{C}$:

$$V_{\bullet\bullet} = \begin{pmatrix} V_{11} & \cdots & V_{1\kappa} \\ \vdots & \ddots & \vdots \\ V_{n1} & \cdots & V_{n\kappa} \end{pmatrix} \tag{D.0.1}$$

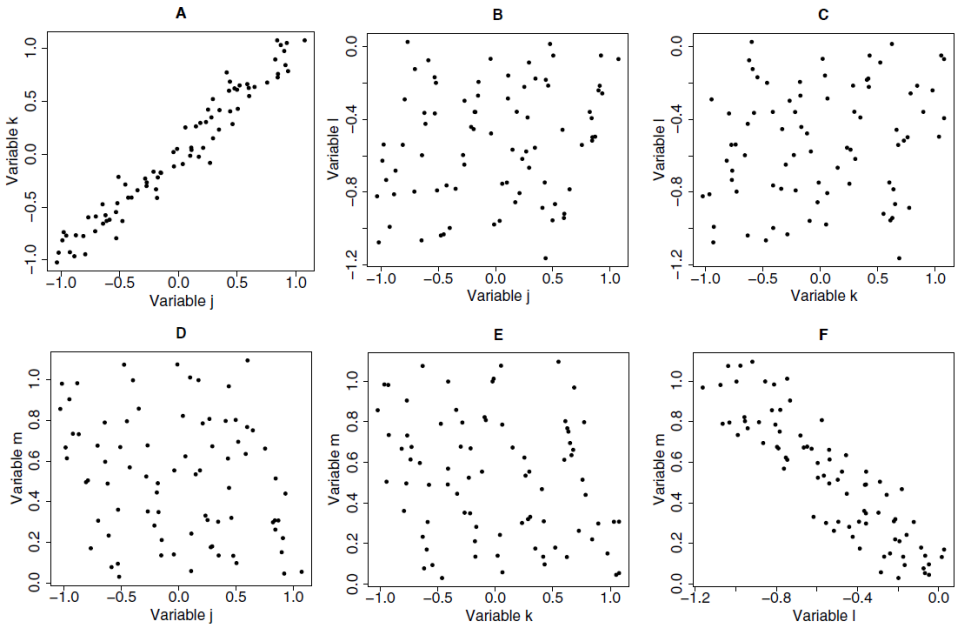

Fig. D.1: Example of a cloud of 40 individuals with 4 variables, from [Husson *et al.* 2011]

We seek to analyze the data set represented by $V_{\bullet\bullet}$, $\mathcal{C}$ being a set of samples from a larger

set (of missions), what we call the targeted market. Therefore, we also need to evaluate the dependency of the results of the analysis on the subpopulation $\mathcal{C}$, should it be replaced by another subpopulation $\mathcal{C}'$ that stems from the same market.

On the one hand, we need to analyze the cloud of individuals, so as to identify similar versus very different individuals. On the other hand, variables might be redundant or complementary to explain individual specificities or subpopulation inertias, therefore we need to evaluate their correlations. Understanding this duality between individual and variable analyses will help us highlight profiles adapted to the description of the tendencies and extreme individuals of the population at stake.

D.1 Cloud of individuals and scaling

We may use the canonical base of $\mathbb{R}^\kappa$ denoted by $(\vec{e}_k)_{k\in[\![1,\kappa]\!]}$ to write:

$$\vec{V}_{c\bullet} = \sum_{k=1}^{\kappa} V_{ck} \cdot \vec{e}_k \tag{D.1.1}$$

In order to reflect dissimilarity between individuals, we determine their Euclidian distance in $\mathbb{R}^\kappa$:

$$d\left(\vec{V}_{c\bullet},\vec{V}_{j\bullet}\right)^2 = \sum_{k=1}^{\kappa} \left(V_{ck} - V_{jk}\right)^2 \tag{D.1.2}$$

However, if variables are heterogeneous, *e.g.* with different units (efforts versus moments), different magnitudes (vertical versus lateral load variations) or very different dispersions (if a path allows freedom of acceleration versus freedom of obstacle avoidance), then the different terms of the sum are not comparable. In order to adjust the set of variables, we can scale them by reducing them.

We define for each variable $V_{\bullet k}$ and on a given population $\mathcal{C}$ the statistical average $\overline{V}_k$ and the standard deviation s_{V_k} by:

$$\overline{V}_k = \frac{1}{n}\sum_{c=1}^{n} V_{ck} \qquad s_{V_k} = \sqrt{\frac{1}{n}\sum_{c=1}^{n}\left(V_{ck} - \overline{V}_k\right)^2} \tag{D.1.3}$$

The variance of the k-th variable is given by $\mathrm{Var}\ (V_{\bullet k}) = \left(\overline{V}_k\right)^2$.

Let us denote $Z^{V,\mathcal{C}}$ the variable V scaled (centered and reduced) over observed population $\mathcal{C}$ and defined by:

$$Z^{V,\mathcal{C}}_{ck} = \frac{V_{ck} - \overline{V}_k}{s_{V_k}} \tag{D.1.4}$$

The centering and reduction step must be kept in mind in order to translate the results of further statistical studies into base variables.

Observing the distance between scaled observations of two individuals amounts to using a new distance:

$$d\left(\vec{V}_{c\bullet},\vec{V}_{j\bullet}\right) = {}^{T}\left(\vec{V}_{c\bullet}-\vec{V}_{j\bullet}\right).{}^{T}(\Sigma)^{-1}.\Sigma^{-1}.\left(\vec{V}_{c\bullet}-\vec{V}_{j\bullet}\right) = \left\|\vec{V}_{c\bullet}-\vec{V}_{j\bullet}\right\|_{S}^{2} \tag{D.1.5}$$

where ${}^{T}(\bullet)$ is the transposition operator and $\Sigma = \begin{pmatrix} s_{V_1} & \cdots & 0 \\ \vdots & \ddots & \vdots \\ 0 & \cdots & s_{V_\kappa} \end{pmatrix}$

The center (of gravity) of the cloud of individuals is given by the joint information of all variables' average values (see Fig. D.2):

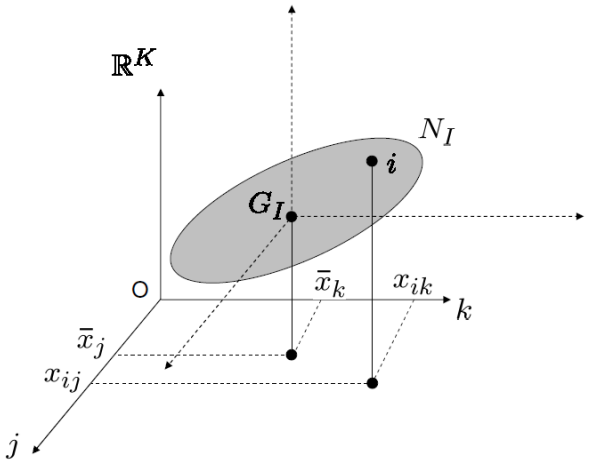

Fig. D.2: Center G of an individual cloud, from [Husson *et al.* 2011]

$$\vec{G}_{\mathcal{C}} = \left(\overline{V}_k\right)_{k\in[\![1,\kappa]\!]} \tag{D.1.6}$$

The inertia of the cloud quantifies the spread of the cloud. It generalizes the variance/dispersion of a scalar variable over a population (see Fig. D.3):

$$I(V_{\bullet\bullet}) = I_{\bullet\bullet}^{V,\mathcal{C}} = \frac{1}{n}\sum_{c=1}^{n} d\left(\vec{V}_{c\bullet},\vec{G}_{\mathcal{C}}\right)^2 = \sum_{k=1}^{\kappa} s_{V_k}^2 \tag{D.1.7}$$

D.2 Correlation of variables

In this section, we assimilate the random variable $V_{\bullet k}$ to the vector of its realization over population $\mathcal{C}$.

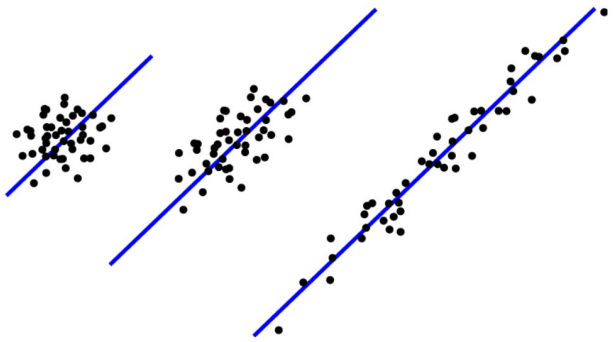

Fig. D.3: The inertia measures the total dispersion of the individual cloud

$$V_{\bullet k} = (V_{ck})_{c\in[1,n]} \tag{D.2.1}$$

The similarity between two variables is evaluated on their joint observations on population $\mathcal{C}$ by their linear correlation coefficient:

$$\begin{aligned} \text{corr}\ (V_{\bullet k},V_{\bullet l}) &= \frac{\text{covar}\ (V_{\bullet k},V_{\bullet l})}{s_{V_k}\cdot s_{V_l}} \\ &= \frac{1}{n}\sum_{c=1}^{n}\frac{\left(V_{ck}-\overline{V}_k\right)\cdot\left(V_{cl}-\overline{V}_l\right)}{s_{V_k}\cdot s_{V_l}} \\ &= {}^{T}(V_{\bullet k})\cdot V_{\bullet l} \end{aligned} \tag{D.2.2}$$

We denote Q the covariance matrix:

$$Q_{\mathcal{C}} = \begin{pmatrix} \text{Var}\ (V_{\bullet 1}) & \text{covar}\ (V_{\bullet 1},V_{\bullet 2}) & \cdots & \text{covar}\ (V_{\bullet 1},V_{\bullet \kappa}) \\ \text{covar}\ (V_{\bullet 1},V_{\bullet 2}) & \text{Var}\ (V_{\bullet 2}) & \cdots & \vdots \\ \vdots & & \ddots & \\ \text{covar}\ (V_{\bullet 1},V_{\bullet \kappa}) & \cdots & & \text{Var}\ (V_{\bullet \kappa}) \end{pmatrix} \tag{D.2.3}$$

Note that $I(V_{\bullet\bullet}) = \text{Tr}(Q)$ and that:

$$\Sigma^{-1}\cdot Q\cdot\Sigma^{-1} = \begin{pmatrix} 1 & \text{corr}\ (V_{\bullet 1},V_{\bullet 2}) & \cdots & \text{corr}\ (V_{\bullet 1},V_{\bullet \kappa}) \\ \text{corr}\ (V_{\bullet 1},V_{\bullet 2}) & 1 & \cdots & \vdots \\ \vdots & & \ddots & \\ \text{corr}\ (V_{\bullet 1},V_{\bullet \kappa}) & \cdots & & 1 \end{pmatrix} \tag{D.2.4}$$

re-using the matrix Σ defined for Eq. D.1.5. The covariance matrix is positive definite. The covariance operation may therefore denote the scalar product of two variables. Note that $\text{covar}\ \left(Z_k^{\bullet,\bullet},Z_l^{\bullet,\bullet}\right) = \text{corr}\ \left(Z_k^{\bullet,\bullet},Z_l^{\bullet,\bullet}\right)$ for any couple of reduced variables.

The (marginal) inertia of a scalar variable is another word to denote its variance:

$$\text{Var}\ (V_{\bullet k}) = I_{\bullet k}^{V,\mathcal{C}} = \frac{1}{n}\sum_{c=1}^{n}\left(V_{ck} - \overline{V}_k\right)^2 = s_{V_k}^2 \tag{D.2.5}$$

The inertia given by a data subset consisting of two uncorrelated variables is the sum of the variances of each variable:

$$\text{If}\ \ \text{covar}\ (A,B) = 0\ \ \text{Then}\ \ I_{\bullet\bullet}^{A\otimes B,\mathcal{C}} = I_{\bullet\bullet}^{A,\mathcal{C}} + I_{\bullet\bullet}^{B,\mathcal{C}} \tag{D.2.6}$$

Let us denote Span $(\vec{a}_l)_{l\in[\![1,p]\!]}$ the set of all linear combinations of a set of vectors $(\vec{a}_l)_{l\in[\![1,p]\!]}$:

$$\text{Span}\ (\vec{a}_k)_{k\in[\![1,p]\!]} = \left\{\vec{x} \mid \exists\vec{\eta}\in\mathbb{R}^p,\ \vec{x} = \sum_{k=1}^{p}\eta_k\cdot\vec{a}_k\right\} \tag{D.2.7}$$

The projection of the an individual joint information $\vec{V}_{c\bullet} \in \mathbb{R}^\kappa$ onto a 1D subspace Span $(\vec{v})$ is given by:

$$\vec{V}_{c\bullet}\Big|_{\vec{v}} = \sum_{k=1}^{\kappa} V_{ck}\cdot\widetilde{v}_k \tag{D.2.8}$$

denoting $\widetilde{v}$ the direction of the vector $\vec{v}$.

The projection of a dataset $V_{\bullet\bullet}$ of dimension $n*\kappa$ onto a linear subspace $W\subset\mathbb{R}^\kappa$ described by a base (*i.e.* p uncorrelated variables) $\left(\widetilde{\vec{v}}_l\right)_{l\in[\![1,p]\!]}$, $p<\kappa$ is a new observation base $V_{\bullet\bullet}|_W$ of dimension $n*p$. Its inertia is given by:

$$I_{\bullet\bullet}^{W,\mathcal{C}} = \sum_{l=1}^{p} I_{\bullet l}^{W,\mathcal{C}} = \sum_{l=1}^{p}\text{Var}\ \left(V_{\bullet\bullet}|_{\widetilde{\vec{v}}_l}\right) \tag{D.2.9}$$

Decomposing the inertia of a dataset on specific subsets of its space is the key to unveil new variables that best explain the variability of the individuals of the sample.

D.3 Principal Component Analysis (PCA)

D.3.1 Why PCA?

The inertia of a finite population represents the amount of distance between individuals in the population. It is a measure of its variability and is important to determine what fraction of a population can be considered large or extreme in terms of a synthetic variable, as well as how distant these extrema will be from the population's average.

In Chapters IV and V, the variables used to study pseudo-fatigue over a population are numerous. However, they are also inter-independent, meaning that a smaller number of variables can be found to evaluate the inertia of the population.

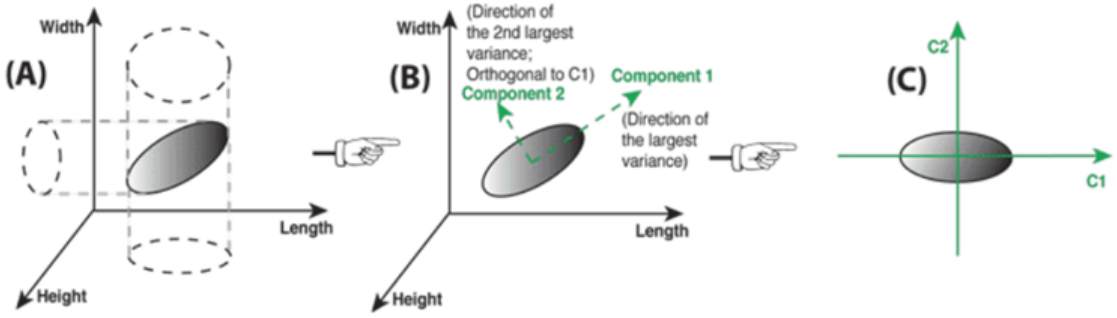

Fig. D.4: PCA seeks the optimal subspace over which to project the individual cloud and save its inertia

PCA is a variable reduction method that seeks an approximate representation of a given observation plan $X_{\bullet\bullet}$ of size $n \otimes \kappa$ using a subspace B of $\mathbb{R}^p$ with $p < \kappa$. In other words, we are looking for an optimal projection of the cloud that minimizes the loss of inertia (see Fig. D.4) while reducing the dimension from κ to p (Fig. D.5).

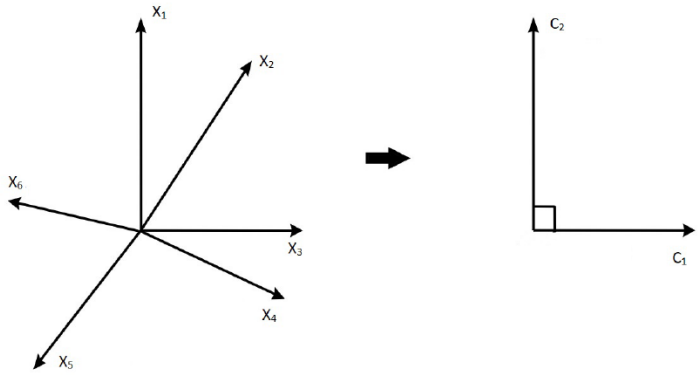

Fig. D.5: PCA helps to determine a smaller number of complementary uncorrelated variables to describe the observations

D.3.2 Principal component determination

Let us denote $A^{\mathcal{C}'}$ the correlation matrix made from the correlations between all scaled variables on the dataset $\mathcal{C}$:

$$A^{\mathcal{C}'} = \left(\text{corr}\ \left(Z^{X,c}\bullet k, Z^{X,c}\bullet h\right)\right)_{(k,h)\in[\![1,\kappa]\!]^2} \tag{D.3.1}$$

Principal components are weighted eigenvectors of the correlation matrix $A^{\mathcal{C}'}$. $\mathcal{C}'$ is the scaled version of the dataset. The eigenvectors of this matrix are denoted $\left(\vec{b}_h\right)_{h\in[\![1,\kappa]\!]}$. The weight of each principal component is its associated eigenvalue $\sqrt{\lambda_h}$:

$$\forall h \in [\![1,\kappa]\!], \quad A^{\mathcal{C}'} \cdot \overrightarrow{b}_h = \lambda_h \cdot \overrightarrow{b}_h \tag{D.3.2}$$

$$\lambda_1 \geq \lambda_2 \geq \cdots \geq \lambda_\kappa \geq 0 \tag{D.3.3}$$

$$\forall h \in [\![1,\kappa]\!], \quad \frac{1}{n}\sum_{c=1}^{n}\left(Z_{c\bullet}^{X,\mathcal{C}}\big|_{\overrightarrow{b}_h}\right)^2 \tag{D.3.4}$$

$$\sum_{h=1}^{\kappa}\lambda_h = I_{\bullet\bullet}^{\bullet,\mathcal{C}'} = \kappa \tag{D.3.5}$$

$$\forall h \neq l, \quad \text{corr}\left(\overrightarrow{b}_h, \overrightarrow{b}_l\right) = 0 \tag{D.3.6}$$

$$\forall h \in [\![1,\kappa]\!], \quad \text{Var}\left(\overrightarrow{b}_h\right) = 1 \tag{D.3.7}$$

denoting $I_{\bullet\bullet}^{\bullet,\mathcal{C}'}$ the inertia of the total scaled dataset $\mathcal{C}'$.

For a given target dimension p, the optimal base for a subspace B^p over which to project and observe the dispersion of the individual cloud is given by $\left(\overrightarrow{b}_h\right)_{h\in[\![1,p]\!]}$. The inertia of the cloud calculated on this new space is given by:

$$I_{\bullet\bullet}^{B^p,\mathcal{C}} = \sum_{h=1}^{p} I_{\bullet h}^{B^p,\mathcal{C}} = \sum_{h=1}^{p}\lambda_h \tag{D.3.8}$$

We denote the coordinates of each principal component $\left(\sqrt{\lambda_h}\cdot\overrightarrow{b}_h\right)$ using the canonical base of $\mathbb{R}^\kappa$ by:

$$\sqrt{\lambda_h}\cdot\overrightarrow{b}_h = \sum_{k=1}^{\kappa}\sqrt{\lambda_h}\cdot b_{hk}\cdot\overrightarrow{e}_k \tag{D.3.9}$$

denoting $\overrightarrow{e}_k$ the k-th elementary vector of $\mathbb{R}^\kappa$.

D.3.3 Individuals on a principal space

An individual joint information is described on $\mathcal{B} = \text{Span}\left(\overrightarrow{b}_h\right)_{h\in[\![1,p]\!]}$ in a fashion similar to Eq. D.1.1 by:

$$\overrightarrow{S}_c = \sum_{h=1}^{\kappa} S_{ch}\cdot\overrightarrow{b}_h \tag{D.3.10}$$

Note that c is the same individual that yields the absolute vector $\overrightarrow{X}_{c\bullet}$, the scaled observations $Z_{c\bullet}^{X,\mathcal{C}}$ and the coordinates in the principal space $\mathcal{B}$ $\overrightarrow{S}_c$.

Let's consider the marginal inertia brought by an individual to the global inertia of the population, calculated in Eq. D.1.7:

$$I_{c\bullet}^{X,\mathcal{C}} = \sum_{k=1}^{\kappa} \left(X_{c,k} - \overline{X}_k \right)^2 \tag{D.3.11}$$

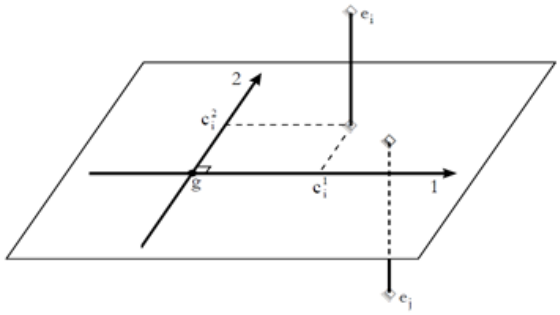

Fig. D.6: An individual is well represented on a subspace if its marginal inertia is saved after projection

The difference between the total inertia borne by one individual, and inertia on the subspace $\mathcal{B}$, can be seen as the distance between the individual's actual observations on the scaled dataset $\mathcal{C}'$ and their projection on the subspace $\mathcal{B}$ (see Fig. D.6). Their ratio denotes the quality of representation of the individual on $\mathcal{B}$ and is given by a cosine-like formula:

$$o_{c,\bullet}^{\mathcal{B}} = \frac{I_{c\bullet}^{\mathcal{B},\mathcal{C}}}{I_{c\bullet}^{Z^{X,\mathcal{C}},\mathcal{C}}} = \frac{\left\| \vec{S}_c \right\|^2}{\left\| Z_{c\bullet}^{X,\mathcal{C}} \right\|^2} = \frac{\sum_{h=1}^{p} \left(S_{ch} \right)^2}{\sum_{k=1}^{\kappa} \left(Z_{ck}^{X,\mathcal{C}} \right)^2} \tag{D.3.12}$$

The ratio between the projected marginal inertia of an individual onto the subspace $\mathcal{B}$ and the inertia of the individual cloud on said subspace denotes the contribution of this individual to creating this subspace.

$$\mathrm{cn}_{c,\bullet}^{\mathcal{B}} = \frac{I_{c\bullet}^{\mathcal{B},\mathcal{C}}}{I_{\bullet\bullet}^{\mathcal{B},\mathcal{C}}} = \frac{\left\| \vec{S}_c \right\|^2}{I_{\bullet\bullet}^{\mathcal{B},\mathcal{C}}} = \frac{\sum_{h=1}^{p} \left(S_{ch} \right)^2}{\sum_{j=1}^{n} \sum_{h=1}^{p} \left(S_{ch} \right)^2} \tag{D.3.13}$$

If an individual surpasses all other individuals to building the inertia of a principal component, it means that this principal component exists mainly because of said individual (see Fig. D.7).

D.3.4 Principal components as variables

From above equations (D.3.2, D.3.4, D.3.6), we can determine that variables $(S_{\bullet h})_{h \in [\![1,\kappa]\!]}$ are centered, that their variance is λ_h, and that they are uncorrelated:

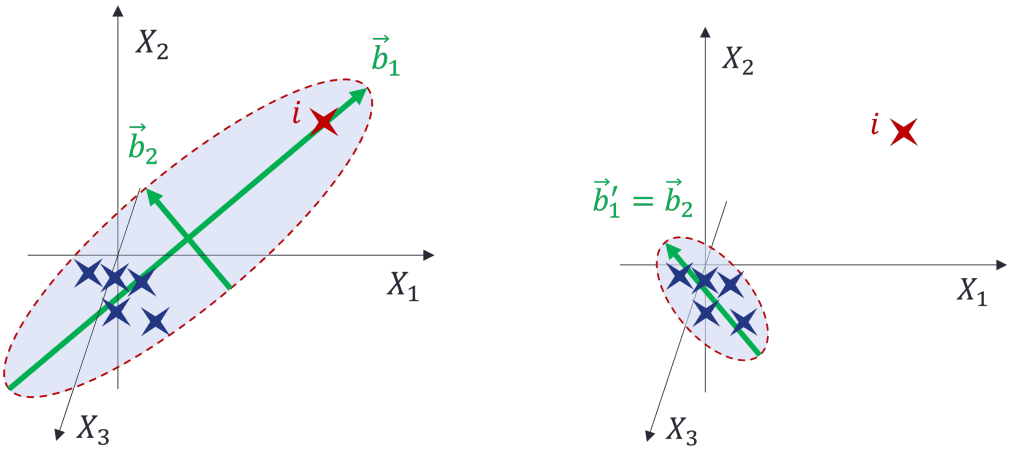

(a) Counting the outlier in PCA

(b) Ignoring the observations of the outlier in PCA

Fig. D.7: An outlier may have a large contribution to the inertia of a component. A preliminary implementation of PCA can aim at routing outliers out of the dataset prior to a second implementation.

$$\forall k, \quad \overline{\mathcal{B}}_h = \sum_{c=1}^{n} S_{ch} = 0 \tag{D.3.14}$$

$$\forall k, \quad s^2_{\mathcal{B}_h} = \sum_{c=1}^{n} (S_{ch})^2 = \lambda_h \tag{D.3.15}$$

$$\forall h \neq k, \quad \text{corr}\ (S_{\bullet h}, S_{\bullet k}) = 0 \tag{D.3.16}$$

Correlations between a centered and reduced base variable $Z^{X,\mathcal{C}}_{\bullet k}$ and profiles $S_{\bullet h}$ are used as the coordinates of said variable described on the principal space. This allows us to draw correlation circles as in Fig. D.8.

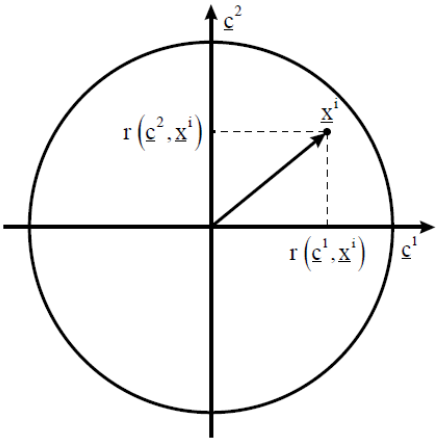

Fig. D.8: The correlations of a variable with two of the principal components is its coordinates on the correlation circle

Note that the correlation between a centered and reduced variable and a profile is similar to the square cosine of the angle between their corresponding vectors in $\mathbb{R}^{\kappa}$.

$$\text{corr}\ \left(Z_{\bullet k}^{X,\mathcal{C}}, S_{\bullet h}\right) = \frac{\text{covar}\ \left(Z_{\bullet k}^{X,\mathcal{C}}, S_{\bullet h}\right)}{I_{\bullet h}^{\mathcal{B},\mathcal{C}}} \tag{D.3.17}$$

$$= \frac{\sum_{c=1}^{n} \left(Z_{ck}^{X,\mathcal{C}} \cdot S_{ch}\right)^2}{\lambda_h} \tag{D.3.18}$$

$$= \frac{Z_{\bullet k}^{X,\mathcal{C}}\big|_{\overrightarrow{b}_h}}{\lambda_h} = \cos^2\left(Z_{\bullet k}^{X,\mathcal{C}}, \overrightarrow{b}_h\right) \tag{D.3.19}$$

denoting $\cos\left(Z_{\bullet k}^{X,\mathcal{C}}, \overrightarrow{b}_h\right)$ the cosinus of the angle between both vectors in the space $\mathbb{R}^{\kappa}$.

Methods to move back and forth from the space of absolute variables or the space of normalized variables to the space of principal components are developed and applied in Section V.4.

Appendix E

The effect of payload

E.1 Difficulties in payload sampling and normalization

In Section IV.2.1, we have identified, along with the knowledge of the vehicle model to design, three main factors determining the loads induced on a vehicle.

The analysis in Section IV.4 has explored the coupled effects of driver behavior and of the composition of the road on the pseudo-fatigue induced on a vehicle during a mission.

The last mission factor, Payload, was set to a fixed value through the whole study, below the maximum admissible payload of the vehicle. This setting corresponds to the vehicle and its driver's total mass, the mass of a few passengers and their associated luggage. The mass and its repartition in the vehicle are controlled and corrected for each new driver of the measurement campaign, by adding dummy weights.

A few individuals of the different measurement campaigns were tried under different mass settings on the same trip. Their payload setting was changed for practical reasons. The number of drivers with an alternative payload setting was insufficient to disambiguate the effect of payload to that of driver. In the absence of verified normalization method for the loads on a vehicle with respect to payload, we had excluded these few drivers from the datasets of interest.

We have previously anonymized the values of load intensity (in Newtons) by the total charge of the vehicle Q_{tot}, *i.e.* the total of all vertical reaction forces on the 4 wheels. However, for a given driver and a given trip, the relationship between the loads - and therefore pseudo-fatigue - and the payload is non-linear in general.

Global loads $\vec{\mathbf{F}}$ on a vehicle following a given spatial trajectory will vary according to the model $\mathcal{V}$ of the vehicle and to its payload $\mathcal{P}$ at the moment of driving.

The loads on a static vehicle are determined by its payload and by the pitch of the vehicle with respect to gravitational acceleration.

During a maneuver, ignoring the asperities of the road, the supplementary loads necessary to brake or to turn with the same maneuvering duration will be proportional to a difference

in payload. We may argue that the general rule for maneuvering in a heavier vehicle is to practice larger braking distances or to reduce speed during cornering, mitigating this effect. We ignore this theoretical effect of payload on appropriate driver behavior.

When the vehicle is in movement, its dynamical response bears a significant influence on its global loads. For a given vehicle model, a change in payload will modify the inertia of the vehicle. When driving on a pothole, the speed and inertia of the vehicle determine the and therefore the reaction forces on the axles. The mechanical response of the vehicle to obstacles is not linearly dependent on payload.

In Chapter III, we have made the hypothesis of quasi-static response of the structure to connect the instantaneous value of its axle loads to the instantaneous values of local Cauchy stresses in any sensible zone of the structure (Eq. III.4.1). We have not made the hypothesis that the complete response of the vehicle to road events was quasi-static.

Two different vehicle models differ, among other things, by the stiffness of their parts, their optimal or mounted wheel parameters and their wheelbase. All these differences make predicting the new efforts on a different vehicle difficult at first sight.

E.2 Payload and vehicle model effects observed on proving grounds

An ambition of the thesis was to seek an invariant of pseudo-fatigue with respect to the payload of a vehicle model. In this section, we present an investigation of loads or pseudo-damages induced by different vehicle models or by different payload settings of the same vehicle model.

Available service data presented in section IV.3 excluded measurement campaigns with set drivers and trips and varying payloads or vehicle models. Their marginal effect on the variability of pseudo-fatigue may yet be observed on proving grounds.

Proving ground tracks are more extensively studied in Chapter VII for the reconstruction of the pseudo-fatigue induced by missions of interest. A track contains one or a series of road events with set geometry. When trying a vehicle on a track, the test driver follows strict rules in terms of speed and trajectory. Therefore, a track is an episode with fixed Driver and Trip factors.

For a given vehicle model $\mathcal{V}$ and a given payload, for each wheel, we define the wheel charge $(Q_j)_{j\in[\![1,4]\!]}$ corresponding to the vertical effort on the vehicle if its pitch is perfectly orthogonal to gravitational acceleration. The total payload Q_{tot} of the vehicle is given by:

$$Q_{\text{tot}} = \sum_{j=1}^{4} Q_j \tag{E.2.1}$$

We have observed the values of magnitudes induced by proving ground tracks on the same vehicle with three different payload settings. The vehicle model of interest is the same as measurement campaigns US18-DT1 and US18-DT2. The three payload settings were driver

only, the reference payload used for the measurement and a larger payload setting used in other situations.

The repartition of mass changed between each payload setting: while the last setting has a slightly larger total payload than the second one, the charges on the front are slightly lighter while the charges on the rear axle are larger.

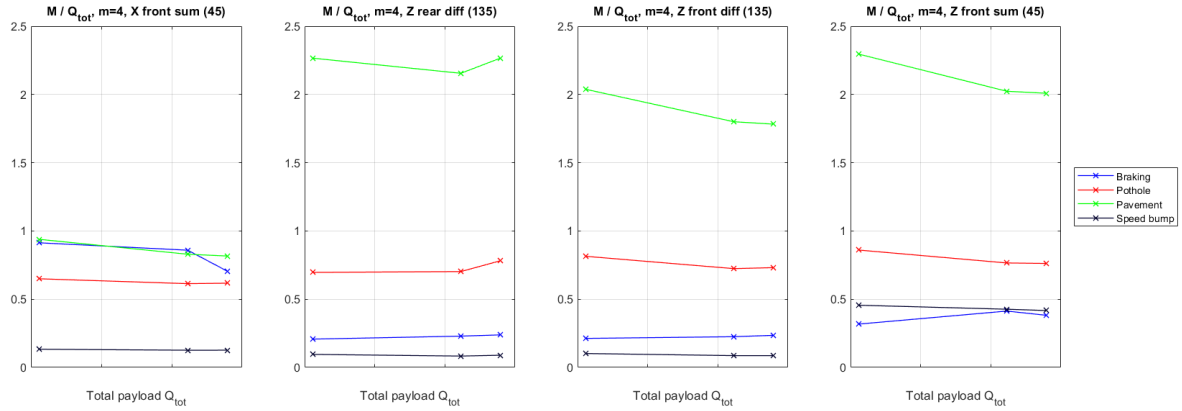

Fig. E.1: Magnitude on 4 local contexts, divided by total payload, observed on 4 tracks for 3 payload settings of the same vehicle. Payloads were hidden for reasons of confidentiality. The leftest payload setting is the driver-only configuration.

Fig. E.1 shows the values of magnitude divided by the total payload Q_{tot} against Q_{tot} for four tracks and on four local contexts. In such a graph, a horizontal line would denote a linear relationship between magnitude and total payload for a given track and a given driver. The number of observations for each track is insufficient to justify or root out such a hypothesis of linearity.

However, we can observe a shift in the trend of the ratio M/Q_{tot} on the pavement and braking tracks for the magnitudes associated with braking ($\widetilde{\alpha}_{X,f,45}$), to rear asymmetrical vertical loads ($\widetilde{\alpha}_{Z,r,135}$) and to front symmetrical vertical loads ($\widetilde{\alpha}_{Z,f,45}$). This switch in trend may be associated with the switch in front-rear repartition of the payload. This bodes ill for the existence of a linear or polynomial relationship between magnitude and total payload.

The same graph was drawn changing the abscissa to the charge associated with the axle of interest for the context, or to the ratio between the charge on the rear axle $Q_r = Q_{r,l} + Q_{r,r}$ and the total charge Q_{tot}, but no significant improve or relationship could be hinted at by these graphs.

Moreover, this observation of trends for different payload settings may not hold from one vehicle model to the other. We have conducted a similarly short study on a pool of different vehicle models from the company. These models may correspond to different motorizations, different suspension technologies and different wheelbases. Each of these parameters is susceptible to increase the complexity of the relationship between vehicle model and global loads. Ideally, the marginal effect of each parameter should be investigated separately.

Fig. E.2 shows graphs of absolute magnitude against total payload for 8 different vehicles on three tracks. The context of interest is chosen according to the event: symmetrical

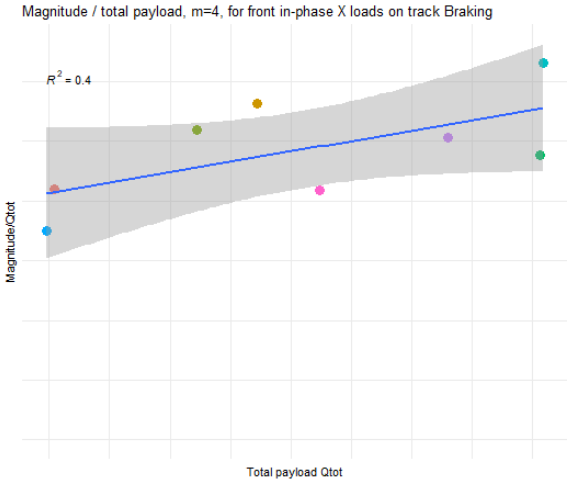

(a) Braking track, front braking loads

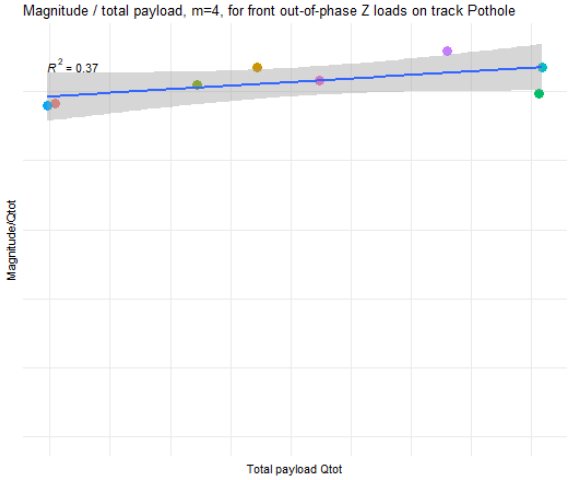

(b) Pothole track, front out-of-phase vertical loads

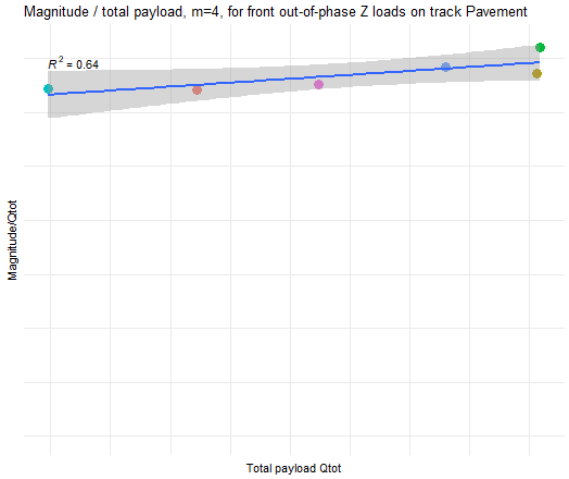

(c) Pavement track, front out-of-phase vertical loads

Fig. E.2: Magnitude (Basquin exponent $m = 4$) against total payload, observed on tracks for the same payload setting of different vehicles. Payloads and vehicle names were hidden for reasons of confidentiality.

front braking loads for the braking track, and asymmetrical vertical loads for potholes and pavements. The values of the magnitudes and payloads are hidden for confidential reasons. A simple linear regression algorithm is implemented to evaluate the relevance of a linear relationship between magnitude and payload. The R-squared coefficient does not allow us to ascertain a linear relationship with a 95% level of confidence. More observations would be required over the database of the company to conclude on this hypothesis of linearity.

If such a linear relationship between magnitude and total payload exists for a given payload setting of all vehicle models, its coefficients may take different values for each local context and for each track. Learning these coefficients may help predict the loads on a new vehicle on proving grounds.

A possible perspective to this analysis of the effect of vehicle model is the transformation of a measurement campaign from a vehicle of interest to a new vehicle model. In order to

adapt the results measured in service with a given vehicle to the design of a new vehicle, we would have to identify, on the trip of the campaign, the number and level of road events and apply an adequate coefficient on the magnitudes or load intensities measured on each road segment.

E.3 A conservative payload setting for the evaluation of service pseudo-fatigue

Payload is an aggravating factor: for given driver and trip, a larger payload generally means larger loads, even if the relation is not linear.

Evaluating service pseudo-fatigue and determining adequate design and validation conditions for a large average payload means designing vehicles for worse than their share. This method is considered to be conservative: it overestimates the pseudo-fatigue induced in service and therefore leads to designs that are more resistant than required.

Let us discuss the limitations of this hypothesis of conservativeness. Driver behavior and the Trip of the vehicle are not independent from Payload. Indeed, Payload is among other things a measure of the number of passengers in the vehicle. A mission with more passengers than usual may serve a specific purpose: drop children to school, to go out with relatives or to go on holidays. Contrariwise, a mission with a low number of passengers may generally be associated with a groceries run or to work commute. An increase in the trend of carpooling may modify these associations. Personal vehicles may be used with larger average payloads in such a transportation paradigm.

We cannot make strong presumptions on the conditional severity of drivers with respect to their passengers. Regionally, some studies show a relationship between number of passengers and more dangerous behaviors [Simons-Morton *et al.* 2005].

ECOLE DOCTORALE

Titre : Dimensionnement fiabiliste sous chargements complexes : de la spécification à la validation

Mots clés : Fatigue, chargements aléatoires, fiabilité, statistiques multivariées

Résumé : Durant l'usage normal (service) d'un véhicule personnel, les pièces de suspension et de la caisse subissent les efforts induits par la route sur les essieux de roue. Ces chargements sont susceptibles d'endommager les soudures et bords de tôles laminées par fatigue polycyclique.

La résistance de ces pièces est assurée par la définition d'exigences sur leur fiabilité. Leur dimensionnement suit une approche probabiliste : leur risque de défaillance avant une durée de vie objective est soumis à un maximum admissible, spécifié au niveau du système et propagé à travers tous ses composants.

Tout au long du développement d'un modèle de véhicule, les prototypes de nouvelles pièces sont soumis à des procédures de validation numériques ou physiques. Les chargements soumis en entrée de ces tests représentent une mission spécifique et artificielle. Celle-ci consiste en une agrégation représentative des situations les plus endommageantes auxquelles le véhicule peut faire face.

L'Interférence Contrainte-Résistance (SSI) est le procédé théorique majeur capable de maîtriser le risque de défaillance des pièces de la suspension et de la caisse d'un véhicule. Une variable aléatoire univariée, la Contrainte, évalue le potentiel d'endommagement qu'une mission du système peut induire sur une ou plusieurs de ses zones sensibles. Cette variable est opposée à la Résistance, qui prend en charge la variabilité du procédé de fabrication.

En théorie, la méthode SSI permet de définir des niveaux (objectifs) de référence pour la conception et la validation de la fiabilité du système. En revanche, son implémentation est actuellement réalisée séparément pour chaque jeu de zones sensibles simultanément endommagées lors de cas de chargement particuliers.

En pratique, une définition préliminaire et générale des conditions et niveaux de chargement pour les tests de validation est donnée par une référence historique. Cette référence peut prendre la forme d'un contrat d'éléments d'une piste d'essai, rencontrés par le véhicule à tester avec trajectoire et vitesse maîtrisées. L'adéquation du contrat piste est vérifiée a posteriori par l'application d'une méthode SSI sur les mesures d'un nouveau marché.

L'objectif de cette thèse est d'améliorer le processus de détermination de chargements de validation adéquats pour la fiabilité de futurs projets de modèles de véhicules. La fatigue induite isolément sur différents jeux de zones sensibles doit être caractérisée par plusieurs variables de comptage distinctes. Nous adaptons donc l'ensemble de la méthode de caractérisation de la Contrainte à l'usage de vecteurs de variables d'intérêt. Cette décomposition complète et minutieuse de la méthode et de ses hypothèses sous-jacentes la transforme en une "boîte blanche" qui révèle pléthore de nouvelles pistes de recherche pour aller plus loin dans la caractérisation des chargements de service du véhicule.

Notre stratégie est de révéler de nouvelles variables de sévérité associées aux différences de comportement conducteur et de contenu des trajets. Ces variables expliquent et quantifient la variabilité du potentiel de fatigue induit sur toutes les zones d'intérêt du véhicule. Elles sont déterminées au cours d'une analyse statistique multivariée sur les pseudo-endommagements induits par un échantillon de chargements en clientèle. Une distribution des conducteurs sur ces variables de sévérité est réalisée à partir d'une restriction motivée de la population des missions du véhicule. Cette distribution multivariée est ensuite traduite en chacune des distributions nécessaires à l'implémentation locale d'une méthode SSI. De nouvelles références de conception peuvent être proposées directement à partir de l'interprétation de la distribution de sévérité.

Enfin, nous formalisons une méthode de détermination de contrats de chargement équivalents qui reproduisent les cas de chargements et pseudo-endommagements de ces références de conception.

Institut Polytechnique de Paris
91120 Palaiseau, France

ECOLE DOCTORALE

Title : Reliable design under complex loads: from specification to validation

Keywords : Fatigue, variable amplitude loads, reliability, multivariate statistics

Abstract : Over the life of a personal vehicle, suspension and body parts are submitted to variable amplitude wheel axle loads caused by user maneuvers and obstacles of the road. In the absence of incident or abuse (service), these variable amplitude loads may lead weld beads, spot welds and metal sheet edges to failure by high cycle fatigue.

The sufficient resistance of vehicle suspension and body parts to service loads is ensured by the validation of requirements on their reliability. Their reliable design follows a probabilistic approach: a maximum admissible risk of failure before an objective lifetime is specified at the system level and propagated into requirements for all parts.

Throughout the development of a new vehicle model, prototypes of new parts are submitted to validation procedures in numerical or physical test environments. Loads input during these trials are the replication of a specific artificial mission that replicates, as much as possible, the most damaging but plausible situations that the vehicle can encounter.

The major theoretical framework to control the risk of failure of a part with respect to its variable population of missions (market) and to the uncertainties inherent to its manufacturing process, is Stress-Strength Interference (SSI). A univariate random variable denoted Stress evaluates indirectly a potential of damage that a mission may induce on one or several locations of the part. Its counterpart, Strength, represents the variable quality of the assembly at such locations. Knowledge of the distribution of Stress and on partial parameters of the distribution of Strength leads to a relationship between risk of failure and nominal part resistance. The method also permits determining adequate design references and validation trials to ensure the sufficient nominal resistance of the part.

In practice, initial load conditions for these trials are determined from a historical reference, such as a schedule of proving ground obstacles encountered with precise trajectory and speed instructions. The adequacy of the schedule is regularly tested against the application of SSI on each new market. New architectures, power technologies and use paradigms will modify the way vehicles are used and loaded in service as well as the stiffnesses and weaknesses of their structure, increasingly questioning design references and the choice of validation loads. A deeper understanding of the factors that underlie the variability of Stress is necessary to adapt such design objectives dynamically.

This thesis aims to improve the determination of adequate load levels and conditions as design references and validation procedures for the reliability of future vehicle projects. The fatigue of locations that are sensible to different kinds of global load cases of the structure must be characterized by different variables. Current (scalar) implementations of SSI manage separately different sets of sensible zones of the structure. In order to tackle their variability altogether, we have adapted the whole framework of service pseudo-fatigue evaluation to the use of vectors of quantities of interest. This led to a complete decomposition of the method and its underlying hypotheses. The resulting “white box” reveals new tracks for further improvement.

Our strategy is to unveil new variables, associated to differences in drivers and trips, underlying the variability of the fatigue induced in service on all locations of interest of the vehicle. These new variables are determined from a multivariate statistical analysis on a sample of service loads in a given region. They define a multidimensional severity, used to achieve a unified distribution, over the market of interest, of all quantities necessary for the implementation of SSI over all parts of the structure.

Finally, we formalize a method to derive fatigue-equivalent proving ground schedules, able to replicate the fatigue induced by a mission or associated with a new design reference.

Institut Polytechnique de Paris
91120 Palaiseau, France